21 April 2006 | $10

Science

INFLUENZA

AAAS

Volume 312, Issue 5772

COVER

Animal health experts, like this ornithologist in Croatia, are on high alert for signs of H5N1 avian influenza. Despite its rapid spread, H5N1 remains primarily a disease of birds. A special section beginning on page 379 examines obstacles to human-to-human transmission and options for responding to a possible pandemic, such as predictive computer models and "universal" vaccines.

Photo: Matko Biljak/Reuters

>> Editorial p. 337; Brevia p. 399; Research Article p. 404; Report p. 447. For related Podcast, see page 331 or go to www.sciencemag.org/about/podcast.dtl

DEPARTMENTS

EDITORIAL

SPECIAL SECTION

Influenza

INTRODUCTION

NEWS

REVIEW

PERSPECTIVES

NEWS OF THE WEEK

NEWS FOCUS

CONTENTS continued **>>**

Science

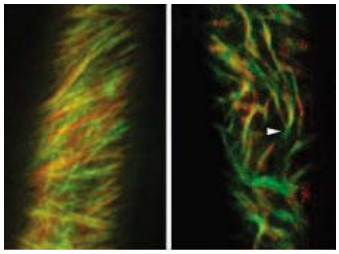

SCIENCE EXPRESS

www.sciencexpress.org

PHYSICS

Flip-Flopping Fractional Flux Quanta
T. Ortlepp et al.
The *d*-wave symmetry of high-temperature superconductors can be manipulated to form a logic gate in an electronic circuit.
10.1126/science.1126041

APPLIED PHYSICS

Atomic-Scale Coupling of Photons to Single-Molecule Junctions
S. W. Wu, N. Ogawa, W. Ho
Resonant tunneling of photoelectrons from the tip of a scanning tunneling microscope allows probing of adsorbed molecules with localized optical spectroscopy.
10.1126/science.1124881

PLANT SCIENCE

Visualization of Cellulose Synthase Demonstrates Functional Association with Microtubules
A. R. Paredez, C. R. Somerville, D. W. Ehrhardt
Cellulose synthase makes and deposits cellulose along plant cell walls as it is carried along microtubules.
10.1126/science.1126551

GEOCHEMISTRY

Drilling to Gabbro in Intact Ocean Crust
D. S. Wilson et al.
A drill core of ocean crust into an underlying solidified magma chamber shows that seismic layers correlate with changes in porosity, not rock type as had been thought.
10.1126/science.1126090

LETTERS

BOOKS *ET AL.*

POLICY FORUM

PERSPECTIVES

TECHNICAL COMMENT ABSTRACTS

EVOLUTION

BREVIA

VIROLOGY

RESEARCH ARTICLES

PLANETARY SCIENCE

VIROLOGY

CONTENTS continued >>

Science

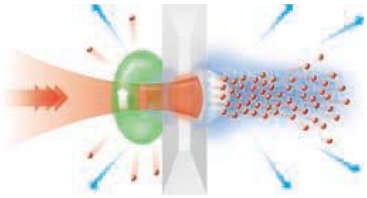

REPORTS

AAAS
ADVANCING SCIENCE, SERVING SOCIETY

SCIENCE (ISSN 0036-8075) is published weekly on Friday, except the last week in December, by the American Association for the Advancement of Science, 1200 New York Avenue, NW, Washington, DC 20005. Periodicals Mail postage (publication No. 484460) paid at Washington, DC, and additional mailing offices. Copyright © 2006 by the American Association for the Advancement of Science. The title SCIENCE is a registered trademark of the AAAS. Domestic individual membership and subscription (51 issues): $139 ($74 allocated to subscription). Domestic institutional subscription (51 issues): $650; Foreign postage extra: Mexico, Caribbean (surface mail) $55; other countries (air assist delivery) $85. First class, airmail, student, and emeritus rates on request. Canadian rates with GST available upon request, GST #1254 88122. Publications Mail Agreement Number 1069624. **Printed in the U.S.A.**

Change of address: Allow 4 weeks, giving old and new addresses and 8-digit account number. **Postmaster:** Send change of address to *Science*, P.O. Box 1811, Danbury, CT 06813–1811. **Single-copy sales:** $10.00 per issue prepaid includes surface postage; bulk rates on request. **Authorization to photocopy** material for internal or personal use under circumstances not falling within the fair use provisions of the Copyright Act is granted by AAAS to libraries and other users registered with the Copyright Clearance Center (CCC) Transactional Reporting Service, provided that $18.00 per article is paid directly to CCC, 222 Rosewood Drive, Danvers, MA 01923. The identification code for *Science* is 0036-8075/83 $18.00. *Science* is indexed in the *Reader's Guide to Periodical Literature* and in several specialized indexes.

CONTENTS continued **>>**

Bio-Rad and RNAi. Come have a look.

From delivery to detection, Bio-Rad supports your RNAi research.

With a broad range of proven delivery technologies, award-winning detection systems, and a suite of high-quality support products, it's clear that Bio-Rad has a vision for RNAi.

- Greatest choice of delivery technologies
- RNA and protein purification products
- Automated microfluidic RNA analysis
- Sensitive, optimized cDNA synthesis kits
- Systems for protein and mRNA detection

For a close look at Bio-Rad's tools for RNAi, visit us on the Web at **www.bio-rad.com/rnai/**

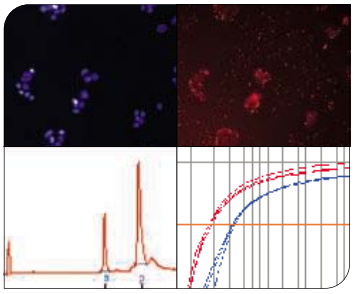

MCF-7 cells transfected using siLentFect™ reagent. RNA purified and analyzed using the Aurum™ total RNA kit and Experion™ system. Detection performed using iScript™ cDNA synthesis kit and the MyiQ™ system.

Visit us on the Web at **discover.bio-rad.com**
Call toll free at 1-800-4BIORAD (1-800-424-6723);
outside the US, contact your local sales office.

BIO-RAD

SCIENCE**NOW**

www.sciencenow.org DAILY NEWS COVERAGE

How Bats Got Off the Ground
Ramping up of bone growth gene may have made flight possible.

A Killer Memory
New findings indicate natural killer cells recall pathogens as well as other immune cells.

The Agony of Defeat
Brain scans of Canadian swimmers hint at how lost races impair future performance.

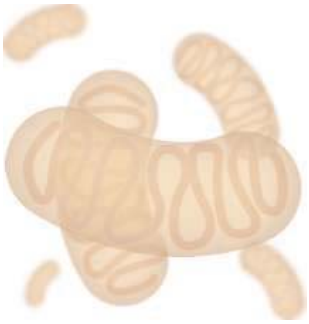

Mitochondria, a source of ROS.

SCIENCE**PODCAST**

Listen to *Science*'s special influenza podcast for 21 April, with segments on antivirals and vaccines, wild birds as an influenza vector, outbreak responses, and more.

www.sciencemag.org/about/podcast.dtl

SCIENCE'S **STKE**

www.stke.org SIGNAL TRANSDUCTION KNOWLEDGE ENVIRONMENT

EDITORIAL GUIDE: Reactive Oxygen Species, Friend or Foe?
N. R. Gough
ROS are implicated in multiple diseases and cell signaling processes.

REVIEW: Reactive Oxygen Species–Mediated Mitochondria-to-Nucleus Signaling—A Key to Aging and Radical-Caused Diseases
P. Storz
ROS serve as cellular signals of mitochondrial metabolism.

PERSPECTIVE: Dopaminergic Neurons Reduced to Silence by Oxidative Stress—An Early Step in the Death Cascade in Parkinson's Disease?
P. P. Michel, M. Ruberg, E. Hirsch
Activation of K_{ATP} by ROS contributes to neuronal cell death.

PROTOCOL: Oxidative Modification of Protein Tyrosine Phosphatases
R. F. Wu and L. S. Terada
A nonradioisotopic method reports on the presence of oxidatively modified (inactive) protein tyrosine phosphatases.

Do checkpoints stop aging?

SCIENCE'S **SAGE KE**

www.sageke.org SCIENCE OF AGING KNOWLEDGE ENVIRONMENT

PERSPECTIVE: Aging in Check
W. Dai and X. Wang
Defects in two spindle checkpoint proteins lead to premature cell senescence and accelerated aging.

PUBLISHED COMMENTS: Making Sense of SENS
A. de Grey
The author responds to criticisms in last week's Perspective on strategies for engineered negligible senescence.

Science opportunities in France.

SCIENCE **CAREERS**

www.sciencecareers.org
CAREER RESOURCES FOR SCIENTISTS

GLOBAL: Living and Working in France—Feature Index
E. Pain
Researchers worldwide get tips about working in France.

FRANCE: Guide to Trouble-Free Landing in France
E. Pain and A. Mauvais
Moving to France can be fun, but you still have to address administrative issues.

US: How to Be an American (Scientist) in Paris
A. Kotok
American scientists doing research in France can turn to a number of specialized funding opportunities.

CANADA: Canadians in France—Funding Programs
A. Fazekas
Next Wave describes two programs funding exchanges between France and Canada.

MISCINET: Should I Stay or Should I Go?
MentorDoctor
A minority postdoc ponders the 'academia or industry' question.

Separate individual or institutional subscriptions to these products may be required for full-text access.

Show Them What You See In Your Research

Announcing SigmaPlot 10

The Simplest and Most Effective Way to Analyze and Graph Data!

Join the more than 100,000 researchers worldwide who use SigmaPlot to easily customize every graphic detail and create compelling publication-quality graphs that clearly present their results for technical publications, presentations, or the web. Gain deeper insight into your data with easy-to-use data analysis tools — from sophisticated curve fitting to advanced mathematical calculations. Add SigmaStat and get 30 of the most frequently used statistical tests to analyze scientific research within SigmaPlot's statistics menu or take advantage of the optional Advisor Wizard that walks the non-statistician through the analysis of their data.

SigmaPlot allows you to:

> Create graphs easily and publish your work anywhere
> Import, analyze & manage data quickly and easily
> Choose over 80 different 2-D and 3-D graph types
> Customize every element of your graphs
> Instantly access SigmaPlot from Microsoft® Excel
> Streamline your work by automating repetitive tasks

SIGMAPLOT
Exact Graphs for Exact Science

Add SigmaStat to get easy-to-use, expert statistical analysis within SigmaPlot:

SigmaStat guides you through your analysis:

> Suggests the appropriate statistical test
> Checks assumptions in the data to avoid errors
> If your data violates any of those assumptions, the Advisor Wizard suggests another test
> Generates an intelligent report that explains your results in plain English – not statistical jargon
> Even handles messy data with missing values

Here are a few of the statistical tests SigmaStat performs:

> Regression (e.g., linear, multiple linear and nonlinear)
> Analysis-of-variance - ANOVA (e.g., independent, paired t-tests)
> Nonparametric statistics (e.g., Mann-Whitney, Wilcoxon)
> Rates and Proportions (e.g., Chi-square, contingency tables)
> Power and sample size (e.g., t-tests and proportions)
> Survival analysis (e.g., Kaplan-Meier, Gehan-Breslow)
> Regression diagnostics (e.g., multicollinearity, homoscedasticity)

FREE
INTERACTIVE DEMOS & 30-DAY TRIAL SOFTWARE AVAILABLE AT
WWW.SYSTAT.COM
OR CALL
1-800-797-7401

adsci

EDITED BY STELLA HURTLEY AND PHIL SZUROMI

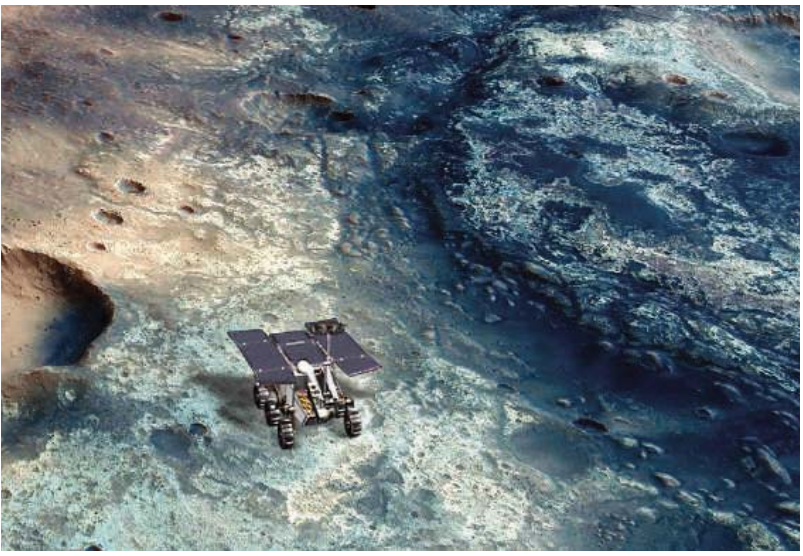

Wet and Dry Martian Processing

The main spectrometer on Mars Express, called OMEGA, has now returned a planet-wide data set, and **Bibring *et al.*** (p. 400) have used these results in combination with related observations by other Mars orbiters and the two rovers to reconstruct the history of water alteration on Mars. Hydrous minerals are abundant only in the oldest rocks; sulfur-rich minerals are present in some younger rocks, but more recent alteration is anhydrous. This record implies that there was likely surface water only early in Mars history, which gave way to more ephemeral acidic alteration. Water-rock interactions are not apparent after about 3.5 billion years ago.

Laser Acceleration Hits the Spot

One application of ultra-intense laser pulses is particle acceleration, but protons and ions accelerated from surfaces tend to have a large spread in energy and spatial extent. **Toncian *et al.*** (p. 410, published online 16 February; see the Perspective by **Dunne**) placed a hollow cylinder in the path of the accelerated protons and hit the cylinder with a well-timed, high-intensity laser pulse. The transit time of the protons is energy dependent, so varying the timing between the ion or proton generation pulse and the cylinder pulse allowed for energy selection and collimation of the protons exiting the cylinder.

Better to Be Left Hanging

The electronic properties of single-walled carbon nanotubes (SWNTs) have been understood in terms of both band and excitonic carrier models. An argument made in favor of the band model is that the photoexcitation spectra of the SWNTs matches their absorption spectra. **Itkis *et al.*** (p. 413) found that by suspending SWNT films, they could increase the photoconductivity response by at least five orders of magnitude, a value large enough to consider these materials as infrared detectors. Because the photoconductivity is bolometric (that is, has a thermal origin), these effects cannot be directly related to photoexcitations and conductivity models.

Faster Than Femtoseconds

The time resolution of chemical dynamics studies has generally been limited by the duration of laser pulses used as probes. Pulse durations now approach 1 femtosecond (fs), but some molecular events occur on even more rapid time scales. **Baker *et al.*** (p. 424, published online 2 March; see the Perspective by **Bucksbaum**) show that an 8-fs laser pulse can be used to observe nuclear dynamics of H_2 and methane after ionization with 0.1-fs (10^{-16} s) resolution. The technique relies on the electrons being ejected from the molecule by the laser pulse with a spread of velocities, which in turn leads to a spread, or chirp, in frequency of the photons released upon electron-ion recombination. The emitted photon frequency acts as a clock that is more precise than the excitation pulse.

Of Gold, Silver, and Diamonds

Nanoparticles can be assembled into a variety of crystalline lattices that are close-packed in nature, but more open structures reminiscent of the diamond lattice are harder to form. **Kalsin *et al.*** (p. 420, published online 23 February; see the Perspective by **Velev**) exploit electrostatic effects to assemble gold and silver nanoparticles, of the same size but coated with oppositely charged monolayers, into the diamond-like sphalerite lattice. Unlike the formation of elemental salt crystals, the screening interactions are on the same scale as the nanoparticles, and so only short-range forces direct the assembly. The presence of smaller charged nanoparticles that act as counterions improved crystalline quality.

Dating the Drake Passage

The opening of the Drake Passage, between the southernmost tip of South America and the Antarctic Peninsula, was an essential step in the development of the Antarctic Circumpolar Current. However, estimates of the age of the passage range from as early as 49 million years to as late as 17 million years ago, so it has been difficult to assess what role the opening played in climate change. **Scher and Martin** (p. 428; see the news story by **Kerr**) present a marine sedimentary record of ocean circulation derived from Nd isotopes in fish teeth found downstream from the Drake Passage for the interval between 46 and 33 million years ago. They find that the passage must have begun to open 41 million years ago, in the middle Eocene. This event long preceded the opening of the last remaining corridor, the Tasmanian Gateway, around 35 million years ago, and major ice sheet growth in Antarctica, which began around 34 million years ago.

Bird Flu H5 Structure Defined

The H5N1 "bird flu" virus is highly contagious and deadly in poultry. To date, infection of humans seems limited to direct bird-to-human transmission, but mortality in humans is high, and the question of whether the virus may adapt into a pandemic human strain is pressing. **Stevens *et al.*** (p. 404, published online 16 March) determined the structure of H5N1 hemagglutinin (HA) at 2.9 angstrom resolution

Continued on page 335

"I think the dosage needs adjusting. I'm not nearly as happy as the people in the ads."

It's time for genetics.

What if you could use DNA to identify patients who respond well to your drug? You might use that knowledge to reach more patients and expand your market, or to get a drug to market faster. Either way – patients win. Perlegen is helping drug companies do just that – today.

Working with you, we can comprehensively analyze the DNA from hundreds of patients taking your drug. Out of the millions of genetic variations between patients, we help you identify the ones that are associated with strong efficacy, poor efficacy, or side effects. Perlegen's unparalleled coverage of the genome and experienced team of analysts mean you get clinically relevant answers, not just data, in a matter of months.

We partner with the top pharmaceutical companies around the world. We also license late-stage drugs. If you have a drug that can benefit from our approach, please contact us.

Patients are waiting.

genetics@perlegen.com
Mountain View, California • 650-625-4500
Tokyo, Japan • +81 (0)3 3444-6080
www.perlegen.com

Targeting today's drugs. Discovering tomorrow's.™

PERLEGEN SCIENCES®

Continued from page 333

and examined the receptor-binding preference of this HA and specific mutants using a glycan microarray system. Mutations that convert avian H2 and H3 HAs to human receptor specificity did not cause a similar specificity switch in the H5N1 HA, but did permit binding to a natural human α2-6 glycan.

Network Interactions in Ecological Communities

Most studies on coevolution and mutualism between plants and animals have focused on interactions between pairs of species and ignore the wider network of interactions at the level of the ecological community. To fill this gap, **Bascompte *et al.*** (p. 431; see the Perspective by **Thompson**) analyzed a large set of coevolved networks, drawing on data from the tropics to the poles, to assess their structure and the implications for their stability and coevolution. Mutualistic networks are dominated by weak, asymmetric interactions, in which one partner in each mutualism depends strongly on the other while the other is only weakly dependent. This network structure confers stability to the wider ecological community.

MicroRNA and Innate Immune Responses in Plants

Plants mount an innate immune response when they detect pathogen-associated molecular markers such as bacterial flagellin. **Navarro *et al.*** (p. 436) now show that in *Arabidopsis*, bacterial flagellin induces the expression of the microRNA miR393, which in turn reduces the expression of three auxin receptors and eventually leads to the down-regulation of auxin signaling pathways that are implicated in disease susceptibility. This down-regulation then increases the plant's resistance to infection. This miRNA expression seems to act in parallel with independent transcriptional repression of the auxin receptors to ensure that an immune response is generated.

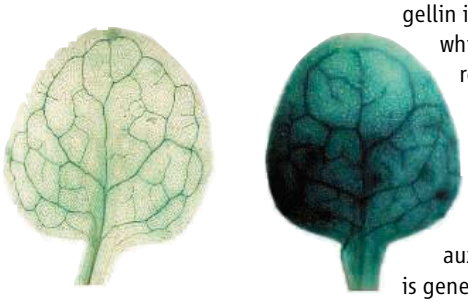

CREDIT: NAVARRO *ET AL.*

Nuclear Pore Production Line

The nucleus of eukaryotic cells is surrounded by a double membrane structure, the nuclear envelope, that is punctuated by nuclear pore complexes. During interphase, nuclear pores represent the exclusive sites of transport between the nucleus and the cytoplasm. Are these nuclear pore complexes generated by splitting of existing pores, or are they produced de novo? **D'Angelo *et al.*** (p. 440) present real-time imaging of nuclear pore complex assembly in living cells and suggest that nuclear pore complexes form de novo and are assembled from both sides of the nuclear envelope.

From in Silico to in Vitro Drug Discovery

Many currently available therapeutic drugs act by modulating signaling through G protein (heterotrimeric GTP-binding protein)–coupled receptors. The G-protein βγ subunit transmits signals from G protein–coupled receptors to their targets, and many crystal structures of such complexes have been solved. **Bonacci *et al.*** (p. 443; see the Perspective by **Tesmer**) used a computer program to predict which chemical compounds would bind to the interaction site on the βγ subunits and obtained potent small molecule inhibitors of protein-protein interactions. Furthermore, these molecules showed specificity for disrupting signaling-specific downstream targets, which suggests that such reagents might be both effective and relatively free of side effects.

Predicting Flu Dynamics

Taking influenza mortality data collected in the United States from 1972 to 2002 as a measure for seasonal influenza virus circulation and disease, **Viboud *et al.*** (p. 447, published online 30 March) investigated the synchrony of influenza epidemics across the United States. They found that severe epidemics were more synchronous than mild ones, and that work-related movement of people correlated with spread of infection better than long-distance travel or geographical distance between states. Adults were the primary transmitters of seasonal influenza, rather than children, as has been previously assumed. These findings have implications for the design of pandemic control strategies.

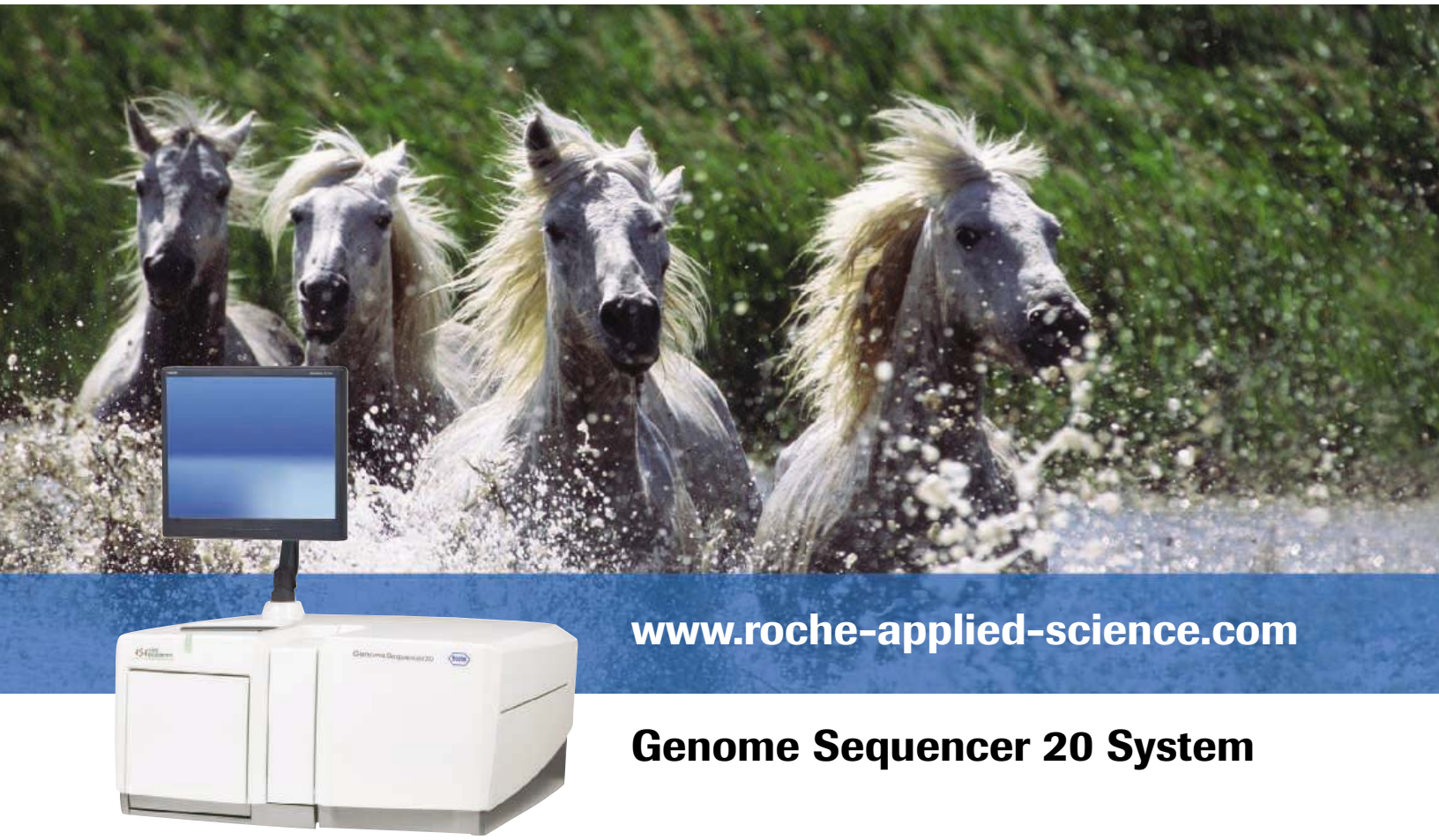

www.roche-applied-science.com

Genome Sequencer 20 System

First to the Finish

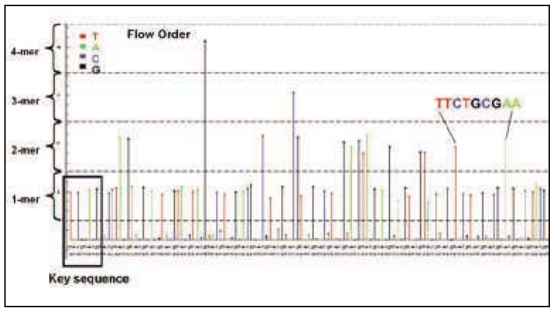

Flowgram of a GS 20 read

Sequence genomes like never before

- **Compare microbial genomes in weeks, not years**
- ***De novo* sequence a bacterial genome in fewer than 5 days**
- **Sequence more than 100 BACs per month**
- **Sequence >200,000 miRNAs, SAGE tags, or ditags (*e.g.*, CAGE) in 5.5 hours**

Coming soon:

Ultra-deep sequencing of amplicons – identify rare SNP patterns or cancer-associated mutations from complex samples

Harness the horsepower of the newest revolution in sequencing today — visit www.roche-applied-science.com/sis/sequencing/genome or contact your local sales representative.

454 LIFE SCIENCES

Roche Diagnostics

Roche Diagnostics GmbH
Roche Applied Science
68298 Mannheim
Germany

Peter S. Lu is the president and chief executive officer of Arbor Vita Corporation in Sunnyvale, CA. The company's focus is the use of PDZ domains in human therapeutics and diagnostics in oncology, neurology, and influenza. He also has patent applications in the area of influenza diagnostics and therapy.

Early Diagnosis of Avian Influenza

THE CURRENT WAVE OF PANDEMIC AVIAN INFLUENZA LOOKS LIKELY TO SPREAD VIA MIGRATING ducks into North America by early fall of this year. Although this form of influenza A virus primarily targets wild birds and poultry, it can infect some mammals. In the few human cases that have been reported (usually only after intimate contact with domestic birds), the infection followed an unusually aggressive course and more than half of the victims have died (on 24 March 2006, the World Health Organization reported 186 human cases and 105 fatalities). The danger is that if the virus adapts sufficiently to allow serial human-to-human transmission, a global human pandemic may rapidly develop.

Vaccination, drug treatment, and containment are all under consideration for influenza preparedness (and are discussed in some detail in the special section in this issue), but their use cannot be optimized unless infection is quickly detected. Early stages of influenza, when transmission first begins, lack distinguishing clinical symptoms and thus require a biochemical test. Because such a test will most likely be used under diverse conditions, ranging, for example, from emergency rooms to airports, it needs to be as straightforward and robust as possible. It should give an answer quickly, ideally in about 5 minutes. It should not require special storage, reagents, instruments, or personnel, nor generate hazardous byproducts such as more virions. It should work on a sample specimen that is easy to obtain and should provide specific information that will distinguish an emerging pandemic strain from seasonal influenza. Perhaps the most challenging requirement is that the test should be resistant to the mutational changes that are characteristic of influenza, allowing us to detect today's virus, not just yesterday's.

Unfortunately, current detection technologies—PCR (polymerase chain reaction), viral culture, and immunoassays—fall short of these requirements. PCR, which analyzes the viral genome, is the most sensitive but is slow (minimum time, 2 hours), requires highly trained personnel, and can miss new viral strains. Viral culture is the gold standard for diagnosis but is even slower (minimum time, several days), is more difficult to perform than PCR, and requires special high-security labs to minimize the risk of release of virions that are formed during the test. Immunoassays, like those used for the familiar home pregnancy test, give rapid results and are easy to perform but currently lack the necessary sensitivity and specificity to distinguish avian from seasonal influenza reliably. The few such immunoassay-based tests that claim to detect avian influenza are purportedly insensitive and are thus unlikely to pick up newly evolving strains.

Is all lost? There are glimmers of hope. Our understanding of the avian influenza virus is growing rapidly, and some of these early insights may be leveraged to facilitate its early detection. Especially important are viral diagnostic targets, such as the abundantly expressed NS1 viral protein that may be used by influenza to inhibit interferon-related host defenses and contribute to its virulence. It appears that this protein exists in a specific form in avian influenza. It could therefore be detected in a rapid diagnostic test by agents that are capable of binding to it but not to the NS1 proteins of typical non-avian human influenza. Such target-based tests will not only permit detection of today's avian influenza but may also be able to detect tomorrow's.

Early diagnosis in the form of a quick point-of-care test is a vital element in our defense against avian influenza. Efforts to develop vaccines and drugs must surely continue, but we cannot rely solely on these interventions. Vaccination presently suffers from the inability to target tomorrow's influenza. Drug treatment can limit influenza's spread, but only when the infection is quickly identified. The power of containment is still our traditional first line of defense against an epidemic, but rapid identification of infectious individuals or animals is crucial to treatment and to containment strategies. Accordingly, we need to put a major effort behind the development of tests that are quick, sensitive, specific, simple, and inexpensive. This may also alleviate the need to extensively train the personnel who administer and interpret these tests. We may or may not need such a test this year, but we will surely have to have it in the future.

– Peter S. Lu

10.1126/science.1128199

EDITED BY GILBERT CHIN AND JAKE YESTON

The fly and the parasite.

BIOMEDICINE

Mounting a Counterattack

Although pathogens display a remarkable ability to outmaneuver host defenses, this struggle has been described as a never-ending arms race. Through antigenic variation of their variant surface glycoproteins (VSGs), trypanosomes successfully evade host immune responses, rendering prevention via vaccination difficult at best. Baral *et al.* have engineered the latest attempt to combat *Trypanosoma brucei*, the causative agent of sleeping sickness, which is transmitted via the tsetse fly. One component of human serum, apoL-I, has been identified as being able to punch holes in most trypanosomes but is stymied by the serum resistance-associated (SRA) protein produced by the resistant strain *T. b. rhodesiense*. The authors chopped off the portion of apoL-I to which SRA binds and attached the rest to an antibody that recognizes VSGs. This conjugate proved efficacious in lysing trypanosomes in vitro and in curing mice suffering from an acute infection by *T. b. rhodesiense*, and it also completely cleared parasites from the bloodstream in chronically infected mice. — GJC

Nat. Med. **12**, 10.1038/nm1395 (2006).

MATERIALS SCIENCE

Bistable Atomic Memories

The conductivity of ferroelectric perovskites, such as strontium titanate, is related to lattice dislocations and local oxygen concentration. $SrTiO_3$ has a simple cubic structure and a high dislocation density at the crystal surfaces, and bistable switching between insulating and metallic states has been observed after doping with chromium.

Szot *et al.* show that bistable switching is possible in undoped $SrTiO_3$ crystals if the oxygen concentration is varied at the surface. For bulk crystals, cycling was achieved by heat treatment under vacuum to lower resistance, followed by reoxidation to a more insulating state at room temperature, and then restoration of the metallic state by exposure to an electric field under vacuum. Individual dislocations could also be switched using an atomic force microscope with a conducting tip; application of the local electric field transported oxygen along the dislocation, thereby varying the conductance. The material therefore holds strong promise for fabrication into memory devices with a bit size of only a few atoms and with state stabilities that would eliminate the current need for refreshing in fast-responding static and dynamic memory chips. — MSL

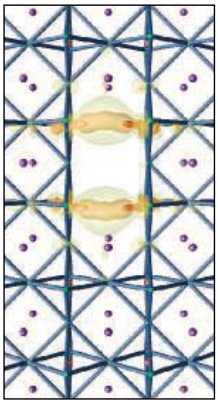

Simulated charge delocalization (orange) in a $SrTiO_3$ lattice defect (Sr, purple; Ti, red; O, green).

Nat. Mater. **5**, 312 (2006).

MOLECULAR BIOLOGY

Surveillance by No-bodies

Within eukaryotic cells, mRNAs that contain errors are subject to strict quality-control measures and are rapidly degraded to prevent any inadvertent molecular catastrophes. Dez *et al.* reveal some of the nuts and bolts of a similar quality-control system that monitors ribosome biogenesis. Ribosomes are built in the nucleolus and nucleoplasm before being exported into the cytoplasm, where they undergo final maturation and function as the protein-synthesizing workhorses of the cell. Dez *et al.* find that preventing the export of "under-construction" pre-ribosomes results in the rapid appearance of ribosomal RNA (rRNA) and protein components in distinct nucleolar foci they christen "No-bodies." Components of the nuclear exosome and the TRAMP polyadenylation complex—molecular assemblies that have been implicated in the elimination of defective nuclear RNAs—are also found to accumulate in the No-body, and furthermore, they seem to be responsible for concentrating the pre-60*S* ribosomes here. The large rRNAs are polyadenylated within the subcellular foci by the TRAMP complex, and this mark seems to tag the rRNAs for destruction by the exosome. Based on these results, the authors suggest that the No-body is the site at which surveillance of pre-ribosomes occurs, and they speculate that defects in maturation might be identified by the failure to displace pre-ribosome–associated factors, resulting in the recruiting of TRAMP. — GR

EMBO J. **25**, 1534 (2006).

CHEMISTRY

Polypropylene Piece by Piece

The properties of polypropylene plastic depend strongly on the relative stereochemistry of the methyl groups appended to every second carbon in the polymer chain. Elasticity, for example, arises from a structure with interspersed segments of random methyl configuration (termed atactic) and strictly parallel configuration (isotactic). Harney *et al.* present a catalytic system to prepare bulk quantities of polypropylene in which isotactic or atactic segments of any specified length can be incorporated in any desired order (demonstrated up to a total polymer molecular weight of ~170,000). The technique is especially promising for studying relations between molecular structure and bulk properties.

The catalyst precursor is a $Zr(CH_3)_2$ complex with amidinate and pentamethylcyclopentadienyl ligands. Scission of a Zr-CH_3 bond by an anilinium borate salt yields a catalyst that selectively produces isotactic polypropylene. The authors previously showed (by adding half an equivalent of borate) that if only half of the precursors lose CH_3, ligand migrations between pre-

CREDITS (TOP TO BOTTOM): PATRICK ROBERT/CORBIS; CDC; SZOT *ET AL.*, *NAT. MATER.* **5**, 312 (2006)

cursor and active catalysts result in atactic polymer. They now find that the CH_3 groups can be restored to the catalyst complexes, regenerating the precursor, by adding another $Zr(CH_3)$ compound bearing a bulky neopentyl substituent. They can thereby tune polymer stereochemistry by successively adding either borate (to prepare an isotactic segment) or the bulky Zr methyl transfer agent (for an atactic segment). — JSY

Angew. Chem. Int. Ed. **45**, 2400 (2006).

CELL BIOLOGY

What Comes In Must Get Out

Certain bacterial toxins, viruses, and proteins enter cells by an atypical form of endocytosis mediated by caveolae, which are cholesterol- and glycolipid-rich membrane invaginations particularly prevalent on the endothelial cells that line blood vessels. The mechanisms involved in caveolar uptake are not well understood. Choudhury *et al*. find that syntaxin 6, a protein known to be involved in membrane fusion events in the secretory pathway, is required. It seems that syntaxin 6 is involved in the recycling and delivery of caveolar components, such as caveolin, GM1 ganglioside, and glycosylphosphatidylinositol-linked proteins, to the cell surface via the Golgi complex.

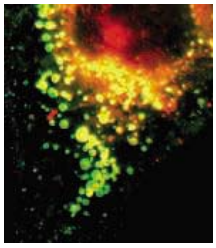

Inhibition of syntaxin 6 results in cytoplasmic accumulation of cholesterol (red) and GM1 (green).

CREDIT: CHOUDHURY *ET AL.*, *NAT. CELL BIOL.* **8**, 317 (2006)

A key factor in the process may be ganglioside trafficking; the addition of GM1 ganglioside to cells with inhibited syntaxin 6 restored caveolin delivery to the cell surface, and caveolar endocytosis. — SMH

Nature Cell Biol. **8**, 317 (2006)

ASTROPHYSICS

Double Take

Most stars exist as binaries, in which two stars orbit one another about their common center of mass. Statistically, individual stars can span a wide range of masses, and there are many more light stars than heavy ones, so if binaries assemble at random, the relative masses of their constituents should generally differ significantly. Moreover, the more massive star in the pair should evolve and die more quickly than its companion.

Pinsonneault and Stanek suggest that a surprisingly high proportion of binaries are twins, with both stars of about the same mass and age. In a spectroscopic sample of the nearby Small Magellanic Cloud galaxy, about half of the well-separated binary pairs are twins, far more than chance would predict. Other literature reports are consistent with twins constituting at least a quarter of all binaries. Because the twin stars are identical, they must both have formed at the same time and evolved at the same rate. This preponderance of twins may impinge upon a range of astrophysical questions related to the interactions, mergers, and deaths of binary stars, including the progenitors of (Type Ia) supernovas and gamma-ray bursts. — JB

Astrophys. J. **639**, L67 (2006).

Science STKE AAAS

www.stke.org

<< Signaling Stress in Asthma

That stress worsens childhood asthma seems paradoxical. Stress promotes the secretion of cortisol (which diminishes airway inflammation) and epinephrine (which acts as a bronchodilator); these chemicals should alleviate asthmatic symptoms. Miller and Chen studied the relationship between life stress and expression of the glucocorticoid receptor (GR) and the β_2-adrenergic receptor (β_2AR). They administered a stress assessment interview to 38 healthy children and 39 who had been diagnosed with asthma, and quantified the expression of the GR and the β_2AR in leukocytes in blood samples. Although the levels of β_2AR and GR mRNA were greater in children with asthma, chronic stress was associated with a decrease in the abundance of β_2AR mRNA in asthmatic children and an increase in β_2AR abundance in healthy children. No effect of chronic stress alone on GR was apparent, and isolated major life events (acute stressors) within the past 3 or 6 months failed to affect the expression of either the β_2AR or the GR. However, major life events that occurred in the context of chronic stress exacerbated the effects of chronic stress on the β_2AR and uncovered a decrease in GR expression in asthmatic children. Thus, the effects of stress on β_2AR and GR expression were in a direction consistent with decreased sensitivity to glucocorticoids and β_2-adrenergic agonists, which could have implications for the clinical management of asthmatic children. — EMA

Proc. Natl. Acad. Sci. U.S.A. **103**, 5496 (2006).

www.sciencemag.org

Science

1200 New York Avenue, NW
Washington, DC 20005
Editorial: 202-326-6550, FAX 202-289-7562
News: 202-326-6500, FAX 202-371-9227

Bateman House, 82-88 Hills Road
Cambridge, UK CB2 1LQ
+44 (0) 1223 326500, FAX +44 (0) 1223 326501

Subscription Services For change of address, missing issues, new orders and renewals, and payment questions: 800-731-4939 or 202-326-6417, FAX 202-842-1065. Mailing addresses: AAAS, P.O. Box 1811, Danbury, CT 06813 or AAAS Member Services, 1200 New York Avenue, NW, Washington, DC 20005

Institutional Site Licenses please call 202-326-6755 for any questions or information

Reprints: Author Inquiries 800-635-7181
Commercial Inquiries 803-359-4578
Corrections 202-326-6501

Permissions 202-326-7074, FAX 202-682-0816

Member Benefits Bookstore: AAAS/BarnesandNoble.com bookstore www.aaas.org/bn; Car purchase discount: Subaru VIP Program 202-326-6417; Credit Card: MBNA 800-847-7378; Car Rentals: Hertz 800-654-2200 CDP#343457, Dollar 800-800-4000 #AA1115; AAAS Travels: Betchart Expeditions 800-252-4910; Life Insurance: Seabury & Smith 800-424-9883; Other Benefits: AAAS Member Services 202-326-6417 or www.aaasmember.org.

science_editors@aaas.org	(for general editorial queries)
science_letters@aaas.org	(for queries about letters)
science_reviews@aaas.org	(for returning manuscript reviews)
science_bookrevs@aaas.org	(for book review queries)

Published by the American Association for the Advancement of Science (AAAS), *Science* serves its readers as a forum for the presentation and discussion of important issues related to the advancement of science, including the presentation of minority or conflicting points of view, rather than by publishing only material on which a consensus has been reached. Accordingly, all articles published in *Science*—including editorials, news and comment, and book reviews—are signed and reflect the individual views of the authors and not official points of view adopted by the AAAS or the institutions with which the authors are affiliated.

AAAS was founded in 1848 and incorporated in 1874. Its mission is to advance science and innovation throughout the world for the benefit of all people. The goals of the association are to: foster communication among scientists, engineers and the public; enhance international cooperation in science and its applications; promote the responsible conduct and use of science and technology; foster education in science and technology for everyone; enhance the science and technology workforce and infrastructure; increase public understanding and appreciation of science and technology; and strengthen support for the science and technology enterprise.

Information for Contributors

See pages 102 and 103 of the 6 January 2006 issue or access www.sciencemag.org/feature/contribinfo/home.shtml

Now! Real-Time PCR results in under 40 minutes!

Real Affordable
Applied Biosystems
7300 Real-Time PCR System

Real Versatile
Applied Biosystems
7500 Real-Time PCR System

Real Fast
Applied Biosystems
7500 Fast Real-Time PCR System

Looking for faster real-time PCR results?

Our new Applied Biosystems 7500 Fast Real-Time PCR System, the choice for labs in a hurry, is the latest addition to the innovative family of real-time PCR systems from Applied Biosystems. It enables 96-well format high-speed thermal cycling, easily integrating into your lab's workflow. Whichever system you choose, you'll get the gold standard combination of TaqMan® assays and the proven performance of the industry leader—plus unbeatable real-time chemistry choices, powerful software, and a comprehensive selection of reagents and consumables. For the real deal in real-time PCR, visit http://info.appliedbiosystems.com/realtimepcr

Applied Biosystems

25 YEARS
ADVANCING SCIENCE

GE & Science Prize for Young Life Scientists

Your essay may be the winner this year

GE & Science Prize for Young Life Scientists was established in 1995, and is presented by *Science*/AAAS and GE Healthcare. The prize was established to help bring science to life by recognizing outstanding PhDs from around the world and rewarding their research in the field of molecular biology.

This is your chance to gain international acclaim and recognition for yourself and your faculty, as well as to turn your scientific ideas into reality. If you were awarded your PhD in molecular biology* during 2005, describe your work in a 1,000-word essay. Then submit it for the 2006 GE & Science Prize for Young Life Scientists. Your essay will be reviewed by a panel of distinguished scientists who will select one grand prizewinner and four regional winners.

The grand prizewinner will get his or her essay published in *Science*, receive US$25,000, and be flown to the awards ceremony in Stockholm, Sweden. Entries should be received by **July 15, 2006**.

GE & Science Prize for Young Scientists: Life Science Re-imagined.

For more information on how to enter, go to www.gehealthcare.com/science

---

Established and presented by:

Science AAAS

* For the purpose of this prize, molecular biology is defined as "that part of biology which attempts to interpret biological events in terms of the physico-chemical properties of molecules in a cell" (McGraw-Hill Dictionary of Scientific and Technical Terms, 4th Edition).

CREDITS (TOP TO BOTTOM): FLORIDA KEYS NATIONAL MARINE SANCTUARY; CANADIAN INSTITUTES OF HEALTH RESEARCH; KURT BENIRSCHKE/UNIVERSITY OF CALIFORNIA, SAN DIEGO

RESOURCES

Species Pointer

Discover Life is a field guide and a biological encyclopedia rolled into one. Sponsored by the Polistes Foundation, a team of biodiversity mavens, teachers, and other experts co-founded by ecologist John Pickering of the University of Georgia, Athens, the site covers some 270,000 species from around the globe. Organized taxonomically, the All Living Things section provides descriptions, photos, and other information on particular species or groups such as the elephant ear sponges (*Agelas clathrodes*; above, a specimen from Florida). Offerings include original pages and compilations from other sites. The IDnature guides section holds interactive keys for North American birds, Jamaican land snails, and more than 20 other groups of organisms. The foundation hopes to amass range maps, identification keys, and other data for 1 million species by the year 2012. >>
www.discoverlife.org

DATABASES

Protein Geography

The heart and the eye depend on different lineups of proteins, and so do a mitochondrion and a lysosome. But scientists haven't compiled a comprehensive list of the proteins residing in each type of organ and organelle. Two databases announced earlier this month in *Cell* take a step in that direction. Using mass spectrometry and other techniques, researchers with the Mouse Proteome Project* at the University of Toronto in Canada pinpointed more than 3200 proteins in six organs. The project's database indicates whether each protein is present in four cellular compartments, such as the cytoplasm and mitochondria. The Organelle Map Database† from the Max Planck Institute for Biochemistry in Martinsried, Germany, focuses on the mouse liver and caches results from a method called protein correlation profiling. The site maps some 1400 proteins to 10 cellular locations. >>

* tap.med.utoronto.ca/~mts
† proteome.biochem.mpg.de/ormd.htm

TOOLS

Hearing Colors, Tasting Shapes

If you listen to the blues and actually see the color, you might have synesthesia, a neurological condition in which senses mingle. Potential synesthetes can assess their perceptions at the Synesthesia Battery, a standard set of questions from neuroscientist David Eagleman of the University of Texas Medical School in Houston. Researchers can send subjects who might have their sensory wires crossed to the site and receive the test results by e-mail. >>
www.synesthete.org

EDUCATION

Around the Brain in 20 Minutes >>

Cocaine occludes the molecular pumps that clear dopamine and other neurotransmitters from brain synapses (right). As a result, the molecular signals jolt neurons again and again, producing euphoria. Students can learn more about how drugs tamper with synapses, how memory works, and other topics at The Brain From Top to Bottom, created by neuroscientist Bruno Dubuc of the Canadian Institutes of Health Research. The primer's eight chapters, which come in three levels of difficulty, explore not only the molecular and cellular mechanisms behind brain functions but also their psychological and social ramifications. In the pleasure and pain section, for example, you can step back for an overview of philosophers' thinking about these two sensory extremes. >>
www.thebrain.mcgill.ca/flash/index_d.html

IMAGES

Wombs With a View

The placenta allows a mammalian mother to speed nutrients to her fast-growing embryos. Pathologists, evolutionary biologists, and other researchers can absorb information about the organ at Comparative Placentation from Kurt Benirschke, a professor emeritus at the University of California, San Diego. For more than 140 mammal species—from the house mouse to the African elephant—the site describes placental anatomy, gestation, implantation, and abnormalities. Accounts feature a wealth of images such as the cross section at left, which shows a 17-day-old mouse fetus in the uterus. >>
medicine.ucsd.edu/cpa

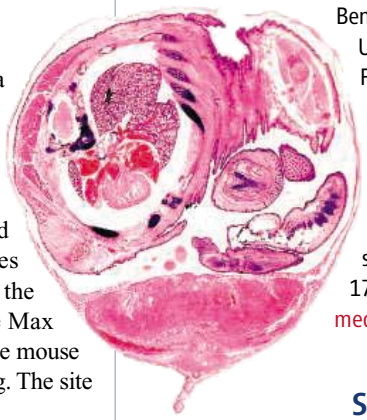

Send site suggestions to >>
netwatch@aaas.org
Archive: www.sciencemag.org/netwatch

Congratulations

to the AAAS Student Poster Winners!

AAAS recognizes the winners of the 2006 Student Poster Competition at the AAAS Annual Meeting in St. Louis, this past February. Their work in a variety of fields displayed originality and understanding that set them apart from their colleagues. This year's winners also will receive cash prizes thanks to the generous support of Subaru; British Consulate General, Chicago; Monsanto; and Sigma-Aldrich. Congratulations!

Brain and Behavior

Jorge Brea, Frank Moss; University of Missouri Saint Louis

Kevin Dolan, Peter Tass; Institute of Medicine, Research Center Juelich

Environment and Ecology

Jonathan P. Knapp, Kathleen C. Benison; Central Michigan University

Math, Technology and Engineering

Gabriel I. Rowe, Alexander V. Mamishev; University of Washington

William R. Ledoux, Glenn K. Klute; U.S. Department of Veterans Affairs

Medicine and Public Health

David A. Martinez, Rafael Gonzalez, Julio Espinosa, Michelle Hickey, Thomas E. Lane, Hans S. Keirstead; University of California, Irvine

Molecular and Cellular

Liang-I Kang, Yan Wang, Vesselina G. Cooke, Ulhas P. Naik, Melinda K. Duncan; University of Delaware

Physical Sciences

Laura L. Vatta, Ron D. Sanderson, Klaus R. Koch; University of Stellenbosch, South Africa

Science in Society

Victoria L. Kramer, Joan S. Thompson; The Pennsylvania State University

Social Sciences

Matthew Herder, Dalhousie University, Canada

Jennifer Brian, Arizona State University

Keep an eye out for information about the AAAS Annual Meeting in San Francisco, 15–19 February 2007.

For more details, visit

www.aaasmeeting.org

AAAS

ADVANCING SCIENCE, SERVING SOCIETY

DECODING THE SPUD

Stamppot—mashed potatoes mixed with bacon and cabbage—may be the Dutch idea of bliss, but for Christian Bachem, a plant scientist at Wageningen University in the Netherlands, it's the potato genome that gets the juices running.

Bachem is spearheading the effort to sequence the potato's 12 chromosomes. A 16-nation consortium, including leading potato producers China, India, Russia, and Poland, has spent the past 6 months trying to come up with money to get started. Now, thanks to $3.6 million from the Dutch government, deciphering of the first chromosome will soon be under way.

Only two other human food staples—rice and tomatoes—have made it into the sequencing pipeline. But potatoes are getting really hot: Consumption in Asia is skyrocketing as rice, wheat, and corn production declines and McDonald's French fries continue to spread, says Bachem. With the genome sequence in hand, researchers will be able to more easily build in resistance to cold, drought, and disease and possibly come up with a healthy potato chip, he says. Sequencers hope to finish the job by 2010.

Red Face for Johns Hopkins

Bad publicity has Johns Hopkins Medicine in Baltimore, Maryland, backpedaling from an alliance it forged with a cosmetics company, New York–based Klinger Advanced Aesthetics. Johns Hopkins is mentioned in promotional material for a new line of skin-care products, sold at Sephora, an upscale chain of beauty stores. The Sephora Web site touted Cosmedicine products as "the only skin-care line" whose clinical testing was done "in consultation with Johns Hopkins Medicine."

But after the agreement was revealed 2 weeks ago in *The Wall Street Journal*, Johns Hopkins announced that it would no longer take equity in Klinger or a seat on the company's board of directors as planned. The university is also forbidding use of its name except "on product packages and in previously printed promotional material."

"The relationship evolved over several years" with "appropriate internal reviews," says Johns Hopkins spokesperson Joann Rogers. "Hopkins did not and does not endorse the products." However, she says, those reviews, which didn't cover conflicts of interest because no Johns Hopkins research is involved, "did not fully anticipate the public's perception" of the relationship. Mildred Cho, a bioethicist at Stanford University in California, says the changes are a "turnaround" but argues that any use of the Johns Hopkins name is "still implicit endorsement." Johns Hopkins is getting consulting fees—it declines to name the amount—for suggesting study designs and reviewing results.

ON THE GO IN CALIFORNIA >>

Things are looking up stem cell–wise in California, which has been stymied by lawsuits in its attempt to become a world stem cell power. Last week, the California Institute for Regenerative Medicine (CIRM) announced that its first-ever grant checks were in the mail.

Although bond sales for the $3 billion stem cell initiative are stalled, CIRM's board chair Robert Klein has rounded up $14 million from buyers of "bond anticipation notes." The first checks went out last week: $12.1 million for research training grants at 16 universities and research institutes. Klein said he had commitments for all but $4 million of the $50 million he is trying to raise. "We expect to have funds for a major new grant program later this year," he said at a 10 April press conference in San Francisco.

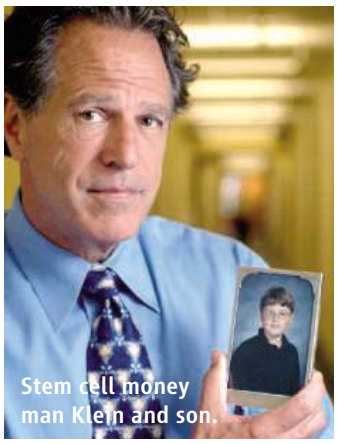

Stem cell money man Klein and son.

The same day, the University of California, San Diego, formalized a research collaboration with Australia's main stem cell matrix: Monash University and the Australian Stem Cell Centre in Melbourne, Victoria. Victoria is putting $35 million into a new Australian Regenerative Medicine Institute at Monash.

Reliving the 'Frisco Quake

Scientists have created a series of simulations that describe in unprecedented detail the shaking and rippling of San Francisco during the massive earthquake that struck on 18 April 1906.

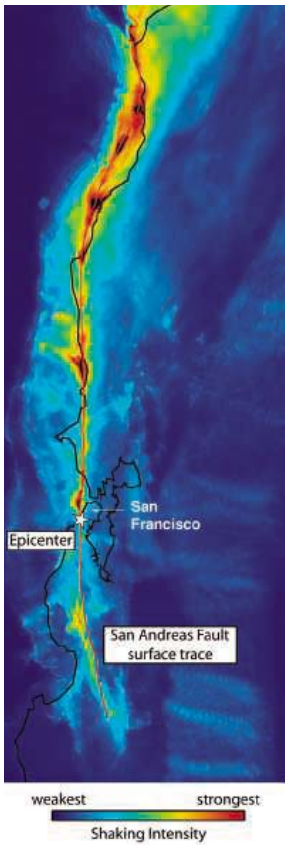

A consortium of government, industry, and university researchers started with a new U.S. Geological Survey (USGS) model of northern California that has geologic data on the nearby faults, including the San Andreas, extending as far as 45 kilometers below the surface. To digitally recreate the event, they added original seismic data, USGS ground measurements taken after the quake, and reports of shaking culled in the aftermath of the event.

Shawn Larsen, a seismologist and computer scientist at Lawrence Livermore National Laboratory who participated in the 2-year effort, says the simulation has yielded a new understanding of how seismic energy traveled east from the quake's epicenter just off the coast and shook California's central valley. Running hypothetical quakes of the same magnitude (roughly 7.8) with epicenters further north yielded terrifying results: "even stronger" ground shaking in San Francisco, Larsen says.

Previous models have given insights into other, smaller quakes, but this one required powerful machines like Livermore's 4000-processor Thunder supercomputer. David Wald of USGS, who was not part of Larsen's team, calls the simulation "the most comprehensive effort to date on this earthquake" and says it lays the groundwork for advances in mitigating future quake damage. The simulation was to be unveiled in San Francisco this week at a conference commemorating the 100th anniversary of the earthquake.

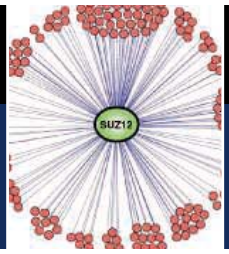

The proteins behind "stemness" 349

Round the horn for the first time 350

BIOMEDICAL RESEARCH

Court Decides Tissue Samples Belong to University, Not Patients

A high-stakes battle pitting a top prostate cancer researcher and his patients against a major research university over who owns the patients' tissue samples was decided last week in a Missouri federal court. The ruling gives Washington University (WU) in St. Louis ownership of tissue samples that urologist William Catalona began collecting 2 decades ago when he was a faculty member at WU. Catalona, who is now at Northwestern University Feinberg School of Medicine in Chicago, Illinois, had sought to establish unprecedented rights for patients by arguing that those who donated to the collection retained control of their tissues.

"The opposite decision would have been disastrous for tissue banks and tissue research," says David Korn, a senior vice president of the Association of American Medical Colleges, which filed an amicus brief supporting WU's position. But some ethicists and legal experts suggest the result could dissuade people from donating tissue samples. "It's a poor precedent for academic researchers and research subjects alike," says Lori Andrews, a professor at the Chicago-Kent College of Law, who advised the patients' attorneys.

Catalona, who has a roster of high-profile patients, is credited with developing the prostate-specific antigen (PSA) test for prostate cancer. He says he began the WU tissue collection in the 1980s with blood and tissue samples from 3000 patients from his private practice, mostly using his own grant funds and departmental money he raised. Other surgeons at WU have since added to the collection, which now has 100,000 serum samples, 3500 prostate tissue samples, and 4400 DNA samples.

The problem began in 2002, Catalona says, when the university changed how the tissue bank operated. "It was just taken from me," he says. The university set up a peer-review panel to decide who could use the samples. When Catalona applied to use samples to test a new PSA assay with a biotech company, the university, he says, "stalled," although the request was granted. Catalona tried to broker a deal to take the tissue collection to the University of Virginia but that fell through, and he eventually decided to leave for Northwestern.

The week before he left, he wrote to all participants in his studies, asking them to send in an enclosed form requesting that WU "release" their samples to him at Northwestern. About 6000 patients signed it. WU refused to transfer the samples, however, and filed a lawsuit in 2003 to resolve the ownership issue. Eight patients later petitioned to join Catalona as defendants.

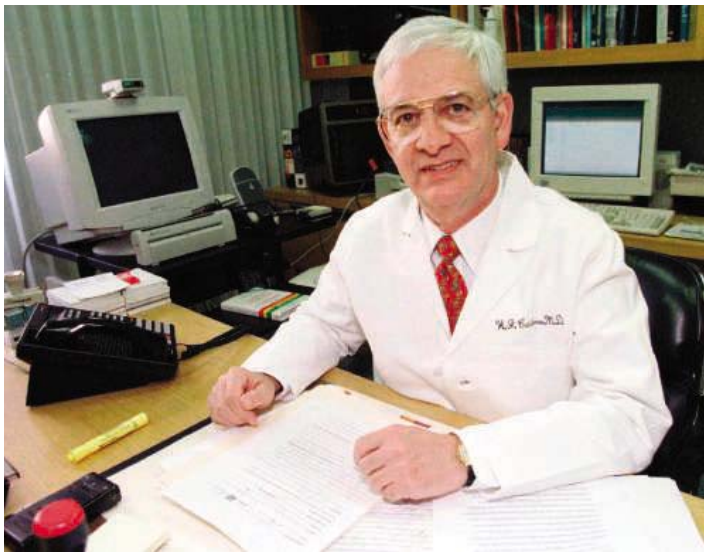

Tissue tussle. Prostate cancer researcher William Catalona is considering whether to appeal the recent court decision that his former university maintains ownership of a tissue collection he established.

In the case, Catalona and the patients argued that the patients' original "intent" was to give their tissue samples to Catalona. The suit also claimed that the patients retained ownership over their tissue because their consent forms said they could ask to withdraw from any WU research.

Judge Stephen Limbaugh of U.S. District Court, Eastern District of Missouri, Eastern Division, showed little sympathy for these arguments. He noted that the tissue donations were a "gift" to WU under Missouri law, which meant the university owned the samples. The judge concluded that the patient consent forms, which typically bore the WU logo, gave the samples to the university. He also noted that many samples didn't come from Catalona's patients and that WU funds had been used to maintain the repository. The decision also cites precedents in two earlier court cases finding that patients do not own biological samples they have donated for research—one involving spleen tissue from a leukemia patient, the other, a study that patented the gene for Canavan disease (*Science*, 10 November 2000, p. 1062).

The court rejected arguments that the patients' request to withdraw consent meant they could get their tissue back. Federal and state regulations simply require that the university had to choose between destroying it, storing it indefinitely without use, or anonymizing the data, Limbaugh noted.

Officials at other universities are relieved by the ruling. Says Ernest Prentice, associate vice chancellor of regulatory and academic affairs at the University of Nebraska Medical Center in Omaha and chair of a federal human research protections advisory board, who testified for WU, "[If] anytime a patient donates tissue … they could say 'I want my tissue back,' that would tie the hands of biomedical research."

Some experts, although sympathizing with the patients, say it should have been no surprise to Catalona that his university owned the samples. "That was the deal. Most researchers realize that," says George Annas, who teaches health law at Boston University. Catalona expects he and the patients will appeal, however. "I don't think this is really informed consent. … A very large number of these patients felt they were giving [tissue] for my research projects," he says.

The decision, say WU officials, should finally allow researchers, even Catalona, to again conduct studies on the tissue samples, which have sat unused since the university filed suit. "We will use the repository for its intended purpose, which is to pursue new information about the development of, and potentially a cure for, prostate cancer," WU said in a prepared statement.

–JOCELYN KAISER

With reporting by Eli Kintisch.

CREDIT: BILL GREENBLATT/UPI/LIAISON AGENCY/GETTY IMAGES

Science connections in a divided land 352

NCI's troubled state 357

WOMEN IN SCIENCE

Progress on Hiring Women Science Faculty Members Stalls at MIT

The number of women faculty members at the Massachusetts Institute of Technology (MIT) in Cambridge has declined or remained flat in five of its six science departments since 2000, whereas the number of women in other areas, such as engineering and architecture, increased significantly during the same period, according to a report released last week. The findings, say academics researching the issue, underscore the difficulty in removing obstacles for female scientists, despite high-level attention by some deans and administrators.

MIT kicked off a nationwide debate in 1999 following publication of a study highly critical of the university's treatment of women scientists (*Science*, 12 November 1999, p. 1272). That study prompted a host of personnel and policy changes at MIT and also led other research institutions across the country to examine their own policies. So when MIT biologist Nancy Hopkins, who chaired the committee that produced that initial report, compiled the most recent statistics, "I couldn't believe my eyes; I dropped my pencil," she says.

In a paper in MIT's most recent faculty newsletter, Hopkins tracks a spike in the hiring of women scientists at MIT between 1996, when the initial findings of her committee were presented to then–dean of science Robert Birgeneau, and 2000, when Birgeneau resigned. From 2000 to 2006, however, the percentage of women increased only in the chemistry department. In biology, brain and cognitive sciences, and earth, atmospheric, and planetary sciences, the percentage decreased, although in physics it remained flat. The story is radically different, however, in the engineering department and in the school of architecture and planning, where the number of women nearly doubled in the past 5 years.

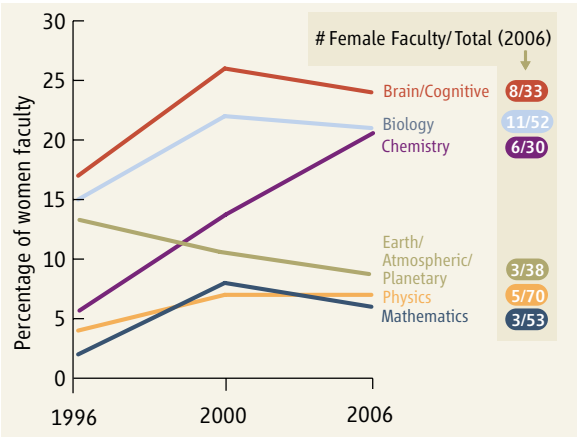

Sliding scale. After rising in the late 1990s, the number of women in most MIT science departments dropped.

Birgeneau's successor, Robert Silbey, says he agrees with Hopkins that MIT has "failed to sustain that initial push," which brought 13 new faculty members into the sciences between 1996 and 2000. "And I'm not happy about it." But he notes that a dozen women scientists were hired between 2000 and 2005, only one less than during Birgeneau's watch. The decreases within departments, Silbey says, are largely due to female faculty members leaving after failing to win tenure or for ▶

SCIENCE POLICY

NSF Begins a Push to Measure Societal Impacts of Research

When politicians talk about getting a big bang for the buck out of public investments in research, they assume it's possible to measure the bang. Last year, U.S. presidential science adviser John Marburger disclosed a dirty little secret: We don't know nearly enough about the innovation process to measure the impact of past R&D investments, much less predict which areas of research will result in the largest payoff to society (*Science*, 29 April 2005, p. 617). He challenged social scientists to do better.

Next month, the National Science Foundation (NSF) will invite the community to pick up the gauntlet. A Dear Colleague letter from David Lightfoot, head of NSF's social, behavioral, and economic sciences (SBE) directorate, will describe an initiative tentatively dubbed "the science of science policy." NSF is also holding three workshops for researchers to lay the intellectual foundations for the initiative. By fall, NSF hopes to have $6.8 million from Congress as a down payment on what Lightfoot envisions as "a significant program" that would eventually support a half-dozen large research centers at U.S. universities and scores of individual grants.

In its 2007 budget request, released in February, NSF says the initiative will give policymakers the ability to "reliably evaluate returns received from past R&D investments and to forecast likely returns from future investments." Lightfoot cautions against expecting too much precision. "One shouldn't overstate this goal," he says. "Nobody is under the illusion that we're going to be able to hand these decisions over to the computers." But he believes that it should be possible to develop "a more evidence-based understanding of what happens to our R&D investments."

NSF officials have outlined a series of steps toward that goal. On 17 to 18 May, some two dozen cognitive scientists, social psychologists, and engineers will discuss the roots of individual and group creativity and innovation in science. On 1 to 2 June, a second workshop will explore the organizational components—how cultural, political, demographic, economic, and scientific patterns affect the creation and application of knowledge. In July, an international group of experts will suggest ways to improve existing surveys that measure various indicators of a nation's technological prowess, from publications to public understanding of science.

If the funding materializes, Lightfoot foresees a collection of interdisciplinary research centers, focused either on a particular discipline or an important technology. "To date, the criteria most commonly used—citation analysis or other bibliometrics—are science-neutral and field-independent," he says. "That strikes me as a mistake and a significant limitation. Chemistry and archaeology have different scientific cultures, and those differences affect innovation."

Lightfoot is in the process of hiring someone to coordinate the initiative within SBE and across NSF. The White House is also forming an interagency task force to oversee the initiative.

–JEFFREY MERVIS

SOURCE: MIT

other reasons. (Nearly half of all junior faculty members, male and female, do not receive MIT tenure.) "Department heads in science are committed to gender diversity, but sustained progress is difficult," he adds. Silbey also notes that he has appointed women to various leadership positions, and that three of the 10 members of MIT's science council are female.

But Hopkins argues that recruitment of distinguished women scientists needs to be more aggressive at the level of the individual science department. "The standard hiring process does not work," she says. Indeed, the pattern found by Hopkins "is really not surprising," says Alice Hogan, who heads a program at the National Science Foundation called Advance, designed to increase women's participation in science and engineering. "If you let the normal processes go their way, you get what happened at MIT." The Advance program has given 19 awards averaging $3 million to $3.5 million during the past 5 years to encourage universities to devise strategies to recruit more women in science and engineering. At the University of Michigan, Ann Arbor, for example, search committees receive extensive briefings on diversity issues. At the University of California, Irvine, faculty members act as "equity advisers" to monitor and assist with searches. And at the University of Washington, Seattle, department chairs are trained to encourage diversity. Abigail Stewart, the principal investigator on Michigan's Advance grant, says there has been a "sharp upturn" in hiring women there since the grant began but adds that her analysis is not yet complete. Representatives from major research universities plan to meet in June in Ann Arbor to compare data and approaches.

Hogan and others say that for now, strong deans willing to push their department chairs may be the most effective tools for recruiting a new generation of female scientists. At MIT, Silbey says he will push harder to find young and excellent women for his departments. Of 10 new hires starting in July, he says four are women.

–ANDREW LAWLER

COSMOLOGY

Skewed Starlight Suggests Particle Masses Changed Over Eons

New measurements suggest that the ratio of the proton's mass to the electron's mass has increased by 0.002% over 12 billion years, a team of astronomers and physicists reports. If so, the ratio and other fundamental "constants" of nature may not be constant after all.

"If this small variation exists, it's a revolution in science," says Victor Flambaum, a theoretical physicist at the University of New South Wales in Sydney, Australia, and a member of a different team that 7 years ago reported that another constant may have changed. But some theorists say inconstant constants may clash with well-established physics.

To spot the change, two groups joined forces to compare starlight to laser light. Using the Very Large Telescope in Atacama, Chile, Alexandre Ivanchik, a theoretical physicist at the Ioffe Physico-Technical Institute in St. Petersburg, Russia, and Patrick Petitjean, an astronomer at the Institute for Astrophysics of Paris, France, and colleagues studied light from two quasars, the hearts of ancient galaxies. The light filtered through clouds of molecular hydrogen billions of light-years away when the universe was in its youth. Meanwhile, physicists Wim Ubachs and Elmar Reinhold of the Free University of Amsterdam, the Netherlands, and colleagues shined laser light through molecular hydrogen in the lab.

Molecular hydrogen absorbs light of distinct wavelengths, and the resulting spectrum of "absorption lines" creates a kind of bar code. The positions of the lines depend on the ratio of the mass of the proton to the mass of the electron. So, by comparing the absorption spectrum from the clouds with the one measured in the lab, the researchers could tell whether the mass ratio had changed.

That's easier said than done. Because of the expansion of the universe, the quasar light is stretched from ultraviolet to visible wavelengths, an effect for which researchers must correct. Measuring the ultraviolet absorption lines in the lab is also challenging. Also, to make a meaningful comparison, Reinhold and Ubachs had to calculate how much each line should shift and in which direction—toward longer or shorter wavelengths—as the mass ratio changed.

Big diff. Researchers compared the absorption of light by ancient hydrogen clouds to absorption in the lab.

The researchers found that the ratio has increased by about 20 parts per million over the past 12 billion years, they report this week in *Physical Review Letters*. The measurement is at the edge of statistical significance. "We have an *indication*," Ubachs says. "I wouldn't call it proof."

The change is plausible, Flambaum says. Such variations arise naturally in "grand unified theories" that attempt to roll the electromagnetic force and the strong and weak nuclear forces into a single unified force, he says. Michael Dine, a theorist at the University of California, Santa Cruz, says that's true in principle. But variable constants would require new particles that generally would either interfere with gravity or cause mind-boggling swings in the energy of the universe, Dine says: "It's very hard to fit varying constants into our conventional notion of how nature works."

Even so, other researchers have turned up occasional hints of inconstancy. In 1999, a team led by John Webb, an astrophysicist at the University of New South Wales, reported measurements of absorption of quasar light by various metal ions. The team found that the "fine-structure constant," which determines the strength of the electromagnetic force, appears to have changed by about six parts in a million. Ironically, Petitjean and colleagues studied that constant and found no change.

To nail down whether the mass ratio has indeed changed, researchers need to study more quasars and clouds, Webb says. He is already working on the problem, so stay tuned for more weighty measurements.

–ADRIAN CHO

CREDITS (TOP TO BOTTOM): ESO; W. UBACH/FREE UNIVERSITY OF AMSTERDAM

DEVELOPMENT

Gene-Suppressing Proteins Reveal Secrets of Stem Cells

Scientists have taken a step toward unlocking the mystery of "stemness": that is, deciphering what makes embryonic stem (ES) cells able to replicate indefinitely and retain the potential to turn into any kind of body cell.

According to papers in *Cell* and *Nature* this week, key guardians of stemness are molecules called polycomb group proteins. A team from the Massachusetts Institute of Technology (MIT) and the Whitehead Institute for Biomedical Research in Cambridge, Massachusetts, reports that these proteins act in concert with others to repress most of the regulator genes whose proteins turn on key developmental genes. This keeps the ES cell in an undifferentiated state.

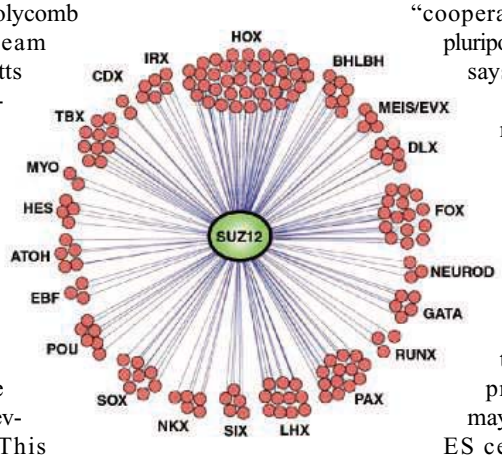

Who regulates the regulators? A polycomb protein silences hundreds of genes that will direct the differentiation and development of ES cells when activated.

Polycomb group proteins are known to play a vital gene-suppressing role in the development of organisms as diverse as fruit flies and humans (*Science*, 29 April 2005, p. 624). Now, the researchers have tracked this role back to the very earliest stage of development. These proteins are "the founding ingredient for development," says Rudolf Jaenisch, an author of both studies. "This is a major step forward in efforts to map the regulatory circuitry of embryonic stem cells, which constitutes the founding circuitry of human beings," adds co-author Richard Young.

In the *Cell* study, the researchers surveyed all 3 billion base pairs in the human genome and identified every gene that a polycomb group protein, Suz12, binds to in ES cells. They started by treating ES cells so that Suz12 remained bound to its DNA targets even after the cells were broken open. They then dumped the cells' contents onto a chip containing DNA representing all of the human genome. The DNA sequences affixed to Suz12, which were labeled with a dye, bound to complementary sequences on the chip, revealing their identity. The scientists also report in *Nature* on a similar study with mouse ES cells using Suz12 and three other polycomb group proteins.

The two efforts identified hundreds of genes targeted by the polycomb group proteins. The vast majority of regulators primed to go into action later in development "are being occupied and repressed by polycomb," says Young. Many of these silenced regulatory genes are also occupied by the ES cell transcription factors Oct4, Sox2, and Nanog. Both sets of proteins "cooperate in keeping a cell pluripotent and self-renewing," says Jaenisch.

"These papers are really exciting because they point the way to one of the next levels of stem cell research," says Princeton University stem cell scientist Ihor Lemischka. The new, fuller picture of polycomb group proteins, adds Young, may help scientists guide ES cell gene expression and push cell populations to develop into desired types, such as neurons or insulin-making pancreatic cells.

The same issue of *Cell* also features a report from the laboratory of Eric Lander at the Broad Institute of Harvard and MIT that highlights the importance of chromatin, the protein package surrounding DNA, in keeping mouse ES cells pluripotent. The scientists, led by Bradley E. Bernstein, found certain chromatin motifs near genes important for development that can repress the genes while at the same time keeping them poised for activation. These chromatin features, which they labeled "bivalent domains," exert control over many of the same regulatory genes targeted by polycomb proteins.

The three papers "provide a wealth of detailed information" on what keeps ES cells pluripotent, says Vincenzo Pirrotta, a molecular biologist at Rutgers University in Piscataway, New Jersey. The polycomb papers demonstrate that those proteins and ES cell transcription factors bind to "a largely common set of genes." The Bernstein paper then addresses how genes silenced by these factors ultimately become activated. Together, says Pirrotta, the papers have "defined the important players and the sites of action" that must be studied to get to the root of what it is to be a stem cell.

–CONSTANCE HOLDEN

CREDIT: LEE *ET AL.*, *CELL* 125, 1-13 (2006)

SCIENCESCOPE

Anthros Happy: No Bones About It

Because $4 million buys a lot of anthropology research, scientists are celebrating a grant of that size from the European Union to promote research into human origins and anatomical variation in primates. "It's the largest ever in Europe for a project centered mostly on paleoanthropology," says Jean-Jacques Hublin of the Max Planck Institute for Evolutionary Anthropology in Leipzig, Germany, a member of the European Virtual Anthropology Network.

The new consortium, launched last month at a meeting in Athens, Greece, will create more than 30 doctoral and postdoctoral positions at 15 participating institutions. The young scientists will learn the latest techniques in 3D imaging, computer modeling, and virtual reconstructions of humans, apes, and their ancestors (*Science*, 3 June 2005, p. 1404).

–MICHAEL BALTER

Super-K A-OK

Japan's Super-Kamiokande neutrino detector is back at full strength, 4.5 years after a shock wave triggered by the implosion of a damaged photomultiplier tube destroyed 7000 of its 11,000 sensors (*Science*, 23 November 2001, p. 1630). Super-Kamiokande made headlines in 1998 by providing evidence that neutrinos have mass, but manufacturing replacement photomultiplier tubes after the subsequent accident took a while. "There is still a lot of neutrino research to be done," says Kamioka Observatory Director Yoichiro Suzuki.

–DENNIS NORMILE

Postdocs off the Docket

Two former postdocs at Harvard Medical School in Boston last week admitted that they took research material from their lab without permission, but charges against them were dropped as part of a deal with prosecutors.

The saga began in early 2000, when Jiang Yu Zhu and his wife Kayoko Kimbara shipped reagents from Harvard to the University of Texas, San Antonio, where Zhu had been offered employment (*Science*, 28 June 2002, p. 2310). Researchers often transfer such materials when they change jobs, but the couple failed to seek permission from their professor, sparking a court case. Prosecutors initially alleged that the couple intended to use the reagents, used in organ-transplant research, to produce a commercial product. After a 2002 arrest, the pair pleaded not guilty. Under a deal with the government, the indictment will be dismissed in 1 year if the pair stays out of trouble.

–ANDREW LAWLER

GEOPHYSICS

Opening the Door to a Chilly New Climate Regime

Earth's early Eocene epoch 50 million years ago was a paradise for warmth-loving life. Back then, alligators basked in the high Arctic on Canada's Ellesmere Island. Today, for better or worse, they cannot venture farther north than the U.S. Deep South. Why did the planet cool so much?

Many paleoclimatologists suspect at least part of the answer lies in the way the supercontinent Gondwanaland fell apart. As the fragments that became South America and Antarctica dispersed, they opened the way for a climate-making ocean current that now encircles Antarctica. By cutting Antarctica off from warm currents flowing from the tropics, the Arctic Circumferential Current (ACC) could have helped bring on the continent's massive, permanent glaciation, with worldwide consequences. On page 428, paleoceanographers report new evidence that the oceanic Drake Passage between the two continents began opening—and changing climate—twice as long ago as once thought.

Paleoceanographers Howie D. Scher of the University of Rochester in New York and Ellen Martin of the University of Florida, Gainesville, found the clues in fossil fish teeth recovered from sediment cores from the far South Atlantic Ocean. Fish teeth, researchers have shown, absorb the rare-earth element neodymium from seawater shortly after they settle to the bottom. But the proportion of two neodymium isotopes in Pacific seawater differs from that in Atlantic seawater, because rivers carry differing isotopic ratios from the rock surrounding the two ocean basins. A varying isotopic ratio in the Atlantic is a sign that Pacific water has managed to mix into the Atlantic.

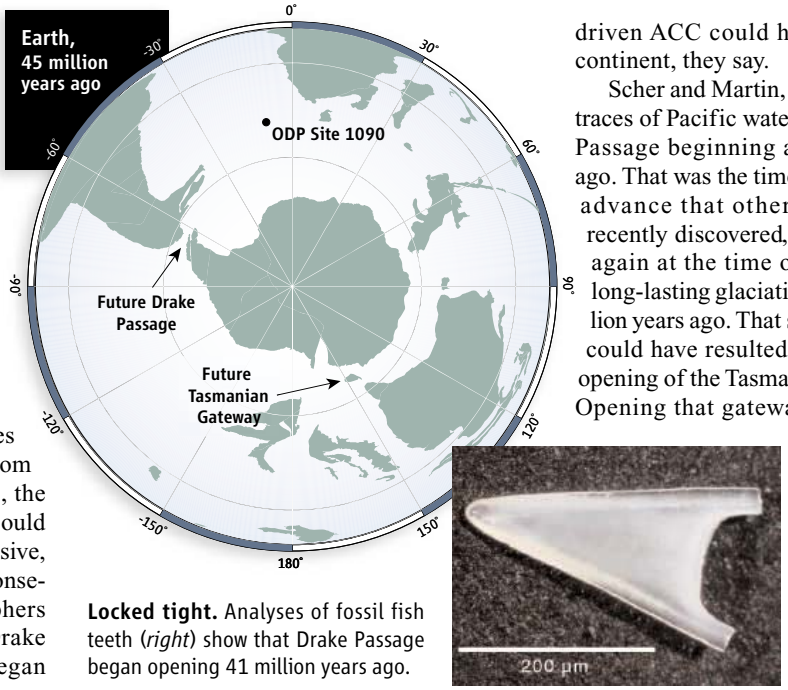

Locked tight. Analyses of fossil fish teeth (*right*) show that Drake Passage began opening 41 million years ago.

Some marine geologists, judging the size of the growing gateway by the crustal record of drifting continents, have argued that Drake Passage did not reach its modern depth and breadth until 20 million years ago. That's the earliest that the ponderous, wind-driven ACC could have first encircled the continent, they say.

Scher and Martin, however, found isotopic traces of Pacific water leaking through Drake Passage beginning about 41 million years ago. That was the time of a short-lived glacial advance that other paleoceanographers recently discovered, they note. Flow surged again at the time of the first substantial, long-lasting glaciation of Antarctica, 34 million years ago. That step, the researchers say, could have resulted from the simultaneous opening of the Tasmanian Gateway upstream. Opening that gateway would have allowed more water into the already-deepening Drake Passage and then the Atlantic.

Paleoceanographer James Kennett of the University of California, Santa Barbara, who suggested the gateway-opening hypothesis of climate change 30 years ago, says the early opening in the neodymium record doesn't really contradict the late opening in the crustal record. "I'd prefer to read the [neodymium] record as a more gradual increase in Pacific waters into the Atlantic," he says. "Everything's progressive; it doesn't all happen at once." Twenty million years or more may well have been required to crank up a full-blown ACC, he says, and to help usher in the global chill felt of late. **–RICHARD A. KERR**

SOUTHEAST ASIA

Thai Scientists Secure Royally Inspired Windfall

BANGKOK—Thailand's king already enjoys wide popularity among his subjects, but now Thai scientists have an extra incentive to pay homage. To mark the 60th anniversary in June of the reign of Bhumibol Adulyadej, the world's longest serving head of state, the Thai government is launching a $500 million, 10-year effort to invigorate Thailand's scientific community by training thousands of researchers and funding hundreds of international collaborations.

The jubilee initiative is not expected to transform Thailand into a global scientific powerhouse. But in a region that has largely paid short shrift to R&D, the "Strategic Research Consortiums" project, if fully implemented, could seed the growth of top-notch research groups and serve as a beacon for other Southeast Asian nations. "What we need most is to form a critical mass of scientists," says biochemist Wanchai De-Eknamkul, adviser to the secretary general of Thailand's Commission on Higher Education.

The pulse of Thai science is weak. In many Asian countries, roughly half of university degrees are awarded in science and engineering, UNESCO reported last year; in Thailand the proportion is just 26%. Less than one in four Thai university faculty members have Ph.D.s. According to the U.S. National Science Foundation's *Science and Engineering Indicators 2006*, Thai researchers published just 1072 articles in citation-indexed journals in 2003—a long way behind its near neighbor Singapore, with 3122. Like oases in the desert, eight Thai universities claim nearly 90% of the country's output. "It's a terrible imbalance," Wanchai says.

Hoping to boost scientific fertility, the higher education commission has laid out 20 strategic research areas, from emerging diseases and basic physics to high-throughput drug screening and Thai specialties such as silk production. Teams will compete for funds; those with international links will have an edge. The 2006 budget, $15 million, will jump to $50 million in 2007. The commission has set ambitious goals. In the next decade, it expects awardees to train 9600 Ph.D.s, hire 2800 academic staff, form 700 international consortia, and establish 60 centers of excellence at Thai universities.

Strengthening Thai science would no doubt please King Bhumibol, who studied science at the University of Lausanne, Switzerland, before ascending to the throne in 1946. During his reign, he has taken a keen interest in agricultural research, setting up six experimental stations throughout the country. Now, the jubilee funds will give Thai researchers a chance to show that the king isn't the only person here with a yen for cutting-edge science. **–RICHARD STONE**

CREDITS: (MAP) ADAPTED FROM H. D. SCHER (PHOTO) H. D. SCHER

CLIMATOLOGY

Latest Forecast: Stand By for a Warmer, But Not Scorching, World

While newly climate-conscious news reporters seek signs of apocalyptic change in hungry polar bears and pumped-up hurricanes, evidence-oriented researchers are working to nail down some numbers. They are concerned with climate sensitivity: how much a given increase in atmospheric carbon dioxide will warm the world. If it's extremely high, continued emissions of greenhouse gases could ignite a climatic firestorm. If it's very low, they might merely raise the global thermostat a notch or two.

Now two new studies that combine independent lines of evidence agree that climate sensitivity is at least moderately strong—moderate enough so that a really scorching warming appears unlikely. Even with the most conservative assumptions, says climate researcher Chris E. Forest of the Massachusetts Institute of Technology in Cambridge, the studies cool the maximum warming. And the reinforced low end of the range, he says, means continued emissions will fuel a substantial warming in this century.

The new studies use a technique called Bayesian statistics to gauge how adding new information improves past estimates of climate sensitivity. Most previous estimates used only a single line of evidence, such as how climate warmed as greenhouse gases increased during the 20th century or how climate cooled right after the debris from a major volcanic eruption shaded the planet. Lately, such analyses have tended to support a 25-year-old guess about climate sensitivity: If the concentration of CO_2 were to double, as is expected by late in the 21st century, the world would warm between a modest 1.5°C and a hefty 4.5°C (*Science*, 13 August 2004, p. 932). The low end of that range looked fairly firm; the negligible warming claimed by greenhouse contrarians looked very unlikely. But no one was sure about the high end. Some studies allowed a real chance that doubling CO_2 could raise temperatures by 7°C, 9°C, or even 11°C (*Science*, 28 January 2005, p. 497).

The two new studies rein in those soaring upper limits for climate sensitivity while reinforcing the substantial lower limit. Climate modeler Gabriele Hegerl of Duke University in Durham, North Carolina, and colleagues started with Northern Hemisphere temperatures between 1270 and 1850 extracted from records such as tree rings. In those preindustrial times, volcanoes, the waxing and waning of the sun, and natural variations in greenhouse gases were changing temperature. Hegerl and her colleagues then combined the preindustrial temperature response to those climate forcings with the global response in the 20th century to volcanoes, rising greenhouse gases, and thickening pollutant hazes. In this week's issue of *Nature*, they report a 5% probability that climate sensitivity is less than 1.5°C and a 95% chance that it's less than 6.2°C. That's still pretty high, but a far cry from 9°C or 11°C.

In a similar study published on 18 March in *Geophysical Research Letters*, climate modelers James Annan and Julia Hargreaves of the Frontier Research Center for Global Change in Yokohama, Japan, found the same lower limit of 1.5°C and a 95% upper limit of 4.5°C. They combined published 20th century warming data with records of coolings after recent volcanic eruptions and estimates of chilling in the depths of the latest ice age.

"Combining multiple lines of evidence is certainly the way to go," says Forest. An extremely high climate sensitivity "is probably less likely than we thought a year ago," agrees climate researcher Reto Knutti of the National Center for Atmospheric Research in Boulder, Colorado. More importantly, "we start to see a much better agreement on the lower bound," says Knutti. "We can be pretty sure the changes will be substantial" by the end of the century, he says.

–RICHARD A. KERR

Constraining Climate Sensitivity

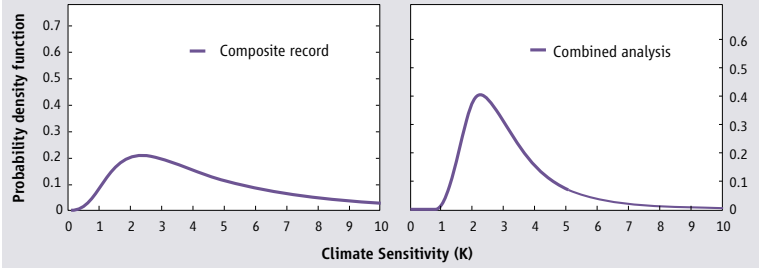

Sharpening the odds. Analyzing how climate forces changed temperature in the past yields a wide range for climate sensitivity (*left*), but combining independent data sets (*right*) narrows the range.

CREDIT: ADAPTED FROM HEGERL *ET AL.*, *NATURE* (2006)

SCIENCESCOPE

EPA Air Review Draws Fire

Activists are criticizing a proposal by the Environmental Protection Agency (EPA) to speed up its regular review of air-quality standards. They fear that some of the changes would allow undue political influence on staff scientists who develop the standards.

By law, EPA must revisit its National Ambient Air Quality Standards every 5 years. Staff scientists evaluate the latest research and propose ranges for new standards, which are then reviewed by the agency's Clean Air Scientific Advisory Committee (CASAC). Because EPA regularly misses its deadline and gets sued, an internal EPA committee proposed several suggestions in April for speeding up the process. Among them, the panel called for "early involvement of EPA senior management and/or outside parties in the framing of policy-relevant issues."

That language set off "flashing red lights" for John Walke of the Natural Resources Defense Council, who worries about political interference. "The idea isn't to have the policy drive the science," counters EPA chief scientist George Gray. Instead, he says, management and CASAC would help experts focus on the most relevant research. EPA is eager to act soon, but Gray says there will be opportunities for public comment.

–ERIK STOKSTAD

Nuke Tests Prove Critical Issue

DELHI—Casting further doubts on the uncertain fate of a landmark nuclear pact, India has rebuffed a U.S. bid for India to forswear further atomic bomb tests.

Under the deal last month, India agreed to place a majority of its power reactors under safeguards in exchange for the right to import nuclear energy technology (*Science*, 10 March, p. 1356). With approval required from legislators skeptical of the deal's nonproliferation merits, the U.S. government earlier this month sent India a draft agreement that includes a clause declaring an end of cooperation if India were to detonate a nuclear device. Although India has adhered to a self-imposed moratorium on nuclear tests since its last round of detonations in 1998, the government deemed the clause a poison pill.

"There was no place for any such provision" in an agreement, says a spokesperson for India's Foreign Office. Negotiations are ongoing, with a team of senior U.S. officials expected in Delhi some time next week to continue talks.

–PALLAVA BAGLA

Israeli and Palestinian scientists are working together in a research program that seems all the more daring now that Hamas has come to power

Bridging the Divide In the Holy Land

JERUSALEM—"This will be the first Palestinian nanotech lab," says Mukhles Sowwan, peering into a dark, empty room at Al-Quds University in East Jerusalem. Making this a reality will be no mean feat. Sowwan, a physicist, needs about $1 million to equip a state-of-the-art laboratory for the kind of science he wants to do, and he can't look to the university for help: Finances at Al-Quds are so precarious that faculty paychecks failed to arrive on time last month—for the third month in a row. "I'm cutting expenses in every way possible," Sowwan says, including designing some of his own devices and software.

But Sowwan, 31, has something that few other Palestinians have: an Israeli research partner. Ever since doing a postdoc in the lab of Danny Porath, a physicist at Hebrew University in West Jerusalem, Sowwan and Porath have teamed up to coax biological molecules to assemble into circuitry and memory devices far

Palestinian Archaeology Braces for a Storm

RAMALLAH—Six years ago, Hamdan Taha, director of the Palestinian Authority's Department of Antiquities and Cultural Heritage, was struggling to make ends meet with a skeleton crew and a $500,000 budget (*Science*, 7 January 2000, p. 33). Then last December, his department got a windfall: The Palestinian Authority offered a $6 million budget boost. Much of the new money was to be for preservation, but some was tagged for the excavation of a freshly uncovered Bronze Age site called Tell Etell, a few kilometers outside Ramallah—the first archaeological project that would be fully Palestinian from start to finish.

But fortunes change fast here. After Hamas was elected to the Palestinian government in January, Israel ceased transferring customs payments. Last week, the European Union announced that it is suspending direct aid to the Palestinian territories. And the United States is asking international agencies to withhold contributions until Hamas recognizes Israel and renounces violence, although few agencies so far have joined the squeeze.

"This will bring terrible impacts on Palestinian archaeology," says Moain Sadeq, antiquities chief in Gaza. The Palestinian Authority may be forced to lay off guards at sites, which could exacerbate a serious looting problem. Some also fear that a Hamas-led government may refocus archaeological efforts on the region's Islamic roots, at the expense of earlier periods. Such controversies are ongoing, such as the alleged destruction of pre-Islamic archaeological material to improve access to a mosque on the Temple Mount in Jerusalem by the previous Palestinian government. Judeh Morkus, the Hamas-appointed minister of tourism and antiquities for the Palestinian Authority, says his government will not require archaeologists to probe only Islamic sites. "The focus will be as it was," he says, adding that the ministry hopes to complete a review of existing agreements by the end of this month.

Taha is at home with turmoil. After Israeli and Palestinian leaders signed the Oslo Accords in 1994, archaeologists from Europe and North America swept in to probe the archaeological riches of the West Bank and Gaza Strip, where layers of continuous occupation go back to the origins of civilization. Taha and his Palestinian colleagues were eager to work with partners from outside. International digs began to uncover archaeological gems, from Canaanite waterworks in the West Bank to Neolithic occupations in the Gaza Strip. But after the second Intifada flared up in 2000, one project after another "came to a standstill," says Taha, who earned his archaeology Ph.D. in Germany. The conflict has restricted access to sites, he says, and in some areas it posed real danger to life and limb.

Making history. For the first time, Palestinian archaeologists are uncovering their heritage—including these Bronze Age pots from Tel Etell—on their own.

CREDITS (TOP TO BOTTOM): K. BUCKHEIT/*SCIENCE* (MAP); GERRIT VAN DER KOOIJ/LEIDEN UNIVERSITY

smaller than present technology allows. Beyond the promise of breakthroughs, however, what makes the collaboration tick, says Porath, is that "we are first of all good friends." This rare fraternity amid one of the world's ugliest conflicts is helping Sowwan realize his dream of bringing nanoscience to the West Bank.

Help has arrived from UNESCO, which 2 years ago laid a challenge before the two communities: Come up with competitive projects involving scientists from both sides of the ethnic divide, and we'll fund you. Last year, UNESCO's Israeli-Palestinian Scientific Organization (IPSO) awarded the first 10 grants. Sowwan and Porath are among the winners.

It's an open question whether such science-for-peace efforts can change communities. Critics say that truly equal scientific exchange will only be possible when Palestinian researchers enjoy university infrastructure on a par with that of their Israeli colleagues. But this is part of the plan, says Dan Bitan, an Israeli historian who co-directs IPSO. The intention, he says, is to build up Palestinian science "one project at a time." The first crop of IPSO projects is receiving raves from observers. "These projects are world-class," says Edouard Brézin, a physicist and president of the French Academy of Sciences.

The fragile endeavor now has a fresh concern: How will the budding collaborations fare under the new Palestinian Authority government led by Hamas, whose leaders have previously called for Israel's destruction? "These Palestinian researchers are so rare to be willing to collaborate," says Brézin. "Will Hamas stop them? That is something we fear." IPSO's saving grace may be that it has been developed "bottom-up" by Israeli and Palestinian scientists rather than as "a top-down imposed cooperation," says Yaakov Garb, an environmental researcher with Ben-Gurion University of the Negev in Beer-Sheva, Israel, and Brown University in Providence, Rhode Island, who co-directs the Brown-based Middle East Environmental Futures Project. IPSO belongs to both communities. And although science and conflict mix poorly, says theoretical economist Menahem Yaari, president of the Israeli Academy of Sciences, "we realized that if we wait for the fighting to end, then we'll wait forever."

Yaari wasn't the only high-profile academic frustrated by the barriers to Arab-Israeli scientific cooperation. Sari Nusseibeh, a philosopher and president of Al-Quds University, and Torsten

Future hope. Palestinian archaeology students at Al-Quds University prepare for fieldwork.

CREDIT: ISSA SARIE

But as partnerships unravel, some archaeologists hold Taha at fault. He is "autocratic," says one archaeologist who has worked on collaborative Palestinian projects and requested anonymity. "When people talk about doing something in Palestine and they learn that it will have to go through Taha, the advice is basically to forget it" because, he says, Taha is "very political" and takes control of projects to consolidate his power.

Taha dismisses such criticisms as "colonial cultural attitudes." He's supported by Gerrit van der Kooij, an archaeologist at Leiden University in the Netherlands and one of the few Westerners who has continued to work with Taha during the recent crisis. "It doesn't surprise me that outsiders become frustrated," he says: Taha "sticks by his policy of equal partnership. That means Palestinians must be involved at every step," from planning and digging to publishing. Van der Kooij says this policy is "fully justified and adds more social value to the project." Markus adds that his ministry will support collaborations "between us and any concerned parties. We believe in partnership," he says.

Palestinian archaeologists say they just want to get on with their work. "But we have an even more basic problem than collaboration and funding," says Issa Sarie, a physical anthropologist at Al-Quds University in Jerusalem. To travel between his home in East Jerusalem, his office at Al-Quds University, and meetings with Taha in Ramallah, Sarie says he risks arrest on a daily basis. His application to renew a permit that allows his movement between Israeli- and Palestinian-controlled areas was declined recently "without explanation" by the Israeli government, he says. To get home to his wife and two children each night, Sarie must cross into Jerusalem illegally, picking his way between fences and mud puddles. "These are the kind of obstacles that keep Palestinian academics from succeeding," he says.

But Sarie and others are quick to point to signs of progress. For one, having sites under Palestinian control is a crucial step toward making Palestinian archaeology "a scientific enterprise," says Taha. For the first time, "we are training our own students in the field," says Hani Nur El-Din, an archaeologist at Al-Quds University. "This makes all the difference for creating the next generation of archaeologists," he says, although "it will probably be 20 years before we can support our own Ph.D. program."

International donors at the first conference on Conservation of Cultural Heritage in Palestine, held in Jericho on 20 February, indicated they will keep funds flowing for archaeological projects in Palestine. Outside help will come even if the Palestinian Authority's budget is frozen, says Sa'id Omar, an officer for the United Nations Development Program in Jerusalem. "Unfortunately, the overall situation remains vague until the dust settles," he says.

–J.B.

Hidden costs. The security barrier may damage agriculture and harm wildlife, critics say.

Breaking Up Bomb Plots—and Habitats?

WADI FUQEEN, WEST BANK—From his village cradled in this ancient valley, Muhammad Manasra (Abu Mazen) can see trouble looming in every direction. Atop the northern hillcrest, the Israeli village of Zur Hadasah spills over the Green Line that has divided Israel from the Palestinian territories since 1967. To the south, the concrete high rises of an Israeli settlement, Beitar Elite, stare down over the rim. A rumbling echo fills the air as bulldozers raze the eastern hilltop to make way for thousands more settlers. But what most worries Abu Mazen, a village council member, is approaching from the north: a 50-meter-wide obstacle course of fences, ditches, and razor wire known as the security barrier. He fears that it will disrupt the flow of rainwater that has recharged the valley's springs for millennia. "Without water, we cannot farm," he says. "Without farming, we cannot live here."

The partially constructed, 670-kilometer barrier has a big value, many Israelis say: It deters suicide bombers. But critics on both sides of the Green Line say it is also wreaking havoc on the environment. "Wadi Fuqeen will not be its only casualty," says Yaakov Garb, an environmental researcher at Ben-Gurion University in Beer-Sheva, Israel, and Brown University. Besides disrupting the flow of surface water, Garb says the barrier could damage the region's unique ecosystems by blocking animal migration. Others are not so sure. "Fragmentation of habitats is our biggest problem, but I don't think [the barrier] is any worse for wildlife than our other roads and fences," says Tamar Dayan, an ecologist at Tel Aviv University in Israel.

To assess the impact of the barrier and other developments, Israeli scientists are assembling a network of long-term environmental monitoring stations. The plan started 7 years ago as a promising U.S.–brokered Israeli-Palestinian collaboration, but after the second intifada, the Palestinians dropped out. Israel has forged ahead with plans to link up 11 existing research stations next year. Data will be pooled on computers at Sandia National Laboratories in Albuquerque, New Mexico, and made freely available on the Internet.

The network's aim is to spot even the subtlest changes in the environment over several decades. "Long-term research is the only way to get the real answers," says Avi Perevolotzky, an ecologist at Israel's Agricultural Research

Wiesel, a Nobel Prize–winning neuroscientist at Rockefeller University in New York City, also felt that it was time for action. At a UNESCO meeting in Paris in 2003, the trio decided that "rather than just talking about peace, we would do it," says Yaari. So with about $3 million cobbled together from UNESCO, the French government, and several nongovernmental organizations, they launched IPSO in 2004. Grants are modest, amounting to about $300,000 for each project over 3 years.

Because tensions were high, says Yaari, "we decided to start cautiously" by embarking on a quiet advertising campaign on the electronic message boards of Israeli and Palestinian universities. Selection criteria were strict: Projects had to be "internationally competitive" and involve "an equal contribution from each side." The organizers expected a couple of dozen applications at most.

But the idea struck a chord. Nearly 100 proposals flooded in, in fields from physics to epidemiology. And far from charity cases, the quality "spoiled us for choice," says Bitan, who has administered the program from the start.

Several IPSO awardees let *Science* shadow them for a week. Their schedules consisted mostly of routines familiar to scientists the world over—from group meetings and grinding departmental paperwork to the coveted hours of isolation at the bench. But they also faced an obstacle course of practical problems that would seem alien to most scientists, any one of which is capable of destroying harmony.

> **"We realized that if we wait for the fighting to end**, then we'll wait forever."
>
> —Menahem Yaari, Israeli Academy of Sciences

Getting from A to B

Shahal Abbo curls his toes on the silky carpet in Mustafa Khamis's East Jerusalem home as he describes how another IPSO team came about. "Our collaboration had an ironic start," he says, cracking a smile beneath his bushy moustache. An agronomist in Rehovot, Abbo recalls talking with his Israeli peers: "You can imagine my colleagues' reactions when I told them I had to write a letter for Jihad." He was not referring to an Islamic holy war, but a young scientist. Jihad is Khamis's Palestinian former graduate student, who needed the power of Abbo's pen to get through army checkpoints.

Their project was a natural for collaboration because it focuses on a problem shared by both Israelis and Palestinians: how to use the precious water in sewage to irrigate crops. "Although [Jihad and I] understood the problem well, we only had a slight idea for a solution," says Khamis, a physical chemist at Al-Quds University, as he fills miniature cups with potent Arab coffee.

Khamis envisioned a two-part answer: a water desalination device that would be small and cheap enough to service a single village and a crop that could thrive on the water it produced. With help from the Euro-

CREDIT: CORBIS

Organization in Bet Dagan. It is unclear how long it will take to assess the barrier's impact. And without equivalent data from the Palestinian territories, researchers will have only half the picture.

"We want to collaborate," says Perevolotzky. A one-sided affair could pose huge problems for decision-makers. "When you work with the environment here, it is impossible to separate politics from science," says Yehoshua Shkedy, an ecologist with the Israel Nature and National Parks Protection Authority.

Shkedy pulls out a rumpled topographic map. "You can see what makes this place so special," he says. Like the spokes of a giant wheel, four slabs of color for different biogeographic zones converge. Each represents a distinct recipe of environmental ingredients, such as rainfall and soil type, that supports a characteristic assemblage of species. This is the only place in the world where the scrublands of Iran and Iraq collide with the oasis palms of eastern Africa, where dense Mediterranean oak groves meet Saharan sand dunes. And altitudes range from the peak of Mount Meron at 1200 meters down to the salt-caked shore of the Dead Sea at 400 meters below sea level, the lowest land on earth. "What's amazing," says Shkedy, "is that, in spite of 10,000 years of agriculture and urbanization, we're still ecologically healthy," with more than 100 species of plant per square kilometer on average and a menagerie of big animals such as leopards, jackals, gazelles, and wolves.

This spot is also the explosive meeting point of two fast-growing populations. "Both Israelis and Palestinians are rushing to claim and develop the land," says Shkedy, "and our job as scientists is to give advice." But sometimes it isn't welcome. For example, he asks, "Which direction should Jerusalem be allowed to expand, east or west?" Many important habitats lie to the west, "so from a conservation standpoint, we should say east." This would delight hawkish politicians who want Israel to expand in that direction, but Shkedy says that outcome "would surely lose the Palestinian cooperation we need to manage the environment over the long term."

The only way to preserve Israel's biological assets, says Shkedy, is to try to get beyond politics and take a long view. "What is most important for conservation is to keep the four biogeographic zones connected," he says. So 6 years ago, he and other ecologists proposed to link them with a network of corridors where development would be off-limits. But then came the second intifada and the security barrier, construction of which started in 2002 (see map on p. 352). "Look, it just could not be worse," says Shkedy, tracing the barrier's jagged course on the map as it slices back and forth through the corridors. Shkedy and others have proposed a "virtual" barrier, an electronic system that detects people but allows wildlife to pass freely. However, the Israeli Ministry of Defense last year shot down that idea on the grounds that it would not provide a sufficient deterrent to interlopers.

A farmer's fears. Abu Mazen (*right*) says his village in Wadi Fuqeen will wither if the security barrier impedes water flow.

The security barrier is part of a larger problem, says Shkedy. With casualties on both sides almost every day, "people say the environment is the least of our concerns," he says. "But if the land becomes ruined, then what are we all fighting for?"

–J.B.

pean Union and an Israeli company, he designed a $50,000 prototype purifier in the 1990s that could process the daily wastewater of 500 people. The output, laden with salts and metals, was not clean enough to drink but did pass muster for agriculture. The next challenge was to find a crop.

A rare friendship. Although difficulties abound, Mukhles Sowwan (*left*) says he is encouraging his students to study nanotechnology at Hebrew University with Danny Porath (*right*).

CREDITS (TOP TO BOTTOM): J. BOHANNON/*SCIENCE*

This is where Abbo's expertise dovetailed. "Chickpeas were the obvious choice," he says, "not only because everyone eats falafel and hummus here, but because the plant is very well adapted to this soil." Since the project began in 1999, Abbo has been breeding chickpea plants that thrive in Khamis's treated water.

On a dusty hill on the edge of the Al-Quds campus, a truck-sized tank quietly hums, churning wastewater with bacteria and straining it through filters. A pipe leads to a lower terrace where neat rows of chickpea plants are sprouting. Khamis dashes indoors to show the extra dimension to this project that helped clinch funding from IPSO. Piece by piece, he is assembling a world-class environmental testing laboratory for the West Bank. Meticulously clean instruments measure nearly everything there is to know about a drop of water. "We don't even have such a facility on the Israeli side," says Abbo. To expand the collaboration, Khamis hopes to add a plant genomics wing within a few years.

But the road ahead is bumpy. Pausing next to a plasma spectroscope, a $120,000 device that identifies heavy-metal contamination, Khamis's cheerful guise clouds over. "This broke down last year, and we have not been able to get a replacement part," he says. Nearby is another expensive instrument that has never been installed. "The companies refuse to send technicians because of security reasons," says Khamis. That's one impediment an IPSO grant has not overcome.

Show me the money

Sowwan checks his watch and gasps. The European sales director of a nanotechnology device company has flown in from the United Kingdom just to meet the Al-Quds physicist for lunch today. "We must rush," says

Sowwan as he passes through a rainbow of hijab veils worn by his female students. Although the meeting is in an hour at Hebrew University, just 5 kilometers away, the road is blocked by the security barrier—which in Jerusalem takes the form of an 8-meter-high concrete wall that chokes traffic and possibly creates ecological problems as well (see sidebar on p. 354). It was built, the Israeli government says, to protect its citizens from terrorist attacks. The best route these days is to drive 45 minutes through outlying Arab villages on narrow, crumbling roads and, inevitably, through a checkpoint. Because Sowwan lives on the Israeli side of Jerusalem, his license plate makes it easier to pass, although he is sometimes stuck for hours in a queue.

The contrast between Al-Quds and Hebrew University is staggering, as if we've teleported from the Middle East to southern California. Bare-shouldered students bask on manicured lawns between stone buildings and a statue of Albert Einstein, a university patron. The campus has also been a haven for Palestinian scientists such as Sowwan, who would otherwise have no equipment to use, let alone experts to learn from. Nanoscience at Hebrew University has been particularly open-armed, producing a string of successful researchers of Palestinian origin publishing in major journals, including *Science*. Although Sowwan has now officially moved to Al-Quds, he retains full membership at the university's Center for Nanoscience and Nanotechnology.

Good chemistry. Mustafa Khamis (*left*) has teamed up with Shahal Abbo (*right*) to tackle the shared problem of water scarcity.

The salesman is waiting in a bustling campus cafe. The meeting proves frustrating. Yet it's typical for Sowwan and other talented but underfunded Palestinian scientists. He spends an hour trying to bargain a $250,000 atomic force microscope down to $50,000, to no avail. (Tip to lab managers: Sowwan did get it to $120,000.) The IPSO grant alone will not be enough to put his new lab at Al-Quds on par with Porath's. Nevertheless, Sowwan says, "it's a start."

Where collaboration is a dirty word

To some critics, IPSO's problems run deeper than a shortage of funds. One Israeli professor, in a series of open letters e-mailed to the Israeli academic community last year, railed against it as "dangerous" and "playing into the hands of terrorists." Yaari responded but was unable to persuade him that the collaborations were worthwhile. "In the end we agreed to disagree," he says.

IPSO scientists have been taking even more flak from the Palestinian side. "Cooperation is viewed as an attempt to normalize the abnormal situation of occupation," says Khamis. "Even the word 'collaboration' is taboo here," adds Viveca Hazboun, a West Bank psychiatrist with a project proposal under review for IPSO funding. Palestinian "collaborators" deemed too helpful to the Israeli government have been murdered by extremist groups, she says.

Hazboun has two strategies for easing tensions on the Palestinian side. Among colleagues, she avoids the term "collaboration." "We call it 'scientific exchange' instead," she says. She also promotes tolerance among her research subjects, the estimated 45% of Palestinians in Bethlehem who suffer from posttraumatic stress disorder. "If you can forgive, you can move on," says Hazboun, whose previous clinic was destroyed 3 years ago by Israeli shells during a siege on Bethlehem.

Ultimately, Israeli and Palestinian scientists will need the consent of their governments to work together. It remains unclear how Hamas will interact with the newly elected Israeli government led by Ehud Olmert, but IPSO is forging ahead. "Creating a culture of peace is our responsibility as Israeli and Palestinian scientists," says Hasan Dweik, a chemist at Al-Quds who co-directs IPSO with Bitan. Another 13 projects have been chosen for the next round of funding later this year, he says.

IPSO researchers, too, are optimistic. Despite the barriers, Sowwan plans to send his Palestinian students to learn in Porath's lab on the Israeli side. "It will be difficult," he admits, but "science is a universal language, like music. It can make people understand each other."

–JOHN BOHANNON

War-zone science. Psychiatrist Viveca Hazboun's Bethlehem offices were destroyed by artillery fire.

CREDITS: J. BOHANNON/*SCIENCE*

CREDIT: RICK KOZAK

CANCER RESEARCH

After Regime Change at the National Cancer Institute

Andrew von Eschenbach, who has been nominated to head FDA, is expected to step down soon as director of NCI after a controversial tenure. His successor will face a big budget squeeze and low morale

Robert Weinberg turned gloomy as he wound up an award lecture earlier this month in Washington, D.C., at the annual meeting of the American Association for Cancer Research. One of the founders of the Whitehead Institute for Biomedical Research in Cambridge, Massachusetts, he flashed a slide of his lab team and gave a warning: Because investigator-initiated grants have become impossible to get, he said, these young researchers don't have "much of a future." Those "who determine funding … have lost sight of [the] most important element." It is "not large research consortia, not new technologies, not cancer centers," Weinberg said, but the young individual investigator. "We have deserted them." His comments drew lengthy applause.

This complaint is echoing across the community as growth at the National Institutes of Health (NIH) comes to a halt. In cancer research, the largest chunk of U.S. biomedical funding, the situation is especially bad. The "payline," or success rate, for bread-and-butter investigator grants (R01s) at the National Cancer Institute (NCI) this year, after peer approval, will drop to 11%, compared to 22% 4 years ago. Already, Weinberg and some other researchers are pointing to this as the main legacy of departing NCI Director Andrew von Eschenbach.

Justly or not, the former urologic surgeon at University of Texas M. D. Anderson Cancer Center in Houston, nominated last month to head the Food and Drug Administration (FDA), will likely be remembered as one of the most controversial NCI directors ever. The pet themes and management methods he adopted—as well as NCI's budget problems—complicated his tenure. Says one leading cancer biologist and former member of an NCI advisory board, "He's been a disaster."

A three-time cancer survivor who came to NCI through connections with President George W. Bush's family, von Eschenbach brought a passion for direct involvement with cancer patients to the $4.8 billion NCI. He introduced prayer to advisory committee meetings and a business model to NCI management. He set a startling goal of ending cancer deaths by 2015. He oversaw several major new technology initiatives to accomplish that. Paying for them, however, has added to the pressure on NCI's budget, which has required painful cuts across NCI that have hit especially hard in the intramural program. One lab chief and 20-year NCI veteran says intramural morale "is as low as I've seen it."

Other researchers are more upbeat. Von Eschenbach "has put a personal face to the problem of cancer," says Robert Young, president of Fox Chase Cancer Center in Philadelphia, Pennsylvania. "That new, different outlook was refreshing and good." John Mendelsohn, president of M. D. Anderson, praises efforts such as working with FDA to speed cancer drug approvals. "His vision is just beginning to be achieved," he says. As for the current budget crisis, "I think it's hard to lay the blame on him," says molecular biologist Albert Fornace of Harvard School of Public Health in Boston, who left NCI's intramural program last year: "It was the perfect financial storm."

Through a spokesperson at FDA, von Eschenbach declined to be interviewed, pending the Senate's vote on his nomination for his new position, but he responded to written questions. The initiatives he oversaw at NCI "will greatly accelerate cancer research" and "hold potential and promise for great advances," von Eschenbach said. Asked about the declining grant award rate, he said NCI "is striving to be the best steward of all its resources" in tough budget times. He also dismissed the critics, saying "the research community has always and consistently been supportive of me and the NCI."

Von Eschenbach is still director of NCI, although he also has been acting chief of the FDA since September. A spokesperson for the Department of Health and Human Services (HHS), NIH's parent agency, says von Eschenbach will leave NCI "soon." This would resolve an apparent conflict, in that he now heads two agencies—one a developer of drugs and the other a regulator. Anticipating a change, leaders in the cancer field have quietly circulated an appeal to the White House for a national search for the next NCI director. (The NIH and NCI directors are both nominated directly by the president.) Whether there will be a search is not known, but this much is clear: The new NCI chief's first challenge will be to solve the agency's massive budget gridlock.

Optimism

Picking the right person to lead cancer research 5 years ago was a high priority for Bush. He named von Eschenbach NCI chief in December 2001, less than 3 months after the departure of former director Richard Klausner, a cell biologist. Von Eschenbach, head of prostate cancer research and later executive vice president at M. D. Anderson, later recalled that he felt both "exhilaration" and "almost … terror" when he first flew into D.C. He was relatively unknown in the NCI world, as a clinical researcher who was president-elect of the American Cancer Society (ACS), an advocacy organization founded by surgeons. He invited controversy by remaining a leader of the National Dialogue on

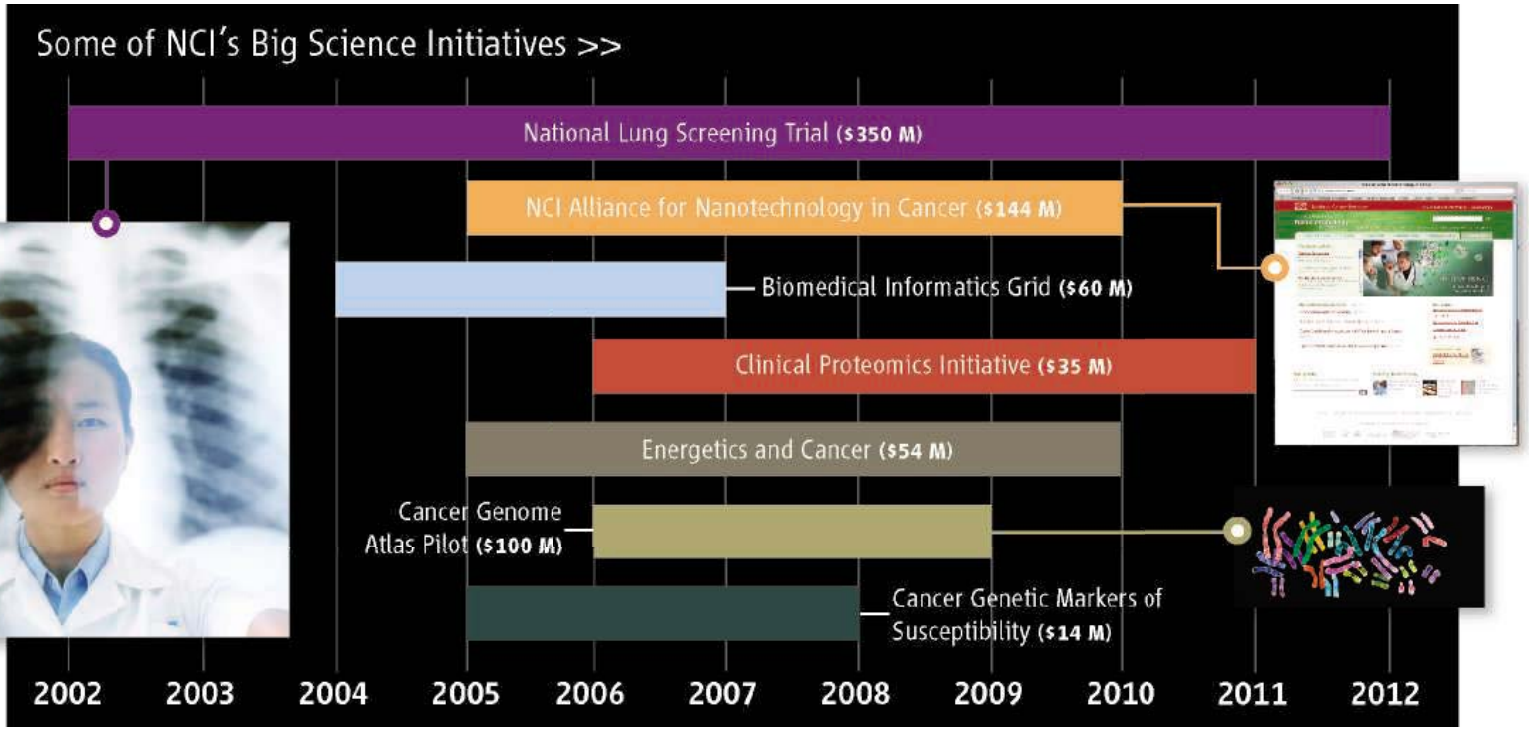

Cancer, a private group funded by ACS and co-chaired by George H. W. Bush. *The Cancer Letter*, a newsletter in Washington, D.C., relentlessly criticized von Eschenbach's ties to the group (now called C-Change) as a conflict of interest. Von Eschenbach resigned from it last September after he became acting chief of FDA. *The Cancer Letter* had reported that C-Change's board members included drug company executives.

Still, von Eschenbach's message of bolstering links between "the three Ds: discovery, development, delivery" was welcome at a time when the NIH budget was booming, says cancer biologist Thomas Curran of St. Jude Children's Research Hospital in Memphis, Tennessee. Von Eschenbach's ties to the Bush family, some hoped, would help boost NCI's budget.

The new chief's style, however, took scientists by surprise. He introduced a moment of silence for cancer patients at NCI's National Cancer Advisory Board (NCAB) meeting. According to one scientist, at a private meeting, von Eschenbach said he was "on a mission from God." The scientist adds: "That was a strange and worrying thing to hear from the director of NCI." Politics, some suspected, was involved in one early incident. A few months into his tenure, several congressional Republicans complained about a fact sheet on NCI's Web site stating that abortion does not raise a woman's risk of breast cancer. Von Eschenbach ordered it removed. He then held a scientific workshop to investigate; it came to the same conclusion—the evidence did not support a link—and the fact sheet went back up.

Von Eschenbach stunned the community in February 2003 when he announced that NCI intended "to eliminate the suffering and death from cancer by 2015." This "challenge goal," reminiscent of President Richard M. Nixon's 1971 launch of the "War on Cancer," was embraced by ACS and some other advocacy groups. But among researchers, it became "a point of some ridicule for Andy and this Administration," says oncologist Richard Schilsky of the University of Chicago in Illinois.

As a manager, von Eschenbach described himself as a corporate CEO. He created four new deputy director positions to run the institute. These deputies became part of a new top level for decision-making, rather than an executive committee that included division directors. This "changed the culture" by adding a new layer of management, says Dinah Singer, director of NCI's Division of Cancer Biology, although she sensed no change in the "commitment of leadership" to her division. And new initiatives often came from these deputies, not from the program staff.

Leading these efforts was one of von Eschenbach's first hires, Anna Barker, former CEO of a biotech company and a C-Change leader. Barker, who has a Ph.D. in immunology and microbiology, had no recent experience as a researcher. She was put in charge of starting new technology initiatives—and soon ran into opposition from extramural scientists.

An idea that ran into early trouble, a national biospecimen network, had first been proposed by C-Change. The ambitious plan was to create a new shared resource of tumor samples with attached patient information. But it was vague on details and disregarded existing tissue banks collected through clinical trials for decades, critics said. It also raised concern that NCI's ideas were coming not from its scientific public advisers but from a group that met behind closed doors. The proposal reflected "naiveté on the part of some of the NCI leadership," says Schilsky. It now survives as a small pilot project collecting prostate cancer specimens.

A second big idea, a $187 million nanotechnology initiative, got a tongue-lashing from skeptics at the June 2004 meeting of NCI's Board of Scientific Advisors (BSA). The reviewers said NCI leaders had failed to demonstrate the scientific promise of nanotech, had not shown that the private sector couldn't carry the ball, and had overlapped with another nanomedicine component launched by NIH Director Elias Zerhouni. BSA soon approved a $144 million, 5-year nano initiative, however.

Two other big initiatives fared better: a proteomics effort to identify proteins in blood and other biomarkers that might work as early warning signs of cancer, and the most recent: a human Cancer Genome Atlas. The latter, presented by Eric Lander of the Broad Institute in Cambridge, Massachusetts, would systematically sequence tumor samples for mutations involved in cancer to speed up the search for new drugs and diagnostics. Some have criticized the Atlas as an employment project for genome centers. Its projected price tag of $1.5 billion over a decade was whittled down to a 3-year, $100 million pilot, to be split between NCI and the National Human Genome Research Institute.

Unlike Barker, who had a contentious beginning, other top recruits enjoyed a relatively gentle welcome. James Doroshow, who oversees the Division of Cancer Treatment and Diagnosis, has made progress with better coordinating clinical trials, says Schilsky. And Mark Clanton,

CREDIT: GETTY IMAGES; NCI

deputy director for cancer care and delivery, started "important" new outcomes research programs, Fox Chase's Young notes. Von Eschenbach never filled a fourth position for basic science deputy.

The crunch

The new projects might have been less controversial had more money been available. But von Eschenbach was working with an ever-tightening NCI budget, much of it tied up in continuing grants and activities. For example, just before von Eschenbach arrived, NCI had agreed to fund a now–$350 million screening trial to see if spiral computed tomography (CT) scans could detect lung tumors missed by x-ray imaging in former smokers. The hope is that by detecting tumors earlier, CT screening could save many lives. The study is controversial: Critics suggest it will lead to a huge increase in biopsies of benign tumors in healthy people, with a relatively minor decline in overall mortality, Curran notes. And the technology is expensive.

Although NCI's budget rose 81% during the 5-year NIH doubling that ended in 2003, the brakes hit hard in 2004, translating into a slight $2.7 million cut in NCI's operating budget after paying grants, salary raises, and contributions to trans-NIH activities. It has been falling in real terms since (see graph, right). To fund the new initiatives and help maintain the payline, von Eschenbach has cut the intramural program 4.4% since 2003.

Because so much of NCI's intramural budget is tied up in salaries, the effect has been severe. The Center for Cancer Research, the main division, is down 43 principal investigators (PIs) to 275, says CCR Director Robert Wiltrout. About 10 labs have been shut down, other PIs have retired, and still others—including several scientific standouts—have left on their own. NCI's advisers recommended cutbacks, but some say without any effort to define the program's mission. Fornace says one reason he left was that remaining labs have lost staff positions; others complain of having no money to refurbish equipment. Von Eschenbach remained "pretty distant," says Fornace, never showing much interest in the labs.

Even so, the cuts haven't been enough to stave off a slide in the portion of basic R01 grant applications that are funded during each round of reviews. The drop in the payline to 11% this year is the lowest level since at least the early 1990s. NIH officials caution that it's not as bad as it seems: The number of applications has been rising, which pushes the success rate down. The total number of funded grants has been fairly steady, roughly 5150 in 2005. Still, the number of new grants dropped by about 200 last year, grants are getting smaller, and some long-term and even midcareer grantees are not being funded. Most worrisome is that young, creative researchers are leaving the field.

Are the big new initiatives to blame? Mendelsohn doesn't think so. "If you eliminated all of the new projects, I don't think it would have solved this problem," says Mendelsohn, noting they only add up to "a few hundred million" dollars spread over several years. Even $100 million annually would only be 2% of NCI's overall budget.

Slippery slope

Worse may be yet to come, however. Paylines are expected to slip to single digits next year when NCI faces a $40 million cut. The sense of crisis is bringing new scrutiny of NCI's large projects, including the 61 cancer center grants and the so-called SPORES, smaller grants to centers that translate science into therapy. At the last BSA meeting in February, advisers agreed that "we will be taking a hard look at many of the major programs," says Young, the committee's chair. That could include scaling back or delaying some of the new initiatives. Schilsky, a BSA member, also hopes NCI will examine an old problem: sprawling infrastructure and relative lack of central coordination. "The background problem is having all this redundancy," says Schilsky.

Cancer research leaders also hope to finesse the awkward 2015 goal. "It's a promissory note that Congress and the public will assume is deliverable," Young says. "My concern is the potential ramifications if it's not reached." A task force of cancer center directors is working on a modified timeline that will be "numbers and data driven," Mendelsohn says. It will look at concrete goals, such as reducing smoking, and may revise what can be achieved by 2015, he says.

Despite the ongoing budget slide and lack of a permanent chief, scientists within NCI seem to be breathing a bit easier lately. "Everybody feels as if … the dust and feathers have settled," says one lab director. Funds freed up by the many departures will allow CCR to recruit some new hires for key positions such as radiation oncology, says Wiltrout. He also hopes to hire a dozen or so "young, smart," tenure-track scientists in the next 2 years.

Some NCI staff members also seem at ease with the person running NCI now, John Niederhuber, deputy director for clinical and translational science. A former director of the University of Wisconsin Cancer Center and NCAB chair, Niederhuber was named NCI's chief operating officer in charge of day-to-day operations when von Eschenbach became acting head of FDA last fall (*Science*, 30 September 2005, p. 2142). Within NCI, Niederhuber has been a "stabilizing force," Wiltrout says. Some are encouraged that he has started a small lab. It shows a "commitment to science," Singer says.

The enormous challenges ahead will require great skill and stamina of the next NCI chief. Many researchers are hoping the White House will conduct a national search for the director. In an unusual step, about 60 prominent cancer researchers sent Bush a letter in March emphasizing the importance of the position and offering their help with finding candidates. Zerhouni, according to an NIH spokesperson, is in touch with HHS and the White House about the position, and the White House "is committed to conducting a broad search so as to identify the best qualified candidates for the president's consideration."

Whether the government can recruit a star is an open question. Any newcomer will have to come to terms not only with the most dismal NCI budget scenario in 3 decades but also with stringent new rules on owning pharmaceutical stock; and because this is a presidential appointment, the director might have less than 2 years to serve. But the hope, says molecular oncologist Michael Kastan of St. Jude, is that there just may be an altruist out there interested in taking on the job.

–JOCELYN KAISER

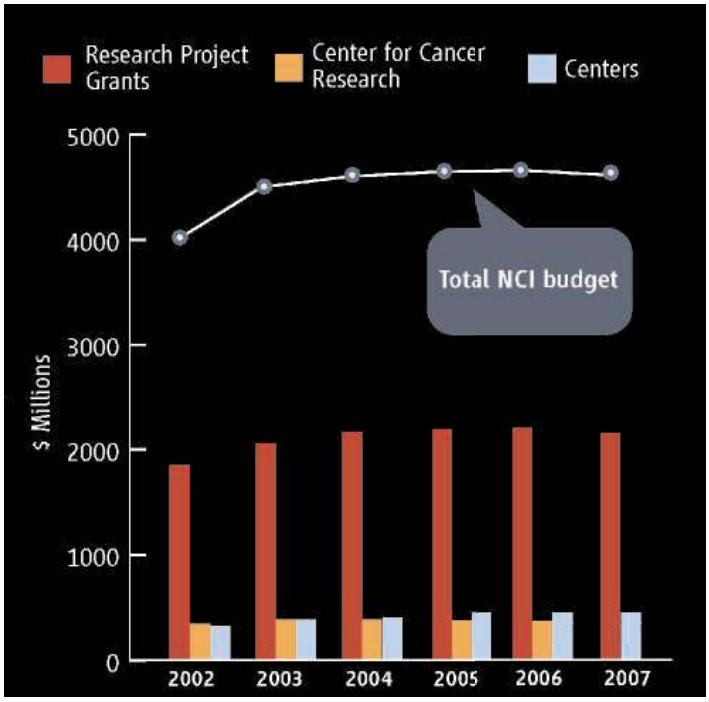

Hard landing. As NCI's budget flattens out and falls short of inflation, the institute is struggling to maintain research grants, centers, and the intramural Center for Cancer Research.

SOURCE: NCI

Graves of the Pacific's First Seafarers Revealed

Little is known about the Lapita peoples, the first settlers of the Western Pacific, other than their ubiquitous calling card: red pottery fragments with intricate designs. But in what's being hailed as one of the most dramatic finds in years, researchers at the meeting offered a glimpse of the first-known early Lapita cemetery. "This is the closest we're going to get to the first Polynesians," says archaeologist Matthew Spriggs of Australia National University (ANU) in Canberra, a member of the excavation team.

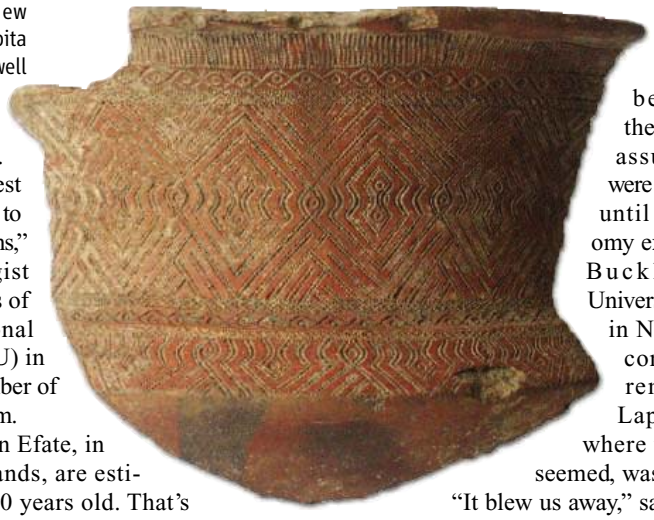

Face to face. A new find reveals the Lapita peoples' bones as well as pottery.

The graves on Efate, in the Vanuatu Islands, are estimated to be 3000 years old. That's around the time that the Lapita peoples began hopscotching across the Pacific from New Guinea's Bismarck Archipelago, fanning out as far as Samoa and Tonga. The site reveals unknown facets of their burial customs, and DNA from the bones may offer clues to their origins. "The find has opened a new window on the Lapita people as a biological population as well as an archaeological culture," says Lapita expert Patrick Kirch of the University of California, Berkeley.

Since the first Lapita shards came to light a half-century ago, more than 200 sites have been found, but skeletal remains are very rare. Then just before Christmas in 2003, workers quarrying soil for a prawn farm came across a chunk of pottery with a complex pattern. They showed it to a field worker with the Vanuatu Cultural Centre, Salkon Yona, who luckily had just been trained in Lapita identification. Yona consulted ANU archaeologist Stuart Bedford, who in a second stroke of luck was on the island for a wedding. Bedford confirmed the shard as early Lapita, skipped the wedding ("my friends understood," he insists), and scrambled to protect the site, near Teouma Bay.

But the biggest surprise came when the team, led by Bedford, Spriggs, and Ralph Regenvanu of the Vanuatu National Museum, began excavating bones. Because so few Lapita burials had been found, the researchers assumed these were recent graves until paleoanatomy expert Hallie Buckley of the University of Otago in New Zealand confirmed the remains were Lapita. Everywhere they dug, it seemed, was a skeleton. "It blew us away," says Bedford.

In two seasons, they excavated 25 graves containing three dozen individuals.

All skeletons were headless, a feature of other Pacific cultures. In some graves, cone shell rings were placed in lieu of the skulls, indicating that the graves were reopened after burial and the heads ceremonially removed, Bedford says. (The rings are 3000 years old, according to radiocarbon dating.) The heads were reburied. In one grave, three skulls (see photo, above) were lined up on the chest of a male skeleton, whose grave the bulldozers missed by centimeters. His bones bear scars of advanced arthritis. "He must have been in a lot of pain and was clearly looked after," says Spriggs.

The pots too are revelatory. Some are burial jars, by far the oldest in the region. The inner rim of one features four clay birds peering into the vessel. The vessels are similar in form to early "red-slip" pottery found in Taiwan and islands of Southeast Asia, bolstering the argument that Lapita peoples at least tarried in this region on their eastward migration. An article on Teouma is in press in *Antiquity*.

After excavations this summer, the team hopes to extract DNA from bones to compare with modern populations. In the meantime, Teouma has become the pride of Vanuatu, which has featured its Lapita heritage in a set of postage stamps.

When in Vietnam, Build Boats as the Romans Do

In December 2004, researchers drained a canal in northern Vietnam in search of ancient textiles from graves. They found that and a whole lot more. Protruding from the canal bank at Dong Xa was a 2000-year-old log boat that had been used as a coffin. After a closer look at the woodwork, archaeologists Peter Bellwood and Judith Cameron of Australia National University in Canberra and their colleagues were astounded to find that the method for fitting planks to hull matched that used by the Roman Emperor Caligula and his contemporaries in the 1st century C.E. That shipwright technique was believed to be unique to the Mediterranean, several thousand kilometers to the west.

"It's very convincing," says Lucy Blue, a maritime archaeologist at the University of Southampton, U.K. "They are absolutely correct in their links with comparable material in the Greco-Roman world." It's impossible to say, however, whether the boatmaking method is a case of technology transfer across vast distances or whether it arose independently in East Asia.

The Dong Xa boat yielded a trove of artifacts: a ramie burial shroud, a cord-marked pot next to the head of the corpse with a red lacquered cup inside, and a couple of Han Dynasty *wushu* coins, minted from 118 B.C.E. to 220 C.E. But the big discovery was courtesy of a remarkably well-preserved hull. Along the gunwale of the 2-meter section are empty mortise and locking peg holes for attaching planks with rectangular fastenings called tenons. In this technique, planks are fitted together before a frame is added.

CREDITS (TOP TO BOTTOM): FREDERIQUE VALENTIN; STUART BEFORD

Java Man's First Tools

About 1.7 million years ago, a leggy human ancestor, *Homo erectus*, began prowling the steamy swamps and uplands of Java. That much is known from the bones of more than 100 individuals dug up on the Indonesian island since 1891. But the culture of early "Java Man" has been a mystery: No artifacts older than 1 million years had been found—until now.

At the meeting, archaeologist Harry Widianto of the National Research Centre of Archaeology in Yogyakarta, Indonesia, wowed colleagues with slides showing stone tools found in sediments that he says were laid down 1.2 million years ago and could be as old as 1.6 million years. The find, at a famous hominid site called Sangiran in the Solo Basin of Central Java, "opens up a whole new window into the lifeways of Java Man," says paleoanthropologist Russell L. Ciochon of the University of Iowa in Iowa City.

Indonesian tool kit. *Homo erectus* used small, finely worked tools on Java.

Although hominids apparently evolved in Africa, Indonesia is a Garden of Eden in its own right, with a wealth of *H. erectus* fossils. The startling discovery 2 years ago of "hobbits"—the diminutive *H. floresiensis* of Flores Island—added a controversial new hominid to the Indonesian menagerie.

In 1998, Widianto found stone flakes in the 800,000-year-old Grenzbank layer at Sangiran, whose well-plumbed sediments reach back 2 million years. Then in September 2004, his team struck gold in a layer dated by extrapolation from the rocks around it to 1.2 million years ago. Over 2 months, they unearthed 220 flakes—several centimeters long, primarily made of chalcedony, and ranging in color from beige to blood red—in a 3-by-3-meter section of sand deposited by an ancient river.

The find, not yet published, could be even more spectacular than Widianto realizes, says Ciochon. His team, which also works at Sangiran, has used ultraprecise argon-argon radiometric methods to date the volcanic strata overlying the levels excavated by Widianto to 1.58 million to 1.51 million years ago—making the flakes at least 1.6 million years old. If the flakes were undisturbed, Ciochon says, they would represent "some of the earliest evidence of the human manufacture of stone artifacts outside of Africa." Their antiquity would match that of the oldest flakes found in China, at Majuangou, dated to 1.66 million years ago and also made of chert.

But not everyone is convinced. Although the chert flakes are abraded, possibly by water, a few limestone flakes are remarkably sharp. "The difference in preservation condition could indicate that we are dealing with secondary deposition," or flakes of different ages mixed together, cautions archaeologist Susan Keates of Oxford University in the U.K., who was at the talk. Others disagree. "I feel their excavation is reliable, because the deposits are thick and undisturbed," says Hisao Baba, curator of anthropology at Japan's National Science Museum and the University of Tokyo, whose team has also uncovered *H. erectus* fossils and flakes on Java.

The Sangiran flakes "are fundamentally different"—smaller—than the stone choppers made by *H. erectus* in Africa, says Ciochon. The evidence, he argues, suggests that Java Man had to range far for small deposits of good flint or chert and so created small, finely worked tools in contrast to the larger tools found in Africa. Considering the scarcity of raw materials on Java, Ciochon says, it's "a remarkably fine technology."

Widianto will resume excavations in June. "I will be going deeper and deeper, older and older," he promises. **–R.S.**

CREDITS (TOP TO BOTTOM): RETNO HANDINI; COURTESY OF PETER BELLWOOD

"The only place in the world where this construction is known is the Mediterranean," says Bellwood, who presented the find in Manila. Shipwreck excavations show that several cultures, including the Egyptians, Greeks, and Romans, employed mortise-and-tenon technology from at least 3300 years ago until around the middle of the first millennium C.E.

Hunting for similar construction in Vietnam, Bellwood and his colleagues found a museum piece made from timbers bearing the same mortise-and-tenon technique. The timbers, part of a mortuary house for an infant coffin made around 200 C.E., are planks from a boat scrapped for burial, Bellwood says. Both the mortuary house and the Dong Xa boat were found in clay deposits near the Red River.

À la Caligula. An ancient boat from Vietnam was built using Roman techniques.

Bellwood doubts that the two cultures ever met face to face. "I don't believe we have Romans sailing to Southeast Asia," he says. "It would be nice to say it was invented independently," he adds, noting that the Chinese used mortise-and-tenon carpentry for houses in the Neolithic, centuries before the technique was applied to Mediterranean ships.

But how the ancient people near the Red River learned their boatmaking remains a mystery. "At present, there is just not enough evidence to support cultural influence in construction choice," says Blue.

Bellwood favors a series of transfers across the ancient world 2 millennia ago, when the Old World was entering its first phase of true globalization. That's the "most attractive hypothesis" for now, he says—at least until a Chinese Neolithic log boat is discovered.

–RICHARD STONE

You could be next

Yes, it *can* happen to you:
If you're making inroads in neurobiology research and you've received your M.D. or Ph.D. within the last 10 years, the Eppendorf & *Science* Prize for Neurobiology has been created for YOU!

$25,000 Prize

This annual research prize recognizes accomplishments in neurobiology research based on methods of molecular and cell biology. The winner and finalists are selected by a committee of independent scientists, chaired by the Editor-in-Chief of *Science*. Past winners include post-doctoral scholars and assistant professors.

If you're selected as next year's winner, you will receive $25,000, have your work published in the prestigious journal *Science* and be invited to visit Eppendorf in Hamburg, Germany.

What are you waiting for? Enter your research for consideration!

Deadline for entries:
June 15, 2006

For more information:
www.eppendorf.com/prize
www.eppendorfscienceprize.org

"This is a unique award because it recognizes young neuroscientists for their work and their ability to communicate with a broad audience. I was surprised and honored to be a winner."

Miriam B. Goodman, Ph.D.
Assistant Professor
Stanford University
School of Medicine
2004 Winner

eppendorf & Science
PRIZE FOR NEUROBIOLOGY

EDITED BY YUDHIJIT BHATTACHARJEE

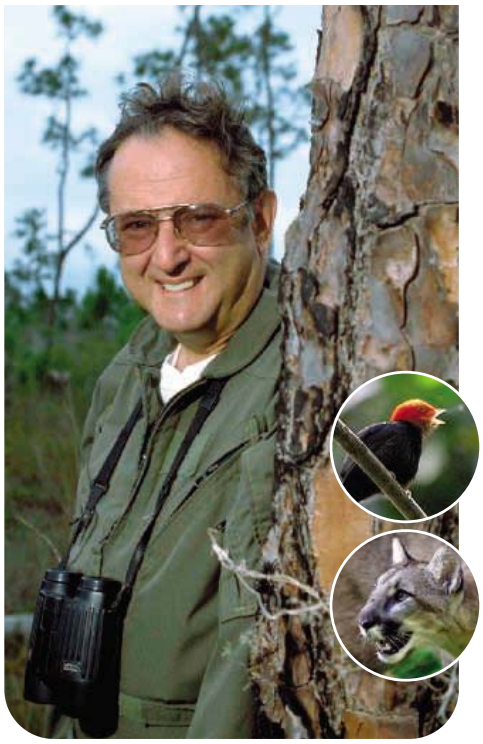

Awards

SAVIOR OF SPECIES. Stuart Pimm's epiphany came almost 30 years ago in Hawaii when the young ecologist discovered that some of the honeycreeper birds he had come to study had vanished. "I realized species are going extinct, and scientists can—and ought—to do something about it," he says.

Since then, Pimm, now at Duke University in Durham, North Carolina, has studied threatened and endangered species around the world and testified for their conservation before the U.S. Congress. This month, he was named winner of the $150,000 Heineken Prize for Environmental Sciences from the Royal Netherlands Academy of Arts and Sciences.

The academy also announced the winners of four other $150,000 prizes: Geneticist Alec Jeffreys of the University of Leicester, U.K., wins the biochemistry and biophysics award for discovering the genetic fingerprint; medical researcher Mary-Claire King of the University of Washington, Seattle, wins the medicine award for linking breast cancer to a gene; psychologist John Anderson of Carnegie Mellon University in Pittsburgh, Pennsylvania, earns the cognitive science award for his theory of human cognition; and economist Joel Mokyr of Northwestern University in Evanston, Illinois, wins the history award for researching the origins of the modern industrial economy.

MOVERS

MOLDING AN AGENCY. Matthias Kleiner has spent a career finding better ways to manufacture new shapes and forms. Now the 50-year-old professor of mechanical engineering at the University of Dortmund will have the chance to shape Germany's research funding agency, DFG.

Last week, the 39-member DFG Senate made Kleiner its unanimous choice to replace outgoing president Ernst-Ludwig Winnacker. The official decision will be made on 31 May, through a vote at DFG's general meeting, but those university professors and research scientists almost always follow the Senate's recommendation.

Kleiner has been a DFG vice president since 2005, winning praise for his management skills and understanding of university and industrial research. He would be the first engineer to lead the $1.8 billion agency, which funds research in all branches of science and the humanities. Winnacker will step down at the end of 2006.

A GRAND HOMECOMING. The British Geological Survey (BGS) has snared the head of earth sciences from France's premier research agency as its next director. John Ludden, a British Canadian who left the United Kingdom after getting his Ph.D. in 1976, will succeed David Falvey, who retires in October.

Taking over an organization founded in 1835 to map the United Kingdom, Ludden sees new technologies such as improved satellite imaging leading to the "rebirth of mapping" along the deep ocean floor and other uncharted areas. Wielding an annual budget of $70 million to $90 million—half of which is government funding—Ludden will continue to forge links between BGS, universities, and commercial companies, focusing on projects such as the Integrated Ocean Drilling Program.

FREEDOM FROM GOVERNMENT. The Bush Administration's restrictions on funding research using human embryonic stem (ES) cells have driven a prominent National Institutes of Health (NIH) researcher into the private sector. Mahendra Rao, who works with ES cells at the National Institute on Aging in Bethesda, Maryland, has been hired by Invitrogen, a biotech company in Carlsbad, California.

"It was clear that the policy was unlikely to change in the next 2 to 3 years, and hence I decided that I needed to move," says Rao. He says his replacement will probably be someone who works on adult tissue.

Sean Tipton of the Coalition for the Advancement of Medical Research in Washington, D.C., says Rao's departure shows "what the results of Bush's restrictive policies are going to be. Good scientists are not going to stay at NIH or even perhaps stay in the country."

At Invitrogen, Rao plans to work on characterization of new ES cell lines not approved by the Administration.

Data Point >>

ZERO ERROR RATE. Perfection is rare. But last year the National Science Foundation (NSF) batted 1.000—35 for 35—in rejecting the final appeals of disgruntled grant applicants.

The appeals represent the fourth try for scientists who think NSF erred in declining their requests for funding. Program managers field the first plea for reconsideration, followed by division directors and the heads of the particular research directorates. If an institution still believes that NSF has made a procedural error—a conflict of interest by a reviewer, for example, says NSF's Nathaniel Pitts—it can ask the NSF deputy director to review the case.

As head of the Office of Integrative Activities, Pitts says that about one-third of the requests sent to him are worthy of reconsideration. But if a losing complainant persists all the way to the final round, "there has to be something egregious" for the top brass to reverse the decisions of its staffers. So last year's batting average suggests to Pitts that the system is working. "I'm actually surprised that any of the requests succeed at that level," he says about the tiny percentage (see graph) of petitioners who have won their appeals in the past.

Asking NSF for a second chance

	2002	2003	2004	2005
No. of appeals	30	26	49	35
Decision reversed	1	2	1	0

Got a tip for this page? E-mail people@aaas.org

CREDITS (TOP TO BOTTOM): COLUMBIA UNIVERSITY EARTH INSTITUTE/(INSETS) STUART PIMM; NIH (PHOTO)

AFFYMETRIX

WORKSHOP SERIES SPRING 2006

APRIL/MAY PROGRAM: GENETICS

READ AFFYMETRIX MICROARRAY BULLETIN INTERVIEWS

April 17, 2006 - **Alan Herbert, Ph.D., and Michael Christman, Ph.D.** Boston University School of Medicine. *Dr. Herbert and Dr. Christman will discuss the discovery of a common genetic variant associated with adult and childhood obesity.* Go to www.microarraybulletin.com/herbert

May 1, 2006 - **Nancy Cox, Ph.D.**, University of Chicago. *Dr. Cox will discuss an improved allele calling algorithm and computational efficiencies for genome-wide association studies.* Go to www.microarraybulletin.com/cox

April 24, 2006 - **Lon Cardon, Ph.D.**, University of Oxford *Dr. Cardon will discuss the development of novel algorthims for analysis of whole-genome association studies.* Go to www.microarraybulletin.com/cardon

May 8, 2006 - **Mehmet Inan**, King Faisal Specialist Hospital and Research Centre. *Mr. Inan will discuss the insights gained into the genetics of inherited familial disorders in Saudi Arabia.* Go to www.microarraybulletin.com/inan

PARTICIPATE IN CONFERENCE CALL SYMPOSIA

April 20, 2006 9:00am PDT - **Alan Herbert, Ph.D., and Michael Christman, Ph.D.** Boston University School of Medicine. *Discovery of a common genetic variation associated with adult and childhood obesity.*

April 27, 2006 9:00am PDT - **Frank A. Middleton, Ph.D.**, State University of New York, Upstate Medical University. *Integrating whole-genome linkage, association and expression data for candidate gene discovery in complex neuropsychiatric disease.*

May 18, 2006 9:00am PDT - **Irshad Sulaiman, Ph.D.**, Center for Disease Control and Prevention. *Characterization of the genomes of two strains of coronavirus infecting humans using Affymetrix severe acute respiratory syndrome resequencing microarrays.*

May 25, 2006 9:00am PDT - **David Gresham, Ph.D.**, Lewis-Sigler Institute for Integrative Genomics, Princeton University. *Genome-wide detection of polymorphisms at nucleotide resolution with a single DNA microarray.*

Visit www.affymetrix.com/genetics to receive print interviews by email and passcodes for symposia.

AFFYMETRIX®

LETTERS

edited by Etta Kavanagh

Assessing Clinical Trial Results

IN HER POLICY FORUM "CLINICAL TRIALS RESULTS DATABASES: UNANSWERED questions" (13 Jan., p. 180), C. B. Fisher warns of several undesirable effects that might result from open access to raw data from clinical trials. Referring to the editorial policy of a new journal, Fisher suggests that "lack of emphasis on the direction of results or size ... risks diluting scientific standards for peer review."

In fact, neither the size of a trial nor the direction of its results in itself determines the trial's scientific validity. Certainly, it is vital that trials based on small numbers of participants and trials delivering negative results should not be overinterpreted. But, if properly conducted and controlled, small trials and trials with negative results can both make important contributions to medical knowledge.

For example, the sample size of a certain trial may be large enough to allow general conclusions to be drawn but may not have sufficient power to distinguish effects on a particular age group. By taking the raw data of several such small trials together, though, it may be possible to safely extend the conclusions beyond those of the original trials. The inclusion of results from trials with both positive and negative results is vital to such meta-analyses to ensure they are not statistically skewed.

Fisher also wonders whether "the availability of large bodies of data from studies that may or may not have scientific merit will improve or distract from the peer-review process." Recent events in South Korea and elsewhere strongly suggest that making additional raw data available to peer reviewers whenever possible would be desirable. While not eliminating the possibility of fraud, it would at least make it less straightforward and so, arguably, less tempting.

Finally, Fisher worries that, by making available early data from clinical trials, drug companies may fall afoul of regulations relating to "forward-looking statements." However, the data from trials are not forward-looking statements, they are reports of concrete past events. It is difficult to see how making these records available in a transparent fashion could be seen as misleading. Of course, some investors may overinterpret promising early results, just as they may overinterpret a profitable first quarter, but if companies clearly warn against overinterpretation, they should not be held accountable for it.

Any science, including published peer-reviewed research, may be abused by misinterpretation. This should not be used as a justification for hiding important data behind closed doors.

MATTHEW JAMES COCKERILL AND MELISSA NORTON

BioMed Central, 34-42 Cleveland Street, London W1T 4LB, UK.

IN HER POLICY FORUM "CLINICAL TRIALS RESULTS databases: unanswered questions" (13 Jan., p. 180), C. B. Fisher equates negative trial results with poorly conducted trials. There is no evidence that this is the case. Rather, the existence of a bias toward the publication of positive outcomes is not only well known (*1*), but documented examples underscore its effects: Inclusion of unpublished data can sometimes shift assessment of a treatment's value from one of overall benefit toward overall harm (*2*).

The new Public Library of Science journal *PLoS Clinical Trials* will address this problem by publishing reports irrespective of a trial's outcome. Fisher suggests that this approach "risks diluting scientific standards for peer review." This statement is not correct; in fact, the journal will ensure the highest standard of reporting by adhering to CONSORT (*3*), by requiring that all trials be registered, and by obtaining a copy of the original trial protocol, which will enable reviewers to compare the final report against what was planned. All trials will be scrutinized by at least one subject-specific reviewer as well as a statistical expert, together with academic editors and in-house editorial staff. In this way, the journal will uphold and advance scientific standards for publication of trial results.

EMMA VEITCH

Publications Manager, PLoS Clinical Trials, Public Library of Science, 7 Portugal Place, Cambridge CB5 8AF, UK. E-mail: eveitch@plos.org

References and Notes

1. K. Dickersin, *AIDS Educ. Prev.* **9** (1 suppl.), 15 (1997).
2. C. J. Whittington *et al.*, *Lancet* **363**, 1341 (2004).
3. A set of guidelines that take an evidence-based approach to improving the quality of reports of randomized trials.

THE INTERESTING POLICY FORUM BY C. B. FISHER "Clinical trials results databases: unanswered questions" (13 Jan., p. 180) contains some misconceptions that warrant comment.

First, the overarching rationale for full disclosure of trial information has been to fulfill ethical obligations to trial participants, who are subjected to potential risks in exchange for the creation of public knowledge. Although potentially important, other competing concerns raised by Fisher must be subsidiary to this fundamental ethical responsibility.

Second, Fisher confounds trial results with trial methods when discussing the validity of peer-reviewed, open-access publications. An appropriately designed study is scientifically valid regardless of its findings or size alone. Small studies may provide less precise yet valid results; precision can be increased by pooling data across studies through meta-analysis. Thus, the publication of all properly conducted trials regardless of the nature or magnitude of their results will help to address the biases associated with selective reporting of research.

Third, an unjustified assumption underlying much of the paper is that peer-reviewed results are inherently better—an unresolved issue that is neither new nor specific to results databases (*1*). On the basis of empiric evidence, the scientific value

of peer review remains unclear (*2*, *3*). Nevertheless, references to trial results should thus continue to indicate their data source to distinguish peer-reviewed and non–peer-reviewed results.

What is clear, however, is that critical appraisal of trial methodology remains vital for placing a set of results into its appropriate context. Sufficient methodological information must therefore accompany all trial results, whether in a results database or journal.

Full results disclosure will improve the status quo of subjective, selective reporting and data suppression. Being fully transparent with numerical data is the only solution free of subjective judgment. As the global, neutral body with legitimacy and international support, the World Health Organization International Clinical Trial Registry Platform (www.who.int/ictrp) will continue its leadership role in consulting all constituencies to define global norms and standards for trial registers and results databases (*4*).

AN-WEN CHAN,[1,3]*† IDA SIM,[1,4]‡
A. METIN GÜLMEZOGLU,[2]
PATRICK UNTERLERCHNER,[1]
GHASSAN KARAM,[1] TIKKI PANG[1]

[1]Department of Research Policy and Cooperation, and [2]Department of Reproductive Health and Research, World Health Organization, Geneva 1211, Switzerland. [3]Department of Medicine, University of Toronto, Toronto, ON M5G 2C4, Canada. [4]Division of General Internal Medicine, Department of Medicine, University of California, San Francisco, San Francisco, CA 94143, USA.

*To whom correspondence should be addressed. E-mail: chana@who.int

†Member of the Editorial Board of *PloS Clinical Trials*
‡Member of the Advisory Board of *PloS Clinical Trials*

References

1. D. J. Cook *et al.*, *JAMA* **269**, 2749 (1993).
2. F. Godlee, K. Dickersin, in *Peer Review in Health Sciences*, F. Godlee, T. Jefferson, Eds. (BMJ Books, London, ed. 2, 2003), pp. 91–117.
3. T. Jefferson *et al.*, *JAMA* **287**, 2784 (2002).
4. T. Evans, M. Gülmezoglu, T. Pang, *Lancet* **363**, 1413 (2004).

Response

I AM PLEASED THAT MY POLICY FORUM HAS prompted discussion on the value of clinical trials databases and ways to ensure that, whether created by industry, government, or international organizations, they benefit all who have a stake in the development of safe and effective health products.

Cockerill and Norton and Chan and colleagues write that small-sample, well-designed studies may have sufficient statistical power to produce scientifically valid results—and that failure to disprove a null hypothesis may sometimes challenge a well-established body of evidence. However, as both Letters admit, there are risks in such data being overinterpreted, especially by patients and physicians with little training in scientific methodology. My Policy Forum is meant to challenge those who create public databases to work to ensure that the equal availability of poorly and well-designed or implemented studies does not create confusion or reduce public trust in medical science. Similarly, although Chan *et al.* criticize my assumption that peer-reviewed results are inherently better, they nonetheless suggest that it will be important to distinguish peer-reviewed from non–peer-reviewed results in clinical trials databases.

Cockerill and Norton and Chan *et al.* emphasize the value of clinical trials for specific types of stakeholders. I agree that medical science benefits when other scientists can evaluate raw data from published studies and that one advantage of transparency is that trial participants can learn how their efforts contributed to public knowledge. However, the range of individuals who will be affected by the quality of clinical trials databases goes beyond these two segments and includes the general public, patients, practitioners, health management organizations and other third party payors, and federal and private sponsors of research. For example, although investigators and sponsors may recognize that reporting of early data is not meant to be "forward-looking statements," various proposals for databases that include public summaries or implications of early results may inadvertently push sponsors in that direction or create a loophole in current regulations meant to protect the public.

In response to Veitch's Letter, it is good to see more detail on the steps that *PLoS Clinical Trials* will take to increase transparency of research reporting. However, the additional information she provides does not change the value of the question posed in my Policy Forum. What will be the effect on established scientific standards of peer review and public confidence in these standards when investigators and the public are inundated with trial results that fail to confirm or disconfirm hypotheses, yield small effect sizes, or use sample sizes insufficiently powered to generate scientifically valid conclusions?

Timely and transparent reporting of clinical trials results is essential to public health and public confidence. To fulfill this mission, those who are lobbying for or creating clinical trials databases must ensure that such sites are of equal benefit to the multiple stakeholders in the development of health products worldwide.

CELIA B. FISHER

Marie Ward Doty Professor of Psychology, Director, Center for Ethics Education, Fordham University, Bronx, NY 10458, USA.

Ethics Issues in Stem Cell Research

THE INTERNATIONAL STEM CELL FORUM (ISCF) supports research on all stem cell types, including adult stem cells, embryonic stem cells, and stem cells from umbilical cord blood (*1*). The Ethics Working Party (EWP) of the ISCF has 19 participants from 17 (*2*) countries. In 2004, the EWP defined its mission as (i) clarification of ethical issues and, where possible, the international harmonization of ethical standards; (ii) the sharing of stem cell lines; and (iii) an agreement on standards for the characterization and registration of lines. As it pursued this mission, by conducting ongoing study of regulatory approaches to human embryonic stem cell research in 50 countries, the EWP identified certain international trends, effective practices, and emerging issues that require further discussion and clarification.

International trends include the following. A small number of countries prohibit all embryonic stem cell research (*3*). Most other countries either permit in vitro research with embryos with no mention of stem cells, limit the creation of stem cell lines to surplus in vitro fertilization (IVF) embryos under certain conditions (such as governance, accreditation, ethics review, and restrictions on research objectives), or limit research to imported cell lines. Seven countries (*4*) explicitly permit the creation of embryos for research purposes, but it must be shown that the research cannot be achieved with the use of other stem cell lines (such as IVF embryos or adult cell lines). All 50 countries studied prohibit or strongly discourage human reproductive cloning (through laws or guidelines). In most countries that allow human embryonic stem cell derivation from human embryos, there are shared principles as well as professional norms and substantive and procedural conditions that further constrain this work. Currently, common principles and procedures include respect for human dignity (*5*); respect for life (limiting growth to 14 days, at which time the primitive streak forms); autonomy (requirement for informed donor consent); donor and/or patient privacy and confidentiality; noncommercialization (prohibiting the buying and selling of embryos); avoidance and declaration of conflicts of interest; limitation to therapeutic purposes (in contrast to reproductive cloning); ethics review before commencement of study; and the traceability of cell lines with respect to their sources.

In the absence of a more formal international ethics framework specific to stem cell research, some countries have added more stringent and effective practices. Licensing requirements ensure the competence of personnel and the quality and safety of stem lines and verify the informed consent of participants. Equivalence requirements ensure that the importation or exportation of stem cell lines is limited to countries that meet the ethical requirements of the host country and are lawful in the importing country. Sunset clauses (*6*) in guidelines or laws ensure continual review of changing scientific and socioeconomic norms. Additional requirements include monitoring the research using the established lines in stem cell banks.

Recent evidence of scientific fraud and unacceptable egg donor procurement practices in South Korea (*7*) highlights the importance of regulation as an emerging issue in this field. Scientific responsibility and integrity must be promoted with attention to possible economic and political influences that might negatively affect researchers. Incentives for open exchange, registration, and validation of results need to be

identified. The conditions (such as financial gain, informed consent, protections of confidentiality, and privacy of the donor) for egg donation for IVF treatment should be distinguished from the conditions surrounding egg donation for research purposes, and potential egg donors should be informed clearly as to the intended uses of their eggs. The failure to follow good ethical practices in egg donation could result in a loss of trust and reluctance to donate among prospective donors. The scarcity of human ova available for research makes human-animal chimeras more attractive, but the application of chimeras to stem cell research requires conceptual clarification and attention to its ethical dimensions. Finally, transparency on the powers and the composition of the necessary oversight bodies is a sine qua non for all stem cell research irrespective of a country's position.

INTERNATIONAL STEM CELL FORUM ETHICS WORKING PARTY

ISCF EWP, Centre de Recherche en Droit Public, Université de Montréal, Montreal, QC H3C 3J7, Canada. The members of the ISCF EWP are B. M. Knoppers (Chair) (Université de Montreal), G. Richardson (King's College London School of Law), E. H. Lee (National University of Singapore), J. Kure (Masaryk University, Czech Republic), G. de Wert (University of Maastricht, Netherlands), J. C. Ameisen (French Institute of Health and Medical Research), L. Lötjönen (National Advisory Board on Research Ethics, Finland), K. Breen (National Health and Medical Research Council, Australia), R. Isasi (Université de Montreal), A. Mauron (University of Geneva), T. Murray (The Hastings Center, New York), and J. Wahlström (University of Gothenburg, Sweden).

References and Notes

1. International Stem Cell Forum (www.stemcellforum.org.uk).
2. Australia, Canada, China, Czech Republic, Denmark, Finland, France, Germany, Italy, Israel, Japan, Netherlands, Singapore, Switzerland, Sweden, United States, and United Kingdom.
3. Austria, Cyprus, Costa Rica, Italy, Ireland, Lithuania, Norway, and Poland.
4. Belgium, Japan, Singapore, South Korea (not an ISCF member), Sweden, United Kingdom, and several U.S. states (MA, CA, and NJ).
5. T. Caulfield, R. Brownsword, *Nat. Rev. Genet.* **7**, 72 (2006).
6. A sunset clause is a provision in a statute or regulation that terminates or mandates review of all or portions of the law after a specific date.
7. C. Holden, *Science* **310**, 1402 (2005).

TECHNICAL COMMENT ABSTRACTS

Comment on "Phylogenetic MCMC Algorithms Are Misleading on Mixtures of Trees"

Fredrik Ronquist, Bret Larget, John P. Huelsenbeck, Joseph B. Kadane, Donald Simon, Paul van der Mark

Mossel and Vigoda (Reports, 30 September 2005, p. 2207) show that nearest neighbor interchange transitions, commonly used in phylogenetic Markov chain Monte Carlo (MCMC) algorithms, perform poorly on mixtures of dissimilar trees. However, the conditions leading to their results are artificial. Standard MCMC convergence diagnostics would detect the problem in real data, and correction of the model misspecification would solve it.

Full text at www.sciencemag.org/cgi/content/full/312/5772/367a

Response to Comment on "Phylogenetic MCMC Algorithms Are Misleading on Mixtures of Trees"

Elchanan Mossel and Eric Vigoda

We presented a tree mixture in which Markov chain Monte Carlo (MCMC) methods have an exponentially slow convergence rate. We expect that many other mixture scenarios will show slow convergence. Ronquist *et al.* show that Metropolis-coupled MCMC (MC^3) converges quickly on our mixture. However, they presented no theoretical or systematic experimental evidence determining the type of mixtures where MC^3 or other methods are efficient.

Full text at www.sciencemag.org/cgi/content/full/312/5772/367b

EDUCATION

Toward Rational Education Policy

Robert L. DeHaan

In his recent State of the Union message, President Bush called upon the United States to bolster mathematics and science education as a means of nurturing corporate innovation. With his plea, he lent urgency to a complex and multifaceted debate over how best to achieve such improvements. That debate—currently raging among academics in fields as dissimilar as cognitive psychology, social change theory, and education research (*1*–*4*)—is the controversy that Michael Feuer refers to in *Moderating the Debate*.

Moderating the Debate
Rationality and the Promise of American Education

by Michael J. Feuer

Harvard Education Press, Cambridge, MA, 2006. 145 pp. $49.95. ISBN 1-891792-70-9. Paper, $24.95. ISBN 1-891792-69-5.

The author developed this small, highly readable book from the 2004–05 Burton and Inglis Lectures that he delivered at the Harvard Graduate School of Education. Feuer, a leading education research and policy analyst and executive director of the Division of Behavioral and Social Sciences and Education at the U.S. National Research Council, focuses on "a mysterious gap in applied social science." Cognitive psychology, he notes, has been central to modern theories of teaching and learning. Indeed, many of the interesting reforms currently being applied in the teaching of reading, mathematics, history, and science are motivated largely by recent cognitive research findings on how people integrate new information with their prior knowledge, how they solve problems, and how they mix learning and memory with discovery and invention (*5*).

Feuer argues forcefully that education policy—including theories of school organization and reform as well as strategies for relevant and useful education research—should benefit from these advances in cognitive science. "It is something of a mystery…," he notes, "that the cognitive revolution has barely touched education policy and the organization of schooling." Given the success of the cognitive revolution as, on the one hand, a tool for understanding human learning and, on the other, for offering insights into organization theory as applied to such policy domains as antitrust law and labor markets, it seems only reasonable that lessons of cognitive psychology should also be applied to the theory and practice of education policy, "where decades of well-intentioned but unrealistic goals suggest the need for a new model of rationality."

After reviewing the contributions of cognitive science to theories of human performance, learning, and assessment, Feuer describes a select few of the many recent developments in organization theory and policy analysis in domains other than education that derive from the cognitive view of rational decision-making. To explore how theories of organization, modified by new cognitive principles, might shed light on critical issues in the education debate, the author (trained as an economist) takes the reader through a "brief digression" to review neoclassical and cognitive economic models. Building on Herbert Simon's notion of "procedural rationality" (*6*), Feuer's analysis of major education policy and reform efforts of the latter half of the 20th century focuses on organizational complexities and the implicit cognitive demands these complexities impose on educators and policy-makers. He emphasizes the view that rational decision-making is a function both of the mental and technological resources available to the decision-makers and of the objective complexity of the decision problem to be solved. Education policy—including the current hot debates (*4*) over standards of evidence, research methodologies, and how to define "scientific" research in education—would be fertile ground for a cognitively inspired theory of action, by which Feuer means "a framework that connects observation to prediction and lays a foundation for reasonable program and policy goals." Such a theory, he believes, would apply principles of cognitive science and procedural rationality to develop reasonable and realistic school reform strategies.

An important element of Feuer's argument about procedural rationality, which he fears may seem counterintuitive, is that "science is furthered, not hindered, by the acknowledgment of complexity and the admission of bounded human problem-solving capacity." Scientific inquiry into questions as complex as those underlying problems of education policy and research methods must be understood to require an incremental process of knowledge accumulation involving the combination of multiple types of data, rather than a single method that promises definitive answers to well-defined causal questions. Procedural rationality, to the author, means something like pragmatism, or "doing the smartest thing possible under the very real constraints of time, resources, and context."

Feuer's exploration of the intersections among cognitive science, economic theory, and education policy is informative, novel, and full of intriguing hints at how to channel the education reform debate in fruitful new directions. But while the author's evident erudition and analytical powers might lead the reader to expect a grand formulation of a new cognitive framework to undergird education policy, that is not his intent. The "moderate proposal" he offers in the last chapter includes a request that researchers and policy-makers alike "lower their rhetorical and political thermostats." His is a call for procedural rationality, for avoiding inflated goals defined extravagantly either for methodological purity or for dramatic effect. Feuer stresses the need for greater communication and cooperation, and he suggests creating a watchdog group to evaluate reform proposals in terms of criteria such as intended and unintended consequences, likely costs, validity of anticipated effects on different populations, reasonableness of timelines, etc. Above all, researchers and policy-makers must "be wary of defining acceptable evidence too narrowly and setting evidentiary standards too high." It makes more sense to seek incrementally better solutions to problems of the organization, production, and use of knowledge for improving educational policy than to wait for the best solutions. Let not the best be the enemy of the better.

References and Notes

1. National Research Council, *Scientific Research in Education* (National Academy of Sciences, Washington, DC, 2002); www.nap.edu/books/0309082919/html.
2. M. J. Feuer, L. Towne, R. J. Shavelson, *Educ. Res.* **31**, 4 (2002).
3. M. Eisenhart, R. L. DeHaan, *Educ. Res.* **34**, 3 (2005).
4. P. Lather, P. A. Moss, Eds., *Teach. Coll. Rec.* **107**, 1–58 (2005).
5. National Research Council, *How Students Learn* (National Academies Press, Washington, DC, 2005); www.nap.edu/books/0309074339/html.
6. H. A. Simon, in *Methods and Appraisal in Economics*, S. J. Latsis, Ed. (Cambridge Univ. Press, Cambridge, 1976), pp. 129–148.

10.1126/science.1127388

The reviewer is at the Division of Educational Studies, Emory University, North Decatur Building, Room 254, 1784 North Decatur Road, Atlanta, GA 30322, USA. E-mail: rdehaan@emory.edu

MATHEMATICS AND ART

CT Scans vs. X-rays

Marjorie Senechal

"In addition to untying a knot in a cord whose ends were sealed together without touching the cord itself, [the 19th-century American spiritualist Henry] Slade claimed to have joined solid wooden rings together, transported objects out of closed containers, and written on pages tightly pressed between two slates—all supposedly under scientific conditions." In an entertaining early chapter of *Shadows of Reality*, Tony

The reviewer is in the Department of Mathematics and Statistics, Smith College, Northampton, MA 01063, USA. E-mail: senechal@science.smith.edu

1979–8. Robbin used multiple perspectives in this painting (acrylic on canvas, 1978) to place the viewer in several positions at once as a depiction of hyperspace.

Robbin discusses Slade's 1876 trial for fraud in London. Physicists argued that such feats could be explained by access to an extraspatial dimension, and the trial "did little to dampen enthusiasm for the spiritualism of the fourth dimension." Yet 19th-century explorers of the then-arcane fourth dimension bequeathed to us a toolkit for imagining and imaging, inter alia, the hypercube, the cross-polytope, and the pentatope.

The principal tools are slices and shadows (*1*). We can, like A. Square in *Flatland* (*2*), train our mind's eye to "see" four-dimensional objects as stacks of lower dimensional cross sections. Or we can study their projected images (in our three-dimensional space) and imagine lifting them back whence they came. Thanks to these tools and to 20th-century revolutions in thought (the physics of space-time) and technology (modern computer graphics), the fourth dimension is no longer a spirit abode, accessible only to magicians and mediums. Physicists can't do without it. Mathematicians have tamed its geometry. Artists, including Robbin, delight in exploring it. Hyperspace has become respectable, even conventional.

Shadows of Reality
The Fourth Dimension in Relativity, Cubism, and Modern Thought

by Tony Robbin

Yale University Press, New Haven, CT, 2006. 151 pp. $40, £30. ISBN 0-300-11039-1.

Shadows of Reality is a fascinating fly-through of the diverse, intellectually rigorous climes in which Robbin finds tracks and traces of hyperspace. Impressed by the power of x-rays to reveal heretofore unglimpsed reality, he tells us, Picasso studied four-dimensional geometry and used it in his 1910 painting *Seated Woman with a Book* "to show his audience the reality they knew existed but could not otherwise see." Hermann Minkowski's formulation of space-time transformed four-dimensional geometry from an idea into truth. Quasicrystals—which Robbin identifies with Penrose tilings—can be derived by projection from four-dimensional space. The intrepid author even tackles Roger Penrose's twistor theory, quantum entanglement, and category theory. The book is a persuasive case for restoring geometry to its once-hallowed place among the liberal arts.

Unfortunately, that is not the case Robbin is trying to make. *Shadows of Reality* is a polemic on behalf of one visualization method and against the other: shadows over slices. According to Robbin, the slicing model, promulgated in *Flatland*, gets all the credit, while the projection model does all the work. "Consider this book a modest proposal to rid our thinking of the slicing model of four-dimensional figures and spacetime in favor of the projection model," he writes, adding that "the proposal means developing a distaste for the slicing model.…" It's hard to tell whether he really believes this—if his doctor orders a CT scan, would he demand an x-ray instead?—or whether he's trying to spice up a book he fears might otherwise be bland. If he does believe it, I fail to understand why. The projection model has received more than equal time for the past 60 years, thanks to the unstinting efforts and ever-widening influence of the great, late geometer H. S. M. Coxeter and his classic *Regular Polytopes* (*3*). In any case, why privilege either of these two invaluable and complementary methods over the other? Most of us poor three-dimensional creatures need all the help we can get.

Robbin's zeal sometimes leads him astray. For example, in the chapter "Patterns, Crystals, and Projections" he briefly considers three methods for generating Penrose tilings: matching the tiles together in accordance with specified rules; cutting the tiles into smaller tiles and then inflating them, ad infinitum, to construct a tiling that repeats on all scales; and projection from a periodic tiling of a higher dimension (four or five) onto a plane. Each of these methods tells us things about Penrose tilings (and many other nonperiodic tilings) that the others do not. All three are powerful and fruitful tools in the study of aperiodic order. Yet Robbin dismisses the first on specious grounds and the second as "of limited use." "It is now understood," he asserts, that N. G. de Bruijn's projection method "is the most general, informative, and foolproof of the three." (By the way, the projection method is a two-step operation: first slice, then project that—so it is also known as "cut and project.")

Robbin is, of course, entitled to his opinions. And let's not quibble over details. Any author of such a bold interdisciplinary adventure is likely to get some details wrong, and he is no exception. (Still, one wishes some of the more egregious had been caught at the proof stage.) The panorama he sketches in *Shadows of Reality* is rich and fascinating. Enjoy the forest, just don't look too closely at the trees.

References and Notes

1. In some special cases, we can also imagine a four-dimensional object as a three-dimensional construction folded up. Thus the hypercube is often "drawn" as an array of six cubes, like the cross in Salvador Dali's *Crucifixion*.
2. [E. A. Abbott], *Flatland: A Romance of Many Dimensions* (London, 1884); see www.alcyone.com/max/lit/flatland.
3. H. S. M. Coxeter, *Regular Polytopes* (Methuen, London, 1948).

10.1126/science.1126513

CREDIT: TONY ROBBIN

GENETICS

No Longer De-Identified

Sequencing human DNA to discover genetic variation should be governed by existing regulations for human subjects.

Amy L. McGuire[1]* and Richard A. Gibbs[2]

As DNA sequencing becomes more affordable and less time-consuming, scientists are adding DNA banking and analysis to research protocols, resulting in new disease-specific DNA databases. A major ethical and policy question will be whether and how much information about a particular individual's DNA sequence ought to be publicly accessible.

Without privacy protection, public trust will be compromised, and the scientific and medical potential of the technology will not be realized. However, scientific utility grows with increased access to sequenced DNA. At present, ethical concerns about the privacy of subjects whose sequenced DNA is publicly released have largely been addressed by ensuring that the data are "de-identified" and that confidentiality is maintained (*1*–*2*). There is a large literature on the various data-management models and computer algorithms that can be used to provide access to genetic data while purportedly protecting privacy (*3*–*6*). We believe that minimizing risks to subjects through new developments in data and database structures is crucial and should continue to be explored, but that additional safeguards are required.

Scientists have been aware for years of the possibility that coded or "anonymized" sequenced DNA may be more readily linked to an individual as genetic databases proliferate (*1*, *3*, *7*, *8*). In 2004, Lin and colleagues demonstrated that an individual can be uniquely identified with access to just 75 single-nucleotide polymorphisms (SNPs) from that person (*9*). Genome-wide association studies routinely use more than 100,000 SNPs to genotype individuals. Although individual identification from the public release of these data would currently require a reference sample, the privacy risk associated with public data release is fueled by the extraordinary pace of technological developments and the rapid proliferation of electronic databases. If protective measures are not adopted now, public trust will be compromised, and genomic research will suffer.

Genetic sequencing typically involves three phases of investigation: (i) subject recruitment and sample collection (primary clinical investigation), (ii) DNA sequencing and data broadcast (genomic sequencing study), and (iii) data retrieval and analysis (secondary-use research) (see figure, above). Institutional Review Board (IRB) oversight and informed consent are unambiguously required for the first phase of sample collection, because it clearly involves human subjects research. There are also detailed consent requirements for some large-scale sequencing studies, such as the HapMap project, that cover the second and third phases. However, it is our experience that, in general, the consent process for most disease-specific genetic research is not protective for these phases and that the privacy risks associated with public data-sharing are not stated. Consent for these studies is highly variable, and in most cases, subjects are simply told that genetic analysis will be performed, without any explanation of what that means or with whom the resulting data will be shared. Further, participants are typically not offered the opportunity to participate in the research if they do not want their data publicly broadcast (*10*).

PHASE 1

Dr. A, from Excel University, is interested in studying whether there are genetic variances associated with Parkinson's disease. Dr. A obtains IRB approval for her study and recruits subjects from her clinic. She explains to potential subjects that she is conducting a genetic study of Parkinson's disease. Subjects are presented with a consent form, which explains that they will be asked to give a blood sample and to fill out a health survey. They are told the risks associated with the blood draw, warned that they may not benefit directly from participation in the study, and assured that confidentiality will be maintained within legal limits.

PHASE 2

Once the subject has consented and her sample collected, the sample is coded and given to Dr. B, a scientist who runs the sequencing center at Excel University. Dr. B does not know who the sample has come from and does not have access to any other patient information. Dr. B sequences the subject's DNA and publishes the sequenced data on a publicly accessible Web site. No additional IRB approval or informed consent is currently federally mandated for this research activity, because Dr. B provides no intervention for and has no interaction with human research subjects.

PHASE 3

Dr. C, at Datamine University, is interested in studying whether patients who have a particular genetic marker for Parkinson's disease also have genetic markers for Alzheimer's-type dementia. Dr. C accesses the public Web site and searches and analyzes the published DNA sequences, looking for associations.

From subject to data analysis. A typical medical genomic sequencing study.

In the United States, there are now two federal regulations that could potentially apply to such studies—the Common Rule, which regulates all federally funded research and sets forth the federal policy for the protection of human research subjects (*11*) and the Health Insurance Portability and Accountability Act (HIPAA) Privacy Rule, which restricts certain unauthorized uses and disclosures of patients' identifiable protected health information by covered entities (*12*). Neither one specifically mandates IRB oversight or subject consent for the public release of sequenced data. The Common Rule would not apply if genomic sequencing studies were not considered to constitute human subjects research. Human subjects research is defined under the Common Rule as research involving "an individual about whom the investigator … obtains data through intervention or interaction with the individual, or identifiable private information" (*11*). According to a guidance document published in 2004 by the Office for Human Research Protections (OHRP), because the data are collected and coded by the primary clinical investigator, and the sequencing investigator is prohibited from deciphering the code, the data are not considered identifi-

[1]Center for Medical Ethics and Health Policy, Baylor College of Medicine, [2]Human Genome Sequencing Center, Baylor College of Medicine, One Baylor Plaza, Suite 310D, Houston, TX 77030, USA. *Author for correspondence. E-mail: amcguire@bcm.edu

able, and the sequencing study is not subject to federal regulation (*13*). Brief IRB review may be necessary to confirm that the research does not involve human subjects, but once that determination is made, no IRB oversight or informed consent is mandated.

Similarly, HIPAA does not provide unambiguous protection because it has not been clear that genomic data constitute readily identifiable protected health information (*14*–*16*), and even if they do, institutions vary in whether the scientists who conduct sequencing studies are considered "covered entities" who must comply with HIPAA. Institutions may choose to impose more stringent requirements on investigators, but there is no federal mandate to do so now.

To resolve the tension between privacy protection and access to DNA data needed for progress in medical research, Lin and colleagues recommend a tiered data-access approach, with sensitive data layers masked from full public view (*9*). This approach has the advantage of minimizing privacy risks without unduly sacrificing progress, but suffers from a lack of flexibility to respond to individual preferences and judgments. It also threatens to slow the pace of research, because current policy calls for sequenced data to be released publicly within 24 hours of their generation (*17*), whereas obtaining approval to access restricted databases could take weeks, if not months. We believe that restricted access should be offered as an option to subjects, but that it not be adopted as a general approach for all genomic sequencing studies.

Kohane and Altman propose that researchers specifically seek out volunteers who are most willing to have their health data publicly shared and that these subjects have explicit control over who has access to their data (*18*). Relying only on such "information altruists" to participate in genetic studies would potentially create subject bias, influencing the ability of investigators to identify disease alleles relevant to the population at large.

We propose that general safeguards be put in place to encourage understanding of and trust in genomic sequencing studies. As an essential first step, genomic sequencing studies should be recognized as human subjects research and brought unambiguously under the protection of existing federal regulation. This would have the effect of mandating informed consent for public release of potentially identifiable sequenced data and requiring IRB oversight to ensure that risks to subjects are minimized and that informed consent, or a waiver of the requirement to obtain informed consent, is obtained (*11*).

Specifically, we recommend a stratified consent process in which all subjects who participate in future genomic sequencing studies are fully informed about how their DNA data may be broadcast and have the authority to decide with whom they want their data shared (*19*). A number of options could be presented; we propose three levels of confidentiality (see table above). A more rigorous assessment of the risks and benefits associated with each of these options will be necessary.

SUGGESTED DATA RELEASE OPTIONS

	Data released	Identifiers	Privacy risk	Benefit
Option 1	Multiple gene loci	>75 SNPs	Higher	Ability to study interactions among different genes
Option 2	Single gene loci	Typically <20 SNPs	Intermediate	Ability to study individual genes
Option 3	No data released	None	Low	Ability to include subjects with low risk tolerance, which increases generalizability and applicability to specific subsets of the population

Some of the practical challenges include providing adequate disclosure and education about a complex risk calculus, ensuring subject comprehension, coordinating a system of restricted access, and managing a complex database that accounts for subjects' informed disclosure preferences. Although it may represent a substantial departure from the traditional model of informed consent in research, stratified consent procedures are commonly used in clinical medicine, where patients frequently make informed choices about treatment options on the basis of individual values and judgments. Stratified consent procedures are also being considered in other areas of research where subjects have to make complicated decisions, such as what type of future research they are willing to participate in and to what extent they want research-related incidental findings reported back to them.

There may be concern about the added burdens on IRBs. McWilliams and colleagues have shown that there is currently considerable variability among local IRBs, particularly in how they deal with DNA banking, risk-benefit analysis, and consent for genetic research (*20*). They recommend centralized IRB oversight for multicenter research.

Although some might fear a negative impact on subject participation in genomic research, stratified consent merely restricts the ability to release sequenced data publicly. If anything, it may boost enrollment by providing an opportunity for even the most risk-averse members of society to participate in research, while ensuring optimal privacy protection.

Empirical study of these and other challenges associated with the implementation of a stratified consent model in research is essential for future policy development. In addition, federal legislation prohibiting genetic discrimination would significantly alter the risk-benefit calculus associated with public data release and should be enacted without delay (*21*). Although it would not obviate the ethical obligation to obtain subject consent, it may foster public trust and positively affect the willingness of subjects to participate in genomic research and to share their genetic data publicly.

References and Notes

1. National Human Genome Research Institute (NHGRI), U.S. National Institutes of Health (NIH), *NHGRI-DOE* [U. S. Department of Energy] *Guidance on Human Subjects Issues in Large-Scale DNA Sequencing* (17 August 1996, updated 27 April 1998) (www.genome.gov/10000921).
2. The International HapMap Consortium, *Nat. Genet.* **5**, 467 (2004).
3. L. Sweeney, *J. Law Med. Ethics* **25**, 98 (1997).
4. B. A. Malin, *J. Am. Med. Inform. Assoc.* **12**, 28 (2005).
5. J. E. Wylie, G. P. Mineau, *Trends Biotechnol.* **21**, 113 (2003).
6. L. Sweeney, Ed., "Navigating computer science research through waves of privacy concerns: Discussions among computer scientists at Carnegie Mellon University" *ACM Comput. Soc.* **34** (April 2004); (http://privacy.cs.cmu.edu/dataprivacy/projects/csresearch1.pdf).
7. B. Malin, L. Sweeney, *J. Biomed. Inform.* **37**, 179 (2004).
8. National Cancer Institute (NCI), NIH, "Confidentiality, data security, and cancer research: Perspectives from the National Cancer Institute" (NCI, Bethesda, MD, 23 March 1999); (www3.cancer.gov/confidentiality.html).
9. Z. Lin, A. B. Owen, R. B. Altman, *Science* **305**, 183 (2004).
10. The International HapMap Consortium, "Template consent form" (www.hapmap.org/consent.html.en).
11. "Protection of human subjects," 45 Code of Federal Regulations (C.F.R.) § 46 (2005).
12. "Security and privacy," 45 C.F.R § 164 (2002).
13. Office for Human Research Protections, U.S. Department of Health and Human Services (HHS), "Guidance on research involving coded private information or biological specimens" (HHS, Washington, DC, 10 August 2004); (www.hhs.gov/ohrp/humansubjects/guidance/cdebiol.pdf).
14. HHS, "Research repositories, databases, and the HIPAA Privacy Rule" (HHS, Washington, DC, January 2004); (http://privacyruleandresearch.nih.gov/pdf/research_repositories_final.pdf).
15. P. A. Roche, *Science* **307**, 1200 (2005).
16. M. A. Rothstein, *J. Law Med. Ethics* **33**, 89 (2005).
17. NHGRI, "Reaffirmation and extension of NHGRI rapid data release policies: Large-scale sequencing and other community resource projects" (NIH, Bethesda, MD, February 2003); (www.genome.gov/10506537).
18. I. S. Kohane, R. B. Altman, *N. Engl. J. Med.* **353**, 2074 (2005).
19. Human Genome Organization (HUGO) Ethics Committee, "Statement on human genomic databases" (HUGO, London, December 2002); (www.gene.ucl.ac.uk/hugo/HEC_Dec02.html).
20. R. McWilliams *et al.*, *JAMA* **290**, 360 (2003).
21. Genetic Information Nondiscrimination Act of 2005, S. 306 (109th Congress).

22. We thank S. E. McGuire, B. A. Brody, L. B. McCullough, M. A. Majumder, and R. R. Sharp. R.A.G. is supported by grants from the NHGRI.

10.1126/science.1125339

ECOLOGY

Mutualistic Webs of Species

Quantitative analysis of a network of plant-animal interactions reveal new organizing principles, including how asymmetric relations stabilize the coevolution of the whole network.

John N. Thompson

As life has diversified over billions of years, so have the ways of extracting a living by exploiting other species. Indeed, no multicellular eukaryotic organism is capable of surviving and reproducing using only its nuclear genes and the gene products it makes. Species coopt the genomes of other species by forming mutualistic, but inherently selfish, alliances. You can grasp the central importance of mutualistic associations in the diversification of life through a simple thought experiment. Try to imagine a plant that can survive and reproduce in a real ecosystem without using, in addition to its nuclear genome, most of the following: a mitochondrial genome (to convert energy); a chloroplast genome (to regulate photosynthesis); one or more mycorrhizal fungal genomes (to improve nutrient and water uptake); the genomes of pollinators (to assist in reproduction); and the genomes of a few birds, mammals, or ants (to move seeds around the ecosystem). Each plant is part of a complex web of interacting mutualists.

One of the major challenges for evolutionary biology is to understand how species coevolve and shape complex webs of mutualistic interaction (see the first figure). On page 431 in this issue, Bascompte *et al*. (*1*) address an important component of this problem by asking if mutualistic interactions involving dozens or even hundreds of plant and animal species coevolve in a way that leads to a predictable pattern of links among species. They focus on some of the most visible, diverse, and quantifiable mutualistic interactions found within terrestrial communities—those between plants and their free-living pollinators and seed-dispersal agents. Some ecosystems, such as tropical rain forests, rely so heavily on these interactions that they would collapse in their absence, because plant reproduction would cease. Within these webs, it is rare for a local plant species and animal species to be so reciprocally specialized that neither interacts with other species (*2*). Instead, species differ greatly within webs in the number of links to other species. For example, some bee species are extreme specialists that visit the flowers of only one or two plant species, but other bee species are generalists that visit the flowers of dozens of plant species. In a previous analysis (*3*), these authors used network theory (*4*) to show that specialization within these mutualistic webs tends to be nested. In a nested web, a core group of generalists all interact with each other, but extreme specialists interact only with the generalist species. The result is a web with many asymmetries in degrees of specialization among the interacting species. In contrast, interactions between predators and prey or herbivores and plants are often more compartmentalized, forming smaller clusters within the broader interaction web (*5*, *6*).

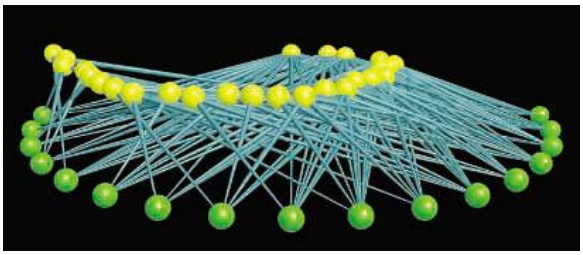

Species interaction web. Asymmetries revealed in the pattern of links among animal (yellow) and plant (green) species.

The new study adds additional ecological realism to these analyses. Most studies of nested and compartmentalized webs have been based on qualitative data, in which all connections between species are given equal weight. Recent studies of food webs with antagonistic interactions between species have begun to explore webs in which the connections among species are weighted by the relative frequency with which a species interacts with other species (*7*). In extending quantitative network analyses to mutualistic webs, Bascompte *et al*. show that the distribution of specialists and generalists within these webs is unlikely to be due to chance. Moreover, they show that asymmetries in specialization among pairs of interacting species are the rule: Strong dependence on a particular interaction in one direction is frequently accompanied by weak dependence in the other direction. Hence, a plant might rely heavily on the seed-dispersal services of a particular frugivore species, but that same frugivore species might consume fruits from multiple plant species (see the second figure).

Using a simple model, they also show that this asymmetry in specialization could promote the coexistence of species within these interactions over evolutionary time. Complex mutualistic webs are therefore not haphazard collections of specialists and generalists. Evolution and coevolution appear to shape these multispecific interactions in a predictable manner regardless of the exact composition of species or the ecosystem, pointing the way to a more tractable theory of coevolution within complex mutualistic webs.

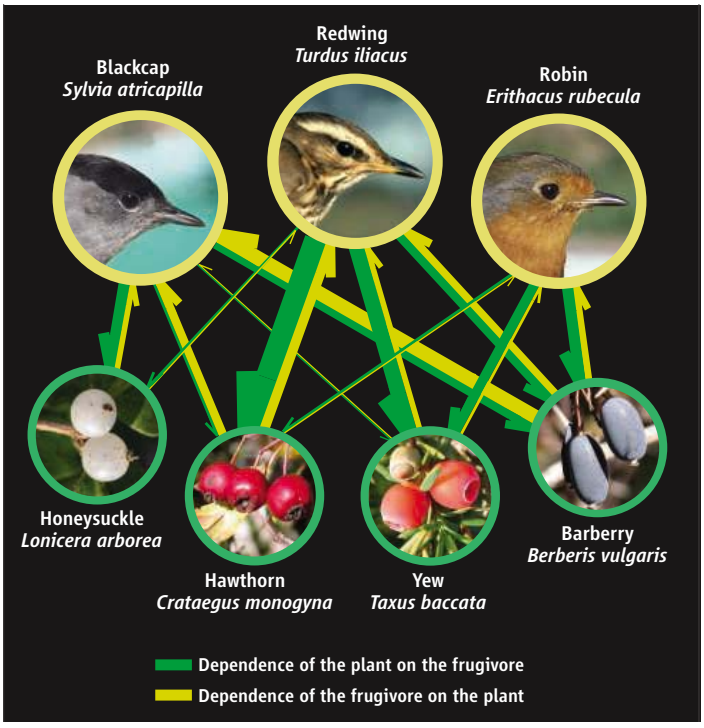

Asymmetric relationships. Part of an interaction web from a montane forest in southeast Spain (*1*). Each interaction between frugivore and fruit illustrates two dependence values (green and yellow arrows). The relative frequency of the interaction is shown by the thickness of the arrows.

Precisely how coevolutionary selection contributes to creating nested mutualistic networks built upon weak and asymmetric links among species is not yet clear. The observed differences in the structure of mutualistic and antagonistic webs, however, are consistent with what is currently known about coevolutionary selection among pairs and small groups of interacting species (*8*). Antagonistic coevolution between predators

The author is in the Department of Ecology and Evolutionary Biology, University of California, Santa Cruz, Santa Cruz, CA 95060, USA. E-mail: thompson@biology.ucsc.edu

CREDITS (TOP TO BOTTOM): J. M. OLESEN/UNIVERSITY OF AARHUS, DENMARK, PRODUCED ACCORDING TO (*10*); P. JORDANO/ESTACIÓN BIOLÓGICA DE DONANA IN SEVILLA, SPAIN

and prey can favor escalating "arms races" among groups of interacting species, producing multispecific clusters that share some reciprocal specialization in defenses and counterdefenses. Amid these arms races, selection continually acts on prey to escape the interaction, preventing predators from incorporating an ever-increasing number of prey species into their diets. In contrast, mutualistic interactions between free-living species often favor incorporation of new species into an interaction, through convergence and complementarity of traits among interacting species. The result is a coevolutionary vortex that grows in the number of interacting species over evolutionary time. Bascompte *et al*. notably extend this general expectation from coevolutionary theory to suggest that species join networks in ways that ultimately create a persistent asymmetric pattern of specialization among interacting species.

The next step in such studies will be to identify the sequence of ecological, evolutionary, and coevolutionary processes that create this pattern as mutualistic webs accumulate species over space and time. Some mutualistic life histories, for example, are not even possible until mutualistic webs include many species. Honeybees, which rely upon a seasonal progression of flowering among species to maintain their hives, could not have evolved until local communities included multiple plant species that flowered at different times. Identifying the evolutionary and coevolutionary processes that shape asymmetries during the assembly of complex mutualistic webs will require studies of how particular pairs and groups of species differ in their patterns of asymmetry in different biological communities.

Studies of complex mutualistic webs are part of an overall scaling up of the fields of coevolutionary biology (*8*) and community ecology (*9*) to encompass the processes shaping the diversity of life across large geographic and temporal scales. These studies are also part of a growing realization that much of the diversification of life is about the diversification of interactions through ongoing coevolution.

References

1. J. Bascompte, P. Jordano, J. M. Olesen, *Science* **312**, 431 (2006).
2. N. M. Waser, J. Ollerton, Eds., *Plant–Pollinator Interactions: From Specialization to Generalization* (Univ. of Chicago Press, Chicago, 2006).
3. J. Bascompte, P. Jordano, C. J. Melián, J. M. Olesen, *Proc. Natl. Acad. Sci. U.S.A.* **100**, 9383 (2003).
4. S. R. Proulx, D. E. L. Promislow, P. C. Phillips, *Trends Ecol. Evol.* **20**, 345 (2005).
5. T. M. Lewinsohn, V. Novotny, Y. Basset, *Annu. Rev. Ecol. Syst.* **36**, 597 (2005).
6. A. E. Krause, K. A. Frank, D. M. Mason, R. E. Ulanowicz, W. W. Taylor, *Nature* **426**, 282 (2003).
7. F. J. F. van Veen, R. J. Morris, H. C. J. Godfray, *Annu. Rev. Entomol.* **51**, 187 (2006).
8. J. N. Thompson, *The Geographic Mosaic of Coevolution* (Univ. of Chicago Press, Chicago, 2005).
9. M. Holyoak, M. A. Leibold, R. D. Holt, Eds., *Metacommunities: Spatial Dynamics and Ecological Communities* (Univ. of Chicago Press, Chicago, 2005).
10. R. J. Williams, Pacific Ecoinformatics and Computational Ecology Lab (www.foodwebs.org).

10.1126/science.1126904

CHEMISTRY

The First Femtosecond in the Life of a Chemical Reaction

Bombardment of reactants with high-order harmonics of a laser reveals the earliest stages of chemical reactions, which occur faster than a single cycle of visible light.

Philip H. Bucksbaum

When light initiates chemical change—such as photosynthesis in plants, or vision in an eye, or the formation of vitamin D in your skin—the first stages happen with breathtaking rapidity. Electrons in molecules can absorb a photon and rearrange in only femtoseconds (a femtosecond is 10^{-15} s). A bedrock of chemical theory known as the Franck-Condon principle assumes that such short times are so infinitesimal that for all practical chemical purposes they are instantaneous: All the atoms in a molecule remain frozen during the critical instant of electron transition. Yet quantum mechanics requires that the atoms in molecules are never truly at rest, and the removal or repositioning of electron charge initiates motion that eventually leads to chemical transformation. These earliest atomic movements have never been observed directly, because they are far too fast and too slight to detect. But this is just what the report by Baker and co-workers shows on page 424 of this issue (*1*). This research comes from the rapidly growing field of attoscience. An attosecond (10^{-18} s) is even shorter than the events that initiate photochemistry, but the name has been taken over to include physical observations on time scales shorter than a single cycle of visible light, or shorter than about two femtoseconds. The specific technique used here is high-harmonic generation (HHG) in molecules illuminated by intense femtosecond pulses of focused laser light.

The report by Baker *et al*. describes and then demonstrates a new method to convert the spectrum of high harmonics into an image of the motion of molecules (such as hydrogen or methane) in the first stages of chemistry. The HHG process, in which visible or infrared laser light is converted to vacuum ultraviolet radia-

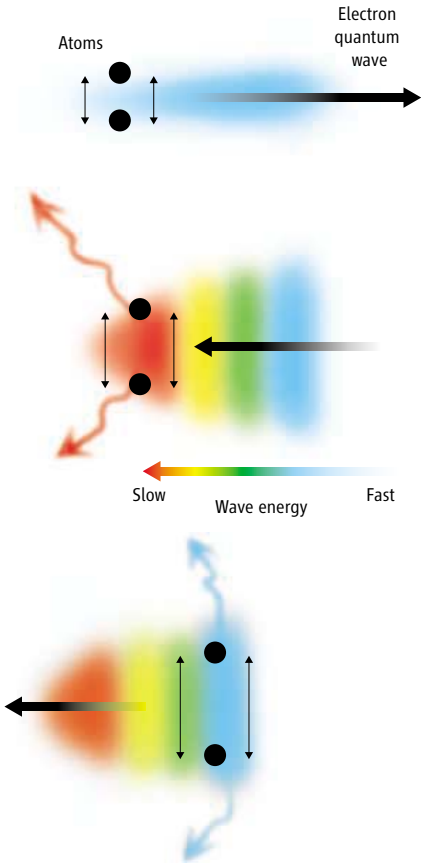

Tracking molecular motion. (**Top**) A laser field (black arrow) pulls an electron quantum wave (blue) away from the molecule, causing the two atoms (black dots) to separate. (**Center**) When the laser field reverses, the quantum wave smashes back into the molecule. Color represents the wave energy, with blue for fast high-energy waves and red for slow low-energy waves. (**Bottom**) The electron wave is absorbed, creating photons with energy corresponding to the wave energy. In this way, each color of light shows the molecule at a different time as the atoms move apart. Total time elapsed is about ½ of an optical cycle, or one femtosecond.

ILLUSTRATION: C. BICKEL/*SCIENCE*

The author is in the Photon Sciences Division, Stanford Linear Accelerator Center, Menlo Park, CA 94025, USA. E-mail: phb@slac.stanford.edu

tion, has been known for nearly two decades (*2*). The light takes the form of odd harmonics —that is, odd multiples of the driving laser frequency. Harmonic frequencies greater than 100 times the laser frequency have been observed in a single spectrum. This extreme phenomenon was not predicted before its initial observation, and it seems to lie outside the reach of conventional nonlinear optics, the theory that predicts parametric processes such as second- or third-harmonic generation in light interacting with atoms and molecules. Yet HHG has an elegant and simple physical explanation, based in part on classical physics (*3*). HHG occurs when an intense laser field pulls an electron away from the molecule in a fraction of one optical cycle, and then sends the electron crashing back into the molecule when the field reverses on the next half-cycle (see the figure). The energy dissipated in the crash of each electron is converted into a single photon of radiation. The HHG spectrum is the forward-directed portion of this light collected from all of the molecules illuminated by the laser.

The research reported by Baker *et al*. takes these ideas one step further. The authors note that according to this classical model, the energy of the photon must be tied to the kinetic energy of the electron that made it, which depends in turn on the precise time that the electron was pulled away from the molecule and the time that it returned. For example, electrons that leave the molecule at the very peak of the oscillating laser electric field take the longest time to return, and the field has slowed them nearly to a stop when they do. Electrons that leave the atoms a bit later will not go as far before turning back, and they return with some excess energy that can be put into a high-harmonic photon. The later an electron leaves in a field cycle, the shorter the duration of its journey, and the higher its energy upon return.

An electron that leaves the molecule about 1/20th of a cycle after the peak (18 degrees of phase) has the highest energy possible when it returns—about three times the average wiggle energy of an electron in the laser field. Electrons that leave still later in the cycle have even shorter total trajectories but return with less than the maximum energy. These "short-trajectory" harmonics were the ones used by the authors to view the just-ionized molecule. The lowest energy part of the spectrum shows the condition of the molecule at the earliest times after the ionization event, and the highest energy part shows longer times. But the total time interval covered by the entire spectral record is extremely short—about a femtosecond.

How should one interpret this spectrum to get any meaningful information, let alone a snapshot image of the molecule? Here the research team deftly switches back to quantum theory for a clue. The returning electron doesn't have to convert its energy to a photon when it crashes back into its home port. It could just as easily scatter from the molecule and careen into another direction from which it never returns. The odds of producing an HHG photon depend on whether the shape of the quantum wave function of the target molecular ion matches the space the neutral molecule needs to occupy when the electron comes back to rest. If the shapes don't match, the electron is likely to just bounce off. This quantum correlation between the ion and the neutral molecule is therefore reflected in the amplitude of the HHG spectrum. More HHG signal at a particular photon energy means a better match at that time. This is not much information, to be sure, but it is just enough to provide important clues used to reconstruct the motion of the molecule in the first femtosecond after ionization. Baker *et al*. report measurements of this motion in hydrogen molecules and in methane ionized by a laser pulse consisting of only a few optical cycles.

Competing effects influence HHG, such as the spatial arrangement of the atoms in the molecule, or the tendency of the molecule to distort under the influence of the laser field even before the moment of electron release. These phenomena also alter the HHG spectrum and could confuse the analysis (*4*). The most important limitation of the new technique is the very short time interval involved. Only the lightest atoms in a molecule move far enough to detect motion over one femtosecond. But hydrogen, the lightest atom, is the critical actor in much photochemistry, and its motion is considerable even over these short times. Furthermore, the continued improvement of ultrafast lasers is leading to infrared sources with longer wavelength and longer cycle periods, and this technique could be extended to longer times in this way.

References

1. S. Baker *et al*., *Science* **312**, 424 (2006); published online 2 March 2006 (10.1126/science.1123904).
2. M. Ferray *et al*., *J. Phys. B* **21**, L31 (1988).
3. P. B. Corkum, *Phys. Rev. Lett.* **71**, 1994 (1993).
4. J. Itatani *et al*., *Nature* **432**, 867 (2004).

10.1126/science.1125514

APPLIED PHYSICS

Laser-Driven Particle Accelerators

Mike Dunne

A new generation of particle accelerators that use laser acceleration can sit on the benchtop. These instruments are being actively developed for widespread applications.

For many years, the high-power–laser community has been pursuing the goal of producing miniaturized particle accelerators. Limitations of conventional technology mean that kilometer-sized accelerators are required for high-energy physics research (see the bottom figure). Similarly, major installations are required for medical applications such as particle beam treatment of tumors, which excludes all but the largest research hospitals. By contrast, laser-plasma–based techniques can support accelerating electric fields at least four orders of magnitude larger than those of conventional techniques, leading to the hope that particle accelerators could one day become a commonplace tool.

Although the goal is attractive, these plasma schemes have, until recently, suffered from many shortcomings, such as poorly controlled particle energy, high divergence, and low luminosity. A host of results in the past year has provided renewed impetus, with demonstrations of quasi monochromatic, high-brightness beams in the multi-MeV energy range. Now, Toncian *et al*. (*1*) at the University of Düsseldorf have demonstrated an imaginative technique for tunable energy selection and focusing of proton beams in the multi-MeV energy range. As reported on page 410 of this issue, they show that the use of a simple capillary lens can lead to dramatic results.

Lens arrangements for proton beams are not new; but until now, there has not been a way to focus picosecond–time-scale beams with currents that are orders of magnitude higher than those of conventional beams and that require focusing over micrometer spatial scales. In the system developed by Toncian *et al.*, a proton beam is created by irradiating a metal foil with laser pulses, and the protons are focused by the electric fields created inside a small cylinder that is irradiated on the side by a second laser (see the top figure). This new idea provides a simple tool to exploit the dramatic advances in laser-driven hadron acceleration seen over recent years.

It is easy to imagine the breadth of science disciplines that would benefit from a new generation of miniature accelerators. Potential applications include the imaging and treatment of cancerous cells, offering scale reductions and far simpler beam orientation compared with conventional cyclotrons. Nearer term applica-

The author is at the Central Laser Facility, Rutherford Appleton Laboratory, Chilton, Oxfordshire OX11 0QX, UK. E-mail: m.dunne@rl.ac.uk

tions involve the use of these ultrashort proton beams to heat matter isochorically (that is, at constant density) to produce extreme thermodynamic states of interest for fundamental atomic physics studies, laboratory astrophysics, and the fast-ignition approach to fusion energy production (*2*). Similarly, such beams have recently been used as a unique probe of electromagnetic field structures in relativistic plasma physics studies (*3*). The technique demonstrated by Toncian *et al*. provides researchers with the means to control these emerging sources to an unprecedented degree.

Laser acceleration of protons occurs as a result of the extremely high electric field gradients created on either the front or rear surface of thin foils illuminated by subpicosecond laser pulses, whose focused intensities exceed 10^{18} W cm^{-2}. The laser ionizes and subsequently accelerates electrons to relativistic velocities. These are confined to form a beam by the azimuthal magnetic field created in the interaction. The ensuing charge separation sets up the electric field to accelerate the proton or ion species in the foil, with an overall energy efficiency between 1 and 10%. Although such laser intensities are incredibly high, they are now routinely produced at high repetition rate on table-top–sized systems. This reflects the dramatic progress seen in laser technology, where an order-of-magnitude increase in peak laser power has been achieved roughly every 3 years.

Over the past few months, we have seen very encouraging experimental results on the production of quasi mono-energetic proton beams in the MeV range (*4*), narrow-band ion acceleration (*5*), and a study of the scaling of proton energy with laser parameters (*6*). This builds on similarly dramatic results with laser-driven electron beams that were reported 18 months ago (*7*–*9*). The results reported by Toncian *et al*. now provide a method for simple control of laser-produced particle beams without having to rely on access to specific plasma physics regimes that are still only partially understood. This should allow greater deployment of controlled particle-beam sources over the near term, at least within the laser research community. This will likely lead to a wealth of new studies using the beams as unique probes and localized heating sources.

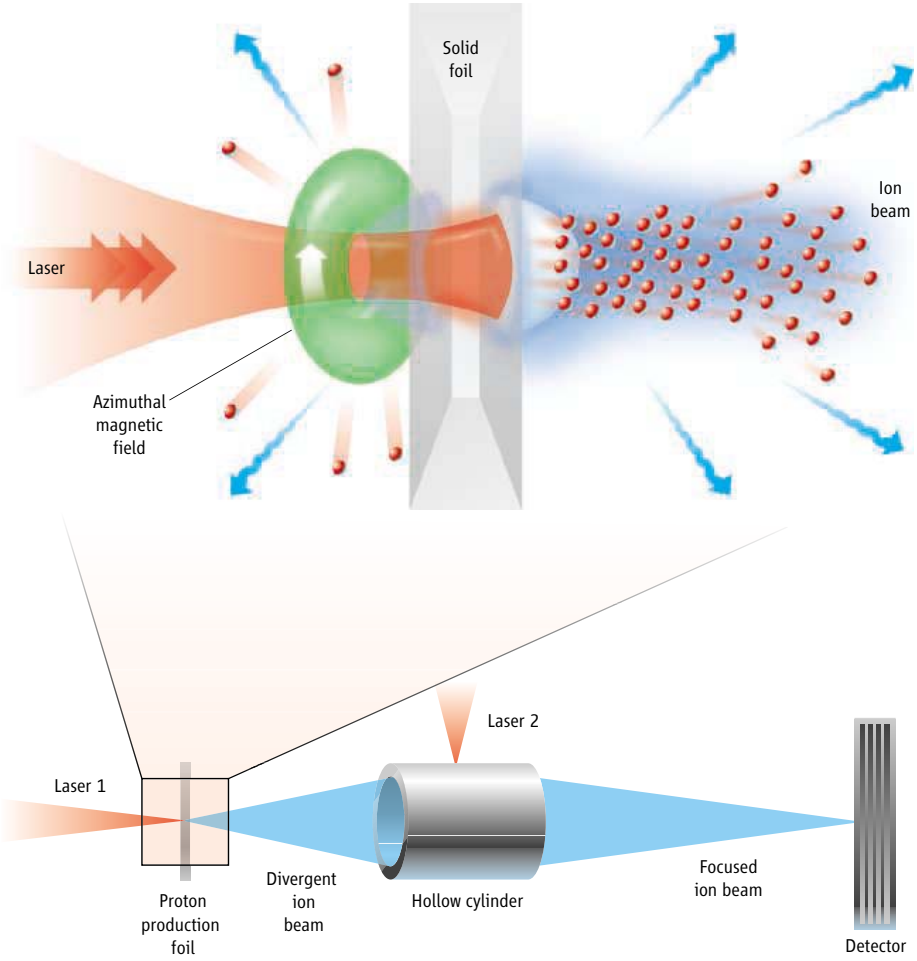

Compact accelerator. (**Top**) Schematic of the laser-plasma interaction process that produces a beam of energetic electrons, protons, and ions. (**Bottom**) Diagram of the cylindrical lens focusing system used by Toncian *et al*. to focus a proton beam.

Such rapid progress demonstrates that laser-driven systems may indeed be able to move from a scientific curiosity to real-world applications in due course. Caution is needed, however, in extrapolating current results to potential applications. Plasma physics has a long history of throwing unwanted surprises at its practitioners, and most of the applications require a level of stability and reproducibility that is a long way from having been demonstrated. Much research across a broad front is still required, but it is now time to start to link this work to the analyses of how such techniques may be developed into reliable systems.

Large and small. (**Left**) Conventional accelerator at Fermilab. (**Center**) Part of the linear accelerator beamline. (**Right**) Benchtop laser particle accelerator for multi-MeV experiments.

CREDITS: (TOP) C. BICKEL/*SCIENCE*; (BOTTOM) FERMILAB

In particular, it will be important to strike an appropriate balance between the basic research needed to progress these ideas and the required industrialization of the techniques. As an example of this balance, European researchers have just been granted funds from the European Union to pursue the development of laser-driven electron accelerators into the GeV energy regime, with a view to creating reproducible monochromatic beams. Alongside this, a demonstration proton oncology laser system known as "ProPulse" is being pursued by a team led by the Laboratoire d'Optique Appliquée (LOA) in France, with the goal of raising the energy of the proton beam to the required 70- to 250-MeV level. These two ambitious projects will help demonstrate whether laser acceleration of particles is a viable route for fundamental physics studies and clinical applications.

Looking further into the future, an exciting new proposal is being developed by a consortium of researchers led by Mourou (at the LOA) for ultrarelativistic particle beam lines based on exawatt-class laser technology. This project, known as Extreme Light Infrastructure, is currently under consideration as part of the European Research Infrastructure roadmap process (*10*). Its goal is to provide multiple accelerator beam lines delivering high-brightness electron, gamma, and proton sources for a wide range of user applications.

It is clear that we are still a number of years away from exploitation of these laser-driven accelerators, but this should not detract from the major advances demonstrated over the past few months. Unprecedented research attention is being paid to this area, which is already paying dividends as demonstrated by the innovative techniques reported here. This is definitely a field to watch.

References and Notes

1. T. Toncian *et al.*, *Science* **312**, 410 (2006); published online 16 February 2006 (10.1126/science.1124414).
2. P. K. Patel *et al.*, *Phys. Rev. Lett.* **91**, 125004 (2003).
3. L. Romagnani *et al.*, *Phys. Rev. Lett.* **95**, 195001 (2005).
4. H. Schwoerer *et al.*, *Nature* **439**, 445 (2006).
5. B. M. Hegelich *et al.*, *Nature* **439**, 441 (2006).
6. J. Fuchs *et al.*, *Nat. Phys.* **2**, 48 (2006).
7. S. Mangles *et al.*, *Nature* **431**, 535(2004).
8. C. Geddes *et al.*, *Nature* **431**, 538 (2004).
9. J. Faure *et al.*, *Nature* **431**, 541 (2004).
10. For information on the European Strategy Forum on Research Infrastructures, see (www.cordis.lu/esfri/home.html).

10.1126/science.1126051

MATERIALS SCIENCE

Self-Assembly of Unusual Nanoparticle Crystals

Regular particles of any size, from atoms to colloids, can form crystals. Manipulation of their charges allows control of crystal structure and can be extended to nanoparticle self assembly.

Orlin D. Velev

The crystallization of matter on any length scale, from atoms and ions to biomolecules to nano- and microparticles, has long been a major thrust in science and technology. On page 420 of this issue, Kalsin *et al.* (*1*) report the cocrystallization of equally sized metallic nanoparticles into large crystals with diamond-like symmetry. The oppositely charged gold and silver nanoparticles attract each other at very short distances and assemble into unusual lattices. This work provides new insights into crystallization on the nanoscale, and fills in a gap in the overall picture of particle and biomolecule crystallization.

It has been known for decades that micrometer- and submicrometer-sized spheres suspended in liquids readily form "colloidal crystals" during sedimentation or drying. The spheres crystallize when their free volume is restricted below a certain threshold, but this occurs only when the interactions between the spheres are repulsive, which allows their rearrangement. Such closely packed crystals allow facile fabrication of materials with controlled porosity and long-range organization (*2*). Volume-restricted repulsive spheres, however, always crystallize in a trivial lattice of hexagonally close-packed layers. This limits the range of their application as other types of crystal symmetries are required for photonic, optoelectronic, and memory storage applications.

The author is in the Department of Chemical and Biomolecular Engineering, North Carolina State University, Raleigh, NC 27695–7905, USA. E-mail: odvelev@unity.ncsu.edu

The formation of colloid crystals with other symmetries can, in principle, be achieved if the particles are assembled by attractive interactions. Two seemingly simple ideas for crystallization by particle attraction have been considered, yet they have proven notoriously difficult to realize experimentally. The first idea is to use binary mixtures of oppositely charged particles that could cocrystallize in a manner broadly similar to crystallization of ionic salts from liquid solutions. The problem with this system is that strongly attractive particles rapidly and irreversibly stick to each other, forming gel-like aggregates. Only recently have Leunissen *et al.* designed a procedure whereby micrometer-sized colloidal spheres having small positive or negative charges are synthesized and cocrystallized in density-matched organic liquids (*3*). The particles, whose attractive interaction energies are estimated to be on the order of a few k_BT units (where k_B is Boltzmann's constant and T is temperature), come together in mixed CsCl-type lattices of alternating positive and negative charges. A variety of crystals of other symmetries and particle compositions have been assembled, and the method could be versatile enough to be used in the routine synthesis of ionic colloidal crystals.

A second idea for particle crystallization by attractive interactions that has also proven difficult to realize is the crystallization of particles by functionalizing them with complementary DNA strands. DNA hybridization locks the particles together when they come into contact; however, the strong irreversible "snapping" into place does not allow crystallization. The key to making this idea work has been to reduce the strength of the interactions by adjusting the temperature of the suspension very near the melting point of DNA, where hybridization is weak and reversible (*4*). Thus, colloidal crystallization may be achieved by various attractive forces, but only when the interaction energy is precisely adjusted within a certain small range (see the figure).

Systems of nanoparticles 1 to 10 nm in size provide a natural link between the areas of molecular and colloidal crystallization. Crystals from such particles can find applications in nanoelectronics, plasmonics, high-density data storage, catalysis, and biomedical materials. The formation of binary crystals from nanoparticle mixtures as a likely result of cocrystallization under restricted volume conditions was reported some time ago (*5*). Only recently has the role of electrostatics in the formation of nanoparticle crystals emerged as a parameter that can be controlled in order to assemble various crystals of new symmetry and composition (*6*). The report by Kalsin *et al.* conclusively proves that large crystals can be produced by controlled electrostatic self-assembly. The crystallization has been achieved by precise adjustment of the attraction between the oppositely charged nanoparticles, but the data also point to the existence of unusual effects of electrostatic screening of the larger particles by the smaller ones that do not scale up to interactions between microspheres.

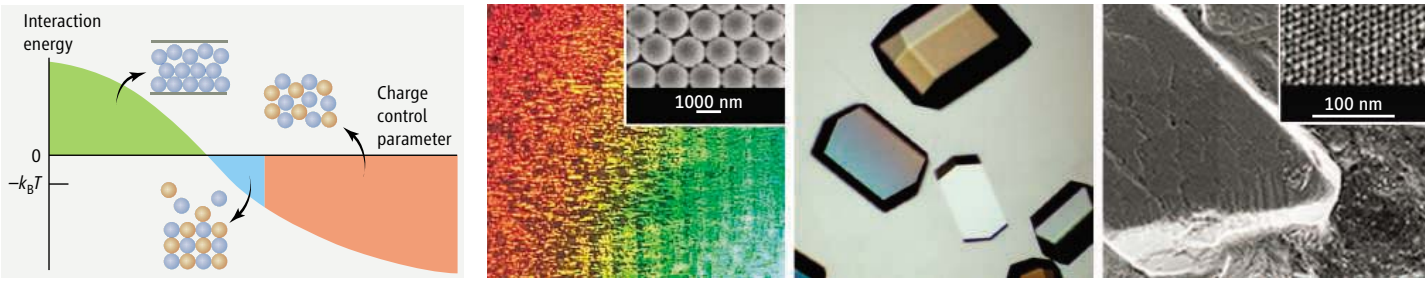

Packing together. The crystallization of colloidal particles and biomacromolecules is intrinsically related to the interactions between the particles, which often can be controlled by their charge (**graph at left**). Repulsive spheres can easily be crystallized by restricting their volume. Proteins and binary mixtures of oppositely charged particles can be crystallized by precise adjustment of the interactions into a weakly attractive regime. However, if the interactions between the particles are strongly attractive, rapid precipitation of amorphous aggregates occurs. The micrograph images are of colloidal crystals assembled by restricting the free volume of repulsive latex spheres (**left**), crystals of the protein lysozyme obtained under slightly attractive interactions (**center**), and a nanoparticle crystal assembled under controlled electrostatic attraction (*1*) (**right**).

Interestingly, the idea that the key to crystallization is achieving a precise balance among weak attractive interactions has been actively explored in the field of protein crystallization for more than a decade. Proteins are large, complex molecules of nonuniform shape and charge, which have been shown to crystallize only under conditions of slightly attractive interactions when both positively and negatively charged groups are present on their surfaces (*7*). The intricate fundamentals of the attractive electrostatic interactions between nanoparticles in a crystal are still not understood in depth. It seems that the concepts developed for proteins may now provide a roadmap for nanoparticle crystallization.

Future research in nanoparticle assembly may bring closer the areas of biomacromolecule and nanoparticle crystallization. Could a similar charge-balancing approach be applied to binary mixtures of proteins, or mixtures of proteins and nanoparticles? A large variety of nanoparticles of special shape and properties have been synthesized in the past few years, but little is yet known about their self-assembly. New "zwitterionic" particles, having patches of negative and positive charges on their surfaces, could soon be synthesized and crystallized by adjustment of the interactions in a manner similar to the crystallization of proteins. Thus, nanoparticle crystallization and assembly may not only yield new nanomaterials, but could also provide insights into how to control colloidal forces on the nanoscale.

References

1. A. M. Kalsin *et al.*, *Science* **312**, 420 (2006); published online 23 February 2006 (10.1126/science.1125124).
2. O. D. Velev, A. M. Lenhoff, *Curr. Opin. Colloid Interface Sci.* **5**, 56 (2000).
3. M. E. Leunissen *et al.*, *Nature* **437**, 235 (2005).
4. P. L. Biancaniello, A. J. Kim, J. C. Crocker, *Phys. Rev. Lett.* **94**, 058302 (2005).
5. C. J. Kiely, J. Fink, M. Brust, D. Bethell, D. J. Schiffrin, *Nature*, **396**, 444 (1998).
6. E. V. Shevchenko, D. V. Talapin, N. A. Kotov, S. O'Brien, C. B. Murray, *Nature* **439**, 55 (2006).
7. A. George, W. Wilson, *Acta Crystallogr. D.* **50**, 361 (1994).

10.1126/science.1125800

PHARMACOLOGY

Hitting the Hot Spots of Cell Signaling Cascades

Small-molecule inhibitors can bind in several different ways to protein interaction sites on signaling proteins, thereby selecting downstream pathways. This type of targeting may be useful therapeutically.

John Joseph Grubb Tesmer

Transient protein-protein interactions are hallmarks of intracellular signaling cascades triggered by heterotrimeric guanine nucleotide-binding proteins, or G proteins (*1*). Hundreds of cell surface receptors for hormones and other extracellular factors activate G proteins, thereby regulating nearly all aspects of cell physiology. These receptors are the targets of a large fraction of the pharmaceutical drugs being used today. Thus, small molecules that negatively or positively modulate the protein-protein interactions of G proteins could likewise be powerful therapeutic agents (*2*, *3*). However, drugs that target protein-protein interfaces are harder to develop than those that target the active sites of enzymes, which are often found in deep, well-defined pockets on the protein surface. Many of the protein-protein interfaces found in signaling cascades are comparatively flat and expansive. They also tend to be adaptive, meaning that a signaling protein can use the same surface to bind to a structurally diverse set of targets (*1*, *2*, *4*). This renders it difficult to find a drug that can turn one particular signaling pathway on or off without affecting the others.

One way to overcome at least some of these hurdles is to identify compounds that target the so-called "hot spot" of the protein-protein interface (*5*). In many transient protein-protein interactions, a majority of the binding energy is contributed by only a few amino acid residues within the interface. These "hot" amino acids tend to cluster together in a relatively small, central region surrounded by a ring of less energetically important and more water-accessible residues (*6*–*8*). Thus, small molecules can disrupt a comparatively large protein-protein interface by binding to the hot spot or, alternatively, to an allosteric site that alters its conformation (*2*).

On page 443 of this issue, Bonacci *et al.* (*9*) use a computer-based "virtual" screen of only 1990 structurally diverse compounds (available from the U. S. National Cancer Institute) to identify molecules that bind to the β_1 and γ_2 subunits of a G protein (G$\beta\gamma$). G proteins consist of three subunits. In the classic G protein signaling cascade, G$\beta\gamma$ subunits are released as a complex from the α subunit (Gα) after activation of an associated receptor at the cell surface. The G$\beta\gamma$ complex can subsequently

The author is in the Department of Pharmacology, Life Sciences Institute, University of Michigan, 210 Washtenaw Avenue, Ann Arbor, MI 48109, USA. E-mail: tesmerjj@umich.edu

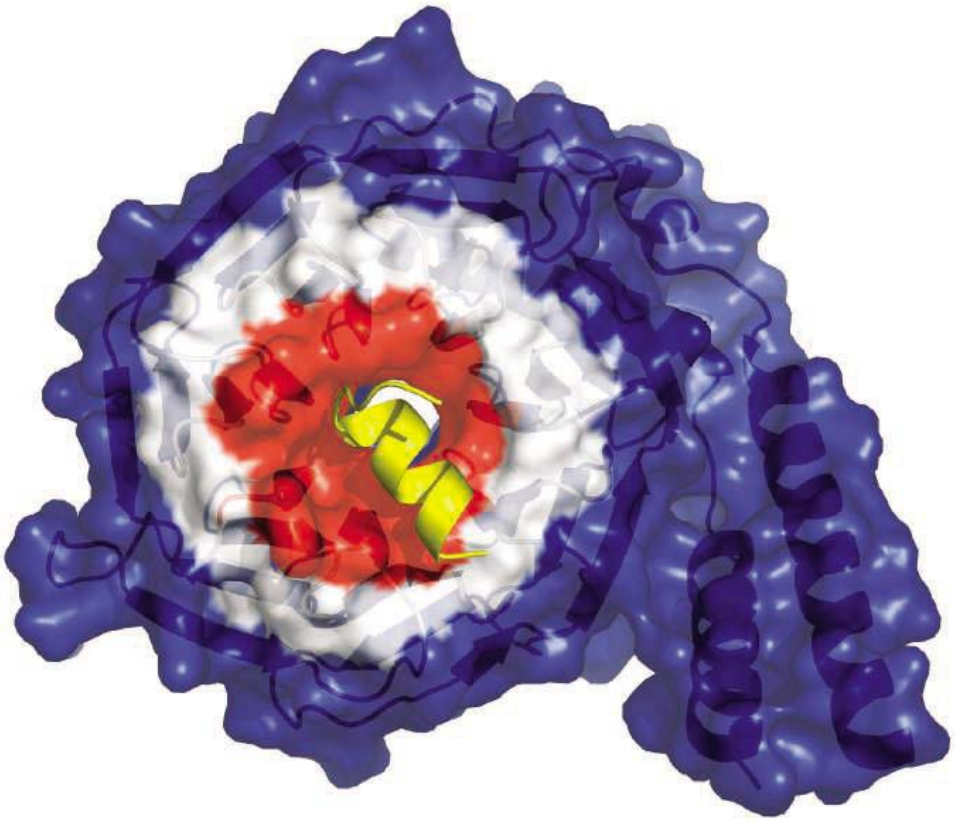

Targeting the Gβγ bull's-eye. Small-molecule compounds that inhibit Gβγ signaling were identified by targeting its "hot spot" in a virtual chemical screen. The structure of Gβγ is depicted as a ribbon diagram superimposed with its molecular surface. The red bull's-eye marks the hot spot that contains residues believed to be important for binding most if not all of the diverse protein targets of Gβγ. The white ring symbolizes regions that can also participate in protein interfaces but may not be as energetically important or are more solvent accessible (however, regions other than those shown in red or white also interact with Gβγ targets). A peptide that helped define the hot spot of Gβγ is shown as a green ribbon (PDB code 1XHM).

interact with and regulate an array of downstream signaling proteins such as phospholipase C–β, G protein–coupled receptor kinase 2 (GRK2), and phosphatidylinositol 3-kinase. These structurally diverse proteins bind (or are expected to bind) to a surface of Gβγ that overlaps the binding site of Gα (*10*–*14*), accounting for the ability of Gα to keep Gβγ from signaling in the absence of extracellular signals (by forming the inactive Gαβγ heterotrimer).

Despite the large surface area of Gβγ that is buried within the Gαβγ complex, it was previously shown that small peptides derived from a phage display library could differentially inhibit the binding of Gβγ to Gα and to its various downstream targets. The peptides bind to a site in Gβγ1 that lies near the center of the surface known to interact with Gα and the effector protein GRK2 (*15*, *16*). Although peptides are not usually good drug candidates, they can still be very useful in defining the functional sites on protein surfaces that can then be targeted by small-molecule drugs (*17*). Accordingly, Bonacci *et al*. used the structure of Gβγ bound to one of the phage display peptides to define the hot spot of Gβγ (see the figure), and then used a molecular modeling computer program to dock compounds of known structure into the hot spot. By evaluating several different metrics, the authors narrowed the library to 85 likely compounds, which they then experimentally tested for Gβγ binding. Of these, nine compounds inhibited the binding of phage-display peptides to Gβγ by 50% at high nanomolar to mid-micromolar concentrations. Several of the most promising inhibitors were then shown to be efficacious at modulating Gβγ function in vivo.

This is not the first example of small-molecule screen, or even a virtual one, that has successfully identified a modulator of a protein-protein interface. For example, a similar virtual screen identified a compound that could inhibit the various protein interactions of the small molecular weight G protein Rac1, a key regulator of the cytoskeleton and cell proliferation (*18*). The remarkable aspect of the work reported by Bonacci *et al*. is that they identified molecules, presumably targeting the same site, that differentially modulate the interactions of Gβγ with its various downstream targets in vitro, in cultured cells, and in an animal model where the physiological effects of one of the compounds was evaluated. Thus, it is possible not only to identify small molecules that directly modulate the function of G proteins, but also to find, with great efficiency, compounds that can turn off one signaling pathway while preserving or even augmenting others. Such compounds could help elucidate the specific pathways regulated by Gβγ under different physiological conditions and may ultimately lead to the development of therapeutic agents for diseases in which Gβγ is expected to play a maladaptive role, such as heart failure (*19*).

It will be important to accurately define the Gβγ binding sites of the compounds identified by Bonacci *et al.*, as they could reside outside of the intended hot spot, either in an allosteric site or in a region of Gβγ that interacts with only a subset of its effectors. Accordingly, high-resolution crystallographic structures of Gβγ in complex with these inhibitors would provide great insight into the specific regions of Gβγ most important for its various protein interactions and facilitate the design of drugs with higher affinity and selectivity. There is also a strong possibility that higher affinity drugs can be identified by a larger survey of chemical compounds, wherein tens of thousands of molecules are typically screened. Finally, it will be interesting to test whether the compounds identified differentially interact with the many possible species of Gβγ (there are genes for at least five isoforms of Gβ and 12 of Gγ in humans). The hunting season for drugs that target other G protein interfaces is now open.

References

1. E. Buck, R. Iyengar, *Sci. STKE* **2003**, re14 (2003).
2. M. R. Arkin, J. A. Wells, *Nat. Rev. Drug Discov.* **3**, 301 (2004).
3. Y. Pommier, J. Cherfils, *Trends Pharmacol. Sci.* **26**, 138 (2005).
4. W. L. DeLano, M. H. Ultsch, A. M. de Vos, J. A. Wells, *Science* **287**, 1279 (2000).
5. W. L. DeLano, *Curr. Opin. Struct. Biol.* **12**, 14 (2002).
6. T. Clackson, J. A. Wells, *Science* **267**, 383 (1995).
7. A. A. Bogan, K. S. Thorn, *J. Mol. Biol.* **280**, 1 (1998).
8. O. Keskin, B. Ma, R. Nussinov, *J. Mol. Biol.* **345**, 1281 (2005).
9. T. M. Bonacci *et al*., *Science* **312**, 443 (2006).
10. M. A. Wall *et al*., *Cell* **83**, 1047 (1995).
11. D. G. Lambright *et al*., *Nature* **379**, 311 (1996).
12. C. E. Ford *et al*., *Science* **280**, 1271 (1998).
13. Y. Li *et al*., *J. Biol. Chem.* **273**, 16265 (1998).
14. D. T. Lodowski, J. A. Pitcher, W. D. Capel, R. J. Lefkowitz, J. J. G. Tesmer, *Science* **300**, 1256 (2003).
15. J. K. Scott *et al*., *EMBO J.* **20**, 767 (2001).
16. T. L. Davis, T. M. Bonacci, S. R. Sprang, A. V. Smrcka, *Biochemistry* **44**, 10593 (2005).
17. S. S. Sidhu, W. J. Fairbrother, K. Deshayes, *Chembiochem* **4**, 14 (2003).
18. Y. Gao, J. B. Dickerson, F. Guo, J. Zheng, Y. Zheng, *Proc. Natl. Acad. Sci. U.S.A.* **101**, 7618 (2004).
19. G. Iaccarino, W. J. Koch, *Assay Drug Dev. Technol.* **1**, 347 (2003).

10.1126/science.1126903

CREDIT: J. TESMER


page 382

INTRODUCTION

Influenza: The State of Our Ignorance

THE STARTLING SPREAD OF H5N1 ACROSS MUCH OF THE GLOBE HIGHLIGHTS OUR vulnerability to the emergence of novel subtypes of influenza virus. Yet despite our fears of pandemic human disease, H5N1 is primarily a disease of birds. Olsen and colleagues (p. 384) outline the unseen network of influenza among migratory birds that spans Earth. H5N1 has engendered alarm not only because it is unusually virulent, laying waste to poultry and causing severe economic losses for farmers, but also because it can, with some difficulty, infect humans and other mammals. So far, the virus has killed more than half of the nearly 200 people known to have been infected. Kuiken and colleagues (p. 394) explore the routes through the obstacles to interspecies transmission (the host species barrier) of viruses. Their analysis focuses on which adaptations are needed to facilitate bird-to-human transfer of H5N1. Examples are provided by Shinya* and in a Brevia by van Riel *et al.* (p. 399). These authors show that the virus preferentially binds to cell types bearing specific surface receptors found deep in the lungs, which may partly explain its poor human-to-human transmissibility.

The combination of ever-unfolding modes of variability (Stevens, p. 404) and symptomless transmission makes identification of the virus slow and hinders the implementation of influenza containment. As Lu outlines in his Editorial (p. 337), we urgently need faster and more robust diagnostic tests for field use (an area we will be covering shortly in our pages). Further articles in this special section describe other tools and approaches for preparedness. Smith (p. 392) summarizes the models that have been developed for tracing the rate and spread of pandemic influenza through human populations, including scenarios for the deployment of drugs and development of vaccines. We might be able to buy some time for vaccine manufacture by stockpiling antiviral drugs for immediate use, but that time may be short. Regoes and Bonhoeffer (p. 389) indicate that the generation and transmission of resistant strains could happen quickly. Unfortunately, our knowledge of influenza transmission is incomplete, and more basic data are needed to make models accurate and to give them predictive weight. Seasonal influenza statistics will provide an important insight into the transmission biology of influenza; Viboud *et al.* (p. 447) have used a large data set from the United States to model annual waves of infection.

In a News story (p. 380), Kaiser explores efforts to develop broader influenza vaccines that protect against new strains and perhaps even all influenza subtypes. Antiviral drugs are also sorely needed to fight a pandemic, but oseltamivir, or Tamiflu, has been in short supply. As Enserink describes (p. 382), Roche and other companies are now ramping up production, while scientists are investigating faster and cheaper synthetic pathways that could make the drug affordable to developing countries. In an accompanying podcast, Wills interviews some of the contributing authors and journalists.

An energetic response to H5N1 does not have to be alarmist. We can marshal existing concern about this particular strain of avian influenza to build a long-lasting international infrastructure to monitor and thwart threats from such emerging infections.

–CAROLINE ASH AND LESLIE ROBERTS

*K. Shinya, *Nature* **440**, 435 (2006).

CREDIT: ROCHE

Influenza

CONTENTS

See also related Editorial p. 337; Brevia p. 399; Research Article p. 404; Report p. 447; and Podcast at www.sciencemag.org/about/podcast.dtl

NEWS

A One-Size-Fits-All Flu Vaccine?

The threat of avian influenza has revived efforts to develop "universal" flu vaccines that protect against all human influenza strains. Although that goal remains elusive, vaccines that protect against seasonal flu variants could be closer

Modern medicine's main weapon against the influenza virus is woefully unsophisticated. Each year, companies have to make a new batch of flu vaccine because unlike, say, polio or chickenpox, flu strains change every year. The vaccine is grown in eggs, a process that takes up to 9 months, and people have to be vaccinated annually, which many don't bother to do. More troubling, if a pandemic strain of influenza came along, the virus could kill millions of people in the time it would take to prepare a matching vaccine.

What scientists dream of is a vaccine that can protect against any flu strain for years or even a lifetime. This so-called universal flu vaccine is still a long way off, if it's even possible. But many labs are dusting off past projects on broad flu vaccines, spurred by new funding and fears that H5N1, the deadly avian influenza that has swept across half the world, could acquire the ability to be transmitted from human to human. Until now, "flu has never been before high enough on the radar screen" for companies in particular to follow through with a strong push for a universal vaccine, says Gary Nabel, director of the Vaccine Research Center at the U.S. National Institute of Allergy and Infectious Diseases (NIAID) in Bethesda, Maryland.

Doing so, however, means coming up with an alternative way to stimulate immunity to the virus. The tried-and-true technique for seasonal flu uses a killed virus vaccine that works mainly by triggering antibodies to hemagglutinin (HA), the glycoprotein on the virus's surface that it uses to bind to human cells. Hemagglutinin and neuraminidase (NA), another surface glycoprotein that helps newly made viruses exit cells, give strains their names (H5N1, for example). The sequences of HA and NA mutate easily, which is why each season's flu strain—although it may be the same in subtype, such as H3N2—"drifts" slightly from the previous year's, and the annual vaccine must be tailor-made.

To make a universal vaccine for influenza A, which includes the main seasonal flu strains and bird flu, as well as past pandemic strains, some scientists are hoping to use "conserved" flu proteins that don't mutate much year to year. (Influenza B, the other type, occurs only in humans and causes milder symptoms.) Some of the conserved protein vaccines in the works stimulate production of antibodies as do conventional flu vaccines, whereas others rouse certain immune system cells to battle the virus.

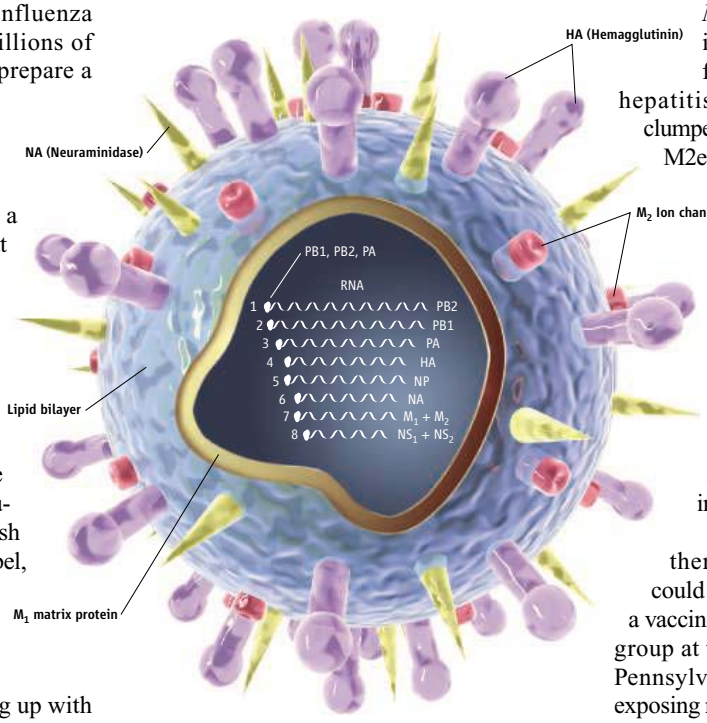

Weak spots. A universal flu vaccine would target "conserved" proteins, such as M2 or NP, an inner protein.

Other scientists are pursuing a slightly less ambitious goal: They are working on vaccines that match a particular HA, such as the H5 in H5N1, but that also protect against "drift" strains that typically emerge from year to year.

It's not yet clear whether any of these broad vaccines will ever work as well as a traditional, HA-matched vaccine. But they could help when the annual vaccine doesn't match the circulating strain exactly, and in a pandemic, they could reduce deaths until a matched vaccine is ready. "Anything that would dampen a pandemic would be useful," says virologist Robert Couch of Baylor College of Medicine in Houston, Texas.

One for all

One of the most hotly pursued strategies for a universal vaccine against influenza A is based on a flu protein called M2. This protein forms an ion channel crossing the membrane of a virus particle or infected cell, barely jutting out from the surface. It's an appealing target because the 23 amino acids that make up the ectodomain, or protruding part, of M2 (known as M2e) scarcely vary from one human flu strain to the next, even back to the 1918 Spanish flu.

Scientists first showed in the late 1980s that antibodies to M2 can slow flu infection in mice. In 1999, biochemist Walter Fiers's team at Ghent University in Belgium reported in *Nature Medicine* that it had reduced flu deaths in mice with a vaccine made of M2e fused to another protein, the core of the hepatitis B virus (HepB). (These proteins clumped into viruslike particles bristling with M2e that stimulated more antibodies to M2e than did the protein by itself.) In its latest paper in *Vaccine* in January, Fiers's lab, now collaborating with the vaccine company Acambis in Cambridge, Massachusetts, has improved the candidate vaccine by attaching three copies of M2e to the HepB core, delivering it nasally—which boosts immune responses compared to injection—and adding an adjuvant, an ingredient that also increases the body's immune response.

Although M2e is typically conserved, there's a small chance that the protein could still evolve, enabling the virus to evade a vaccine. To assess that risk, Walter Gerhard's group at the Wistar Institute in Philadelphia, Pennsylvania, pushed the virus to mutate by exposing mice with weak immune systems to an H1N1 seasonal flu strain while giving them antibodies specific to M2e. As they reported last June in the *Journal of Virology*, M2e mutants appeared in some mice after 3 weeks, but there were only two types—fewer than might have been expected. "To us, that was reassuring," Gerhard says, because it should be possible to make an M2e vaccine to match the few anticipated variants.

Another major caveat is that although M2 vaccines may prevent deaths from flu, they may not keep people from getting sick, the way conventional vaccines normally do, notes Couch. That's because M2 antibodies seem to work by binding to infected cells and promoting their clearance, instead of blocking the virus (which

CREDITS (TOP TO BOTTOM): C. BICKEL/*SCIENCE*

sports few M2 surface proteins) from infecting new cells, as traditional vaccines are thought to do. Fiers's mice, for instance, still get sick and lose some weight, although they do survive. Fiers argues that, given the limitations of current seasonal flu vaccines—a regular flu vaccine matches the circulating strain only 80% to 90% of the time and often doesn't work at all in the elderly, whose immune systems aren't good at making new antibodies—M2 vaccines are a possible replacement. Others, including Gerhard, see M2 vaccines as a backup to regular vaccines, perhaps as an added component in annual flu shots.

Some experts caution that it's too early to say that M2 vaccines will work in people, as opposed to mice. Retired New York Medical College virologist Edwin Kilbourne, for instance, questions whether Fiers challenged mice with sufficiently high doses of virus.

Despite the skepticism, several companies hope to commercialize M2 flu vaccines, including Switzerland-based Cytos Biotechnology; Acambis expects to submit a clinical trial application to the U.S. Food and Drug Administration (FDA) this year. Acambis's Ashley Birkett agrees that "we need to see how it performs in the clinic." Another contender is Merck, which has done animal tests on an M2 vaccine combined with an influenza B vaccine made from a conserved stretch of the virus's HA, says Merck researcher Antonello Pessi.

Looking inside

Another approach to a universal flu vaccine uses conserved internal proteins such as nucleoprotein (NP) to elicit a different kind of immunity, one based on a type of T cell called a cytotoxic T lymphocyte (CTL) rather than on antibodies. CTLs recognize and kill infected cells expressing viral antigens, fragments of proteins such as NP.

Researchers at Merck and Vical Inc., a biotech company in San Diego, California, reported 13 years ago that a vaccine based on NP partially protected mice from seasonal influenza A, although some animals still died. Instead of immunizing the animals with NP itself, the researchers used DNA encoding the protein as the vaccine, a strategy that often generates a more powerful cellular immune response. Last year, FDA researcher Suzanne Epstein and others showed that mice survived seasonal flu and could be partially protected against dying from H5N1 by an NP-based DNA vaccine boosted by ferrying the DNA into cells inside an adenovirus disabled so it can't replicate.

Broad thinker. Belgian biochemist Walter Fiers hopes to take advantage of the similarities among flu viruses.

Like M2 vaccines, vaccines based on internal viral proteins won't prevent infection altogether because CTLs target already infected cells. Still, says Epstein, they could offer some protection until a pandemic vaccine is produced. Her group is now looking at a DNA vaccine that combines NP and M2, a strategy also being pursued by Vical with NIAID support. Others are considering the inner proteins not for a standalone vaccine but as adjuvants that could broaden the immune response to HA-based vaccines.

One overarching question is whether long-lasting immune protection against different flu subtypes—whether through CTLs, M2, or some other mechanism—is possible in humans. The epidemiological data have been scanty. But Epstein recently found suggestive evidence by analyzing old records from a study of 60 Cleveland, Ohio, families who experienced the 1957 H2N2 flu pandemic. Epstein reports in the January 2006 *Journal of Infectious Diseases* that adults (but not children) who had lab-verified H1N1 flu in the years before that pandemic were one-third as likely to get sick with the 1957 H2N2 flu.

Narrowing in

With the two main approaches to making a truly universal flu vaccine still a question mark, some investigators are working on a seemingly more approachable goal: making HA-specific vaccines that protect against drift strains within the same HA family.

One way to achieve this broad immunity is with a live attenuated vaccine, which consists of a virus that can still infect cells and thus should induce CTL responses. A live attenuated nasal vaccine made each year for annual flu, FluMist, has been on the market since 2003 in the United States. Manufacturer MedImmune says that it protects against mismatched strains. MedImmune and NIAID will soon begin clinical testing of FluMist versions for potential pandemic strains such as H5N1 and H9N2. The downside of live vaccines, however, is that there is a small risk that the virus could revert to a dangerous form, perhaps even creating a new pandemic strain.

A safer way to achieve protection against drift pandemic strains may be with DNA encoding the HA surface protein delivered by means of a viral vector. Compared to the traditional killed virus vaccine, this should stimulate broadly protective CTL responses to conserved parts of the HA protein that are shared by related strains. Separate teams at the University of Pittsburgh in Pennsylvania and Purdue University in West Lafayette, Indiana, both collaborating with the U.S. Centers for Disease Control and Prevention (CDC) in Atlanta, Georgia, reported in *The Lancet* and the *Journal of Virology* in February that an adenovirus-delivered vaccine based on H5 DNA protected against both the 1997 Hong Kong strain of H5N1 and the 2004 Vietnam strain. One advantage compared to conventional egg-grown vaccines: The manufacturing of the vaccine is done with cells, and "you can make millions of doses in a month's time," says

Some Proposed Universal or Broad Flu Vaccines

	Vaccine Type	Antibodies	Cytotoxic T lymphocytes	Who	Clinical trials
All HA Strains	M2e	✓		Acambis, Merck, Cytos Biotech., Wistar Inst., Wash. U./Vaccine Res. Inst.	Acambis 2007? Merck 2006?* Cytos 2007?
	Conserved HA (influenza B)	✓		Merck	Merck 2006?*
	DNA vaccine with NP, sometimes M2 genes†	✓		FDA, Vical/St. Jude	
HA Drift Strains	DNA vaccine with HA gene	✓	✓	PowderMed	Seasonal flu 2005; H5N1 2006
	Adenovirus-based with H5 HA gene	✓	✓	U. Pittsburgh/CDC, Purdue/CDC	2007?
	Live attenuated	✓	✓	MedImmune/NIAID	FluMist (seasonal flu) on market; pandemic vaccine trials 2006

* Merck is testing a new flu vaccine but has not disclosed which one. † FDA vaccine included adenoviral boost.

CREDITS: WALTER FIERS (PHOTO)

Suryaprakash Sambhara of CDC, senior author on the *Lancet* study.

Both universities are seeking funding for clinical tests from NIAID and companies. Sambhara plans to give the Purdue team an adenovirus-based vaccine containing genes for NP and M, which codes for M2 and an inner protein, as well as H5HA; and Andrea Gambotto of Pittsburgh hopes his vaccine, which also worked in chickens, may be picked up as a bird vaccine. A company called PowderMed avoids using adenoviruses to deliver the DNA, which have some drawbacks, instead using gold-coated particles and high-speed injection to get HA-based DNA vaccines into a person's skin cells.

Although the variety of approaches to broader flu vaccines can be dizzying, "having all of those efforts moving forward gives us more weapons in the arsenal and makes us more likely to find the best platform," NIAID's Nabel says. Even if one approach rises to the top, there are many obstacles ahead, such as persuading regulatory agencies—who now approve flu vaccines based only on HA antibody responses—to use CTL responses as a measure of efficacy instead, notes virologist Albert Osterhaus of Erasmus University in Rotterdam, the Netherlands. Still, if universal—or at least broader—flu vaccines can make it to the market, they could save lives during regular flu season and stave off disaster when the next pandemic strikes.

–JOCELYN KAISER

NEWS

Oseltamivir Becomes Plentiful—But Still Not Cheap

The shortage of oseltamivir may soon be a thing of the past. But whether the drug will become cheap enough for developing countries and how well it will work against a pandemic remain to be seen

For more than 6 months, German physician Tido von Schoen-Angerer has "desperately" tried to order oseltamivir from Roche, the Swiss company that produces the anti-influenza drug. "But I've given up," he says. Von Schoen-Angerer, research and development director of the Campaign for Access to Essential Medicines at Médecins sans Frontières in Berlin, wanted 100,000 treatment courses to protect MSF personnel and to treat patients, should the organization ever find itself at the cradle of a pandemic. But Roche kept saying it simply didn't have enough of the drug, Von Schoen-Angerer says. He eventually picked up 500 treatments from a Dutch wholesaler last month, at a price he says was too high.

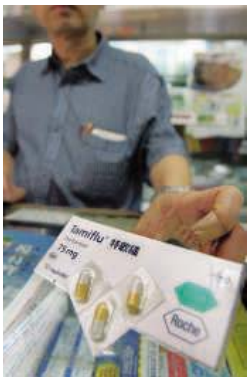

Drug of choice. More than 65 countries are stockpiling oseltamivir, better known as Tamiflu.

As global demand for oseltamivir, better known by Roche's brand name Tamiflu, reached the stratosphere, many clients found themselves at the end of a long queue. But their frustrating wait should soon be over. Last month, Roche announced a series of deals with other companies to dramatically ramp up production of oseltamivir; in 2007, it says it will be capable of producing 400 million treatment courses (each consisting of 10 capsules) yearly. That's up from just 6 million 3 years ago and much more than the expected demand. Supply will be boosted further because a handful of generic drug makers have started producing their own versions of oseltamivir—some with a sublicense from Roche, others without.

Although production may finally meet worldwide demand, several questions remain. It's unclear whether oseltamivir's price will drop enough for poor countries to stockpile the drug; many fear that they will be left behind (*Science*, 18 November 2005, p. 1103). That's why it's essential to find simpler ways to produce the drug, some say. One such method may be a revolutionary, easy, and cheap synthetic pathway that Harvard University chemist and Nobel laureate Elias Corey and his team are now reporting.

Also unanswered is the question of how well oseltamivir will work against a pandemic virus. The drug is effective against seasonal flu strains, but there aren't solid data about its efficacy against H5N1, the avian influenza strain that some suspect is a prime candidate to evolve into the next flu pandemic. "We think it's effective" against H5N1, says Nikki Shindo, a medical officer at the World Health Organization (WHO) in Geneva, Switzerland, "but that's a feeling. We would like to have more evidence." Some studies on the drawing board aim to get just that.

Change of heart

Until less than a year ago, Roche routinely dismissed suggestions that it sublicense oseltamivir, saying it needed tight control over the complex production process, which includes a risky step involving an explosive intermediate compound called an azide. It also refused to say how much oseltamivir it produced or how much it was charging governments for it.

But the company did an about-face last fall. In the past 6 months, it has signed deals with more than 15 companies, each of which will help carry out a step in Tamiflu's production process. In addition, Roche has sublicensed Shanghai Pharmaceuticals and HEC, both in China, and Hetero in India, to make oseltamivir from beginning to end. Those companies will produce generic versions for local use; they won't be named Tamiflu, and Roche will not control quality, production volume, or pricing policy, says David Reddy, Roche's pandemic task force leader.

CREDITS (TOP TO BOTTOM): ROCHE; PAUL YEUNG/REUTERS

But does it work? Exactly how effective oseltamivir is against H5N1 infection in humans is unclear.

Two Indian generic drug makers—Ranbaxy and Cipla—have started making oseltamivir without a deal with Roche; they can sell it in India and other places where Tamiflu is not covered by a patent, Roche says, such as Thailand, Vietnam, Indonesia, and sub-Saharan Africa. Cipla—which has dubbed its drug Antiflu—can currently produce about half a million treatments per month and plans to double capacity soon, says the company's joint managing director, Amar Lulla; the production process is "difficult but not impossible," he adds. Ranbaxy also hopes to double its current production, to over half a million treatments per month. Generic drug makers in Taiwan, Bangladesh, and Algeria also make oseltamivir.

For now, the generic companies aren't offering much of a discount. Roche charges governments in developing countries roughly $15 for a treatment course (rich nations pay $18); Cipla will sell Antiflu for about $12, says Lulla, and other generic drug makers have quoted prices in the same ballpark. "We're not seeing generic [drug] prices that are vastly dissimilar to ours," says Reddy. But Von Schoen-Angerer is confident that competition from the generics will cause prices to plummet, as happened with HIV drugs. At $12, he says, "developing countries still cannot stockpile in any meaningful way."

Innovation could further drive down prices. The Achilles' heel of oseltamivir production is its starting point, a compound called shikimic acid. It was originally derived from star anise, an herb grown in China and Vietnam that quickly became scarce as oseltamivir demand surged. However, Roche says it now gets roughly one-third of its shikimic acid through fermentation by genetically engineered *Escherichia coli* bacteria, developed by John Frost of Michigan State University in East Lansing; it would like to increase that proportion further to two-thirds.

New chemistry could do away with the need for shikimic acid altogether, some scientists say. Harvard's Corey says his synthesis route, described in a paper accepted for publication by the *Journal of the American Chemical Society* (*JACS*), starts with butadiene and acrylic acid, "two of the cheapest chemicals you can buy." As an added bonus, the synthesis route is easy to scale up and avoids the explosive intermediate, says Corey. Organic chemist K. C. Nicolaou of the University of California, San Diego, and the Scripps Research Institute, who is familiar with the work, says, "The synthesis is strikingly short and efficient." Corey, who serves on Roche's bioscience scientific advisory board, says he has told Roche about the findings, which he did not patent in hope that they will become widely used. "My hope is that this work will save lives, especially in poor countries," he says.

If it holds up, Corey's production method would have to garner regulatory approval and would need to be scaled up. What's more, other companies couldn't simply start using it, because patents for oseltamivir cover the compound itself, not just the way it is made, says Vid Mohan-Ram, a patent agent with Foley & Lardner in Chicago. But generic drug makers could adopt the process, he says, which could drive their prices down. And an easier production route could also encourage Roche to lower its price. Reddy says that Roche is "always looking at new types of technologies" but declined to discuss Corey's work or that of chemist Masakatsu Shibasaki of the University of Tokyo, who, in another paper accepted by *JACS*, claims to have found a second new route to oseltamivir. (Shibasaki says that "Roche chemists are examining the details" of his findings.)

Clinical study

As oseltamivir stashes begin to grow, several international efforts are under way to answer basic questions about the drugs' effects on avian influenza in humans. Animal studies have suggested, for instance, that H5N1's virulence may call for a higher dose than the 150 milligrams used daily to treat ordinary flu. Now, 11 hospitals in Indonesia, Thailand, and Vietnam have teamed up with the U.S. National Institutes of Health for a randomized trial to test whether patients with serious influenza—either from H5N1 or a human strain—fare better when they receive 300 milligrams per day. The logistics are complex, says Menno de Jong of the Hospital for Tropical Diseases in Ho Chi Minh City, but the study could start in a few months.

WHO, too, is working on study protocols, says Shindo, and on agreements with countries to implement them when new human cases show up. They're looking into the efficacy of prophylactic use in health care workers and other high-risk groups as well as the usefulness of combining an older influenza drug, amantadine, with oseltamivir.

But with human cases so rare—so far there have been fewer than 200, scattered across nine countries—any such trial will be extremely difficult to conduct. In Turkey, for instance, where WHO had relatively good access when human cases popped up in January, Shindo says there wasn't really an opportunity to study prophylaxis; communication problems and practical concerns got in the way. "Our primary objective during an outbreak is not doing science," she says. "It's to save people's lives and stop the outbreak."

–MARTIN ENSERINK

Supply surge. With help from other companies, Roche says it can produce 400 million treatment courses of oseltamivir next year. Generic drug makers plan to make millions more.

CREDITS (TOP TO BOTTOM): ROCHE

REVIEW

Global Patterns of Influenza A Virus in Wild Birds

Björn Olsen,[1,2] Vincent J. Munster,[3] Anders Wallensten,[4,5] Jonas Waldenström,[6] Albert D. M. E. Osterhaus,[3] Ron A. M. Fouchier[3]*

The outbreak of highly pathogenic avian influenza of the H5N1 subtype in Asia, which has subsequently spread to Russia, the Middle East, Europe, and Africa, has put increased focus on the role of wild birds in the persistence of influenza viruses. The ecology, epidemiology, genetics, and evolution of pathogens cannot be fully understood without taking into account the ecology of their hosts. Here, we review our current knowledge on global patterns of influenza virus infections in wild birds, discuss these patterns in the context of host ecology and in particular birds' behavior, and identify some important gaps in our current knowledge.

Influenza A viruses have been isolated from many species, including humans, pigs, horses, mink, felids, marine mammals, and a wide range of domestic birds, but wildfowl and shorebirds are thought to form the virus reservoir in nature. The influenza A virus genome consists of eight segments of negative-stranded RNA, which code for 11 proteins. Influenza viruses are classified on the basis of two of these proteins expressed on the surface of virus particles; the hemagglutinin (HA) and neuraminidase (NA) glycoproteins (*1*). In wild birds and poultry throughout the world, influenza viruses representing 16 HA and 9 NA antigenic subtypes have been detected (*2*), which can be found in numerous combinations (also called subtypes, e.g., H1N1, H16N3).

The HA protein is initially synthesized as a single polypeptide precursor (HA0), which is cleaved into HA_1 and HA_2 subunits by proteases. The mature protein mediates binding of the virus to host cells, followed by fusion with endosomal membranes (*1*). Influenza viruses of subtypes H5 and H7, but not other HA subtypes, may become highly pathogenic after introduction into poultry and can cause outbreaks of highly pathogenic avian influenza (HPAI, formerly termed "fowl plague"). The switch from a low pathogenic avian influenza (LPAI) virus phenotype, common in wild birds and poultry, to the HPAI virus phenotype is achieved by the introduction of basic amino acid residues into the HA0 cleavage site, which facilitates systemic virus replication. HPAI isolates have been obtained primarily from commercially raised poultry (*3*).

In the past decade, HPAI outbreaks have occurred frequently, caused by influenza viruses of subtype H5N1 in Asia, Russia, the Middle East, Europe, and Africa (ongoing since 1997); H5N2 in Mexico (1994), Italy (1997), and Texas (2004); H7N1 in Italy (1999); H7N3 in Australia (1994), Pakistan (1994), Chile (2002), and Canada (2003); H7N4 in Australia (1997); and H7N7 in the Netherlands (2003) (*3*, *4*).

Migratory Birds as a Natural Reservoir of LPAI Viruses

LPAI viruses have been isolated from at least 105 wild bird species of 26 different families (Table 1) (*5*). All influenza virus subtypes and most HA/NA combinations have been detected in the bird reservoir and poultry, whereas relatively few have been detected in other species. Although many wild bird species may harbor influenza viruses, birds of wetlands and aquatic environments such as the Anseriformes (particularly ducks, geese, and swans) and Charadriiformes (particularly gulls, terns, and waders) constitute the major natural LPAI virus reservoir (*1*). Anseriformes and Charadriiformes are distributed globally, except for the most arid regions of the world (*6*).

In birds, LPAI viruses preferentially infect cells lining the intestinal tract and are excreted in high concentrations in their feces. It has been shown that influenza viruses remain infectious in lake water up to 4 days at 22°C and more than 30 days at 0°C (*7*), and the relatively high virus prevalence in birds living in aquatic environments may be due in part to efficient transmission through the fecal-oral route via surface waters (*1*, *7*).

Migration is a common strategy for birds occupying seasonal habitats and may range from short local movements to intercontinental migrations. Migratory birds can carry pathogens, particularly those that do not significantly affect the birds' health status and consequently interfere with migration. Many Anseriformes and Charadriiformes are known to perform regular long-distance migrations (*6*), thereby potentially distributing LPAI viruses between countries or even continents. Birds breeding in one geographic region often follow similar migratory flyways, e.g., the East Asian–Australian flyway from eastern Siberia south to eastern Asia and Australia (Fig. 1A). However, the major flyways are simplifications, and there are numerous exceptions where populations behave differently from the common patterns (*6*, *8*). Within the large continents and along the major flyways, migration connects many bird populations in time and space, either at common breeding areas, during migration, or at shared nonbreeding areas (Fig. 1). As a result, virus-infected birds can transmit their pathogens to other populations that subsequently may bring the viruses to new areas.

It is important to realize that the transmission of the viruses and their geographical spread is dependent on the ecology of the migrating hosts. For instance, migrating birds rarely fly the full distance between breeding and nonbreeding areas without stopping over and "refueling" along the way. Rather, birds make frequent stopovers during migration and spend more time eating and preparing for migration than actively performing flights (*9*). Many species aggregate at favorable stopover or wintering sites, resulting in high local densities. Such sites may be important for transmission of LPAI viruses between wild and captive birds and between different species.

Influenza Viruses in Ducks

Extensive surveillance studies of wild ducks in the Northern Hemisphere have revealed high LPAI virus prevalence primarily in juvenile—presumably immunologically naïve—birds with a peak in early fall before southbound migration. In North America, the prevalence falls from ~60% in ducks sampled at marshalling sites close to the Canadian breeding areas in early fall, to 0.4 to 2% at the wintering grounds in the southern U.S.A., and ~0.25% on the ducks' return to the breeding grounds in spring. Similar patterns have been observed in Northern Europe, but influenza virus detection during spring migration can be significantly higher, up to 6.5%. Surveillance of the nesting grounds of ducks in Siberia before winter migration revealed the presence of influenza viruses in up to 8% of birds (*10*).

Such year-round prevalence raises the possibility that LPAI virus can persist in ducks alone. This hypothesis complements earlier ones, in which additional host species or preservation of infectious influenza viruses in frozen lakes over the winter play a role in the perpetuation of avian influenza viruses (*1*, *7*).

All HA and NA subtypes, with the exception of H13 to H16, circulate in wild ducks in North America and Northern Europe. In a 26-year longitudinal study performed in Canada, influenza viruses of subtypes H3, H4, and H6 were isolated from ducks most frequently; H1, H2, H7, H10,

[1]Department of Infectious Diseases, Umeå University, SE-90187 Umeå, Sweden. [2]Section for Zoonotic Ecology and Epidemiology, Department of Biology and Environmental Science, University of Kalmar, SE-39182 Kalmar, Sweden. [3]Department of Virology, Erasmus Medical Center, Rotterdam, Netherlands. [4]Smedby Health Center, Kalmar County Council, SE-39471 Kalmar, Sweden. [5]Division of Virology, Department of Molecular and Clinical Medicine (IMK) Faculty of Health Sciences, Linköping University, SE-581 85 Linköping, Sweden. [6]Department of Animal Ecology, Lund University, SE-22362 Lund, Sweden.

*To whom correspondence should be addressed. E-mail: r.fouchier@erasmusmc.nl

and H11 less frequently; and H5, H8, H9, and H12 only sporadically. Although in other North American and European studies, influenza viruses of subtypes H3, H4, and H6 were also detected frequently, the detection of other virus subtypes was not significantly different (*4*, *11*). Thus, the prevalence of influenza virus in general, as well as the specific distribution of subtypes, may vary between different surveillance studies depending on species, time, and place.

In the Canadian studies, cyclic patterns of influenza virus subtypes were reported: Peaks in virus isolation of an HA subtype were followed 1 to 2 years later by reduced rates of isolation of this subtype. This observation awaits confirmation in other surveillance studies but is of particular interest in relation to findings for other infectious diseases: Cyclic patterns described for measles and whooping cough in humans have provided new insights in the role of spatial factors, herd immunity, and population age-structure on epidemiology (*12*). Cycling of influenza virus in wild birds could provide similar new insights into the ecology of influenza viruses in their natural hosts.

Influenza virus surveillance of ducks has been performed in Japan since the late 1970s. As in other studies, influenza virus prevalence and isolated subtypes varied between years and locations (*5*). The prevalence of influenza virus in wild birds elsewhere in Asia is largely unknown, but several studies have been conducted in live bird markets, where most HA and NA subtypes were found in poultry (*1*, *13*). It is plausible that the circulation of the LPAI virus subtypes in poultry at least partially reflects that in wild birds, but no direct connection has yet been established.

Dabbling ducks of the *Anas* genus, with Mallards (*Anas platyrhynchos*) as the most extensively studied species, have been found to be infected with influenza viruses more frequently than other birds, including diving ducks (Table 1) (*5*). Differences in virus prevalence between ecological guilds of ducks are likely in part related to behavior. Dabbling ducks feed primarily on food in surface waters; diving ducks forage at deeper depths and more often in marine habitats (*6*). Dabbling ducks display a propensity for abmigration, the switching of breeding grounds between years, which is in part due to mate choice (*6*). This behavior could provide an opportunity for influenza viruses to be transmitted between different host subpopulations. LPAI virus infection generally causes no major clinical signs in dabbling ducks, and experimental infections indicate that animals only produce a transient, low-level humoral immune response, which may be sufficient to provide partial protection against reinfection with viruses of the same subtype but is unlikely to confer protection against heterologous reinfections (*14*). Different influenza virus subtypes can also infect ducks concomitantly, creating the opportunity for genetic mixing (*15*).

Table 1. Prevalence of influenza A virus in wild birds. Influenza virus prevalence in specific species is given only if tests on >500 birds have been reported; lower numbers in individual species are included in the total. See (*5*) for additional comments and original data. Of the 36 species of ducks, 28,955 were dabbling ducks and 1011 were diving ducks, with influenza virus prevalence of 10.1 and 1.6%, respectively.

Family	Species	Sampled	Positive	
			(*n*)	(%)
Ducks	36 species	34,503	3275	9.5
	Mallard (*Anas platyrhynchos*)	15,250	1965	12.9
	Northern Pintail (*Anas acuta*)	3,036	340	11.2
	Blue-winged Teal (*Anas discors*)	1,914	220	11.5
	Common Teal (*Anas crecca*)	1,314	52	4.0
	Eurasian Wigeon (*Anas penelope*)	1,023	8	0.8
	Wood Duck (*Aix sponsa*)	926	20	2.2
	Common Shelduck (*Tadorna tadorna*)	881	57	6.5
	American Black Duck (*Anas rubripes*)	717	130	18.1
	Green-winged Teal (*Anas carolinensis*)	707	28	4.0
	Gadwall (*Anas strepera*)	687	10	1.5
	Spot-billed Duck (*Anas poecilorhyncha*)	574	21	3.7
Geese	8 species	4,806	47	1.0
	Canada Goose (*Branta canadensis*)	2,273	19	0.8
	Greylag Goose (*Anser anser*)	977	11	1.1
	White-fronted Goose (*Anser albifrons*)	596	13	2.2
Swans	3 species	5,009	94	1.9
	Tundra Swan (*Cygnus columbianus*)	2,137	60	2.8
	Mute Swan (*Cygnus olor*)	1,597	20	1.3
	Whooping Swan (*Cygnus cygnus*)	930	14	1.5
Gulls	9 species	14,505	199	1.4
	Ring-billed gull (*Larus delawarensis*)	6,966	136	2.0
	Black-tailed Gull (*Larus crassirostris*)	1,726	17	1.0
	Black-headed Gull (*Larus ridibundus*)	770	17	2.2
	Herring Gull (*Larus argentatus*)	768	11	1.4
	Mew Gull (*Larus canus*)	595	0	0.0
Terns	9 species	2,521	24	0.9
	Common Tern (*Sterna hirundo*)	961	16	1.7
Waders	10 species	2,637	21	0.8
Rails	3 species	1,962	27	1.4
	Eurasian Coot (*Fulica atra*)	1,861	23	1.2
Petrels	5 species	1,416	4	0.3
	Wedge-tailed Shearwater (*Puffinus pacificus*)	794	4	0.5
Cormorants	1 species	4,500	18	0.4
	Great Cormorant (*Phalacrocorax carbo*)	4,500	18	0.4

Little is known about the prevalence of influenza viruses in wild ducks in the Southern Hemisphere or potential transmission between the hemispheres. There is little connectivity between northern and southern Anatidae species, and most species stay year round within each breeding continent. The Blue-winged Teal (*Anas discors*) is one of the few North American species that has a winter distribution that includes South America (Fig. 1C) (*6*). There are several other duck species that could serve as hosts for influenza virus in South America (*6*), but surveillance data are not available. Similarly, only 6 of 39 Anatidae species breeding in Eurasia winter with at least part of the population south of the Sahara desert in Africa, e.g., the Garganey (*Anas querquedula*) (Fig. 1C) and the Northern Pintail *(Anas acuta)*, each have African winter populations in excess of one million birds (*16*). As in South America, none of the 22 Anatidae species that breed in sub-Saharan Africa spend the nonbreeding season outside the continent. However, there are several species with large, widespread populations in Africa (*16*), and some migrate within Africa (*17*). Potential areas for mixing of Eurasian and African ducks are in West Africa, near the Senegal and Niger Rivers, the floodplains of the Niger River in Nigeria and Mali, and Lake Chad (*16*), and influenza viruses in African Anatidae populations may thus be linked to Eurasia through migrating species. Anatidae of Oceania are mainly resident and do not perform regular seasonal migrations (*6*).

Influenza Viruses in Gulls and Terns

The first recorded isolation of influenza virus from wild birds was from a Common Tern (*Sterna*

hirundo) in 1961. This HPAI H5N3 virus was responsible for an outbreak in South Africa where at least 1300 of these birds died (*3*). The most frequently detected LPAI virus subtype in gulls is H13, a subtype rarely found in other birds. Recently, a "novel" virus subtype (H16), related to H13, was described in Black-headed Gulls (*Larus ridibundus*) in Sweden. The genes of H13 and H16 viruses are genetically distinct from those of influenza viruses from other hosts, which suggests they have been genetically isolated for sufficient time to allow genetic differentiation (*2*). This concurs with the observation that gull influenza viruses do not readily infect ducks when they are inoculated experimentally (*1*). Although other influenza virus subtypes are also occasionally detected in terns and gulls (Table 1) (*5*), it is plausible that the viruses that are genetically indistinguishable from viruses of other avian hosts are most likely not endemic in gulls and terns.

Influenza viruses can be detected in a small proportion of gulls, with the highest virus prevalence reported in late summer and early fall. Most gull species breed in colonies (*6*), with adults and juveniles crowded in a small space, creating good opportunities for virus spread. This situation contrasts with that in dabbling ducks that do not breed in dense colonies (*6*), and epizootics could be more easily initiated when birds congregate in large numbers during molt, migration, or wintering.

Influenza Viruses in Waders

Waders in the Charadriidae and Scolopacidae families are adapted to either marine or freshwater wetland areas and often live side-by-side with ducks (*18*). Long-term influenza virus surveillance studies are still sparse, but data from North America suggest a distinct role of these birds in the perpetuation of certain virus subtypes. Influenza viruses of subtypes H1 to H12 have been isolated in birds migrating through the eastern U.S.A., with a high prevalence of certain HA subtypes (H1, H2, H5, H7, H9 to H12) and a larger variety of HA/NA combinations as compared with ducks in Canada, suggesting that waders maintain a wider spectrum of viruses. Moreover, the seasonal prevalence of influenza viruses in waders seems to be reversed as compared with ducks, with higher virus prevalence (~14%) during spring migration (*19*). This has led to the hypothesis that different families of wetland birds are involved in perpetuation of LPAI virus and suggests a role for waders, which may carry the virus north to the duck breeding grounds in spring. Recent genetic analyses have not revealed striking differences between influenza viruses from ducks and waders in the Americas, suggesting that these viral gene pools are not separated (*20*, *21*). Although the wader-duck link may be a plausible scenario based on the North American data, studies in waders in Northern Europe have failed to produce similar results. Nevertheless, many wader species of the Northern Hemisphere are long-distance intercontinental migrants (*8*) and may, therefore, have the potential to distribute influenza viruses around the globe.

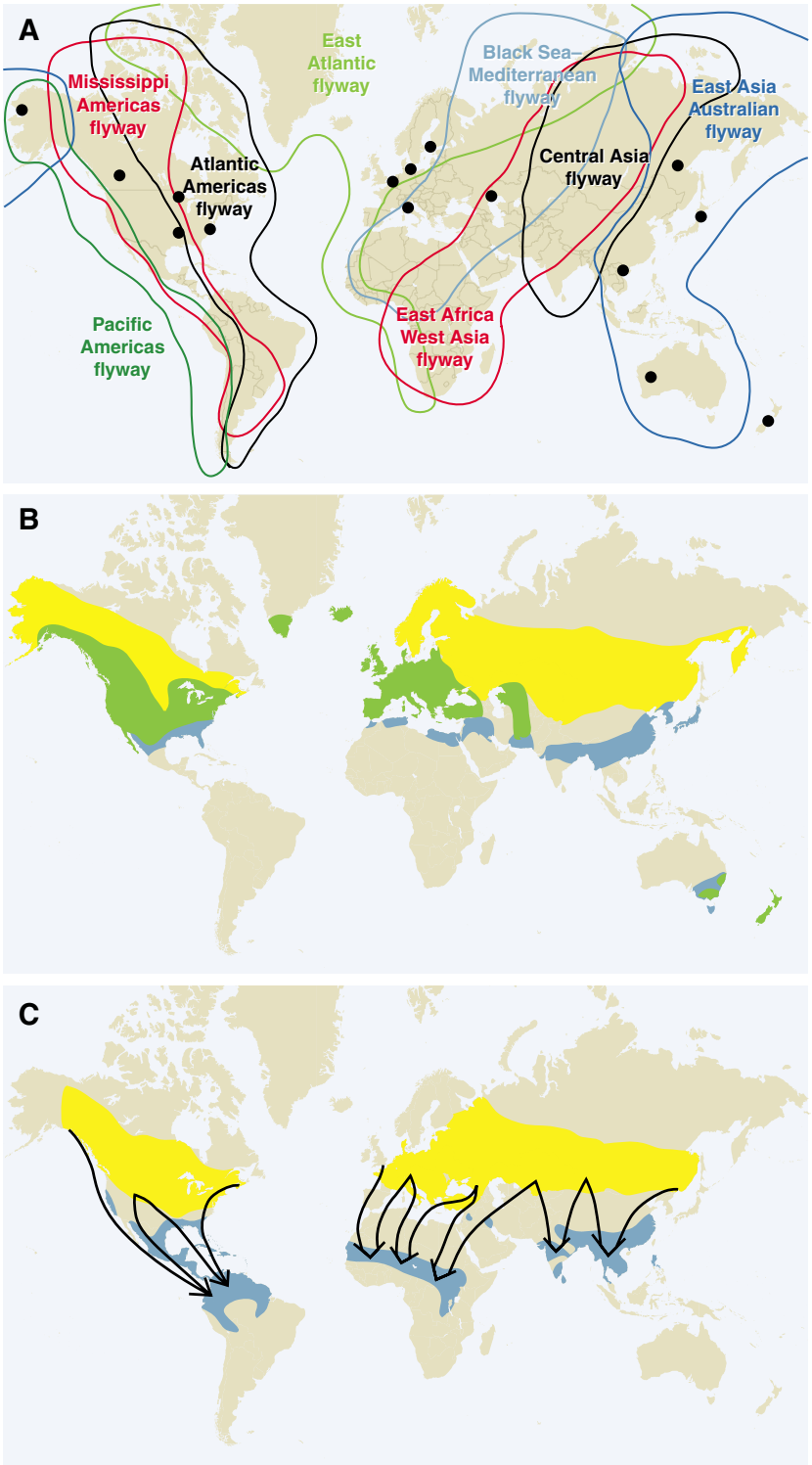

Fig. 1. Migratory flyways of wild bird populations. A world map with the main general migratory flyways of wild bird populations is shown (adapted from information collected and analyzed by Wetlands International). (**A**) Black dots indicate the locations of historical and current influenza virus surveillance sites from which data have been used in this manuscript. These global migration flyways are simplifications, and there are situations where populations behave differently from the common patterns. Migration patterns of Mallard (*Anas platyrhynchos*) (**B**) and Garganey (*Anas querquedula*) in Eurasia and Africa and Blue-winged Teal (*Anas discors*) in the Americas (**C**) (right and left parts of the map, respectively) are provided. Yellow color indicates breeding areas in which species are absent during winter, green indicates areas in which species are present around the year, and blue indicates areas in which species are only present in winter and do not breed. Arrows indicate the seasonal migration patterns.

Influenza Viruses in Other Wild Birds

LPAI viruses can be found in numerous other bird species (Table 1) (*5*), but it is unclear in which of these species influenza viruses are endemic and in which the virus is a temporary pathogen. Species in which influenza viruses are endemic share the same habitat at least part of the year with other species in which influenza viruses are frequently detected, including geese, swans, rails, petrels, and cor-

morants. In these birds and others (*5*), influenza virus prevalence seems to be lower than in dabbling ducks (Table 1), but it should be noted that studies on these species are limited, and it is possible that peak prevalence has been missed because of its seasonal nature or location.

As for ducks, gulls, and waders, their behavior and ecology may be an important determinant of their role as host species. For instance, geese are mainly herbivorous and often congregate in large flocks for grazing in pastures and agricultural fields, especially during the nonbreeding season. Such flocks may reach tens of thousands of birds in optimal areas and often contain several different species. Colonial breeding occurs in some goose species, but most are solitary nesters or nest in loose groups with little interaction between pairs. Given that wild geese and ducks are the ancestors of today's domestic goose and duck species and that these domestic animals in parts of the world are frequently kept alongside chickens, wild geese and ducks may form the bridge for influenza viruses between wild and domestic birds.

Genetic Variation of Influenza Viruses in Wild Birds

Evolution of avian influenza viruses in their natural hosts is slow, but not negligible. Avian influenza viruses can be divided into two lineages, Eurasian and American (Fig. 2), probably as a result of long-term ecological and geographical separation of hosts. However, the avifauna of North America and Eurasia are not completely separated; some ducks and shorebirds cross the Bering Strait during migration or have breeding ranges that include both the Russian Far East and northwestern North America (*6*). The majority of tundra shorebirds from the Russian Far East winter in Southeast Asia and Australia, but some species winter along the west coast of the Americas (*22*). The overlap in distribution of ducks is not as profound as that of shorebirds, but a few species (e.g., Northern Pintail, *Anas acuta*) are common in both North America and Eurasia (*6*) and could also provide an intercontinental bridge for influenza virus. Indeed, influenza viruses carrying a mix of genes from the American and Eurasian lineages have been isolated, indicating that allopatric speciation is only partial (*23*–*25*). The partial ecological isolation of influenza virus hosts seems sufficient to facilitate divergent evolution of separate gene pools, but allows occasional spillover of gene segments from one gene pool to the other.

Within each genetic lineage, multiple sublineages of viral genes cocirculate, but there appear to be no consistent temporal or spatial correlations. Moreover, genetic data from duck and shorebird influenza virus isolates from the Americas suggest an active interplay between these host species (*20*, *21*). Although certain HA subtypes are reported to be more prevalent in either shorebirds or ducks in North America, this also does not seem to have resulted in differences in the genetic composition of influenza viruses obtained from these two reservoirs (*19*, *26*).

The segmented nature of the influenza virus genome enables evolution by a process known as genetic reassortment, i.e., the mixing of genes from two or more influenza viruses. A recent study of 35 influenza virus isolates obtained from ducks in Canada indicates that genetic "sublineages" do not persist, but frequently reassort with other viruses (*27*). Influenza viruses of a particular subtype do not necessarily have the same genetic make-up, even within a single year or a single host species. The high prevalence of influenza virus in some wild bird species and the sporadic detection of concomitant infections in single birds (*15*) support the notion that reassortment may occur in nature. Gaining information on the actual frequency of reassortment in the wild bird reservoir and the impact of these events on LPAI virus evolution will be of considerable interest.

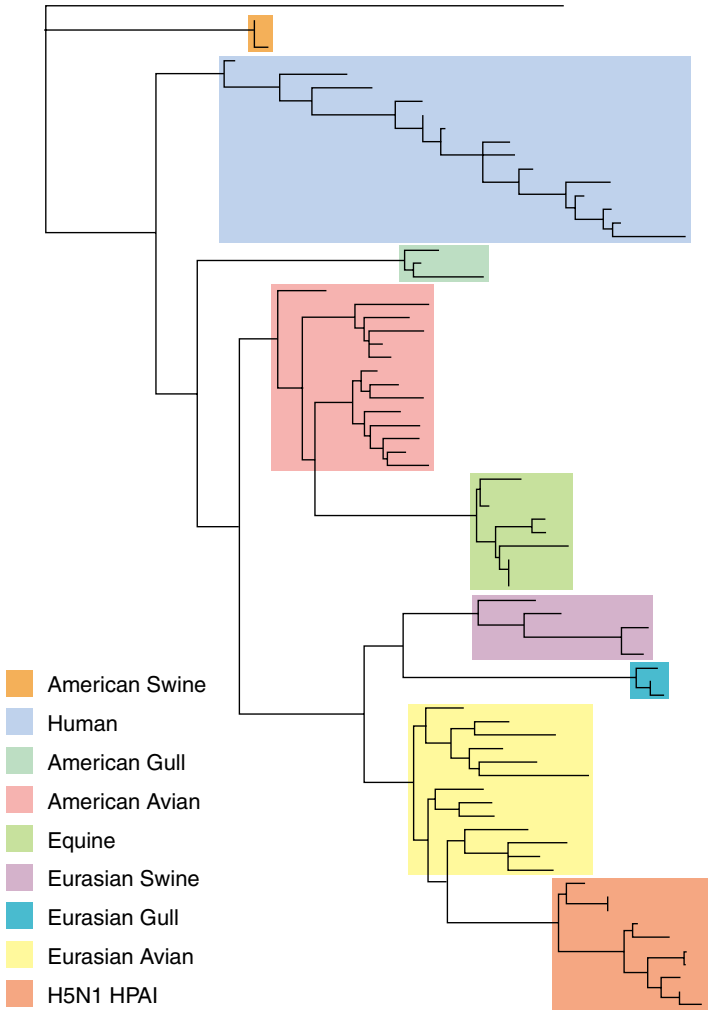

Fig. 2. Phylogenetic tree for the matrix gene of influenza A viruses from a variety of hosts. Nucleotide sequences were selected from public databases and aligned, after which a maximum likelihood tree was generated using influenza virus A/Equine/Prague/57 (H7N7) as outgroup. Sequences were selected from each host to reflect the longest possible time frame and variation in locations of virus isolation. The avian influenza viruses are divided in an American lineage (pink) and a Eurasian lineage (yellow), and there are no clear patterns of host, temporal, or spatial correlation within these lineages. In contrast, the human influenza A virus lineage (light blue), the Eurasian swine lineage (purple), and the HPAI H5N1 lineage (orange) display clear temporal patterns of virus evolution.

HPAI H5N1 Viruses in Wild Birds

In 1997, an HPAI outbreak caused by H5N1 influenza virus occurred in chicken farms and the live bird markets of Hong Kong, which also resulted in the first reported case of human influenza and fatality attributable directly to avian influenza virus (*28*). The H5N1 HPAI virus reappeared in 2002 in waterfowl at two parks in Hong Kong and was also detected in other captive and wild birds (*29*). It resurfaced again in 2003 and has devastated the poultry industry in large parts of Southeast Asia since 2004. In 2005, the virus was isolated during an outbreak among migratory birds in Qinghai Lake, China, affecting large numbers of wild birds (*30*). This single epizootic caused an estimated 10% decrease of the global population of Bar-headed Geese (*Anser indicus*), highlighting the potential devastating effects on vulnerable wildlife. Subsequently, the virus has appeared across Asia, Europe and the Middle East, and in several African countries. Wild bird deaths have been reported in several of these countries, in Europe, particularly affecting Mute Swans (*Cygnus olor*) and Whooper Swans (*Cygnus cygnus*), but mortality has also been recorded in other waterfowl species, and occasionally in raptors, gulls, and herons. So far, the HPAI H5N1 strain that originated in poultry in Southeast Asia has caused mortality in >60 wild bird species (*29*–*31*). In addition, during the devastating outbreaks in poultry, the H5N1 virus was transmitted to 175 humans, leading to 95 deaths (as of 6 March 2006), and has also

been isolated from pigs, cats, tigers, and leopards.

It is most likely that the H5N1 virus has circulated continuously in domestic birds in Southeast Asia since 1997 and, as a consequence, has evolved substantially (Fig. 2). Surveillance studies in Mainland China from 1999 onward indicated that H5N1 viruses have become endemic in domestic birds in the region and that multiple genetic lineages of the virus are cocirculating (*32*, *33*). Poultry trade and mechanical movement of infected materials are likely modes for spreading HPAI in general (*3*). For the H5N1 virus, it is without doubt that domestic waterfowl, specific farming practices, and agroecological environments played a key role in the occurrence, maintenance, and spread of HPAI for many affected countries (*34*, *35*). Although numerous wild birds have also become infected, it has been much debated whether they play an active role in the geographic spread of the disease. It has been argued that infected birds would be too severely affected to continue migration and thus unlikely to spread the H5N1 virus. Although this may be true for some wild birds, it has been shown that, in experimental infections, several bird species survive infection and shed the H5N1 virus without apparent disease signs (*31*, *32*, *36*). In addition, many wild birds may be partially immune owing to previous exposures to LPAI influenza viruses, as has been shown for chickens (*37*). Finally, recent studies suggest that HPAI viruses may become less pathogenic to ducks infected experimentally, while retaining high pathogenicity for chickens (*32*, *36*, *38*). The present situation in Europe, where infected wild birds have been found in several countries that have not reported outbreaks among poultry, suggests that wild birds can indeed carry the virus to previously unaffected areas. Although swan deaths have been the first indicator for the presence of the H5N1 virus in several European countries, this does not necessarily imply a role as predominant vectors; they could merely have functioned as sentinel birds infected via other migrating bird species.

Prospects

Despite the relatively intense surveillance studies that have been performed for many years in North America and Eurasia, our understanding of the global distribution of LPAI viruses in wild bird populations is still limited. Serological evidence indicates that influenza viruses occasionally circulate in Antarctica (*39*), and it is reasonable to assume that influenza viruses are distributed globally, wherever competent host species are present. It is possible that some subtypes are rare or not detected annually in current surveillance studies. Simply because of the limitations of our studies, we are currently biased toward species that are easy to sample during migration or wintering. Second, to understand the global patterns of LPAI viruses in wild birds, it will be crucial to integrate virus and host ecology with long-term surveillance studies to provide more insight on the year-round perpetuation of influenza viruses in wild birds. Possible intercontinental contacts among ducks and shorebirds in areas where migrating birds from the northern and southern latitudes mix are of particular interest. Can influenza viruses be perpetuated in ducks alone, or does the interface between ducks and shorebirds, as seems to occur in North America (*19*), also occur on other continents? With high-throughput sequencing technology, it should be possible to gain more insight into the genetic variability and evolution of LPAI viruses in wild birds and to integrate this information with epidemiology and virus-host ecology.

The recent H5N1 outbreaks in Eurasia have identified additional gaps in our knowledge of avian influenza viruses in wild birds in general. It should be realized that our knowledge of LPAI viruses in wild birds cannot simply be extrapolated to HPAI viruses; for instance, the most important host species or routes of transmission may be quite different (Table 1) (*29*–*31*, *38*). It is clear that influenza virus surveillance of wild birds could provide "early warning" signals for the introduction of HPAI H5N1 virus in new regions and may provide access to strains for characterization. For proper risk assessment studies, however, we also need a better understanding of the interface between wild and domestic birds, the possible transmission of influenza viruses between these populations, bird behavior, age-structures of populations, and detailed migration routes. We further need better understanding of the transmission and pathogenesis of H5N1 virus in wild birds, as well as identification of virus-permissive host species and their relative likelihood to develop disease, patterns of virus secretion, and temporal and spatial variations in virus prevalence.

With our current limited knowledge on HPAI in wild birds, there is no solid basis for including wild birds in control strategies beyond the physical separation of poultry from wild birds. Even in areas with significant outbreaks in poultry, virus prevalence in wild birds is low (*32*), and the role of these wild birds in spreading the disease is unclear. It is clear that the H5N1 problem originated from outbreaks in poultry and that the outbreaks and their geographical spread probably cannot be stopped without implementation of proper control measures in the global poultry industry. However, there is at present no scientific basis for culling wild birds to control the outbreaks and their spread, and this is further highly undesirable from a conservationist perspective.

The current increased interest in influenza virus surveillance in wild and domestic birds provides a unique opportunity to increase our understanding not only of HPAI epidemiology but also of the ecology of LPAI viruses in their natural hosts, at the same time and for the same cost.

References and Notes

1. R. G. Webster, W. J. Bean, O. T. Gorman, T. M. Chambers, Y. Kawaoka, *Microbiol. Rev.* **56**, 152 (1992).
2. R. A. M. Fouchier *et al.*, *J. Virol.* **79**, 2814 (2005).
3. D. J. Alexander, *Vet. Microbiol.* **74**, 3 (2000).
4. V. J. Munster *et al.*, *Emerg. Infect. Dis.* **11**, 1545 (2005).
5. Table S1 and references are available as supporting material on *Science* Online.
6. J. Del Hoyo, A. Elliot, J. Sargatal, Eds., *Handbook of the Birds of the World* (Lynx Edicions, Barcelona, 1996), vols. 1 and 3.
7. R. G. Webster, M. Yakhno, V. S. Hinshaw, W. J. Bean, K. G. Murti, *Virology* **84**, 268 (1978).
8. J. van de Kam, B. Ens, T. Piersma, L. Zwarts, *Shorebirds: An Illustrated Behavioural Ecology* (KNNV Publishers, Utrecht, Netherlands, 2004).
9. T. Alerstam, A. Lindstrom, in *Bird Migration: Physiology and Ecophysiology*, E. Gwinner, Ed. (Springer-Verlag, Berlin, 1990), pp. 331–351.
10. K. Okazaki *et al.*, *Arch. Virol.* **145**, 885 (2000).
11. B. A. Hanson, D. E. Stallknecht, D. E. Swayne, L. A. Lewis, D. A. Senne, *Avian Dis.* **47**, 867 (2003).
12. P. Rohani, D. J. Earn, B. T. Grenfell, *Science* **286**, 968 (1999).
13. D. C. Nguyen *et al.*, *J. Virol.* **79**, 4201 (2005).
14. H. Kida, R. Yanagawa, Y. Matsuoka, *Infect. Immun.* **30**, 547 (1980).
15. G. B. Sharp *et al.*, *J. Virol.* **71**, 6128 (1997).
16. D. A. Scott, P. M. Rose, *Atlas of Anatidae Populations in Africa and Western Eurasia* (Publ. no. 41, Wetlands International, Wageningen, Netherlands, 1996).
17. L. H. Brown, E. K. Urban, K. Newman, *The Birds of Africa* (Academic Press, London, 1982), vol. 1.
18. T. Piersma, *Oikos* **80**, 623 (1997).
19. S. Krauss *et al.*, *Vector Borne Zoonotic Dis.* **4**, 177 (2004).
20. L. Widjaja, S. L. Krauss, R. J. Webby, T. Xie, R. G. Webster, *J. Virol.* **78**, 8771 (2004).
21. E. Spackman *et al.*, *Virus Res.* **114**, 89 (2005).
22. R. E. Gill, R. W. Butler, P. S. Tomkovich, T. Mundkur, C. M. Handel, *Trans. North Am. Wildlife Nat. Resources Conf.* **59**, 63 (1994).
23. A. Wallensten *et al.*, *Arch. Virol.* **150**, 1685 (2005).
24. N. V. Makarova, N. V. Kaverin, S. Krauss, D. Senne, R. G. Webster, *J. Gen. Virol.* **80**, 3167 (1999).
25. J. H. Liu *et al.*, *Virus Genes* **29**, 81 (2004).
26. J. C. Obenauer *et al.*, *Science* **311**, 1576 (2006).
27. T. F. Hatchette *et al.*, *J. Gen. Virol.* **85**, 2327 (2004).
28. J. C. de Jong, E. C. Claas, A. D. Osterhaus, R. G. Webster, W. L. Lim, *Nature* **389**, 554 (1997).
29. T. M. Ellis *et al.*, *Avian Pathol.* **33**, 492 (2004).
30. J. Liu *et al.*, *Science* **309**, 1206 (2005).
31. K. M. Sturm-Ramirez *et al.*, *J. Virol.* **78**, 4892 (2004).
32. H. Chen *et al.*, *Proc. Natl. Acad. Sci. U.S.A.* (2006).
33. K. S. Li *et al.*, *Nature* **430**, 209 (2004).
34. V. Martin *et al.*, *Dev. Biol.* **124**, 23 (2006).
35. M. Gilbert *et al.*, *Emerg. Infect. Dis.* **12**, 227 (2006).
36. D. J. Hulse-Post *et al.*, *Proc. Natl. Acad. Sci. U.S.A.* **102**, 10682 (2005).
37. S. H. Seo, M. Peiris, R. G. Webster, *J. Virol.* **76**, 4886 (2002).
38. K. M. Sturm-Ramirez *et al.*, *J. Virol.* **79**, 11269 (2005).
39. F. J. Austin, R. G. Webster, *J. Wildl. Dis.* **29**, 568 (1993).

40. We apologize to the scientists whose original contributions have not been cited here due to space restrictions. We thank G. Rimmelzwaan, D. Smith, T. Piersma, J. de Jong, and E. de Wit for fruitful discussions and helpful comments.

Supporting Online Material

www.sciencemag.org/cgi/content/full/312/5772/384/DC1
Table S1
References and Notes

10.1126/science.1122438

PERSPECTIVE

Emergence of Drug-Resistant Influenza Virus: Population Dynamical Considerations

Roland R. Regoes and Sebastian Bonhoeffer*

Given the considerable challenges to the rapid development of an effective vaccine against influenza, antiviral agents will play an important role as a first-line defense if a new pandemic occurs. The large-scale use of drugs for chemoprophylaxis and treatment will impose strong selection for the evolution of drug-resistant strains. The ensuing transmission of those strains could substantially limit the effectiveness of the drugs as a first-line defense. Summarizing recent data on the rate at which the treatment of influenza infection generates resistance de novo and on the transmission fitness of resistant virus, we discuss possible implications for the epidemiological spread of drug resistance in the context of an established population dynamic model.

Two classes of drugs are currently available for chemoprophylaxis and treatment of influenza. The neuraminidase (NA) inhibitors oseltamivir (brand name Tamiflu) and zanamivir (brand name Relenza) impair the efficient release of virus from infected cells. The M2 protein inhibitors amantadine (known under several brand names) and rimantadine (brand name Flumadine) target the viral M2 protein, which is required for efficient uncoating of the virus inside the cell. The NA inhibitors are effective against all NA subtypes of influenza, whereas the M2 inhibitors are effective only against influenza A virus (*1*).

In the absence of transmitted drug resistance, the efficacy of chemoprophylaxis is comparable to that of vaccines. The efficacy of vaccines in preventing laboratory-confirmed illness is around 80% in children and adults but is substantially lower in elderly people and depends on how well the vaccine matches the antigenic characteristics of the circulating virus. The efficacy of prophylaxis with amantadine against the development of illness is around 80 to 90% during interpandemic influenza (*2*, *3*) but may be only 60 to 70% for pandemic influenza (*4*). Among NA inhibitors, only oseltamivir is approved for chemoprophylaxis, but both types of NA inhibitors have been shown to be similarly effective (zanamivir, 84%; oseltamivir, 82%) (*5*). Thus, if available in sufficient quantities, anti-influenza drugs could play an important role as a first-line defense in the case of a new pandemic.

Institute of Integrative Biology, ETH Zürich, ETH Zentrum CHN K12.1, Universitätsstrasse 16, CH 8092 Zürich, Switzerland.

*To whom correspondence should be addressed. E-mail: sebastian.bonhoeffer@env.ethz.ch

The typical course of influenza is self-limiting and lasts for about a week. Antiviral treatment has only a moderate effect on shortening the infection. Aggregate analysis of a large number of trials shows that the time to alleviation of symptoms is shortened by 1 day by M2 inhibitors (*6*) and by 1.3 days by NA inhibitors (*7*). However, treatment of patients within the first 30 hours of the onset of symptoms can lead to a more substantial reduction of the time to alleviation of symptoms (*8*).

High-level drug resistance to both types of inhibitors is typically conferred by single amino acid substitutions in the M2 protein and the NA (*9*, *10*). Mutations conferring resistance to M2 inhibitors generally provide full cross-resistance to both amantadine and rimantadine (*11*), whereas several mutations conferring resistance to NA inhibitors are drug-specific (*12*).

Two key factors affect the epidemiology of drug resistance in influenza. The first factor is the rate at which treatment generates resistance de novo. M2 inhibitor–resistant mutants have been reported to occur in about 30% of treated patients (*5*), but the estimates may be even higher if more rigorous detection techniques are used (*13*). Until recently, it seemed that de novo resistance against NA inhibitors occurs only rarely. Resistance against zanamivir has been found only in one immunocompromised child (*14*), whereas resistance against oseltamivir was found in 0.7 to 4% (*15*, *16*) of adults and in 4 to 8% of children (*15*, *17*). However, a more recent study found resistant isolates in 18% of oseltamivir-treated children (*18*).

The second factor is the fitness costs associated with drug resistance mutations. Studies of the transmission of amantadine-resistant virus in birds in the absence of the drug suggest that M2 inhibitor resistance mutations incur no or little cost in terms of transmissibility and pathogenicity (*19*). Moreover, M2 inhibitor–resistant mutants have been shown to be transmissible in humans (*2*). Several studies suggest that resistance to NA inhibitors typically involves high fitness costs (*20*–*22*), nourishing the hope that in comparison to M2 inhibitors, resistance against NA inhibitors will be less of an epidemiological concern (*23*, *24*). However, recent studies in ferrets show that transmission and growth characteristics vary substantially between different oseltamivir-resistant mutants (*25*). Although the $Arg^{292}\rightarrow Lys^{292}$ (R292K) and $His^{274}\rightarrow Tyr^{274}$ (H274Y) mutations in NA were associated with substantially impaired growth and transmission (*21*, *26*), the $Glu^{119}\rightarrow Val^{119}$ (E119V) mutant displayed growth and transmissibility similar to that of wild-type virus (*25*), demonstrating that fitness costs for resistance to NA inhibitors need not be high. Moreover, it is conceivable that with increased use of NA inhibitors, compensatory mutations could arise that restore fitness without affecting drug resistance.

Despite the high level of de novo resistance and the apparently low transmissibility cost of resistance mutations for M2 inhibitors, resistance among circulating isolates was generally rare until 5 years ago (approximately 1 to 2% of isolates globally) (*3*). However, over the recent years, resistance to M2 inhibitors has grown rapidly. In 2004, 12% of globally collected isolates were resistant [with 70 to 74% of isolates being resistant in Hong Kong or China (*3*)]. During the initial months of the 2005/2006 influenza season in the United States, 92% of the H3N2 isolates tested were resistant (*27*). This rapid rise of M2 inhibitor resistance is presumably due to high rates of de novo resistance and low transmission fitness costs. Therefore, the recent findings regarding NA inhibitors that de novo resistance may be higher and fitness costs may be lower than previously thought raise justifiable concerns that the extensive use of NA inhibitors may induce a greater resistance problem than anticipated so far.

Epidemiologists frequently use the concept of the basic reproductive number, R_0, as a measure of the transmission fitness of an infectious pathogen (*28*). R_0 is defined as the expected number of secondary cases generated by the primary case in a wholly susceptible population. Consequently, a pathogen with $R_0 < 1$ cannot sustain transmission, and thus an epidemic caused by such a pathogen would inevitably die out. Estimates of

R_0 for pandemic influenza strains range from 1.8 to 3 for the 1918 Spanish flu (*29*, *30*) and are around 1.9 for the H3N2 pandemic (*31*). Clearly, the R_0 of a novel pandemic strain cannot be predicted, but it is conceivable that a novel strain would at least initially be poorly adapted for human-to-human transmission and hence that its R_0 would be only marginally larger than 1. On the other hand, such a strain could rapidly acquire higher values of R_0 after only a few rounds of transmission (*32*). Considering that treatment leads to only a modest shortening of the course of disease, it is highly unlikely that a new pandemic could be contained solely by treatment of symptomatic individuals. Indeed, detailed computer simulations modeling the outbreak of pandemic influenza in Southeast Asia suggest that even with targeted prophylaxis, a pandemic can only be contained if $R_0 < 1.6$ to 1.8 (*29*, *33*).

Given that a large number of individuals will need treatment or prophylaxis in the case of a new pandemic, it is relevant to study the rise of resistance under conditions of high drug selection pressure. Mathematical models have been used to study the epidemiology of drug resistance for both amantadine (*34*), and oseltamivir (*23*) treatment, but these models have not accounted for the recently described higher de novo resistance rates and low transmission fitness costs of oseltamivir-resistant mutants. To illustrate some general principles of the effects of treatment and prophylaxis, we show simulation results based on a model developed by Stilianakis *et al*. (*34*), adapted here to model interventions with oseltamivir (Fig. 1). This model describes the dynamics of resistance in a closed population, such as a school or a nursing home, and thus allows analysis of the effects of drug intervention for the control of small epidemic foci. A detailed description of the simulations is provided in the supporting online material (SOM) (*35*).

In the following discussion, we use the term "prophylaxis" to describe the use of prophylaxis in addition to treatment. Figure 1A shows a simulated local outbreak in a closed population of 500. For the chosen parameters, the simulation shows that using prophylaxis in addition to treatment reduces both the total number of infected cases and the absolute number of resistant cases. However, prophylaxis increases the fraction of resistant cases (Fig. 1B). Figure 2, A and B, shows the fraction of resistant cases accumulated over the entire outbreak as a function of the rate at which treatment generates de novo resistance and the relative transmission fitness of resistant and sensitive virus. The simulations shown in Fig. 2A suggest that

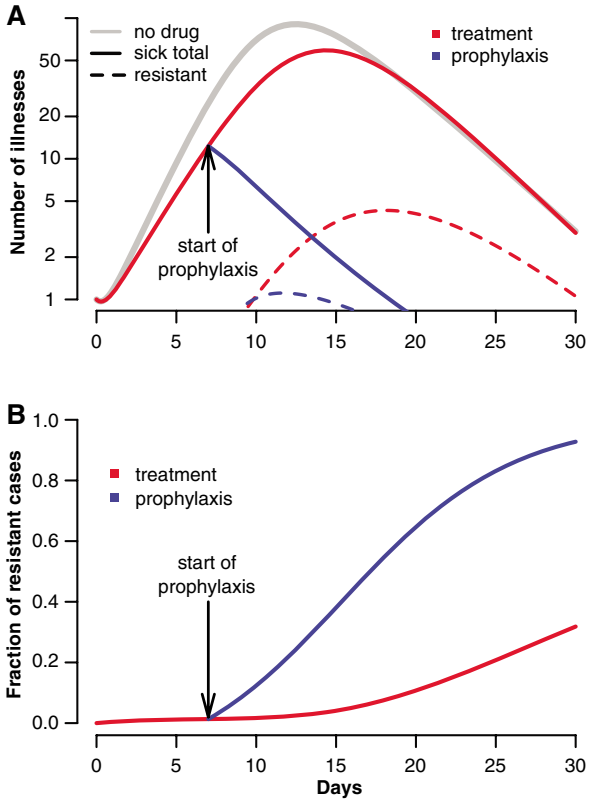

Fig. 1. Epidemic curves as predicted by the model of Stilianakis *et al*. (*34*) for parameters characterizing interventions with oseltamivir. [For model equations and parameter values, see the SOM (*35*).] (**A**) Number of infected individuals using treatment only (red) or using prophylaxis in addition to treatment (blue) over the first 30 days of the epidemic. The gray line shows the course of the epidemic without any intervention. The solid lines depict the total number of infected individuals, whereas the dashed lines depict the number of individuals infected with resistant virus. The total number of illnesses during the 30-day period is 247, 227, or 26 in the epidemic with no intervention, with treatment, or with prophylaxis, respectively. (We assume that there is no pre-existing immunity in the population.) All symptomatic individuals receive treatment on average 1.4 days after the onset of symptoms. Prophylaxis starts at day 7. (**B**) Fraction of individuals infected with resistant virus under treatment (red) and prophylaxis (blue).

when only symptomatic individuals are treated, the fraction of resistant cases increases only slowly with both increasing rate of de novo resistance and increasing levels of relative transmission fitness. The reason is that treatment has only a moderate effect in terms of shortening the period of viral shedding, and therefore its effect on the transmission fitness of the sensitive strain is limited. Sensitive virus spreads rapidly in the unprotected population and interferes with the transmission of resistant virus, because individuals who are or have been infected with sensitive virus are protected against infection by resistant virus. However, if prophylaxis is used in addition to treatment, then changes in the rate of de novo resistance and the relative transmission fitness have markedly different effects (Fig. 2B). Although the fraction of resistant cases increases only slowly with increasing rate of de novo resistance, small changes in relative transmission fitness can lead to a substantial increase of the fraction of resistant cases. The reason for this abrupt increase is that once the resistant strain has sufficiently high transmission fitness (that is, once it has an $R_0 > 1$), it can generate a self-sustaining epidemic in the population receiving prophylaxis (fig. S2). In this case, using prophylaxis in addition to treatment leads to a marked increase in resistance in terms of both the fraction (Fig. 2B) and the absolute number (fig. S1) of resistant cases.

Prophylaxis has two important effects on the epidemiology of resistance. First, prophylaxis has a more pronounced effect than treatment on the relative transmission fitness, because it greatly reduces the number of individuals susceptible to the sensitive strain. Second, prophylaxis reduces the competitive interference between sensitive and resistant strains, because only resistant virus can infect individuals receiving prophylaxis. The simulations illustrate the critical role of transmission fitness in determining the epidemiology of resistance. If the transmission fitness of the resistant virus is sufficiently low, then prophylaxis will reduce the incidence of resistance. Conversely, if the transmission fitness of the resistant strain is high, then prophylaxis will enhance the spread of resistance, in contrast to the common notion that treatment but not prophylaxis generates resistance.

The mathematical model discussed here was developed to describe epidemiological data from a small outbreak in a boarding school in 1978 (*34*). To extrapolate the above points to a pandemic, we need to consider the limitations of the model. First, the model assumes a single well-mixed homogeneous

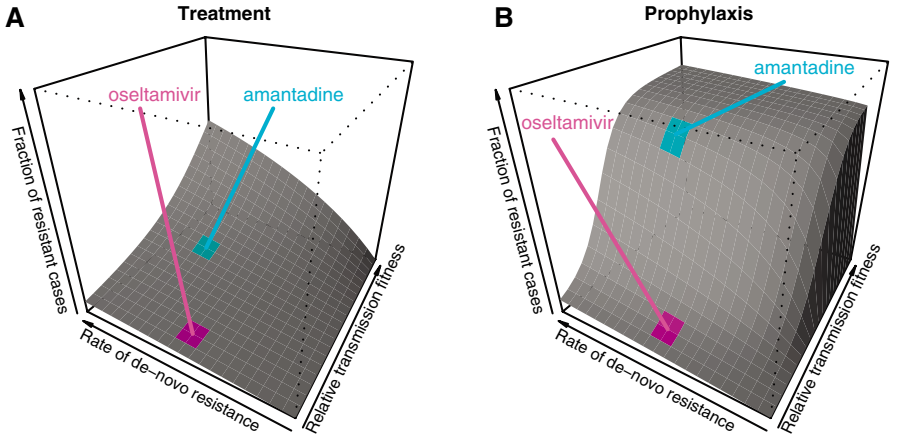

Fig. 2. Fraction of resistant cases as a function of the relative transmission fitness of resistant virus and the rate at which treatment generates de novo resistance with (**A**) treatment of symptomatic individuals and (**B**) prophylaxis in addition to treatment. The top of the *z* axis corresponds to 100%, which is the theoretical maximum. The relative transmission fitness ranges from 0 to 1, and the rate of de novo resistance ranges from 0 to 0.072 per day. For other parameters, see the SOM (*35*). The most likely parameter ranges for oseltamivir (violet) and amantadine (cyan) are indicated on the resistance surfaces. (For oseltamivir, these are also the parameters used in Fig. 1.) Because of our rudimentary knowledge with regard to these parameters, these ranges need to be regarded with caution.

population rather than a network of interconnected heterogeneous subpopulations, as would be more appropriate to model a large-scale outbreak. However, the threshold behavior when resistant virus is capable of causing a self-sustaining epidemic (Fig. 2B and fig. S2) has also been observed in models with a more complex population structure (*23*). Second, the model makes the simplifying assumption that all individuals in the population receive prophylaxis. In a pandemic, prophylaxis will be targeted only at exposed individuals. However, it is only these individuals that generate a selection pressure for resistance, because individuals who receive prophylaxis but are never exposed will obviously not contribute to the development and spread of resistance. Hence, the simplifying assumption is expected to be of little consequence for the extrapolation to the pandemic situation. However, to go beyond the conceptual points we make here and to quantitatively predict the emergence of resistance will require more detailed models.

Assessing the transmissibility of resistant virus in human infection remains a challenge and currently provides only rough estimates. To date, it is therefore difficult to predict exactly how intensive drug use for treatment and prophylaxis will affect the epidemiology of resistance. Should the R_0 of a new pandemic strain be lower than 2, then a 50% reduction in transmission fitness of the resistant strain would be sufficient to render the resistant virus incapable of causing a self-sustaining epidemic. The observation that resistance to M2 inhibitors has increased substantially in recent years (*3*, *27*) suggests that these strains do indeed have sufficiently high transmission fitness to cause a self-sustaining epidemic. For NA inhibitors, however, the situation is less clear. The more common R292K or H274Y mutations may be associated with sufficiently impaired transmission fitness (*21*, *26*). However, the comparatively high transmissibility of the E119V mutant (*25*) and the possibility of compensatory mutations raise the concern that intense use of NA inhibitors for treatment and prophylaxis could also generate a large number of resistant cases. Unfortunately, taking a broader view of the use of novel anti-infective drugs against microbial pathogens reinforces this concern, because resistance has typically emerged faster than anticipated when the drugs were first introduced (*36*).

To get a better understanding of the consequences associated with the use of antiviral drugs as a first-line defense against a novel pandemic strain, we see a need for further research in two specific areas. (i) Experimental and epidemiological studies need to be intensified to allow a more accurate quantification of the transmission fitness of resistant virus. (ii) Computer models, based on a realistic human population structure, are required to simulate the emergence of resistance at the outset of a pandemic for various scenarios of drug use. Such models would also allow the testing of alternative intervention strategies such as combination therapy/prophylaxis or the use of different drugs for treatment and prophylaxis.

References and Notes

1. A. Moscona, *N. Engl. J. Med.* **353**, 1363 (2005).
2. F. G. Hayden, *Philos. Trans. R. Soc. London Ser. B* **356**, 1877 (2001).
3. R. A. Bright *et al.*, *Lancet* **366**, 1175 (2005).
4. World Health Organization, in *WHO Guidelines on the Use of Vaccines and Antivirals During Influenza Pandemics* (World Health Organization, Geneva, Switzerland, 2004).
5. S. A. Harper, K. Fukuda, T. M. Uyeki, N. J. Cox, C. B. Bridges, *MMWR Recomm. Rep.* **54**, 1 (2005).
6. T. Jefferson, J. J. Deeks, V. Demicheli, D. Rivetti, M. Rudin, *Cochrane Database Syst. Rev.* **2004**, CD001169 (2004).
7. K. G. Nicholson, J. M. Wood, M. Zambon, *Lancet* **362**, 1733 (2003).
8. F. G. Hayden *et al.*, *N. Engl. J. Med.* **337**, 874 (1997).
9. A. J. Hay, in *Antiviral Drug Resistance*, D. D. Richman, Ed. (Wiley, Chichester, UK, 1996), pp. 43–58.
10. L. V. Gubareva, L. Kaiser, F. G. Hayden, *Lancet* **355**, 827 (2000).
11. R. B. Belshe, M. H. Smith, C. B. Hall, R. Betts, A. J. Hay, *J. Virol.* **62**, 1508 (1988).
12. J. McKimm-Breschkin *et al.*, *Antimicrob. Agents Chemother.* **47**, 2264 (2003).
13. K. Shiraishi *et al.*, *J. Infect. Dis.* **188**, 57 (2003).
14. L. V. Gubareva, M. N. Matrosovich, M. K. Brenner, R. C. Bethell, R. G. Webster, *J. Infect. Dis.* **178**, 1257 (1998).
15. H. C. Jackson, N. Roberts, Z. M. Wang, R. B. Belshe, *Clin. Drug Invest.* **20**, 447 (2000).
16. L. V. Gubareva, L. Kaiser, M. N. Matrosovich, Y. Soo-Hoo, F. G. Hayden, *J. Infect. Dis.* **183**, 523 (2001).
17. N. A. Roberts, *Philos. Trans. R. Soc. London Ser. B* **356**, 1895 (2001).
18. M. Kiso *et al.*, *Lancet* **364**, 759 (2004).
19. W. J. Bean, S. C. Threlkeld, R. G. Webster, *J. Infect. Dis.* **159**, 1050 (1989).
20. J. Carr *et al.*, *Antiviral Res.* **54**, 79 (2002).
21. M. L. Herlocher *et al.*, *Antiviral Res.* **54**, 99 (2002).
22. J. A. Ives *et al.*, *Antiviral Res.* **55**, 307 (2002).
23. N. M. Ferguson, S. Mallett, H. Jackson, N. Roberts, P. Ward, *J. Antimicrob. Chemother.* **51**, 977 (2003).
24. A. S. Monto, *Vaccine* **21**, 1796 (2003).
25. H. L. Yen *et al.*, *Antimicrob. Agents Chemother.* **49**, 4075 (2005).
26. M. L. Herlocher *et al.*, *J. Infect. Dis.* **190**, 1627 (2004).
27. R. A. Bright, D. K. Shay, B. Shu, N. J. Cox, A. I. Klimov, *JAMA* **295**, 891 (2006).
28. R. M. Anderson, R. M. May, *Infectious Diseases of Humans* (Oxford Univ. Press, Oxford, 1991).
29. N. M. Ferguson *et al.*, *Nature* **437**, 209 (2005).
30. C. E. Mills, J. M. Robins, M. Lipsitch, *Nature* **432**, 904 (2004).
31. L. A. Rvachev, I. M. Longini, *Math. Biosci.* **75**, 3 (1985).
32. R. Antia, R. R. Regoes, J. C. Koella, C. T. Bergstrom, *Nature* **426**, 658 (2003).
33. I. M. Longini Jr. *et al.*, *Science* **309**, 1083 (2005).
34. N. I. Stilianakis, A. S. Perelson, F. G. Hayden, *J. Infect. Dis.* **177**, 863 (1998).
35. Supporting material is available on *Science* Online.
36. D. L. Heymann, *Cell* **124**, 671 (2006).

37. We gratefully acknowledge R. Antia, F. Débarre, M. Kopf, B. Levin, M. Lipsitch, and A. Trkola for critical reading of the manuscript and valuable discussion and the Swiss National Science Foundation for financial support.

Supporting Online Material

www.sciencemag.org/cgi/content/full/312/5772/389/DC1
SOM Text
Figs. S1 and S2
Tables S1 and S2
Flu-Scripts Compressed Archive
References

10.1126/science.1122947

PERSPECTIVE

Predictability and Preparedness in Influenza Control

Derek J. Smith

The threat of pandemic human influenza looms as we survey the ongoing avian influenza pandemic and wonder if and when it will jump species. What are the risks and how can we plan? The nub of the problem lies in the inherent variability of the virus, which makes prediction difficult. However, it is not impossible; mathematical models can help determine and quantify critical parameters and thresholds in the relationships of those parameters, even if the relationships are nonlinear and obscure to simple reasoning. Mathematical models can derive estimates for the levels of drug stockpiles needed to buy time, how and when to modify vaccines, whom to target with vaccines and drugs, and when to enforce quarantine measures. Regardless, the models used for pandemic planning must be tested, and for this we must continue to gather data, not just for exceptional scenarios but also for seasonal influenza.

Few would be surprised if there were an influenza H5 (bird flu) pandemic in humans. The source and basic mechanisms of the threat are clear, yet there is much we cannot predict: how severe such a pandemic would be, how fast it would spread, where it would start, whether it would become resistant to existing drugs, what strain to use in a vaccine, or whether a vaccine would be available in time to protect a large proportion of the population. Most important, we do not know how close the virus is to sustained human-to-human transmission, and thus to initiating a pandemic.

How can there be this much uncertainty when many of the best virologists, molecular biologists, epidemiologists, and public health scientists work or have worked on the influenza virus, when so much is already known, and when the global surveillance system is better than the system for any other pathogen? The answer lies in the inherent variability of influenza viruses, in their seemingly endless capacity to continue to change, and, in the case of type A viruses, in their rich and diverse ecology in many species and their ability to cross species barriers and adapt to new hosts (*1*, *2*).

An influenza H5 virus capable of causing a pandemic in humans is likely to differ from the avian H5 viruses that have caused a pandemic in birds and have occasionally caused highly pathogenic infections in humans. A human-adapted H5 virus, by definition, should be able to transmit effectively among humans; it might have antigenic differences compared with avian strains and would possibly be less pathogenic in humans. Adaptation to the human host may occur as a result of either mutation or a combination of mutation and reassortment with an existing human virus. A key event would probably be a change in the binding specificity of the virus from a receptor in the lower respiratory tract to one in the upper respiratory tract. This may result in a decrease in at least the initial pathogenicity, as the infection would be more likely to start with a tracheal bronchitis rather than pneumonia (*3*, *4*). In addition, if human adaptation resulted from reassortment with a human virus, pathogenicity factors on gene segments not in the resulting reassortment would be lost, and there may be a degree of prior immunity in the population to the human virus–derived gene segments, both further reducing pathogenicity in humans.

The large possible range for pathogenicity is also evident in the differences in mortality during the three influenza pandemics of the past century: The 1918 pandemic killed an estimated 40 to 50 million people, the 1957 pandemic killed an estimated 2 million people, and the 1968 pandemic an killed an estimated 1 million people.

Despite these uncertainties, national and international public health bodies have to prepare for a potential influenza pandemic. Mathematical and computational methods can provide valuable quantitative information for influenza preparedness in the face of uncertainty. Here, I discuss how such methods are being used to improve preparedness.

The Dynamics of Spread and Effect of Interventions

Because of the delay before a pandemic vaccine will be available, the immediate defenses against pandemic influenza are the neuraminidase-inhibitor antiviral drugs, oseltamivir and zanamivir. The World Health Organization (WHO) has a stockpile of oseltamivir to use in early cases of human-to-human transmissions of a potential pandemic virus to attempt to slow the outbreak and create more time for vaccine production and other preparations. However, the unknowns regarding a potential pandemic virus, including how quickly the virus spreads, the efficacy of the drugs, and the rate of acquisition of drug resistance by the virus, make it difficult to predict how useful a drug stockpiling strategy would be.

A better use of resources may be to pursue alternative routes to vaccine development, vaccine stockpiling, or prepandemic vaccination. Here, mathematical models can be valuable to help decide strategy, particularly for quantifying the variability of possible outcomes for a range of estimates of critical parameters, such as the transmission rate of the virus. Detailed epidemiological models have recently been developed to make quantitative predictions of the spread of an unchecked outbreak (Fig. 1), and how effective an antiviral stockpile could be in slowing or stopping an outbreak before it causes a pandemic (*5*, *6*). Taking Thailand as the scenario, the models show what it would take to stop an outbreak in terms of speed and accuracy of detection, speed of delivery, delivery strategy (contact-based or geographic-based), and the total quantity of drugs required. Thus, if the

Department of Zoology, University of Cambridge, Downing Street, Cambridge, CB2 3EJ, UK and National Influenza Center and Department of Virology, Erasmus Medical Center, Doctor Molewaterplein 50, 3015GE Rotterdam, Netherlands. E-mail: dsmith@zoo.cam.ac.uk

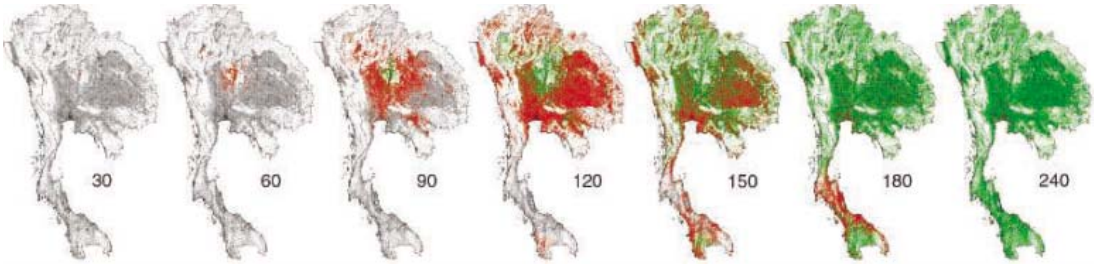

Fig. 1. Expected pattern of spread of an uncontrolled influenza epidemic in Thailand. Time sequence (in days) of an epidemic, showing spread in a single simulation of an epidemic parameterized such that, on average, in a fully susceptible population, each person infects 1.5 others (i.e., $R_0 = 1.5$). Red indicates presence of infected individuals, green the density of people who have recovered from infection or died. [Reprinted from (*5*).]

delivery of antivirals is rapid enough, and the transmission rate of the virus is approximately the same as that observed for previous pandemic viruses, then it should be possible to stop a single outbreak with a realistically sized stockpile of antiviral drugs. The models also predict that for effective control, antiviral prophylaxis would have to be started within about 3 weeks of the first human-to-human transmissions and within 2 days of the onset of a new case after an outbreak is underway; in practice, this would be extremely difficult to achieve in rural Southeast Asia. These examples show how models can reveal weaknesses, inform plans for training, indicate ways of deploying an antiviral stockpile, and estimate its necessary size (*7*). However, it is important to recognize that even if drug intervention were successful, it may only temporarily stall a potential pandemic (*8*).

The Thailand scenario was also used to predict the effect of control measures such as quarantine, restriction of movement, the closing of schools and workplaces, vaccination, and their effects on slowing an outbreak. Likewise, such models can be adjusted for geographic, demographic, and movement patterns in other countries, and be used to update national pandemic preparedness plans before and even during the course of a pandemic.

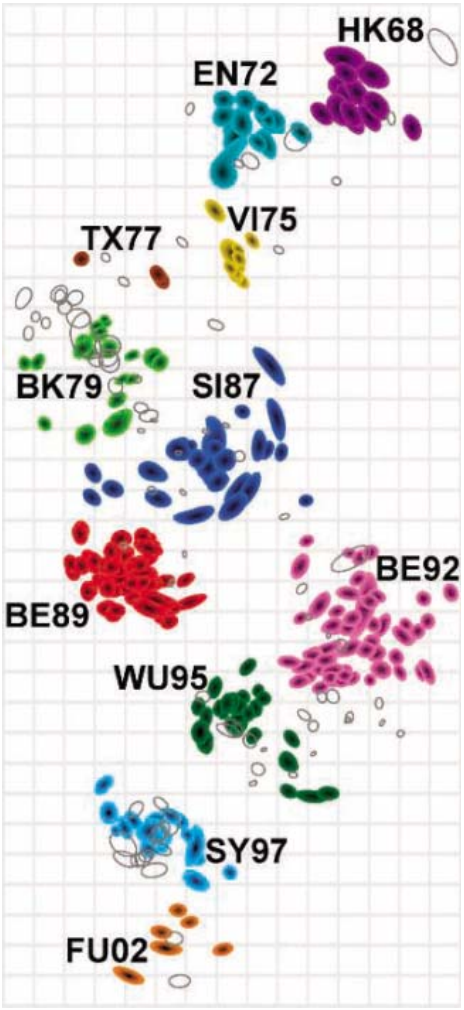

Fig. 2. Antigenic evolution of human influenza A (H3N2) virus from 1968 to 2003. The relative positions of strains (colored shapes) and antisera (open shapes) were adjusted such that the distances between strains and antisera in the map represent the corresponding hemagglutination inhibition (HI) measurements with the least error. The periphery of each shape denotes a 0.5 unit increase in the total error and is a measure of confidence in the placement of the strain or antiserum. Strain color represents the antigenic cluster to which the strain belongs; antisera are not colored. Clusters were identified by a *k*-means clustering algorithm and named after the first vaccine strain in the cluster. Two letters refer to the location of isolation: HK, Hong Kong, China; VI, Victoria, Australia; TX, Texas, United States; BK, Bangkok, Thailand; SI, Sichuan, China; BE, Beijing, China; WU, Wuhan, China; SY, Sydney, Australia; and FU, Fujian, China) and the two digits refer to year of isolation. The grid represents one unit of antigenic distance (i.e., a two-fold dilution in HI titer). [Reprinted from (*10*).]

Antigenic Evolution and Vaccine Strain Selection

The mainstay of seasonal influenza control is vaccination. The primary target for the human immune response is the viral hemagglutinin protein. Consequently, the hemagglutinin of the strain of influenza virus used to produce the vaccine needs to be a good antigenic match to that of the wild-type strains. The hemagglutinin of human influenza viruses evolves sufficiently rapidly that an extensive global surveillance network is necessary to track the evolution of the virus, and the strains used in the seasonal influenza virus vaccine have to be updated, often annually, to maintain antigenic similarity between wild-type and vaccine strains (*9*).

Antigenic differences among viral isolates are measured by the hemagglutination inhibition assay, but these data are sometimes difficult to interpret. Antigenic cartography resolves many of these difficulties, increases the resolution at which antigenic data can be interpreted, makes the interpretation more quantitative, and provides a visualization of antigenic differences among strains (*10*) (Fig. 2). These methods are now integrated into the biannual WHO seasonal vaccine strain-selection process. They are also being used to map the antigenic evolution of H5 viruses and will be used to evaluate the breadth of immunity offered by pandemic vaccines.

Although the hemagglutinin of avian influenza viruses is usually antigenically stable compared with that of human influenza viruses, the antigenic properties of the hemagglutinin of avian H5 viruses have changed substantially since 1997; the magnitude of the change is similar to that seen in human H3 over the same period. Thus, as with seasonal vaccine strain selection, the choice of strains for a pandemic vaccine will be critical.

The somewhat regular patterns seen in the human H3 antigenic map (Fig. 2) suggest that some aspects of its antigenic evolution are predictable. Less is known about the predictability of the antigenic evolution of avian H5 viruses. It is not clear whether the mutations in the hemagglutinin that have caused the antigenic changes in avian H5 since 1997 are directly selected for escape from prior immunity (i.e., allowing re-infection) or if the mutations accompany other changes in the virus and are selectively neutral for the hemagglutinin; if the latter, they would be difficult to predict.

Improving Predictions

Models are approximations of the systems they represent; by necessity, they are built with incomplete knowledge and need to be tested against either experimental or observational data. Thus, it is important to be aware of potential inaccuracies and parameter sensitivities when interpreting their results and to assess the accuracy of the models. Hence, to test the robustness of antigenic cartography (*11*), the human H3 antigenic map was repeatedly constructed from a random subset of the data and the constructs used to predict the omitted data. Predicted measurements for specific antigen-antiserum combinations not present in the original data were also checked by subsequent laboratory measurements. Testing models by prediction has not yet become standard practice in epidemiological modeling.

The pandemic influenza models discussed here are tours de force of painstaking gathering and synthesis of relevant details, but their predictions have not yet been tested by comparison with real outbreak data. This does not mean that the models are not useful in their current form; similar models were instrumental in shaping successful control policies during the Foot and Mouth Disease virus outbreak in the United Kingdom in 2001 (*12*, *13*) and were valuable in supplying rapid estimates of key epidemiological parameters including the mortality rate and transmissibility during the severe acute respiratory syndrome outbreak in 2003 (*14*, *15*). Nevertheless, we need data sets, such as those of seasonal influenza in regions with good surveillance data, that can be used to test the model predictions.

Experimental epidemiological studies, such as the vaccination of school children (*16*), or those that follow family units (*17*), provide core information for model design and parameterization, and (especially if there are multiple independent studies) for model testing. The large-scale study proposed to test the herd

immunity effect of vaccinating school children against influenza (*18*) would be extremely valuable in this context. Not only would the study test an important prediction for seasonal influenza, but it would also provide information about whom to prioritize for vaccination when vaccine is scarce, as it could be during a pandemic, and it also could provide repeated data sets for model testing.

A Final Caveat

We do not know that a human-adapted H5 will have similar epidemiology to human H3. We do know that when in humans, avian H5 infections currently have a substantially different clinical picture than that of human-adapted H3 infections. Hence, even a perfect epidemiological model for human H3 might be a poor model for human H5. Nevertheless, a well-understood and accurate human H3 model would be extremely valuable in its own right and would be a good starting point for any reparameterization necessary for a human H5 epidemiological model once the characteristics of the virus are known.

As we focus attention and funds on preparedness for a pandemic, we must not lose sight of the necessity for medium-term and longer term investments to expand basic understanding of influenza viruses at the molecular, immunological, evolutionary, epidemiological, and ecological levels. Such increases in our basic understanding, some already within reach, will increase our options both to control seasonal influenza and our ability to predict and thus increase preparedness for the next influenza pandemic—regardless of whether it is imminent or many years away.

References and Notes

1. R. G. Webster, W. J. Bean, O. T. Gorman, T. M. Chambers, Y. Kawaoka, *Microbiol. Rev.* **56**, 152 (1992).
2. T. Kuiken *et al.*, *Science* **312**, 394 (2006).
3. K. Shinya *et al.*, *Nature* **440**, 435 (2006).
4. D. van Riel *et al.*, *Science* **312**, 399 (2006); published online 23 March 2006 (10.1126/science.1125548).
5. N. M. Ferguson *et al.*, *Nature* **437**, 209 (2005).
6. I. M. Longini Jr. *et al.*, *Science* **309**, 1083 (2005).
7. World Health Organization, ***WHO Pandemic Influenza Draft Protocol for Rapid Response and Containment*** (www.who.int/csr/disease/avian_influenza/guidelines/pandemicfluprotocol_17.03a.pdf).
8. C. E. Mills, J. M. Robins, C. T. Bergstrom, M. Lipsitch, *PLoS Biol.* **3**, e135 (2006).
9. A. W. Hampson, in *Influenza*, C. W. Potter, Ed. (Elsevier, London, 2002), pp. 49–85.
10. D. J. Smith *et al.*, *Science* **305**, 371 (2004).
11. B. Efron, R. J. Tibshirani, *An Introduction to the Bootstrap* (Chapman & Hall, London, 1993).
12. N. M. Ferguson, C. A. Donnelly, R. M. Anderson, *Science* **292**, 1155 (2001).
13. M. J. Keeling *et al.*, *Science* **294**, 813 (2001).
14. M. Lipsitch *et al.*, *Science* **300**, 1966 (2003).
15. S. Riley *et al.*, *Science* **300**, 1961 (2003).
16. A. S. Monto, F. M. Davenport, J. A. Napier, T. Francis Jr., *Bull. World Health Org.* **41**, 537 (1969).
17. L. H. Taber, A. Paredes, W. P. Glezen, R. B. Couch, *J. Hyg. London* **86**, 303 (1981).
18. M. E. Halloran, I. M. Longini Jr., *Science* **311**, 615 (2006).

19. I thank S. Cornell, D. Farmer, R. Fouchier, C. Gilligan, B. Grenfell, T. Jones, A. Lapedes, B. Larder, A. Mosterin, N. Ferguson, P. Rohani, C. Russell, D. Smith, and C. Viboud for useful discussions. Funding was provided by the European Union grant EC 503350, and the NIH Director's Pioneer Award Program, part of the NIH Roadmap for Medical Research, through grant number DP1-OD000490-01.

10.1126/science.1122665

PERSPECTIVE

Host Species Barriers to Influenza Virus Infections

Thijs Kuiken,[1]* Edward C. Holmes,[2] John McCauley,[3] Guus F. Rimmelzwaan,[1] Catherine S. Williams,[2] Bryan T. Grenfell[2,4]

Most emerging infectious diseases in humans originate from animal reservoirs; to contain and eradicate these diseases we need to understand how and why some pathogens become capable of crossing host species barriers. Influenza virus illustrates the interaction of factors that limit the transmission and subsequent establishment of an infection in a novel host species. Influenza species barriers can be categorized into virus-host interactions occurring within individuals and host-host interactions, either within or between species, that affect transmission between individuals. Viral evolution can help surmount species barriers, principally by affecting virus-host interactions; however, evolving the capability for sustained transmission in a new host species represents a major adaptive challenge because the number of mutations required is often large.

The highly pathogenic avian influenza H5N1 virus is just one example of a zoonotic pathogen capable of transmission from animal reservoir species to humans (*1*). If we are to contain and eradicate such emerging infectious diseases (EIDs), we need to understand how and why some pathogens become capable of infecting and being maintained in novel host species. Here, we review the interaction of factors that collectively limit the transmission of an infection from a donor host species to a recipient species and that constitute the host species barrier. We discuss these factors specifically as they apply to influenza, but the underlying principles apply to any EID.

The host species barrier is not a simple concept; the likelihood of a virus becoming endemic in a new host species depends on the interaction of three sets of processes (Fig. 1): interspecific interactions between hosts of the donor and recipient species, host-virus interactions within individual hosts of the recipient species, and host-host interactions within the recipient species. For any type of species transfer, there must be sufficient contact between donor and recipient species and enough compatibility between the virus and the new host to allow replication and the possibility of transmission to other members of the recipient species. If this transmission can occur, the contact network structure of the recipient species, together with variations in transmission through this network, are critical in determining whether the virus will persist or die out. As the history of influenza pandemics and epidemics illustrates, viral evolution can help considerably in lowering the species barrier. However, we argue below that the relative rarity of successful species jumps testifies to the complex adaptations often required to achieve sustained transmission in a new species. We also review the components and evolutionary dynamics of the species barrier as they apply to influenza and then suggest areas for future work.

The Virus-Host Interaction: Within-Host Barriers

Cell entry-exit and receptor biology. For a virus shed by one host to infect another, it must breach entry barriers (e.g., mucus, alveolar macrophages, and epithelium) and find its way to tissues in which it can replicate. For example, chimpanzees are relatively resistant to experimental respiratory exposure to human influenza viruses, possibly because their respiratory tract secretions contain mucins that can specifically bind viruses before they reach airway epithelial cells (*2*). Once in appropriate

[1]Department of Virology, Erasmus Medical Center, 3015 GE Rotterdam, Netherlands. [2]Center for Infectious Disease Dynamics, Department of Biology, Pennsylvania State University, University Park, PA 16802, USA. [3]Institute for Animal Health, Compton Laboratory, Compton, Newbury, Berkshire RG20 7NN, UK. [4]Fogarty International Center, National Institutes of Health, Bethesda, MD 20892, USA.

*To whom correspondence should be addressed. E-mail: t.kuiken@erasmusmc.nl

tissues, a virus must attach to and enter cells before it can replicate. The specificity of receptor molecules governs virus entry into cells (*3*). For example, hemagglutinin molecules on the viral coats of avian influenza viruses preferentially bind to one form of molecule in the host cell membrane [sialic acid (SA)-α-2,3-Gal–terminated saccharides], whereas the hemagglutinins on human influenza viruses prefer another (SA-α-2,6-Gal–terminated saccharides) (*4*). This difference, together with the predominance of SA-α-2,6-Gal–terminated saccharides in the human trachea, may explain why replication of avian influenza viruses in humans generally tends to be restricted (*5*). The rare occurrences of fatal pneumonia in humans infected with the current H5N1 virus from Asia (*6*) and the H7N7 virus from the Netherlands in 2003 (*7*) are likely due to the ability of these viruses to attach to and replicate in lower respiratory tract cells, which do have SA-α-2,3-Gal–terminated saccharides (*8*, *9*).

Replication and spread within tissues. Once it has entered a cell of the new host, the virus must successfully co-opt host cell processes to replicate there. Many avian influenza viruses can infect mouse cells but cannot replicate, frequently because amino acid residue 627 of the PB2 protein of the viral polymerase differs between avian and mammalian influenza viruses. In the avian virus, this residue is usually glutamic acid, whereas in mammalian influenza virus it is lysine (*4*), suggesting that PB2 residue 627 might be important in determining species range. In experimentally infected mice, a glutamic acid–to–lysine mutation at this position in the PB2 protein of H5N1 virus results in increased virulence and the ability to invade extrarespiratory organs (*10*). It is notable that both H5N1 virus from human patients in Asia (*10*) and H7N7 virus from a fatal human case in the Netherlands (*7*) possess a lysine at this site, suggesting rapid evolution within humans of a virus originating in poultry. Strikingly, though, and worryingly, lysine is the PB2 residue in H5N1 viruses isolated from wild waterfowl in mid-2005 from Qinghai Lake, in China (*11*, *12*).

If a virus does succeed in replicating, it needs to be released from the host cell to infect more cells or be shed from the host. In influenza, progeny virus particles are bound to host cell sialosaccharides by their hemagglutinin. Viral neuraminidase cleaves these sialosaccharides, thus releasing newly produced virus from the cell surface. Like the respective hemagglutinins, neuraminidases from avian influenza viruses have a preference for SA-α-2,3-Gal–terminated saccharides, whereas those from many human influenza viruses prefer SA-α-2,6-Gal–terminated saccharides (*4*). Interestingly, the H2N2 virus that caused the 1957 pandemic initially retained a binding preference for "avian" SA-α-2,3-Gal–terminated sialosaccharides but switched affinity to "human" SA-α-2,6-Gal–terminated saccharides during subsequent influenza seasons in the human population (*13*).

Even if progeny virus exits one host cell, host innate immune responses may hinder infection of other cells. Interferons may induce uninfected cells to enter an antiviral state that inhibits viral replication (*4*). To counter host responses, influenza virus has developed strategies for evading innate immunity: The viral NS1 polypeptide acts as an antagonist of interferon induction in infected cells by sequestration of double-stranded RNA or suppression of host posttranscriptional processing of mRNAs (*4*). NS1 also may help influenza viruses to replicate in interferon-treated cultured cells, as has been reported for H5N1 virus isolates from 1997 (*14*); whether currently isolated H5N1 viruses have retained this property remains to be determined.

Sometimes infection is restricted to particular tissues; in other cases, it can be systemic. For influenza virus to spread from the respiratory tract to other susceptible tissues, it needs to enter the lymph and/or blood system, be successfully transported, and exit at tissue-blood junctions (*15*). In poultry, whether infection is localized or systemic depends on the amino acid sequence at the cleavage site of the precursor hemagglutinin. This cleavage is required for the hemagglutinin to become fully functional. Low pathogenicity influenza viruses require extracellular proteases limited to the respiratory and gastrointestinal tracts to cleave the precursor hemagglutinin, whereas highly pathogenic avian influenza viruses have changes in the cleavage site that allow the precursor hemagglutinin to be processed by ubiquitous intracellular proteases, resulting in fatal systemic infection (*4*). In mammals, the viral factors determining systemic infection are less clear, although cleavability of the precursor hemagglutinin plays an important role (*10*).

From their sites of replication, viruses need ultimately to be transmitted to new hosts. In general, dissemination of progeny viruses from the infected host occurs through shedding in respiratory, enteric, or urogenital secretions. Human influenza virus replicates mainly in the upper respiratory tract and is usually readily transmitted via droplets formed during coughing or sneezing (*16*). By contrast, the H5N1 influenza virus typically infects human cells in the lower respiratory tract (*8*, *9*) and so may be less easily shed from the infected patient; this may partly explain why so far there has been little human-to-human transmission observed.

Host-Host Interactions: Cross-Species Contacts

Human population growth and consumption patterns are now reducing the magnitude of many geographical, environmental, or behavioral barriers that limit contact and potential virus transmission between donor and recipient species. The spread of viral diseases through international travel and trade is a major concern, although natural modes of spread can be important too. H5N1 virus was spread from Southeast Asia to Western Europe in 2005 and 2006, most likely by a combination of migratory wild birds (*11*, *12*) and trade in poultry and poultry products. Even when donor and recipient species live in the same area, spread of infection from the one to the other can be hampered by differences in habitat use or by environmental barriers. The massive increase in poultry production in Southeast Asia has certainly reduced some of the obstacles to interspecific transmission of avian influenza virus.

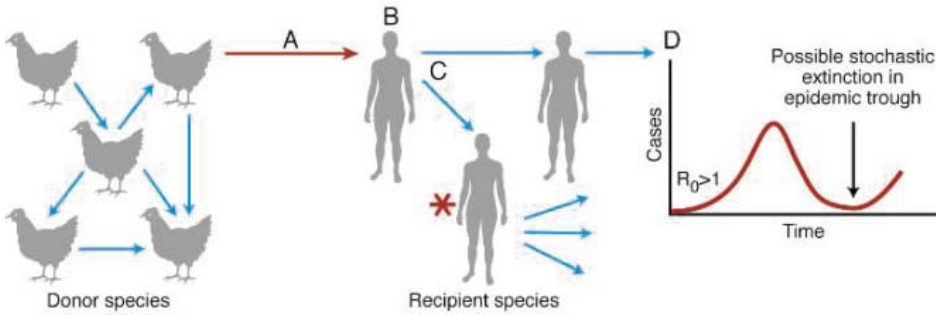

Fig. 1. Schematic illustrating phases in overcoming species barriers. (**A**) Interspecific host-host contact must allow transmission of virus from donor species to recipient species. (**B**) Virus-host interactions within an individual of recipient species affect the likelihood of the virus replicating and being shed sufficiently to infect another individual of recipient species. (**C**) Intraspecific host-host contact in recipient species must allow viral spread ($R_0 > 1$) in the presence of any preexisting immunity. Superspreader events (red asterisk) early in the transmission chain can help this process. (**D**) The pathogen must persist in the recipient species population even during epidemic troughs (after most susceptible individuals have had the disease) so that subsequent epidemics can be seeded: If few susceptibles are left, the virus may (stochastically) go extinct in epidemic troughs. Viral variation and evolution can aid invasion and persistence, particularly by affecting host-virus interactions.

Increasing numbers of poultry are kept in close proximity to wild waterfowl (*17*) and are brought into contact with other species at live animal markets (*18*). Even if two host species share the same geographical area and habitat, host behavior may limit pathogen transmission by, for instance, restricting infective contacts. Conversely, certain behaviors can predispose hosts to increased pathogen exposure. For example, consumption of raw poultry products resulted in fatal H5N1 virus infection in both humans and felids (*19*, *20*), and racing greyhounds may have contracted equine influenza virus A/H3N8 after being fed meat from infected horses (*21*).

Host-Host Interactions: Intraspecific Contacts in the Recipient Population

Assuming that a virus can be transmitted between individuals of the recipient host species, persistence of infection then depends on how it is spread through the host's contact network, and successful invasion depends on the network structure and the likelihood of particular individuals in the network transmitting the virus. The basic reproduction ratio of infection, R_0, represents the number of secondary cases produced when an infected individual is introduced into a well-mixed local population of wholly susceptible individuals (*22*, *23*). It is well established that, as the proportion of susceptibles in the population, s, drops (as individuals become infected, then recover), the number of secondary cases per infection, R, also drops: $R = sR_0$. If $R < 1$, as is currently the case for H5N1 virus in humans, an infection will not cause a major epidemic. But if R is even modestly greater than unity, a novel infection may spread locally, with potential for further spread in the absence of control (*24*).

For some novel infections that jump the species barriers, there is no preexisting immunity; however, preexisting immune protection can sometimes reduce the number of susceptibles, and hence R. For instance, humans who had previously encountered an influenza virus with the N2 neuraminidase may have been partially protected in the 1968 H3N2 pandemic that followed the global circulation of H2N2 viruses (*25*). There is also indirect evidence of short-term immunity between subtypes of influenza viruses (*24*, *26*), which could play a role in the early spread of pandemics (*24*). In addition, cross-reactive T cells also may contribute to heterosubtypic immunity to influenza and reduce viral shedding (*27*).

The biological characteristics and evolutionary potential of the invading virus can also affect the longer term persistence of the infection. Acute immunizing infections are typified by initial steep increases in the number of infected individuals. This type of epidemic depletes the supply of susceptibles, leading to deep epidemic troughs (Fig. 1D) when local stochastic extinction of infection is possible, especially after a major epidemic typical of an invasion of a new host species. This effect creates a barrier to sustained transmission that applies especially to infections with strong, stable immunity, such as morbilliviruses (*28*); however, it is less of a handicap to infections such as influenza, in which the viruses can evolve quickly to overcome prevailing herd immunity (*29*). Teasing out what combination of immune escape and spatial dynamics allows interpandemic influenza to persist, despite its short infectious period and strongly seasonal transmission, is an important area for future work (*29*).

Overall, the likelihood of an EID persisting in a new species depends in a complex way on the population sizes and the degrees of mixing of donor and recipient host species as well as the values of R_0 in each (*30*). At every geographical level, whether local, regional, or global, the rate and the pattern of disease spread depend on the spatial distribution and mixing of the host population. Long-range spatial spread is in general facilitated by high

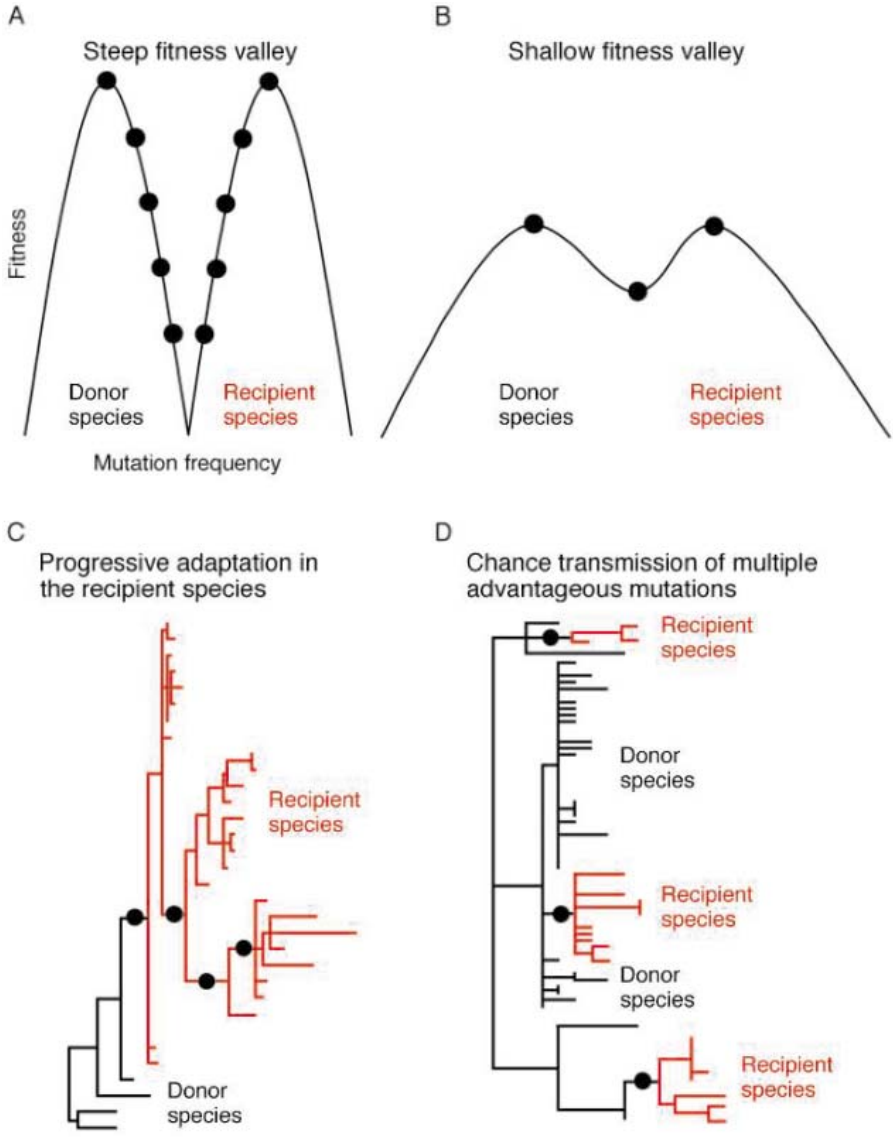

Fig. 2. Evolutionary models for the cross-species transmission of pathogens. (**A**) The donor and recipient species represent two distinct fitness peaks separated by a steep fitness valley. Multiple adaptive mutations (solid circles) are therefore required for the virus to successfully establish onward transmission in the recipient host species. (**B**) The donor and recipient species are separated by a far shallower fitness valley. This facilitates successful cross-species transmission because only a small number of advantageous mutations are required. (**C**) When multiple mutations are required for a virus to adapt to a new host, these may evolve progressively in the recipient species. However, this necessarily requires some onward transmission. (**D**) It is also possible that many of the mutations required to allow adaptation to a new host species were preexisting in the donor species and transmitted simultaneously. This will accelerate successful viral emergence.

infectivity, a long infectious period, and (at least in human influenza) a period of transmission before symptoms become apparent and quarantine measures can be taken. This contrasts with severe acute respiratory syndrome (SARS), in which the period of infectiousness begins with the onset of symptoms, allowing quarantine measures to be taken before maximum infectiousness is attained (*31*). The fate of an epidemic can also depend strongly on heterogeneities in R_0, particularly on the role of "superspreaders" early in the epidemic (*32*). For example, some superspreader individuals may be more infective per contact for some reason; other superspreaders may not have higher per-contact transmission, but have many more contacts and therefore greatly multiply the rate of spread (*22*). If superspreaders become infected early in an outbreak, the epidemic is more likely to take off, which can have substantial implications for disease control (*32*).

The Role of Pathogen Evolution

In evolutionary terms and from the perspective of the pathogen, the host species barrier for infection can be thought of as a fitness valley lying between two distinct fitness peaks representing donor and recipient hosts, respectively (Fig. 2). The more mutations required for a virus to move between these peaks, the deeper the valley and the less likely that this can occur in a single step, particularly if adaptation involves changes at multiple loci, as in the case of avian influenza virus transmitting in human populations (*33*). Such a model has two important implications for our understanding of viral disease emergence.

First, the effective rate of virus adaptation is not simply determined by the overall rate at which mutations arise, but by the fitness of these mutations, particularly the proportion that are advantageous in multiple hosts. Hence, although RNA viruses often show prodigious levels of genetic variation, reflecting their high rates of mutation and immense intrahost population sizes (*34*), a large proportion of the mutations that arise within an individual viral population will be deleterious or slightly so (*35*). As a case in point, vector-borne RNA viruses seem to be characterized by a particularly high proportion of deleterious mutations because of the fitness trade-offs that are inherent in replication in hosts as distant as mammals and arthropods (*36*) and that thereby constitute a major constraint on their adaptability (*23*). Further, there is growing evidence that mutations, both advantageous and deleterious, often show complex epistatic interactions, which can also have major effects on the rate and the progress of adaptation (*37*).

Second, the critical parameters determining when successful onward transmission will occur include not only the time it takes to optimize fitness ($R_0 > 1$) in the new host species (*38*) but also the probability that the recipient population is exposed to a viral strain that, by chance, already harbors several mutations required for successful onward transmission. For example, of the myriad influenza viruses produced by faulty replication within an individual, some, by chance, may possess those mutations that affect the receptor binding site to alter sialic acid binding capacity. This was highlighted recently (January 2006) in samples from a patient infected with H5N1 virus in Turkey. This individual had a mixed population of viruses, some of which expressed hemagglutinin with an amino acid sequence associated with an increased affinity for SA-α-2,6-Gal–terminated saccharides. Because intrahost genetic diversity has rarely been examined in RNA viruses, it is unclear how much adaptively important genetic variation rests within hosts.

Reassortment and recombination further complicate the picture. These processes will allow some viruses to acquire many of the key adaptive mutations in a single step and hence make a major jump in fitness space. However, whereas reassortment may allow viruses to traverse the adaptive landscape faster than through mutation alone, the optimal epistatic interactions among genes are likely to be broken by reassortment, and most reassortments, like most point mutations, are also expected to be largely deleterious.

Future Research Needs

Although there is a vast body of literature on influenza, only a few studies consider the barriers for influenza viruses to cross from one species to another. There are several important questions in this area that need to be addressed. Which genetic changes would allow the currently circulating H5N1 virus to acquire the characteristic to spread efficiently among humans? Such a study would require a combination of reverse genetics to generate potential virus candidates and a suitable animal model to simulate human-to-human transmission. If such a virus were to evolve, which factors at the population level would allow it to cause a pandemic? Investigating this requires epidemiological models that take into account not only the properties of the donor and recipient populations but also the characteristics of the newly emerged virus. What is the within-host diversity of influenza viruses, and does it include mutants that are able to replicate in a new host species? The current status of viral genome sequencing makes such studies possible, although studies of intrahost viral diversity are notable for their rarity. We have a detailed understanding of the replication cycle of influenza virus in a cell culture system, but what, at the tissue and organ level in vivo, are the barriers that limit human influenza virus to the respiratory tract while allowing H5N1 virus to cause systemic disease? To understand this requires a multidisciplinary approach based on a combination of laboratory investigation and human clinical studies. Apart from the specific application to influenza virus, answering these questions will also result in a better understanding of the general principles that prevent viruses from jumping the species barrier.

References

1. T. Kuiken *et al.*, *Science* **309**, 1680 (2005).
2. S. Olofsson, U. Kumlin, K. Dimock, N. Arnberg, *Lancet Infect. Dis.* **5**, 184 (2005).
3. J. Stevens *et al.*, *Science,* in press; published online 20 March 2006 (10.1126/science.1124513).
4. S. J. Baigent, J. W. McCauley, *Bioessays* **25**, 657 (2003).
5. Y. Suzuki, *Biol. Pharm. Bull.* **28**, 399 (2005).
6. J. H. Beigel *et al.*, *N. Engl. J. Med.* **353**, 1374 (2005).
7. R. A. Fouchier *et al.*, *Proc. Natl. Acad. Sci. U.S.A.* **101**, 1356 (2004).
8. D. van Riel *et al.*, *Science,* in press; published online 23 March 2006 (10.1126/science.1125548).
9. K. Shinya *et al.*, *Nature* **440**, 435 (2006).
10. M. Hatta, P. Gao, P. Halfmann, Y. Kawaoka, *Science* **293**, 1840 (2001).
11. H. Chen *et al.*, *Nature* **436**, 191 (2005).
12. J. Liu *et al.*, *Science* **309**, 1206 (2005); published online 6 July 2005 (10.1126/science.1115273).
13. D. Kobasa *et al.*, *J. Virol.* **73**, 6743 (1999).
14. S. H. Seo, E. Hoffmann, R. G. Webster, *Nat. Med.* **8**, 950 (2002).
15. H. Smith, C. Sweet, *Rev. Infect. Dis.* **10**, 56 (1988).
16. B. R. Murphy, R. G. Webster, in *Fields Virology*, B. N. Fields *et al.*, Eds. (Lippincott-Raven, Philadelphia, 1996), vol. 1, ch. 46.
17. J. I. Slingenbergh, M. Gilbert, K. I. de Balogh, W. Wint, *Rev. Sci. Tech.* **23**, 467 (2004).
18. R. G. Webster, *Lancet* **363**, 234 (2004).
19. J. Keawcharoen *et al.*, *Emerg. Infect. Dis.* **10**, 2189 (2004).
20. G. F. Rimmelzwaan *et al.*, *Am. J. Pathol.* **168**, 176 (2006).
21. P. C. Crawford *et al.*, *Science* **310**, 482 (2005); published online 26 September 2005 (10.1126/science.1117950).
22. R. M. Anderson, R. M. May, *Infectious Diseases of Humans: Dynamics and Control* (Oxford Univ. Press, Oxford, 1991).
23. M. E. J. Woolhouse, D. T. Haydon, R. Antia, *Trends Ecol. Evol.* **20**, 238 (2005).
24. N. M. Ferguson *et al.*, *Nature* **425**, 681 (2003).
25. C. Viboud, R. F. Grais, B. A. Lafont, M. A. Miller, L. Simonsen, *J. Infect. Dis.* **192**, 233 (2005).
26. Y. Xia, J. R. Gog, B. T. Grenfell, *Appl. Statist.* **54**, 659 (2005).
27. A. J. McMichael, F. M. Gotch, G. R. Noble, P. A. Beare, *N. Engl. J. Med.* **309**, 13 (1983).
28. B. T. Grenfell *et al.*, *Science* **303**, 327 (2004).
29. N. M. Ferguson, A. P. Galvani, R. M. Bush, *Nature* **422**, 428 (2003).
30. A. Fenton and A. B. Pedersen, *Emerg. Infect. Dis.* **11**, 1815 (2005).
31. M. Lipsitch *et al.*, *Science* **300**, 1966 (2003); published online 23 May 2003 (10.1126/science.1086616).
32. J. O. Lloyd-Smith, S. J. Schreiber, P. E. Kopp, W. M. Getz, *Nature* **438**, 355 (2005).
33. J. K. Taubenberger *et al.*, *Nature* **437**, 889 (2005).
34. E. Domingo, J. J. Holland, *Annu. Rev. Microbiol.* **51**, 151 (1997).
35. R. Sanjuan, A. Moya, S. F. Elena, *Proc. Natl. Acad. Sci. U.S.A.* **101**, 8396 (2004).
36. C. H. Woelk, E. C. Holmes, *Mol. Biol. Evol.* **19**, 2333 (2002).
37. R. Sanjuan, A. Moya, S. F. Elena, *Proc. Natl. Acad. Sci. U.S.A.* **101**, 15376 (2004).
38. R. Antia, R. R. Regoes, J. C. Koella, C. T. Bergstrom, *Nature* **426**, 658 (2003).

10.1126/science.1122818

GE Healthcare

Faster protein purification? It's not rocket science.

HiTrap™ columns give you pure proteins with less effort. They come prepacked with the widest choice of media, ensuring results you can depend on in a broad range of applications, and the highest level of convenience.

But we're never content to stand still. We constantly strive for new innovations for tomorrow's research and drug development. And thanks to our technological achievements and global presence, we're able to help you turn your scientific ideas into reality – bringing science to life and helping transform healthcare.

We call it Life Science Re-imagined.

Discover how HiTrap columns can help power your protein purification.
Visit www.gehealthcare.com/life

imagination at work

GE Healthcare Bio-Sciences AB, a General Electric Company.
Björkgatan 30, 751 84 Uppsala, Sweden.

GE05-06

H5N1 Virus Attachment to Lower Respiratory Tract

Debby van Riel, Vincent J. Munster, Emmie de Wit, Guus F. Rimmelzwaan, Ron A. M. Fouchier, Ab D. M. E. Osterhaus, Thijs Kuiken*

Highly pathogenic avian influenza virus of the subtype H5N1 may cause infection of the lower respiratory tract (LRT) and severe pneumonia in humans (*1*). However, the cell types in the LRT to which the virus attaches are unknown for both humans and experimental animals. Although attachment is not the only factor required for virus replication, this information is important both to better understand the pathogenesis of H5N1 influenza and to assess the suitability of animal models. Therefore, we compared the pattern of H5N1 virus attachment to the LRT of humans and four animal species.

Influenza viruses attach to host cells by binding of the hemagglutinin to sialosaccharides on the host cell surface. Human influenza viruses prefer sialic acid (SA)–α-2,6-Gal–terminated saccharides, whereas avian influenza viruses prefer those terminating in SA-α-2,3-Gal (*2*). The use of lectins that specifically detect α-2,6– and α-2,3–linked sialosaccharides is an indirect measure of influenza virus attachment to host tissues and does not account for other variables that influence the binding avidity, such as type of SA, and glycosylation and sialylation of the hemagglutinin close to the receptor binding site (*2*). For a more direct method, which was modified from a previously used technique (*3*), we incubated formalin-fixed, paraffin-embedded tissue sections with formalin-inactivated fluorescein isothiocyanate (FITC)–labeled H5N1 virus (A/Vietnam/1194/04) and detected virus with a peroxidase-labeled rabbit antibody to FITC that was amplified with a tyramide signal amplification system. Tissues comprised histologically normal LRT (including alveolus, bronchiole, and bronchus), as well as trachea from three individuals of each of the following species: human, mouse (C57BL/6), ferret, cynomolgus macaque, and domestic cat (*4*).

In the human LRT, H5N1 virus attached predominantly to type II pneumocytes, alveolar macrophages, and nonciliated cuboidal epithelial cells in terminal bronchioles. Attachment became progressively rarer toward the trachea (Fig. 1 and table S1). The identity of type II pneumocytes was confirmed by double staining with antibody to human surfactant apoprotein A (fig. S1). These findings fit with the limited pathology data for H5N1 virus infection in humans, which show diffuse alveolar damage (*1*) and the presence of H5N1 virus antigen in type II pneumocytes (*5*). However, they contrast with the idea that avian influenza viruses generally have little affinity for human respiratory tissues (*2*).

The predilection of H5N1 virus for type II pneumocytes and alveolar macrophages may contribute to the severity of the pulmonary lesion. Because type II pneumocytes are metabolically active and are the most numerous cell type lining the alveoli, targeting of this cell type may lead to abundant virus production. Damage to type II pneumocytes may impair their functions, including re-epithelialization after alveolar damage, ion transport, and surfactant production, and so may inhibit tissue repair. Targeting of alveolar macrophages may be important because of their role in limiting viral replication and in the immune response to viral infection.

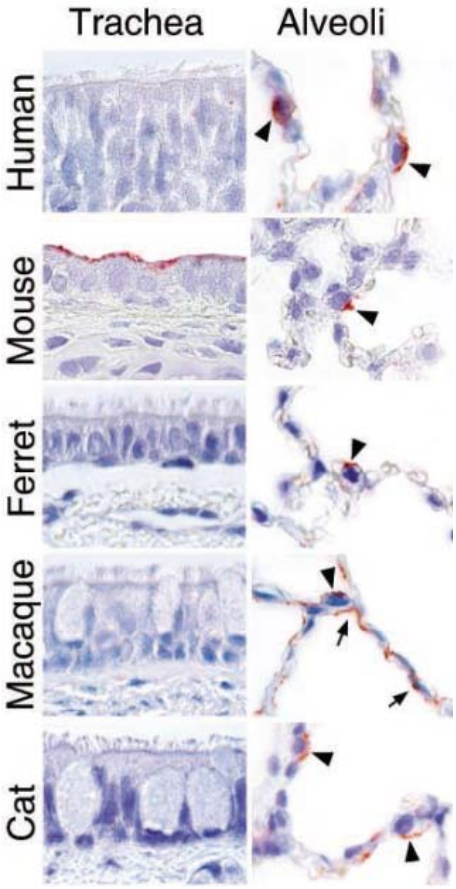

Fig. 1. Attachment of H5N1 virus to respiratory tissues of humans and four animal species. In the trachea, H5N1 virus—visible as red-brown staining—attached only to epithelial cells of mice. In the alveoli, H5N1 virus attached predominantly to type II pneumocytes (arrowheads) in humans and all animal species except the macaque, where attachment was predominantly to type I pneumocytes (arrows).

The pattern of H5N1 virus attachment to cat LRT and, to a lesser extent, ferret LRT most closely resembled that in human tissues (Fig. 1 and table S1). Based on this criterion, we considered these two species as the most suitable models for H5N1 viral pneumonia in humans. However, other factors also need to be considered, such as the availability of reagents and immunologic similarity. In macaque alveoli, H5N1 virus attached predominantly to type I pneumocytes instead of type II pneumocytes, as in human tissues. In mice, H5N1 virus attachment to cells was most abundant in the trachea and became progressively rarer toward the alveoli, whereas the opposite trend was observed in human tissues. The observed pattern of H5N1 virus attachment to the LRT is consistent with the respective pathology and immunohistochemistry results of experimental H5N1 virus infection in mice (*6*), ferrets (*7*), macaques (*8*), and cats (*9*).

This study demonstrates the attachment of H5N1 virus to the human LRT in a pattern that corresponds with autopsy findings. It also identifies cat and ferret as the most suitable animal models for human H5N1 viral pneumonia, on the basis of the similarity of viral attachment pattern. This technique also could be applied to further determine H5N1 virus attachment to the upper respiratory tract. Failure to attach to this site may be a limiting factor in human-to-human transmissibility of H5N1 virus.

References and Notes

1. J. H. Beigel *et al.*, *N. Eng. J. Med.* **353**, 1374 (2005).
2. S. J. Baigent, J. W. McCauley, *Bioessays* **25**, 657 (2003).
3. J. N. Couceiro, J. C. Paulson, L. G. Baum, *Virus Res.* **29**, 155 (1993).
4. Materials and methods are available as supporting material on *Science* Online.
5. M. Uiprasertkul *et al.*, *Emerg. Infect. Dis.* **11**, 1036 (2005).
6. C. W. Lee *et al.*, *J. Virol.* **79**, 3692 (2005).
7. T. R. Maines *et al.*, *J. Virol.* **79**, 11788 (2005).
8. G. F. Rimmelzwaan *et al.*, *J. Virol.* **75**, 6687 (2001).
9. G. F. Rimmelzwaan *et al.*, *Am. J. Pathol.* **168**, 176 (2006).
10. We thank W. Lim for providing the H5N1 virus isolate; M. den Bakker, H. Sharma, M. Vermeij, and J. van den Brand for providing tissues; and F. van der Panne for technical assistance.

Supporting Online Material

www.sciencemag.org/cgi/content/full/1125548/DC1
Materials and Methods
Figs. S1 and S2
Table S1
References

30 January 2006; accepted 21 March 2006
Published online 23 March 2006;
10.1126/science.1125548
Include this information when citing this paper.

Department of Virology, Erasmus Medical Center, 3015 GE Rotterdam, Netherlands.

*To whom correspondence should be addressed. E-mail: t.kuiken@erasmusmc.nl

Global Mineralogical and Aqueous Mars History Derived from OMEGA/Mars Express Data

Jean-Pierre Bibring,[1] Yves Langevin,[1] John F. Mustard,[2] François Poulet,[1] Raymond Arvidson,[3] Aline Gendrin,[1,2] Brigitte Gondet,[1] Nicolas Mangold,[4] P. Pinet,[5] F. Forget,[6] the OMEGA team[7]

Global mineralogical mapping of Mars by the Observatoire pour la Mineralogie, l'Eau, les Glaces et l'Activité (OMEGA) instrument on the European Space Agency's Mars Express spacecraft provides new information on Mars' geological and climatic history. Phyllosilicates formed by aqueous alteration very early in the planet's history (the "phyllocian" era) are found in the oldest terrains; sulfates were formed in a second era (the "theiikian" era) in an acidic environment. Beginning about 3.5 billion years ago, the last era (the "siderikian") is dominated by the formation of anhydrous ferric oxides in a slow superficial weathering, without liquid water playing a major role across the planet.

The earliest observations of Mars by spacecraft showed that water had caused substantial erosion of the surface, including extensive channeling and associated transport and deposition of material (*1*). However, fundamental questions remain. Was water-driven activity on its surface transient or persistent, the latter being a prerequisite to sustain habitable surface environments? When and where did that activity take place, and when did it end? Mineralogical thermal infrared mapping from the Mars Global Surveyor Thermal Emission Spectrometer (MGS TES) suggests that Mars must have been cold and dry over most of its history (*2*–*4*). In a few locations, however, gray hematite was detected and was interpreted to result from aqueous processes (*2*, *5*, *6*). In Terra Meridiani, the Mars Exploration Rover (MER) Opportunity revealed that sulfates formed in the presence of water and that the hematite found by TES consists of concretions weathered from the sulfate deposits (*7*). New data from the Mars Express OMEGA (Observatoire pour la Minéralogie, l'Eau, les Glaces et l'Activité) instrument (*8*, *9*), in combination with local ground information from the MERs, provide extensive information on the aqueous history of Mars and the mineralogical evolution of its crust.

Surface mineralogy. After 1 martian year of operation in orbit around Mars, OMEGA has mapped 90% of the surface at a spatial sampling of 1.5 to 5 km and ~5% of the surface at a sampling of <0.5 km; on each pixel, the spectrum from 0.35 to 5.1 μm is acquired. OMEGA spectral data allow the identification of a variety of mafic and altered minerals, typically at a volume concentration of 5% or greater. For hydrated minerals and a few others, the sensitivity is even higher.

Fe-bearing pyroxene is the most widely distributed mineral detected by OMEGA (*10*) (Fig. 1) and previous instruments (*2*–*4*); both high-calcium pyroxene (HCP) and low-calcium pyroxene (LCP) have been identified by OMEGA through their spectral features from 0.7 to 2.5 μm. LCP-rich areas are observed within the ancient Noachian crust. HCP-rich areas are mapped in more recent lava flows. Olivine is also found either in these pyroxene-rich terrains or in localized areas in which olivine dominates, mostly within crater floors and rims, and proximal to large impact basins (*11*). The identification and distribution of these mafic minerals are consistent with and extend previous observations using thermal infrared measurements (*12*). On a global scale, both pyroxene and olivine are still present at the surface in the older terrains, including within sand dunes. However, much of the younger surface, particularly within the large lowlands of the northern hemisphere (Fig. 1), does not exhibit the spectral signatures of these Fe-bearing mafic minerals: The exposed original constituents have been heavily altered or covered by heavily altered dust. This alteration of the martian surface material has not occurred merely through physical weathering, such as through the grinding of bedrock into sand and dust. Surface texture from high-resolution imaging [by the MGS Mars Orbiter Camera (MOC) and Mars Express High-Resolution Stereo Camera (HRSC)], thermal inertia from infrared (IR) behavior [from the MGS TES and the Mars Odyssey Mission Thermal Emission Imaging System (Odyssey THEMIS)], and pyroxene content from near-IR hyperspectral imagery (from OMEGA) are not systematically coupled: Terrains of similar pyroxene content are found as both bedrock and dunes, and terrains with similar soil properties are found with different pyroxene content. Laboratory data and remote sensing of the Moon (*13*) demonstrate that mafic regolith grains can exhibit their diagnostic spectral signatures after extended exposure that includes meteoritic impact (forming high concentrations of glasses) and solar wind irradiation. In the wide areas of Mars with no mafic signatures, the surface material is thus made of grains and rocks that have been chemically altered, as mobile dust and/or in situ–processed bedrock.

OMEGA data contribute to the identification of these altered phases and to the search for the potential role that water played in that alteration: OMEGA allows discrimination among gas, frost, ice, water absorbed, and water bound in hydrated minerals. High-albedo regions distributed across Mars show specific absorption features from 0.4 to 1.3 μm attributed to Fe^{3+} (Fig. 1) and are thus oxidized. These results extend previous observations made from Earth (*14*), and from the rovers on Mars (*15*). The OMEGA spectra of these oxidized minerals lack the absorption signatures of hydrated minerals (Fig. 2A): The minerals are not hydrated nor do they require the presence of liquid water to form. The alternative interpretation that they result from a dehydration of hydroxides (such as goethite or palagonite) is not validated by the OMEGA detection of a variety of hydrated silicates (clay minerals) and sulfates in old terrains. Liquid water is not responsible for Mars being red.

The grain size of these anhydrous ferric oxides that dominate in the bright areas is likely

[1]Institut d'Astrophysique Spatiale (IAS), Bâtiment 121, 91405 Orsay Campus, France. [2]Department of Geological Sciences, Brown University, Providence, RI 02912, USA. [3]Department of Earth and Planetary Sciences, Washington University, St. Louis, MO 63130, USA. [4]Interactions et Dynamique des Environnement de Surface (IDES), Bâtiment 509, 91405 Orsay Campus, France. [5]Observatoire Midi-Pyrénées, Toulouse, France. [6]Laboratoire de Météorologie Dynamique (LMD), Université Paris 6, Paris, France. [7]The OMEGA co-investigator team: Michel Berthé,[1] Jean-Pierre Bibring,[1] Aline Gendrin,[1] Cécile Gomez,[1] Brigitte Gondet,[1] Denis Jouglet,[1] François Poulet,[1] Alain Soufflot,[1] Mathieu Vincendon,[1] Michel Combes,[2] Pierre Drossart,[2] Thérèse Encrenaz,[2] Thierry Fouchet,[2] Riccardo Merchiorri,[2] GianCarlo Belluci,[3] Francesca Altieri,[3] Vittorio Formisano,[3] Fabricio Capaccioni,[4] Pricilla Cerroni,[4] Angioletta Coradini,[4] Sergio Fonti,[5] Oleg Korablev,[6] Volodia Kottsov,[6] Nikolai Ignatiev,[6] Vassili Moroz,[6] Dimitri Titov,[6] Ludmilla Zasova,[6] Damien Loiseau,[7] Nicolas Mangold,[7] Patrick Pinet,[8] Sylvain Douté,[9] Bernard Schmitt,[9] Christophe Sotin,[10] Ernst Hauber,[11] Harald Hoffmann,[11] Ralf Jaumann,[11] Uwe Keller,[12] Ray Arvidson,[13] John F. Mustard,[14] Tom Duxbury,[15] François Forget,[16] G. Neukum,[17] [Affiliations for the OMEGA team: [1]IAS, Orsay Campus, France. [2]Laboratoire d'Etudes Spatiales et d'Instrumentation en Astrophysique, Observatoire de Paris, Meudon, France. [3]Istituto di Fisica della Spazio Interplanetario–Istituto Nazionale di Astrofisica (IFSI-INAF), Rome, Italy. [4]IAS-INAF, Rome, Italy. [5]University of Lecce, Italy. [6]Institut Komichiski Issledovanie, Moscow, Russia. [7]IDES, Orsay Campus, France. [8]Observatoire Midi-Pyrénées, Toulouse, France. [9]Laboratoire de Planétologie, Grenoble, France. [10]Departement de Planétologie, Université de Nantes, France. [11]Deutsches Zentrum für Luft- und Raumfahrt, Berlin, Germany. [12]Max-Planck-Institut für Sonnensystemforschung, Lindau, Germany. [13]Department of Earth and Planetary Sciences, Washington University, St. Louis, MO, USA. [14]Department of Geological Sciences, Brown University, Providence, RI, USA. [15]Jet Propulsion Laboratory, Pasadena, CA, USA. [16]LMD, Université Paris 6, Paris, France. [17]Freie Universität, Berlin, Germany.]

very small, and they might be nanocrystalline red hematite α-Fe_2O_3 or possibly maghemite γ-Fe_2O_3. Such small particles would be easily transported, stick on most grains, and account for the magnetic properties of the soil measured by the MERs (*16*). Ferric oxides are also detected in localized areas with a variety of albedo (such as within Terra Meridiani, Valles Marineris, or Aram Chaos).

Two types of hydrated minerals have been identified from OMEGA data: phyllosilicates (*10*, *17*) (Fig. 2B) and sulfates (*10*, *18*–*20*) (Fig. 2C), but in only a few locations (*17*) (Fig. 3). Carbonate-rich areas have not been found by OMEGA, although a low concentration of carbonate is interpreted from TES data on martian dust (*21*), and carbonates are recognized in martian meteorites (*22*).

From their near-IR (0.8 to 2.6 μm) spectra, we infer that most of the phyllosilicate minerals are Fe-rich (such as chamosite and nontronite), although Al-rich phyllosilicates (such as montmorillonite) are locally dominant (*17*). These clay minerals are found in a variety of light-toned outcrops and scarps, primarily in rocks and soils north of the Hesperian-aged Syrtis Major volcanic plateau, Nili Fossae, and the Marwth Vallis regions. In all these regions, phyllosilicates are mapped associated with ancient Noachian-aged surfaces. For example, in Nili Fossae, thin Noachian-aged but unaltered mafic units rest directly on phyllosilicate-bearing outcrops. Information from the Mars Express HRSC, the MGS MOC, and the Odyssey THEMIS images clearly indicates that the phyllosilicates are in rocks buried by more recent deposits; the hydrated silicate-bearing bedrock has been exposed through erosion. The surface material of Noachian terrains, which are identified as being heavily cratered, does not necessarily all date from the Noachian times. Rocks of Noachian age are exposed in spots because of impact, faulting, or erosion.

In the Syrtis Major and Nili Fossae regions, phyllosilicate-rich rocks are detected in both ancient craters and material recently excavated from ancient terrains beneath a later volcanic cover. These relations demonstrate that these impacts did not dehydrate the minerals. In contrast, no hydrated minerals are detected in the lobate craters (thought to form by impact into volatile-rich substrates) within the lava flows from Nili Patera, which embay the ancient terrains (*10*). This relation suggests that mineralization of hydrated minerals occurred before the emplacement of the Hesperian-aged lavas from Nili Patera and that these lavas are essentially water-free. In the Marwth Vallis region (Fig. 4), hydrated minerals are not found in the channel nor in its opening but rather on the surrounding plateau and its eroded flanks. Thus, water associated with the formation of the channel did not lead to phyllosilicate formation, although this outflow was sufficient to produce severe erosion, including exposing the ancient clay-rich minerals. So far, none of the major and minor outflow channels or the valley networks show evidence of hydrated minerals.

Sulfates, including Mg sulfates (such as kieserite) and Ca sulfates (such as gypsum), constitute the second major class of hydrated minerals mapped by OMEGA and detected by the NASA rovers (*7*). OMEGA has shown that the sulfate-rich areas are not restricted to the gray hematite-rich regions detected by the MGS TES (*2*, *5*, *6*). We have detected three principal types of hydrated sulfate deposits: layered deposits within Valles Marineris, extended deposits exposed from beneath younger units as in Terra Meridiani, and the dark dunes of the northern polar cap (*10*, *18*–*20*).

Sequential mineral formation. Environments conducive to clay mineral formation may have existed at or near the surface or in the deeper subsurface. Surface or near-surface conditions would not require high-temperature conditions (hydrothermal, for example). Surface formation of these clay minerals would indicate a long-lasting wet episode, with large surface aqueous reservoirs and alkaline water resulting from this chemical alteration, occurring during the Noachian.

Clay minerals could also have been formed primarily in the subsurface, by one of the three following processes: hydrothermal activity (*23*); cratering, supplying subsurface water (liquid and/or ice) to the impacted minerals (*24*); or during the cooling of the mantle, if not thoroughly depleted of volatile compounds. These deep scenarios would not require a warm Mars to have existed over extended time scales, and they could have taken place even if Mars never sustained a dense atmosphere. In addition, the formation of clay minerals could have continued at greater depths long after conditions at the surface became unfavorable.

Sulfate mineral formation requires substantial quantities of water to account for the broad distribution of minerals seen by OMEGA. Because sulfate precipitation requires water to evaporate, it is essentially a surface process. For at

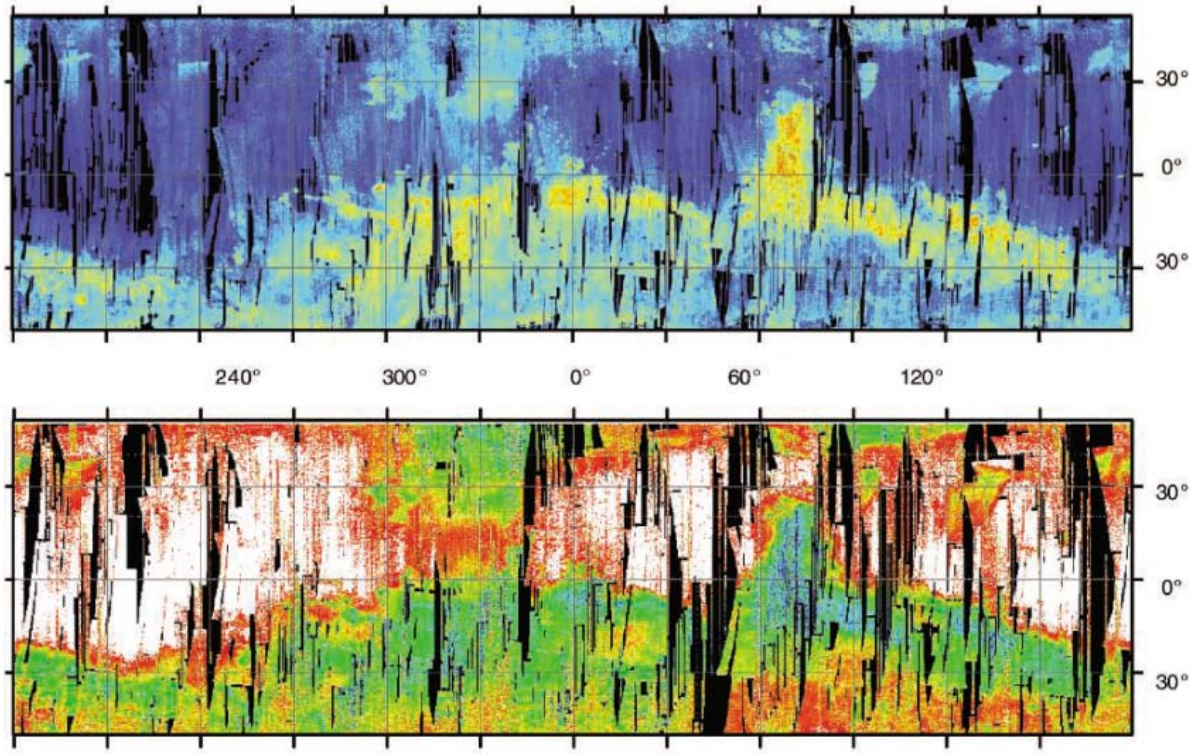

Fig. 1. Global maps of pyroxene (**top**) and anhydrous nanophase ferric oxides (**bottom**), exhibiting the anticorrelation between surface mafics and altered minerals (in the form of ferric oxides). The cratered crust with large pyroxene content (top, yellow to red) is not covered with altered minerals (bottom, blue to green). Conversely, the large areas with no mafics (top, blue) correspond to the higher concentration of ferric oxides (bottom, red to white).

least some of the sulfates identified, an acidic environment is also required. On this basis, we infer that extensive sulfate minerals formed from the late Noachian to the Hesperian, after the surface formation of phyllosilicates, which indicates a substantial change in the global aqueous chemistry of Mars. In addition to their younger age, the sulfate-rich deposits observed by OMEGA extend over a large region. Their size requires a large source of sulfur that we propose is a direct consequence of the extensive outpourings of lavas and associated degassing that primarily formed Tharsis Plateau, as well as the northern plains (in a lunar mare–like process) and Hesperian ridged plains (*25*, *26*). This period of peak volcanism was probably accompanied by a huge release of volatiles, including sulfur and water. This sulfur would have been rapidly oxidized in the atmosphere to form H_2SO_4, which then precipitated on the surface. Surface water would result from a combination of outgassing, hydrothermal activity, the rise of the water table, and massive outflows as Valles Marineris opened, over extended periods of time. All the ingredients were in place for extensive sulfate deposition, either by means of acidic alteration or by weathering of both mafic minerals and, locally, their phyllosilicate alteration products.

Although carbonate minerals have been invoked as a possible reservoir for an early thick CO_2 atmosphere in contact with persistent liquid water (*27*), none have been detected above the OMEGA sensitivity limit of 4% in volume abundance. This result indicates that (i) the era during which surface liquid water remained stable did not last long enough to enable large amounts of CO_2 from the primordial denser atmosphere to be transformed into carbonates; or (ii) clay minerals were formed by impact or subsurface hydrothermal processes rather than by slow surface alteration within liquid water, leaving most of the primordial CO_2 in the atmosphere; or (iii) carbonates have been eliminated from the near surface by acidic weathering or decomposition; or (iv) Mars never sustained a dense CO_2-rich atmosphere. OMEGA data indicate no present major CO_2 reservoirs other than in the atmosphere or the thin CO_2 permanent ice cap over the southern pole (*10*, *28*). This cap is only a thin veneer, typically some meters deep, thus accounting for a small fraction (~10% at most) of the present atmospheric CO_2. On board the NASA Mars Reconnaissance Orbiter, the Compact Reconnaissance Imaging Spectrometers for Mars will perform hyperspectral near-IR mapping with 10 times better spatial resolution than OMEGA: The potential detection of carbonates in association with either phyllosilicates or rocks exposed by impacts should provide constraints against these different possibilities.

After the formation of phyllosilicates and sulfates, the third alteration era began and has continued up to the present, in which liquid water did not play an important role. This is evidenced by the lack of hydration of the ferric oxides, in contrast with the detection of hydrated phyllosilicates and sulfates. Liquid water was probably present during transient and local events (such as the release of volatiles by impacts or the melting of ice deposits), but these episodes were too short to leave a substantial mark on the surface composition. Thus, these transient water events are not responsible for the global alteration, which has mostly been caused by surface oxidation and the production of nanophase ferric oxide, without hydration (Fig. 1). Formation of this alteration product could result from gas/solid reactions (such as atmospheric weathering), mainly through peroxide reactivity or perhaps by frost/rock interactions. This type of alteration probably occurred throughout the three eras. However, it became dominant only in the latter era, when the other sources, which led to the formation of phyllosilicates then sulfates, faded out. The low current H_2O_2 content (*29*), if representative of the entire third era, makes this a slow process, affecting only the superficial layer. This hypothesis is supported by observations of a thin alteration rind on basaltic rocks observed by the Spirit rover at the Gusev landing site (*7*, *30*, *31*). This rind is at most a few millimeters thick and the underlying rock is unaltered. It is also consistent with the low albedo of the material within the trenches made by the MERs in the PanCam images (*31*), indicating that the covering soil and the alteration layer together are a few millimeters thick at most. This slow atmospheric alteration process also accounts for the presence of unaltered mafic minerals in areas either recently brought to the surface (by impact or erosion) or consisting of ancient high-altitude terranes, which have been exposed to much-reduced atmospheric peroxide activity. The presence of nanophase ferric oxide materials across broad regions such as Tharsis, Arabia, and Hellas indicates that these alteration products have been

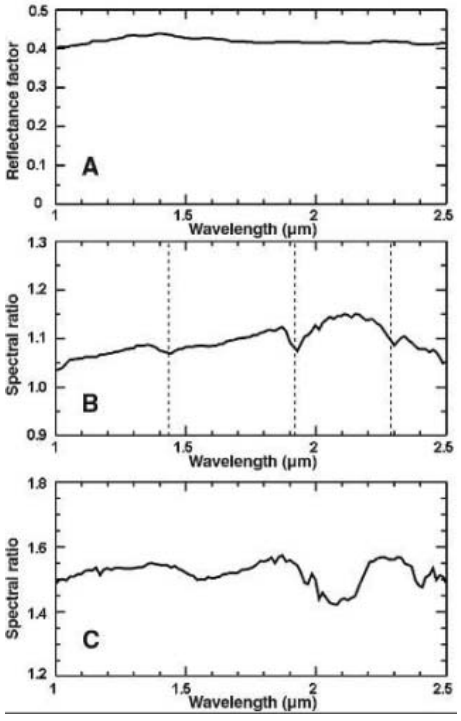

Fig. 2. OMEGA spectra of (**A**) a bright anhydrous soil, rich in nanophase ferric oxides; (**B**) a typical Fe-rich phyllosilicate area; and (**C**) a Mg-sulfate deposit.

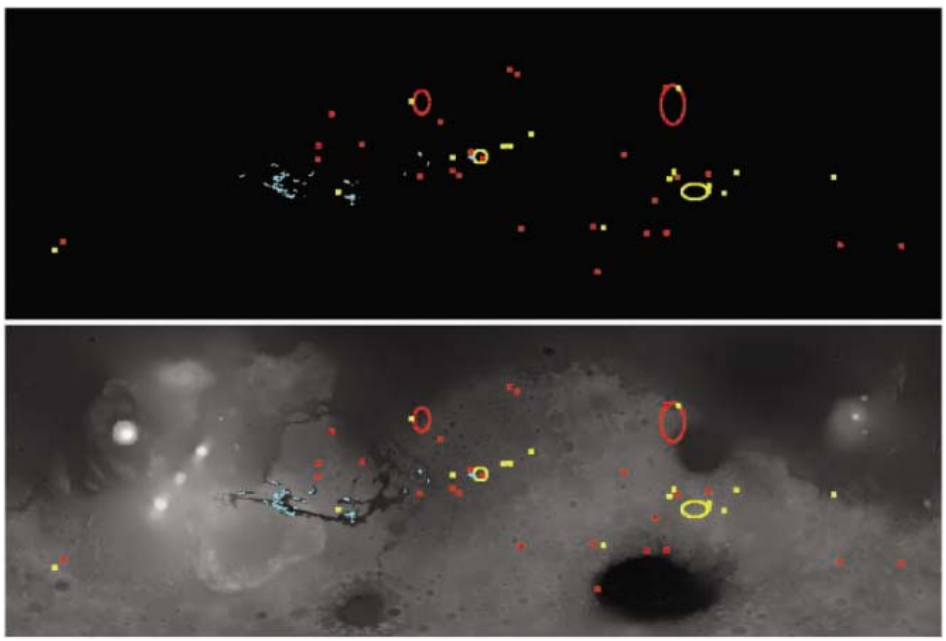

Fig. 3. Global map of hydrated minerals (**top**) plotted over a MGS Mars Orbiter Laser Altimeter (MOLA) altitude reference map (**bottom**). Red, phyllosilicates; blue, sulfates; yellow, other hydrated minerals, with no marked feature (such as being driven by metal-OH vibration) enabling the identification.

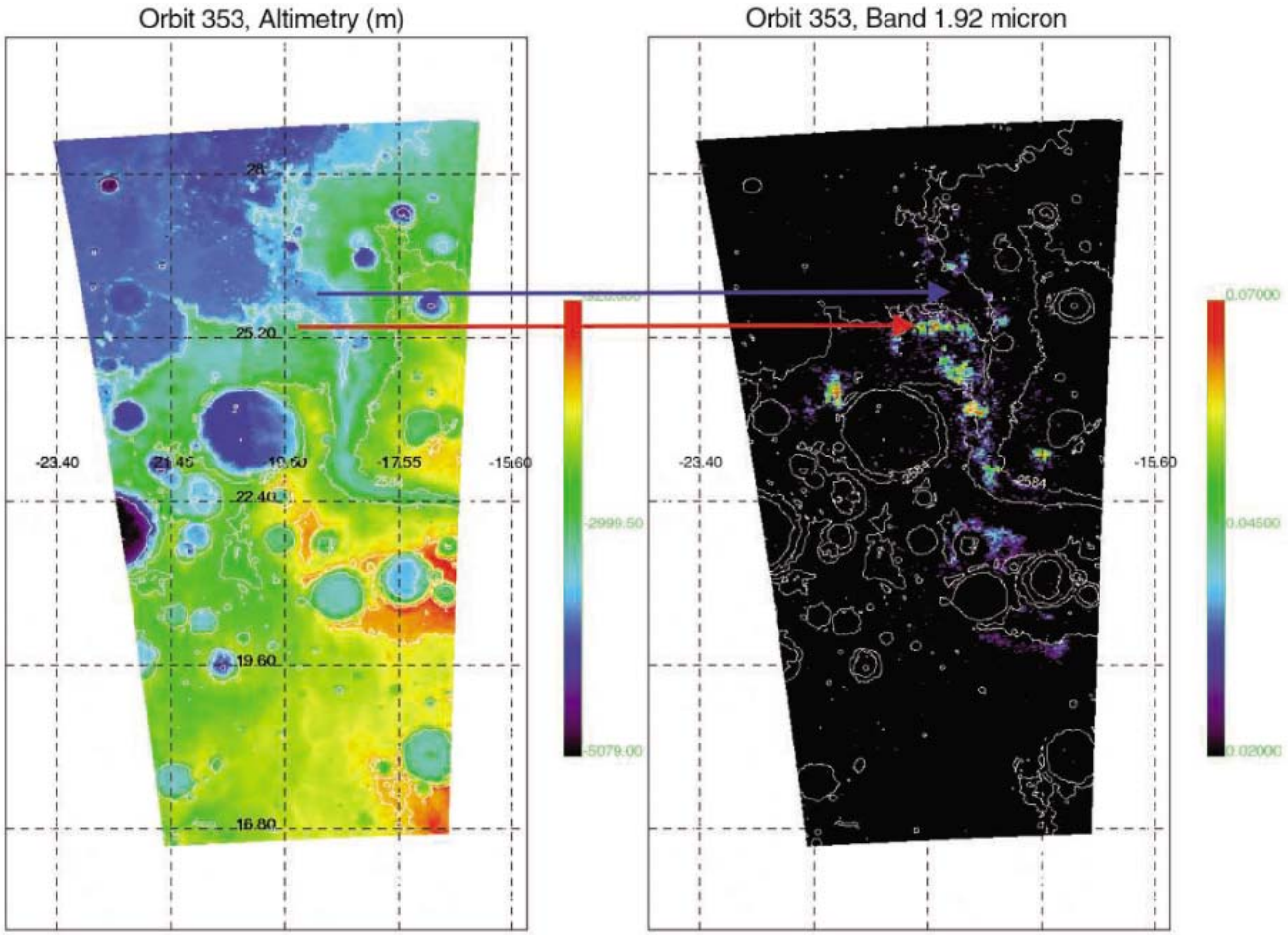

Fig. 4. Magnification of one area of the global map of hydrated minerals (Fig. 3), mapping the hydrated sites in the Marwth Vallis region, with its context in a MGS MOLA altimetry map. Hydrated minerals are not found in the channel (blue arrow) but in the eroded flanks and the cratered plateau (red arrow).

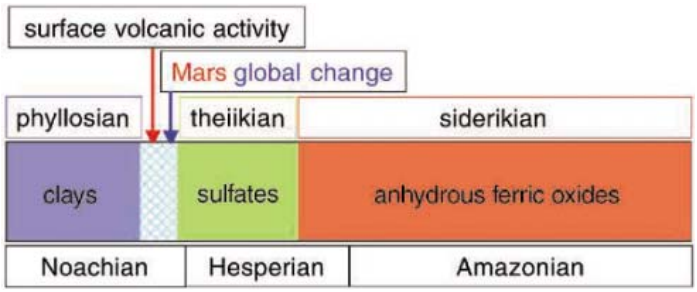

Fig. 5. Sketch of the alteration history of Mars, with phyllosilicates formed first, then sulfates, then anhydrous ferric oxides.

redistributed by atmospheric and aeolian processes across the planet.

Derived Mars history. Our analysis of OMEGA mineralogical assignments in the context of the geologic history of Mars indicates three sequential eras characterized by the surface alteration products (Fig. 5): (i) a nonacidic aqueous alteration, traced by phyllosilicates (the "phyllosian" era); (ii) an acidic aqueous alteration, traced by sulfates (the "theiikian" era); and (iii) an atmospheric aqueous-free alteration, traced by ferric oxides (the "siderikian" era)

The transition between the first two eras occurred early in time and during a critical episode of Mars global climate change from an alkaline, possibly moist, environment to an acidic environment. This change was driven by the extensive outgassing of volatiles, including sulfur, coupled to the volcanic activity that modeled Mars' surface. If phyllosilicates had formed in the subsurface, the Mars environment might have always been tenuous, cold, and dry, except for transient episodes.

If instead phyllosilicates formed at or close to the surface, this would require the Mars early atmosphere to be dense. The global change to an acidic environment would then have been coupled to a rapid drop in atmospheric pressure. A number of processes can be invoked to account for it. The heavy bombardment of Mars, given its low mass, could have resulted in an efficient escape of its early atmosphere (*32*). The global change could also have been triggered by a rapid drop of the internal dynamo and its resulting magnetic shield, favoring efficient atmospheric sputtering (*32*, *33*).

The era during which Mars might have been most likely to have hosted habitable conditions is the first one, indicated by the presence of phyllosilicates. If indeed living organisms formed, these clay minerals could be the sites in which this biochemical development took place (*34*). The low level of the further surface alteration, in perennial cold and dry conditions, under a tenuous atmosphere, could have preserved most of the record of biological molecules, structures, or other diagnostic features in clay-rich surface or subsurface rocks. These areas of high habitability potential offer exciting targets for future in situ exploration.

References and Notes

1. M. H. Carr, *Water on Mars* (Oxford Univ. Press, New York, 1996).
2. P. R. Christensen *et al.*, *J. Geophys. Res.* **106**, 23 (2001).
3. P. R. Christensen *et al.*, *J. Geophys. Res.* **106**, 823 (2001).
4. P. R. Christensen *et al.*, *J. Geophys. Res.* **106**, 871 (2001).
5. P. R. Christensen, R. V. Morris, M. D. Lane, J. L. Bandfield, M. C. Malin, *J. Geophys. Res.* **106**, 873 (2001).
6. P. R. Christensen, R. V. Morris, M. D. Lane, J. L. Bandfield, M. C. Malin, *J. Geophys. Res.* **106**, 885 (2001).

7. S. W. Squyres *et al.*, *Science* **306**, 1709 (2004).
8. J.-P. Bibring *et al.*, *Eur. Space Agency Spec. Publ.* **1240**, 37 (2004).
9. A. Chicarro, P. Martin, R. Trautner, *Eur. Space Agency Spec. Publ.* **1240**, 3 (2004).
10. J.-P. Bibring *et al.*, *Science* **307**, 1576 (2005).
11. J. Mustard *et al.*, *Science* **307**, 1594 (2005).
12. J. L. Bandfield, *J. Geophys. Res.* **107**, 5092 (2002).
13. C. M. Pieters, in *Remote Geochemical Analysis: Elemental and Mineralogic Composition*, C. M. Pieters, P. A. J. Englert, Eds. (Cambridge Univ. Press, New York, 1993), pp. 309–340.
14. P. Pinet, S. Chevrel, *J. Geophys. Res.* **95**, 14435 (1990).
15. J. F. Bell III *et al.*, *J. Geophys. Res.* **105**, 1721 (2000).
16. P. Bertelsen *et al.*, *Science* **305**, 827 (2004).
17. F. Poulet *et al.*, *Nature* **438**, 623 (2005).
18. A. Gendrin *et al.*, *Science* **307**, 1587 (2005).
19. Y. Langevin, F. Poulet, J.-P. Bibring, B. Gondet, *Science* **307**, 1584 (2005).
20. R. Arvidson *et al.*, *Science* **307**, 1591 (2005).
21. J. L. Bandfield, T. D. Glotch, P. R. Christensen, *Science* **301**, 1084 (2003).
22. J. C. Bridges *et al.*, *Space Sci. Rev.* **96**, 365 (2001).
23. L. L. Griffith, E. L. Shock, *J. Geophys. Res.* **102**, 9135 (1997).
24. H. E. Newson, *Icarus* **44**, 207 (1980).
25. X. Phillips *et al.*, *Science* **291**, 2587 (2001).
26. S. C. Solomon *et al.*, *Science* **307**, 1214 (2005).
27. R. Kahn, *Icarus* **62**, 175 (1985).
28. J.-P. Bibring *et al.*, *Nature* **428**, 627 (2004).
29. T. Encrenaz *et al.*, *Icarus* **170**, 424 (2004).
30. R. V. Morris *et al.*, *Science* **305**, 833 (2004).
31. See plates in (*35*).
32. E. Chassefière, F. Leblanc, *Planet. Space Sci.* **52**, 1039 (2004).
33. B. M. Jakovsky, R. J. Phillips, *Nature* **412**, 237 (2001).
34. J. D. Bernal, *The Physical Basis of Life* (Routledge & Kegan Paul, London, 1951).
35. J. F. Bell III *et al.*, *Science* **305**, 800 (2004).

36. The OMEGA instrument was developed with the support of the Centre National d'Etudes Spatiales (CNES), Agenzia Spatiale Italiana (ASI), and Russian Space Agency. The scientific activity is funded by national space and research agencies and universities in France, Italy, Russia, Germany, and the United States. We are very grateful to all of the European Space Agency (ESA) teams who, together with industry, enable this mission. Public OMEGA data are accessible on the ESA Planetary Science Archive Web site. This paper benefited from very valuable comments from S. Murchie.

15 November 2005; accepted 20 March 2006
10.1126/science.1122659

Structure and Receptor Specificity of the Hemagglutinin from an H5N1 Influenza Virus

James Stevens,[1]* Ola Blixt,[1,2] Terrence M. Tumpey,[4] Jeffery K. Taubenberger,[5] James C. Paulson,[1,2] Ian A. Wilson[1,3]*

The hemagglutinin (HA) structure at 2.9 angstrom resolution, from a highly pathogenic Vietnamese H5N1 influenza virus, is more related to the 1918 and other human H1 HAs than to a 1997 duck H5 HA. Glycan microarray analysis of this Viet04 HA reveals an avian α2-3 sialic acid receptor binding preference. Introduction of mutations that can convert H1 serotype HAs to human α2-6 receptor specificity only enhanced or reduced affinity for avian-type receptors. However, mutations that can convert avian H2 and H3 HAs to human receptor specificity, when inserted onto the Viet04 H5 HA framework, permitted binding to a natural human α2-6 glycan, which suggests a path for this H5N1 virus to gain a foothold in the human population.

The H5N1 avian influenza virus, commonly called "bird flu," is a highly contagious and deadly pathogen in poultry. Since late 2003, H5N1 has reached epizootic levels in domestic fowl in a number of Asian countries, including China, Vietnam, Thailand, Korea, Indonesia, Japan, and Cambodia, and has now spread to wild bird populations. More recently, the H5N1 virus has spread to infect bird populations across much of Europe and into Africa. However, its spread to the human population has so far been limited, with only 191 documented severe infections, but with a high mortality accounting for 108 deaths in Indonesia, Vietnam, Thailand, Cambodia, China, Iraq, Turkey, Azerbaijan, and Egypt [as of 4 April 2006, see the World Health Organization Web site (*1*)]. Of these, evidence suggests direct bird-to-human transmission, although indirect transmission, perhaps through contaminated water supplies, cannot be ruled out.

Of the three influenza pandemics of the last century, the 1957 (H2N2) and 1968 (H3N2) pandemic viruses were avian-human reassortments in which three and two of the eight avian gene segments, respectively, were reassorted into an already circulating, human-adapted virus (*2*, *3*). The origin of the genes of the 1918 influenza virus (H1N1), which killed about 50 million people worldwide (*4*), is unknown. The extinct pandemic virus from 1918 has recently been reconstructed in the laboratory and was found to be highly virulent in mice and chicken embryos (*5*, *6*). With continued outbreaks of the H5N1 virus in poultry and wild birds, further human cases are likely, and the potential for the emergence of a human-adapted H5 virus, either by reassortment or mutation, is a threat to public health worldwide.

Hemagglutinin (HA), the principal antigen on the viral surface, is the primary target for neutralizing antibodies and is responsible for viral binding to host receptors, enabling entry into the host cell through endocytosis and subsequent membrane fusion. As such, the HA is an important target for both drug and vaccine development. Although 16 avian and mammalian serotypes of HA are known, only three (H1, H2, and H3) have become adapted to the human population. HA is a homotrimer; each monomer is synthesized as a single polypeptide (HA0) that is cleaved by host proteases into two subunits (HA1 and HA2). HA binds to receptors containing glycans with terminal sialic acids, where their precise linkage determines species preference. A switch in receptor specificity from sialic acids connected to galactose in α2-3 linkages (avian) to α2-6 linkages (human) is a major obstacle for influenza A viruses to cross the species barrier and to adapt to a new host (*7*, *8*). On H3 and H1 HA frameworks, as few as two amino acid mutations can switch human and avian receptor specificity.

Of the H5N1 viral isolates studied to date, A/Vietnam/1203/2004 (Viet04) is among the most pathogenic in mammalian models, such as ferrets and mice (*9*, *10*). This virus was originally isolated from a 10-year-old Vietnamese boy who died from bird flu. Because of the importance of HA in viral pathogenesis and host response to viral infection, we cloned and expressed the ectodomain (HA0) of its HA gene (fig. S1) in a baculovirus expression system, using the same strategy that led to the crystal structure of the 1918 influenza virus HA0 (*11*, *12*). Viet04 HA0 was cleaved during protein production into its activated form (HA1/HA2) and was crystallized at pH 6.55 (*13*). Its structure was determined by molecular replacement (MR) to 2.95 Å resolution (table S1) (*14*). In addition, we have investigated the potential of this H5 HA to acquire human receptor specificity by introducing mutations known to effect such a specificity switch on H1 and H3 frameworks.

Structural overview. The overall fold of the Viet04 HA trimer (Fig. 1, A and B) is very similar to other published HAs, as expected, with a globular head containing the receptor binding domain (RBD) and vestigial esterase domain, and a membrane proximal domain with its distinctive, central α-helical stalk and HA1/HA2 cleavage site (essential for viral pathogenicity). Although Viet04 HA and the only other avian H5 HA structure, Sing97 [A/Duck/Singapore/3/1997; Protein Data Bank (PDB) entry 1jsm (*15*)], are closely related in sequence (HA1, 90%; HA2, 98%), the best molecular replacement (MR) solutions were sur-

[1]Department of Molecular Biology, [2]Glycan Array Synthesis Core-D, Consortium for Functional Glycomics, [3]Skaggs Institute for Chemical Biology, The Scripps Research Institute, 10550 North Torrey Pines Road, La Jolla, CA 92037, USA. [4]Influenza Branch, Division of Viral and Rickettsial Diseases, Centers for Disease Control and Prevention, Atlanta, GA 30333, USA. [5]Department of Molecular Pathology, Armed Forces Institute of Pathology, Rockville, MD 20306, USA.

*To whom correspondence should be addressed. E-mail: wilson@scripps.edu (I.A.W.) and jstevens@scripps.edu (J.S.)

prisingly achieved by using the 1918 H1 structure (sequence identity: HA1, 58%; HA2, 85%) as a search model (*16*). Superimposition of human, avian, and swine HA structures by using their HA2 domains (table S2) or individual domains (table S3) confirms that the Viet04 HA is more closely related to human 1918 H1 HA [root mean square deviation (RMSD) 1.2 Å] than to Sing97 H5 HA (RMSD 1.7 Å). For example, an interhelical loop between the two major helices in HA2 is stabilized by a hydrogen bond between HA2 Arg^{68} and HA2 Asn^{81}, resulting in its having an overall conformation much more akin to the 1918 H1 loop than to that of Sing97 or H3 (Fig. 1C).

The amino acid sequence of Viet04 HA predicts seven possible glycosylation sites per monomer, although one is in the cytoplasmic tail and unlikely to be glycosylated. Interpretable electron density is observed at 16 of the possible 54 glycosylation sites in the asymmetric unit (nine monomers), which represents carbohydrates at two sites, Asn^{34} and Asn^{169} in HA1 (*17*).

Hemagglutinin is synthesized as a single-chain precursor (HA0) in the endoplasmic reticulum, where it is assembled as a trimer, and is then exported to the cell surface via the Golgi network. On the cell surface, HA0 is cleaved by specific host proteases, such as tryptase Clara (*18*), into HA1 and HA2 (*19*). For the majority of HAs, the specific cleavage site (Q/E-X-R) (*20*) and the narrow tissue distribution of the relevant proteolytic enzymes restricts infection to the lung in mammals. However, for H5 and H7 subtypes, a polybasic sequence has been associated with high virulence in birds (*21*), because of enhanced cleavage susceptibility by a broader range of cellular proteases, as seen with our baculovirus-expressed Viet04 HA (fig. S1) (*22*). Consequently, the tissue tropism for H5 viruses in mammals is not restricted to the lungs, but extends to other organs, including the brain (*10*). In the Viet04 structure, the C-terminal HA1 cleavage site region could be interpreted only as far as Pro^{324} and does not account for the remaining QRERRRKKR residues before Gly^{1} at the N terminus of HA2 (fig. S3). As in other HAs, the HA2 N terminus is stabilized within an electronegative cavity by hydrogen bonds from its backbone amide groups to Asp^{112} and to Ser^{113} of the adjacent HA2 (fig. S3).

From our previous 1918 HA0 structure, we proposed that a pH-sensitive histidine patch (His^{A18}, His^{A38}, and His^{B111}) (*14*), together with the adjacent HA2 Trp^{B21}, could play a role in fusion peptide destabilization and release (Fig. 1A) (*11*). This structural feature is conserved in other avian and human H1, H2, and H5 serotypes, as well as in Viet04 HA (fig. S3). In 1918 HA0, a second patch of four exposed histidines within the vestigial esterase domain (Fig. 1A and fig. S4A), together with a nearby lysine, was also implicated in pathogenicity via enhanced membrane fusion (*11*). Of the five HA1 residues in this basic patch (His^{47}, Lys^{50}, His^{275}, His^{285}, and His^{298}), only three are conserved in avian H5 structures (His^{47}, Lys^{50}, and His^{298}) (fig. S4, B to D), but Viet04 and Sing97 HAs have an additional lysine (Lys^{45}) and histidine (His^{295}) (fig. S4, B, C, and E). Furthermore, Viet04 has yet another lysine (Lys^{46}), which renders this patch even more basic and is found in two strains (1203/1204) that were isolated from the same patient (*10*) (fig. S5). The contribution of this region to virulence, if any, is as yet unknown, but is worthy of further investigation.

H5N1 antigenic variation. Phylogenetic analysis of H5 HA genes from 2004 and 2005 has revealed two distinct lineages, termed clades 1 and 2 (*23*); Viet04 belongs to the Indochina peninsula lineage (clade 1). Comparison of their amino acid sequences identified 13 positions of antigenic variation that are mainly clustered around the receptor-binding site; the rest are within the vestigial esterase domain (Fig. 2). Escape mutants of H5 HAs (*24*, *25*) can be clustered into three epitopes (*24*), as follows: site 1, an exposed loop (HA1 140 to 145) that overlaps with antigenic sites A (*26*) of H3 (*27*) and Ca2 of H1 (*28*); site 2, HA1 residues 156 and 157, which correspond to antigenic site B in H3 serotypes; and site 3, HA1 129 to 133, which is restricted to the Sa site in H1 HAs (*28*) and H9 serotypes (*29*). Thus, natural variation

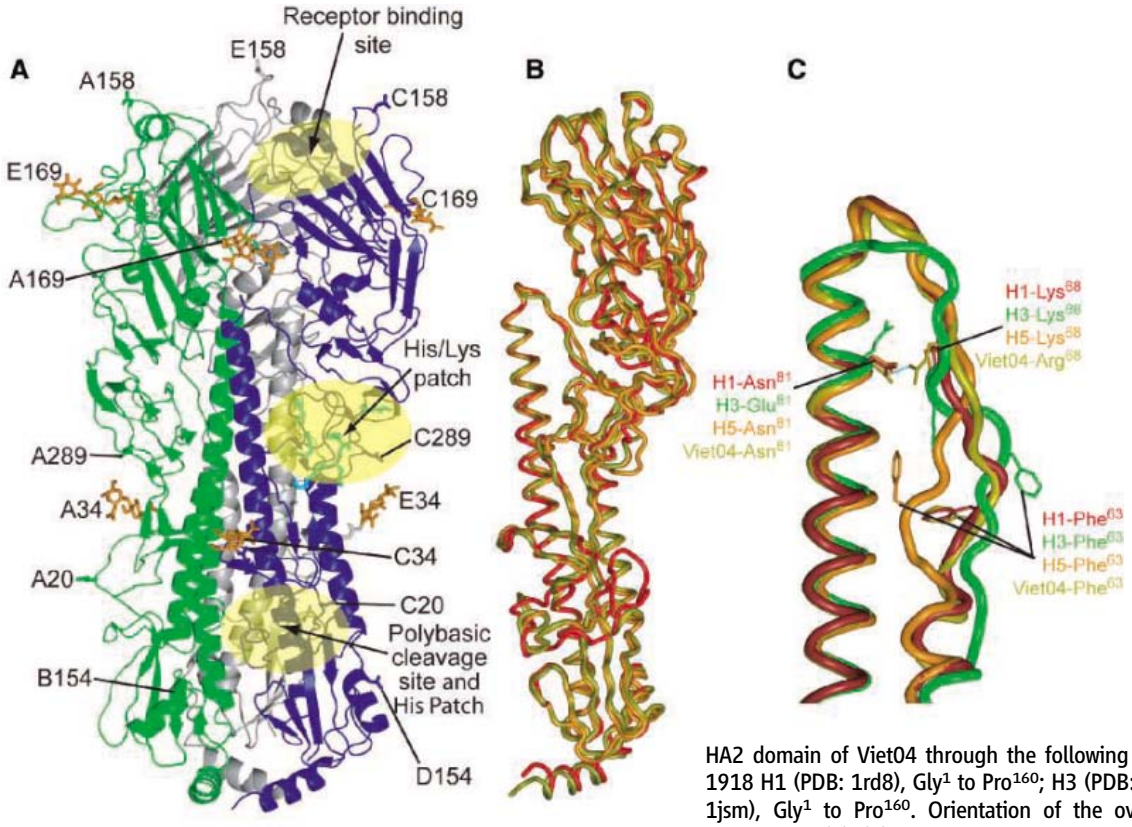

Fig. 1. Crystal structure of Viet04 HA and comparison with 1918 human H1, duck H5, and 1968 human H3 HAs. (**A**) Overview of the Viet04 trimer, represented as a ribbon diagram. For clarity, each monomer has been colored differently. Carbohydrates observed in the electron-density maps are colored orange, and all the asparagines that make up a glycosylation site are labeled. Only Glu^{20}, Glu^{289}, and Phe^{154} are not labeled, as these are on the back of the molecule. The location of the receptor binding, cleavage, and basic patch sites are highlighted only on one monomer. All the figures were generated and rendered with the use of MacPymol (*66*). (**B**) Structural comparison of the Viet04 monomer (olive) with duck H5 (orange) and 1918 H1 (red) HAs. Structures were first superimposed on the HA2 domain of Viet04 through the following residues: Viet04, Gly^{1} to Pro^{160}; 1918 H1 (PDB: 1rd8), Gly^{1} to Pro^{160}; H3 (PDB: 2hmg), Gly^{1} to Pro^{160}; H5 (PDB: 1jsm), Gly^{1} to Pro^{160}. Orientation of the overlay approximates to the blue monomer in (A). (**C**) Superimposition of the two long α-helices of HA2 for 1918 H1 (PDB: 1rd8), avian H5 (PDB: 1jsm), human H3 (PDB: 2hmg), and Viet04 reveal that the extended interhelical loop of Viet04 is more similar to the 1918 H1 than to the existing avian H5 structure. The side chain of Phe^{63} is illustrated as an example of the close proximity of the two structures.

(yellow in Fig. 2), as well as escape mutants (blue in Fig. 2, green in both 2004 and 2005 viral isolates), suggests continued evolution of the virus that impacts decisions on which strain should be considered for a bird flu vaccine. One mutation that has alanine at residue 160 replaced by threonine (A160T), which is present in all 2004–05 strains, introduces a new glycosylation site at Asn^{158}, consistent with a strategy commonly used by influenza viruses to mask and unmask antigenic sites from the immune system (*30*, *31*). This glycosylation likely results in steric hindrance to antigenic site 2 (around residues 156 and 157), thus reducing the ability of the host to mount an effective immune response to these more recent H5N1 viruses.

Receptor binding domain. The RBD is at the membrane distal end (HA1) of each HA monomer (Fig. 1A) and binds to its sialic acid–containing receptors with very weak (millimolar) affinity (*32*). However, influenza virus can increase its avidity to host cells through multivalent binding via a high density of HA trimers on the virus surface. Avian viruses bind to sialosides with an α2-3 linkage in the intestinal tract, whereas human-adapted viruses are specific for the α2-6 linkage in the respiratory tract (*7*), although H5 viruses have also been reported in human intestine (*33*). A switch from α2-3 to α2-6 receptor specificity is a critical step in the adaptation of avian viruses to a human host and appears to be one of the reasons why most avian influenza viruses, including current avian H5 strains, are not easily transmitted from human to human after avian-to-human infection.

All HA structures, including Viet04 (Fig. 3A), have similarly configured RBDs. The binding site comprises three structural elements, namely an α-helix (190-helix, HA1 188 to 190) and two loops (130-loop, HA1 134 to 138, and 220-loop, HA1 221 to 228) (Fig. 3A). A number of conserved residues are involved in receptor binding, including Tyr^{98}, Trp^{153}, and His^{183} (Table 1) (*19*). Superimposition of the RBD structural elements of Viet04 with Sing97 H5 reveals a very close relation (RMSD 0.3 Å) (Fig. 3B). Indeed, all key residues implicated in receptor specificity [reviewed in (*19*)] (Table 1) are conserved between structures, although loop 210 to 221 is displaced ~1 Å from its equivalent in Sing97 (Fig. 3B). Otherwise, only two RBD residues differ between these two H5 HAs (Viet04, Arg^{216} and Ser^{221}; Dk97, Glu^{216} and Pro^{221}). Thus, the question arises as to how a current H5 virus could adapt its HA for binding to human receptors.

Receptor binding specificity of Viet04 HA. Our cloning and expression strategy produces HA with a His-tag at the C terminus, which facilitates receptor-binding studies using a glycan microarray (*34*–*37*). Glycan binding analyses of Viet04 HA reveal an avian α2-3 specificity in which the highest affinity is for glycans with sulfate on the 6 position of the *N*-acetylglucosamine (GlcNAc) residue at the third position in the glycan chain (Fig. 4A and table S4) (*38*, *39*). Considerable binding to only one α2-6–linked sialoside was observed (6′-sialyllactose, no. 49), but this glycan is only found in milk and is not a receptor candidate for influenza (*40*). We also expressed and investigated the glycan-binding properties of A/Duck/Singapore/Q-F119-3/1997 (Dk97), whose sequence is identical to that of Sing97, for correlation with its structure (*15*). Binding of glycoproteins (nos. 1 to 6) and sulfated glycans was comparable to those of Viet04, but binding to other α2-3 sialosides was reduced relative to Viet04 (Fig. 4B).

Mutational analysis of the RBD. Previous studies using whole virus identified a number of key RBD mutations that were implicated in avian-human receptor specificity switching in H1, H2, and H3 serotypes. However, adaptation of avian H1 and H2/H3 serotypes for human receptor binding occurs by different mecha-

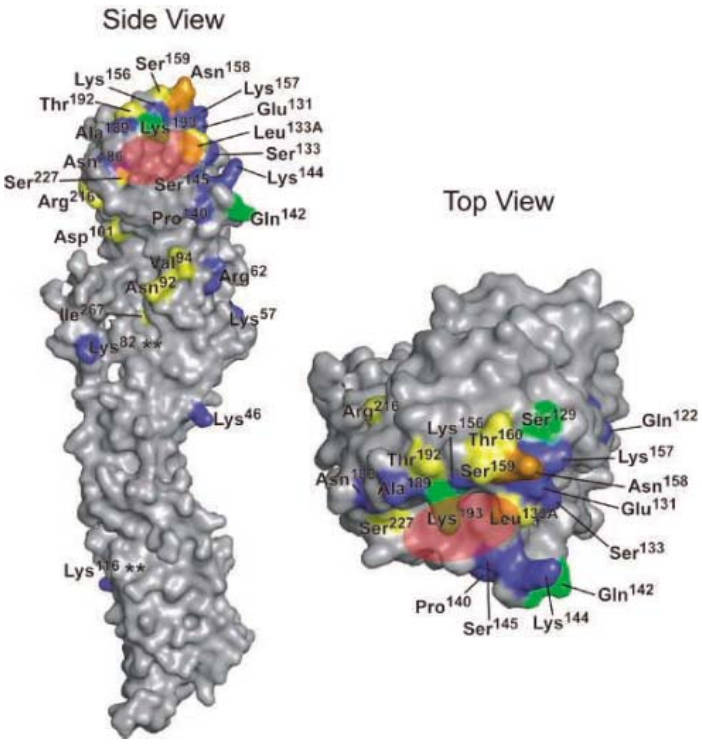

Fig. 2. Antigenic variation in recent H5N1 viruses mapped onto the Viet04 structure. (**Left**) Side view of the Viet04 structure in which natural mutations identified by comparison of 2005 with 2004 isolates (*23*) are colored yellow; escape mutants (*24*, *25*) are blue; and those that overlap in both analyses are green. All of the 2004 and 2005 strains have a new potential glycosylation site at position 158 in the HA1 chain (orange). The receptor binding site is highlighted with a red oval. (**Right**) Top view looking down onto the globular membrane distal end of the trimer around the RBD showing that the mutations mainly cluster around the RBD.

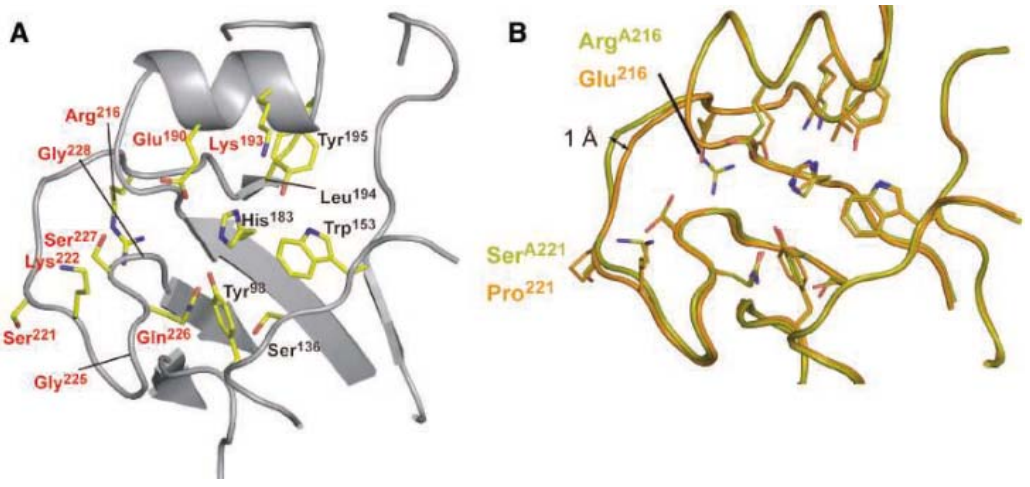

Fig. 3. Analysis of Viet04 receptor binding site. (**A**) The Viet04 receptor-binding domain (RBD) with the side chains of key residues for receptor binding labeled. The binding site comprises three structural elements: an α-helix (190-helix) and two loops (130-loop and 220-loop). Residues mutated in this study are labeled red. (**B**) Overlay of the RBDs of Viet04 with Sing97 structure (PDB: 1jsm) reveals a similar RBD. The most divergent part of the pocket is the loop made up of residues 210 to 221, in which the Viet04 loop is displaced ~1 Å farther away from the binding pocket compared with the 1997 avian H5. Only two residues, at position 216 and 221, differ in these two RBDs.

nisms. For H2 and H3, mutation of Gln^{226} and Gly^{228} in avian strains to Leu^{226} and Ser^{228} in human viruses correlates with a shift to human receptor specificity (*41*, *42*). In H1 serotypes, the avian Gln^{226} and Gly^{228} framework is maintained and a Glu^{190} to Asp^{190} mutation now appears critical for adaptation to human α2-6 receptors (*43*, *44*). Indeed, glycan microarray and cell-based assays revealed that the 1918 HA could be readily converted from classic α2-6 receptor specificity to classic avian α2-3 specificity by only two mutations (D190E and D225G) (*35*, *45*). Here, the reverse experiment was performed with an avian H1 virus [A/Duck/Alberta/35/1976 (Dk76)] in which the same two residues were mutated to the "human" sequences (E190D and G225D), which completely converted Dk76 to exclusive α2-6 specificity, similar to that seen for the South Carolina 1918 virus (Figs. 4C and 5, A to C; and table S4) (*11*, *46*).

However, which mutations are likely to modulate receptor specificity in the H5 serotype is not so obvious. Based on sequence similarity, H5 is in the same clade as H1, H2, and H6 serotypes (*47*). So, to address that issue, we analyzed glycan binding of Viet04 HA (Fig. 5 and fig. S6) by generating a panel of mutants

Table 1. Conserved residues within the RBDs of H1 and H5 serotypes that are implicated in receptor specificity. Accession numbers for each wild-type HA are listed in supporting online material. Residues mutated in this study are highlighted in gray. The last two columns give a qualitative assessment of α2-3/α2-6 binding preferences for each mutant with the glycan array. Qualitative binding assessments were based on a combination of the signal strength and the number of glycans bound for a given linkage. The binding of Viet04 was used as a standard for strong binding to the α2-3 linkage (✓✓✓), and the double mutant for Dk76 (E190D,G225D) was used for strong binding (✓✓✓) to the α2-6 linkage.

Viral strain	Amino acid position														Specificity	
	98	136	153	183	190	193	194	216	221	222	225	226	227	228	α2-3	α2-6
H1 serotype																
A/Duck/Alberta/35/1976	Y	T	W	H	E	S	L	E	P	K	G	Q	A	G	✓✓	O
A/Duck/Alberta/35/1976 (E190D)	Y	T	W	H	D	S	L	E	P	K	G	Q	A	G	✓	O
A/Duck/Alberta/35/1976 (G225D)	Y	T	W	H	E	S	L	E	P	K	D	Q	A	G	O	O
A/Duck/Alberta/35/1976 (E190D,G225D)	Y	T	W	H	D	S	L	E	P	K	D	Q	A	G	O	✓✓✓
H5 serotype																
A/Duck/Singapore/Q-F119-3/1997	Y	S	W	H	E	K	L	E	P	K	G	Q	S	G	✓✓	O
A/Vietnam/1203/2004	Y	S	W	H	E	K	L	R	S	K	G	Q	S	G	✓✓✓	✓
A/Vietnam/1203/2004 (E190D)	Y	S	W	H	D	K	L	R	S	K	G	Q	S	G	✓✓	O
A/Vietnam/1203/2004 (G225D)	Y	S	W	H	E	K	L	R	S	K	D	Q	S	G	✓✓✓	✓
A/Vietnam/1203/2004 (E190D,G225D)	Y	S	W	H	D	K	L	R	S	K	D	Q	S	G	O	O
A/Vietnam/1203/2004 (Q226L)	Y	S	W	H	E	K	L	R	S	K	G	L	S	G	✓	O
A/Vietnam/1203/2004 (S227N)	Y	S	W	H	E	K	L	R	S	K	G	Q	N	G	✓✓✓	✓
A/Vietnam/1203/2004 (G228S)	Y	S	W	H	E	K	L	R	S	K	G	Q	S	S	✓✓✓	✓✓*
A/Vietnam/1203/2004 (Q226L,G228S)	Y	S	W	H	E	K	L	R	S	K	G	L	S	S	✓✓	✓✓*
A/Vietnam/1203/2004 (R216E)	Y	S	W	H	E	K	L	E	S	K	G	Q	S	G	ND	ND
A/Vietnam/1203/2004 (S221P)	Y	S	W	H	E	K	L	R	P	K	G	Q	S	G	✓✓✓	✓
A/Vietnam/1203/2004 (R216E,S221P)	Y	S	W	H	E	K	L	E	P	K	G	Q	S	G	✓✓✓	✓

*Although Viet04 mutants (G228S and Q226L,G228S) only bound a limited number of α2-6 ligands, they bound strongly to these glycans and were, therefore, assessed as ✓✓ for α2-6 specificity. No binding is represented by "O"; ND indicates binding to the array was not determined.

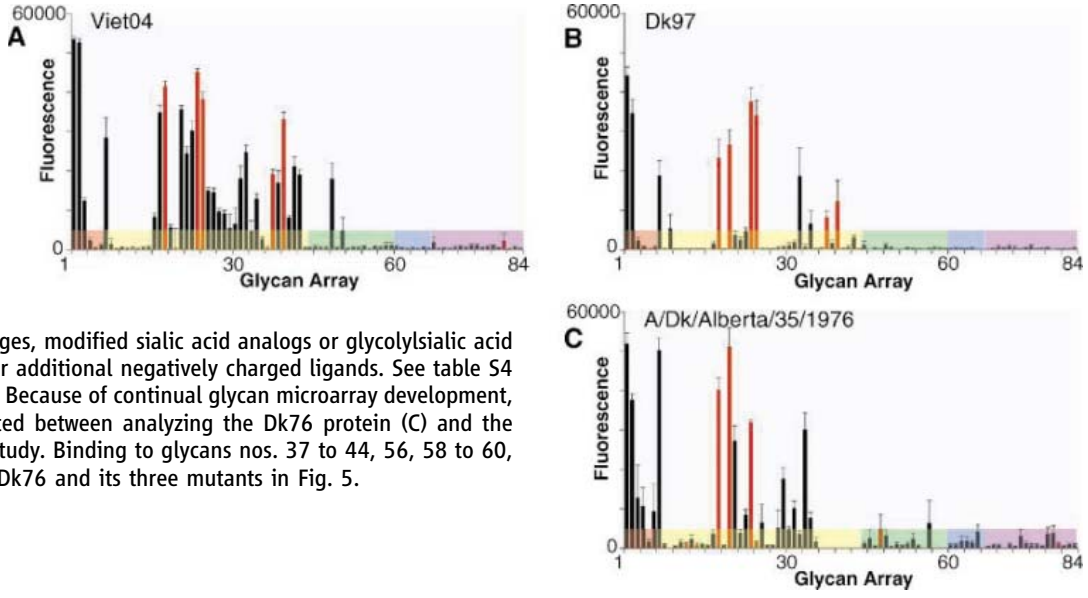

Fig. 4. Glycan microarray analyses of (**A**) Viet04, (**B**) Dk97, and (**C**) an avian H1, Dk76. The Dk97 HA sequence is identical to that in the published structure of duck virus Sing97, so a direct structural comparison can be made. Binding to different types of glycans on the array are highlighted where orange represents glycoproteins; yellow, α2-3 ligands; green, α2-6 ligands; blue, α2-8 ligands; and purple, other ligands such as β-linkages, modified sialic acid analogs or glycolylsialic acid glycans. Red bars indicate sulfated or additional negatively charged ligands. See table S4 for list and tabulated binding results. Because of continual glycan microarray development, a number of new ligands were printed between analyzing the Dk76 protein (C) and the remaining samples reported in this study. Binding to glycans nos. 37 to 44, 56, 58 to 60, 67, and 70 was not determined for Dk76 and its three mutants in Fig. 5.

(Fig. 3A and Table 1) in and around the RBD to explore whether this H5 HA can readily become adapted to humans through mutations that are known to change receptor specificity in H1 and H3 serotypes. Mutations at positions 190 and 225 did not reveal any adaptation of Viet04 to human receptor analogs (Fig. 5, D to F) (*48*), in contrast to H1 Dk76 (Fig. 5, A to C) and 1918 HAs (*35*). Indeed, the single E190D mutation on the Viet04 framework reveals markedly reduced affinity to α2-3 sialosides (Fig. 5D), whereas the double mutant (E190D,G225D) did not interact at all with the glycan microarray (Fig. 5F) (*49*, *50*). However, sulfated glycans bound equally well to the single E190D mutant and to the wild type (Figs. 4A and 5D), which suggests that other residues within the Viet04 RBD, such as Lys^{193} or Lys^{222} (Fig. 3A), may enhance interaction with charged glycans.

Mutation of residues 226 and 228, which enable H3 viruses to switch from avian to human specificity, was also evaluated as a potential route for H5 viruses to acquire human receptor specificity. Although a dramatic switch to a classic α2-6 human receptor binder was not observed (*51*), the double mutant (Q226L,G228S) showed substantially reduced affinity to α2-3 sialosides, as noted for mutants of the H3 A/Hong Kong/156/1997 virus (*52*). But it was notable that significant binding to a natural, branched α2-6 biantennary glycan (nos. 56 and 57) was observed for both the double mutant and the single G228S mutant (Fig. 5H). Although the glycan composition of lung epithelia have not been analyzed in detail, the mammalian sialyltransferase that produces α2-6–linked structures on many human tissues (*53*, *54*) is found in lung epithelial cells (*55*–*57*). Thus, these two effects could offer advantages for an H5N1 virus to adapt to a human host. Decreased binding to α2-3–linked glycans would help circumvent the inhibitory effects of respiratory mucins (*58*), whereas increased binding to biantennary N-linked glycans with α2-6–linked sialic acids would allow the virus to attach to the surface of epithelial cells that express this carbohydrate receptor (*55*–*57*). In this regard, human H1 viruses before 1957 were reported to bind sialic acid receptors with both α2-3 and α2-6 linkages; post 1957 viruses were specific only for α2-6 linkages (*37*). These binding patterns suggest that, once a foothold in a new host species is made, the virus HA optimizes its specificity to the new host. It is noteworthy that, of the HAs tested on the array, the humanized avian H1 (Dk76) double mutant (E190D,G225D) (Fig. 5C) and the human H3 HA (A/Moscow/10/1999) (*35*) did not bind α2-6 biantennary glycans, in contrast to 1918 South Carolina H1 HA and human H1, A/Texas/36/1991 (*35*). Therefore, the HAs of some viruses may be able to increase avidity through interaction with such bivalent structures on N-linked glycans, whereas, for others, the geometry of the bivalent structure appears to restrict binding to linear sequences containing α2-6

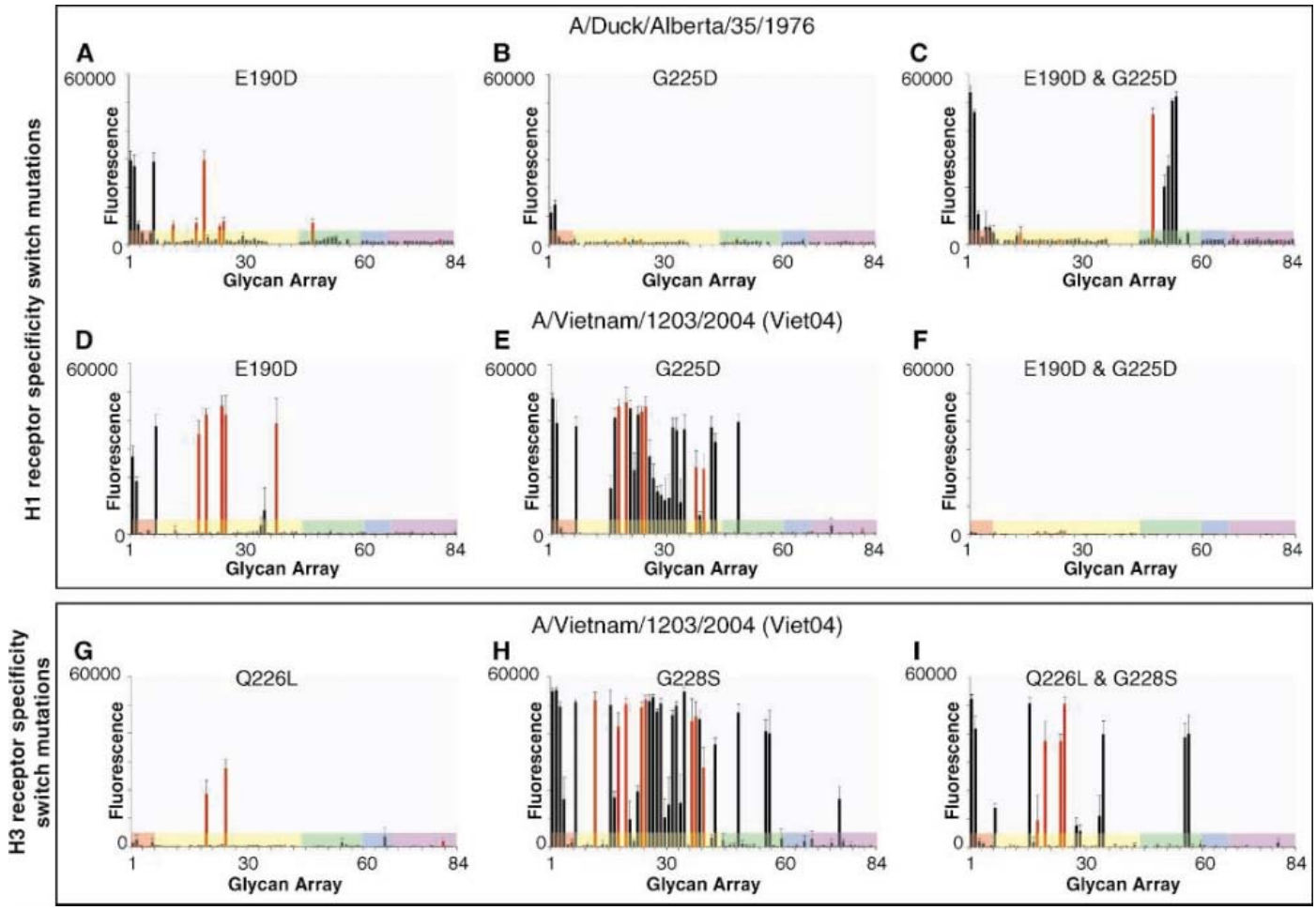

Fig. 5. Glycan microarray analysis of mutants of Viet04 and Dk76. Mutations of an avian H1, Dk76: (**A**) E190D, (**B**) G225D, and (**C**) E190D and G225D were generated and subjected to glycan microarray analysis. Both positions were reported to be important for conversion of α2-6 receptor specificity of the human 1918 virus HA to avian α2-3 specificity (*35*, *45*). These mutations did indeed result in exclusive α2-6 specificity for this avian H1 HA. (**D** to **F**) Consequently, Viet04 mutations were generated at the same positions, but did not result in a switch of receptor specificity, except to 6′-sialyllactose, although they did result in decreased α2-3 binding, particularly to nonsulfated glycans (compare Fig. 4A). (**G** to **I**) Viet04 was mutated at positions 226 and 228, known to be important for H3 HA α2-6 receptor adaptation. Again, no clear switch in receptor specificity was observed, although binding to biantennary α2-6 moieties was observed, as well as reduced α2-3 binding in the double and single (Q226L) mutant. Graphs are generated as described in the legend for Fig. 4 and labels to the introduced mutations.

linkages. Thus, although human viral HAs have a primary specificity for α2-6 linkages, each may use a different spectrum of glycan receptors for cell entry.

All key residues within the RBD are conserved in the majority of H5 strains that have infected humans (fig. S5). However, two A/Hong Kong/2003 (HK2003) isolates acquired a S227N mutation within the binding site, whereas a double mutation (E216R,P221S) in the 220-loop is observed in all 2003–05 isolates (fig. S5). The possible effect of these natural mutations on Viet04 HA binding specificity (Table 1) was, therefore, assessed. The S227N mutation had comparable specificity to that of Viet04, with the exception of increased binding, particularly for branched α2-3 fucosylated glycans (nos. 26 to 29) and for 6-sialylated *N*-acetylgalactosamine (GalNAc) (no. 20) (fig. S6A) (*59*, *60*), contrary to previous reports that HK2003 isolates had increased affinity toward α2-6 analogs, but decreased affinity toward α2-3 analogs (*39*). However, in a previous study from a 1997 isolate, such changes were also not observed (*52*), although Viet04 differs at a number of other positions around the RBD compared with the Hong Kong isolates that could account for this difference (*61*) (Fig. 3A). Reverse R216E and S221P mutants were also generated, as well as the double mutant (R216E,S221P), but the R216E mutant expressed poorly and could not be analyzed. However, only the double mutant is found in natural isolates, suggesting a pressure to select for both mutations, which possibly are related to the HA stability. Whereas Viet04 HA binds to branched fucosylated sialosides (nos. 26 to 29) (Fig. 4A), the S221P mutation showed weaker binding, whereas the double mutant abrogated binding to all branched fucosylated glycans unless sulfated (no. 25) (fig. S6, B and C). In the Viet04 HA structure, these residues hydrogen bond to an adjacent monomer in the trimer (Arg^{216} with Asn^{210} and Ser^{221} with Asp^{241}) (*15*) and stabilize the displaced 210 to 229 loop (Fig. 3B), which, therefore, could possibly enhance binding to branched fucosylated glycans.

So how might H5 avian HA adapt to human receptors? Knowledge of genetic changes in circulating viral isolates (*39*) by themselves obviously cannot be used to predict the impact on receptor specificity, let alone predict the effect of future mutations. Here, we use a completely recombinant system for structural and functional analyses that enables such investigation in the laboratory. Our conclusion is that the mutations that cause a shift from the avian-type to human-type specificity on the H1 and H3 frameworks do not cause an equivalent shift in specificity on the H5 framework of the Viet04 isolate. However, the mutations that give rise to α2-6 specificity in H3 HAs do in fact reduce avidity to α2-3 sialosides and increase specificity for α2-6–linked biantennary N-linked glycans that could serve as receptors for the virus on lung epithelial cells. These combined effects could allow the Viet04 virus to escape entrapment by mucins and increase the likelihood of binding to and infection of susceptible epithelial cells (*52*). Thus, such mutations provide one possible route by which H5 viruses could gain a foothold in the human population, although it is possible that other, as yet unidentified, mutations may allow the H5N1 virus to effect a switch in receptor specificity.

This glycan microarray technology can, therefore, be used to analyze not only existing viral HAs, but as we show here, to identify mutations that enable adaptation of the remaining influenza serotypes into the human population. Monitoring such changes in the "receptor binding footprint" in the field on whole viruses using the glycan microarray could be invaluable in the identification of emerging viruses that could cause new pandemics or epidemics.

References and Notes

1. WHO (www.who.int/en/).
2. C. Scholtissek, W. Rohde, V. Von Hoyningen, R. Rott, *Virology* **87**, 13 (1978).
3. Y. Kawaoka, W. J. Bean, R. G. Webster, *Virology* **169**, 283 (1989).
4. N. P. Johnson, J. Mueller, *Bull. Hist. Med.* **76**, 105 (2002).
5. J. K. Taubenberger *et al.*, *Nature* **437**, 889 (2005).
6. T. M. Tumpey *et al.*, *Science* **310**, 77 (2005).
7. C. R. Parrish, Y. Kawaoka, *Annu. Rev. Microbiol.* **59**, 553 (2005).
8. Y. Suzuki *et al.*, *J. Virol.* **74**, 11825 (2000).
9. E. A. Govorkova *et al.*, *J. Virol.* **79**, 2191 (2005).
10. T. R. Maines *et al.*, *J. Virol.* **79**, 11788 (2005).
11. J. Stevens *et al.*, *Science* **303**, 1866 (2004).
12. Materials and Methods are available as supporting material on *Science* Online.
13. Viet04 HA at a concentration of 9 mg/ml was used to grow crystals in sitting drops with a precipitant solution of 22% polyethylene glycol 2000 and 0.1 M Hepes, pH 6.55 (see also supporting online material).
14. 1918 H1 HA0 (PDB: 1rd8), truncated to remove residues around the cleavage site, was used as the initial MR model. The final R_{cryst} and R_{free} values are 26.9 and 31.9% respectively, at 2.9 Å resolution. The crystal asymmetric unit contains nine hemagglutinin monomers (six HA monomers in two noncrystallographic trimers and three HA monomers that each form one-third of three crystallographic trimers) with an estimated solvent content of 57% based on a Matthews' coefficient (V_m) of 2.9 $Å^3$/dalton (fig. S2). For comparison with previous structures, the Viet04 sequences are numbered as for the H3 subtype. A, C, E, G, I, K, M, O, and Q refer to the nine HA1 subunits in the asymmetric unit, and B, D, F, H, J, L, N, P, and R refer to the nine HA2 subunits; e.g., His^{A18} refers to HA1 residue 18 in the A subunit and His^{B11} refers to HA2 residue 111 in the B subunit of the same monomer. Insertions in Viet04 relative to H3 are labeled by the preceding residue with a letter (e.g., Asn^{19A}).
15. Y. Ha, D. J. Stevens, J. J. Skehel, D. C. Wiley, *EMBO J.* **21**, 865 (2002).
16. Scores from the molecular replacement program PHASER revealed superior scores for the 1918 H1 structure (*Z* score: 37.2; and log-likelihood gain, 3412), as compared with the Sing97 structure (*Z* scores, 33.8; and log-likelihood gain, 768).
17. Two *N*-acetyl glucosamines were interpretable at 13 of these sites (Asn^{A34}, Asn^{C34}, Asn^{C169}, Asn^{E34}, Asn^{G34}, Asn^{I34}, Asn^{I169}, Asn^{K34}, Asn^{K169}, Asn^{M34}, Asn^{M169}, Asn^{O34}, Asn^{O169}), but an additional mannose residue could be interpreted at a further three sites (Asn^{A169}, Asn^{E169}, Asn^{G169}). The glycans are stabilized at Asn^{34} by a neighboring residue (Gln^{24}) in the same chain, whereas at Asn^{169}, an additional mannose was visualized because of stabilization with Lys^{56} and main-chain amide of Val^{57}, in a symmetry-related monomer.
18. H. Kido *et al.*, *J. Biol. Chem.* **267**, 13573 (1992).
19. J. J. Skehel, D. C. Wiley, *Annu. Rev. Biochem.* **69**, 531 (2000).
20. Single-letter abbreviations for the amino acid residues are as follows: A, Ala; C, Cys; D, Asp; E, Glu; F, Phe; G, Gly; H, His; I, Ile; K, Lys; L, Leu; M, Met; N, Asn; P, Pro; Q, Gln; R, Arg; S, Ser; T, Thr; V, Val; W, Trp; X, any amino acid; and Y, Tyr.
21. D. J. Hulse, R. G. Webster, R. J. Russell, D. R. Perez, *J. Virol.* **78**, 9954 (2004).
22. H. D. Klenk, W. Garten, *Trends Microbiol.* **2**, 39 (1994).
23. WHO Global Influenza Program Surveillance Network, *Emerg. Infect. Dis.* **11**, 1515 (2005).
24. N. V. Kaverin *et al.*, *J. Gen. Virol.* **83**, 2497 (2002).
25. M. Philpott, C. Hioe, M. Sheerar, V. S. Hinshaw, *J. Virol.* **64**, 2941 (1990).
26. Regions of antigenic variation have been identified in H1 and H3 serotypes. For H1, these sites were designated Sa, Sb, Ca, and Cb; for H3, sites were designated A, B, C, and D.
27. D. C. Wiley, I. A. Wilson, J. J. Skehel, *Nature* **289**, 373 (1981).
28. A. J. Caton, G. G. Brownlee, J. W. Yewdell, W. Gerhard, *Cell* **31**, 417 (1982).
29. N. V. Kaverin *et al.*, *J. Virol.* **78**, 240 (2004).
30. M. L. Perdue, D. L. Suarez, *Vet. Microbiol.* **74**, 77 (2000).
31. S. J. Baigent, J. W. McCauley, *Virus Res.* **79**, 177 (2001).
32. N. K. Sauter *et al.*, *Biochemistry* **31**, 9609 (1992).
33. J. H. Beigel *et al.*, *N. Engl. J. Med.* **353**, 1374 (2005).
34. O. Blixt *et al.*, *Proc. Natl. Acad. Sci. U.S.A.* **101**, 17033 (2004).
35. J. Stevens *et al.*, *J. Mol. Biol.* **355**, 1143 (2006).
36. HA binding can be analyzed not only for sialic acid–linkage preference, but also for additional features, such as charge; glycan length; or additional sulfation, fucosylation, and sialylation. Of the 265 glycans currently imprinted on the array, 6 are glycoproteins; 38 have sialic acids with α2-3 linkages; 16 have α2-6 linkages; 7 have α2-8 linkages; and a further 16 are β-linkages, modified sialic acid analogs, or glycolylsialic acid glycans. (See table S4 for the glycans analyzed in this study. Of the α2-6 sialosides, only natural full-sized N-linked glycans represented on the array are the biantennary structures (nos. 56 and 57). The remaining sialosides are fragments or terminal sequences found on glycoproteins. For full information on the array, contact the Consortium for Functional Glycomics (*62*). Previous binding data using this technology and cell-based assays with whole viruses show that N-linked glycans close to the receptor-binding site can affect receptor binding through steric hindrance (*35*, *63*). Insect cells do not produce complex glycans containing terminal galactose and/or sialic acids, as seen in mammalian cells, although high-mannose glycans are produced (*64*). However, because of the presence of the influenza sialidase, complex glycans of influenza HAs usually terminate only in galactose, and thus the size of the N-glycans elaborated by insect cells approximate to the size of the complex N-glycans in mammalian host cells. Thus, any importance of complex glycans for HA function is still unknown. Indeed, results for the avian H3 HA (A/Duck/Ukraine/1/1963), published recently (*35*), are in agreement with previous whole viral studies (*65*). However, independent studies are ongoing to develop the array for whole-virus analyses so that a direct comparison can be made. Such initial experiments are promising, because the strict α2-3 specificity observed here for Dk76 is also seen with whole-virus studies (*37*) and preliminary experiments with A/Puerto Rico/8/1934 virus that reveal both α2-3 and α2-6 specificity (*34*), in agreement with experiments from cell-based assays (*37*).
37. G. N. Rogers, B. L. D'Souza, *Virology* **173**, 317 (1989).
38. Whole-virus studies, including those for Viet04 virus, also revealed α2-3 specificity with a preference for sulfation in current H5N1 strains (*39*). However, this assay used only seven ligands (one α2-6 and six α2-3), which is considerably fewer than the 84 sialosides, sialoside analogs, and glycoproteins analyzed here. In our glycan array,

sulfation on the second galactose was not tolerated (no. 37) for Viet04, although binding was apparent for sialosides with Gal in either β1-3 or β1-4 linkage to a GlcNAc or GalNAc (nos. 21 to 23, 32, 33), as well as to fucosylated glycans (nos. 26 to 29).
39. A. Gambaryan *et al.*, *Virology* **344**, 432 (2006).
40. H. Debray, D. Decout, G. Strecker, G. Spik, J. Montreuil, *Eur. J. Biochem.* **117**, 41 (1981).
41. R. J. Connor, Y. Kawaoka, R. G. Webster, J. C. Paulson, *Virology* **205**, 17 (1994).
42. G. N. Rogers *et al.*, *Nature* **304**, 76 (1983).
43. M. Matrosovich *et al.*, *J. Virol.* **74**, 8502 (2000).
44. E. Nobusawa, H. Ishihara, T. Morishita, K. Sato, K. Nakajima, *Virology* **278**, 587 (2000).
45. L. Glaser *et al.*, *J. Virol.* **79**, 11533 (2005).
46. Avian H1 bound only to nonbranched glycans and to sulfated and/or negatively charged glycans (Figs. 4C and 5, A to C). The single E190D mutation reduced binding to most α2-3 glycans, except to sulfated sialosides (Fig. 5A). These results suggest mutation at both 190 and 225 positions is always a requirement for H1 serotypes to adapt to a human host.
47. R. A. Fouchier *et al.*, *J. Virol.* **79**, 2814 (2005).
48. The E190D mutation (Fig. 5D) reduced overall binding of α2-3 ligands and glycoproteins, except for the sulfated and/or negatively charged glycans (nos. 18, 20, 24, 25, and 38). The G225D mutation (Fig. 5E) appeared to have little effect on the binding profile, in contrast to avian H1, where binding was not detected (Fig. 5B). The double mutant (E190D,G225D) did not bind to any glycan on the array (see Fig. 5F).
49. S. J. Gamblin *et al.*, *Science* **303**, 1838 (2004).
50. For the human H1 HA from A/Puerto Rico/8/1934, the longer side chain of Glu^{190} can form hydrogen bonds to sialic acid of both α2-6 and α2-3 sialosides, whereas for structures of A/Swine/Iowa/1930, H1 HA bound to human receptor analogs, the shorter side chain of Asp^{190} can only interact with the GlcNAc to stabilize the α2-6 conformation (*49*). Binding data, with the 1918 South Carolina H1 HA (*35*) and the Dk76 double mutation (E190D,G225D) (Fig. 5C), show that some sulfated glycans with α2-6 sialic acid linkages can bind. However, this situation does not arise for the Viet04 double mutant. Although the G225D mutation would have been expected to enhance α2-6 specificity, the additional stabilizing influence of the E190D mutation toward the GlcNAc may not be possible because of the neighboring Lys^{193}, which could inhibit interaction of Asp^{190} with the glycan either by steric hindrance or by direct interaction with Asp^{190}. Experiments are in progress to test this notion.
51. The Q226L mutation eliminated binding to the microarray, except for two negatively charged α2-3 glycans [with either an extra sialic acid on the 6-position of a GalNAc (no. 20) or 6-sulfation on GlcNAc with a branched fucose (no. 25)]. The G228S mutation did not have any significant effect compared with Viet04, except that sialosides with sulfation on the 6-position of the galactose, with or without branched fucosylation on the GlcNAc (nos. 12, 37) were tolerated. Stronger binding was observed for fucosylated glycans (nos. 26 to 29), and reduced binding was observed for sialosides with β1-3 linkages between the galactose and GlcNAc/GalNAc (nos. 21 to 23) (Fig. 5H). In addition to 6′-sialyllactose (no. 49), as seen for Viet04, binding was observed for α2-6 biantennary structures (nos. 56 and 57). The double mutant (Q226L,G228S) showed reduced binding to α2-3 sialosides. Only sulfated and long-chain glycans were tolerated (nos. 16, 20, 24, 25, 35), but binding to α2-6 biantennary structures (nos. 56 and 57), as with the G228S mutation, was also maintained.
52. R. Harvey, A. C. Martin, M. Zambon, W. S. Barclay, *J. Virol.* **78**, 502 (2004).
53. D. H. Joziasse *et al.*, *J. Biol. Chem.* **262**, 2025 (1987).
54. See glycan structure database (www.functionalglycomics.org).
55. L. G. Baum, J. C. Paulson, *Acta Histochem. Suppl.* **40**, 35 (1990).
56. P. Gagneux *et al.*, *J. Biol. Chem.* **278**, 48245 (2003).
57. M. N. Matrosovich, T. Y. Matrosovich, T. Gray, N. A. Roberts, H. D. Klenk, *Proc. Natl. Acad. Sci. U.S.A.* **101**, 4620 (2004).
58. G. Lamblin *et al.*, *Glycoconj. J.* **18**, 661 (2001).
59. Attenuated viruses with a S227N mutation led to higher hemagglutinin inhibition titers in ferrets (*60*). Thus, enhanced binding to α2-3 ligands, especially to 6-sulfated GalNAc, could lead to an increased uptake into antigen-presenting cells and subsequent antibody production.
60. E. Hoffmann, A. S. Lipatov, R. J. Webby, E. A. Govorkova, R. G. Webster, *Proc. Natl. Acad. Sci. U.S.A.* **102**, 12915 (2005).
61. The 2003 isolates contain Ala^{160}, Arg^{193}, Lys^{216} and Asn^{227}, whereas Viet04 has Thr^{160} (which introduces a glycosylation site at Asn^{158}), Lys^{193}, Arg^{216}, and Ser^{227}.
62. Consortium for Functional Glycomics (www://functionalglycomics.org).
63. H. D. Klenk, R. Wagner, D. Heuer, T. Wolff, *Virus Res.* **82**, 73 (2002).
64. T. A. Kost, J. P. Condreay, D. L. Jarvis, *Nat. Biotechnol.* **23**, 567 (2005).
65. G. N. Rogers, J. C. Paulson, *Virology* **127**, 361 (1983).
66. W. L. Delano (2002); (www.pymol.org).
67. The work was supported in part by National Institute of Allergy and Infectious Diseases grant AI058113 (I.A.W., T.T., J.K.T.); National Institute of General Medical Sciences grants GM062116 (to J.C.P., I.A.W.) and GM060938 (to J.C.P.); and partial support from NIH grants to I.A.W. (CA55896 and AI42266). We thank P. Palese and L. Glaser (Mount Sinai School of Medicine, New York) for providing the full-length clone of A/Vietnam/1203/2004; the staff of the Advanced Light Source Beamline 8.2.2 for the beamline assistance; X. Dai, S. Ferguson, P. Carney, and J. Vanhnasy (The Scripps Research Institute) for expert technical assistance; and R. Stanfield and M. Elsliger (The Scripps Research Institute) for helpful discussions. This is publication 17916-MB from The Scripps Research Institute. Coordinates and structure factors have been deposited in the Protein Data Bank (code 2FK0) and will be released on publication.

Supporting Online Material

www.sciencemag.org/cgi/content/full/1124513/DC1
Materials and Methods
Figs. S1 to S6
Tables S1 to S4
References

3 January 2006; accepted 28 February 2006
Published online 16 March 2006;
10.1126/science.1124513
Include this information when citing this paper.

REPORTS

Ultrafast Laser–Driven Microlens to Focus and Energy-Select Mega–Electron Volt Protons

Toma Toncian,[1] Marco Borghesi,[2] Julien Fuchs,[3] Emmanuel d'Humières,[3,4] Patrizio Antici,[3] Patrick Audebert,[3] Erik Brambrink,[3] Carlo Alberto Cecchetti,[2] Ariane Pipahl,[1] Lorenzo Romagnani,[2] Oswald Willi[1]*

We present a technique for simultaneous focusing and energy selection of high-current, mega–electron volt proton beams with the use of radial, transient electric fields (10^7 to 10^{10} volts per meter) triggered on the inner walls of a hollow microcylinder by an intense subpicosecond laser pulse. Because of the transient nature of the focusing fields, the proposed method allows selection of a desired range out of the spectrum of the polyenergetic proton beam. This technique addresses current drawbacks of laser-accelerated proton beams, such as their broad spectrum and divergence at the source.

The recent development of ultra-intense laser pulses (*1*) has opened up opportunities for applications in many areas, including particle acceleration (*2*–*5*), inertial fusion energy (*6*), generation of intense x-ray pulses (*7*), laser-driven nuclear physics (*8*), and laboratory astrophysics (*9*). In particular, the acceleration of mega–electron volt ions from the interaction of high-intensity laser-pulses with thin solids has major applicative prospects because of the high beam quality of these ion bursts (*10*, *11*). Such proton beams are already applied to produce high-energy density matter (*12*) or to radiograph transient processes (*13*), and they offer promising prospects for tumor therapy (*14*), isotope generation for positron emission tomography (*15*), fast ignition of fusion cores (*16*), and brightness increase of conventional accelerators. However, because these proton beams are polyenergetic and divergent at the source, reduction and control of their divergence and energy spread are essential requirements for most of these applications.

[1]Heinrich Heine Universität Düsseldorf, D-40225 Düsseldorf, Germany. [2]School of Mathematics and Physics, The Queen's University of Belfast, Belfast BT7 1NN, Northern Ireland, UK. [3]Laboratoire pour l'Utilisation des Lasers Intenses, UMR 7605 CNRS-CEA-Ecole Polytechnique-Université Paris VI, 91128 Palaiseau, France. [4]Centre de Physique Théorique, UMR 7644 CNRS-Ecole Polytechnique, 91128 Palaiseau, France.

*To whom correspondence should be addressed. E-mail: oswald.willi@laserphy.uni-duesseldorf.de

Focusing of energetic proton beams is usually achieved with electrostatic or magnetic lenses (*17*), which have several drawbacks, including slow switching times, large sizes, asymmetry in the transverse plane for the focused beam, aberrations, inability to focus large currents, and large heat dissipation. It has been proposed that particle selection and beam collimation of laser-produced protons applicable for tumor therapy could be achieved by means of superconducting magnet systems (*18*). Relativistic laser-plasma devices appear in principle more suitable for achieving the required angular and spectral control of laser-accelerated ion beams because they can withstand large ion beam currents, can be switched over picosecond time scales, and can support large deflecting fields on microscales.

Advances in ion beam tailoring have been achieved so far mainly with the use of target engineering techniques. Geometrical focusing of laser-driven protons has been attained with the use of curved targets (*12*). Demonstration of this technique has been limited so far to focal distances of a few millimeters and to the low-energy component of the proton spectrum. Very recently, quasi-monochromatic acceleration from laser irradiated microstructured targets has been reported (*19*, *20*). In these approaches, the focusing or energy-selection effect is achieved by directly acting on the source. As a consequence, these techniques rely on relatively complex target fabrication or preparation procedures.

We describe here an alternative approach, which provides tunable, simultaneous focusing and energy selection of mega–electron volt proton beams. Furthermore, our approach decouples the beam tailoring stage from the acceleration stage, allowing for their independent optimization. This leads to a system with higher flexibility than the methods above, considerably relaxing the target fabrication constraints. The method uses a compact laser-driven microlens arrangement (Fig. 1A). The underlying physical process begins with relativistic electrons injected through the cylinder's wall produced by the laser operating in chirped pulse amplification (CPA) mode, which spread evenly on the cylinder's inner walls and initiate hot plasma expansion (Fig. 1, B and C). The transient electric fields associated with the expansion are used in a radial geometry to focus protons accelerated by a separate CPA laser pulse from a thin planar foil. The microlens operation was demonstrated in experiments carried out at the Laboratoire pour l'Utilisation des Lasers Intenses (LULI), which used the 100-TW laser (*21*) operating at a wavelength of 1 μm. After amplification, the laser pulse was split into two separate pulses (CPA_1 and CPA_2), which were recompressed in separate grating compressors to a 350-fs duration. The delay between the two pulses was controlled optically with picosecond precision. The CPA_1 pulse (irradiance $I = 5 \times 10^{19}$ W/cm^2) was used to accelerate a high-current, diverging beam of up to 15-MeV protons from a 25-μm-thick Al foil target [the protons are produced from hydrocarbon impurities (*22*) on the target rear surface (*23*, *24*)]. The CPA_2 pulse ($I = 3 \times 10^{18}$ W/cm^2) was focused onto the outer wall of a hollow cylinder. The proton beam from the first foil was directed through the cylinder and detected with a stack of radiochromic films (RCF), a dosimetric detector (*25*), positioned at a variable distance (from 2 to 70 cm) from the proton source. The RCF stack was used to measure the proton beam divergence. It also provided a coarse energy resolution due to the energy deposition properties of the ions (*3*) (most of the energy of a proton is released in the so-called Bragg peak, located at a distance in the detector which depends on the incident proton energy). It was shielded with an 11-μm Al foil allowing protons with energies greater than 1.5 MeV to be recorded. In some cases, a central millimeter-sized hole was bored through the RCF to allow downstream high spectral resolution measurements with the use of a magnetic spectrometer with a 0.6-T permanent magnet. The spectral resolution determined by the slit width and the dispersion of the spectrometer is 0.2 MeV at 6 MeV and 0.7 MeV at 15 MeV. The distance between the proton production foil and cylinder and the distance between the cylinder and detector were varied throughout the experiment. At a source-cylinder distance of 1 mm, the proton flux increase due to focusing by the microlens was so strong that saturation of the film occurred. Quantitative data could only be obtained when the cylinder was moved to 4 mm from the proton foil, in order to collect a smaller part of the diverging proton beam.

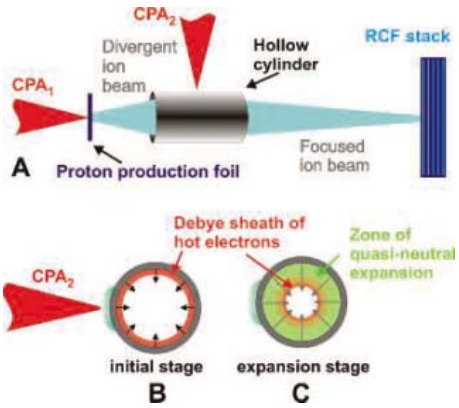

Fig. 1. (**A**) Schematic of the microlens device. A proton beam is accelerated from a planar foil by the CPA_1 laser pulse. The proton beam propagates through a hollow cylinder side irradiated by the CPA_2 laser pulse. (**B** and **C**) Schematic of the operation's principle of the microlens. The CPA_2 laser pulse injects hot electrons within the cylinder. These spread evenly onto the cylinder's inner wall. In the early stage (B), these electrons, confined over a Debye length on the cylinder's surface, generate a space-charge field (indicated by the radially pointing arrows), which then induces plasma expansion (C) from the cylinder's inner walls. The resulting radial electric field, still indicated by the arrows and decreasing in time as the plasma expands, focuses the protons. The field is peaked at the front but extends toward the cylinder's wall.

An RCF pack placed 9.5 cm away from the proton target recorded the proton beam after its propagation through a laser-irradiated dural cylinder 3 mm in length, 700 μm in diameter, and 50 μm in wall thickness. The fifth and sixth in the stack, corresponding to protons of 9 and 7.5 MeV, respectively, are shown in Fig. 2A. The entrance plane of the cylinder was placed 4 mm from the proton-producing foil. The distance from the proton-producing foil to the CPA_2 irradiation point on the cylinder was 5 mm. As expected, no focusing effect is observed for the 9 MeV protons. Indeed, the electric field is triggered by the CPA_2 laser pulse ~20 ps after these protons exit the cylinder. For the 7.5-MeV protons, the electric field develops while these protons are close to exit the cylinder, and a small spot about 600 μm [full width at half

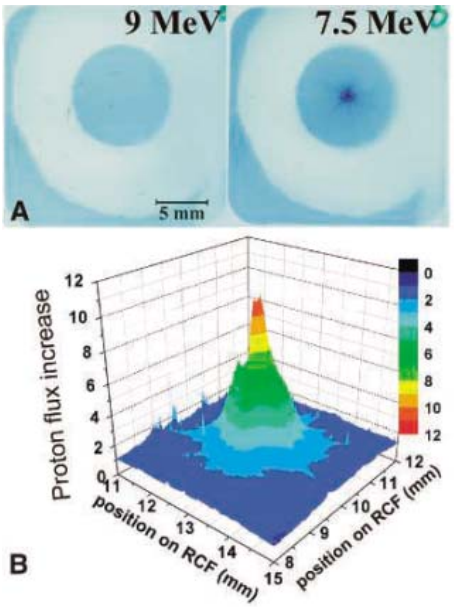

Fig. 2. (**A**) RCF layers showing the proton beam focusing effect due to a 3-mm-long, 700-μm-diameter dural (95% Al, 4% Cu, and 1% Mg) laser–irradiated cylinder with 50-μm wall thickness. For the energies reaching the Bragg peak in the two layers shown, the protons with an energy of 9 MeV pass through the cylinder before the electric field is present, showing no focusing, whereas the divergence of the protons with an energy of 7.5 MeV is strongly reduced by the electric field that has developed inside the cylinder. The shadow of the cylinder and of the 50-μm tungsten holding wire can be seen clearly. The cylinder was positioned far from the proton source intentionally to reduce the number of protons entering the cylinder and avoid RCF saturation. The distance between the entrance plane of the cylinder and the proton production foil was 4 mm. (**B**) Flux increase with respect to the unfocused flux for 7.5-MeV protons as deduced from the layer shown in (A).

maximum (FWHM)] in diameter is seen on the RCF at the center of the cylinder's shadow (spots as small as 200 μm have been observed, depending on the detector position). In this case, the proton flux within the spot at the film plane is increased as many as 12 times compared with the unfocused part not captured by the cylinder (Fig. 2B). Based on the known properties of the proton source and on the decay time of the focusing fields [inferred to be ~ 10 ps from particle-in-cell (PIC) simulations and experimental results (*26*)], a focused current of about 5 A can be estimated for the conditions of Fig. 3. We also studied the evolution of the beam size, as a function of the propagation distance from the cylinder. This was done under the same conditions of Fig. 2. The behavior of the 7.5-MeV proton component is shown in Fig. 3. For this energy, the beam size is only 8 mm after 70 cm of propagation, whereas when freely propagating, the size of the beam would have been ~260 mm. An energy spectrum was obtained, in the same experimental configuration, with the use of the magnetic spectrometer, having an entrance slit of 250 μm positioned 70 cm away from the proton source (Fig. 4). As a reference, we also show a typical exponential spectrum collected in the same conditions but without the microlens. The data clearly shows the energy-selection capability of the microlens: Because of selective collimation of the 6.25-MeV protons, these could be transmitted efficiently through the spectrometer slit (acting as an angular filter), and their density after the slit in the spectrally dispersed plane is enhanced as compared with the free-space expansion case. For this shot, the 6.25-MeV protons experience the focusing fields for ~5 ps before exiting the cylinder. We obtained an energy spread of 0.2 MeV—limited by the spectrometer energy resolution—for the peak located at 6.25 MeV. The numerical simulations performed in the same conditions as in the experiment suggest that the spectral width of the peak is about 0.1 MeV and hence narrower than demonstrated by the experimental spectrum shown (Fig. 4). By varying the optical delay between the laser beams, the location of this peak on the energy axis can be tuned selectively (as demonstrated experimentally), thereby allowing us to tailor the energy distribution of the transmitted beam, a necessary step for many applications. Notably, with this approach, focusing and energy selection are provided simultaneously.

We performed one-dimensional (1D) and 2D PIC simulations of field generation at the microlens's walls and 3D test-particle simulations of proton propagation through the microlens. The simulations were performed in three steps with the use of the CALDER code (*27*). First, we verified with 2D simulations that the laser pulse triggering the microlens by irradiating the cylinder's outer wall generated a population of hot electrons that spread evenly on the cylinder's walls. We then used a 1D code to simulate the plasma expansion within the cylinder (i.e., we simulated the expansion of two slabs of plasma separated by the cylinder's diameter of 700 μm). The expansion is driven by a hot-electron population that has a Boltzmann distribution with a temperature of 400 keV, as given by the ponderomotive potential at the irradiance of CPA_2 (*28*). The initial electron density at the cylinder's wall was estimated by considering that a 40% fraction of the laser energy [inferred from experimental measurements (*29*)] is converted into hot electrons and that these are then spread evenly on the cylinder's walls. This results in a hot-electron density of ~6 × 10^{16} cm^{-3}. We assumed that when the plasma expansion starts, the field obtained in the PIC simulation is the same along the whole cylinder. Finally, we simulated the propagation of a proton beam in the cylinder through the space- and time-dependent fields obtained from the PIC simulation. The proton source used in the simulations has a divergence and energy spectrum as measured in the experiment.

The successful comparison between the simulations and the data (Figs. 3 and 4) supports the scenario in which laser-triggered transient fields drive the selective deflection of the protons. The transient field (*30*) is associated with a hot-electron sheath that extends over a Debye length ahead of the plasma, expanding toward the cylinder's axis (*26*, *31*). The different energy components present in the proton beam spectrum transit through the cylinder at different times depending on their different velocities, with higher energy protons crossing the cylinder at earlier times. Protons passing through the microlens before it is triggered (as in Fig. 2A for the 9-MeV layer) do not experience any fields and are therefore not deflected. Protons which are crossing the cylinder and are close to its end when it is triggered and that therefore experience the fields for only a short time will exit the cylinder with a very low divergence (as in Fig. 2A for the 7.5-MeV layer). Lower energy protons will experience a larger cumulated field along their propagation through the cylinder. The particle-tracing simulations suggest that they are therefore focused at a short distance from the exit plane of the microlens and diverge strongly after focus. This is consistent with the diluted beam observed on the RCF stack positioned a few centimeters away and with the strong dip observed in the spectrum of Fig. 4 below 6 MeV. Finally, protons that have very low energy (i.e., below 4 MeV in the case of Fig. 4) pass through the microlens after the fields have vanished and do not experience any deflection. Additional simulations were performed to test the scalability of the microlens to higher proton energies, as needed for applications such as proton therapy. We computed that, using the same cylinder as in our experiment and a slightly more intense CPA_2 triggering laser pulse (10^{19} W/cm^2), one could reduce the divergence of 270-MeV protons. Protons of such high energy transit through the microlens in a short time (13 ps); therefore, even higher laser intensities, on the order of 10^{20} W/cm^2, would be required to focus them. The focusing device described in this paper has potential use in all applications of energetic protons in which reduced divergence, large flux, or narrow energy range are required. These include most of the proposed applications in scientific, medical, and technological areas. For

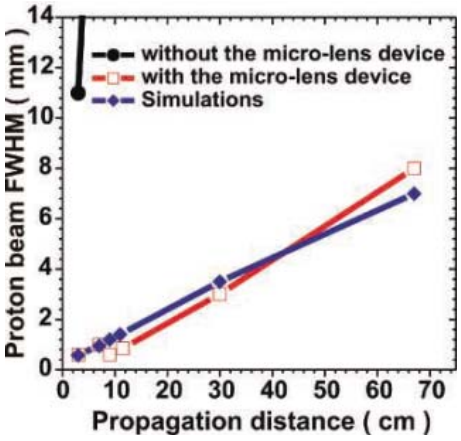

Fig. 3. Evolution of the FWHM of the proton beam along its propagation, for protons with energy of 7.5 MeV (the propagation distance is calculated from the proton source). The black circles correspond to the case without the microlens (free-space divergence), the blue diamonds to the particle-tracer simulation in the fields given by the PIC simulation, and the red squares to the experimental results with the use of the microlens. The RCF shown on the right of Fig. 2A corresponds to the red point at 9.5 cm.

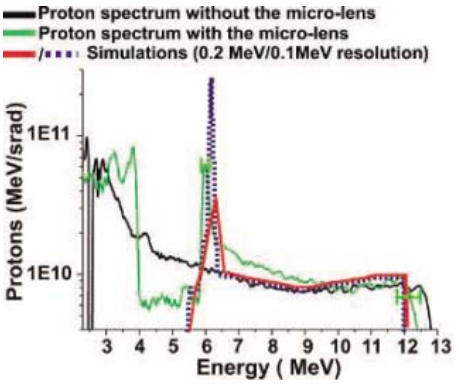

Fig. 4. Experimental proton spectra measured with a magnetic spectrometer without the microlens (black line) and with the microlens (green line), and proton spectra obtained from simulations (red and blue lines) performed with the use of the experimental proton beam parameters and the magnetic spectrometer parameters (i.e., distance from the source and slit characteristics). The red and blue curves were obtained with the use of energy bins of 0.2 and 0.1 MeV, respectively. The simulated spectrum was obtained by tracing, for each energy bin, 5000 protons through the fields predicted by the PIC simulation.

example, focusing ion beams provides a different perspective, which may lead to further developments in areas such as hadron therapy for cancer treatment, accelerator physics, and inertial fusion physics. In addition to applications that use laser-driven ion beams, such a device might find application in conventional accelerator beams as a focusing or fast-switching tool.

References and Notes

1. M. D. Perry, G. Mourou, *Science* **264**, 917 (1994).
2. E. Clark *et al.*, *Phys. Rev. Lett.* **84**, 670 (2000).
3. R. Snavely *et al.*, *Phys. Rev. Lett.* **85**, 2945 (2000).
4. A. Maksimchuk, S. Gu, K. Flippo, D. Umstadter, V. Yu. Bychenkov, *Phys. Rev. Lett.* **84**, 4108 (2000).
5. V. Malka, J. Faure, Y. Glinec, A. F. Lifschitz, *Plasma Phys. Control. Fusion* **47**, B481 (2005).
6. M. Tabak *et al.*, *Phys. Plasmas* **1**, 1626 (1994).
7. A. Rousse *et al.*, *Phys. Rev. Lett.* **93**, 135005 (2004).
8. K. W. D. Ledingham, P. McKenna, R. P. Shinghal, *Science* **300**, 1107 (2003).
9. B. A. Remington, D. Arnet, R. P. Drake, H. Takabe, *Science* **284**, 1488 (1999).
10. M. Borghesi *et al.*, *Phys. Rev. Lett.* **92**, 055003 (2004).
11. T. Cowan *et al.*, *Phys. Rev. Lett.* **92**, 204801 (2004).
12. P. Patel *et al.*, *Phys. Rev. Lett.* **91**, 125004 (2003).
13. M. Borghesi *et al.*, *Phys. Plasmas* **9**, 2214 (2002).
14. S. V. Bulanov, T. Zh. Esirkepov, V. S. Khoroshkov, A. V. Kuznetsov, F. Pegoraro, *Phys. Lett. A* **299**, 240 (2002).
15. I. Spencer *et al.*, *Nucl. Inst. Meth. Phys. Res. B* **183**, 449 (2001).
16. M. Roth *et al.*, *Phys. Rev. Lett.* **86**, 436 (2001).
17. M. Szilagyi, *Electron and Ion Optics* (Plenum Press, New York, 1988).
18. W. Luo, E. Fourkal, J. Li, Ch. Ma, *Med. Phys.* **32**, 794 (2005).
19. B. M. Hegelich *et al.*, *Nature* **439**, 441 (2006).
20. H. Schwoerer *et al.*, *Nature* **439**, 445 (2006).
21. B. Wattellier *et al.*, *Opt. Lett.* **29**, 2494 (2004).
22. S. J. Gitomer *et al.*, *Phys. Fluids* **29**, 2679 (1986).
23. M. Allen *et al.*, *Phys. Rev. Lett.* **93**, 265004 (2004).
24. J. Fuchs *et al.*, *Phys. Rev. Lett.* **94**, 045004 (2005).
25. GAFCHROMIC radiochromic dosimetry films (www.ispcorp.com/products/dosimetry/index.html).
26. L. Romagnani *et al.*, *Phys. Rev. Lett.* **95**, 195001 (2005).
27. E. Lefebvre *et al.*, *Nucl. Fusion* **43**, 629 (2003).
28. S. C. Wilks *et al.*, *Phys. Plasmas* **8**, 542 (2001).
29. M. Key *et al.*, *Phys. Plasmas* **5**, 1966 (1998).
30. These fields have been studied in detail, in planar geometry, in a previous experiment (*26*) and figure 3 of reference (*26*) shows their spatial and temporal evolution.
31. S. Gordienko, A. Pukhov, personal communication.

32. We thank L. Gremillet, T. Grismayer, S. Gordienko, E. Lefebvre, P. Mora, A. Pukhov, and V.Malka for fruitful discussions; E. Lefebvre for allowing us to use his PIC code CALDER; and the Commissariat à l'Energie Atomique/Direction des Applications Militaires (CEA/DAM) for the simulations we performed on Le Centre de Calcul Recherche et Technologie (CCRT) computers. We acknowledge the support from the technical teams at LULI. This work was supported by European Union grant no. HPRICT 1999-0052, grant no. E1127 from Région Ile-de-France, and DFG TR18 and GK1203, and partly by the Queen's University of Belfast–International Research Centre for Experimental Physics (QUB-IRCEP) Distinguished Fellowship Visiting scheme and Deutscher Akademischer Austausch Dieust (DAAD).

28 December 2005; accepted 9 February 2006
Published online 16 February 2006;
10.1126/science.1124412
Include this information when citing this paper.

Bolometric Infrared Photoresponse of Suspended Single-Walled Carbon Nanotube Films

Mikhail E. Itkis, Ferenc Borondics,* Aiping Yu, Robert C. Haddon†

The photoresponse in the electrical conductivity of a single-walled carbon nanotube (SWNT) film is dramatically enhanced when the nanotube film is suspended in vacuum. We show here that the change in conductivity is bolometric (caused by heating of the SWNT network). Electron-phonon interactions lead to ultrafast relaxation of the photoexcited carriers, and the energy of the incident infrared (IR) radiation is efficiently transferred to the crystal lattice. It is not the presence of photoexcited holes and electrons, but a rise in temperature, that results in a change in resistance; thus, photoconductivity experiments cannot be used to support the band picture over the exciton model of excited states in carbon nanotubes. The photoresponse of suspended SWNT films is sufficiently high that they may function as the sensitive element of an IR bolometric detector.

The optical properties of SWNTs, including photoconductivity, suggest outstanding potential for applications in nanoscale-sized optoelectronics (*1–4*). Prominent absorption features in the optical spectra of SWNTs have been widely ascribed to interband transitions associated with the series of van Hove singularities in the one-dimensional (1D) electronic density of states (*5–7*). However, more-recent studies suggest that the electron-hole pairs are strongly coupled in the SWNT 1D crystal lattice and that major photoexcitations are excitons, rather than free carriers (*8–11*). Experiments on the relaxation of photoexcitations in SWNTs (*11*) and two-photon excitation spectroscopy (*12*) support the exciton model and provide a large value for the exciton binding energy (0.4 eV) (*12*).

In the interband transition (band) model, free electrons and holes are produced upon photoexcitation, and, providing the lifetime of these carriers is sufficiently long, the spectral features in absorption and photoconductivity match the optical transitions associated with the van Hove singularities (Fig. 1A). In the exciton model, the photoexcitations occur at energies lower than the direct bandgap and give rise to neutral species that cannot directly contribute to the photoconductivity (Fig. 1A). In this situation, the excitons would have to be dissociated thermally (*13*) or by a large electric field (*12*) to produce free electrons and holes that could contribute to the photoconductivity. Exciton-related low-energy spectral features in the photoresponse would be substantially suppressed, especially at low temperatures, compared with the features corresponding to the interband transitions, and differences should arise in the absorption and photoconductivity spectra.

There are a number of reports on the photoconductivity of SWNT films deposited on optical substrates (*13–15*). In all cases, a very weak photoresponse with low signal-to-noise (S/N) ratio was observed despite the use of high laser powers. Nevertheless, the photoconductivity showed spectral features that coincided with the optical absorption spectrum in support of the original band model, with free carriers as the major photoexcitations (*13–15*). Recent photoconductivity experiments on individual SWNTs (laser power intensity of 1 kW/cm^2) in a field-effect–transistor configuration gave a weak sideband in addition to the primary resonance, and the result was interpreted in a favor of the exciton model (*16*).

We report here on the photoconductivity of suspended SWNT films, and we are able rationalize contradictory reports to date, as well as shed light on the nature of the optical excitations in SWNTs and the origin of the photoresponse. The extremely large photoresponse that is observed for suspended SWNT films also makes them attractive candidates for the sensitive element of an infrared (IR) bolometer.

Photoconductivity experiments were carried out with semitransparent SWNT films prepared by two different techniques. A network of as-prepared (AP) SWNTs can form in the electric arc discharge process. The network growth was initiated by the placement of stainless steel wire grids of cell size 2.54 × 2.54 cm near the plasma zone inside the electric arc chamber. The growing SWNTs drift from the plasma core toward the water-cooled walls of the arc reactor, and the wire grid nucleates the growth of an extended SWNT network that forms a continuous semitransparent SWNT film after 1 to 5 min of operation of the electric arc (fig. S1). This process leads to a high-purity film, because the SWNTs are trapped in the growing network with high probability; but typical impurities, such as nanoparticles and amorphous carbon, penetrate the thin network without becoming entangled. We

Center for Nanoscale Science and Engineering, Departments of Chemistry and Chemical and Environmental Engineering, University of California, Riverside, CA 92521–0403, USA.

*Present address: Magyar Tudományos Akadémia, Szliárdtestfizikai és Optikai Kutatóintézete, Budapest, H 1525, Hungary.

†To whom correspondence should be addressed. E-mail: haddon@ucr.edu

have used this type of film as a reference standard for SWNT purity evaluation based on near-IR spectroscopy (*17*). In the second case, purified (P) SWNTs were used, and a free standing P-SWNT film was obtained by vacuum filtration of a SWNT dispersion (*3*, *7*).

The SWNT film was suspended between two supporting blocks that also function as the electrical contacts (Fig. 1B) by placing a 0.5-mm-wide ribbon of the SWNT film across the 3.5-mm opening of a sapphire ring attached to the cold finger of the optical cryostat (Fig. 1C). At 50 K, the dc photoresponse of the AP-SWNT film to 0.04-Hz square-wave pulses (Fig. 2A) shows a resistance drop of 0.7% under an incident power of 0.12 μW of radiation from an IR light-emitting diode (peak emission λ_p = 940 nm), and the photoresponse is easily detectable with S/N ~ 100. The power level used in our experiments is 5 to 10 orders of magnitude lower than in previously reported photoconductivity measurements (*13*–*16*). We did not observe any detectable change of resistance in a control experiment carried out with a SWNT film supported directly on the substrate. This latter result is in agreement with the very low level of the steady-state photoconductivity signal previously reported in experiments that used much higher incident power levels (*13*–*16*). The suspension of the SWNT film in vacuum led to an enhancement of the photoconductivity response by at least 5 orders of magnitude.

The enhancement of the photoresponse of the suspended SWNT film allowed us to conduct spectral measurements with a commercial spectrophotometer at an IR power intensity of 0.1 to 1 μW. Figure 2B shows the photoresponse of a 40-nm-thick AP-SWNT film along with its absorption spectrum. The absorption spectrum is typical of electric arc SWNTs with average diameter 1.4 nm (*6*), and it shows two characteristic bands that have been associated with the first and second interband transitions in semiconducting SWNTs (Fig. 2B) (*5*–*7*). The photoconductivity spectrum is virtually identical and exhibits no shift in the observed spectral positions within an accuracy of 10 meV.

To identify the nature of the photoexcitations in SWNTs, it is necessary to confirm the mechanism of the observed change in resistance. Direct photoconductivity can contribute photoexcited carriers to the electric current, or the response can be bolometric in nature, in which case the absorbed radiation heats the sample. The dramatic enhancement of the photoresponse when the thermal contact of the SWNT film with the environment is minimized by suspension supports a bolometric origin of the photoresponse, although the interaction of the SWNTs with the substrate can modify the electronic states.

There are several features that distinguish bolometric responses from free-carrier photoconductivity: (i) The bolometric response is strongly decreased by thermal coupling between the sensitive element and the environment. (ii) The typical time constant of the bolometric response is 1 to 100 ms. (iii) The magnitude of the bolometric response depends on the temperature derivative of the resistance *dR/dT* (*18*).

Increasing the pressure in the sample chamber of the cryostat (Fig. 3A) strongly reduced the signal at pressures above 1 mtorr. The effect of the gas in thermally coupling the SWNT film to its surroundings is consistent with the bolometric nature of the photoresponse. The frequency dependence and time trace of the photosignal and the device (Fig. 3B) show a typical bolometric response time (≈50 ms). The temperature dependence of the resistance $R(T)$ of the suspended 1-μm-thick film of P-SWNTs (Fig. 3C) reveals a transition at $T \sim 230$ K from the metallic behavior, observed at high temperatures with positive *dR/dT*, to semiconducting behavior, with negative *dR/dT* at low temperatures. The photoresponse of this film presented in the form of the resistance change (*dR*) under constant incident radiation (Fig. 3D) reverses sign at the resistance minimum, from positive ($T > 230$ K) to negative ($T < 230$ K), which is in agreement with the behavior expected for a bolometric response. If the photocarriers were responsible for the photoconductivity, the sample resistance would be expected to decrease irrespective of the sign of *dR/dT*. Taken together, the data establish the bolometric origin of the photoconductivity observed in suspended SWNT films.

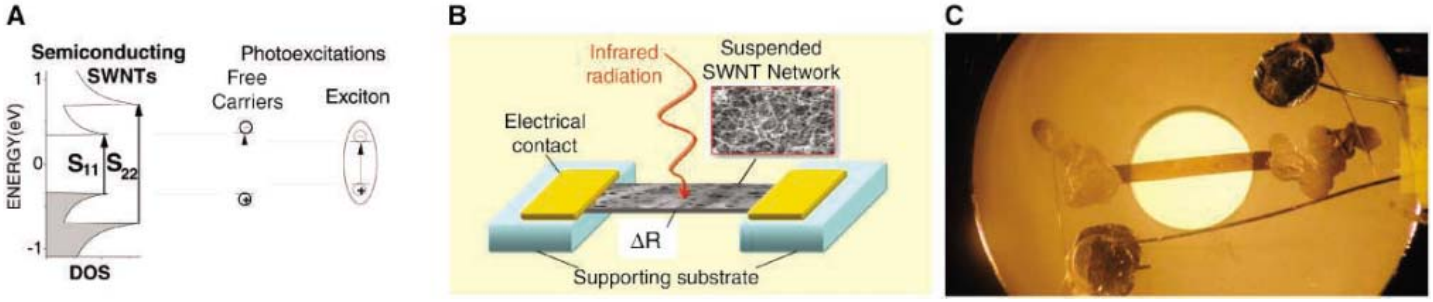

Fig. 1. (**A**) Schematic diagram of electronic density of states (DOS) and corresponding interband transitions S_{11} and S_{22} in semiconducting SWNTs (left) and schematic representation of the two types of photoexcitations: free carrier electrons and holes in the interband transition (band) model and low-energy coupled electron-hole pairs in exciton model (right). (**B**) Diagram of SWNT network suspended between electrical contacts. (**C**) 100-nm-thick SWNT film suspended across 3.5-mm opening of a sapphire ring.

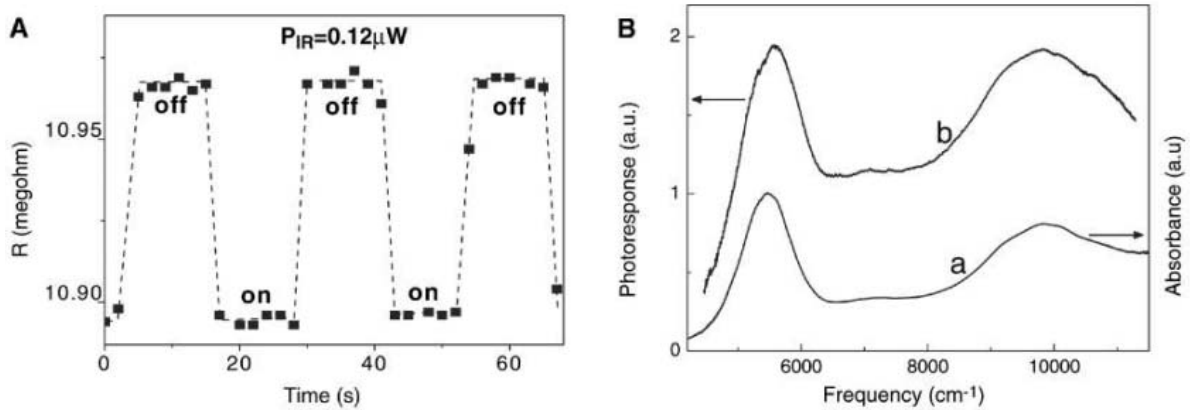

Fig. 2. (**A**) Modulation of resistance of SWNT film at 50 K under square-wave pulses of power P = 0.12 μW IR radiation. (**B**) Spectra of near-IR absorption (curve a) and electrical photoresponse (curve b) of AP-SWNT film. a.u., arbitrary units.

The direct photoconductivity component in SWNT films is likely limited by the ultrafast relaxation time of the photocarriers (10^{-10} to 10^{-14} s) (*11*, *19*). The energy of the absorbed IR radiation is efficiently transferred to the crystal lattice through strong electron-phonon interactions that increase the temperature of the film, which is observed as a photoresponse due to the temperature dependence of the resistance. In the suspended configuration, bolometric spectroscopy of long, individual SWNTs is applicable to the study of the fundamental aspects of the electronic density of states of SWNTs, which has been accomplished for single crystals of 1D compounds in charge-density–wave states (*20*, *21*).

The absence of a spectral shift between the absorption and photoconductivity spectra (Fig. 2B) cannot be used as an argument for the band model, because the strongest bolometric response is expected at the spectral maximum of the absorbed power. Our conclusions regarding the bolometric nature of the photoresponse in SWNT films suggests that previous arguments in favor of the band model, which are based on an interpretation of direct photoconductivity (contribution of photoexcited electrons and holes to the transport properties), should be reexamined. It is possible that direct photoconductivity may be observable in individual SWNTs (*16*); in this configuration, the bolometric response is suppressed by the efficient dissipation of the heat, because the thermal conductivity of the SWNTs is not limited by the intertube junctions, which dominate the thermal and electrical resistance in the case of SWNT films (*22*, *23*).

Thin films of SWNTs have already demonstrated outstanding performance in gas and biosensing applications (*24*–*26*) and as a semitransparent conducting coating for large-area flexible optoelectronics (*3*, *22*, *27*, *28*). The strong bolometric response reported here shows the potential of SWNT thin films to function as the sensitive elements of infrared bolometers; in our experiments, we found that in the absence of the cold optical filter that is used to block the blackbody radiation from the environment, the temperature of the SWNT sample rose more than 100 K above the temperature of the supporting sapphire ring at 10 K. The strong thermal response of SWNTs to incident radiation may be responsible for the ignition of SWNTs that has been observed when the material is exposed to a conventional photographic flashlight (*29*). The absorption coefficient of SWNTs is extremely high (10^4 to 10^5 cm^{-1}) (fig. S2), at least 1 order of magnitude greater than that of mercury-cadmium-telluride, the most popular photoconductor for 2D arrays of IR photodetectors (*18*). Furthermore, the strong absorption of SWNT thin films extends from the ultraviolet to the far-IR region, (*6*) and a 100-nm-thick film absorbs >70% of the incident radiation. At this thickness, the SWNT film has an extremely low mass (ng), thus satisfying the low–heat capacity requirement of the bolometer sensitive element (*18*).

A high negative value of the temperature coefficient of resistance (TCR) of the bolometer sensitive element is required to efficiently transfer temperature modulation into an electrical signal (*18*). The temperature dependence of resistance $R(T)$ of three thin SWNT films used in laboratory prototype SWNT IR bolometers is given in Fig. 4A, and Fig. 4B shows the corresponding voltage responsivities (ratio of output voltage to incident power). The resistance of the film of P-SWNTs of 1-μm thickness shows a very weak temperature dependence with a change in the sign of the slope from metallic to semiconducting around 230 K (Fig. 3C), and this film shows a low responsivity especially at high temperatures (Fig. 4B, curve a). By decreasing the thickness of the film to 100 nm and annealing the film in vacuum at 670 K, it was possible to eliminate the metallic behavior, increase the TCR, and substantially enhance the responsivity over the entire temperature range. The strongest change of resistance with temperature [R(4.2 K)/R(300 K) = 100], and highest responsivity (up to 1000 V/W), was obtained for a 40-nm-thick film of AP-SWNTs. We registered a noise power density of less than 10^{-14} V^2/Hz in the frequency range 1 to 100 Hz, which is comparable to the lowest noise levels reported for carbon nanotube films (*27*, *30*).

The AP-SWNT film shows a TCR between 1 and 2.5% in the 330 to 100 K temperature range (fig. S3); these values are comparable with the TCR of vanadium dioxide, the most common thermistor material used in the fabrication of micromachined silicon bolometers (*18*). The TCR can be further increased by reducing the film thickness, modifying the processing conditions, and by chemical functionalization of the SWNTs (*23*). The SWNT film can be envisioned as a network of individual SWNTs or small bundles in which electrical resistance and its temperature dependence are dominated by tunneling at the intertube junctions (*22*, *23*). Modification

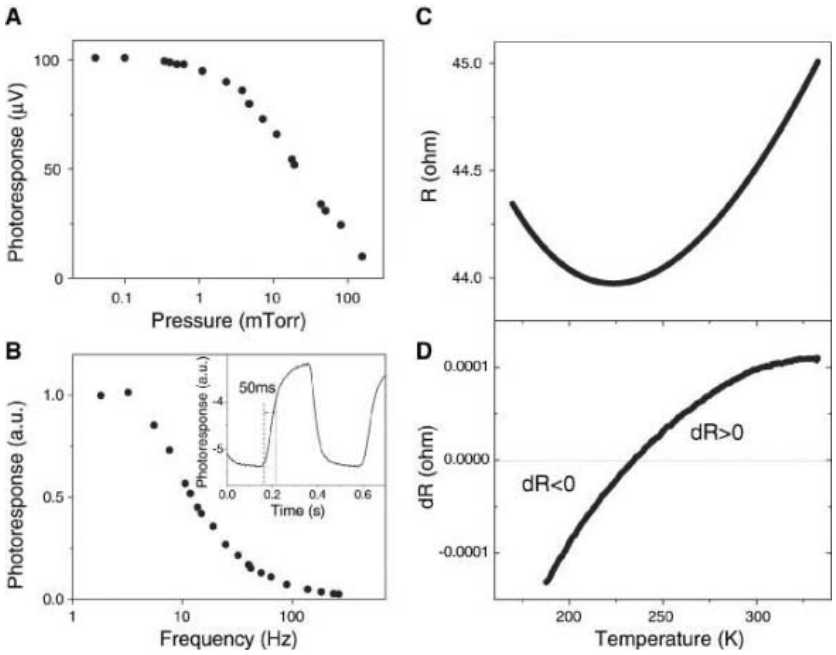

Fig. 3. Demonstration of bolometric nature of photoresponse. (**A**) Dependence of photoresponse on pressure in the cryostat. (**B**) Dependence of photoresponse on chopping frequency. (Inset) Time trace of square-wave modulated photoresponse with characteristic rise time of 50 ms. (**C**) Temperature dependence of resistance of 1-μm-thick film of purified SWNTs with minimum at 230 K caused by transition from metallic to semiconducting behavior. (**D**) Reverse of the sign of photoresponse dR at the resistance minimum.

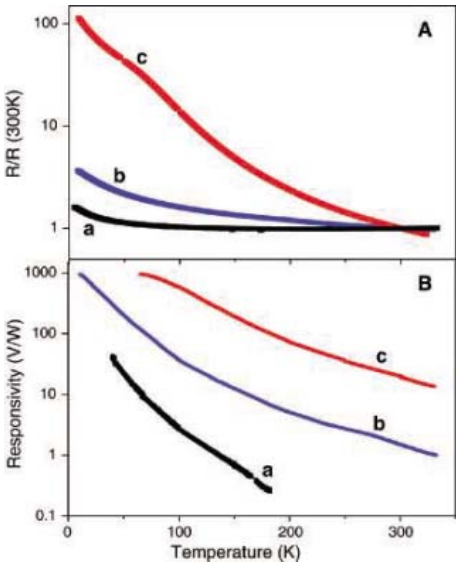

Fig. 4. (**A**) Temperature dependences of resistance of three SWNT films: (i) 1-μm-thick film of purified SWNTs (curve a); (ii) 100-nm-thick film of purified SWNTs annealed in vacuum at 670 K (curve b); and (iii) 40-nm-thick AP-SWNTs film (curve c). (**B**) Corresponding voltage responsivity of infrared bolometers made from these films.

of these junctions by chemical functionalization (*23*) or physical processing can markedly increase the TCR as shown in the annealing experiment (fig. S3). The presence of intertube junctions dramatically decreases the efficiency of heat transport along the SWNT film, thereby thermally insulating the sensitive element from the supporting substrate, which enhances the temperature response (*18*). Optimization of the room-temperature performance of the SWNT-based bolometer may provide a cost-efficient alternative to pyroelectric detectors, vanadium dioxide, and amorphous silicon–based bolometer arrays (*18*).

The SWNT networks used here are a mixture of semiconducting and metallic SWNTs; metallic pathways present within such networks reduce the temperature dependence of the resistance (*23*). The ultimate enhancement of the TCR would be achieved by the exclusive use of semiconducting SWNTs, but even with current preparations, the implementation outlined above in conjunction with recent advances in carbon nanotube thin film preparation technology (*3*, *7*, *22*, *27*, *28*) allows the manufacture of high-density 2D arrays of SWNT bolometers that are suitable for applications in thermal imaging, spectroscopy, and infrared astronomy (*18*).

References and Notes

1. J. A. Misewich *et al.*, *Science* **300**, 783 (2003).
2. M. Freitag *et al.*, *Phys. Rev. Lett.* **93**, 076803 (2004).
3. Z. Wu *et al.*, *Science* **305**, 1273 (2004).
4. P. W. Barone, S. Baik, D. A. Heller, M. S. Strano, *Nat. Mater.* **4**, 86 (2005).
5. M. S. Dresselhaus, G. Dresselhaus, P. Avouris, Eds., *Carbon Nanotubes: Synthesis, Structure, Properties and Applications*, vol. 80 (Springer-Verlag, Berlin, 2001).
6. M. E. Itkis *et al.*, *Nano Lett.* **2**, 155 (2002).
7. F. Hennrich *et al.*, *Phys. Chem. Chem. Phys.* **4**, 2273 (2002).
8. T. Ando, *J. Phys. Soc. Jpn.* **66**, 1066 (1997).
9. C. D. Spataru, S. Ismail-Beigi, L. X. Benedict, S. G. Louie, *Phys. Rev. Lett.* **92**, 077402 (2004).
10. V. Perebeinos, J. Tersoff, P. Avouris, *Phys. Rev. Lett.* **92**, 257402 (2004).
11. C.-X. Sheng, Z. V. Vardeny, A. B. Dalton, R. H. Baughman, *Phys. Rev. B* **71**, 125427 (2005).
12. F. Wang, G. Dukovic, L. E. Brus, T. Heinz, *Science* **308**, 838 (2005).
13. Y. Matsuoka *et al.*, *Sci. Technol. Adv. Mater.* **4**, 47 (2003).
14. A. Fujiwara *et al.*, *Carbon* **42**, 919 (2004).
15. A. Mohite, S. Chacraborty, P. Gopinath, G. U. Sumanasekera, B. W. Alphenaar, *App. Phys. Lett.* **86**, 061114 (2005).
16. X. Qiu, M. Freitag, V. Perebeinos, P. Avouris, *Nano Lett.* **5**, 749 (2005).
17. M. E. Itkis *et al.*, *Nano Lett.* **3**, 309 (2003).
18. M. Henini, M. Razeghi, *Handbook of Infrared Detection Technologies* (Elsevier Advanced Technology, Kidlington, Oxford, UK, 2002).
19. F. Wang, G. Dukovic, L. E. Brus, T. Heinz, *Phys. Rev. Lett.* **92**, 177401 (2004).
20. S. L. Herr, G. Minton, J. W. Brill, *Phys. Rev. B* **33**, 8851 (1986).
21. M. E. Itkis, F. Y. Nad', *JETP Lett.* **39**, 448 (1984).
22. E. Artukovic, M. Kaempgen, D. S. Hetch, S. Roth, G. Gruner, *Nano Lett.* **5**, 757 (2005).
23. E. Bekyarova *et al.*, *J. Am. Chem. Soc.* **127**, 5990 (2005).
24. E. Bekyarova *et al.*, *J. Phys. Chem. B* **108**, 19717 (2004).
25. E. S. Snow, F. K. Perkins, E. J. Houser, S. C. Badescu, T. L. Reinecke, *Science* **307**, 1942 (2005).
26. A. Star, T.-R. Han, V. Joshi, J.-C. P. Gabriel, G. Gruner, *Adv. Mater.* **16**, 2049 (2004).
27. M. Zhang *et al.*, *Science* **309**, 1215 (2005).
28. M. Kaempgen, G. S. Duesberg, S. Roth, *Appl. Surf. Sci.* **252**, 425 (2005).
29. P. M. Ajayan *et al.*, *Science* **296**, 705 (2002).
30. P. G. Collins, M. S. Fuhrer, A. Zettl, *Appl. Phys. Lett.* **76**, 894 (2000).

31. Supported by the U.S. Department of Defense/Defense Advanced Research Projects Agency/Defense Microelectronics Activity grants DMEA90-02-2-0216, H94003-04-2-0404, and H94003-05-2-0504. F.B. was supported by a Fulbright Association and Hungarian Scientific Research Fund (OTKA) T049338.

Supporting Online Material

www.sciencemag.org/cgi/content/full/312/5772/413/DC1
Materials and Methods
Figs. S1 to S3

1 February 2006; accepted 21 March 2006
10.1126/science.1125695

Atomic Pillar–Based Nanoprecipitates Strengthen AlMgSi Alloys

J. H. Chen,* E. Costan, M. A. van Huis, Q. Xu, H. W. Zandbergen

Atomic-resolution electron microscopy reveals that pillarlike silicon double columns exist in the hardening nanoprecipitates of AlMgSi alloys, which vary in structure and composition. Upon annealing, the Si_2 pillars provide the skeleton for the nanoparticles to evolve in composition, structure, and morphology. We show that they begin as tiny nuclei with a composition close to $Mg_2Si_2Al_7$ and a minimal mismatch with the aluminum matrix. They subsequently undergo a one-dimensional growth in association with compositional change, becoming elongated particles. During the evolution toward the final Mg_5Si_6 particles, the compositional change is accompanied by a characteristic structural change. Our study explains the nanoscopic reasons that the alloys make excellent automotive materials.

Aluminum is essential to modern civilizations because of its light weight, strength, and workability. Its many applications include fuel-efficient transportation vehicles (e.g., it comprises about 80% of a commercial aircraft's unloaded weight), building construction, and food packaging. Pure aluminum is soft and has little strength or resistance to plastic deformation. However, alloyed with small amounts of other elements, it can provide the strength of steel at only half the weight. With thermal treatments, the added alloying elements can form nanometer-sized precipitates, which act as obstacles to dislocation movement in the crystal (atomic matrix), strengthening the aluminum. This phenomenon is known as precipitation hardening, and the hardening nanoprecipitates are named GP zones after the pioneer work by Guinier and Preston on AlCu alloys (*1*, *2*).

AlMgSi accounts for a large percentage of the total aluminum production in the world. With appropriate pre-aging treatments, AlMgSi alloys can be pressed easily into a given form and then strengthened rapidly by annealing for a very short duration (<30 min) at about 180°C [i.e., by a characteristic two-step age-hardening process (*3*)]. This important property of AlMgSi alloys, called the quick-bake hardening response, has led to increased applications in the automotive industry (*3*–*7*), such as outer panel materials that have a strength/weight ratio optimal for fuel efficiency and environmental protection. It has long been understood that AlMgSi alloys are strengthened when needlelike monoclinic precipitates form (*5*–*14*), but to date little is known about the structures of the particles responsible for the quick-bake hardening response (*5*–*7*). Whereas the final structure of the needlelike particles has been determined (*8*, *9*), their early-stage development is difficult to characterize.

Because the nanoprecipitate structures are not well understood, the hardening nanoparticles in AlMgSi alloys are named ambiguously: They are referred to as GP(I) and GP(II) zones, pre-β″ and β″ phases, or Si/Mg co-clusters and GP zones in the early stages (*4*–*11*). The essential questions remain: How many different hardening particles exist, and how do they transform from one to another? To answer these questions, we used high-resolution transmission electron microscopy (HRTEM) and computational analysis to assess their initial structures.

We studied aluminum that was alloyed with 0.43% Mg and 1.2% Si (*15*). The homogenized alloy was heated at 560°C and then water quenched to 20°C. The best quick-bake hardening response can be achieved if the hardening annealing is performed immediately after water quenching. However, this is not practical for automotive body sheet applications, because the sheets have to be stored (up to months) and shipped at room temperature. Any storage (natural aging) will quickly degrade the alloy's quick-bake hardening response because of the formation of natural-aging clusters, which delay the formation of the hardening particles upon annealing (*4*–*7*). Hence, for advanced applications, pre-aging has

Netherlands Institute for Metals Research and Kavli Institute of Nanoscience, Delft University of Technology, Lorentzweg 1, 2628 CJ Delft, Netherlands.

*To whom correspondence should be addressed. E-mail: j.h.chen@tnw.tudelft.nl

to be applied in aluminum factories to make the quick-bake hardening response largely independent of the storage time. Therefore, we studied samples with and without pre-aging (*15*). The specimens were prepared by electropolishing for HRTEM investigations (*15*).

For straight annealing at 180°C, the hardening particles start appearing in ~1 to 5 min and then grow rapidly along the Al⟨100⟩ directions into needles. Slightly elongated particles ~2 to 6 nm in length and ~2 nm in width lead to a hardness increase of the alloy from 75 to 85 Vickers hardness (HV) (Fig. 1A). In 30 min, they become needles of 18 nm long on average without coarsening in width (Fig. 1B), and the hardness increases to ~120 HV. As annealing continues, the needles grow rather slowly and still do not change notably in width. A peak hardness of ~130 HV can be reached after annealing for ~3 hours. With continued annealing, coarsened needles ~4 nm in width can appear (Fig. 1C), and the hardness decreases slowly. The final-stage hardening particles have been identified as the Mg_5Si_6 (β″) phase (*8*, *9*).

After appropriate pre-aging, most of the particles formed are spherical and ~2 nm or smaller (small round particles in Fig. 1A). Typical hardening particles formed after two-step age-hardening processes (*15*) yield quick-bake hardening responses with hardness increases between ~75 to 85 HV and ~110 to 120 HV (Fig. 1D). Although shorter than those seen in Fig. 1, B and C, these particles are also elongated along the Al⟨100⟩ directions. If many particles become elongated after pre-aging, the alloy may demonstrate the quick-bake hardening response but lose the good formability necessary for automotive parts.

Analysis of many HRTEM images of these nanoparticles reveals that they all have the same monoclinic lattice (Fig. 1, E to H, and figs. S1 and S2). These lattice images show that (i) most particles have only ~1 to 2 monoclinic unit cells in width (~2 nm), whereas the final particles can be up to 4 nm in width (Fig. 1G) and (ii) most particles are coherent with the matrix, but final particles can be semicoherent and some of them may include stacking faults.

It is difficult to determine the monoclinic nature of these particles, especially the short ones, for several reasons. (i) The image delocalization due to microscopic aberrations leads to mixing of the particle image with the matrix image (*16*). As a result, the particles appear as disordered clusters under most imaging conditions (*15*). (ii) The differences between Mg, Al, and Si columns in electron-scattering power are small for the specimen thicknesses used (typically ~5 to 15 nm). (iii) For thick specimens, particles are likely covered by the matrix. Hence, longer particles (>5 nm) and atomic imaging in HRTEM must be used to reveal the structure of early-stage precipitates.

We used through-focus exit-wavefunction (EW) reconstruction (*15*–*21*) to image the atomic structure of early-stage needles (Fig. 1B). From a recorded through-focus series of 20 HRTEM images, we retrieved the electron wavefunction at the exit plane of the specimen. The EW's phase was then used as an atomic image of the specimen. The obtained image clearly resolves all of the atom columns in the precipitate (Fig. 2).

To deduce the precipitate structure through modeling and image simulation, we considered the following. (i) The early precipitates are the result of the Mg/Si aggregation and substitution of Al in the matrix. (ii) Previous studies indicate that atoms in such precipitates should take the coordinates of either $y = 0$ or $y = ½$ (*8*, *9*). (iii) The known atomic sizes of Mg, Si, and Al allow us to exclude unreasonable configurations (e.g., the Mg–Mg bonds should not be the shortest bonds). We first assumed that our specimen was a weak-phase object, for which the EW's phase is proportional to the projected potentials of atom columns (*21*, *22*). Therefore, the brightest spots in Fig. 2 are Si (the heaviest), the least bright spots are Mg, and the others are Al. Using these guidelines, we obtained an initial structure model.

The model was repeatedly adjusted such that the phase image of the EW calculated from the model matched well with the phase image of the EW reconstructed from the experimental image series. The refinement took into account all parameters that may influence the image contrast (Fig. 2A). The EW calculations were performed with the MacTempas image simulation software

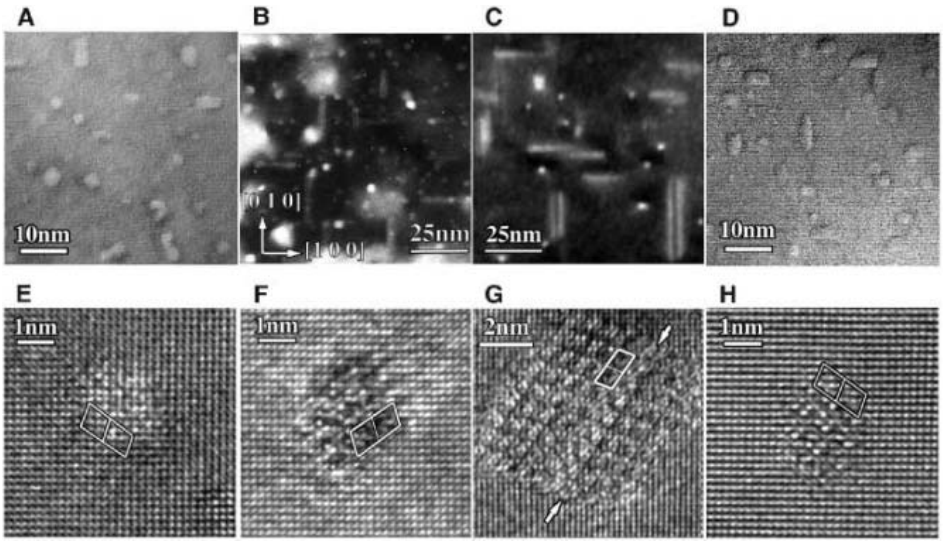

Fig. 1. HRTEM images of typical hardening precipitates in AlSiMg alloys. (**A** to **D**) Overviews of these ⟨100⟩-oriented particles after direct annealing at 180°C for 5 min (A), 30 min (B), and 4 hours (C), and after a characteristic two-step age-hardening process (*15*) (D). (**E** to **H**) The lattice images of the particles shown in (A) to (D), showing that these particles have the same monoclinic unit cells. To see the morphology of short particles clearly [(A) and (D)], the high-resolution imaging mode in HRTEM has to be used, whereas the diffraction-contrast imaging mode provides better overviews of the needlelike particles [(B) and (C)]. The arrows in (G) indicate a stacking fault in the particle.

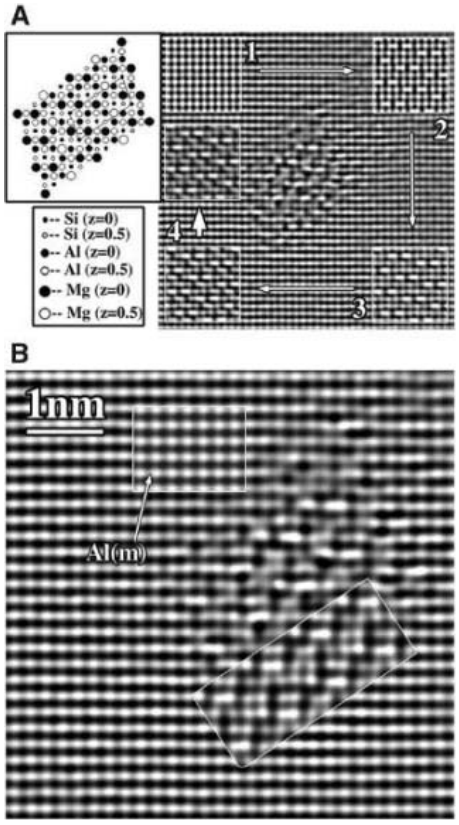

Fig. 2. Deduction of the precipitate structure. (**A**) The phase-image of the reconstructed EW of a precipitate in the matrix. The bright dots represent atom columns. The insets are the calculated images from a structure model (left) with varying specimen parameters: 1, changing the Si-Si distances in the model; 2, adjusting the crystal tilt and thickness; 3, adjusting the positions and compositions of atomic columns; 4, including the DW factors of atoms. (**B**) Refinement results: The calculated images (insets) match with the reconstructed images for both the precipitate and the matrix [Al(m)].

(*23*). Furthermore, it was necessary to match the phase images not only for the precipitate but also for the matrix (as an internal standard) under the same conditions (Fig. 2B) (*15*).

The obtained structural data (including the specimen thickness and tilt) are shown in table S1. Comparing the deduced $Mg_2Si_{2.6}Al_{6.4}$ structure with the β″ structure (*8*, *9*) and with an intermediate structure proposed for the so-called pre-β″ phase (Fig. 3A) (*11*), we made several observations. (i) $Mg_2Si_{2.6}Al_{6.4}$ has a high Al content (58%), and its Al atoms are ordered nearly in the same way as they are in the matrix. (ii) The common components of these structures are the Si double atoms. They remain unchanged not only in their location and orientation, but also in their interatomic distance (0.256 nm). This implies that a transformation from $Mg_2Si_{2.6}Al_{6.4}$ to Mg_5Si_6 may occur without having to break down the monoclinic frame kept by these Si_2 components. Two changes are required for such a transformation: replacing all Al by Si/Mg and rearranging atom positions, including a $b_{GP}/2$ shift of 2 (out of 22) atoms (where b_{GP} is the b lattice parameter of the precipitates, i.e., GP zones) (Fig. 3A). (iii) Notably, all the Si_2 atoms have a small Debye-Waller (DW) factor, whereas all the atoms that are expected to change have large DW factors (which describe the displacements of atoms from their average positions resulting from thermal vibration and other local random movements) (table S1). The large DW factors imply that atoms are less evenly aligned along in these columns because of their compositional variations.

In its first stage, a hardening precipitate can be considered a one-dimensional (1D) crystal containing MxNxQ unit cells (where the cell number in one width direction M = 1 and that in another width direction Q = ~1 to 2, whereas that in length N equals the needle length divided by 0.405 nm) (Fig. 3B). A 20-nm-long needle contains ~50 to 100 cells. The main feature of such 1D crystals is the Si double columns. They are not only the common components of different precipitates, but also the stable components of an evolving precipitate (i.e., they act as atomic pillars of the precipitate). All columns between the Si_2 pillars can change.

We propose that the hardening precipitates have a dynamic structure, which changes upon annealing but does not break down its skeleton of Si_2 pillars. Its initial format can be assumed as $Mg_2Si_2Al_7$ rather than as the deduced $Mg_2Si_2Si_{0.6}Al_{6.4}$, where Si_2 indicates the Si_2 pillar. Its dynamic composition can be described as $[Mg_{1-u-v}(Si_uAl_v)]_2Si_2[Al_{1-x-y}(Si_xMg_y)]_7$ [0 <

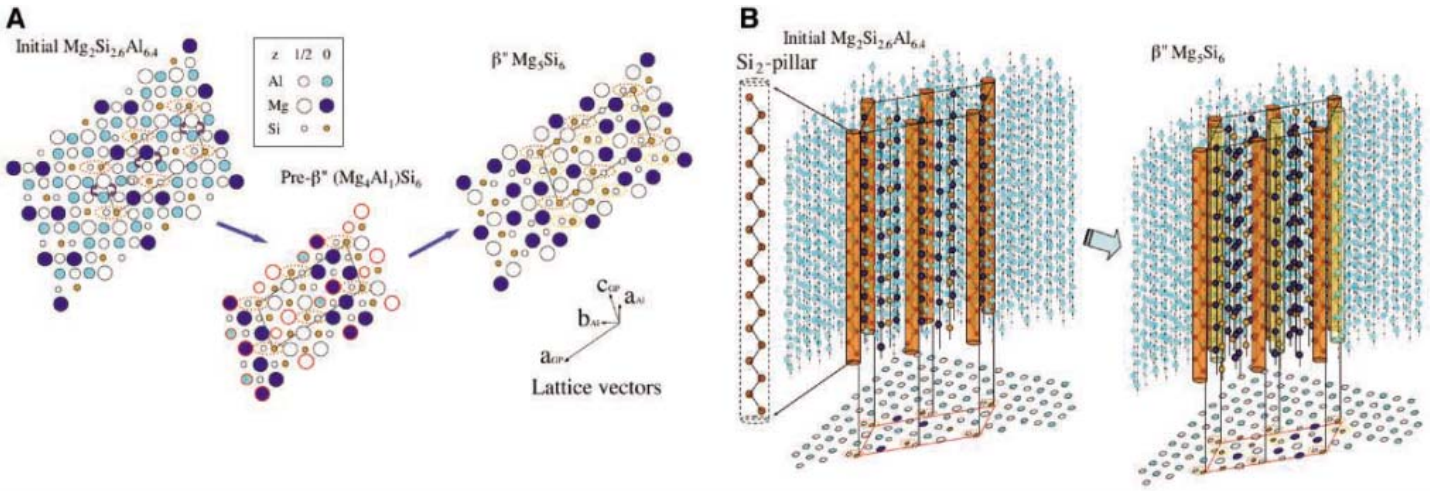

Fig. 3. The structures of different hardening precipitates. (**A**) The structures projected along c_{Al} (=b_{GP}). (a_{Al} b_{Al} c_{Al}) and (a_{GP} b_{GP} c_{GP}) denote the Al and precipitate lattice vectors, respectively. The Al atoms in $(Mg_4Al_1)Si_6$ are outlined with red circles. The Mg atoms outlined with red circles indicate the special positions at which the Mg atoms have to shift $b_{GP}/2$ to become Mg_5Si_6 (*11*). (**B**) The 3D view of $Mg_2Si_{2.6}Al_{6.4}$ and Mg_5Si_6 particles surrounded by Al, showing that the Si double columns are the common structural components of these precipitates and may serve as the stable pillars in the structure evolution. More Si_2 components (yellow ones) can be found in Mg_5Si_6, but they no longer act as pillars for Mg_5Si_6 to evolve.

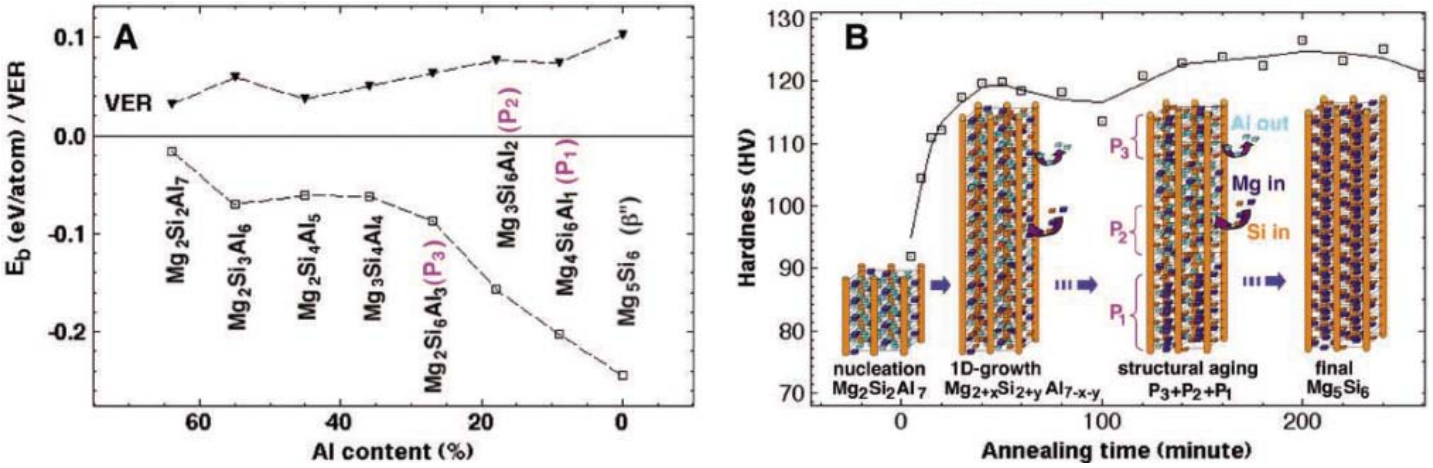

Fig. 4. The evolution of a Si_2 pillar–based nanoprecipitates upon annealing. (**A**) VERs with respect to the Al lattice and the bulk formation enthalpies (E_b) with respect to the solid solution, calculated for a few ordered structural configurations plotted against the Al content in the precipitate (atom %). The total energy calculations were performed with the use of the first-principles Vienna ab initio simulation package (VASP) code (*24*, *25*). (**B**) Schematic illustration of four featured stages of an evolving nanoprecipitate with respect to the hardness profile of the alloy being annealed at 180°C.

$u(t) < ½$, $v(t) \approx 0$, $0 < x(t) + y(t) < 1$, where t is annealing time]. Compositionally, the particle starts with $[Mg]_2Si_2[Al]_7$ and then undergoes a continuous substitution of the Al and (partially) Mg atoms by other atoms, until it reaches $[Mg_{½}(Si_{½})]_2Si_2[(Si_{½}Mg_{½})]_7$ ($Mg_5Si_6 = \beta''$). The energy gradients for a compositional change and the local availability of Si/Mg atoms drive the evolution. This model implies that each nanoprecipitate has its own composition and its own stages in evolution.

To qualitatively understand some aspects of the structure dynamics of such nanoparticles, we performed first-principles calculations without directly including the particle-matrix interactions (*24*, *25*). Figure 4A plots the bulk formation enthalpies (E_b) and the volume expansion ratios (VERs) for different structures against their Al content. The larger the VERs, the higher the particle-matrix interaction energies (E_i) (including the interface-energy increase due to the mismatch of atom bonds). VERs, therefore, qualitatively indicate the relative levels of E_i for these structures (if embedded in the matrix). At least for a sufficiently long precipitate, ΣE_b (total E_b) is dominant over ΣE_i (total E_i), because such particles would not have existed otherwise. Figure 4A shows that (i) the evolution is indeed energetically favored. (ii) $Mg_2Si_2Al_7$ has the highest E_b but a minimal mismatch with the matrix; i.e., it is least effective for strengthening the alloys [supporting online material (SOM) text]. (iii) E_b markedly decreases, first upon the change from $Mg_2Si_2Al_7$ to $Mg_2Si_3Al_6$, and then upon the appearance of β″-type structures (the P_1, P_2, and P_3 structures shown in Fig. 4), in which two specific (AlMg) atoms in the unit cell are shifted by $b_{GP}/2$ (Fig. 3A).

The reality is more complex, in that the precipitates start with a small size and the compositional evolution is accompanied by a morphology (length) change (Fig. 1, A and B). This is understandable. For any particle with a certain structure there is a critical size (length) below which ΣE_i is dominant over ΣE_b and the particle is unstable. Because it is mostly coherent with the matrix, $Mg_2Si_2Al_7$ has the smallest critical length of all. Once stabilized, a $Mg_2Si_2Al_7$ particle can grow in one dimension (because along b_{GP} the particles are most coherent with the matrix), but its ΣE_b gain will be small (Fig. 4A). However, if the 1D growth is combined with the compositional change from $Mg_2Si_2Al_7$ to $Mg_{2+x}Si_{2+y}Al_{7-x-y}$ ($1 < x + y < 3$), the substantial lowering in ΣE_b will allow the particle to grow rapidly. It is not surprising that a short $Mg_2Si_2Al_7$ particle will not evolve to β″ without a substantial growth in advance, given that Mg_5Si_6 (β″) has the largest critical length of all.

Further compositional changes in a needle-like particle result in the development of β″-type structures. In this stage, because all changes from P1 toward β″ markedly lower E_b (Fig. 4A), one segment of the needle would proceed with further changes rather than wait for the rest of the needle to develop the same composition. At this point, four featured stages of the evolving nanoprecipitate can be identified (Fig. 4B), which is in agreement with the alloy's hardness profile (SOM text).

The dynamic behavior of the nanoparticles changes with temperature. At lower temperatures (e.g., ~70° to 80°C), the particle's critical lengths at different compositions become larger, such that the nucleation at $Mg_2Si_2Al_7$ and particularly the further evolution to $Mg_{2+x}Si_{2+y}Al_{7-x-y}$ become slower, or even impossible. This prevents the rapid 1D growth and therefore the further evolution toward β″. At room temperature, even the particle's nucleation at $Mg_2Si_2Al_7$ becomes impossible. Hence, for automotive application, our study suggests that the particles at $Mg_2Si_2Al_7$ and at $Mg_{2+x}Si_{2+y}Al_{7-x-y}$ are key particles and are directly responsible for the quick-bake hardening response of AlMgSi alloys. Appropriate pre-aging should nucleate a large number of $Mg_2Si_2Al_7$ particles but prevent their further evolution. Two mechanisms coexist for quickly strengthening the alloys upon a second heating: (i) the quick evolution of the nuclei from $Mg_2Si_2Al_7$ to $Mg_{2+x}Si_{2+y}Al_{7-x-y}$ (leading to effective obstacles for dislocation movement), and (ii) the 1D growth of the particles (leading to a rapid increase of the total precipitate volume fraction) (SOM text).

We show that upon annealing, the hardening nanoprecipitates in AlMgSi alloys undergo a rather complex evolution, involving changes in composition, structure, and morphology. Yet, they do not break down their Si_2 pillar skeleton. We analyze two complementary points of view to provide a complete explanation of these nanoparticles and their evolution. On the one hand, we consider them as dynamic objects in a nonequilibrium evolution process, analogous to a living process, involving nucleation, growth, and maturation. A hardening nanoprecipitate undergoes various physical changes with age (annealing time), but it remains fundamentally the same object because of its stable identity—the Si_2 pillar skeleton. On the other hand, we treat the nanoparticles as distinct phases in a series of transformations; different particles are formed in different stages, and one may transform into another (if energetically favored). This approximation allows an analysis on the driving forces for the evolution. Additional computer power will allow direct incorporation of the particle-matrix interactions in energy calculations (requiring the inclusion of ~10^4 atoms in the particle-matrix system), which will lead to an even better understanding of the nanoparticle evolution.

References and Notes

1. A. Guinier, *Nature* **142**, 569 (1938).
2. G. D. Preston, *Philos. Mag.* **26**, 855 (1938).
3. For automotive outer panel application, a characteristic two-step age-hardening process is beneficially employed for AlMgSi alloys (*26*), in which the "seeds" of the precipitates are prepared with appropriate pre-aging in Al factories, whereas the effective hardening precipitates will form rapidly upon a short annealing (paint bake cycles) in car manufacturing plants. After pre-aging, the alloys must (i) be sufficiently soft for good formability and (ii) form certain particles for the quick-bake hardening response upon the second heating.
4. L. Zhuang *et al*., Proceedings of the *2001 TMS Annual Meeting: Automotive Alloys*, New Orleans, LA, 11 to 15 February (The Minerals, Metals, and Materials Society, New Orleans, LA, 2001), pp. 77–91.
5. M. Murayama, K. Hono, *Acta Mater.* **47**, 1537 (1999).
6. G. A. Edwards, K. Stiller, G. L. Dunlop, M. J. Couper, *Acta Mater* **46**, 3893 (1998).
7. P. Ringer, K. Hono, *Mater. Charact.* **44**, 101 (2000).
8. H. W. Zandbergen, S. J. Andersen, J. Jansen, *Science* **277**, 1221 (1997).
9. S. J. Andersen *et al.*, *Acta Mater.* **46**, 3283 (1998).
10. A. Perovic, D. D. Perovic, G. C. Weatherly, D. J. Lloyd, *Scripta Mater.* **41**, 703 (1999).
11. C. D. Marioara, S. J. Andersen, J. Jansen, H. W. Zandbergen, *Acta Mater.* **49**, 321 (2001).
12. C. Ravi, C. Wolverton, *Acta Mater.* **52**, 4213 (2004).
13. G. Thomas, *J. Inst. Met.* **90**, 57 (1961).
14. A. Guinier, *Heterogeneities in Solid Solutions in Solid State Physics*, F. Seitz, D. Turnbull, Eds. (Academic Press, London, 1959), vol. 9, pp. 293–398.
15. Materials and methods are available as supporting material on *Science* Online.
16. W. Coene, A. Jansen, *Scanning Microsc. Suppl.* **6**, 379 (1992).
17. W. O. Saxton, *Computer Techniques for Image Processing in Electron Microscopy* (Academic Press, London, 1978).
18. W. Coene, G. Janssen, M. Op De Beeck, D. Van Dyck, *Phys. Rev. Lett.* **69**, 3743 (1992).
19. C. L. Jia, A. Thust, *Phys. Rev. Lett.* **82**, 5052 (1999).
20. W. Coene, A. Thust, M. Op de Beeck, D. Van Dyck, *Ultramicroscopy* **64**, 109 (1996).
21. J. H. Chen, H. W. Zandbergen, D. Van Dyck, *Ultramicroscopy* **98**, 81 (2004).
22. J. M. Cowley, *Diffraction Physics* (North-Holland Publishing, New York, 1981).
23. M. A. O'Keefe, R. Kilaas, *Scanning Microsc. Suppl.* **2**, 225 (1988).
24. G. Kresse, J. Furthmuller, *Phys. Rev. B* **54**, 11169 (1996).
25. The formation enthalpy of a precipitate $Mg_xSi_yAl_z$ is defined with respect to the energies of Mg and Si atoms in solid solution in Al, as $\Delta H = E_{MgSiAl} - xE_{Mg} - yE_{Si} - zE_{Al}$, where E_{MgSiAl} is the calculated precipitate energy. E_{Mg}, and E_{Si} are, respectively, the (Gibbs-free) energies of single substitutional Mg and Si atoms in bulk Al, which are calculated with the use of a supercell consisting of 3-by-3-by-3 conventional face-centered cubic cells. E_{Al} is the energy of single bulk Al atoms. By *k*-point sampling and energy cutoff, it was ascertained that all the energy calculations are converged to <1 meV/atom (0.1 kJ/mol). Allowing both cell dimensions and atom positions to relax, the first-principles calculations also yield the free volume expansion ratios of different structures with respect to the Al lattice.
26. D. W. Pashley, M. H. Jacobs, J. T. Vietz, *Philos. Mag.* **16A**, 51 (1967).

27. This research was carried out under the project number MC4.98047 of the Netherlands Institute for Metals Research. We thank K. Urban and M. Lentzen for the use of their aberration-corrected HRTEM facility; L. Zhuang for providing Al alloy samples; and I. M. Richardson for constructive discussions. J.H.C. would like to thank the National Science Fund of China (grant no. 10474102) for supporting part of the image analysis work.

Supporting Online Material

www.sciencemag.org/cgi/content/full/312/5772/416/DC1
Materials and Methods
SOM Text
Figs. S1 and S2
Table S1
References

22 December 2005; accepted 21 March 2006
10.1126/science.1124199

Electrostatic Self-Assembly of Binary Nanoparticle Crystals with a Diamond-Like Lattice

Alexander M. Kalsin, Marcin Fialkowski, Maciej Paszewski, Stoyan K. Smoukov, Kyle J. M. Bishop, Bartosz A. Grzybowski*

Self-assembly of charged, equally sized metal nanoparticles of two types (gold and silver) leads to the formation of large, sphalerite (diamond-like) crystals, in which each nanoparticle has four oppositely charged neighbors. Formation of these non–close-packed structures is a consequence of electrostatic effects specific to the nanoscale, where the thickness of the screening layer is commensurate with the dimensions of the assembling objects. Because of electrostatic stabilization of larger crystallizing particles by smaller ones, better-quality crystals can be obtained from more polydisperse nanoparticle solutions.

Crystalline aggregates composed of one or more types of metallic and/or semiconductor nanoparticles (NPs) are of great interest for the development of new materials with potential applications in areas such as optoelectronics (*1*), high-density data storage (*2*), catalysis (*3*), and biological sensing (*4*). To date, methods for the crystallization of two-dimensional (2D) and 3D NP superlattices have relied on the differences in the sizes of component particles and on attractive van der Waals or hard-sphere interactions between them. This strategy has been successful in preparing several types of lattices [such as AB (*5*), AB_2 (*6*), AB_5 (*7*), and AB_{13} (*6*)], but the all-attractive nature of the interparticle potentials limits its applicability to relatively few and usually (*8*) close-packed structures.

To overcome this limitation, we and others (*8*, *9*) have focused on systems of NPs interacting via electrostatic forces; such forces provide a basis for ionic, colloidal (*9*), or even macroscopic (*10*) crystals, but, despite promising attempts (*8*, *11*), have not been successfully exploited for controllable or predictable long-range organization of matter at the nanoscale. Here, we report electrostatic self-assembly (*10*) (ESA) of oppositely charged, nearly equally sized metallic NPs of different types into large 3D crystals characterized by sphalerite (diamond-like) (*12*) internal packing, and of overall morphologies identical to those of macroscopic diamond or sphalerite crystals (Figs. 1 to 4). Formation of these non–close-packed structures results from the change in electrostatic interactions in the nanoscopic regime, where the thickness of the screening layer becomes commensurate with the dimensions of the assembling particles, and is facilitated by the presence of smaller, charged NPs in the crystallizing solutions that stabilize larger NPs by what can be termed a nanoscopic counterpart of Debye screening.

We used Ag and Au NPs coated with ω-functionalized alkane thiols (*13*): $HS(CH_2)_{10}COOH$ (MUA) and $HS(CH_2)_{11}NMe_3^+Cl^-$ (TMA) (Fig. 1A). These NPs were prepared according to a modified procedure (*14*) [see Supporting Online Material (*15*)] and had average diameters of 5.1 nm (with dispersity σ = 20%) for Au and 4.8 nm (σ = 30%) for Ag (Fig. 1B). We chose this pair as a model system, because the average sizes of Au NPs passivated with MUA [self-assembled monolayer (SAM) thickness = 1.63 nm (*16*)] and Ag NPs covered with TMA (SAM thickness ~ 1.9 nm) were very similar overall (~8.36 nm versus ~8.60 nm).

Both types of NPs were stable and unaggregated when kept in separate aqueous solutions. At the concentration used (2 mM), the pH of AuMUA solution was 9.7, so the NPs presented deprotonated carboxylate groups, and the ratio of

Department of Chemical and Biological Engineering and The Northwestern Institute on Complex Systems, Northwestern University, 2145 Sheridan Road, Evanston, IL 60208, USA.

*To whom correspondence should be addressed. E-mail: grzybor@northwestern.edu

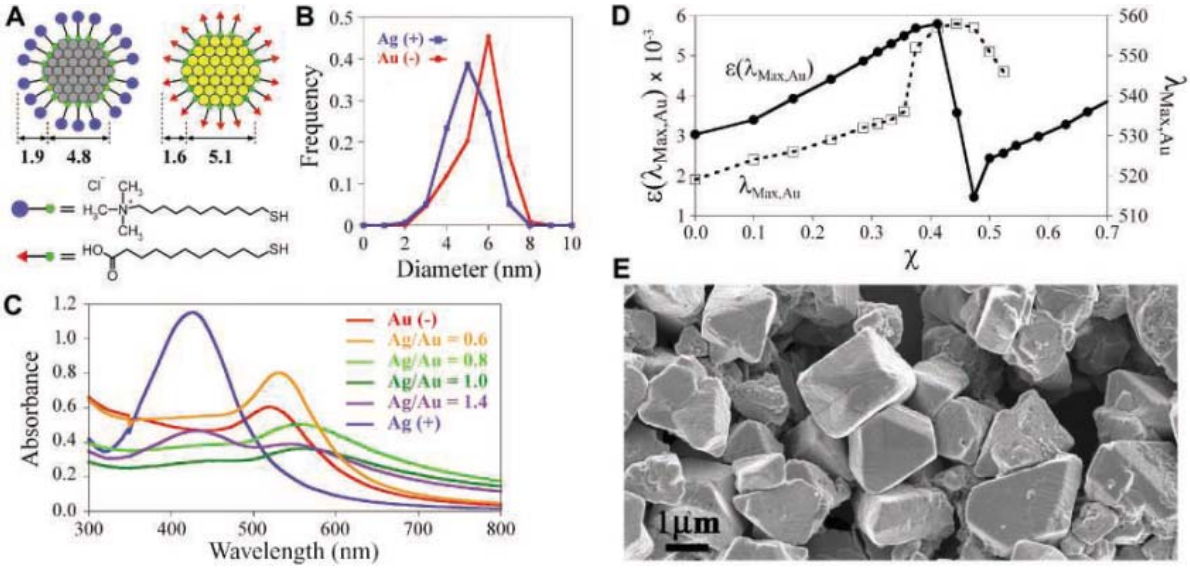

Fig. 1. (**A**) Scheme and average dimensions (in nm) of AuMUA and AgTMA nanoparticles used as the model system. Particle compositions estimated using the method from (*39*) are $Au_{4100}L_{380}$ (where L is MUA) and $Ag_{3400}L_{340}$ (where L is TMA); the ratio of the particles' charges Q(AgTMA)/Q(AuMUA) = −0.90. (**B**) Experimental, normalized size distributions of metallic cores of Ag and Au NPs; statistics are based on high-resolution TEM images of at least 500 NPs of each type. (**C**) Typical UV-Vis spectra for the titration of AuMUA solution (here, 2 mM, 0.4 ml) with small aliquots (40 μl = 0.1 equiv.) of AgTMA solution (2 mM; concentrations are given in moles of metal atoms). The legend gives numbers of AgTMA equivalents added. Initially, absorption of the SPR band of gold ($\lambda_{max,Au}$ = 520 nm) rises and that of the SPR band of silver ($\lambda_{max,Ag}$ = 424 nm) is extinguished. Precipitation begins at ~ 0.7 equiv. AgTMA and is complete when [AgTMA]/[AuMUA] ~ 0.9. The precipitation point corresponds to the formation of charge-compensated (electroneutral) complex and is consistent with an estimate derived from particle compositions: $([AgTMA]/[AuMUA])_{neutral} = (N_{Ag}/N_{Au})|Q_{AuMUA}/Q_{AgTMA}| = (3400/4100)/0.9 = 0.92$, where N_{Ag} and N_{Au} are the numbers of Ag and Au atoms in one AgTMA and one AuMUA particle, respectively). Further addition of silver NPs solubilizes the precipitate, as evidenced by the increasing intensities of SPR bands of both types of NPs (and also by visual examination of the sample). (**D**) (Solid curve) Progress of the titration represented by absorption coefficient $\varepsilon(\lambda_{max,Au})$ defined in (*15*). The initial increase in ε is the result of close proximity of oppositely charged particles within soluble aggregates (*15*). Aggregation is confirmed by the red shift of the Au plasmon band maximum, $\lambda_{max,Au}$, from 520 to ~558 nm (dashed curve). For $\chi \gtrsim 0.5$, precipitate redissolves, and $\lambda_{max,Au}$ decreases. (**E**) Large-area SEM image of binary crystals obtained from AuMUA/AgTMA precipitates.

NP charges was Q(AgTMA)/Q(AuMUA) = −0.90 (compare Fig. 1A). When the solutions were mixed, the positively charged AgTMAs interacted with the negatively charged AuMUAs. As suggested by the absence of the silver plasmon band centered at λ_{max}^{Ag} = 424 nm and concomitant growth of the gold band at λ_{max}^{Au} = 520 nm (Fig. 1C), the interaction involved close proximity of particles of the two types within small, soluble aggregates (*15*). These aggregates precipitated rapidly when the molar ratio of the NPs was near unity and the overall charge of the NPs was neutralized (Fig. 1D).

Crystals were obtained from the NP precipitate, from which the excess of ammonium salt hindering the crystallization process was removed by washing with water. Subsequently, the precipitate was dissolved in a 1:4 v/v mixture of water and dimethyl sulfoxide (DMSO), and crystals were grown by slow (~12 hours) evaporation of water at 70°C (*17*). This procedure yielded large numbers of regularly faceted crystals, each composed of several million NPs and with dimensions up to 3 μm in each direction (Figs. 1 and 4). When the crystals were partly dissolved in water, the ultraviolet-visible (UV-Vis) spectra showed no blue-shift of the surface plasmon resonance (SPR) of Au and an extinguished SPR band of Ag. These data suggest that (i) Ag and Au NPs in the crystals were in close proximity and (ii) that they did not amalgamate (*18*) during crystallization. Amalgamation was also ruled out by performing successful crystallization without heating.

The crystal structure was solved by small-angle, powder x-ray diffraction (XRD) (*15*). The XRD spectrum in Fig. 2A shows three peaks located at 2θ = 0.801°, 1.308°, and 1.539°. This diffraction pattern characterizes the sphalerite [or diamond (*15*)] structure with the lattice constant a = 19.08 ± 0.53 nm and with peak positions corresponding to Bragg reflections on planes specified by Miller indices (111), (220), and (311), respectively. The lattice constant agrees with the value of $a \approx$ 18.5 nm based on scanning electron microscopy (SEM) measurements (Fig. 2B). Also, the interparticle distance along the body-diagonal axis calculated from XRD data is 8.27 ± 0.26 nm, near the value of ~8.48 nm estimated from hard-sphere radii of individual NPs (compare Fig. 1A) and 8.5 nm from the SEM image (Fig. 2C). Finally, both the bulk composition of the crystals as well as the identities of NPs on crystalline faces were examined via energy dispersive spectroscopy (EDS) in SEM and in transmission electron microscopy (TEM); it was found that the bulk contents of Ag and Au were approximately equal [compare (*15*)] and that the arrangement of surface particles was congruent with the XRD analysis (Fig. 3).

All of these experiments indicate that NPs are arranged on a diamond lattice with each NP surrounded by four oppositely charged neighbors at the vertices of a tetrahedron (Fig. 2D). This structure is closely related to that of ZnS, except that the NP "ions" have nearly identical radii. Not surprisingly, the overall crystal morphologies—including octahedral, truncated tetrahedral, truncated and twinned octahedral, and triangular—are identical to those observed for their macroscopic diamond or sphalerite (ZnS) counterparts (Fig. 4).

Crystallization of NPs into a diamond-like structure is mediated by screened electrostatic interactions. Screening occurs because (i) the NP cores are metallic and (ii) each charged NP is surrounded by a layer of counterions. As a result, the particles interact by short-range electrostatic potentials. To show why such interactions do not lead to more closely packed NaCl or CsCl structures that might have been expected on the basis of NP charges alone, we first note that the screening length, κ_C^{-1}, for the crystallized NPs is ~2.7 nm (*19*, *20*). This short distance relative to the interparticle distance means that the electrostatic

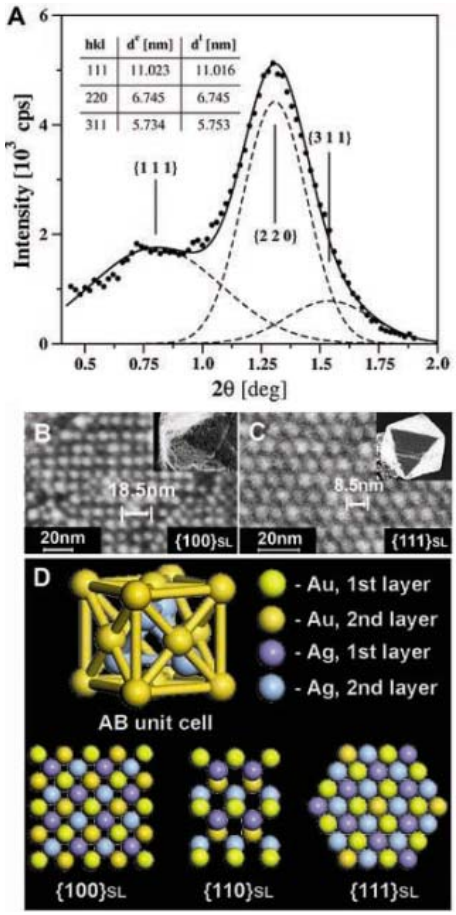

Fig. 2. Structure of AuMUA-AgTMA binary crystals. (**A**) Small-angle powder XRD spectrum of the crystals. Bragg reflections on planes specified by Miller indices shown are characteristic of a diamond-like structure. (Inset) Comparison between experimental (d^e) and theoretical (d^t) spacing between crystal planes with Miller indices {*hkl*}. Values of d^t were calculated based on the lattice constant a = 19.08 nm. The center-to-center distance between nanoparticles on the (100) face, calculated as $D = \sqrt{2}a/2$, is D = 13.49 ± 0.37 nm; interparticle distance along body-diagonal axis calculated from XRD data is 8.27 ± 0.26 nm. (**B**) An SEM image of a $\{100\}_{SL}$ square face taken from a twinned-octahedron crystal (inset); estimated lattice constant a = 18.5 nm. (**C**) An SEM image of a $\{111\}_{SL}$ plane of a triangular face of an octahedron (inset) with estimated interparticle distance of 8.5 nm. (**D**) Scheme of an AB unit cell and the projections of $\{100\}_{SL}$, $\{110\}_{SL}$, $\{111\}_{SL}$ planes. NPs of one type are positioned in the nodes of a face-centered cubic lattice, whereas the others occupy half of the tetrahedral voids. The crystals are isostructural with sphalerite ZnS (SG 216) or, for crystals made of only one type of metal cores (compare Fig. 5B), with the diamond lattice (SG 227).

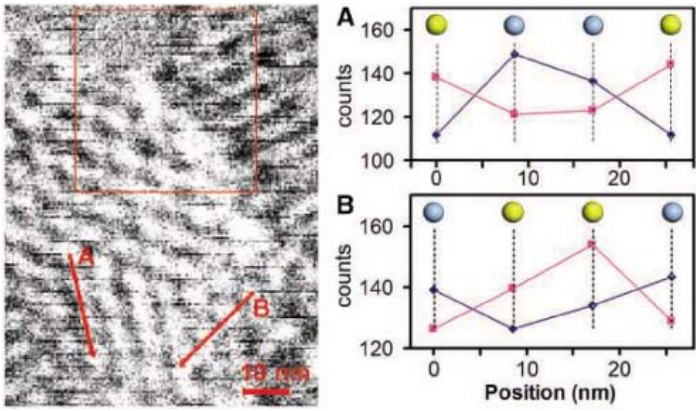

Fig. 3. Compositional analysis of the NP crystal faces. The left panel shows a typical scanning TEM (STEM) image of a hexagonal {111} face recorded on Hitachi HF2000 instrument. The EDS analysis was performed in the STEM mode with small aperture and 2-nm electron probe size. The aperture settings (#3) were chosen such as to minimize scattering from neighboring/underlying particles while retaining sufficient image contrast. Drift correction area is delineated by the red box. Graphs in (**A**) and (**B**) give typical EDS data collected along directions indicated in the STEM image at 60° with respect to one another (compare Fig. 2D). Because a measurement at each nanoparticle took 30 s and the residual drift of the instrument (inherent and due to sample heating) was ~1 nm/min, it was possible to collect reliable data over up to four successive NPs and two scans. EDS data were obtained from the x-ray emission lines of AgLα (2.98 keV, blue line) and of AuLα (9.71 keV, magenta line). The graph in (A) corresponds to the Au-Ag-Ag-Au sequence of NPs and that in (B), to Ag-Au-Au-Ag that can be expected at these relative locations. The counts are relatively high because the beam penetrates into the crystal beyond the top layer of NPs. Although x-ray emission is thus collected from several layers, signal undulation is due to the top layer—when the aperture is increased (to #1 or #2) and signal is collected from an even larger volume/depth, the counts for Ag and Au equalize, giving the ~1:1 bulk composition of the crystal (*15*).

energy of the crystals is well approximated by accounting only for the interactions between nearest oppositely and like-charged NPs.

With this simplification, crystal energies (per NP) of structures, in which each NP has n oppositely and m like-charged neighbors [e.g., $n = 4$, $m = 12$ for diamond; 6 and 12 for NaCl; 8 and 6 for CsCl (*21*)], can be written as a sum of favorable, nE_{op}, and unfavorable, $mE_{like}(d)$, contributions. Here, E_{op} and E_{like} denote, respectively, the energy of two oppositely charged NPs brought into contact, and two nearest like-charged NPs. The value of E_{like} depends on the separation, $d(m)$, between the surfaces of like-charged NPs. If $d > 2\kappa^{-1}$, the electrostatic interaction is screened and $E_{like} \approx 0$; for smaller separations, E_{like} increases rapidly with decreasing d (*20*, *22*). In particular, for diamond structure (Fig. 4A, left), $2\kappa^{-1} \approx d_d = 5.3$ nm, and only E_{op} contributes effectively to the crystal energy, which is thus favorable (i.e., negative). In contrast, for NaCl and CsCl lattices (Fig. 5A, right), the values of $d(m)$ are considerably smaller (3.5 and 1.3 nm, respectively), and the like-charge repulsions offset the energetic gain compared to that of the diamond lattice ($2E_{op}$ for NaCl and $4E_{op}$ for CsCl). Overall, the diamond structure has the lowest energy.

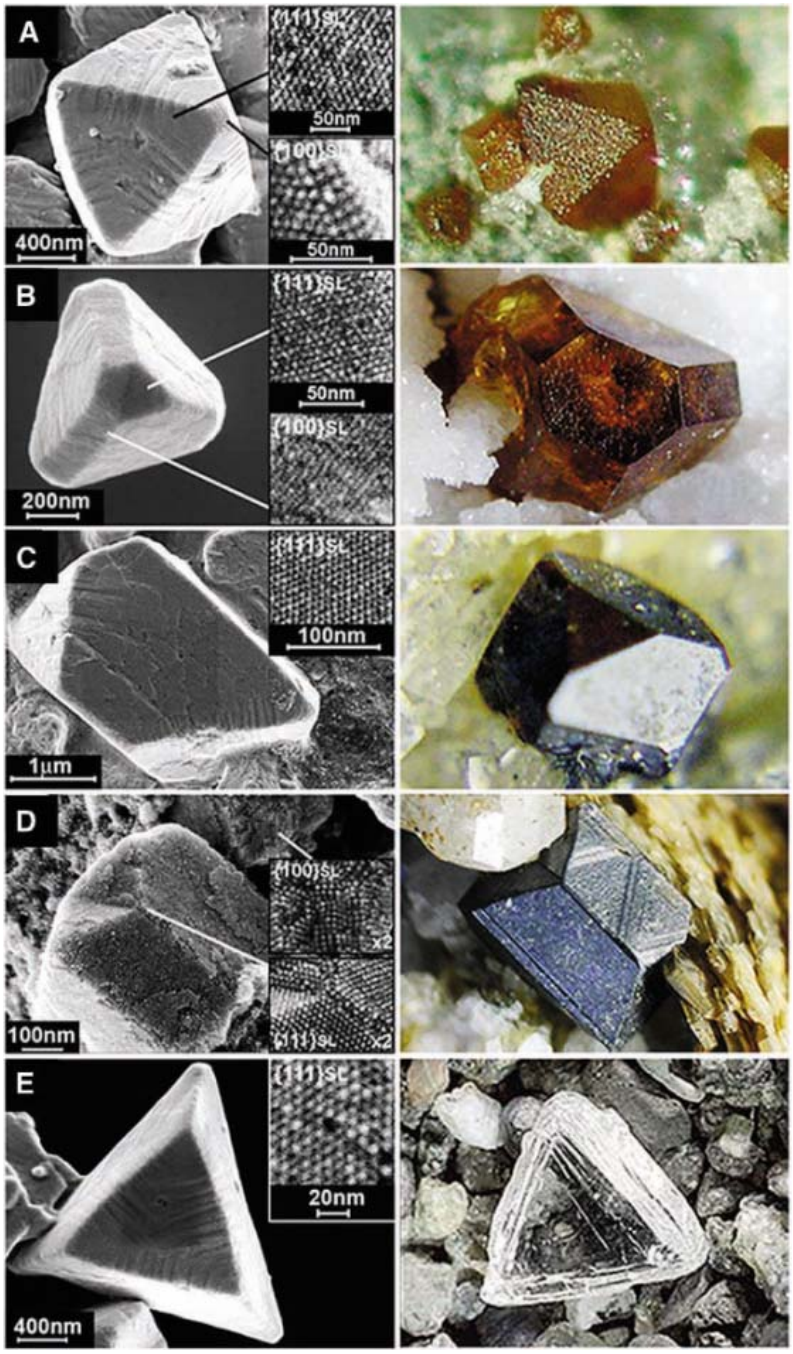

Fig. 4. Different morphologies of the AuMUA-AgTMA crystals (left column) and their macroscopic sphalerite (SL) (**A** to **D**) and diamond (**E**) counterparts (right column). (A) Octahedron; insets show $\{111\}_{SL}$ and $\{100\}_{SL}$ faces. (B) Cut tetrahedron; insets show $\{111\}_{SL}$ and $\{100\}_{SL}$ faces from cut top and from cut edge, respectively. (C) Octahedron with two triangular faces cut; inset shows the $\{111\}_{SL}$ face. (D) Twinned octahedron; insets magnify $\{111\}_{SL}$ faces at the location of twinning and the $\{100\}_{SL}$ face of a broken neighboring crystal. (E) Truncated tetrahedron; inset shows top view of the $\{111\}_{SL}$ face.

We emphasize that this effect does not scale with the size of the assembling objects. For example, with larger particles such as those recently described in (*9*) and (*23*), the characteristic separation distance between like-charged particles is much larger than the screening length, and close-packed lattices are favored. We also note that theoretical models without screening but accounting for either entropic effects (*24*) and/or van der Waals interactions (*25*–*28*) cannot justify the formation of a diamond lattice.

Progress of the crystallization process depends on the degree of monodispersity of the nanoparticles used. Surprisingly, polydispersity skewed toward smaller particles facilitated crystallization and gave rise to crystals of better quality. To understand this effect, we performed a series of experiments under identical experimental conditions (solvent and temperature) but with NPs characterized by various size distributions (Fig. 5B). When Au particles taken from the same, narrow distribution ($\sigma = 20\%$) but functionalized with either MUA or TMA were cocrystallized, the quality of crystals was poor, and a large proportion of NPs formed amorphous aggregates (Fig. 5B, left). In contrast, when one of the distributions was broader (e.g., AgTMA with $\sigma = 45\%$) than the other (as with the AuMUAs that we used in the model system; $\sigma = 20\%$), large numbers of high-quality crystals were obtained (Fig. 5B, middle). Finally, when both distributions were broad (e.g., AgTMA with $\sigma = 45\%$ and AuMUA with $\sigma = 30\%$), particles stayed in solution and did not crystallize at all (Fig. 5B, right). That is, some polydispersity—but not too much—aided crystallization.

These observations can be explained qualitatively on the basis of screening of electrostatic forces acting between large NPs by smaller particles present in solution. The electrostatic interaction between two large NPs can be approximated by a screened potential (*29*), in which the effective screening length decreases with increasing concentration of screening charge carriers (here, small NPs) and determines the stability of dispersed nanoparticles. When large NPs are surrounded by smaller, oppositely charged ones, the effective screening length is small, and the NPs interact weakly and do not aggregate (*30*, *31*). In contrast, when no small particles are present, the screening length is large, long-range attractive electrostatic forces are strong, and flocculation (*32*) ensues.

Thermodynamically, the presence of small NPs shifts the equilibria between dispersed (D), amorphous-aggregate (A), and crystalline (C) phases (Fig. 5C). In the absence of small particles, the chemical potential of the dispersed phase,

μ_1, is—due to the electrostatic interactions—very high compared to both μ_A and μ_C. In this case, the NPs either condense via flocculation or nucleate to the crystalline phase. Because the nucleation processes are less likely to occur, the condensed phase consists mostly of amorphous aggregates. Addition of small particles weakens the electrostatic interactions substantially and lowers the potential of the dispersed phase to μ_2, which is only slightly higher than the potentials of condensed phases A and C. Here, the effective attractive forces are sufficient to overcome the energetic barrier accompanying aggregation, but are weak enough to allow the aggregates to anneal into low-energy crystals (*9*, *33*). The formation of the crystalline phase occurs via the nucleation/aggregation processes (*34*), in which a stable nucleus is formed if its radius, R, is large enough and if the gain in the bulk energy, $\Delta E_{bulk} \propto \Delta\mu_{2C} R^3$, dominates over the surface energy $\Delta E_{surf} \propto \sigma R^2$, where $\Delta\mu_{2C}$ and σ denote, respectively, the difference in chemical potentials and the surface energy between dispersed and crystalline phases. The critical size, R_{crit}, of the nucleus that remains in suspension and serves as a seed for further crystallization is determined by the condition that the sum $\Delta E_{bulk} + \Delta E_{surf}$—inversely proportional to $|\Delta\mu|$—reaches its maximum value (*34*). Because $|\Delta\mu|_{2C} \ll |\Delta\mu|_{1C}$, crystals obtained from suspension "2" were much larger than those formed from phase "1." Finally, if large numbers of small particles of both types are present, the chemical potential of the dispersed phase is lower than both μ_A and μ_C, and no aggregation or crystallization is observed.

Several comments are in order. We emphasize that the experimental trends cannot be explained by entropic "depletion" forces (*35*). In such cases, the presence of small particles would destabilize the free-floating, large particles and would lead to phase separation. The electrostatic stabilization of large NPs by small ones is analogous to the Debye screening affected by high–ionic strength solutions (*36*, *37*); in this respect, small, charged nanoparticles behave like ions. However, if the sizes and charges of the crystallizing particles were increased, one would need proportionally more small particles to provide efficient electrostatic stabilization (*30*). We have seen this effect in collections of 6- and 12-nm NPs that we tried to cocrystallize, where the particles kept in solution could not be stabilized even by broad distributions of small NPs. Although the screening can, in principle, be modulated by increasing the ionic strength of the crystallization medium by adding salts, these salts stabilize isolated particles and also crystallize themselves—as we verified experimentally, both of these effects hinder the formation of NP crystals.

Finally, from a practical standpoint, extension of the ESA approach to other types and combinations of NPs (e.g., magnetic or photoluminescent) may open new avenues to nanostructured materials of composite properties deriving from the unique properties of the diamond lattice (*38*).

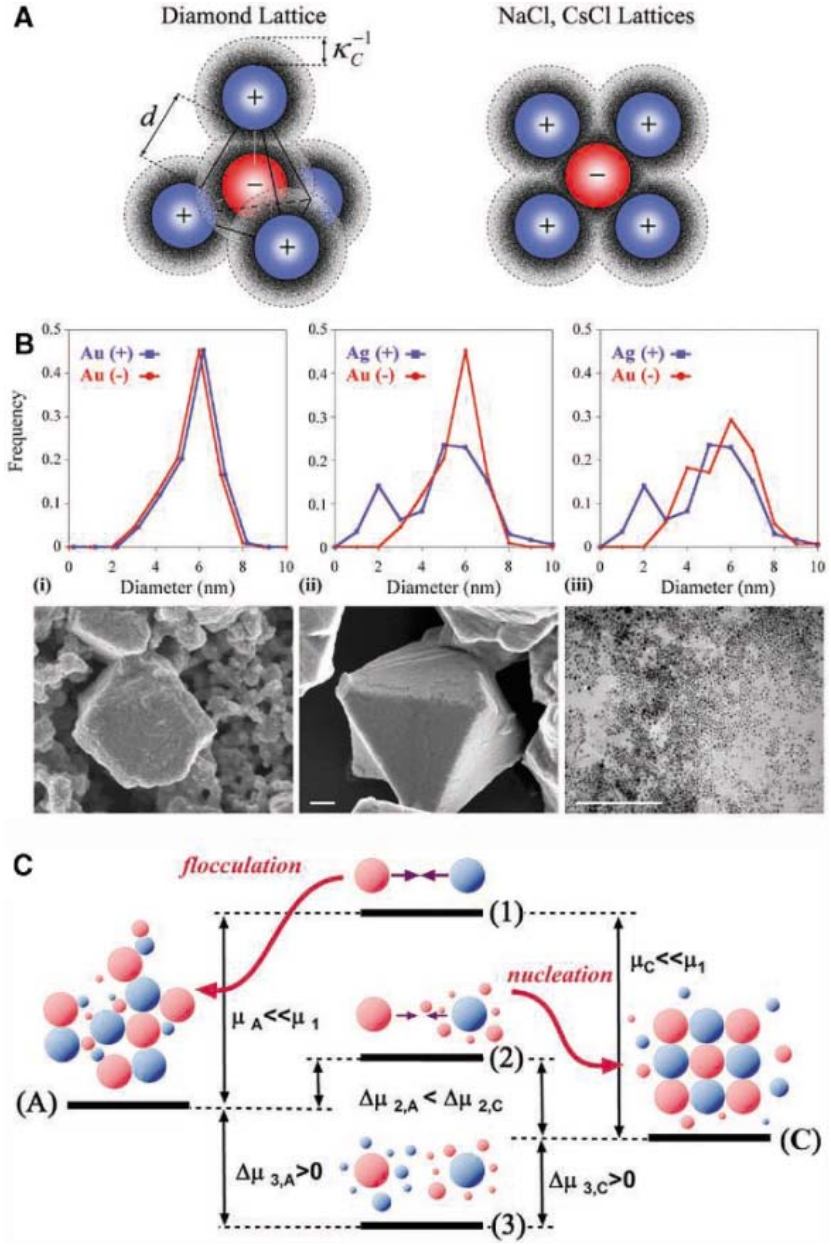

Fig. 5. (**A**) Qualitative schemes of NP arrangements and counterion "atmospheres" in lattice structures considered [more realistic drawings of the lattices and the discussion of the *m* and *n* values defined in the main text can be found in (*20*)]. For diamond, the separation between the like-charged particles, *d*, is larger than the sum of screening lengths, $2\kappa_C^{-1}$, and the energy of repulsive electrostatic interactions is negligible. For NaCl and CsCl lattices $d < 2\kappa_C^{-1}$, and the repulsions between like-charged NPs offset the energetic gain of oppositely charged interactions. (**B**) Effect of NP polydispersity on the quality of crystals. Graphs (i) to (iii) give normalized size distributions of the metallic cores of oppositely charged NPs used in crystallization experiments; typical outcomes of these experiments are illustrated by SEM or TEM images shown in the bottom row (scale bars correspond to 200 nm). In all cases, experimental conditions were the same, and crystallization was attempted at least five times. (i) Cocrystallization of similarly sized AuTMA and AuMUA gave mostly amorphous aggregates. Sparse, poor-quality crystals (100 to 800 nm) were observed in only one out of five experiments. (ii) Crystals grown from narrowly distributed AuMUA (σ = 20%) and polydisperse AgTMA (σ = 45%, bimodal distribution with a large fraction of smaller particles of sizes 1 to 3 nm) were large (up to 3 μm) and regularly shaped. (iii) Broadly distributed AuMUAs (σ = 30%) and AgTMAs (σ = 45%) did not aggregate or crystallize at all. (**C**) Effect of small particles on the stability of the dispersed, large NPs. In the absence of small particles (phase "1"), large NPs of opposite charges interact by relatively strong electrostatic forces, and the dispersed phase has a high chemical potential, μ_1. In this case, the NPs instantly flocculate to form amorphous aggregates (A). If small NPs of one type are present (phase "2"), they surround large NPs of the opposite charge and effectively screen electrostatic interactions between them. Phase "2" is characterized by a chemical potential, μ_2, much lower than that of phase "1"—as a result, large NPs nucleate and aggregate into ordered crystal structures. If small NPs of both types are present in the suspension (phase "3"), all large NPs are screened and interact very weakly. Thus, phase "3" has chemical potential lower than phases A and C, and NPs remain stable in solution.

References and Notes

1. S. A. Maier *et al.*, *Nat. Mater.* **2**, 229 (2003).
2. J. Hoinville *et al.*, *J. Appl. Phys.* **93**, 7187 (2003).
3. J. Grunes, J. Zhu, E. A. Anderson, G. A. Somorjai, *J. Phys. Chem. B* **106**, 11463 (2002).
4. M. Zayats *et al.*, *J. Am. Chem. Soc.* **125**, 16006 (2003).
5. A. E. Saunders, B. A. Korgel, *ChemPhysChem* **6**, 61 (2005).
6. F. X. Redl, K. S. Cho, C. B. Murray, S. O'Brien, *Nature* **423**, 968 (2003).
7. A. L. Rogach, *Angew. Chem. Int. Ed.* **43**, 148 (2004).
8. E. V. Shevchenko, D. V. Talapin, N. A. Kotov, S. O'Brien, C. B. Murray, *Nature* **439**, 55 (2006).
9. M. E. Leunissen *et al.*, *Nature* **437**, 235 (2005).
10. B. A. Grzybowski, A. Winkleman, J. A. Wiles, Y. Brumer, G. M. Whitesides, *Nat. Mater.* **2**, 241 (2003).
11. J. Kolny, A. Kornowski, H. Weller, *Nano Lett.* **2**, 361 (2002).
12. For crystals composed of Ag and Au nanoparticles, the lattice is isostructural with sphalerite ZnS (SG 216). For crystals made of only one type of metal cores (compare Fig. 5B), the lattice is best described as diamond (SG 227). To account for both of these possibilities we use "diamond-like" nomenclature in the text.
13. D. Witt, R. Klajn, P. Barski, B. A. Grzybowski, *Curr. Org. Chem.* **8**, 1763 (2004).
14. N. R. Jana, X. G. Peng, *J. Am. Chem. Soc.* **125**, 14280 (2003).
15. Supporting material is available on *Science* Online.
16. C. V. K. Sharma, G. A. Broker, G. J. Szulczewski, R. D. Rogers, *Chem. Commun.* **2000**, 1023 (2000).
17. After the evaporation of the "good" solvent, the NP crystals constituted only ~0.01% v/v of the remaining solution, so crystallization cannot be attributed to confinement effects that might have been operative had all liquid been evaporated.
18. S. Link, Z. L. Wang, M. A. El-Sayed, *J. Phys. Chem. B* **103**, 3529 (1999).
19. This estimate is based on the Deryagin-Landau-Verwey-Overbeek (DLVO) theory and for a 1:1 electrolyte. Specifically, $\kappa_C^{-1} = (\varepsilon\varepsilon_0 k_B T/2ce^2)^{1/2}$, where c denotes the number density of ions, e is the charge of an electron, ε is the static dielectric constant of the medium, and ε_0 is the permittivity of vacuum. Using EDS, we determined the content of Cl^- to be ~5%, which corresponds to a concentration $c \sim 10^{-2}$ M of the residual ammonium salt ($NMe_4^+Cl^-$) present in the crystal. Assuming that the effective dielectric constant of a mixture of water and DMSO filling the free space between the NPs in the crystal can be approximated as $\varepsilon_{eff} = (\varepsilon_{water} + \varepsilon_{DMSO})/2 \approx 65$, $\kappa_C^{-1} \sim 2.7$ nm. We emphasize that this number can only be treated as an estimate, because with NPs several nanometers in diameter, we are at the limit of applicability of the DLVO mean-field approach. At the same time, our approximation is qualitatively correct as verified by recent numerical Monte Carlo simulations of pairs of nanometer-sized charged particles (*20*).
20. J. Z. Wu, D. Bratko, H. W. Blanch, J. M. Prausnitz, *J. Chem. Phys.* **111**, 7084 (1999).
21. C. Kittel, *Introduction to Solid State Physics* (Wiley, Hoboken, NJ, ed. 8, 2005).
22. J. N. Israelachvili, *Intermolecular and Surface Forces* (Academic Press, San Diego, ed. 2, 1992).
23. A.-P. Hynninen, M. E. Leunissen, A. van Blaaderen, M. Dijkstra, *Phys. Rev. Lett.* **96**, 018303 (2006).
24. P. Ziherl, R. D. Kamien, *J. Phys. Chem. B* **105**, 10147 (2001).
25. Because each NP is covered with a SAM, the only dispersion (van der Waals) interaction that needs to be considered is that between alkyl chains of MUA and TMA thiols that form the SAMs. This attractive interaction is important only if the SAMs interpenetrate; it vanishes at distances larger than ~1 nm, and its characteristic energy—assuming ideal parallel alignment of two alkyl chains—is on the order of k_BT per CH_2 group (*26*, *27*). TEM images of the charged NPs that we used reveal that the SAMs are "rigid" (i.e., their thicknesses between aggregated NPs are the same as those on isolated ones) and that no interpenetration takes place. This observation is easily rationalized by noting that possible interpenetration of the alkyl chains would have to take place at the expense of favorable electrostatic interactions between oppositely charged head groups. Overall, the van der Waals forces in our system can be neglected even if two NPs touch each other. At such small separations, the interactions are dominated by attractive electrostatic forces. Finally, we note that entropic forces due to SAM squeezing (*28*) are also negligible, because the SAMs are not "compressible."
26. L. Salem, *J. Chem. Phys.* **37**, 2100 (1962).
27. C. D. Bain *et al.*, *J. Am. Chem. Soc.* **111**, 321 (1989).
28. P. Ziherl, R. D. Kamien, *Phys. Rev. Lett.* **85**, 3528 (2000).
29. Results of recent molecular dynamics simulations (*21*) indicate that mean-field screening concepts can be extended to the nanoscale and can be used to approximate electrostatic forces acting between nanoparticles screened by counterions comparable in size (within one order of magnitude) and present in small quantities (a few layers). Although quantitative analogies could thus be justified, we restrict our discussion to qualitative arguments that are sufficient to explain experimental observations.
30. V. Tohver, J. E. Smay, A. Braem, P. V. Braun, J. A. Lewis, *Proc. Natl. Acad. Sci. U.S.A.* **98**, 8950 (2001).
31. M. Rasa, A. P. Philipse, J. D. Meeldijk, *J. Colloid Interface Sci.* **278**, 115 (2004).
32. R. C. Ball, D. A. Weitz, T. A. Witten, F. Leyvraz, *Phys. Rev. Lett.* **58**, 274 (1987).
33. P. C. Ohara, D. V. Leff, J. R. Heath, W. M. Gelbart, *Phys. Rev. Lett.* **75**, 3466 (1995).
34. P. M. Chaikin, T. C. Lubensky, *Principles of Condensed Matter Physics* (Cambridge Univ. Press, Cambridge, ed. 1, 2000).
35. S. Sanyal, N. Easwar, S. Ramaswamy, A. K. Sood, *Europhys. Lett.* **18**, 107 (1992).
36. J. Lyklema, *Fundamentals of Interface and Colloid Science* (Academic Press, London, San Diego, 1995).
37. E. J. W. Verwey, J. T. G. Overbeek, *Theory of the Stability of Lyophobic Colloids* (Dover, Mineola, NY, 1999).
38. Z. Zhang, A. S. Keys, T. Chen, S. C. Glotzer, *Langmuir* **21**, 8383 (2005).
39. S. Stoeva, K. J. Klabunde, C. M. Sorensen, I. Dragieva, *J. Am. Chem. Soc.* **124**, 2305 (2002).

40. We thank J.-G. Zheng and M. Kowski for helpful discussions. B.A.G. gratefully acknowledges financial support from the Camille and Henry Dreyfus New Faculty Awards Program, NSF (grant 0503673), and the American Chemical Society Petroleum Research Fund (Award 42953-AC5). K.J.M.B. was supported by the NSF Graduate Fellowship.

Supporting Online Material

www.sciencemag.org/cgi/content/full/1125124/DC1
Materials and Methods
Figs. S1 and S2
References and Notes

18 January 2006; accepted 8 February 2006
Published online 23 February 2006;
10.1126/science.1125124
Include this information when citing this paper.

Probing Proton Dynamics in Molecules on an Attosecond Time Scale

S. Baker,[1] J. S. Robinson,[1] C. A. Haworth,[1] H. Teng,[1] R. A. Smith,[1] C. C. Chirilă,[2] M. Lein,[2] J. W. G. Tisch,[1] J. P. Marangos[1]*

We demonstrate a technique that uses high-order harmonic generation in molecules to probe nuclear dynamics and structural rearrangement on a subfemtosecond time scale. The chirped nature of the electron wavepacket produced by laser ionization in a strong field gives rise to a similar chirp in the photons emitted upon electron-ion recombination. Use of this chirp in the emitted light allows information about nuclear dynamics to be gained with 100-attosecond temporal resolution, from excitation by an 8-femtosecond pulse, in a single laser shot. Measurements on molecular hydrogen and deuterium agreed well with calculations of ultrafast nuclear dynamics in the H_2^+ molecule, confirming the validity of the method. We then measured harmonic spectra from CH_4 and CD_4 to demonstrate a few-femtosecond time scale for the onset of proton rearrangement in methane upon ionization.

There is currently great interest in the development of methods to probe the dynamical behavior of matter on the attosecond (1 as = 10^{-18} s) time scale (*1*–*3*). It is known that the ionization of an atom or molecule by an intense laser field and subsequent electron acceleration in the field results in the formation of a chirped electron wavepacket—a "burst" of electrons with a broad range of kinetic energies that recollide with the parent ion over a range of time delays (*4*). However, the chirp of the electron wavepacket is a hitherto unexploited property in the measurement of ultrafast dynamical behavior.

The technique demonstrated here is based on high-harmonic generation (HHG) from molecules. HHG is well understood within the framework of a semiclassical model (*5*), which separates the process into three distinct steps. In the first step, an intense laser pulse ionizes an atom or molecule, launching an electron wavepacket into the continuum. In the next step, the electron wavepacket moves in response to the laser electric field; it is first accelerated away from the parent ion and then returns at some later time (typically 0.5 to 1.6 fs for a laser field at a wavelength of ~800 nm) as the laser field reverses direction. The third step is the recombination of the electron with the parent ion and the emission of a high-energy photon (~10 to 500 eV) that carries away, at discrete multiples of the laser frequency (*6*), the kinetic energy gained by the electron in the process.

The intensity of the radiation emitted at the moment of recombination depends upon the transition amplitude between the wave function de-

[1]Blackett Laboratory, Imperial College London, Prince Consort Road, South Kensington, London SW7 2BZ, UK. [2]Max Planck Institute for Nuclear Physics, Saupfercheckweg 1, 69117 Heidelberg, Germany.

*To whom correspondence should be addressed. E-mail: j.marangos@imperial.ac.uk

scribing the electron and ion at this instant and the initial molecular ground state. Lein (*7*) showed theoretically that the harmonic signal in a molecule will be approximately proportional to the squared modulus of the nuclear autocorrelation function, which is the overlap between the initial and final nuclear parts of the molecular wave function that evolves from the moment of ionization until the point of recollision. Details of the nuclear dynamics are therefore encoded in the HHG signal, which is blind to all other competing channels because the quantum mechanical path for the molecule starts and ends in the same state.

Our method (Fig. 1) can be viewed as a pump-probe technique. The ionization step of harmonic emission is the pump, because in the case of a molecule, a nuclear wavepacket is simultaneously launched at the moment of ionization. The probe is the recollision of the electron wavepacket with the parent ion, with the nuclear wavepacket information encoded in the emitted harmonics.

The use of the recollision as a probe is broadly related to earlier experiments by Niikura *et al*., who used the correlation of electron and nuclear wavepackets (*1*, *2*) to provide information about the instantaneous average internuclear separation with subfemtosecond temporal resolution. In that work, the kinetic energy released in recollision-induced fragmentation was used for the probe signal, and thus the temporal resolution was limited to >0.5 fs by the inherent temporal spread of the recolliding electron bunch. A further limitation was the requirement to tune the laser wavelength over a wide range to vary the pump-probe delays. The kinetic energy release technique has so far been restricted to observing motion along the internuclear axis of diatomic molecules; it is also affected by competing excitation channels. In contrast, our method measures the quantum mechanical nuclear dynamics by determining the overlap integral between the wave function at two times, so it is sensitive to motion in any direction. Further, by using the chirp associated with harmonic emission (*4*) to probe the nuclear motion, we attain ~100-as time resolution as well as access to a range of pump-probe time delays for a single laser pulse at fixed wavelength.

The high temporal resolution available in our technique arises from the chirped nature of the recolliding electron wavepacket (Fig. 2). Electrons born into the continuum between ~1/20th of an optical cycle after the laser field maximum and the next zero of the field follow so-called "short trajectories" (*8*) that return quickly to the core. Each of these short trajectories returns to the parent ion at a different delay time Δt, and each is associated with a different electron kinetic energy at the point of recollision. This temporal spread leads to a frequency-chirped harmonic emission, with successively higher harmonics being generated at longer time delays, as has been directly measured by Mairesse *et al*. (*4*). This property of HHG is fundamental to the technique demonstrated here, because it allows a range of pump-probe delays to be accessed by analysis of a single harmonic spectrum. In principle, a second set of longer trajectories can contribute to the HHG spectrum, with the electron born earlier and returning later to the core, but in this experiment these long trajectories are filtered out from the spectrum, yielding a one-to-one mapping between delay and photon frequency (Fig. 2). Simply recording the harmonic spectrum therefore allows us to probe the nuclear motion over a range of pump-probe time delays set by the temporal spread of the recolliding electron wavepacket.

We implement this method by observing the ratio of the harmonic spectra generated in gaseous H_2 and D_2, or CH_4 and CD_4. The use of isotopes ensures that the variation in HHG spectra is due primarily to differing nuclear dynamics, because the electronic states are very similar. The variation of this ratio with harmonic order then yields information concerning the differing nuclear (proton or deuteron) dynamics in the ions of the two species, with the 100-as time resolution encoded in the frequency of the emitted radiation over a range of ~1 fs for laser light of ~800 nm wavelength. The HHG efficiency decreases more over a given range of harmonic orders for H_2 than for D_2 because of faster nuclear motion in the lighter molecule.

We used very short laser pulses in this experiment to freeze rotational motion. We generated 8-fs pulses centered at a wavelength of ~775 nm with the use of a gas-filled hollow fiber and chirped mirrors to compress ~0.75-mJ, 30-fs pulses. The laser beam was focused by an off-axis paraboloid mirror (focal length 400 mm) into a pulsed gas jet (Fig. 1A). The focus was located 9 mm before the gas jet to ensure that short electron trajectories dominated the harmonic signal. The intensity at the interaction region was estimated to be 2×10^{14} W cm^{-2}. The harmonic signal was spectrally dispersed in a grazing-incidence, angularly resolving, flat-field spectrometer and was detected by an extreme ultraviolet–sensitive imaging microchannel plate detector, with a charge-coupled device (CCD) camera used for readout. The harmonic spectrum was extracted by angular integration of the CCD images. Because the first ionization potential in the two species is very similar [15.43 eV for H_2, 15.46 eV for D_2 (*9*)], differences in phase-matching conditions for harmonic generation in the two cases were negligible: The harmonics generated in H_2 and D_2 had identical far-field angular distributions.

It was essential that each gas (e.g., H_2 or D_2) was delivered to the interaction region at an equal

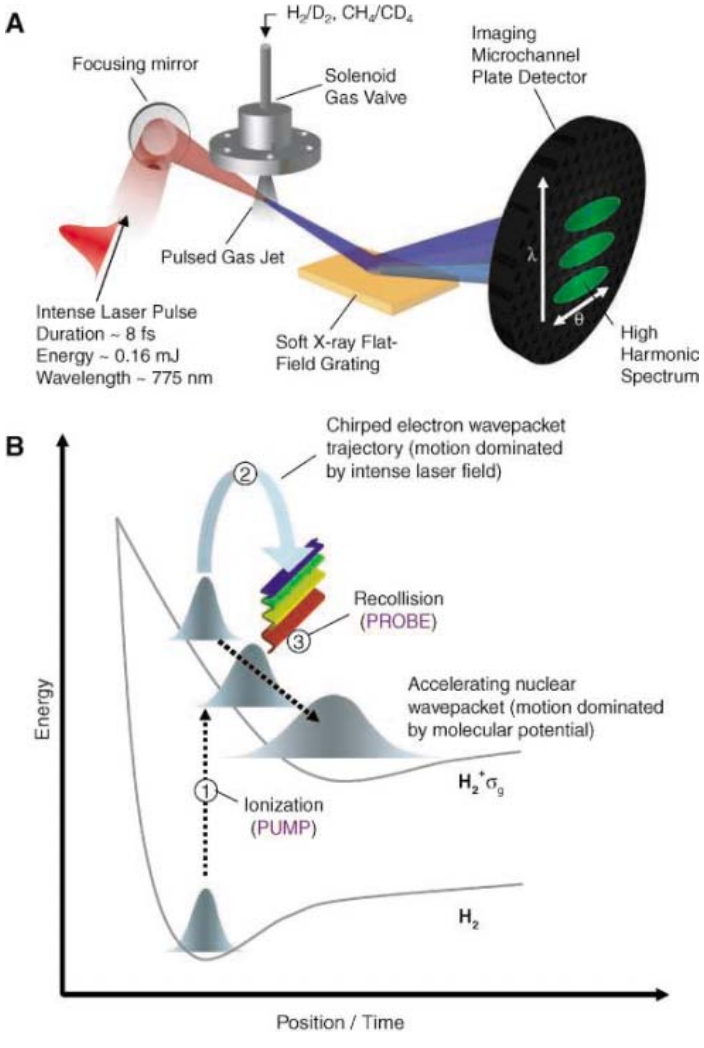

Fig. 1. Pump-probe method for measuring proton dynamics in molecules. **(A)** The experimental setup required to observe high-harmonic emission. **(B)** Ionization serves as the pump process because it launches an electron wavepacket into the continuum simultaneously with a nuclear wavepacket on the H_2^+ ground state potential surface (σ_g). The electron wavepacket then moves in response to the laser field, returning to the parent ion with an increased kinetic energy at some later time. The recollision acts as the probe of the nuclear motion that has occurred in the time delay since ionization occurred.

density. We ensured this condition by using a high-intensity, 800-fs laser field at 1053 nm to fully ionize the gas, and performing interferometric measurements and Abel inversion to characterize the electron density. The experimentally determined backing pressure ratio, $P(D_2)/P(H_2)$, that was found to equalize the electron (and therefore molecular) density was 1.3 ± 0.1. This ratio was measured with a species-independent piezoelectric gauge in the gas jet backing line and agrees, within experimental error, with gas flow calculations and other tests based on the pressure jump in the interaction chamber after pulsing the valve a fixed number of times with the vacuum pumps off.

Typical high-harmonic spectra from H_2 and D_2 at equal density are shown in Fig. 3A. Spectra were averaged over 400 laser shots, although it should be noted that the full dynamical information is encoded in each spectrum recorded. In agreement with Lein's predictions, Fig. 3A shows that the harmonic signal at all orders detected is higher in D_2 than in H_2—a clear signature of the slower nuclear motion occurring in D_2. As expected from the different speeds of nuclear motion, we see a significant increase in the D_2/H_2 HHG intensity ratio as the frequency of the harmonic, and therefore the time delay, increases (Fig. 3B).

We compared our experimental results with a calculation based on the strong-field approximation, which collects the effect of the nuclear motion in the compact nuclear correlation function (*10*). The harmonics are approximately proportional to the squared modulus of the nuclear autocorrelation function, $c(\tau) = \int \chi(R,0)\chi(R,\tau)dR$, where $\chi(R,0)$ and $\chi(R,\tau)$ are the initial and propagated vibrational wavepackets in the molecular ion, R is the internuclear distance, and τ is the electron travel time (equivalent to our delay time, Δt). For geometrical reasons, most of the molecules in the randomly aligned sample in our experiment have their molecular axes nearly perpendicular to the laser electric field direction, which reduces the effect of two-center interference (*11*) and minimizes Stark shifts (*12*). We have confirmed in test calculations that the influence of the Stark shifts in the Born-Oppenheimer potential is negligible for the present set of parameters. Two-center interference gives rise to a small but clearly discernable shift and has been included in our analysis. For random orientation, this effect can be taken into account by using the nuclear correlation function $c(\tau,k) = \int \chi(R,0)\chi(R,\tau)f(k,R)dR$ including the interference kernel $f(k,R) = \sin(kR/2)/(kR/2)$. Here, k is the wave vector of the recolliding electron, evaluated using the relation $\hbar^2k^2/(2m) = \hbar\omega$ (*13*), where $\hbar$ is Planck's constant divided by 2π, and $\hbar\omega$ is the energy of the harmonic being emitted upon recombination. The ratio of harmonic intensities D_2/H_2 is calculated by taking the ratio of the squared modulus of the two correlation functions for D_2 and H_2. The calculated curve is scaled to account for the slight difference in photoionization cross sections for H_2 and D_2 (*14*). We found good quantitative agreement between our measurements and the calculation (Fig. 3B).

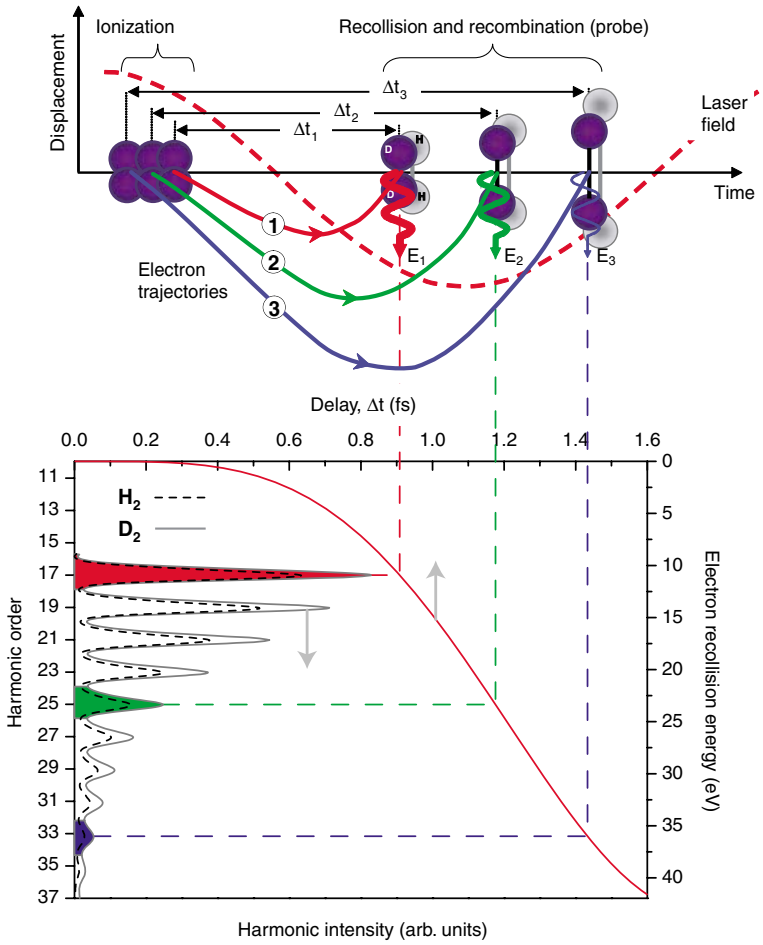

Fig. 2. Encoding of nuclear dynamics within harmonic spectra. Upper panel: The trajectory of the ionized electron differs depending on the exact time of ionization. Three possible electron trajectories labeled 1, 2, and 3 are shown, which recollide with the molecular ion after delays Δt_1, Δt_2, and Δt_3, with increasing kinetic energy E_1, E_2, and E_3, resulting in the emission of increasingly higher frequency photons after recombination (shown as the 17th, 25th, and 33rd harmonics for the purpose of this illustration). Note: Although the curves in the lower panel are physically accurate, the electron trajectories shown in the upper panel have been slightly altered to improve clarity.

The nuclear wave function $\chi(R,t)$ and, from this, the time evolution of the expectation value of R [$\langle R(t)\rangle$] in each molecule was reconstructed from the recorded intensity spectra and their ratio by use of a genetic algorithm (*7*, *10*). Agreement with the exact calculation is good (Fig. 3C). Therefore, the measurement of the harmonic spectrum ratio can be used to determine proton (deuteron) motion in H_2 and D_2 molecules ~1 fs after ionization, with a temporal resolution of ~100 as (the difference in recollision times between successive harmonic orders). Here we use the data from H_2/D_2 primarily to test and confirm the method, as the potential surface and thus the calculated dynamics of the proton are known in the case of H_2. Therefore, the agreement between the measurement and the calculated ratio of the nuclear correlation function (Fig. 3B) is confirmation that the chirp of the electron is satisfactorily given by the semiclassical treatment, validating the frequency-to-time mapping. With this confirmation, we can apply the technique to other molecules for which the potentials are not fully known.

The HHG spectrum is determined by the squared moduli of $c(\tau)$ and of the remaining parts $\bar{d}(\omega)$ of the transition dipole moment that do not depend on the nuclear motion. Similar to Itatani *et al.* (*15*), we write $\bar{d}(\omega) = a[k(\omega)]r[k(\omega)]$, where $a[k(\omega)]$ is the amplitude for an electron of wave vector k, and $r[k(\omega)]$ is the recombination part of $\bar{d}(\omega)$. It is feasible to directly calibrate the factor $\bar{d}(\omega)$ by measuring a given harmonic over a range of laser intensities (so that $r[k(\omega)]$ would be fixed but the recollision time would be changing with laser intensity). An auxiliary measurement on an atom of similar ionization potential would be used to establish the variation of $a[k(\omega)]$ with recollision time. In our implementation of the method, the equivalence of $\bar{d}(\omega)$ for the protonated and deuterated species has been used to remove the spectral variation of this factor. This simplification is experimentally convenient, as then the main technical difficulty is simply to ensure equal particle densities in the comparison, with only a single set of measurements being required at a fixed and known laser intensity.

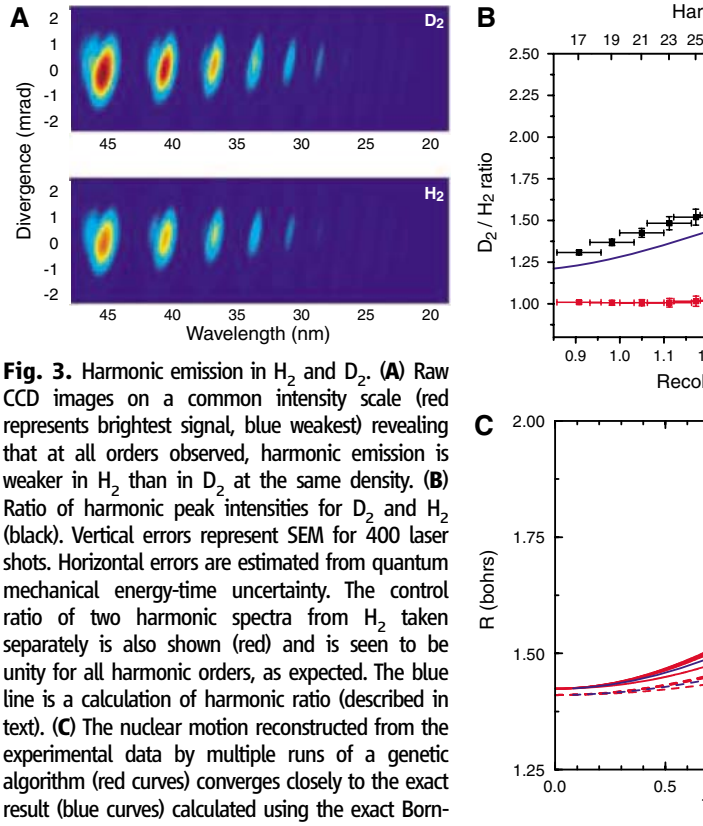

Fig. 3. Harmonic emission in H_2 and D_2. (**A**) Raw CCD images on a common intensity scale (red represents brightest signal, blue weakest) revealing that at all orders observed, harmonic emission is weaker in H_2 than in D_2 at the same density. (**B**) Ratio of harmonic peak intensities for D_2 and H_2 (black). Vertical errors represent SEM for 400 laser shots. Horizontal errors are estimated from quantum mechanical energy-time uncertainty. The control ratio of two harmonic spectra from H_2 taken separately is also shown (red) and is seen to be unity for all harmonic orders, as expected. The blue line is a calculation of harmonic ratio (described in text). (**C**) The nuclear motion reconstructed from the experimental data by multiple runs of a genetic algorithm (red curves) converges closely to the exact result (blue curves) calculated using the exact Born-Oppenheimer potentials for H_2^+ and D_2^+.

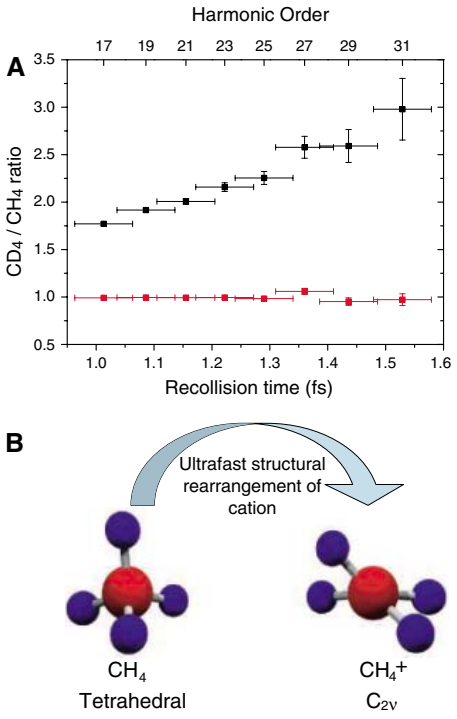

Fig. 4. Probing structural rearrangement in CH_4 and CD_4. (**A**) Ratio of harmonic signals in CD_4 and CH_4 (black). The error represents SE over 200 laser shots. Also shown is the control ratio of two harmonic spectra from CD_4 taken separately (red). (**B**) Known structures of CH_4 and CH_4^+ at equilibrium. Upon removal of an electron, it is anticipated that CH_4 will rapidly evolve toward the CH_4^+ structure shown.

To further explore the application of this technique, we compared harmonic spectra obtained in CH_4 and CD_4 (Fig. 4A). We observed behavior consistent with our studies of D_2 and H_2: The harmonic yield is found to be greater in the heavier isotope whose nuclei are expected to move more slowly, and this effect is found to be enhanced for the higher order harmonics, which probe the parent molecule at a longer time delay. The differing photoabsorption cross sections in CH_4 and CD_4 (*16*), although making a small contribution to the measured ratio, cannot account for the increase in the ratio that we observe. These results therefore confirm that this technique is not limited to probing nuclear wavepackets in diatomic molecules.

It is known from theory (*17*) and experiment (*18*, *19*) that although the CH_4 molecule has the well-known tetrahedral structure (with 109.50° bond angles), CH_4^+ adopts a C_{2v} geometry, with some bond angles diminishing to <60° (Fig. 4B). It is anticipated that these structural rearrangements at the moment of ionization must be fast, as the tetrahedral structure of methane is far from the equilibrium bond angles of the ion. Our measurements provide direct evidence that the time scale for the onset of this structural rearrangement is on the order of a few femtoseconds. The measured ratio (Fig. 4A) is the square of the ratio of the nuclear autocorrelation functions for the two species, a quantity that can be calculated directly from the molecular potentials. Therefore, the measurement can be used to test the correctness of computed potentials.

Several extensions of the technique are possible. Use of a driving laser field of a longer wavelength would extend the time window over which information on the nuclear dynamics can be gained; for instance, a field at a wavelength of 2 μm would allow motion to be followed for up to 4 fs after ionization. This could also be achieved by selection of the long-trajectory component of the chirped electron wavepacket for harmonic emission without affecting the temporal resolution of the measurement. A further extension of the technique may be to study neutral molecular dynamics by starting from negative molecular ions formed through electron attachment.

Our technique is sensitive to the initial few femtoseconds after the electronic change (e.g., photoionization) that drives the motion of the protons toward a new equilibrium position. In contrast, conventional methods only provide data for the potential energy surface around the equilibrium position and do not access the extremely fast proton rearrangement that follows directly from electronic changes. Our technique may therefore provide new insights into some of the most fundamental events in chemistry.

References and Notes

1. H. Niikura *et al.*, *Nature* **417**, 917 (2002).
2. H. Niikura *et al.*, *Nature* **421**, 826 (2003).
3. R. Kienberger *et al.*, *Nature* **427**, 817 (2004).
4. Y. Mairesse *et al.*, *Science* **302**, 1540 (2003).
5. P. B. Corkum, *Phys. Rev. Lett.* **71**, 1994 (1993).
6. A. L'Huillier, L.-A. Lompré, G. Mainfray, C. Manus, in *Atoms in Intense Laser Fields*, M. Gavrila, Ed. (Academic Press, New York, 1992), pp. 139–201.
7. M. Lein, *Phys. Rev. Lett.* **94**, 053004 (2005).
8. P. Antoine, A. L'Huillier, M. Lewenstein, *Phys. Rev. Lett.* **77**, 1234 (1996).
9. Y. Liang, S. Augst, S. L. Chin, Y. Beaudoin, M. Chaker, *J. Phys. B* **27**, 5119 (1994).
10. See supporting material on *Science* Online.
11. M. Lein, N. Hay, R. Velotta, J. P. Marangos, P. L. Knight, *Phys. Rev. Lett.* **88**, 183903 (2002).
12. H. Stapelfeldt, H. Sakai, E. Constant, P. B. Corkum, *Phys. Rev. Lett.* **79**, 2787 (1997).
13. M. Lein, N. Hay, R. Velotta, J. P. Marangos, P. L. Knight, *Phys. Rev. A* **66**, 023805 (2002).
14. C. J. Latimer, K. F. Dunn, F. P. O'Neill, M. A. Macdonald, N. Kouchi, *J. Chem. Phys.* **102**, 722 (1995).
15. J. Itatani *et al.*, *Nature* **432**, 867 (2004).
16. C. J. Latimer, R. A. Mackie, A. M. Sands, N. Kouchi, K. F. Dunn, *J. Phys. B* **32**, 2667 (1999).
17. R. F. Frey, E. R. Davidson, *J. Chem. Phys.* **88**, 1775 (1988).
18. Z. Vager *et al.*, *Phys. Rev. Lett.* **57**, 2793 (1986).
19. L. B. Knight, J. Steadman, D. Feller, E. R. Davidson, *J. Am. Chem. Soc.* **106**, 3700 (1984).

20. We thank J. Lazarus and M. Hohenberger for assistance with the interferometric measurements of the gas densities; L. Chipperfield, P. L. Knight, R. Torres, and C. Latimer for valuable scientific discussions; and P. Ruthven, A. Gregory, and B. Ratnasekara for technical assistance. Supported by the Research Councils UK through the Basic Technology Programme and the Engineering and Physical Sciences Research Council.

Supporting Online Material

www.sciencemag.org/cgi/content/full/1123904/DC1
Materials and Methods
Fig. S1
References

15 December 2005; accepted 13 February 2006
Published online 2 March 2006;
10.1126/science.1123904
Include this information when citing this paper.

Timing and Climatic Consequences of the Opening of Drake Passage

Howie D. Scher* and Ellen E. Martin

Age estimates for the opening of Drake Passage range from 49 to 17 million years ago (Ma), complicating interpretations of the relationship between ocean circulation and global cooling. Secular variations of neodymium isotope ratios at Agulhas Ridge (Southern Ocean, Atlantic sector) suggest an influx of shallow Pacific seawater approximately 41 Ma. The timing of this connection and the subsequent deepening of the passage coincide with increased biological productivity and abrupt climate reversals. Circulation/productivity linkages are proposed as a mechanism for declining atmospheric carbon dioxide. These results also indicate that Drake Passage opened before the Tasmanian Gateway, implying the late Eocene establishment of a complete circum-Antarctic pathway.

Over the past 50 million years (My), deterioration of the early Cenozoic greenhouse climate occurred in a series of steps, the largest being widespread and permanent glaciation of Antarctica ~34 Ma (*1*). Changes in ocean circulation and decreasing carbon dioxide (CO_2) levels may have both contributed to the "greenhouse-icehouse" climate transition; however, their relative roles in planetary cooling are currently a matter of debate (*2*). The separation of South America from Antarctica and subsequent formation of Drake Passage are widely believed to have influenced Cenozoic cooling because these events enabled the development of the Antarctic Circumpolar Current (ACC) (*3*). This wind-driven current facilitates interocean exchange of seawater, contributes to upwelling-induced productivity in the Southern Ocean, and is speculated to have reduced poleward heat transport to Antarctica (*4*). However, age estimates for the development of this Pacific-Atlantic connection range from the middle Eocene (*5*) to early Miocene (*3*), obscuring the ACC's role in Antarctic glaciation. Uncertainty over the history of Drake Passage's origin represents a major gap in our knowledge of the primary mechanisms leading to Cenozoic global cooling.

Previous studies have interpreted widespread increases in the biological productivity of the Southern Ocean in terms of the efficiency of circulation-driven nutrient upwelling during the Eocene (*6*, *7*). However, attempts to infer the onset of the ACC from proxies for productivity in the Atlantic sector's sedimentary record are criticized for being equivocal with respect to the opening of Drake Passage (*8*). Ideally, characteristic signatures of Pacific seawater entering the Atlantic sector of the Southern Ocean would provide a sound basis for establishing an age for the Pacific-Atlantic connection.

Neodymium (Nd) isotopes can be used to track changes in ocean circulation because seawater Nd has a short residence time [500 to 1000 years (*9*)] relative to ocean mixing time scales (~1500 years). Water masses are imprinted with the signature of Nd isotope ratios ($^{143}Nd/^{144}Nd$, expressed as ε_{Nd} values) from their source regions, and seawater ε_{Nd} values (*10*) can be used to detect Pacific seawater in the Atlantic sector. Seawater ε_{Nd} values reflect the age of continental Nd inputs to the ocean. The geologic distribution of young volcanic rocks in the circum-Pacific and much older terrains around the Atlantic results in distinct ε_{Nd} values for each basin. Specifically, Pacific ε_{Nd} values are more radiogenic (i.e., positive) than Atlantic values, creating a steep Pacific-Atlantic gradient (*11*).

Ferromanganese (Fe-Mn) crusts and fossil fish teeth preserve ε_{Nd} values of bottom water on tectonic time scales. Early Cenozoic ε_{Nd} values reported for the Pacific Ocean range from –3 to –5 (*12*), whereas values for deep water in the Atlantic sector were less radiogenic [$\varepsilon_{Nd} = -9$ (*13*)]. These records indicate that a steep Pacific-Atlantic ε_{Nd} gradient also existed during the Eocene; thus, an influx of Pacific seawater after the opening of Drake Passage should be clearly resolvable in Atlantic sector ε_{Nd} records. In this study, Nd isotopes in fossil fish teeth from a sediment core on Agulhas Ridge [Ocean Drilling Program (ODP) Site 1090; 3700 m Eocene paleodepth (Fig. 1)] (*14*) are used to evaluate middle Eocene to early Oligocene Atlantic sector ε_{Nd} values (*10*). Fossil fish teeth preserve the same benthic Nd signal as Fe-Mn crusts, but at higher resolution and with better chronologic control (*15*) (table S1).

Nd isotope data from middle to late Eocene fossil fish teeth from Site 1090 (table S2) reveal a transition from nonradiogenic to radiogenic ε_{Nd} values (Fig. 2). From 43 to 41.3 Ma, ε_{Nd} values average –8.2. Between 41.3 and 39.6 Ma, values increase by 2.2 ε_{Nd} units. Late middle Eocene ε_{Nd} values average –6.4. After the transition to more Pacific-like compositions, ε_{Nd} values do not decrease below –6.7 for the remainder of the Eocene, with the most radiogenic ε_{Nd} values occurring during the late Eocene (averaging –6.0).

This paper focuses on the prominent middle Eocene transition to radiogenic ε_{Nd} values. It is the largest ε_{Nd} shift documented in an early Cenozoic Nd isotope record. Low yields of fossil fish teeth during the late middle Eocene limit dating of the onset of the shift to 41.3 to 39.6 Ma. A smaller increase in ε_{Nd} values has also been documented on Maud Rise (ODP Site 689; 1600 m Eocene paleodepth) over this same time interval (*16*) (Fig. 2). Radiogenic ε_{Nd} values do not evolve identically at these locations because of vertical and horizontal offsets; within the limitation of age constraints (*10*), the onset of radiogenic values occurred up to 1.7 My earlier at the shallower site. Regardless, the nearly coeval onset of radiogenic ε_{Nd} values suggests that the shift reflects a regional event.

To place Atlantic sector ε_{Nd} variability in a global paleoceanographic framework, average ε_{Nd} values were calculated from published Nd isotope records for all major ocean basins during three time slices corresponding to the early middle, late middle, and late Eocene (table S3). Resulting values were mapped onto tectonic reconstructions (Fig. 1). Although average ε_{Nd} values at ODP Site 1090 increase from –8.2 to –6, ε_{Nd} values in other ocean basins fluctuate by less than 1 ε_{Nd} unit, and average values in the Pacific and Atlantic Oceans decrease slightly. Thus, the onset of radiogenic ε_{Nd} values in the Atlantic sector of the Southern Ocean was clearly not driven by changes originating in other ocean basins. Rather, the Nd isotopic results provide evidence for the direct introduction of radiogenic Nd into the Atlantic sector during the late middle Eocene.

Seawater ε_{Nd} values can be altered by a change in weathering inputs to the ocean or by water mass mixing. A change in weathering inputs is not likely to account for the required addition of radiogenic material, because major sources of riverine and eolian material to the Atlantic sector are predominantly nonradiogenic (*17*). The only exception is volcanogenic ash derived from sources in the Scotia Sea; such ash is highly reactive and has extremely radiogenic ε_{Nd} values. Ash dispersal into Southern Ocean deep water formation areas (such as the Atlantic sector) may have raised the ε_{Nd} value of deep waters, ultimately carrying the radiogenic signal to Agulhas Ridge. Two observations argue against this mechanism as an explanation for our results. First, there is no evidence of ash deposition in middle Eocene sections of Atlantic sector sediment cores. Second, the ε_{Nd} value of Antarctic Bottom Water (AABW), as recorded by a Fe-Mn crust in Cape Basin (6854-6; Fig. 1) (*18*), changed very little during the late Neogene, despite extensive ash deposition in the Weddell Sea from Scotia Sea volcanism (*19*).

The preferred explanation for the middle Eocene onset of Atlantic sector radiogenic ε_{Nd} values is a change in ocean circulation that brought radiogenic Pacific seawater into the Atlantic sector. Nonradiogenic ε_{Nd} values in the Atlantic sector during the early middle Eocene ($\varepsilon_{Nd} = -8.2$) are consistent with $\delta^{13}C$ and ε_{Nd} reconstructions of deep water circulation that indicate a predominant, Southern Ocean–sourced, deep water mass in the Atlantic (*13*, *20*). Pacific seawater is the only water mass that could have mixed with deep water

Department of Geological Sciences, University of Florida, Gainesville, FL 32611, USA.

*To whom correspondence should be addressed at the Department of Earth and Environmental Sciences, University of Rochester, Rochester, NY 14627, USA. E-mail: howie@earth.rochester.edu

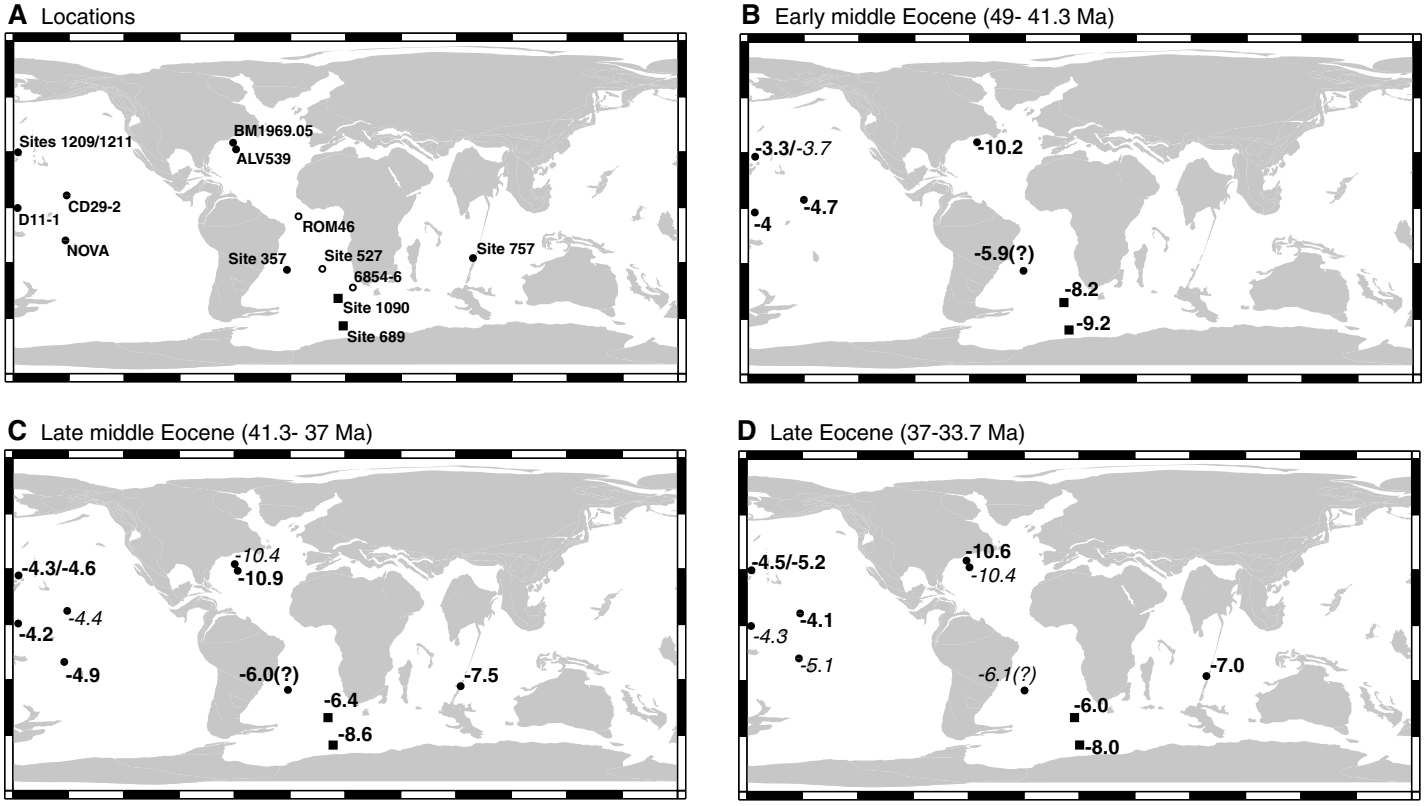

Fig. 1. Plate tectonic reconstructions illustrating locations of ε_{Nd} records and the time-progressive evolution of worldwide seawater ε_{Nd} values from the early middle Eocene, late middle Eocene, and late Eocene. Atlantic sector ODP Sites 1090 and 689 are designated by solid squares. (**A**) Locations of ODP Site 1090 and other relevant sediment cores and Fe-Mn crusts on a late Eocene plate tectonic reconstruction. Solid circles distinguish locations with middle to late Eocene Nd isotope records. Open circles correspond to locations of older and younger Nd isotope records that are discussed in the text. (**B** to **D**) Numbers represent the arithmetic mean of Nd isotope data from samples falling within the corresponding time interval. Numbers in italics represent a linear interpolation through the midpoint of the time interval using adjacent data points (table S3). Sources of the Nd isotope data used in this figure are contained in table S3.

sourced in the Southern Ocean to generate ε_{Nd} values as high as –6.0 on Agulhas Ridge.

Based on Eocene paleogeography, Pacific seawater could have entered the Atlantic sector through the Indian Ocean or via the Central American Seaway (CAS); however, there are arguments against these pathways. Benthic foraminiferal $\delta^{13}C$ records from the Indian Ocean indicate that the Ninetyeast Ridge was an effective barrier to deep water communication between the western and eastern Indian Ocean for depths below 2000 m (*21*). Furthermore, ε_{Nd} values from a shallow location on Ninetyeast Ridge (ODP Site 757; Fig. 1) do not suggest the influence of Pacific water (*22*). Similarly, South Atlantic ε_{Nd} records from the Romanche Fracture Zone (ROM46; Fig. 1) (*23*) and Walvis Ridge [Deep Sea Drilling Program (DSDP) Site 527; Fig. 1] (*13*) do not suggest a Pacific influence during the early Cenozoic. The Rio Grande Rise (DSDP Site 357; Fig. 1) exhibits radiogenic ε_{Nd} values during the Eocene (Fig. 1) (*24*); however, these values are called into question because there is a volcanic breccia layer in middle Eocene sediments that may have contributed radiogenic Nd to Fe-Mn coatings on uncleaned foraminifera.

It is likely that the abrupt appearance of Pacific-like ε_{Nd} values in Atlantic sector records reflects the early opening of Drake Passage ~41 Ma. This conclusion corroborates recent findings of an eightfold increase in spreading rate that accompanied a change in spreading direction between South America and Antarctica ~50 Ma (*5*). Positive shifts in ε_{Nd} records from the Atlantic sector, ~9 My after the new phase of spreading, indicate that crustal extension and thinning led to the development of a Pacific-Atlantic connection that could be exploited by wind-driven Pacific seawater throughflow. We believe that the strong radiogenic signal observed at Agulhas Ridge reflects the influx of radiogenic Nd through Drake Passage into deep water production areas of the Southern Ocean. The observation that ODP Site 689 shows a weaker response to the early opening of Drake Passage, despite being located closer to Pacific throughflow and having a shallower Eocene paleodepth, implies that water masses were vertically stratified in the Atlantic sector, with Southern Ocean deep water lying below intermediate depths on Maud Rise. Pronounced vertical gradients in water mass properties have been previously documented between intermediate and deep locations in the Atlantic sector during the middle to late Eocene (*25*).

Today 60% of AABW forms in the Atlantic sector, mostly in the Weddell Sea. From there, the bottom water is exported to the north via the Scotia Sea, though some is recirculated within the Weddell gyre and carried toward Maud Rise (*26*). It is possible that Pacific seawater entered the Atlantic sector, sank during deep water production in the Weddell Sea, and was transported to Agulhas Ridge. However, this seawater may have had less of an effect at Maud Rise because (i) the Weddell gyre was absent or not well organized in the Eocene, or (ii) the relatively shallow paleodepth of ODP Site 689 meant that it was influenced by water masses forming elsewhere; i.e., in areas less affected by Pacific seawater. It is also possible that the development of fronts, which are water mass boundaries for surface water, influenced the distribution of ε_{Nd} values in Atlantic sector surface waters. Reconstructions of Eocene paleofront positions based on microfossil distributions indicate a proto-Polar Front very close to Maud Rise (*27*), a front whose existence is supported by large variations in paleoproductivity during the middle Eocene (*6*).

Changes in Atlantic sector ε_{Nd} values outline the history of the opening of Drake Passage more directly than previous studies that relied on other paleoceanographic proxies to infer a Pacific-Atlantic connection. The early opening ~41 Ma is documented by the onset of radiogenic values in the Atlantic sector. Under the assumption that a greater volume of Pacific throughflow resulted in more radiogenic Atlantic sector ε_{Nd} values, subsequent ε_{Nd} increases during the late Eocene most

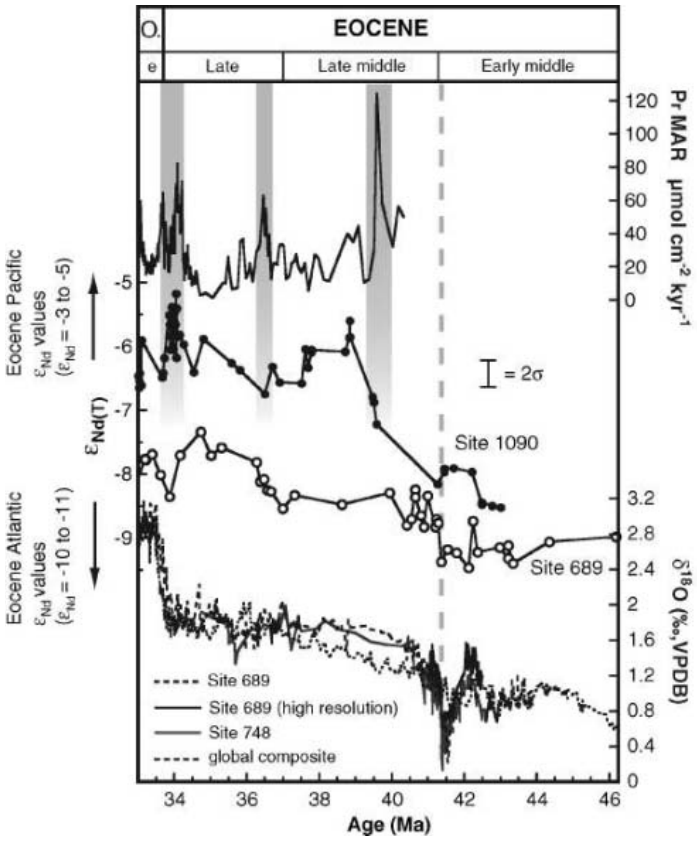

Fig. 2. Nd isotope records, temperature and ice volume, and productivity proxy records from Atlantic and Indian sector sediment cores, and the global composite $\delta^{18}O$ record for the middle Eocene to early Oligocene. (**Top**) Reactive phosphorus mass accumulation rate (P_r MAR) data for ODP Site 1090 from Anderson and Delaney (*14*), including early middle Eocene data from their auxiliary material that has been plotted according to the extended chronology for ODP Site 1090 described in table S1. (**Middle**) ε_{Nd} records for Sites 1090 (solid circles) and 689 (open circles). The error bar represents 2σ external reproducibility (*10*). The Eocene range of Pacific and Atlantic ε_{Nd} values are noted on the left *y* axis. (**Bottom**) $\delta^{18}O$ values for the global composite and ODP Sites 689 (Maud Rise) and 748 (Kerguelen Plateau). All Southern Ocean $\delta^{18}O$ data are from *Cibicidoides* spp. reported relative to the Vienna Pee Dee belemnite standard (‰ VPDB) and have been adjusted by + 0.64 ‰ to account for vital effects. Sources of $\delta^{18}O$ data are as follows: ODP Site 689 (*6*); ODP Site 689, high resolution; and ODP Site 748 (*31*), global composite (*1*). Gray bars highlight inferred associations between changes in ocean circulation and sea surface productivity in the Atlantic sector. The vertical dashed gray line highlights the onset of radiogenic ε_{Nd} values and the termination of the MECO (*31*).

likely represent progressive widening and deepening of the gateway. A pronounced ε_{Nd} increase at Maud Rise ~37 Ma has been previously interpreted as an opening of Drake Passage to intermediate depths (*16*). An increase in Pacific throughflow ~34 Ma is indicated by a shift to the most radiogenic values observed at Agulhas Ridge and is interpreted as the establishment of a deeper Pacific-Atlantic connection in the late Eocene. This conclusion is supported by tectonic reconstructions (*28*). Alternatively, increased deepening of the Tasmanian Gateway from 35.5 to 33.5 Ma (*29*) may have initiated greater throughflow via Drake Passage without a substantial change in its dimensions. Lower ε_{Nd} values during the earliest Oligocene are part of a long-term decrease in ε_{Nd} in response to global circulation changes. This trend was also observed at ODP Site 689 (*16*).

Chemical proxies for export productivity (*7*) and organic carbon burial (*14*) in middle to late Eocene Atlantic sector sediments demonstrate a long-period cycle. High values, centered around 39, 36.5, and 34.6 to 33.6 Ma (*14*, *30*), coincide with increasing ε_{Nd} values (Fig. 2). We speculate that changes in circulation, initiated by the early opening and successive deepening of Drake Passage, enhanced nutrient upwelling. These changes appear to have stimulated the biological pump, which is an important link between short- and long-term carbon cycles. This mechanism may have been a factor in lowering atmospheric CO_2 during the Paleogene. The influence of this mechanism on global climate may be evident during the middle Eocene, when an ephemeral glaciation, associated with changes in carbon cycling (*31*), followed an enigmatic climate reversal called the middle Eocene climatic optimum (MECO) (*32*). Cooling coincided with the early opening of Drake Passage (Fig. 2).

Nd isotope results suggest that Drake Passage opened before the Tasmanian Gateway. Reduction of oceanic heat flux after ACC development (*4*) is not unanimously accepted as a mechanism for global cooling (*29*); however, our results imply that a circum-Antarctic pathway could have existed by the late Eocene. Additionally, the proposed circulation-induced productivity increase may have sequestered atmospheric CO_2, contributing to global cooling and Antarctic glaciation.

References and Notes

1. J. Zachos, M. Pagani, L. Sloan, E. Thomas, K. Billups, *Science* **292**, 686 (2001).
2. R. M. DeConto, D. Pollard, *Nature* **421**, 245 (2003).
3. P. F. Barker, *Earth Sci. Rev.* **55**, 1 (2001).
4. J. P. Kennett, *J. Geophys. Res.* **82**, 3843 (1977).
5. R. Livermore, A. Nankivell, G. Eagles, P. Morris, *Earth Planet. Sci. Lett.* **236**, 459 (2005).
6. L. Diester-Haass, R. Zahn, *Geology* **24**, 163 (1996).
7. J. C. Latimer, G. M. Filippelli, *Palaeogeogr. Palaeoclimatol. Palaeoecol.* **182**, 151 (2002).
8. P. Barker, E. Thomas, *Earth Sci. Rev.* **66**, 143 (2004).
9. K. Tachikawa, V. Athias, C. Jeandel, *J. Geophys. Res.* **108**, 3254 (2003).
10. Materials and methods are available as supporting material on *Science* Online.
11. S. L. Goldstein, S. R. Hemming, in *The Oceans and Marine Geochemistry*, H. Elderfield, Ed. (Elsevier, Oxford, 2003), pp. 453–489.
12. H. F. Ling *et al.*, *Earth Planet. Sci. Lett.* **146**, 1 (1997).
13. D. J. Thomas, T. J. Bralower, C. E. Jones, *Earth Planet. Sci. Lett.* **209**, 309 (2003).
14. L. D. Anderson, M. L. Delaney, *Paleoceanography* **20**, PA1013 (2005).
15. E. E. Martin, H. D. Scher, *Earth Planet. Sci. Lett.* **220**, 25 (2004).
16. H. D. Scher, E. E. Martin, *Earth Planet. Sci. Lett.* **228**, 391 (2004).
17. S. L. Goldstein, R. K. O'Nions, P. J. Hamilton, *Earth Planet. Sci. Lett.* **70**, 221 (1984).
18. M. Frank, N. Whiteley, S. Kasten, J. R. Hein, K. O'Nions, *Paleoceanography* **17**, 10.1029/2000PA000606 (2002).
19. H. W. Hubberten, W. Morche, F. Westall, D. K. Fuetterer, J. Keller, *Proc. Ocean Drilling Program Sci. Res.* **114**, 733 (1991).
20. K. G. Miller, in *Eocene-Oligocene Climatic and Biotic Evolution*, D. Prothero, W. A. Berggren, Eds. (Princeton Univ. Press, Princeton, NJ, 1992), pp. 160–177.
21. J. C. Zachos, D. K. Rea, K. Seto, R. Nomura, N. Niitsuma, in *The Indian Ocean: A Synthesis of Results from the Ocean Drilling Program*, R. A. Duncan, D. K. Rea, R. B. Kidd, U. von Rad, J. K. Weissel, Eds. (American Geophysical Union, Washington, DC, 1992), pp. 351–386.
22. H. D. Scher, E. E. Martin, A. A. Haase, *Geochim. Cosmochim. Acta* **66**, A677 (2002).
23. M. Frank *et al.*, *Paleoceanography* **18**, PA1091 (2003).
24. M. R. Palmer, H. Elderfield, *Geochim. Cosmochim. Acta* **50**, 409 (1986).
25. G. A. Mead, D. A. Hodell, P. F. Cielcielski, in *The Antarctic Paleoenvironment: A Perspective on Global Change*, J. P. Kennett, D. A. Warnke, Eds. (American Geophysical Union, Washington, DC, 1993), pp. 27–48.
26. A. H. Orsi, G. C. Johnson, J. L. Bullister, *Prog. Oceanogr.* **43**, 55 (1999).
27. P. J. Cooke, C. S. Nelson, M. P. Crundwell, D. Spiegler, *Palaeogeogr. Palaeoclimatol. Palaeoecol.* **188**, 73 (2002).
28. L. A. Lawver, L. M. Gahagan, *Palaeogeogr. Palaeoclimatol. Palaeoecol.* **198**, 11 (2003).
29. C. E. Stickley *et al.*, *Paleoceanography* **19**, PA4027 (2004).
30. The peak in reactive phosphorus mass accumulation rate (P_r MAR) at 39 Ma may be an artifact of a change in sedimentation rate that is not resolved in the extended age model (*10*) but is possibly indicated by other proxy records (*33*). However, the occurrence of the peak at 39 Ma appears to be part of a cycle of high- and low-productivity intervals observed at this location (*14*).
31. A. Tripati, J. Backman, H. Elderfield, P. Ferretti, *Nature* **436**, 341 (2005).
32. S. M. Bohaty, J. C. Zachos, *Geology* **31**, 1017 (2003).
33. L. Anderson, personal communication.

34. This manuscript benefited from discussions with P. Barker, S. Blair, S. Bohaty, D. Hodell, A. Piotrowski, and J. Smellie; laboratory assistance from A. Heatherington and R. Thomas; and thoughtful reviews by three anonymous referees. This study was supported by NSF grant OCE-962970 to E.E.M. Samples used in this study were provided by the ODP.

Supporting Online Material

www.sciencemag.org/cgi/content/full/312/5772/428/DC1
Materials and Methods
Tables S1 to S3

12 September 2005; accepted 21 March 2006
10.1126/science.1120044

Asymmetric Coevolutionary Networks Facilitate Biodiversity Maintenance

Jordi Bascompte,[1]* Pedro Jordano,[1] Jens M. Olesen[2]

The mutualistic interactions between plants and their pollinators or seed dispersers have played a major role in the maintenance of Earth's biodiversity. To investigate how coevolutionary interactions are shaped within species-rich communities, we characterized the architecture of an array of quantitative, mutualistic networks spanning a broad geographic range. These coevolutionary networks are highly asymmetric, so that if a plant species depends strongly on an animal species, the animal depends weakly on the plant. By using a simple dynamical model, we showed that asymmetries inherent in coevolutionary networks may enhance long-term coexistence and facilitate biodiversity maintenance.

It is widely acknowledged that mutualistic interactions have molded biodiversity (*1*, *2*). In the past decade, much has been learned about how communities shape coevolutionary interactions across time and space (*3*). However, although most studies on coevolution focus on pairs or small groups of species, recent work has highlighted the need to understand how broader networks of species coevolve (*4*–*7*). Such knowledge is critical to understanding the persistence and coevolution of highly diverse plant-animal assemblages.

Recent research on the architecture of plant-animal mutualistic networks has been based mostly on qualitative data, assuming that all realized interactions are equally important (Fig. 1A) (*5*–*7*). This has precluded a deeper assessment of network structure (*8*) and strongly limited our understanding of its dynamic implications. To understand how mutualistic networks are organized and how such an organization affects species coexistence, we compiled from published studies and our own work 19 plant-pollinator and 7 plant-frugivore quantitative networks (Fig. 1 and Database S1). These networks range from arctic to tropical ecosystems and illustrate diverse ecological and biogeographical settings. Each network displays information on the mutual dependence or strength between each plant and animal species, mainly measured as the relative frequency of visits (*9*). Thus, our networks describe ecological interactions, and evolutionary inferences should be made with caution. However, frequency of visits has been shown to be a surrogate for per capita reproductive performance (*10*). Our results could be more directly related to coevolution when the reproductive success of one species depends directly on visitation frequency. This seems to be the case when there is a high variation of dependences among species (*10*). Unlike previous studies on food webs (*11*–*16*), for each plant-animal species pair, we have now two estimates of mutual dependence (defined in two adjacency matrices P and A): the dependence d_{ij}^{P} of plant species i on animal species j (i.e., the fraction of all animal visits coming from this particular animal species) and the dependence d_{ji}^{A} of animal species j on plant species i (i.e., the fraction of all visits by this animal species going to this particular plant species) (Fig. 1, B and C). Therefore, one can calculate an index of asymmetry for each pairwise interaction (*17*), depicting the relative dissimilarity between the two mutual dependences (Fig. 1, B and C).

Regardless of the type of mutualism, the frequency distribution of dependences is right-skewed, mostly with weak dependences and a few strong ones (Fig. 2). This is in agreement with previous work on ecological networks (*9*, *11*–*16*). This heterogeneous distribution is highly significant and cannot be predicted on the basis of an independent association between plants and animals. On the contrary, the distribution of animal visits is highly dependent on plant species ($P < 0.00001$, G-test in all nine communities in which the test can be performed). To illustrate the effect of such weak dependences on community coexistence, we used a mutualistic model (*18*–*21*). For the simplest case, there is a positive community steady state (community coexistence) if the following inequality holds (*21*)

$$\alpha\beta < \frac{ST}{mn}$$

where α and β are the average per capita effects of the animals on the plants, and of the plants on the animals, respectively. Hereafter, such per capita effects are estimated by the mutual dependence values (*21*). S and T are the average intraspecific competition coefficients of plants and animals, and n and m are the number of plant and animal species, respectively.

As community size increases, the product of mutual dependences has to become smaller for the community to coexist (fig. S1). Two situations fulfill this requirement: (i) either both dependences are weak; or (ii) if one dependence is strong, the accompanying dependence is very weak (so the product remains small). The dominance of weak dependences (Fig. 2) contributes to situation i. To assess the likelihood of scenario ii, we next look at the asymmetry of mutual dependences.

For each pair of plant species i and animal species j, we calculated the observed asymmetry of mutual dependences using (*17*). The frequency distribution of asymmetry values is also very skewed, with the bulk of pairwise interactions being highly asymmetric (Fig. 3). The question now is whether dependence pairs are more asymmetric than expected by chance. To answer this question, we calculated a null frequency distribution of asymmetry values to compare with the observed one by means of a χ^2 test. We achieved this by fixing the observed dependence d_{ij}^{P} of plant species i on animal species j and randomly choosing d_{ji}^{A} without replacement from the set of all dependences of the animals on the plants in this particular community. This procedure was repeated 10,000 times; the null asymmetry frequency distribution is the average of these replicates.

For pollination, only seven out of 19 communities (36.8%) showed a frequency distribution of asymmetry values that deviates significantly from the null frequency distribution (46.1% when considering only networks with at least 100 pairs). For seed dispersal, only one out of seven communities (14.3%) showed a frequency distribution of asymmetry values that deviates significantly from the null frequency distribution (20.0% when considering only networks with at least 100 pairs). These results show that in the bulk of the cases, the frequency distribution of asymmetry values originates exclusively from the skewed distribution of dependences. That is, most communities show mutual dependences that are asymmetric, but no more asymmetric than what we would expect by chance, given the distribution of dependence values.

Because strong interactions have the potential to destabilize ecological networks (*16*, *18*, *22*–*24*), we repeated the above calculations considering only dependence pairs in which at least one value is larger than or equal to 0.5 (other threshold values do not significantly affect our results). The fraction of large pollination networks (at least 100 pairs) with a frequency distribution of asymmetry significantly departing from expectation increased to 87.5% (seven out of eight communities). Similarly, for seed dispersal, the three largest communities ($n \geq 20$ pairs) also have frequency distributions of asymmetry values significantly departing from random (100%). Overall, these results suggest that there are constraints in the combination of strong mutual dependence values. Next, from the significant comparisons, we explored which intervals of asymmetry contribute to significance.

Asymmetry values range from 0 to 1 (Fig. 3). Within this range, some values may be over-

[1]Integrative Ecology Group, Estación Biológica de Doñana, Consejo Superior de Investigaciones Científicas, Apartado 1056, E-41080 Sevilla, Spain. [2]Department of Ecology and Genetics, University of Aarhus, Ny Munkegade, Building 540, DK-8000 Aarhus, Denmark.

*To whom correspondence should be addressed. E-mail: bascompte@ebd.csic.es

represented and some underrepresented, relative to random expectation (again comparing the null frequency distribution with the observed frequency distribution by using a χ^2 probability distribution). We found that the first half of the range (low to moderate asymmetry) is significantly underrepresented ($P = 3.81 \times 10^{-6}$ for pollination and $P = 0.0156$ for seed dispersal; binomial test). This underrepresentation of low asymmetry values implies that a strong dependence value for one of the partners in the mutualistic interaction tends to be accompanied by a weak dependence value of the other partner. That is, two strong interactions tend to be avoided in a pair, which agrees with the analytic prediction (scenario ii).

Our above analysis of mutual dependences, however, is based on isolated analysis of pairwise interactions and thus provides only limited information on the complexity of the whole mutualistic network (*25*). For example, how does the pattern of skewed dependences and strong asymmetries scale up to account for properties at the community level? A more meaningful measure of network complexity is provided by the concept of species strength (*25*). The strength of an animal species, for example, is defined as the sum of dependences of the plants relying on this animal. It is a measure of the importance of this animal from the perspective of the plant set (Fig. 1, D and E). This measure is a quantitative extension of the species degree, which is the number of interactions per species in qualitative networks (*5*). Previous work showed that mutualistic networks are highly heterogeneous (i.e., the bulk of species have a few interactions, but a few species have many more interactions than expected by chance) (*5*). Next, we considered how this result stands when quantitative information is considered.

In all but one case, there is a significant positive relationship between species strength and species degree (Fig. 4). To explore deviations from linearity, we performed a quadratic regression and tested for the significance of the quadratic term. The quadratic term is significant in 35 out of the 52 cases (for each community, we looked at both plants and animals independently). This fraction increases to 24 out of 30 cases when considering only communities with at least 30 species. That is, species strength increases faster than species degree (Fig. 4), a pattern previously found for the worldwide airport network, but not for the scientific collaboration network (*25*). The strength of highly connected species is even higher than expected based on their degree, because specialists tend to interact exclusively with the most generalized species (*6*, *7*) and so depend completely on them. Thus, specialists contribute disproportionately to increase the overall strength of the generalists they depend on.

Overall, previous results based on qualitative networks (i.e., their high heterogeneity in the number of links per species) (*5*) are confirmed by our analysis of quantitative networks. Second, previous work (i.e., asymmetry at the species level) (*6*, *7*) provides a mechanistic explanation for some of the new results presented here as the higher-than-expected strength of generalist species. However, our results go a step further, because we show here that asymmetry is also a property at the link level based on species-specific mutual dependences.

Our results suggest that the architecture of quantitative mutualistic networks is characterized by the low number of strong dependences, their asymmetry, and the high heterogeneity in species strength, all of which may promote community coexistence. Community coexistence, in turn, may favor the long-term persistence of reciprocal selective forces required for the coevolution of these species-rich assemblages (*2*, *3*). By considering mutualistic networks as coevolved structures rather than as diffuse multispecific interactions, we can better understand how these networks develop (*3*). There are two forces that, acting in combination, may lead to networks with the reported architecture: coevolu-

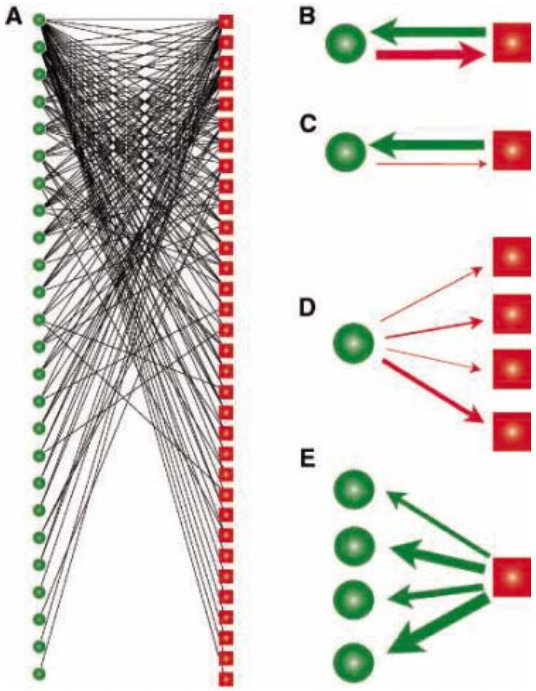

Fig. 1. A network approach to plant-animal mutualisms. (**A**) Example of a community of plants and their seed dispersers in Cazorla, SE Spain (see Database S1 for references and data sets). Green circles represent plant species and red squares represent animal species. A plant and an animal interact if there is a qualitative link between them. (**B** and **C**) Each of the above plant-animal interactions is described by two weighted links (arrows) depicting the relative dependence of the plant on the animal (green arrow) and the animal on the plant (red arrow). The asymmetry of the pairwise interaction is proportional to the difference between the thickness of both arrows. Here we show a symmetric (B) and an asymmetric (C) example. (**D** and **E**) A species degree is the number of interactions it has with the other set. Species strength is the quantitative extension of species degree, and can be defined as the sum of dependences of the animals on the plant (D) and the plants on the animal (E). Although the degree is four in both (D) and (E), the strength of the animal (E) is higher than that of the plant (D).

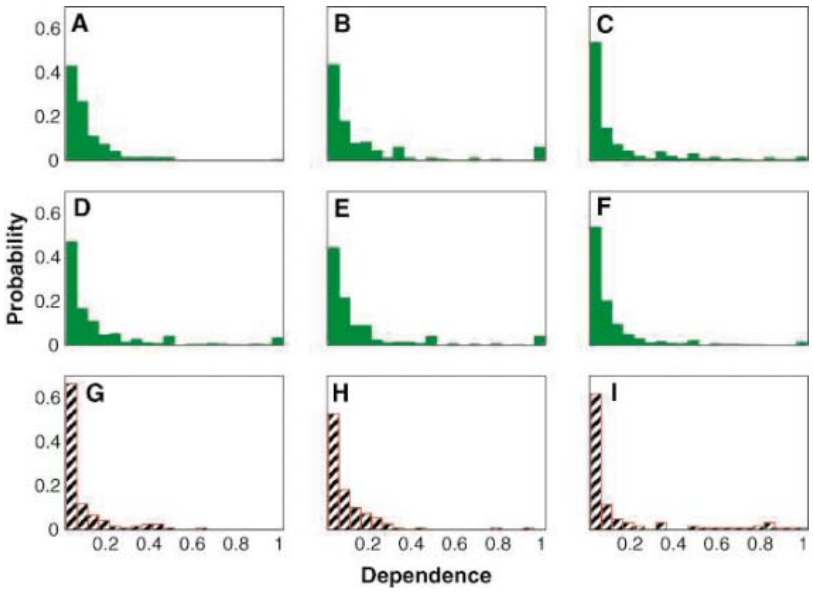

Fig. 2. Frequency distributions of dependence values within a mutualistic community. Green solid histograms (**A** to **F**) represent dependences of plants on pollinators, and red dashed histograms (**G** to **I**) represent dependences of seed dispersers on plants. See Database S1 for references and data sets.

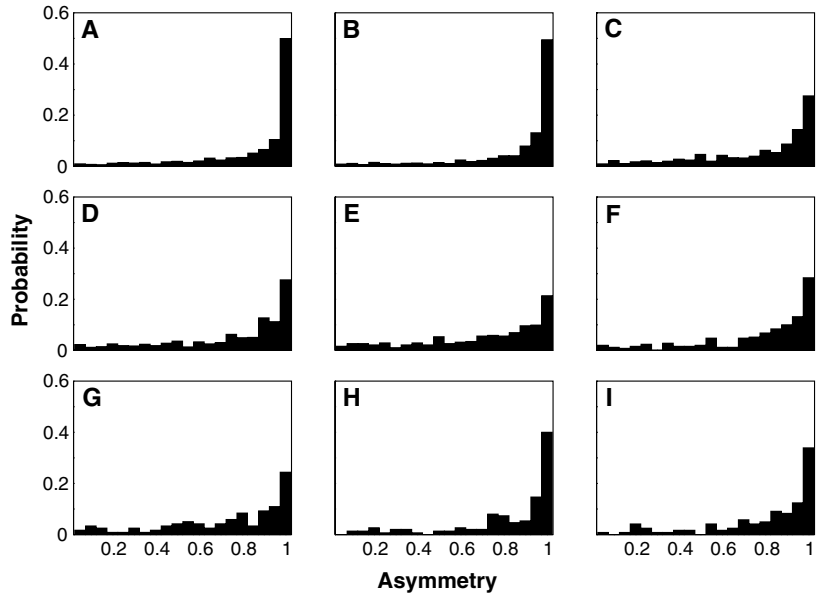

Fig. 3. Frequency distributions of asymmetry values of mutual dependences within a mutualistic community. (**A** to **F**) Plant-pollinator communities. (**G** to **I**) Plant seed–disperser communities. See Database S1 for references and data sets.

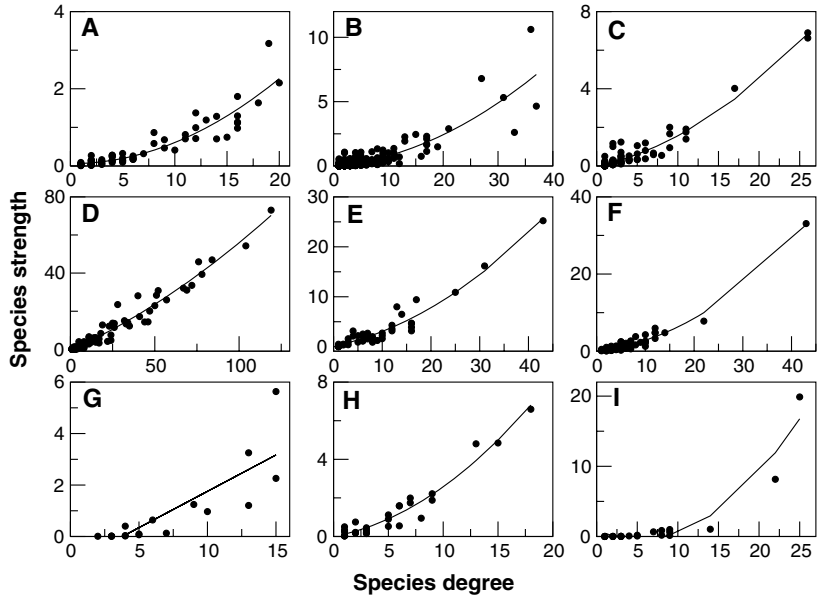

Fig. 4. Relationship between the number of interactions per species (degree) and its quantitative extension, species strength. (**A** to **C**) Pollinator species in plant-pollinator communities. (**D** to **F**) Plant species in plant-pollinator communities. (**G** and **H**) Animal species in plant seed–disperser communities. (**I**) Plants in a plant seed–disperser community. A quadratic regression is represented when the quadratic term is significant; otherwise a linear regression is plotted (G). As noted, in all cases but (G), species strength increases faster than species degree. See Database S1 for references and data sets.

tionary complementarity and coevolutionary convergence (*3*). Pairwise interactions build up on complementary traits of the plants and the animals (e.g., corolla and pollinator tongue lengths), whereas the convergence of traits allows other species to attach to the network as this evolves (e.g., convergence in fruit traits among plants dispersed by birds rather than mammals) (*3*). These forces differ from those shaping antagonistic interactions such as coevolutionary alternation (i.e., selection favoring herbivores attacking less defended plants) (*2*, *3*). Thus, one could predict differences in the architecture of mutualistic and antagonistic networks. Other types of biological interactions also show high asymmetry values. For example, a large fraction of competitive interactions are asymmetric, especially in the marine intertidal (*26*, *27*). Our results highlight the importance of asymmetric interactions in mutualistic networks. Asymmetry seems to be the key to both their diversity and coexistence. Whether asymmetry extends to other types of complex networks remains to be seen.

References and Notes

1. P. R. Ehrlich, P. H. Raven, *Evolution* **18**, 586 (1964).
2. J. N. Thompson, *The Coevolutionary Process* (Univ. of Chicago Press, Chicago, IL, 1994).
3. J. N. Thompson, *The Geographic Mosaic of Coevolution* (Univ. of Chicago Press, Chicago, IL, 2005).
4. J. Memmott, *Ecol. Lett.* **2**, 276 (1999).
5. P. Jordano, J. Bascompte, J. M. Olesen, *Ecol. Lett.* **6**, 69 (2003).
6. J. Bascompte, P. Jordano, C. J. Melián, J. M. Olesen, *Proc. Natl. Acad. Sci. U.S.A.* **100**, 9383 (2003).
7. D. P. Vázquez, M. A. Aizen, *Ecology* **85**, 1251 (2004).
8. L.-F. Bersier, C. Banasek-Richter, M.-F. Cattin, *Ecology* **83**, 2394 (2002).
9. P. Jordano, *Am. Nat.* **129**, 657 (1987).
10. D. P. Vázquez, W. F. Morris, P. Jordano, *Ecol. Lett.* **8**, 1088 (2005).
11. R. E. Ulanowicz, W. F. Wolff, *Math. Biosci.* **103**, 45 (1991).
12. R. T. Paine, *Nature* **355**, 73 (1992).
13. W. F. Fagan, L. E. Hurd, *Ecology* **75**, 2022 (1994).
14. D. Raffaelli, S. Hall, in *Food Webs, Integration of Patterns and Dynamics*, G. Polis, K. Winemiller, Eds. (Chapman & Hall, New York, 1995), pp. 185–191.
15. J. T. Wootton, *Ecol. Monogr.* **67**, 45 (1997).
16. J. Bascompte, C. J. Melián, E. Sala, *Proc. Natl. Acad. Sci. U.S.A.* **102**, 5443 (2005).
17. The asymmetry of a pairwise mutualistic interaction is estimated as follows: $AS(i, j) = |d^{P}_{ij} - d^{A}_{ji}|/\max(d^{P}_{ij}, d^{A}_{ji})$, where d^{P}_{ij} and d^{A}_{ji} are the relative dependences of plant species i on animal species j and of animal species j on plant species i, respectively; $\max(d^{P}_{ij}, d^{A}_{ji})$ refers to the maximum value between d^{P}_{ij} and d^{A}_{ji}. Related measures of asymmetry are highly correlated to this equation, so results are insensitive to the particular asymmetry measure used.
18. R. M. May, *Stability and Complexity in Model Ecosystems* (Princeton Univ. Press, Princeton, NJ, 1973).
19. R. M. May, in *Theoretical Ecology*, R. M. May, Ed. (Sinauer, Sunderland, MA, ed. 2, 1981), pp. 78–104.
20. M. S. Ringel, H. H. Hu, G. Anderson, M. S. Ringel, *Theor. Pop. Biol.* **50**, 281 (1996).
21. Materials and methods are available as supporting material on *Science* Online.
22. K. McCann, A. Hastings, G. R. Huxel, *Nature* **395**, 794 (1998).
23. G. D. Kokkoris, A. Y. Troumbis, J. H. Lawton, *Ecol. Lett.* **2**, 70 (1999).
24. A. Neutel, J. A. P. Heesterbeek, P. C. Ruiter, *Science* **296**, 1120 (2002).
25. A. Barrat, M. Barthélemy, R. Pastor-Satorras, A. Vespignani, *Proc. Natl. Acad. Sci. U.S.A.* **101**, 3747 (2004).
26. R. T. Paine, *J. Anim. Ecol.* **49**, 667 (1980).
27. T. W. Schoener, *Am. Nat.* **122**, 240 (1983).

28. We thank P. Amarasekare, J. E. Cohen, W. Fagan, M. A. Fortuna, P. Guimarães, T. Lewinsohn, N. Martinez, R. M. May, C. J. Melián, R. T. Paine, A. G. Sáez, G. Sugihara, J. N. Thompson, and A. Valido for comments on a previous draft. J. E. Cohen and M. A Fortuna provided technical assistance. Funding was provided by the Spanish Ministry of Science and Technology (grants to J.B. and P.J.), the Danish Natural Sciences Research Council (to J.M.O.), and the European Heads of Research Councils and the European Science Foundation through an EURYI award (to J.B.).

Supporting Online Material

www.sciencemag.org/cgi/content/full/312/5772/431/DC1
Materials and Methods
Fig. S1
Database S1
References

5 December 2005; accepted 27 February 2006
10.1126/science.1123412

Stability via Asynchrony in *Drosophila* Metapopulations with Low Migration Rates

Sutirth Dey and Amitabh Joshi*

Very few experimental studies have examined how migration rate affects metapopulation dynamics and stability. We studied the dynamics of replicate laboratory metapopulations of *Drosophila* under different migration rates. Low migration stabilized metapopulation dynamics, while promoting unstable subpopulation dynamics, by inducing asynchrony among neighboring subpopulations. High migration synchronized subpopulation dynamics, thereby destabilizing the metapopulations. Contrary to some theoretical predictions, increased migration did not affect average population size. Simulations based on a simple non–species-specific population growth model captured most features of the data, which suggests that our results are generalizable.

Natural populations often exhibit some degree of spatial structuring into metapopulations: ensembles of local populations (subpopulations) connected by migration (*1*). The effects of migration rate on the dynamics and stability of metapopulations have been extensively investigated theoretically (*1*). Analytical (*2*, *3*) and simulation (*4*) studies have shown that even a simple system, consisting of two subpopulations (modeled by a pair of logistic maps) with a constant rate of to-and-fro migration, can exhibit rich dynamic behavior. In such systems, low, intermediate, and high migration rates have been shown to lead to complex, stable, and unstable dynamics, respectively (*2*–*4*). Similar results have been obtained with a variety of more realistic models (*5*–*8*). Potential stabilizing effects of migration have also been shown in studies on more complex systems (*9*–*12*). Although it has been empirically shown that migration can stabilize dynamics (*13*, *14*), most metapopulation experiments have been carried out within the classical extinction-recolonization framework (*15*), which ignores the dynamics of population size. Thus, rigorous tests of theoretical predictions regarding the effects of migration rate on metapopulation dynamics are rare (*13*). Similarly, despite a large corpus of theoretical studies (*16*–*18*), the effects of migration rates on mean population size have rarely been investigated experimentally (*19*).

Here, we report the effects of low (10%) and high (30%) migration rates on the dynamics of replicated laboratory metapopulations of the fruit fly *Drosophila melanogaster* in a 21-generation experiment (*20*). We quantified constancy stability (*21*) of the metapopulations and subpopulations with the use of a dimensionless measure of amplitude of fluctuation in population size over time (*22*). This statistic, which we call the fluctuation index (FI), is inversely related to stability. We also performed simulations (*20*) using a simple non–*Drosophila*-specific model to test whether the results reflect a simple effect of migration rates on typical population dynamics, or are due to some specific features of the life history and ecology of *Drosophila* cultures.

Metapopulations with low levels of migration (henceforth LMMs) had lower FI values for metapopulation size than did either the control metapopulations (CMs; no migration) or those experiencing high migration levels (HMMs) (Fig. 1A). Nonetheless, the FI for subpopulation size was significantly higher in LMMs than in HMMs or CMs (Fig. 1B). Thus, low levels of migration caused global metapopulation stability, despite increased local instability in the subpopulations. The underlying mechanism was revealed by examining cross-correlations at lag zero of the first differenced time series of log abundance [$\ln(N_{t+1}) - \ln(N_t)$, where N_t is the population size at time t] of all subpopulation pairs in a metapopulation (*23*). The mean cross-correlation across all subpopulation pairs was significantly positive in CMs and HMMs but was close to zero in LMMs (Fig. 2A). This indicates that in CMs and HMMs, the subpopulations tended to reach peak and trough population sizes together, leading to high-amplitude oscillations at the metapopulation level (*20*) (fig. S1). However, there was no such synchrony in subpopulation sizes in LMMs, rendering the metapopulation dynamics relatively more stable.

We further investigated the spatial patterns of subpopulation synchrony by examining the cross-correlations for all nearest neighbor pairs. LMMs showed a significantly negative mean cross-correlation (Fig. 2B), indicating that immediate neighboring subpopulations were often out of phase; this result confirmed some theoretical predictions (*2*–*4*, *10*). CMs and HMMs, however, showed significantly positive mean cross-correlations between nearest neighbors (Fig. 2B). Although high migration rate is predicted to induce synchrony (positive correlation) between subpopulations (*7*–*9*), zero migration (as in our CMs) is not expected to do so, particularly under constant-environment laboratory conditions. With no migration, the subpopulations are independent of one another, and their dynamics should not become synchronized without external environmental forcing (*24*), which is unlikely under laboratory conditions. However, subpopulations in our CMs suffered frequent extinctions, averaging 3.35 out of 9 subpopulations per generation. Upon extinction, these subpopulations were restarted by introducing eight flies (*25*). Thus, about one-third of the subpopulations in each CM were equalized for population size every generation, potentially leading to artifactual positive cross-correlations among them. Overall, our results on the effects of migration rate on subpopulation synchrony, and therefore

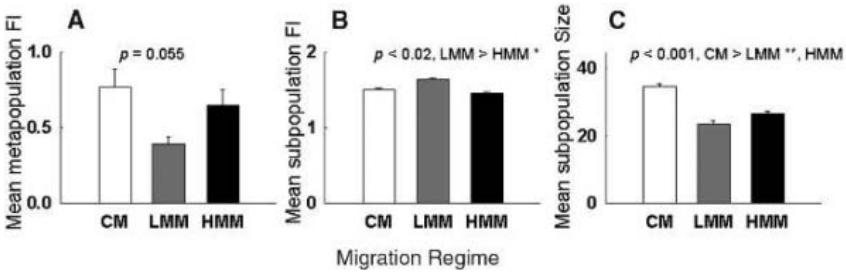

Fig. 1. Experimental results. The *P* values indicate the significance level from the corresponding mixed-model analysis of variance. The inequalities denote the means that were found different at the 0.05 (*) or 0.01 (**) level of significance using Tukey's HSD test. CM, no migration; LMM, low levels of migration (10%); HMM, high levels of migration (30%). Error bars are SEM for four replicate metapopulations. (**A**) Mean fluctuation index (FI) of LMMs is lower than that of either CMs or HMMs, indicating higher constancy stability. (**B**) Mean FI of the subpopulations is highest in the LMMs, suggesting lower stability at that migration rate. (**C**) Mean subpopulation size of CMs is higher than for both LMMs and HMMs, which is unexpected. See text for possible explanations.

Evolutionary Biology Laboratory, Evolutionary & Organismal Biology Unit, Jawaharlal Nehru Centre for Advanced Scientific Research, Jakkur P.O., Bangalore 560 064, India.

*To whom correspondence should be addressed. E-mail: ajoshi@jncasr.ac.in

metapopulation stability, seem to confirm the existing theoretical predictions.

Contrary to a previous report that migration leads to increase in population size (*19*), the mean subpopulation and metapopulation sizes of CMs in our study were significantly higher than those of LMMs or HMMs (Fig. 1C). However, the controls used in that study (*19*) underwent no subpopulation extinctions, whereas subpopulations in our CMs frequently went extinct and were restarted (*25*). This influx of flies is the probable reason for increased mean subpopulation size in our CMs. Mean subpopulation size in our LMMs and HMMs did not differ significantly, thus contradicting predictions that local population size should decrease (*17*) or increase (*19*) monotonically with increase in migration rate. This may be attributed to the specific model assumptions and restricted parameter range (*17*), or differences in experimental protocol (*19*), of these studies. Thus, the effects of migration rate on metapopulation and subpopulation size seem to depend critically on model assumptions and the biology of the organisms, making generalized predictions difficult.

The generality of our findings depends largely on whether they reflect a simple effect of migration rates on typical population dynamics, or an interaction of migration rate with some specific features of the life history and ecology of *Drosophila* cultures. One way to address this issue is to simulate the experimental system with a simple model of population dynamics that does not include these specific features of *Drosophila* cultures. Populations with uniform random spatial distribution and scramble competition exhibit simple Ricker dynamics (*26*). Because *Drosophila* cultures more or less satisfy both conditions, we modeled subpopulation dynamics with the one-dimensional, discrete version of the Ricker map (*20*). The qualitative behavior of the Ricker map is determined solely by the intrinsic rate of growth, r, and the model exhibits a period-doubling route to chaos with increase in r (*27*).

The simulation of our experimental system yielded results very similar to the empirical observations. The FI values of LMMs in the simulations were lower than those of both CMs and HMMs (compare Figs. 3A and 1A), whereas at the subpopulation level, FI values for LMMs were the highest (compare Figs. 3B and 1B). The mean all-pair and nearest neighbor cross-correlations were also found to be similar to the experimental data (compare Figs. 2 and 4), with nearest neighbors in LMMs showing significantly negative correlations. However, in the simulations, subpopulation size exhibited the trend CMs < HMMs < LMMs (Fig. 3C), which does not agree with the observed trend in the experiment (CMs > LMMs ~ HMMs). The subpopulation time series revealed that the number of extinctions in the simulations was much less than in the experiment (*28*). The subpopulation extinction criteria for simulations and experiment were zero individuals and the absence of at least one male-female pair, respectively (*20*, *25*). Consequently, there were fewer resets to $N_r = 8$ in the CM subpopulations of the simulations, ultimately leading to lower mean subpopulation size relative to the experiments. Thus, Ricker-based simulations in a biologically meaningful parameter range recovered almost all major features of the experimental data. Scramble competition for resources is experienced across a wide range of animal taxa, including most microbes, invertebrates, fishes, and amphibians, and the Ricker model is known to be a good descriptor of scramble competition–driven dynamics (*26*, *29*, *30*). Our experimental results are therefore likely to hold true for a variety of species.

Besides verifying several existing theoretical predictions, our results have potential practical implications. A major concern in conservation biology is the designing of migration corridors for stabilizing the dynamics of populations in isolated, patchy habitats. Our results show that too much migration can actually increase the amplitude of fluctuations in metapopulation size, thus potentially endangering the metapopulation

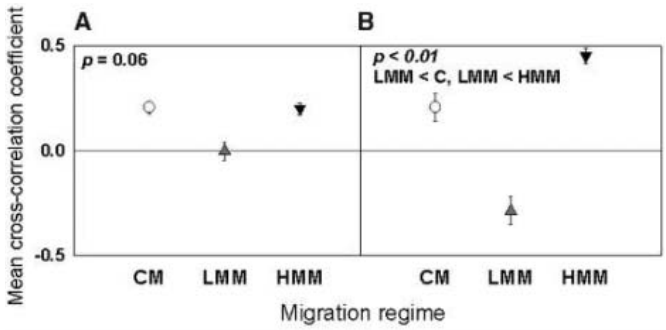

Fig. 2. Mean (±SE) cross-correlation coefficients from the experimental data. (**A**) The means for all possible pairs of subpopulations are positive for CMs and HMMs, indicating synchrony between the subpopulations. (**B**) The mean nearest neighbor cross-correlation coefficient is significantly negative for the LMMs. This indicates that neighboring subpopulations are oscillating out of phase with each other, leading to the observed patterns of stability.

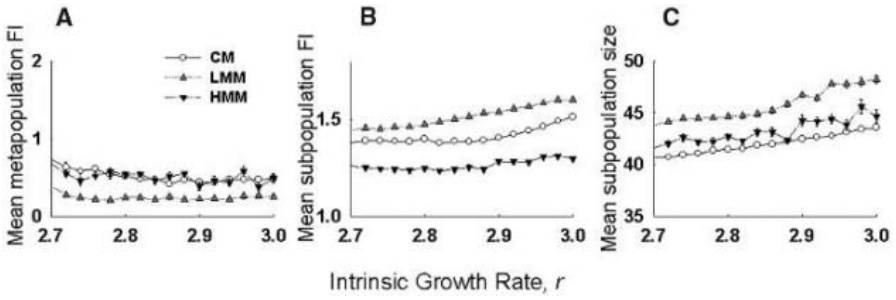

Fig. 3. Simulation results averaged over 10 independent runs (error bars represent SEM). (**A**) Mean metapopulation FI values are lowest for LMMs and are similar for CMs and HMMs (compare Fig. 1A). (**B**) Mean subpopulation FI values are highest for LMMs (compare Fig. 1B). (**C**) The average subpopulation size of CMs is the lowest, contrary to the experimental findings (Fig. 1C). See text for a possible explanation.

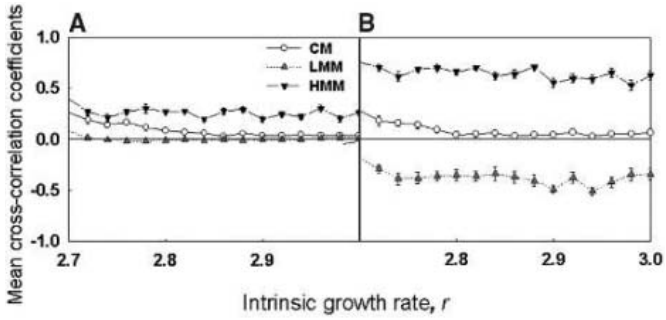

Fig. 4. Mean (±SE) cross-correlation coefficients from the simulations. (**A**) The average cross-correlation coefficient between all possible subpopulation pairs is close to zero for both CMs and LMMs. This indicates an overall lack of synchrony and contradicts the corresponding empirical observation for CMs (compare Fig. 2A). See text for a possible explanation. (**B**) The average cross-correlation coefficient between the nearest neighbors is negative for LMMs but is close to zero for CMs. This shows that although the LMM subpopulations were out of phase with each other, there was little synchrony among the CM subpopulations.

in the long run. However, migration rate in our experiment was density independent and migration was confined to the two nearest neighbors, whereas it is known that the dynamics of a metapopulation can vary depending on the exact form of density dependence (*31*) and scheme of migration (*11*). Moreover, growth rates of *Drosophila* (and most insects, microbes, and fishes) are higher than those of mammals and birds, which are generally of greater concern for conservation. The intrinsic growth rates of subpopulations are also known to interact strongly with migration rate in producing observed metapopulation dynamics (*12*). Therefore, due caution should be exercised when extrapolating our results to natural populations.

References and Notes

1. I. Hanski, *Metapopulation Ecology* (Oxford Univ. Press, New York, 1999).
2. M. Gyllenberg, G. Söderbacka, S. Ericsson, *Math. Biosci.* **118**, 25 (1993).
3. B. E. Kendall, G. A. Fox, *Theor. Popul. Biol.* **54**, 11 (1998).
4. A. Hastings, *Ecology* **74**, 1362 (1993).
5. J. C. Allen, W. M. Schaffer, D. Rosko, *Nature* **364**, 229 (1993).
6. G. D. Ruxton, *Proc. R. Soc. London Ser. B* **256**, 189 (1994).
7. E. Ranta, V. Kaitala, P. Lundberg, *Oikos* **83**, 376 (1998).
8. J. Ripa, *Oikos* **89**, 175 (2000).
9. G. Nachman, *J. Anim. Ecol.* **56**, 267 (1987).
10. G. Nachman, *Biol. J. Linn. Soc.* **42**, 285 (1991).
11. D. J. D. Earn, S. A. Levin, P. Rohani, *Science* **290**, 1360 (2000).
12. S. Dey, S. Dabholkar, A. Joshi, *J. Theor. Biol.* **238**, 78 (2006).
13. L. D. Mueller, A. Joshi, *Stability in Model Populations* (Princeton Univ. Press, Princeton, NJ, 2000).
14. J. Lecomte, K. Boudjemadi, F. Sarrazin, K. Cally, J. Clobert, *J. Anim. Ecol.* **73**, 179 (2004).
15. R. Levins, *Bull. Entomol. Soc. Am.* **15**, 237 (1969).
16. G. D. Ruxton, *J. Anim. Ecol.* **65**, 161 (1996).
17. I. Hanski, D. Y. Zhang, *J. Theor. Biol.* **163**, 491 (1993).
18. G. Nachman, *Oikos* **91**, 51 (2000).
19. A. R. Ives, S. T. Woody, E. V. Nordheim, C. Nelson, J. H. Andrews, *Am. Nat.* **163**, 375 (2004).
20. In the experiment, the nine subpopulations (single-vial *Drosophila* cultures) were arranged on the periphery of a circle, with each vial exchanging migrants only with its two nearest neighbors (i.e., a one-dimensional array with periodic boundary conditions). In nature, such metapopulations might exist, for example, on the shorelines of lakes or along the edges of ecosystems. The simulations mimicked the experimental system and focused on the behavior of nine coupled Ricker maps, with periodic boundary conditions. See supporting material on *Science* Online.
21. V. Grimm, C. Wissel, *Oecologia* **109**, 323 (1997).
22. We define a population whose size fluctuates with higher amplitude across time to be less stable than one that has lower amplitude of fluctuation ["constancy" attribute of stability (*21*)]. We introduce a measure of stability, the fluctuation index (FI) of a series, given as

$$\mathrm{FI} = \frac{1}{T\overline{N}} \sum_{t=0}^{T-1} \mathrm{abs}(N_{t+1} - N_t)$$

where $\overline{N}$ is the mean population size over T generations. FI thus reflects the mean one-step change in population size, scaled by average population size, over the study duration.
23. O. N. Bjørnstad, R. A. Ims, X. Lambin, *Trends Ecol. Evol.* **14**, 427 (1999).
24. P. A. P. Moran, *Aust. J. Zool.* **1**, 291 (1953).
25. In the experiment, a subpopulation was deemed extinct when it did not contain at least one male and one female fly. When a CM subpopulation became extinct, it was restarted using four males and four females from a backup vial. The backup vials were maintained in parallel to the three treatments, under high larval crowding and yeast supplement to the adults. There were no restarts in LMMs or HMMs; extinct subpopulation vials remained empty until recolonized by migrants from a neighboring subpopulation.
26. Å. Brännström, D. J. T. Sumpter, *Proc. R. Soc. London Ser. B* **272**, 2065 (2005).
27. R. M. May, G. F. Oster, *Am. Nat.* **110**, 573 (1976).
28. For example, in simulations with $r = 2.8$, comparable to the estimated r in our CM subpopulations, the mean extinction rate was 0.75 out of 9 subpopulations per generation, versus 3.35 out of 9 for experimental CMs.
29. R. A. Cheke, J. Holt, *Ecol. Entomol.* **18**, 109 (1993).
30. V. Sheeba, A. Joshi, *Curr. Sci.* **75**, 1406 (1998).
31. R. A. Ims, H. P. Andreassen, *Proc. R. Soc. London Ser. B* **272**, 913 (2005).

32. We thank V. K. Sharma for useful discussions; three anonymous reviewers for helpful comments on the manuscript; M. Shakarad, M. Rajamani, and N. Raghavendra for crucial help in fly handling; and J. Mohan, S. Ghosh, K. M. Satish, N. Rajanna, and M. Manjesh for help in diverse ways during the experiment. Supported by a senior research fellowship from the Council for Scientific and Industrial Research, Government of India (S.D.) and by grants from Department of Science and Technology, Government of India.

Supporting Online Material

www.sciencemag.org/cgi/content/full/312/5772/434/DC1
Materials and Methods
SOM Text
Fig. S1
References

24 January 2006; accepted 16 March 2006
10.1126/science.1125317

A Plant miRNA Contributes to Antibacterial Resistance by Repressing Auxin Signaling

Lionel Navarro,[1,2] Patrice Dunoyer,[2] Florence Jay,[2] Benedict Arnold,[3] Nihal Dharmasiri,[4] Mark Estelle,[4] Olivier Voinnet,[2]*† Jonathan D. G. Jones[1]*†

Plants and animals activate defenses after perceiving pathogen-associated molecular patterns (PAMPs) such as bacterial flagellin. In *Arabidopsis*, perception of flagellin increases resistance to the bacterium *Pseudomonas syringae*, although the molecular mechanisms involved remain elusive. Here, we show that a flagellin-derived peptide induces a plant microRNA (miRNA) that negatively regulates messenger RNAs for the F-box auxin receptors TIR1, AFB2, and AFB3. Repression of auxin signaling restricts *P. syringae* growth, implicating auxin in disease susceptibility and miRNA-mediated suppression of auxin signaling in resistance.

Plants perceive a 22–amino acid peptide (flg22) from the N terminus of eubacterial flagellin (*1*). In *Arabidopsis*, flg22 triggers rapid changes in transcript levels, including down-regulation of a gene subset, potentially by posttranscriptional mechanisms (*2*). One posttranscriptional mechanism is RNA silencing, a sequence-specific mRNA degradation process mediated by 20- to 24-nucleotide (nt) RNAs known as short interfering RNAs (siRNAs) and microRNAs (miRNAs). Both are made from double-stranded RNA (dsRNA) by the ribonuclease III enzyme Dicer. Four paralogs (Dicer-likes, or DCLs) are found in *Arabidopsis*. DCL2 produces viral-derived siRNAs (*3*) and siRNAs from antisense overlapping transcripts (*4*). DCL3 generates DNA repeat–associated siRNAs (*3*), whereas DCL4 synthesizes trans-acting siRNAs and mediates RNA interference (*5*–*7*). DCL1 excises miRNAs from intergenic stem-loop transcripts to promote cleavage of cellular transcripts carrying miRNA-complementary sequences (*8*).

We examined whether small RNAs—especially miRNAs—contribute to the rapid changes elicited by flg22. We analyzed transgenic *Arabidopsis* expressing the P1-Hc-Pro, P19, and P15 viral proteins that suppress miRNA- and siRNA-guided functions (*9*, *10*), anticipating that transcripts repressed by flg22-stimulated small RNAs would be more abundant in these lines. Comparative transcript profiling of untreated

[1]The Sainsbury Laboratory, John Innes Centre, Colney Lane, Norwich NR4 7UH, UK. [2]Institut de Biologie Moléculaire des Plantes du Centre National de la Recherche Scientifique, 67084 Strasbourg Cedex, France. [3]John Innes Centre, Colney Lane, Norwich NR4 7UH, UK. [4]Department of Biology, Indiana University, Bloomington, IN 47405, USA.

*These authors contributed equally to this work.
†To whom correspondence should be addressed. E-mail: jonathan.jones@sainsbury-laboratory.ac.uk (J.D.G.J.); olivier.voinnet@ibmp-ulp.u-strasbg.fr (O.V.)

transgenic seedlings and flg22-elicited wild-type seedlings identified a subset of mRNAs that fulfilled this criterion, including TIR1 (Transport Inhibitor Response 1) and two of its three functional paralogs, AFB2 and AFB3 (Auxin signaling F-Box proteins 2 and 3) (fig. S1, A and B). However, accumulation of AFB1, the third TIR1 paralog, was not discernibly altered in the suppressor lines (fig. S1B).

The F-box proteins TIR1, AFB1, AFB2, and AFB3 are receptors for the plant hormone auxin (*11*–*13*). Additionally, TIR1 and AFB transcripts are targets of miR393, a conserved miRNA (fig. S2) (*14*, *15*). A modified rapid amplification of cDNA ends (RACE) assay confirmed that TIR1, AFB2, and AFB3 mRNAs are specifically cleaved by miR393 in a DCL1-dependent manner (Fig. 1A and fig. S3). However, polymerase chain reaction (PCR)–amplified cleavage products derived from AFB1 were hardly detectable and rarely cloned (Fig. 1A and fig. S3), confirming that AFB1 is partially resistant to miR393-directed cleavage. Presumably, this is due to a single mismatch in the miR393 complementary site found specifically in AFB1 mRNA (fig. S3).

Quantitative reverse transcription–polymerase chain reaction (RT-qPCR) analyses with primers flanking the miR393 target sites revealed a two- to threefold reduction in the levels of TIR1, AFB1, AFB2, and AFB3 30 min after flg22 elicitation of wild-type seedlings (Fig. 1B). Repression of TIR1, AFB2, and AFB3 was partially compromised in *dcl1-9* seedlings (Fig. 1B), suggesting that a miRNA-directed pathway, probably involving miR393, contributes to TIR1, AFB2, and AFB3 down-regulation. However, flg22-triggered down-regulation of AFB1 was unaffected in *dcl1-9*, in agreement with its reduced sensitivity to miR393 (Fig. 1A and fig. S3). Therefore, repression of AFB1 is miRNA-independent and may exclusively occur at the transcriptional level.

We analyzed miR393 levels in flg22-elicited *Arabidopsis* seedlings. Northern analysis showed a twofold increase in miR393 accumulation after 20 and 60 min, whereas levels of the unrelated miR171 remained unaltered (Fig. 2A). Similarly, miR393 levels were unaltered in seedlings treated with control flg22$^{A.tum}$ inactive peptide (Fig. 2A) (*1*). The *Arabidopsis* genome contains two miR393 precursors, on chromosomes 2 (*At-miR393a*) and 3 (*At-miR393b*) (*16*). We fused 1.5-kb DNA fragments upstream of *At-miR393a* and *At-miR393b* to the *enhanced Green Fluorescence Protein* (*eGFP*) and transformed them into *Arabidopsis*, producing transgenic lines *AtmiR393a-p*::*eGFP* and *AtmiR393b-p*::*eGFP*. Using RT-qPCR, we observed a twofold increase in eGFP mRNA level in three independent flg22-treated *AtmiR393a-p*::*eGFP* lines (Fig. 2B), consistent with the miR393 Northern analysis (Fig. 2A). However, eGFP levels were unaltered in three independent *At-miR393b-p*::*eGFP*–elicited lines (Fig. 2B). These data suggest that up-regulation of miR393 by flg22 results from enhanced transcription of *At-miR393a*.

To assay TIR1 protein levels after flg22 treatment, we used *Arabidopsis* transformants expressing a Myc epitope–tagged TIR1 under the dexamethasone (Dex)-inducible promoter (Dex::TIR1-Myc) (*12*). Western blotting revealed a rapid reduction in TIR1-Myc levels upon flg22, but not flg22$^{A.tum}$, treatment (Fig. 3A). Because TIR1 is part of the ubiquitin-ligase complex SCF^{TIR1} that interacts with Aux/IAA proteins to promote their degradation (*17*), we investigated whether Aux/IAA proteins became stabilized upon flg22 treatment. We used transgenic lines expressing a

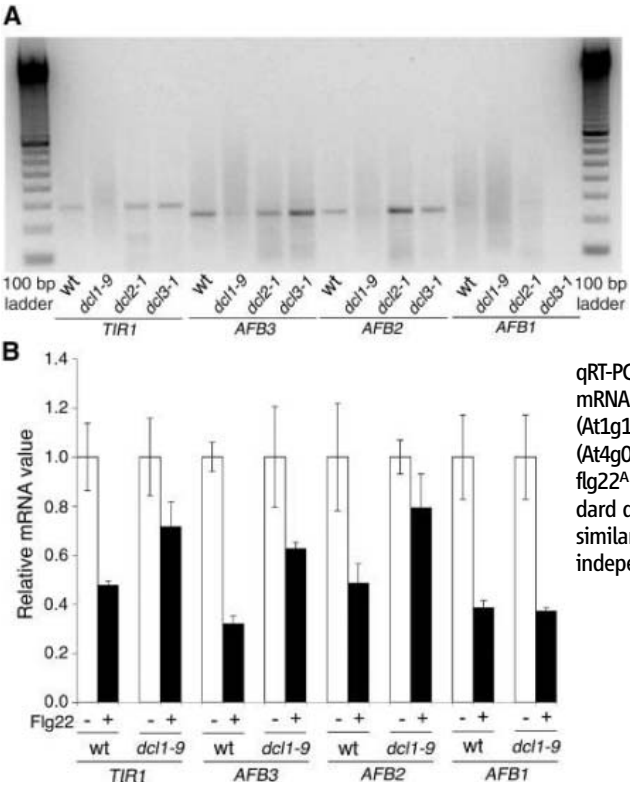

Fig. 1. Flg22 triggers a reduction in TIR1 and AFB mRNAs through miRNA-dependent and miRNA-independent regulatory mechanisms. (**A**) PCR-amplified cleavage products from TIR1 and AFB mRNAs. Col-0 samples are not shown (*27*). (**B**) Repression of TIR1, AFB1, AFB2, and AFB3 mRNAs in response to flg22. Seedlings were treated for 30 min with either 10 μM flg22 (+) or 10 μM flg22$^{A.tum}$ (−). qRT-PCRs were done to assess the relative mRNA levels of TIR1 (At3g62980), AFB3 (At1g12820), AFB2 (At3g26810), and AFB1 (At4g03190) upon treatment with flg22 or flg22$^{A.tum}$. Error bars represent the standard deviation from four PCR results, and similar results were obtained in three independent experiments.

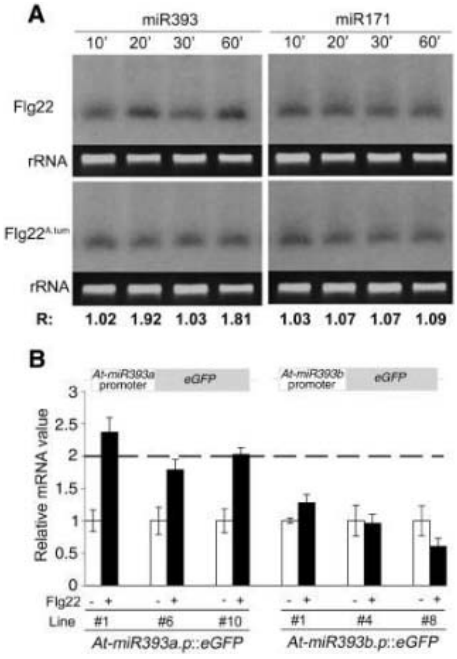

Fig. 2. Flg22 triggers miR393 induction mainly through transcriptional activation of *At-miR393a*. (**A**) Northern analysis of miR393 (left panels) and miR171 (right panels) upon treatment with flg22 (upper panels) or flg22$^{A.tum}$ (bottom panels). Col-0 seedlings were treated with either 10 μM flg22 or 10 μM flg22$^{A.tum}$. rRNA, ethidium bromide staining of ribosomal RNA; R, miRNA signal ratio between flg22-treated versus flg22$^{A.tum}$-treated samples at each time point. (**B**) Transcriptional activation of *At-miR393a* in response to flg22. T2 transgenic lines were treated for 60 min with either 10 μM flg22 (+) or 10 μM flg22$^{A.tum}$ (−). Bar graph representing the relative mRNA level of eGFP upon treatment with flg22 (+) versus flg22$^{A.tum}$ (−) as assayed by qRT-PCR. Error bars represent the standard deviation from three PCR results, and similar results were obtained in two independent experiments. *At-miR393a-p::eGFP* and *At-miR393b-p::eGFP* represent transgenic lines expressing miR393a and miR393b promoter-eGFP fusions, respectively. The dashed line indicates the twofold threshold induction observed in three independent flg22-treated *At-miR393a-p::eGFP* lines.

heat shock–inducible AXR3/IAA17 protein fused to the β-glucuronidase (GUS) reporter (HS::AXR3NT-GUS) (*17*). Seedlings were treated with either flg22 or flg22$^{A.tum}$ for 2 hours at 37°C and then stained for GUS. Flg22, but not flg22$^{A.tum}$, triggered stabilization of AXR3NT-GUS (Fig. 3B), starting from 1.5 hours after flg22 elicitation (Fig. 3C), which coincided with the TIR1-Myc repression (Fig. 3A).

Aux/IAA proteins repress auxin signaling through heterodimerization with Auxin Response Factors (ARFs) (*18*). Those transcription factors ARFs bind to auxin-responsive elements (AuxREs) in promoters of primary auxin-response genes and activate (or repress) transcription (*19*). The flg22-induced stabilization of AXR3/IAA17 prompted us to determine whether flg22 inhibits auxin-response gene activation. Seedlings were treated for 1.5 hours with either flg22 or flg22$^{A.tum}$, and transcripts of the primary auxin-response genes *GH3-like*, *BDL/IAA12*, and *AXR3/IAA17* were monitored by RT-qPCR. This time point was chosen on the basis of the flg22-induced stabilization profile of AXR3/IAA17 (Fig. 3C). All three auxin-response genes were repressed at this time point (Fig. 3D). Thus, flg22 triggers events that contribute to rapid down-regulation of primary auxin-response genes.

Does repression of auxin signaling enhance bacterial disease resistance? We tested, in a *tir1-1* mutant background, resistance in *Arabidopsis* transgenic lines that constitutively overexpress Myc epitope–tagged *AFB1* (*20*). These lines contain higher levels of AFB1 mRNA as compared with *tir1-1*, and exhibit high AFB1-Myc protein accumulation (Fig. 4A). The partial resistance of AFB1 mRNA to miR393, together with its constitutive overexpression, suggested that both AFB1 mRNA and AFB1-Myc would remain unaffected by flg22 treatment, which was confirmed in semiquantitative RT-PCR and Western analysis (Fig. 4, B and C). We anticipated that constitutive overexpression of AFB1 would prevent the miR393-mediated suppression of auxin signaling, perhaps resulting in enhanced disease sensitivity. When AFB1-Myc–overexpressing plants were inoculated with virulent *P. syringae* pv. tomato (Pto) DC3000, they had bacterial titers that were about 20-fold higher than those of nontransformed or *tir1-1* plants and they displayed enhanced disease symptoms (Fig. 4D, fig. S4A). Furthermore, no difference was observed with avirulent Pto DC3000 carrying *AvrRpt2*, which triggers race-specific resistance via resistance gene *RPS2* (Fig. 4E) (*21*). Thus, suppression of auxin signaling, mediated at least partly by miR393, might specifically promote resistance to virulent Pto DC3000 but is not implicated in race-specific resistance.

We also transformed *Arabidopsis* with a construct with *At-miR393a* constitutively transcribed from the strong 35*S* promoter (Fig. 4F). Three independent T2 transgenic lines were selected for high miR393 accumulation (Fig. 4F). These lines showed lower TIR1 mRNA levels than controls (Fig. 4F), and in older plants, they displayed reduced apical dominance with multiple shoots, reminiscent of auxin signaling mutants. However, these developmental alterations were minor compared with those observed in *tir1/afb* multiple mutants (*20*). Four days after inoculation with virulent Pto DC3000, all three miR393-overexpressing lines, but not the controls, displayed fivefold lower bacterial titer, confirming that miR393 restricts Pto DC3000 growth (Fig. 4G). There was no difference in bacterial growth on transgenic lines overexpressing an artificial miRNA directed against GFP (*22*) (Fig. 4G).

We show here that a bacterial PAMP down-regulates auxin signaling in *Arabidopsis* by targeting auxin receptor transcripts. Augmenting auxin signaling through overexpressing a *TIR1* paralog that is partially refractory to miR393 enhances susceptibility to virulent Pto DC3000, and, conversely, repressing auxin signaling through miR393 overexpression increases bacterial resistance. These results indicate that down-regulation of auxin signaling, resulting in ARF inactivation, is part of a plant-induced immune response (fig. S5). They also suggest that auxin promotes susceptibility to bacterial disease. This is consistent with other published findings. The tumorigenic *P. syringae* pv. *savastonoi* synthesizes high levels of indole-3-acetic acid (IAA) (*23*). Also, most *P. syringae* strains can produce IAA, and Pto DC3000 infection triggers increased IAA levels in *Arabidopsis* (*24*, *25*). Consistent with these observations, exogenous application of the auxin analog 2,4-dichlorophenoxyacetic acid enhances Pto DC3000 disease symptoms (fig. S4B).

In addition to the contribution of miR393 in flg22-triggered repression of auxin signaling, our analysis also reveals a miR393-

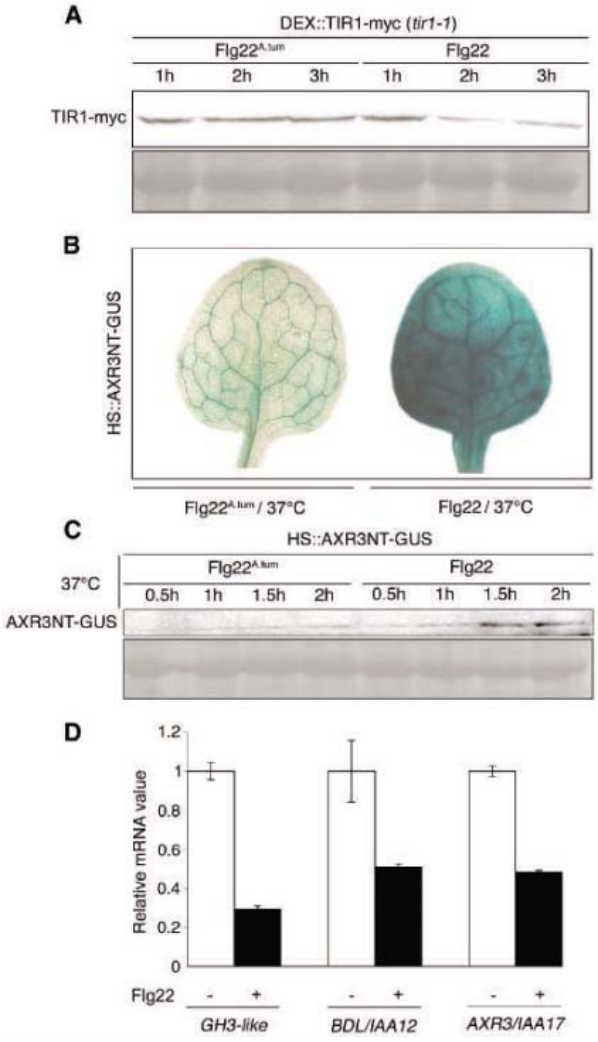

Fig. 3. Flg22 triggers repression of TIR1 protein, stabilization of AXR3/IAA17, and repression of three primary auxin-response transcripts. (**A**) TIR1-Myc repression in response to flg22. (Upper panel) Western analysis using a Myc-specific antibody (anti-Myc). (Bottom panel) Ponceau staining of total proteins. Similar results were obtained in two independent experiments. (**B**) AXR3/IAA17 stabilization in leaves. HS::AXR3NT-GUS seedlings were transferred for 2 hours at 37°C with either 10 μM flg22 (right leaf) or 10 μM flg22$^{A.tum}$ (left leaf). Similar results were obtained in five independent experiments. (**C**) Kinetics of AXR3/IAA17 stabilization. HS::AXR3NT-GUS seedlings were treated as in (B). (Upper panel) Western analysis using anti-GUS. (Bottom panel) Ponceau staining of total proteins. Similar results were obtained in two independent experiments. (**D**) Flg22 reduces accumulation of three primary auxin-response genes. Col-0 seedlings were treated for 1.5 hours with either 10 μM flg22 (+) or 10 μM flg22$^{A.tum}$ (−). qRT-PCRs were done to assess the relative mRNA level of GH3-like (At4g03400), BDL/IAA12 (At1g04550), and AXR3/IAA17 (At1g04250) upon flg22 as compared with flg22$^{A.tum}$ treatment. Error bars represent the standard deviation from four PCR results, and similar results were obtained in three independent experiments.

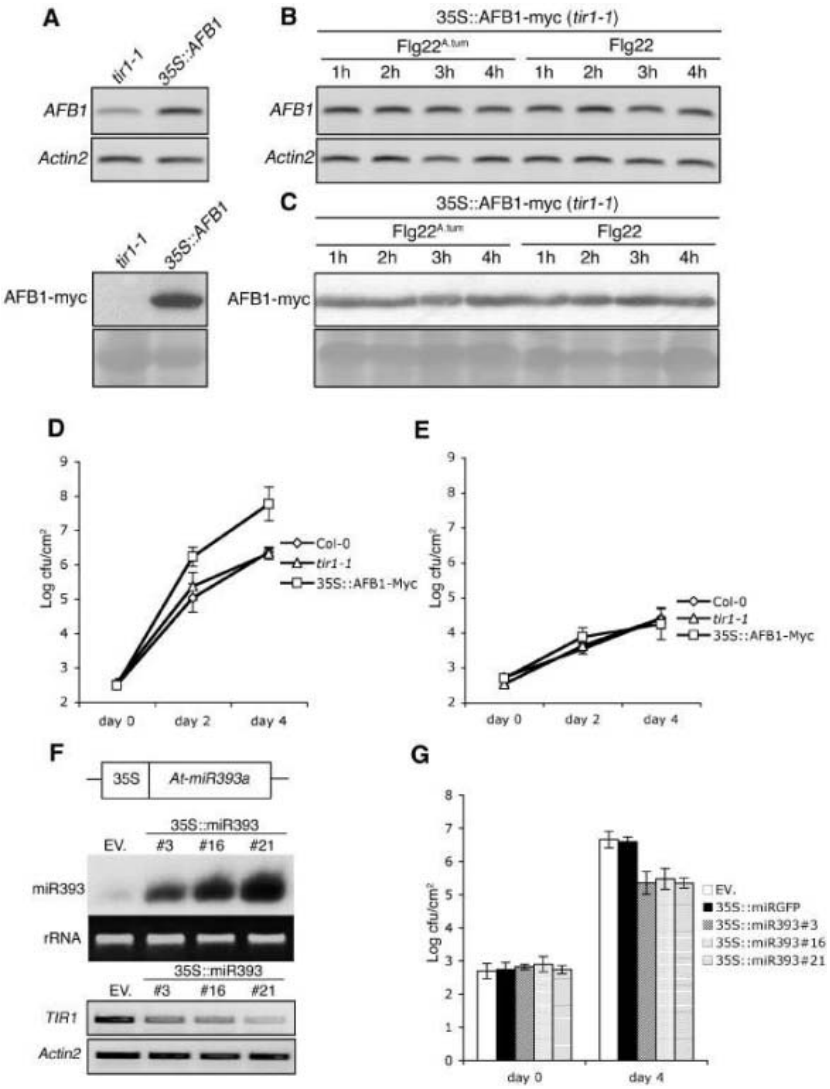

Fig. 4. Down-regulation of auxin signaling is required for Pto DC3000 disease resistance. (**A**) Molecular characterization of AFB1-overexpressing lines. (Upper panel) RT-PCR analysis of AFB1 transcript. (Bottom panel) Western analysis using anti-Myc. (**B**) AFB1 mRNA levels are not altered in AFB1-overexpressing lines treated with flg22. The 35S::AFB1-Myc seedlings were treated with either 10 μM flg22 or 10 μM flg22$^{A.tum}$. RT-PCR analysis was done as in (A). (**C**) AFB1-Myc protein levels are not altered in AFB1-overexpressing challenged lines. The 35S::AFB1-Myc seedlings were treated as in (B). (Upper panel) Western analysis using anti-Myc. (Bottom panel) Ponceau staining of total proteins. (**D**) Growth of Pto DC3000 on AFB1-overexpressing lines. Six-week-old plants were inoculated with 10^5 colony-forming units (cfu/ml) of bacteria. Error bars represent the standard error of log-transformed data from five independent samples, and similar results were obtained in three independent experiments. (**E**) Growth of Pto DC3000 (AvrRpt2) on AFB1-overexpressing lines. Inoculation was performed as in (D), and results are presented as in (D). Similar results were obtained in two independent experiments. (**F**) Molecular characterization of miR393-overexpressing lines. (Top panel) Schematic representation of the 35S::*At-miR393a* construct. (**G**) Growth of Pto DC3000 on miR393-overexpressing lines. Inoculation was performed as in (D). Similar results were obtained in two independent experiments. (Middle panel) Northern analysis of miR393 overexpression in independent T2 transgenic lines; EV, empty vector; rRNA, ethidium bromide staining of ribosomal RNA. (Bottom panel) RT-PCR of the TIR1 transcript.

independent pathway that probably involves transcriptional repression of *TIR1* and its paralogs. This is consistent with "mutual exclusion" in *Drosophila*, whereby miRNAs prevent unwanted expression of genes that become transcriptionally repressed in the miRNA-producing cells (*26*). Rapid induction of miR393 by flg22 might deplete TIR1 mRNAs present at the time of elicitation and thus confer robustness to the transcriptional repression provoked during elicitation. This regulatory feature has not previously been reported for plant miRNAs involved in development, and it will be interesting to establish if these observations on miR393 hold for other stress-induced miRNAs.

References and Notes

1. G. Felix, J. D. Duran, S. Volko, T. Boller, *Plant J.* **18**, 265 (1999).
2. L. Navarro *et al.*, *Plant Physiol.* **135**, 1113 (2004).
3. Z. Xie *et al.*, *PLoS Biol.* **2**, E104 (2004).
4. O. Borsani, J. Zhu, P. E. Verslues, R. Sunkar, J. K. Zhu, *Cell* **123**, 1279 (2005).
5. Z. Xie, E. Allen, A. Wilken, J. C. Carrington, *Proc. Natl. Acad. Sci. U.S.A.* **102**, 12984 (2005).
6. V. Gascioli, A. C. Mallory, D. P. Bartel, H. Vaucheret, *Curr. Biol.* **15**, 1494 (2005).
7. P. Dunoyer, C. Himber, O. Voinnet, *Nat. Genet.* **37**, 1356 (2005).
8. D. P. Bartel, *Cell* **116**, 281 (2004).
9. P. Dunoyer, C. H. Lecellier, E. A. Parizotto, C. Himber, O. Voinnet, *Plant Cell* **16**, 1235 (2004).
10. E. J. Chapman, A. I. Prokhnevsky, K. Gopinath, V. V. Dolja, J. C. Carrington, *Genes Dev.* **18**, 1179 (2004).
11. N. Dharmasiri, S. Dharmasiri, M. Estelle, *Nature* **435**, 441 (2005).
12. W. M. Gray *et al.*, *Genes Dev.* **13**, 1678 (1999).
13. S. Kepinski, O. Leyser, *Nature* **435**, 446 (2005).
14. M. W. Jones-Rhoades, D. P. Bartel, *Mol. Cell* **14**, 787 (2004).
15. R. Sunkar, J. K. Zhu, *Plant Cell* **16**, 2001 (2004).
16. A. M. Gustafson *et al.*, *Nucleic Acids Res.* **33**, D637 (2005).
17. W. M. Gray, S. Kepinski, D. Rouse, O. Leyser, M. Estelle, *Nature* **414**, 271 (2001).
18. E. Liscum, J. W. Reed, *Plant Mol. Biol.* **49**, 387 (2002).
19. G. Hagen, T. Guilfoyle, *Plant Mol. Biol.* **49**, 373 (2002).
20. N. Dharmasiri *et al.*, *Dev. Cell* **9**, 109 (2005).
21. M. C. Whalen, R. W. Innes, A. F. Bent, B. J. Staskawicz, *Plant Cell* **3**, 49 (1991).
22. E. A. Parizotto, P. Dunoyer, N. Rahm, C. Himber, O. Voinnet, *Genes Dev.* **18**, 2237 (2004).
23. T. Yamada *et al.*, in *Molecular Strategies of Pathogens and Host Plants*, D. L. Mills, C. Vance, S. Ouchi, S. S. Patil, Eds. (Springer, New York, 1991), pp. 83–94.
24. E. Glickmann *et al.*, *Mol. Plant Microbe Interact.* **11**, 156 (1998).
25. P. J. O'Donnell *et al.*, *Plant J.* **33**, 245 (2003).
26. A. Stark, J. Brennecke, N. Bushati, R. B. Russell, S. M. Cohen, *Cell* **123**, 1133 (2005).
27. Materials and methods are available as supporting material on *Science* Online.

28. We thank B. Kunkel and P. Brodersen for helpful comments and L. Buhot for technical advice. Supported by the Gatsby Foundation (J.D.G.J); a long-term Fellowship from the Federation of European Biochemical Societies and by the Gatsby Foundation (L.N.); an Action Thématique Incitative sur Programme grant from the CNRS and a grant from the trilateral génoplante–German Plant Genome Research Program–Spanish ministry of Research (P.D, F.J, and O.V); and by grants from NIH, NSF, and the U.S. Department of Energy (N.D and M.E.)

Supporting Online Material

www.sciencemag.org/cgi/content/full/312/5772/436/DC1
Materials and Methods
SOM Text
Figs. S1 to S5
References

10 February 2006; accepted 23 March 2006
10.1126/science.1126088

Nuclear Pores Form de Novo from Both Sides of the Nuclear Envelope

Maximiliano A. D'Angelo,* Daniel J. Anderson,* Erin Richard, Martin W. Hetzer†

Nuclear pore complexes are multiprotein channels that span the double lipid bilayer of the nuclear envelope. How new pores are inserted into the intact nuclear envelope of proliferating and differentiating eukaryotic cells is unknown. We found that the Nup107-160 complex was incorporated into assembly sites in the nuclear envelope from both the nucleoplasmic and the cytoplasmic sides. Nuclear pore insertion required the generation of Ran guanosine triphosphate in the nuclear and cytoplasmic compartments. Newly formed nuclear pore complexes did not contain structural components of preexisting pores, suggesting that they can form de novo.

Nuclear pore complexes (NPCs) are the exclusive sites of trafficking between the nucleus and the cytoplasm (*1*, *2*), and their biogenesis is crucial for the differentiation and metabolic activity of eukaryotic cells (*3*). In proliferating cells, the number of pores doubles during interphase before mitosis (*4*, *5*). It is unclear whether NPC assembly occurs from the nucleoplasmic and/or cytoplasmic side(s) of the nuclear envelope (NE) (*6*). It is also unknown whether existing NPCs serve as templates for new pores or whether NPCs assemble de novo (*7*–*9*).

To distinguish between these possibilities, we analyzed NPC assembly into intact NEs in vitro and in vivo. First, we established a cell-free NPC insertion assay using *Xenopus* egg extracts (*10*). We preassembled nuclei (NE-0) by incubating sperm chromatin and cytosol together with fluorescently labeled membranes (*11*). NE-0 nuclei were incubated for an additional period of 80 min (NE-80), during which growth and NE expansion occurred (Fig. 1A). Both NE-0 and NE-80 nuclei were intact and excluded 70-kD dextran (Fig. 1A). NPCs were monitored with monoclonal antibody mAb414, which recognizes four nucleoporins (Fig. 1A) (*12*). During nuclear growth, the density of NPCs remained constant at 4.9 ± 0.6 NPCs/μm^2, indicating that new NPCs had been inserted into the expanding NE.

Using three-dimensional (3D) reconstructions of entire nuclei and visualization of individual NPCs by immunofluorescence (fig. S1, A to C), we found that the NE expanded from 920 ± 104 μm^2 in NE-0 to 3100 ± 229 μm^2 in NE-80, and the number of NPCs increased from 4400 ± 651 to 15800 ± 1054 NPCs (Fig.

Salk Institute for Biological Studies, Molecular and Cell Biology Laboratory, 10010 North Torrey Pines Road, La Jolla, CA 92037, USA.

*These authors contributed equally to this work
†To whom correspondence should be addressed. E-mail: hetzer@salk.edu

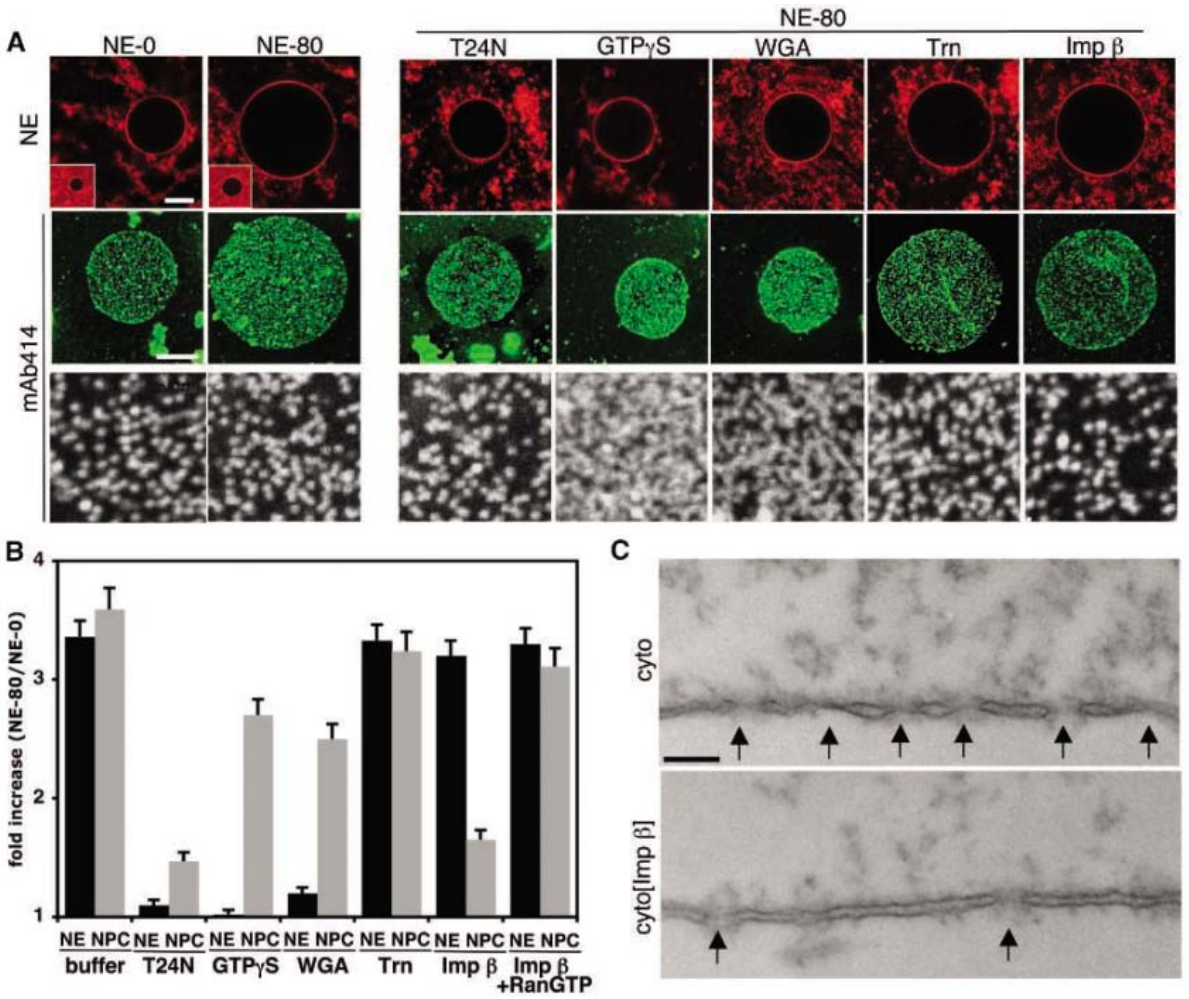

Fig. 1. Transport-independent role of Importin β in NPC insertion. (**A**) Nuclei (NE-0) were preassembled in 5-μl reactions including egg extracts, membranes, and sperm chromatin for 40 min (*17*), and diluted with 50 μl fresh cytosol in the absence or presence of 5 μM RanT24N, 2 mM GTPγS, WGA (20 μg/ml), 2 μM transportin (Trn), or Importin β (Imp β) (±10 μM RanGTP), for an additional 80 min (NE-80) and analyzed by confocal microscopy. The formation of a closed NE was analyzed in unfixed nuclei using the membrane stain $DiIC_{16}$ (1,1′dihexadecyl-3,3,3′,3′-tetramethylindocarbocyanine perchlorate) (*27*) and 70-kD dextran (small insert). Individual NPCs were visualized by immunofluorescence with mAb414 on the surface of the nuclei at low magnification (middle row) and with 8× zoom (bottom row). Scale bars, 10 μm. (**B**) NE surface area and total number of pores were calculated using five independent experiments as described in (*28*). The relative increase of surface area (black) and pore numbers (gray) during 80 min were plotted. Error bars indicate SD. (**C**) Nuclei were assembled in the absence (buffer) and presence of 2 μM Importin β, sectioned, and analyzed by transmission electron microscopy (*17*). Scale bar, 200 nm. Cyto, cytosol.

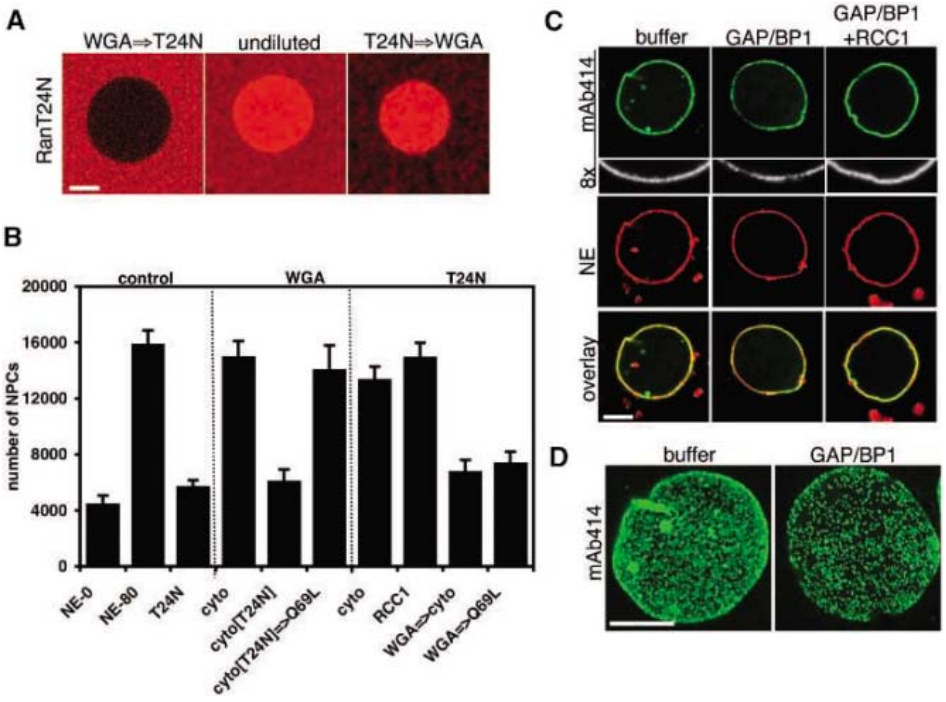

Fig. 2. RanGTP-mediated incorporation of Nup107-160 complex occurs from the nucleoplasmic and cytoplasmic side of the NE. (**A**) Fluorescently labeled RanT24N accumulated in assembled nuclei and was trapped in the nucleoplasm of WGA-sealed nuclei after dilution (T24N ⇒ WGA). RanT24N was excluded from the nucleoplasm when added after the NPCs were blocked with WGA (WGA ⇒ T24N). Scale bar, 10 μm. (**B**) The area labeled "control" shows the quantification of total pore numbers of NE-0 and NE-80 nuclei. The area labeled "T24N" shows data for NE-0 nuclei that were incubated with 5 μM RanT24N for 10 min. NPC insertion was induced with 200 volumes of cytosol (cyto) or 5 μM RCC1. To trap RanT24N inside the nucleus, NPCs were sealed with WGA (20 μg/ml) for 10 min, and NPC insertion was then induced by adding cytosol (WGA ⇒ cyto) or 5 μM RanGTP (WGA ⇒ RanQ69L). The area labeled "WGA" shows data for NE-0 nuclei that were incubated with WGA (20 μg/ml) for 10 min before the addition of cytosol (cyto), cytosol that contained 5 μM RanT24N (cyto[T24N]), or RanT24N and RanQ69L (cyto[T24N] ⇒ Q69L). The number of NPCs was quantified as described in Fig. 1. (**C**) NE-0 nuclei were incubated in the absence or presence of 5 μM RanGAP-RanBP1 or RanGAP-RanBP1 plus 5 μM RCC1 as indicated. Nuclei were stained with mAb414 (green) and $DiIC_{16}$ (red) and analyzed in cross sections or (**D**) on the NE surface to visualize individual NPCs. Scale bars, 10 μm.

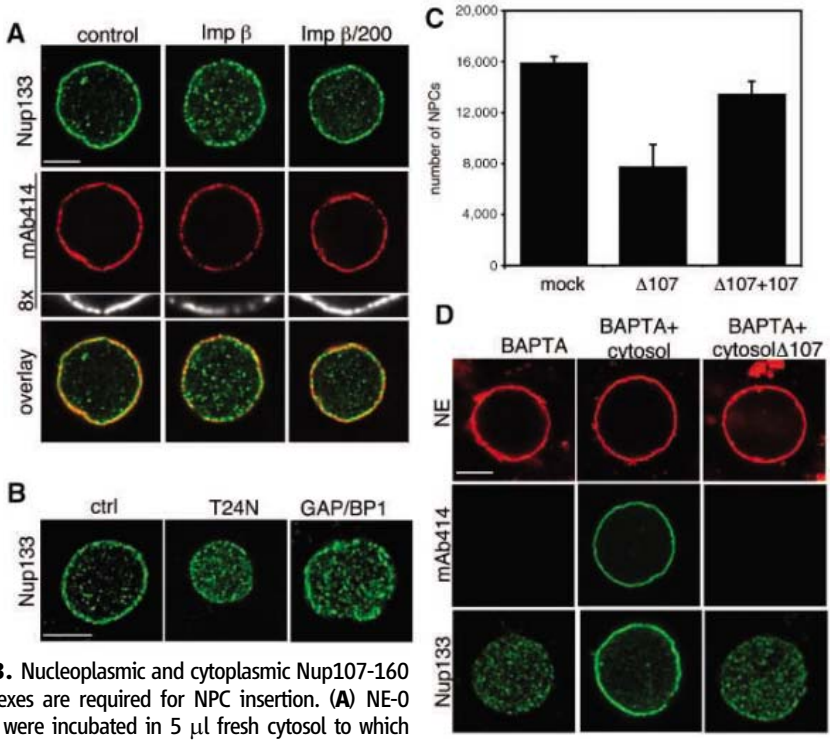

Fig. 3. Nucleoplasmic and cytoplasmic Nup107-160 complexes are required for NPC insertion. (**A**) NE-0 nuclei were incubated in 5 μl fresh cytosol to which buffer or 2 μM Importin β had been added, and nuclei were analyzed after 80 min by immunofluorescence using αNup133 and mAb414. To reverse the inhibitory effect of Importin β, NE-80 nuclei were diluted in 200 volumes of cytosol. Scale bar, 10 μm. (**B**) Nuclei were assembled in the presence of Importin β, and subsequently diluted in 200 volumes of cytosol (buffer), cytosol containing 5 μM RanT24N, or 10 μM RanGAP-RanBP1 for 30 min. Nuclei were analyzed by immunofluorescence using αNup133. Scale bar, 10 μm. (**C**) NE-0 nuclei were incubated at room temperature with mock-depleted or Nup107-160–depleted cytosol (in the absence or presence of purified Nup107-160 complex), and the total number of NPCs was quantified as in Fig. 1. Error bars indicate SD. (**D**) Nuclear assembly was performed using $DiIC_{16}$-labeled NE membranes, sperm chromatin, and cytosol in the presence of 5 mM BAPTA for 60 min, and the nuclei were diluted with mock-depleted cytosol or Nup107-160–depleted cytosol. NPCs were visualized with mAb414 and αNup133. Scale bar, 10 μm.

1, A and B). NPC insertion occurred steadily at a rate of 142 ± 11 NPCs/min.

The insertion of new pores into intact nuclei occurs in the presence of nucleo-cytoplasmic transport, which is driven by the small guanosine triphosphatase (GTPase) Ran (*2*, *13*). To test whether Ran-mediated transport was required for pore formation, we incubated NE-0 nuclei with cytosol in presence of RanT24N, a Ran mutant (where Thr^{24} is replaced by Asn) that blocks the generation of RanGTP (*14*). NPC insertion, NE expansion (Fig. 1, A and B), and Ran-mediated nuclear transport (fig. S1D) were all strongly inhibited. The addition of two transport inhibitors—a nonhydrolyzable GTP analog (GTPγS) and wheat germ agglutinin (WGA), which blocks pores by binding to nucleoporins that contain *N*-acetylglucosamine residues (*12*, *15*)—both inhibited nuclear import of bovine serum albumin–nuclear localization signal (BSA-NLS) (fig. S1D) and NE expansion (Fig. 1B). However, new NPCs were still efficiently inserted (Fig. 1, A and B), and the NPC density increased from 4.9 ± 0.6 to 10.3 ± 1.4 NPCs/μm² in the presence of GTPγS and to 8.3 ± 0.5 NPCs/μm² in the presence of WGA (Fig. 1, A and B). Thus, NPC insertion in vitro requires RanGTP but can occur in the absence of the nuclear transport activity of existing pores and NE expansion.

NPC assembly into the reforming NE at the end of mitosis is negatively regulated by the nuclear transport receptor Importin β (*16*, *17*). We wanted to test Importin β's effect on new NPC insertion. In the presence of 2 μM Importin β, neither NE expansion (Fig. 1, A and B) nor nuclear import of BSA-NLS (fig. S1D)

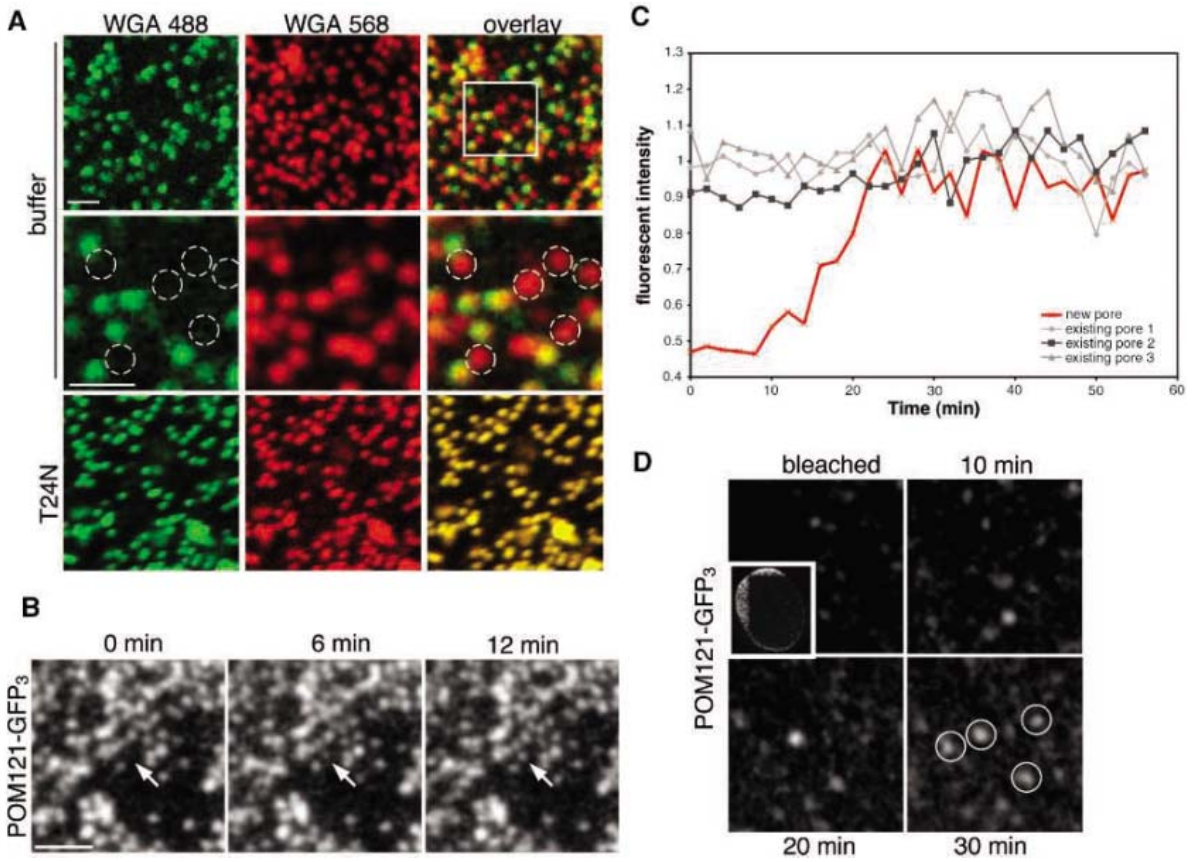

Fig. 4. NPC insertion occurs by a de novo mechanism. (**A**) NE-0 nuclei were labeled with fluorescently labeled WGA-488 (10 μg/ml) for 10 min and subsequently incubated with 400 volumes of cytosol in the absence or presence of 5 μM RanT24N for 30 min. Fluorescently labeled WGA-568 was added for 10 min, and nuclei were analyzed by confocal microscopy. Newly formed pores are visible as red dots; they do not contain a detectable green signal. Scale bar, 1 μm. (**B**) HeLa cells expressing POM121-(GFP_3) were analyzed in real time by confocal microscopy on the NE surface every 2 min. Arrows indicate new NPC assembly site. (**C**) Relative fluorescence intensity of preexisting pores (gray) and new pores (red) was plotted against time. (**D**) Large areas of NEs were photobleached (inset), and the formation of few pores was monitored by 4D confocal microscopy. Bleached POM121-(GFP_3) did not recover for more than 4 hours, similar to previously published report (*29*).

were affected. However, NPC insertion was strongly inhibited when compared with control reactions containing transportin, an import receptor not involved in NPC assembly (Fig. 1, A and B) (*17*). The pore density dropped from 4.9 ± 0.6 NPCs/μm² in control reactions to 2.2 ± 0.4 NPCs/μm² in the presence of Importin β, an effect that was restored by 10 μM RanGTP (Fig. 1, A and B). Thus, Importin β negatively regulates NPC insertion into intact nuclei in a transport-independent manner.

To analyze from which sides of the NE nucleoporins were inserted, RanGTP production had to be blocked only in the cytoplasm or only in the nucleoplasm. First, NE-0 nuclei were assembled, and the existing pores were sealed with WGA at a concentration of 20 μg/ml before adding either cytosol or cytosol-containing 5 μM RanT24N. RanT24N inhibited NPC insertion (Fig. 2B), even though it was excluded from the nucleus (Fig. 2A). NPC assembly was restored by the addition of 5 μM RanQ69L (where Gln^{69} is replaced by Leu), a GTPase-deficient mutant of Ran (*18*, *19*), or by 5 μM Ran's nucleotide exchange factor RCC1 (Fig. 2B), demonstrating that RanT24N specifically inhibited endogenous cytoplasmic RCC1.

Second, we added recombinant RanGAP-RanBP1 complex [Ran's GTPase activating protein (GAP) and its co-factor RanBP1 (*14*)], which are excluded from the nucleus (*20*) to deplete cytoplasmic RanGTP. NPC insertion was blocked, but unlike the case with RanT24N, neither nuclear transport (fig. S1D) nor NE expansion were affected (Fig. 2C), and consequently, the pore density decreased (Fig. 2D). Thus, RanGTP, as previously suggested [see discussion in (*21*)], plays a cytoplasmic role in NPC insertion in vitro.

To inhibit nuclear RCC1, we incubated NE-0 nuclei with RanT24N, which accumulated in the nucleoplasm (Fig. 2A) and inhibited NPC insertion (Fig. 2B). After 10 min, either buffer or WGA was added to the reactions to seal the pores. When the WGA-treated nuclei were incubated with 200 volumes of fresh cytosol, RanT24N in the cytosol was diluted to noninhibitory levels. The concentration of RanT24N trapped inside the nucleus was unaffected (Fig. 2A), and NPC insertion was not restored (Fig. 2B). In contrast, nuclei that were diluted in the absence of WGA efficiently inserted new NPCs (Fig. 2B). Thus, the generation of RanGTP inside the nucleus is required for NPC insertion. Taken together, these results suggest that NPC assembly in egg extracts involves Ran-dependent steps on both sides of the NE. Whether somatic cells, which do not appear to have cytoplasmic RCC1 and RanGTP, use a different NPC insertion mechanism remains to be analyzed.

Our results imply a model in which RanGTP-mediated release of nucleoporins from Importin β (*17*) occurs in both the nucleoplasmic and cytoplasmic compartment. To test whether soluble Importin β–binding nucleoporins, such as the Nup107-160 complex (*17*), are indeed present in both compartments, we stained NE-80 nuclei with antibodies against several nucleoporins (Fig. 3A and fig. S2). We detected a strong NE rim staining for all of them and an additional nucleoplasmic signal specifically with antibodies to Nup133 and Nup160, two components of the Nup107-160 complex, which has been shown to be essential for NPC formation (Fig. 3A) (*22*, *23*). When the assembly of new pores into NE-0 nuclei was blocked by adding Importin β, an increase in nucleoplasmic Nup107-160 signal was observed, whereas the rim signal was reduced (Fig. 3A and fig. S2A). Diluting the nuclei with 200 volumes of fresh cytosol or the addition of RanGTP (*24*) reversed this effect, even when nuclear transport was blocked by WGA (Fig. 3B and fig. S2B). Similarly, the nucleoplasmic Nup107-160 signal increased when NPC insertion was blocked with RanT24N or RanGAP-RanBP1 (Fig. 2B), suggesting that the nucleoplasmic pool of Nup107-160, which is essential for pore formation (*23*), was not incorporated into the NE when RanGTP production was blocked.

Next we analyzed whether Nup107-160 complexes were incorporated from the cytoplasmic side of the NE. We assembled NE-0

nuclei and subsequently added WGA to seal the existing pores. A nucleoplasmic signal was detectable when these nuclei were stained with αNup133 and αNup160 (*24*). In contrast to mock-depleted cytosol, Nup107-160–depleted cytosol did not induce the assembly of new pores (Fig. 3C). This lack of activity was caused by the absence of Nup107-160, because the addition of purified Nup107-160 complex (fig. S2C) restored NPC insertion (Fig. 3C).

Nuclei were formed in the presence of BAPTA (1,2-bis(2-aminophenoxy)ethane-*N*,*N*,*N*′,*N*′-tetraacetic acid), a calcium chelator that inhibits NPC formation (*25*), and a strong nucleoplasmic Nup133 signal was detected (Fig. 3D). When the BAPTA nuclei were diluted in mock-depleted cytosol, NPC insertion was restored, whereas Nup107-160–depleted cytosol failed to do so (Fig. 3D). Consistent with the cytoplasmic RanGTP-mediated release of Importin β from the Nup107-160 complex, we found that the addition of 5 μM RanT24N resulted in a 60% increase of Importin β associated with immunoprecipitated Nup107-160 complex (*24*). Thus, the incorporation of the Nup107-160 complex into new assembly sites occurs from both sides of the NE. Because nuclear transport is not required for NPC insertion in vitro, the nucleoplasmic pool of Nup107-160 complexes might be generated via chromatin association during nuclear assembly (*17*).

Next we wanted to analyze if pores assemble de novo or by the splitting of existing pores (*7*–*9*). We assembled NE-0 nuclei and subsequently fluorescently labeled individual pores with WGA-488 (green) (Fig. 4A). Upon dilution, WGA-488 remained stably bound to NPCs while new unlabeled pores were inserted (fig. S3A), which could be labeled with WGA-568 (red). Newly formed pores were only labeled with WGA-568 and appeared as red dots, whereas old pores were labeled with both dyes resulting in a yellow overlay. The new pores did not exhibit green signal from existing pores, suggesting that NPCs form de novo (Fig. 4A). When the formation of new pores was blocked by the addition of 5 μM RanT24N, all pores appeared yellow in the overlay (Fig. 4A), indicating that red dots represented newly formed pores. Furthermore, the average fluorescence intensity of WGA-488–labeled NPCs remained constant after dilution of the dye, and it was indistinguishable between nuclei that inserted new pores and nuclei where the formation of new NPCs was blocked by 5 μM RanT24N (fig. S3B). These results suggest that newly formed pores do not incorporate nucleoporins from existing NPCs, and they support a de novo mechanism, because in a splitting process, the intensity of the old pores would be expected to decrease. Additionally, we were able to detect pores that stained with αPOM121, a transmembrane nucleoporin, and Nup133, but not with mAb414 (fig. S3C). POM121 colocalized with mAb414 when the formation of new NPCs was blocked by RanT24N (fig. S3C). This indicates that phenyl-glycyl–repeat nucleoporins are recruited to new assembly sites after POM121 and Nup107-160 complexes have been incorporated and further supports de novo formation.

To determine whether NPC formation in vivo also occurs by a de novo mechanism, we generated a stable HeLa cell line expressing low, nontoxic levels of POM121 containing multiple copies of green fluorescent protein (GFP) to visualize individual NPCs in living cells (*26*). Four-dimensional confocal time-lapse microscopy was used to follow NPC assembly during interphase and new pores became visible as single dots in areas where initially no GFP signal was detectable (Fig. 4B and Movie S1) and in areas where preexisting pores have been photobleached (Fig. 4D). New NPCs colocalized with neighboring, preexisting pores along the *z* axis (fig. S4, A and B), showing that they were inserted into the NE. Consistent with de novo formation, existing pores did not change fluorescence intensity over time (Fig. 4C). These findings further support a de novo mechanism for NPC biogenesis.

References and Notes

1. S. R. Wente, *Science* **288**, 1374 (2000).
2. D. Gorlich, U. Kutay, *Annu. Rev. Cell Dev. Biol.* **15**, 607 (1999).
3. G. G. Maul, L. L. Deaven, J. J. Freed, G. L. Campbell, W. Becak, *Cytogenet. Cell Genet.* **26**, 175 (1980).
4. G. G. Maul *et al.*, *J. Cell Biol.* **55**, 433 (1972).
5. M. Winey, D. Yarar, T. H. Giddings Jr., D. N. Mastronarde, *Mol. Biol. Cell* **8**, 2119 (1997).
6. B. Burke, J. Ellenberg, *Nat. Rev. Mol. Cell Biol.* **3**, 487 (2002).
7. M. Hetzer, T. C. Walther, I. W. Mattaj, *Annu. Rev. Cell Dev. Biol.* (2005).
8. K. Bodoor *et al.*, *Biochem. Cell Biol.* **77**, 321 (1999).
9. G. Rabut, P. Lenart, J. Ellenberg, *Curr. Opin. Cell Biol.* **16**, 314 (2004).
10. M. J. Lohka, Y. Masui, *Science* **220**, 719 (1983).
11. M. Hetzer, D. Bilbao-Cortes, T. C. Walther, O. J. Gruss, I. W. Mattaj, *Mol. Cell* **5**, 1013 (2000).
12. L. I. Davis, G. Blobel, *Proc. Natl. Acad. Sci. U.S.A.* **84**, 7552 (1987).
13. M. Dasso, *Curr. Biol.* **12**, R502 (2002).
14. C. Klebe, H. Prinz, A. Wittinghofer, R. S. Goody, *Biochemistry* **34**, 12543 (1995).
15. D. R. Finlay, E. Meier, P. Bradley, J. Horecka, D. J. Forbes, *J. Cell Biol.* **114**, 169 (1991).
16. A. Harel *et al.*, *Mol. Biol. Cell* **14**, 4387 (2003).
17. T. C. Walther *et al.*, *Nature* **424**, 689 (2003).
18. F. R. Bischoff, C. Klebe, J. Kretschmer, A. Wittinghofer, H. Ponstingl, *Proc. Natl. Acad. Sci. U.S.A.* **91**, 2587 (1994).
19. C. Klebe, F. R. Bischoff, H. Ponstingl, A. Wittinghofer, *Biochemistry* **34**, 639 (1995).
20. D. Gorlich, *Curr. Opin. Cell Biol.* **9**, 412 (1997).
21. K. J. Ryan, J. M. McCaffery, S. R. Wente, *J. Cell Biol.* **160**, 1041 (2003).
22. A. Harel *et al.*, *Mol. Cell* **11**, 853 (2003).
23. T. C. Walther *et al.*, *Cell* **113**, 195 (2003).
24. M. A. D'Angelo, D. J. Anderson, E. Richard, M. W. Hetzer, data not shown.
25. C. Macaulay, D. J. Forbes, *J. Cell Biol.* **132**, 5 (1996).
26. N. Daigle *et al.*, *J. Cell Biol.* **154**, 71 (2001).
27. M. Hetzer *et al.*, *Nat. Cell Biol.* **3**, 1086 (2001).
28. Materials and methods are available as supporting material on *Science* Online.
29. G. Rabut, V. Doye, J. Ellenberg, *Nat. Cell Biol.* **6**, 1114 (2004).

30. Antibodies against Importin β were kindly provided by L. Gerace. We thank the members of our laboratory and T. Hunter for helpful discussions and W. Eckhart, J. Karlseder, V. Lundblad, J. Young, B. Sefton, and M. Weitzman for critically reading the manuscript. M.A.D and M.H. were supported by The Pew Charitable Trust.

Supporting Online Material

www.sciencemag.org/cgi/content/full/312/5772/440/DC1
Materials and Methods
Figs. S1 to S4
Movie S1

22 December 2005; accepted 14 March 2006
10.1126/science.1124196

Differential Targeting of Gβγ-Subunit Signaling with Small Molecules

Tabetha M. Bonacci,[1] Jennifer L. Mathews,[1] Chujun Yuan,[2] David M. Lehmann,[1] Sundeep Malik,[1] Dianqing Wu,[3] Jose L. Font,[1] Jean M. Bidlack,[1] Alan V. Smrcka[1,2]*

G protein βγ subunits have potential as a target for therapeutic treatment of a number of diseases. We performed virtual docking of a small-molecule library to a site on Gβγ subunits that mediates protein interactions. We hypothesized that differential targeting of this surface could allow for selective modulation of Gβγ subunit functions. Several compounds bound to Gβγ subunits with affinities from 0.1 to 60 μM and selectively modulated functional Gβγ-protein-protein interactions in vitro, chemotactic peptide signaling pathways in HL-60 leukocytes, and opioid receptor–dependent analgesia in vivo. These data demonstrate an approach for modulation of G protein–coupled receptor signaling that may represent an important therapeutic strategy.

The βγ subunits of heterotrimeric guanine nucleotide binding proteins (G proteins) are released upon ligand activation of G protein–coupled receptors (GPCRs). Free Gβγ subunits bind and regulate multiple target proteins within the cell—including phospholipase C (PLC) β2 and PLC β3, phosphoinositide 3 kinase (PI3K) γ, adenylyl cyclase, N-type Ca^{2+} channels, and inwardly rectifying K^+ channels—and mediate physiological

processes such as neutrophil chemotaxis, vascular cell proliferation, and cardiac chronotropy (*1*, *2*).

To investigate the molecular nature of Gβγ-target recognition, we screened random-peptide phage display libraries for binding to $G\beta_1\gamma_2$ and identified a series of peptides that bound to a single preferred protein-protein interaction surface ("hotspot") on Gβ (*3*). One of the peptides (SIRK) blocked Gβγ-dependent regulation of PLCβ2 and PI3Kγ but not regulation of type I adenylyl cyclase or N-type Ca^{2+} channels, thus demonstrating the potential for selective targeting of Gβγ signaling. The crystal structure of $G\beta_1\gamma_2$ in a complex with a SIRK peptide derivative (SIGK) reveals the preferred interaction surface as a region overlapping the Gα-switch II domain binding surface on top of the Gβ propeller (*4*–*6*). Subclasses of peptides appeared to bind distinct subsurfaces of the hotspot and differentially affect G protein subunit interactions. Many Gβγ effectors also use diverse mechanisms for binding within this surface (*7*, *8*), and because peptides showed some selectivity, we hypothesized that small organic molecules also might selectively modulate Gβγ-target interactions.

We used FlexX virtual screening software (*9*) in the Sybyl molecular modeling package to dock 1990 compounds in the chemical diversity set from the National Cancer Institute (NCI) to the interaction hotspot of $G\beta_1\gamma_2$. The diversity library was designed to contain chemical core structures representative of the larger 250,251-compound library from NCI. The docked models were ranked using five scoring functions in C-Score: D-score, G-score, F-score, Chemscore, and PMF-score (*10*). Two consensus scores that equally weight the five scoring functions were also used to rank the compounds. The top 1% of compounds from each scoring function (85 compounds total) were tested for their ability to compete with phage-displaying SIGK for binding to biotinylated $G\beta_1\gamma_2$ ($bG\beta_1\gamma_2$) in an enzyme-linked immunosorbent assay (ELISA) (*3*). Nine of the 85 compounds inhibited SIGK binding with median inhibitory concentration (IC_{50}) values ranging from 100 nM to 60 μM (Fig. 1B and table S1).

One compound, M119, with a high apparent affinity for $bG\beta_1\gamma_2$ (ELISA IC_{50} = 200 nM) (Fig. 1, B and C, and table S1) was selected as a lead to define structure-activity requirements (SAR) for binding to $G\beta_1\gamma_2$. Twenty-one compounds from the NCI library with similar structures to M119 were tested for relative $G\beta_1\gamma_2$ binding affinities (Fig. 1C and table S2). For example, the apparent affinity of M119B for $bG\beta_1\gamma_2$ is $^1/_{1000}$ that of M119, with the key chemical difference being the loss of two hydroxyl groups. Thus, specific chemical characteristics may be required for interactions with the Gβγ hotspot. We next tested whether M119 could disrupt protein interactions with a bona fide Gβγ binding partner, $G\alpha_{i1}$. The hotspot for protein interaction overlaps with the Gα switch II binding surface on Gβγ. The overall $G\alpha_{i1}$-βγ interaction surface spans 1800 $Å^2$ (*5*, *6*), and the dissociation constant (K_d) for $G\alpha_{i1}$ binding to Gβγ is ~1 nM (*11*). M119 competed with fluorescein isothiocyanate (FITC)–α_{i1} ($F\alpha_i$) for binding to $bG\beta_1\gamma_2$ with an IC_{50} value of 400 nM (Fig. 1D). However, unlike SIGK and related peptides that bind to this surface (*12*), M119 did not promote dissociation of $G\alpha_i$ from Gβγ (fig. S1).

FlexX docking software predicted that compounds M201 and M119 (Fig. 1C) bound to distinct subsurfaces in the hotspot, but M201 did not compete for SIGK binding. Nevertheless, we tested M119 and M201 in in vitro reconstitution assays of Gβγ-dependent activation of PLCβ2, PLCβ3, and PI3Kγ and binding to GRK2. M119 attenuated $G\beta_1\gamma_2$-dependent activation of PLCβ2 (IC_{50} value of 3 μM), PLCβ3, and PI3Kγ (Fig. 2, A to C, left panels). M201, on the other hand, did not affect PLCβ2 activation by $G\beta_1\gamma_2$ but potentiated $G\beta_1\gamma_2$-dependent activation of both PLCβ3 and PI3Kγ (Fig. 2, A to C, right panels). M119 also inhibited direct binding of $bG\beta_1\gamma_2$ to PLCβ2 and PLCβ3, whereas M201 did not block binding of PLCβ2 and enhanced binding of PLCβ3 to $G\beta_1\gamma_2$ (fig. S2). M119 and M201 both inhibited GRK2 binding to $bG\beta_1\gamma_2$ with similar IC_{50} values of approximately 5 μM (Fig. 2D). A weakly binding compound M119B (Fig. 1C and table S2) did not have effects in these assays (fig. S3). These

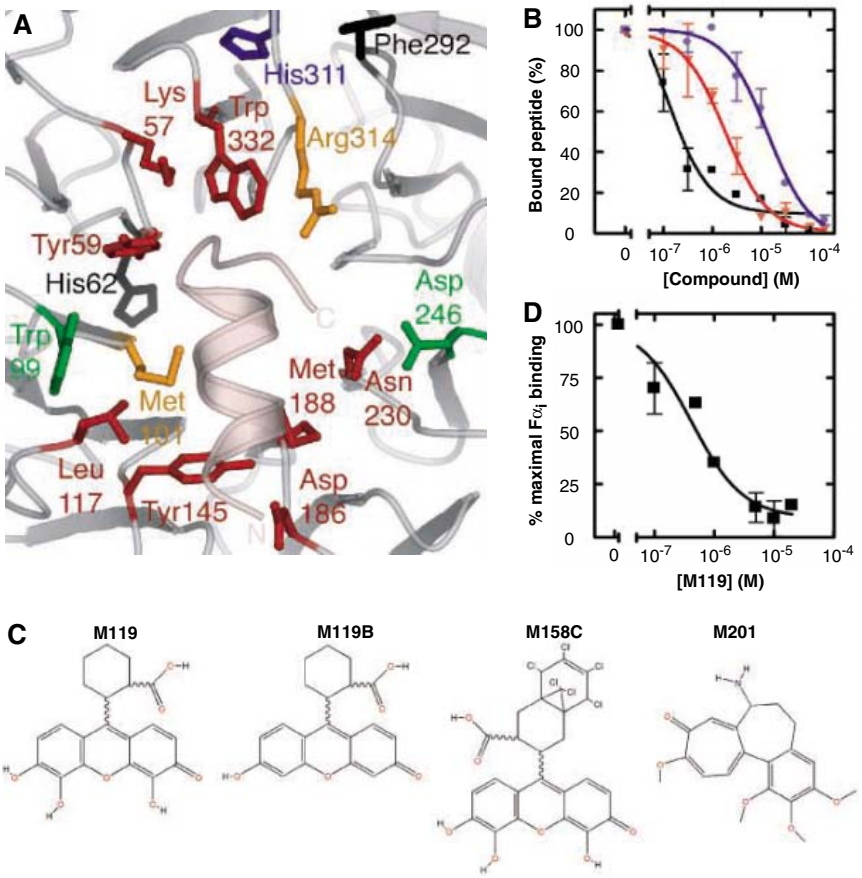

Fig. 1. Small molecule binding to the hotspot on Gβγ. (**A**) Structure of SIGK bound to Gβγ at the hotspot. Amino acids within 6.5 Å of SIGK were targeted with the FlexX module of Sybyl virtual docking software. (**B**) Competition ELISA data for three of the compounds identified in the virtual screen. Compounds were tested for their ability to inhibit binding of a phage displaying the peptide SIGKAFKILGYPDYD (*3*, *4*). M119 (NSC119910) (squares); M109 (NSC109208) (triangles); M117 (NSC117079) (circles). Data for all the binding compounds are summarized in table S1. (**C**) Structures of representative βγ-binding compounds. (**D**) Competition of M119 for interactions between $G\alpha_{i1}$ and $G\beta_1\gamma_2$. F-α_{i1} and M119 were simultaneously added to $bG\beta_1\gamma_2$ immobilized on streptavidin beads. The amount of bead-based fluorescence was assessed by flow cytometry as described (*11*, *12*).

[1]Department of Pharmacology and Physiology and [2]Department of Biochemistry and Biophysics, University of Rochester School of Medicine and Dentistry, Rochester, NY 14642, USA. [3]Department of Genetics and Developmental Biology, University of Connecticut Health Center, Farmington, CT 06030, USA.

*To whom correspondence should be addressed. E-mail: Alan_Smrcka@URMC.rochester.edu

data suggest that both M201 and M119 bind to Gβγ but differentially modulate Gβγ interactions with effectors. These are only two of multiple diverse compounds identified, which suggests the potential for multiple modes of Gβγ-dependent target modulation by these small molecules.

To test the effects of differentially targeting Gβγ on GPCR signaling in intact cells, M119 (and a similar compound, M158C) (Fig. 1C and table S2) and M201 were tested for their ability to modulate fMLP receptor–dependent signaling in differentiated HL-60 leukocytes. The fMLP receptor couples to Gi in these cells and activates PLCβ2 (PLCβ3 is a minor isoform in these cells), PI3Kγ, and ERK through Gβγ signaling (*13*, *14*). Pretreatment of differentiated HL-60 cells with M119 and M158C (Fig. 3A and fig. S4A), but not M201 (Fig. 3B and fig. S4B), attenuated fMLP-induced Ca^{2+} increases. M119 had no effect on carbachol-dependent increases in Ca^{2+} in HEK293 cells stably expressing the Gq-linked M3-muscarinic receptor, confirming a specific effect of M119 on Gβγ-dependent Ca^{2+} mobilization (fig. S4C). fMLP-dependent GRK2 translocation to the membrane fraction of HL-60 cells, on the other hand, was substantially inhibited by incubation with either M119 or M201 (Fig. 3C). Thus, M119 and M201 differentially modulate PLCβ2 regulation by Gβγ, yet both inhibit GRK2 binding in intact cells.

To assess the ability of M119 and M158C to inhibit fMLP receptor–dependent regulation of PI3Kγ activation, we stimulated HL-60 cells stably overexpressing a green fluorescent protein (GFP)–tagged pleckstrin homology (PH) domain from Akt (*15*) with fMLP and assessed translocation of the GFP-PHAkt to the membrane by subcellular fractionation and Western blotting. The PH domain from Akt binds to PIP_3 produced by PI3K activity at the membrane. Pretreatment of the cells with 10 μM of M119 or M158C inhibited fMLP-dependent translocation of GFP-PHAkt to the membrane (Fig. 3D), consistent with the ability of these compounds to inhibit activation of PI3Kγ by Gβγ.

Stimulation of differentiated HL-60 cells with fMLP also results in pertussis toxin–sensitive activation of various MAP kinases, including ERK1 and ERK2, p38, and JNK (*16*). However, pretreatment of HL-60 cells with M119, M158C, and M201 did not block fMLP-induced activation of ERK1 and ERK2 (Fig. 3E). Ca^{2+} mobilization occurred at low fMLP (100 nM) concentrations relative to that required to observe ERK1 and ERK2 (1 μM) activation, indicating that the selective lack of effect of M119 on ERK activation is not due to excess G protein activation.

We tested the efficacy of our compounds in an in vivo model. Compared with wild-type animals, PLCβ3$^{-/-}$ mice are 10 times as sensitive to the antinociceptive effects of the μ-agonist morphine (*17*). Because M119 blocks Gβγ-dependent activation of PLCβ3, we tested whether coadministration of M119 with morphine would also increase morphine-induced antinociception. Coadministration of M119 with morphine intracerebroventricularly resulted in an 11-fold increase in the analgesic potency of morphine (Fig. 4A) [ED_{50} values and 95% confidence limits: 0.069 (0.023 to 0.201) nmol and 0.743 (0.341 to 1.62) nmol, respectively], whereas administration of 100 nmol M119 alone had no effect on baseline antinociception (table S3). M119 also had no effect on morphine-dependent antinociception in PLCβ3$^{-/-}$ mice (Fig. 4B). These data highlight the specificity of M119 actions and the selective nature of M119 both in vitro and in vivo. Gβγ subunits regulate many aspects of signaling critical for the actions of opioid agonists (*18*). If M119 were globally blocking Gβγ subunit functions, we expect that morphine-induced antinociception would have been attenuated rather than potentiated with M119 coadministration.

Protein interaction interfaces present difficult drug targets because of the generally large interaction surface area and flat topology of the interaction surfaces. Hotspots at protein interfaces comprise a small fraction of the overall interaction surface, yet are responsible for most of the energetics of binding, and it has been proposed that targeting such surfaces could successfully disrupt protein-protein binding (*19*). As a result of extensive screening, some protein interaction interfaces have been targeted with small molecules (*19*–*21*). Our screen of only 1990 molecules identified multiple compounds with apparent affinities in the high nM

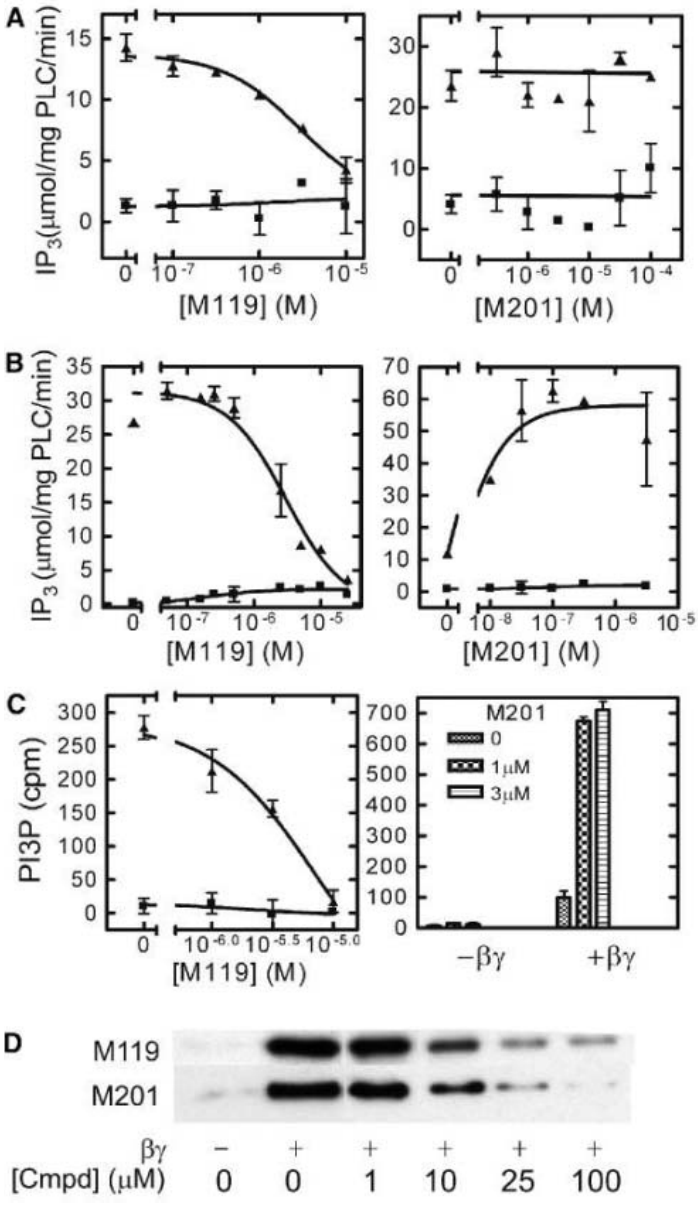

Fig. 2. Differential effects of M119 and M201 on βγ-dependent regulation of downstream targets. (**A**) Effects of M119 and M201 (NSC201400) on Gβγ-activation of PLCβ. Purified PLCβ2 (0.25 ng) was assayed in the presence (triangles) or absence (squares) of 100 nM purified $Gβ_1γ_2$. (**B**) Effects of M119 and M201 effects on purified PLCβ3 (0.5 ng) activity in the presence (triangles) or absence (squares) of 100 nM purified $Gβ_1γ_2$. (**C**) Effects of M119 and M201 on activation of PI3Kγ by $Gβ_1γ_2$. Assays contained 10 ng of purified p101/p110 PI3Kγ heterodimer with or without 100 nM purified $Gβ_1γ_2$. Left,: (triangles) 100 nM $Gβ_1γ_2$ or (squares) no βγ. (**D**) Effects of M119 and M201 on Gβγ-GRK2 interactions. M119 or M201 and 25 nM purified GRK2 were added simultaneously to 250 nM $bGβ_1γ_2$ immobilized on streptavidin agarose. Associated GRK2 was detected with antibody to GRK2. Data are representative experiments [mean ± SEM, except (D)] and were repeated at least three times each. The concentrations of compound required for these assays are apparently higher than predicted by the phage ELISA assays, but may reflect the different assay conditions and protein concentrations required for each assay.

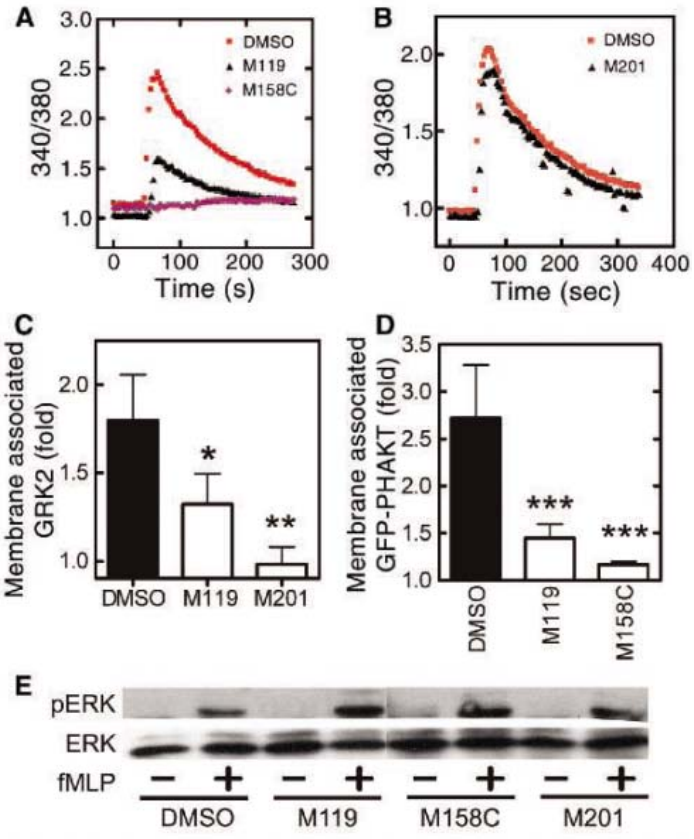

Fig. 3. Effects of M119 and related compounds on Gβγ signaling in dimethyl sulfoxide (DMSO)–differentiated HL-60 cells. (**A**) M119 and related compounds block fMLP-dependent Ca^{2+} release in differentiated HL-60 cells, loaded with 1 μM Fura2-AM. Cells were pretreated with DMSO or 10 μM compounds for 5 min before stimulation with 250 nM fMLP. The change in fluorescence was monitored at 340/380 nm. Data are representative of five independent experiments. Compounds are significantly different than DMSO control, $P < 0.01$. See fig. S4A for dose dependence. (**B**) Same as A except 10 μM M201 was tested. Data are representative of four independent experiments. See fig. S4B for pooled data. (**C**) M119 and M201 inhibition of GRK2 translocation. Differentiated HL-60 cells were treated with 10 μM compound before stimulation with 250 nM fMLP. Translocation of endogenous GRK2 was determined by Western blotting with a GRK2 antibody and quantitative chemiluminescence. Data are mean ± SEM from five experiments, $*P < 0.05$, $**P < 0.01$ analysis of variance (ANOVA). (**D**) M119 and M158C (NSC158110) inhibition of GFP-PHAkt translocation. Differentiated HL-60 cells stably overexpressing GFP-PHAkt were treated with 10 μM compound before stimulation with 100 nM fMLP. Translocation of GFP-PHAkt to the membrane was determined by Western blotting with antibody to GFP and quantitative chemiluminescence. Data are mean ± SEM from four experiments. $***P < 0.001$ ANOVA. (**E**) Lack of effect of M119, M158C, and M201 on fMLP-induced ERK1 and ERK2 activation. Differentiated HL-60 cells were pretreated with 10 μM of compound prior to stimulation with 1 μM fMLP for 5 min. Levels of phosphorylated and total ERK were determined by Western blotting. This experiment was repeated three times with similar results.

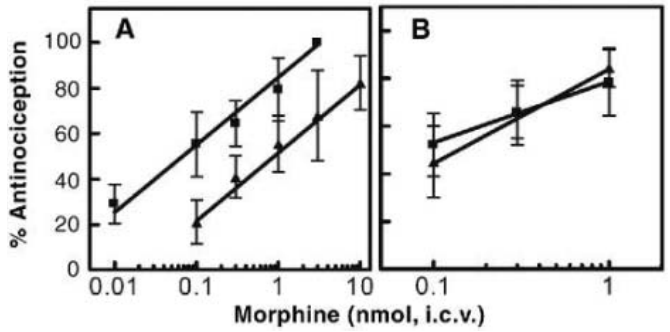

Fig. 4. M119 effects on morphine-induced antinociception in (**A**) wild-type and (**B**) PLCβ3$^{-/-}$ mice. Increasing concentrations of morphine were administered intracerebroventricularly to mice with (squares) or without (triangles) concomitant administration of 100 nmol M119. Antinociception was measured 20 min after injection using the 55°C tail-flick test. Data are mean ± SEM from 7 to 10 animals at each point.

to low μM range. These molecules demonstrate that multiple small molecule binders of Gβγ could be developed that differentially modulate functions downstream of GPCRs. Numerous studies in animal models have implicated Gβγ-subunit targeting as a therapeutic strategy in diseases such as heart failure (*22*), prostate cancer (*23*), vascular disease (*24*), and inflammatory disease (*13*). Thus, more extensive screening for molecules that bind to the Gβγ hotspot will yield a repertoire of potentially therapeutically useful small molecules.

References and Notes

1. D. E. Clapham, E. J. Neer, *Annu. Rev. Pharmacol. Toxicol.* **37**, 167 (1997).
2. T. M. Cabrera-Vera *et al.*, *Endocr. Rev.* **24**, 765 (2003).
3. J. K. Scott *et al.*, *EMBO J.* **20**, 767 (2001).
4. T. Davis, T. M. Bonacci, A. V. Smrcka, S. R. Sprang, *Biochem.* **44**, 10593 (2005).
5. M. A. Wall *et al.*, *Cell* **83**, 1047 (1995).
6. D. G. Lambright *et al.*, *Nature* **379**, 311 (1996).
7. C. E. Ford *et al.*, *Science* **280**, 1271 (1998).
8. Y. Li *et al.*, *J. Biol. Chem.* **273**, 16265 (1998).
9. M. Rarey, B. Kramer, T. Lengauer, G. Klebe, *J. Mol. Biol.* **261**, 470 (1996).
10. R. D. Clark, A. Strizhev, J. M. Leonard, J. F. Blake, J. B. Matthew, *J. Mol. Graph. Model.* **20**, 281 (2002).
11. N. A. Sarvazyan, A. E. Remmers, R. R. Neubig, *J. Biol. Chem.* **273**, 7934 (1998).
12. M. Ghosh, Y. K. Peterson, S. M. Lanier, A. V. Smrcka, *J. Biol. Chem.* **273**, 34747 (2003).
13. Z. Li *et al.*, *Science* **287**, 1046 (2000).
14. E. R. Neptune, H. R. Bourne, *Proc. Natl. Acad. Sci. U.S.A.* **94**, 14489 (1997).
15. G. Servant *et al.*, *Science* **287**, 1037 (2000).
16. M. J. Rane, S. L. Carrithers, J. M. Arthur, J. B. Klein, K. R. McLeish, *J. Immunol.* **159**, 5070 (1997).
17. W. Xie *et al.*, *Proc. Natl. Acad. Sci. U.S.A.* **96**, 10385 (1999).
18. M. Connor, M. J. Christie, *Clin. Exp. Pharmacol. Physiol.* **26**, 493 (1999).
19. M. R. Arkin, J. A. Wells, *Nat. Rev. Drug Discov.* **3**, 301 (2004).
20. A. G. Cochran, *Curr. Opin. Chem. Biol.* **5**, 654 (2001).
21. T. Oltersdorf *et al.*, *Nature* **435**, 677 (2005).
22. G. Iaccarino, W. J. Koch, *Assay Drug Dev. Technol.* **1**, 347 (2003).
23. Y. Daaka, *Sci. STKE* **2004**, re2 (2004).
24. G. Iaccarino, L. A. Smithwick, R. J. Lefkowitz, W. J. Koch, *Proc. Natl. Acad. Sci. U.S.A.* **96**, 3945 (1999).

25. We thank the Developmental Therapeutics Program at the NCI/NIH for providing the compounds used in this study, J. Benovic for providing purified GRK2, H. Bourne for providing HL-60 cells stably overexpressing GFP-PHAkt, and S. Sprang for evaluation of this manuscript. Supported by NIH grants GM60286 (A.V.S.), K05-DA00360 (J.M.B.), HL080706 (D.W.), Predoctoral Training grant in Cardiovascular Biology HL-T3207949 (T.M.B.), and NIDA Drug Abuse Training grant T32DA07232 (J.L.M.).

Supporting Online Material

www.sciencemag.org/cgi/content/full/312/5772/443/DC1
Materials and Methods
Tables S1 to S3
Figs. S1 to S4
References

20 September 2005; accepted 28 February 2006
10.1126/science.1120378

Synchrony, Waves, and Spatial Hierarchies in the Spread of Influenza

Cécile Viboud,[1]* Ottar N. Bjørnstad,[1,2,3] David L. Smith,[1] Lone Simonsen,[4] Mark A. Miller,[1] Bryan T. Grenfell[1,3]

Quantifying long-range dissemination of infectious diseases is a key issue in their dynamics and control. Here, we use influenza-related mortality data to analyze the between-state progression of interpandemic influenza in the United States over the past 30 years. Outbreaks show hierarchical spatial spread evidenced by higher pairwise synchrony between more populous states. Seasons with higher influenza mortality are associated with higher disease transmission and more rapid spread than are mild ones. The regional spread of infection correlates more closely with rates of movement of people to and from their workplaces (workflows) than with geographical distance. Workflows are described in turn by a gravity model, with a rapid decay of commuting up to around 100 km and a long tail of rare longer range flow. A simple epidemiological model, based on the gravity formulation, captures the observed increase of influenza spatial synchrony with transmissibility; high transmission allows influenza to spread rapidly beyond local spatial constraints.

Influenza epidemics occur every year during the winter season in temperate areas of the world and result in considerable morbidity, mortality, and economic burden (*1*). The virological basis for these recurrent epidemics is a continual process of small changes in influenza surface antigens to escape host immunity (antigenic drift) (*2*). A/H3N2 viruses have the highest rate of evolution among the three influenza subtypes currently circulating (*3*), with antigenically distinct strains emerging on average every 2 to 5 years (*2*); influenza-related mortality and severe morbidity are highest in seasons where A/H3N2 viruses predominate, as compared with A/H1N1 or B (*4*). Infrequently, viruses with novel surface antigens (so that all hosts are effectively susceptible) appear through antigenic shifts that lead to pandemics (*1*).

The spatial spread of influenza has been much studied, particularly with respect to pandemic invasion waves (*5*–*11*). Simulation models incorporating air and surface transportation have generated important insights into the spread of influenza (*6*, *7*, *10*, *11*); however, the key underlying relationship between human movement and disease spread has not been verified across wide spatial scales nor contrasted among multiple interpandemic seasons of varying severity and viral subtype dominance.

We address this gap by analyzing the spatial dynamics of interpandemic influenza epidemics between 1972 and 2002, using vital statistics for the lower 49 contiguous "states" in the United States (48 continental U.S. states and the District of Columbia) (Fig. 1) (*12*). To study these influenza epidemics, we use weekly state-specific "excess" mortality rates from pneumonia and influenza (P&I) (Fig. 1 and fig. S1) (*4*, *13*). [See (*12*) for a discussion of calibration against influenza morbidity data.] The weekly time series of excess mortalities appear to be useful indicators of (i) timing of epidemics, (ii) spatial spread and, with caution, (iii) incidence within each state (fig. S2).

The relative timing and correlation of epidemic trajectories can provide critical insights into the tempo and mode of spatial spread (*9*, *14*, *15*). On average, interpandemic influenza took 5.2 weeks to spread across the lower United States during 1972 to 2002

[1]Fogarty International Center, National Institutes of Health, Bethesda, MD 20892, USA. [2]Department of Entomology, Pennsylvania State University, University Park, Pennsylvania 16802, USA. [3]Center for Infectious Disease Dynamics, Department of Biology, Pennsylvania State University, University Park, Pennsylvania 16802, USA. [4]National Institute of Allergy and Infectious Diseases, National Institutes of Health, Bethesda, MD 20818, USA.

*To whom correspondence should be addressed. E-mail: viboudc@mail.nih.gov

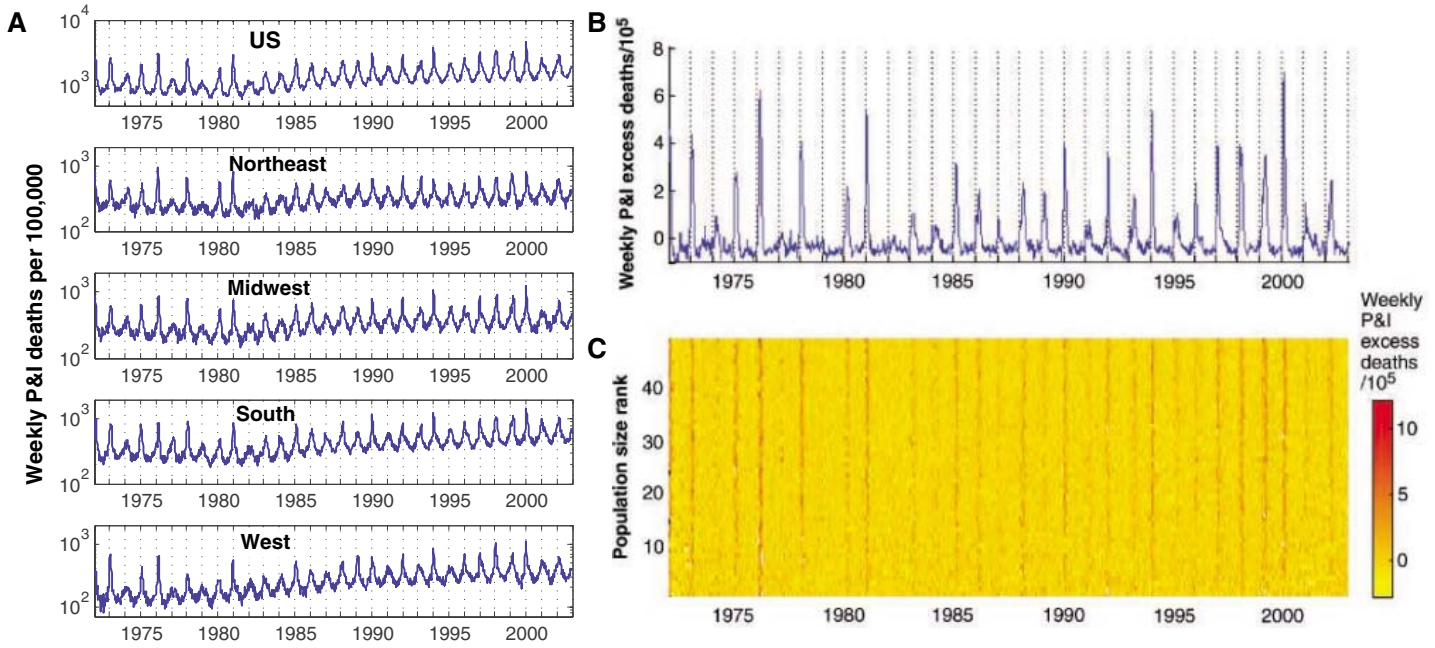

Fig. 1. Weekly epidemic time series. (**A**) Death rates from pneumonia and influenza (P&I) in the United States (excluding Hawaii and Alaska) and each of the four administrative regions (Northeast, Midwest, South, and West). Deaths are shown per 100,000 population on a log10 scale. (**B** and **C**) Death rates in excess attributed to influenza in the United States (B) and by state as a color intensity plot (C). Rates are normalized to have zero mean and unit variance. (C) The 49 "states" are arranged by decreasing population sizes (from top = California to bottom = Wyoming). Vertical bands in red correspond to synchronized epidemics, which occur in the most populated states or during larger epidemics, suggesting that synchrony increases with population size and epidemic size. (See also fig. S1.)

(range 2.7 to 8.4 weeks) (table S2). We use wavelet phase analysis to study the spatial synchrony in timing of epidemics through the spatial phase coherence function (*12*, *14*). This analysis reveals pronounced synchrony in the timing of epidemics across the continental United States, superimposed on a spatial correlation signature (Fig. 2A). This strong epidemiological "regionalization" is also reflected by marked correlation in the amplitude of excess mortality at the weekly and seasonal time scale (Fig. 2B and fig. S3A). The synchronous timing of epidemics is in part due to the strong winter seasonality of influenza; however, across seasons, the statewise U.S. epidemics are more synchronized than expected based on seasonality alone (table S1) (*12*).

The decay in epidemic synchrony with distance is broadly consistent with diffusive disease spread (*14*, *16*). However, pairwise synchrony and phase coherence are also significantly associated with state population sizes. To visualize this, we ranked the states by size and computed correlations in amplitude and phase within and among size quartiles (ignoring distance) (Fig. 2, C and D). The hierarchy of spread is immediately apparent: The most populous states exhibit synchronized epidemics, whereas less populated states exhibit more erratic patterns, both relative to each other and to the continental norm.

In addition to the spatial and hierarchical within-season patterns, interpandemic spread also varies with disease prevalence and predominant virus subtype. The severe epidemics, dominated by A/H3N2, are more synchronous than milder, generally A/H1N1 and B, seasons (Fig. 2E) (*17*). The median difference in the date of the local and national peak is 3.8 weeks in A/H3N2 seasons versus 6.3 weeks in A/H1N1 and B seasons (Wilcoxon test, $P < 0.01$). Interestingly, the relationship between severity and synchrony holds within as well as between subtypes (Fig. 2E). Additional analyses indicate that the slower spread in A/H1N1 and B seasons cannot be explained by the inevitably more error-prone "sampling" resulting from the lower case-fatality of A/H1N1 or B infection (*12*). Furthermore, the apparent relationship between epidemic synchrony and mortality impact is apparent in the more limited flu morbidity data available for the United States: Epidemic synchrony increases with influenza virus prevalence ($P < 0.01$) (fig. S3B) and is generally higher in seasons where the prevalence of A/H3N2 is high. These patterns echo the general theoretical principle that enhanced disease transmission facilitates spatial spread (*14*, *18*).

To understand the relationship between disease spread and severity, distance, and population size, we need to compare the key epidemic metrics (timing and incidence) to relevant measures of human movement. From the U.S. Census Bureau and Department of Transportation, we compiled a variety of potential a priori predictors of influenza spread. In particular, we compared the matrix of relative timing and amplitude of epidemics among the states with Euclidian distance between the population centers of each state, as well as various measures of domestic transportation such as workflows (rates of movement of people to and from their workplaces), long-distance travel, and rates of air transportation (*6*, *10*–*12*, *19*). Mantel

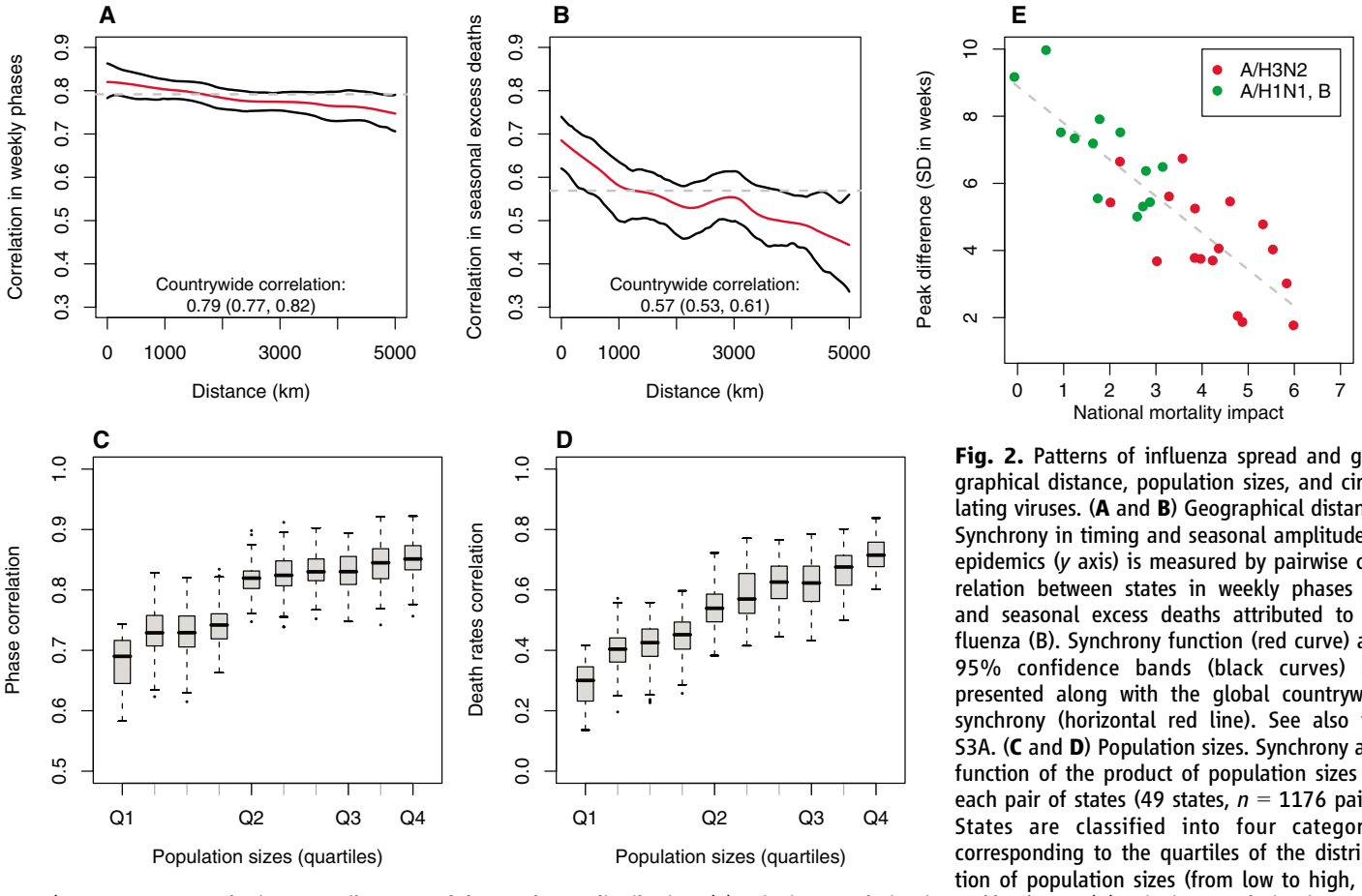

Fig. 2. Patterns of influenza spread and geographical distance, population sizes, and circulating viruses. (**A** and **B**) Geographical distance. Synchrony in timing and seasonal amplitude of epidemics (*y* axis) is measured by pairwise correlation between states in weekly phases (A) and seasonal excess deaths attributed to influenza (B). Synchrony function (red curve) and 95% confidence bands (black curves) are presented along with the global countrywide synchrony (horizontal red line). See also fig. S3A. (**C** and **D**) Population sizes. Synchrony as a function of the product of population sizes for each pair of states (49 states, $n = 1176$ pairs). States are classified into four categories corresponding to the quartiles of the distribution of population sizes (from low to high, Q1 to Q4). Boxes represent the interquartile range of the synchrony distribution. (C) Pairwise correlation in weekly phases. (D) Pairwise correlation in weekly death rates. (**E**) Circulating virus. Epidemics associated with high mortality impact, generally dominated by A/H3N2 viruses, spread more quickly than mild ones. Spread is measured by the standard deviation (SD in weeks, *y* axis) of the difference in the timing of epidemic peaks between national and local P&I mortality time series. National mortality impact (*x* axis) is measured as seasonal P&I excess death rates per 100,000 population for the whole United States, 1972 to 2002 (30 seasons). Epidemics are classified according to the predominant viral subtype in the United States (green dots: A/H1N1 or B; red dots: A/H3N2). Gray line: linear fit, $R^2 = 0.72$, $P < 0.0001$.

tests (*20*) based on rank correlation reveal a significant association between disease dynamics and all the metrics (Table 1). Partial Mantel tests (*20*), however, show that workflow is the key predictor of influenza spread among those tested (Table 1). In absolute (nonrank) terms, the relation to U.S. workflows is nonlinear and conspicuously sigmoidal (Fig. 3A).

Because excess-mortality proxies for influenza incidence are only available at the statewise scale for the whole United States, a comparison with movement metrics can only be made at this scale. However, we can develop a more spatially and demographically refined model for the best fit workflow data, using county-level information (Fig. 3B and fig. S4). As a starting point, we use a general gravity model from transportation theory; this allows flexible dependence of flow on distance and the sizes of "donor" and "recipient" communities [location of residence and workplace, respectively (*15*)]. A gravity model for workflow (or disease spread) (C_{ij}) between community i (of size P_i) and j (of size P_j) takes the form (*21*)

$$C_{ij} = \theta \frac{P_i^{\tau_1} P_j^{\tau_2}}{d_{ij}^{\rho}}$$

where θ is a proportionality constant and the exponents τ_1, τ_2 and ρ, respectively, tune the dependence of dispersal on donor and recipient sizes, and the distance between the two communities, d_{ij}.

We found that a thresholded version of this gravity formulation captures key features of workflows in the United States. There is a rapid decline (distance exponent > 3) in movement to work up to 119 km; beyond this threshold, a small flux of movements is nearly independent of distance (distance exponent small but > 0) [Table 2 and Fig. 3B; see also (*19*) for Thailand]. The gravity formulation also allows us to explore the scaling of workflows with donor and recipient population sizes (fig. S4). The two population exponents are less than unity, indicating that smaller populations are more important per capita, both in donating and receiving workers (Table 2). Below 119 km, the population exponents are relatively high, and larger for the "recipient" of workers.

As a crude validation of the gravity like spread of influenza among states, we superimpose a model of between-state workflow movements (Table 2) on a set of standard stochastic susceptible-infected-recovered (SIR) models at the state level (*12*). To calibrate transmission in the model for interpandemic years, we estimate

Table 1. Correlation between matrices of epidemic synchrony, Euclidian distance, and population movements between U.S. states. Workflows show a strong and independent correlation with influenza spread. Epidemic matrices representing influenza dispersal in 49 continental U.S. states are based on pairwise Spearman correlation in Pneumonia and Influenza (P&I) weekly death rates and weekly phases. P&I death rates have been logged and normalized by population size before calculating pairwise correlation between states. All movement matrices are symmetric; this is done by adding movements from state i→j and state j→i. The correlation between the two matrices of epidemic synchrony is 0.85 (Mantel $P < 0.0001$).

Distance or movement matrix	Correlation with epidemic synchrony based on	
	P&I weekly phases	P&I weekly death rates
Mantel correlations		
Workflows	0.61***	0.67***
Long-distance trips	0.55***	0.60***
Air travel	0.37*	0.42***
Euclidian distance†	−0.31***	−0.26**
Partial Mantel correlations		
Workflows, adjusting for:		
Long-distance trips	0.31***	0.39***
Air travel	0.52***	0.54***
Euclidian distance	0.55***	0.65***
Long-distance trips, adjusting for:		
Workflows	0.004 ($P = 0.47$)	−0.03 ($P = 0.30$)
Air travel, adjusting for:		
Workflows	0.024 ($P = 0.39$)	0.17 ($P = 0.07$)
Euclidian distance,† adjusting for:		
Workflows	0.003 ($P = 0.51$)	0.13 ($P = 0.08$)

P values for Mantel test given by 10,000 permutations of the original matrices: * <0.01, ** < 0.001, *** < 0.0001. †Euclidian distance between state population centers. The Euclidian distance matrix is a "dissimilarity" matrix, whereas all other matrices are "similarity" matrices, hence the negative sign for the correlation with the epidemic data. Only the absolute value of the correlation coefficient is tested.

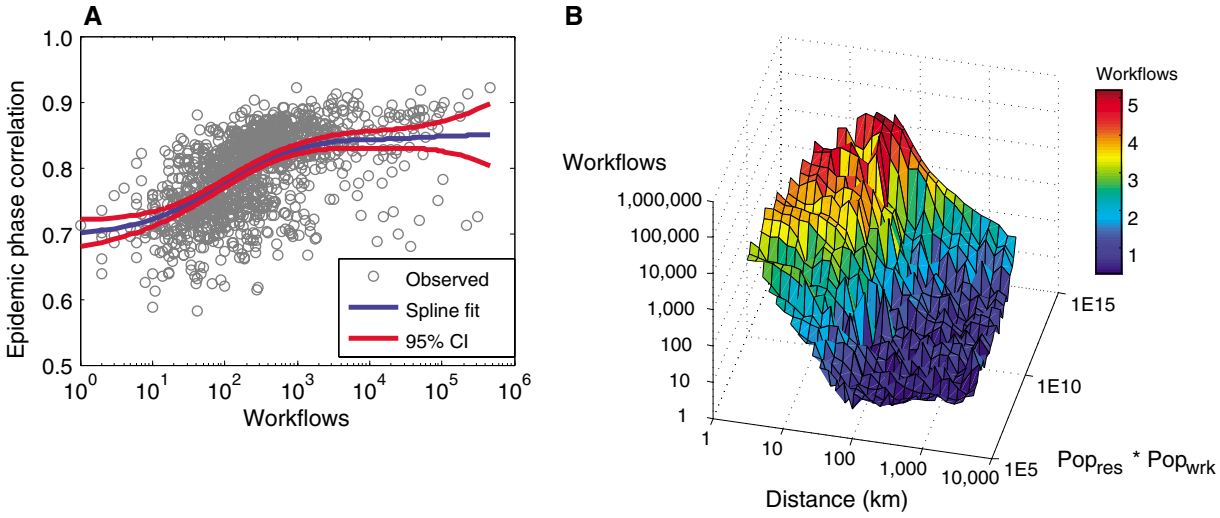

Fig. 3. Influenza spread and workflows. (**A**) Gray dots represent the observed phase synchrony in influenza epidemics (*y* axis) plotted against the total number of individuals commuting between each (pair of) states (*x* axis, log10 scale). Superimposed is the best fit statistical model (spline, red curve) and 95% confidence intervals (CI, blue curve). (**B**) Relationship between total workflows (*z* axis), population sizes (*y* axis), and distance (*x* axis) as in the gravity framework. The spatial unit in (B) is the county. (See also fig. S4.)

the effective reproduction ratio of infection, R, from observed epidemics, based on the weekly increase in the cumulative number of P&I excess deaths (*12*, *22*). We find a mean R of 1.35 in A/H3N2 epidemics (95% confidence interval 1.10 to 1.60). Figure 4A uses this model to illustrate how increasing disease transmission [reflected in increased prevalence, for example, A/H3N2 epidemics versus A/H1N1 or B (Fig. 2E)] will raise the probability of a synchronized and widespread epidemic. Here, we manipulate transmission by varying R; this formulation is dynamically equivalent to using a fixed basic reproduction number, R_0, and raising average susceptibility [for example, through the faster evolution rate of A/H3N2 (*3*)]. Both approaches account for a partially immune population and give similar model results (*23*).

Figure 4A explores the predicted spatiotemporal spread of typical epidemics starting in a populous, highly connected state (California), compared with a smaller, more isolated one (Wyoming). Because of the topology of gravity-like spread, epidemics beginning in California are both more spatially synchronized and widespread; infection disseminates through strong long-range connections. For the mean observed value of R (1.35), the duration of spread across the United States matches that seen in real epidemics (predicted mean 4.7 weeks, range 1.0 to 9.0 weeks) (Fig. 4B and table S2). [See (*12*) for further evaluations of the gravity model predictions.] By contrast, if epidemics ever were to arise from a less populous and very isolated state like Wyoming, spread is predicted to be slower and more local (Fig. 4C) [mean time to epidemic onset = 6.9 weeks (range 1.0 to 14.0 weeks)]; the national outbreak does not gain momentum until the epidemic hits a better connected state.

Turning to the onset of the national epidemic, there is a tendency for the influenza season to start in California more often than in any other state (with an average lead of 1 week for California, $P < 0.01$). This is consistent with California's being the most populous state; however, additional analyses indicate that population factors alone cannot explain the early epidemic onset in California (*12*). Teasing out the causes of this interesting geographical trend in the initial epidemic focus—in terms of population size, international connectivity, and preferred destinations (in particular Asia and Australia)—may have important implications for understanding the intercontinental spread of influenza.

We can also use the model to explore how the higher reproduction ratios of infection seen during pandemics might affect the speed of spread across the United States. Figure 4D

Table 2. Parameter estimates for the piecewise gravity model fitted to U.S. workflow data by county. Models are fitted separately for distances above and below 119 km, following: $Flow_{Residence \to Work} \propto \frac{P_{Resident}^{\tau_1} P_{Work}^{\tau_2}}{d_{Residence,Work}^{\rho}}$; where P is the county population size; d is the Euclidian distance between the population centers of two counties; τ_1, τ_2, and ρ, respectively, tune the dependence of dispersal workflows on the population size of the donor (resident county) and recipient (work county) and the distance between them. A total of 3109 counties in 49 continental U.S. states are used, yielding 161,710 pairs of counties with nonzero flow of workers.

Parameter	Point estimate (standard error)	
	Distances < 119 km*	Distances ≥ 119 km*
τ_1: population of residence county (donor)	0.30† (0.004)	0.24† (0.001)
τ_2: population of work county (recipient)	0.64† (0.004)	0.14† (0.001)
ρ: distance (km)	3.05 (0.012)	0.29 (0.003)

*Cut-off at 119 km chosen as the distance that minimized the residual sum of square of a piecewise (log) linear gravity model. †$\tau_1 \neq \tau_2$ in both models; $P < 0.01$.

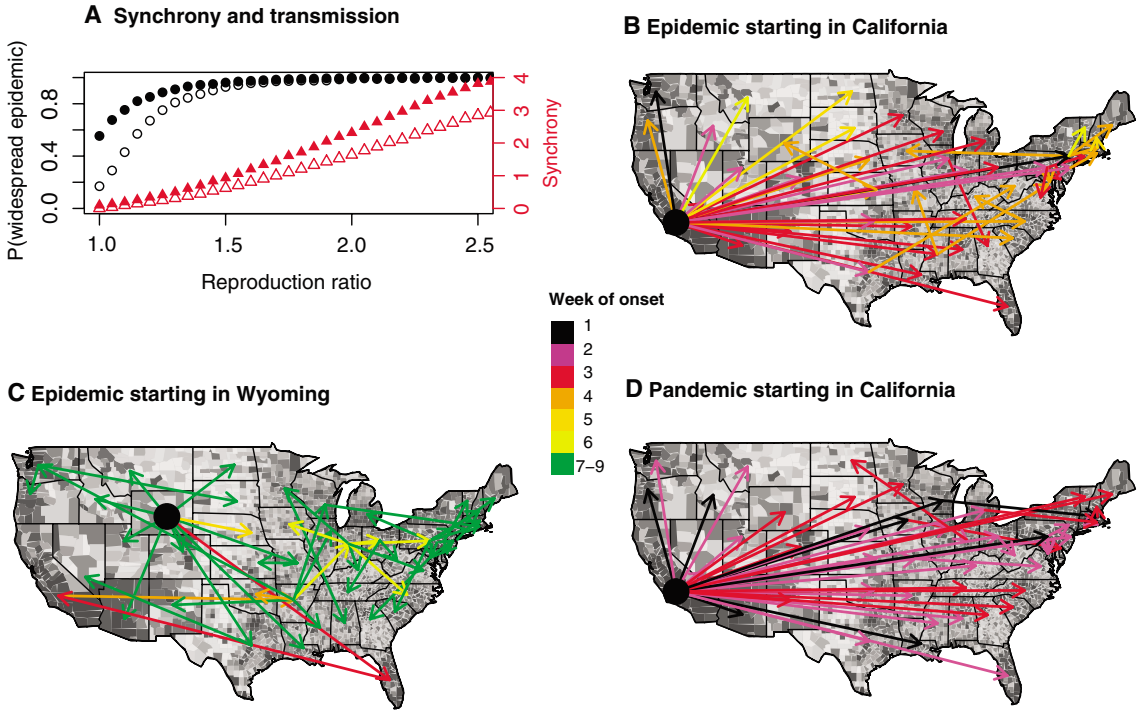

Fig. 4. Simulated spread of influenza by a gravity model based on work movements, for epidemics originating in California or Wyoming. (**A**) Synchrony and geographical extent of epidemics increases with higher transmission. Transmission is manipulated through the reproduction ratio, R (x axis). Epidemics originating in California (filled symbols), a highly populated and connected state, are more synchronous and widespread than those originating in Wyoming, the least populated state (open symbols). Synchrony is measured by the inverse of the variance in dates of epidemic onsets (in weeks) in the 49 continental U.S. states (red triangles, right y axis). The probability of having a widespread epidemic, where infection has reached all 49 states, is represented by black circles (left y axis). Coupling between states follows a gravity model, fitted to work movement data (*12*). Results are based on 1000 simulations; 95% confidence intervals are ± 5% of indicated values. (**B** to **D**) Maps of simulated spread out of California or Wyoming for epidemic seasons [(B and C), intermediate R = 1.35] and pandemic seasons [(D), R = 1.89, as in the 1968 pandemic (*6*)]. The background in grayscale indicates county population sizes [from light gray (<1,000 inhabitants) to dark gray (>400,000)]. Filled black circles represent the location of initial cases. Arrows indicate the source of infection for individual states; arrows originate from, and point to, a state population center. Arrows are color coded, based on the date of epidemic onset in individual states, from black = early onset to green = late onset; see color bar.

illustrates this for a reproduction ratio of 1.89, corresponding to the reported estimate for the 1968 A/H3N2 pandemic (*6*). Spread of pandemic influenza is predicted to be more rapid than in interpandemic seasons (2.2 weeks rather than 4.7, starting from California) (Fig. 4D and table S2). Interestingly, the projected spread is also faster than the reports from the 1968 pandemic [6 to 7 weeks (*24*)]. The discrepancy may be due to an increase in the flow of movements since 1968, although there is no obvious corresponding trend of increasing synchrony in observed epidemics between 1972 and 2002. Differences in the contact network of pandemic and interpandemic influenza might also play a role, because the relative importance of adults versus school-age children may differ (*12*). Interestingly, the observed interpandemic data (on which our model was calibrated) indicate that the spread of influenza was substantially slower in the 1968 pandemic than in several subsequent epidemics. Comparing the spread of influenza in pandemic and interpandemic seasons is an important topic for future studies.

An essential step in generating realistic epidemic models is calibrating them against historical spread of outbreaks and underlying patterns of host movement. Here, we investigate statistical and dynamic models of large-scale spread of influenza at the state level for the United States; these models explicitly incorporate data on human movements and are calibrated against long-term disease statistics. We find that workflows capture the spread of influenza better than simple Euclidean distance or other movement metrics. Workflow data have been used previously to simulate disease spread (*19*), but here, long-term historical disease data have allowed us to calibrate flows of infection against flows of people. A gravity model (*21*) demonstrates a strong decay in county-level workflows (and therefore potentially the flux of infection) with distance up to ~100 km. The population exponents for the gravity model are less than unity, suggesting that cases (and susceptibles) in small populations may be proportionately more important for disease spread.

A recurring problem for influenza epidemiology is a lack of detailed spatiotemporal incidence or prevalence data, exacerbated by the poor specificity of clinical diagnosis and relative scarcity of laboratory testing (*1*). Here, good agreement between influenza-related mortality and indicators of the prevalence of infection allows us to use mortality to study disease spread (fig. S2) (*12*). There are still caveats; for example, A/H1N1 and B viruses cause less mortality and severe morbidity than A/H3N2 viruses (*4*), so our estimates may be less precise for the milder A/H1N1-B seasons. However, other studies confirm that A/H1N1 and B virus prevalence do contribute to P&I mortality (*25*), corroborating the observed quantitative relationship between disease dispersal and mortality, for all three subtypes (Fig. 2E). In addition, detailed analyses confirm that subtype differences are not simply due to sampling biases and indicate a true difference in spread between A/H1N1-B and A/H3N2 epidemics (*12*).

We illustrate the epidemiological implications of the gravity framework with the simplest dynamical description, a statewise SIR model. Despite its simplicity and spatial coarseness, this model reproduces the observed timing and spread of seasonal influenza, capturing observed changes in synchrony with transmission, population size, and distance. As more spatially disaggregated mortality and morbidity data become available, more detailed models may help elucidate within-state spread and consequences of demographic heterogeneities. Interestingly, we did not find any association between local transmission (measured by the estimated effective reproduction ratio at the state level) and population density or population size (*12*). This lack of association echoes earlier work on the dynamics of the 1918 pandemic across U.S. cities (*26*)—as well as patterns in other disease (*27*)—that for some infections, reproduction ratios can be surprisingly invariant across a wide range of population sizes.

Our study indicates a likely increase of influenza spread and synchrony with increasing transmission. A key area for future research is how the combination of quicker evolution of the virus and intrinsic differences in viral transmissibility drives the faster geographical spread of A/H3N2 epidemics. The data-based models described here should also help us understand in a more mechanistic way the well-known spread of viral novelty (antigenic drift) that drives the ongoing pattern of partial immunity against interpandemic influenza (*2*). Understanding local spatial spread is also an important step in refining existing phylodynamic models for influenza evolution (*3*, *28*).

More generally, our results have a number of implications for the comparative dynamics of acute infections. The strong dependence of interpandemic influenza spread on workflows, coupled with a steep decline in workflows with distance [exponent >3; see also (*19*)], implies a key role for adults in the regional dissemination of infection. This is not necessarily contrary to the current consensus that children drive the local spread of influenza [within school, households, and cities in general (*29*, *30*)]. At the same time, the long-distance dissemination of influenza, between cities or states, is captured by movements linked to adults. By contrast, the spread of prevaccination measles was more local, with a distance exponent of unity (*21*); this child-focused infection was presumably entirely driven by contacts between schools. Investigating the specific role of children and adults in the spread of influenza would require not only age-specific disease data but also data on movements of children in the United States. This is a crucial area for future data collection, as pandemic influenza would probably be spread through both child and adult social networks. In essence, disease dissemination is a complex function of host movement, filtered by the age structure of susceptibility.

References and Notes

1. L. Simonsen, *Vaccine* **17** (suppl. 1), S3 (1999).
2. D. J. Smith *et al.*, *Science* **305**, 371 (2004).
3. N. M. Ferguson, A. P. Galvani, R. M. Bush, *Nature* **422**, 428 (2003).
4. L. Simonsen *et al.*, *Arch. Intern. Med.* **165**, 265 (2005).
5. M. Smallman-Raynor, N. Johnson, A. D. Cliff, *Trans. Inst. Br. Geogr.* **27**, 452 (2004).
6. I. M. Longini Jr., P. E. Fine, S. B. Thacker, *Am. J. Epidemiol.* **123**, 383 (1986).
7. R. F. Grais, J. H. Ellis, G. E. Glass, *Eur. J. Epidemiol.* **18**, 1065 (2003).
8. E. Bonabeau, L. Toubiana, A. Flahault, *Proc. R. Soc. Lond. B* **265**, 2421 (1998).
9. A. D. Cliff, P. Haggett, J. K. Ord, *Spatial Aspects of Influenza Epidemics* (Pion, London, 1986).
10. R. F. Grais, J. H. Ellis, A. Kress, G. E. Glass, *Health Care Manag. Sci.* **7**, 127 (2004).
11. A. Flahault *et al.*, *Stat. Med.* **7**, 1147 (1988).
12. Methods and supplementary analyses are available as supporting material on *Science* Online.
13. C. Viboud, R. F. Grais, B. A. Lafont, M. A. Miller, L. Simonsen, *J. Infect. Dis.* **192**, 233 (2005).
14. B. T. Grenfell, O. N. Bjornstad, J. Kappey, *Nature* **414**, 716 (2001).
15. A. D. Cliff, P. Haggett, M. Smallman-Raynor, *Spatial Processes* (Blackwell, New York, 1994).
16. O. N. Bjornstad, R. A. Ims, X. Lambin, *Trends Ecol. Evol.* **14**, 427 (1999).
17. S. K. Greene, E. L. Ionides, M. L. Wilson, *Am. J. Epidemiol.* **163**, 316 (2006).
18. D. Mollison, *Math. Biosci.* **107**, 255 (1991).
19. N. M. Ferguson *et al.*, *Nature* **437**, 209 (2005).
20. P. Legendre, L. Legendre, *Numerical Ecology* (Elsevier, Amsterdam, 1998).
21. Y. Xia, O. N. Bjornstad, B. T. Grenfell, *Am. Nat.* **164**, 267 (2004).
22. M. J. Ferrari, O. N. Bjornstad, A. P. Dobson, *Math. Biosci.* **198**, 14 (2005).
23. D. J. Earn, P. Rohani, B. M. Bolker, B. T. Grenfell, *Science* **287**, 667 (2000).
24. *Morb. Mortal. Wkly. Rep.* **18**, 217 (1969).
25. J. Dushoff, J. B. Plotkin, C. Viboud, D. J. Earn, L. Simonsen, *Am. J. Epidemiol.* **163**, 181 (2006).
26. C. E. Mills, J. M. Robins, M. Lipsitch, *Nature* **432**, 904 (2004).
27. O. N. Bjornstad, B. Finkenstadt, B. T. Grenfell, *Ecol. Monogr.* **72**, 169 (2002).
28. B. T. Grenfell *et al.*, *Science* **303**, 327 (2004).
29. C. Viboud *et al.*, *Br. J. Gen. Pract.* **54**, 684 (2004).
30. A. S. Monto, *Epidemiol. Rev.* **16**, 351 (1994).

31. This study was funded by the Fogarty International Center, NIH.

Supporting Online Material

www.sciencemag.org/cgi/content/full/1125237/DC1
Methods
SOM Text
Figs. S1 to S4
Tables S1 to S3
References

23 January 2006; accepted 20 March 2006
Published online 30 March 2006;
10.1126/science.1125237
Include this information when citing this paper.

RNA Interference Directs Innate Immunity Against Viruses in Adult *Drosophila*

Xiao-Hong Wang,[1]* Roghiyh Aliyari,[2]* Wan-Xiang Li,[2] Hong-Wei Li,[2] Kevin Kim,[4] Richard Carthew,[4] Peter Atkinson,[3] Shou-Wei Ding[1,2]†

Innate immunity against bacterial and fungal pathogens is mediated by Toll and immune deficiency (Imd) pathways, but little is known about the antiviral response in *Drosophila*. Here, we demonstrate that an RNA interference pathway protects adult flies from infection by two evolutionarily diverse viruses. Our work also describes a molecular framework for the viral immunity, in which viral double-stranded RNA produced during infection acts as the pathogen trigger whereas *Drosophila* Dicer-2 and Argonaute-2 act as host sensor and effector, respectively. These findings establish a *Drosophila* model for studying the innate immunity against viruses in animals.

RNA interference (RNAi) silences gene expression through small interfering RNAs (siRNAs) and microRNAs (miRNAs). In *Drosophila melanogaster* (*1*), Dicer-2 (Dcr-2) produces siRNAs, whereas Dicer-1 (Dcr-1) recognizes precursors of miRNAs. The small RNAs are assembled with an Argonaute (Ago) protein into related effector complexes, such as RNA-induced silencing complex (RISC), to guide specific RNA silencing (*1*).

RNA silencing provides an antiviral mechanism in plants and animals (*2*–*6*). Plant viruses have evolved diverse strategies for evading the RNA silencing immunity, and expression of viral suppressors of RNAi (VSRs) is essential for infection and virulence (*6*). However, it is unknown whether antiviral silencing in plants is controlled by a specific small RNA pathway targeted by plant VSRs. Bacterial and fungal infections of *D. melanogaster* induce Toll and immune deficiency (Imd) pathways, leading to transcriptional induction of antimicrobial peptide effectors via nuclear factor κB (NF-κB)–like signaling processes (*7*). However, it has been unclear whether either pathway plays a role in *Drosophila* innate immunity against viruses (*8*, *9*). Our previous work in cell culture has indicated that RNAi might mediate viral immunity in *D. melanogaster* (*3*). Here, we investigated whether RNAi indeed provides protection against virus infection in *Drosophila* embryos and adults.

Flock house virus (FHV) contains an RNA genome (*10*) divided among two plus-strand molecules, RNAs 1 and 2. RNA2 (R2) encodes the single virion structural protein, whereas RNA1 (R1) encodes protein A, the viral RNA–dependent RNA polymerase (RdRP), and B2, a VSR (*3*, *4*, *11*) expressed after RNA1 replication from its own mRNA, RNA3 (fig. S1). In the absence of R2, R1 replicated autonomously, accumulated to high levels, and produced abundant RNA3 in wild-type (WT) *D. melanogaster* embryos 30 hours after injection with R1 transcripts synthesized in vitro (Fig. 1, lane 2). No FHV RNAs accumulated in WT embryos injected with R1fs transcripts that contain a frameshift mutation in the RdRP open reading frame (ORF) (Fig. 1, lane 1). FHV RNAs were also not readily detected in WT embryos injected with a second mutant of R1, R1ΔB2, which does not express the VSR (Fig. 1, lane 3). However, abundant accumulation of R1ΔB2 (Fig. 1, lane 9) but not FR1fs (Fig. 1, lane 7) occurred in mutant *Drosophila* embryos that carried a homozygous null mutation in *ago-2* (*ago-2*^{414}), which is essential for RNAi in *Drosophila* (*1*, *12*, *13*). These data indicated that viral RNA replication in *Drosophila* embryos triggers an RNAi-mediated virus clearance in an *Ago-2*–dependent manner and that effective RNAi suppression by B2 is necessary to achieve normal accumulation of FHV RNAs.

In *Drosophila*, Ago-2 acts downstream of Dicer-2 (Dcr-2) to recruit siRNAs, the products of Dcr-2 activity, into the siRNA-dependent RISC (siRISC) (*1*, *14*). Thus, a genetic requirement for *ago-2* in FHV RNA clearance implicates Dcr-2 in the RNAi antiviral effector mechanism. To test this hypothesis, we injected R1, R1fs, and R1ΔB2 transcripts into embryos carrying a homozygous *dcr-2* null mutation, *dcr-2*^{L811fsX}. Northern blot hybridizations showed that, although FHV RNAs remained undetectable in *dcr-2*^{L811fsX} embryos injected with R1fs (Fig. 1, lane 4), viral RNA accumulation was rescued in the *dcr-2*^{L811fsX} embryos injected with R1ΔB2 transcripts (Fig. 1, lane 6). This result shows that Dcr-2 is required to initiate RNAi-mediated clearance of FHV RNAs in *Drosophila* embryos.

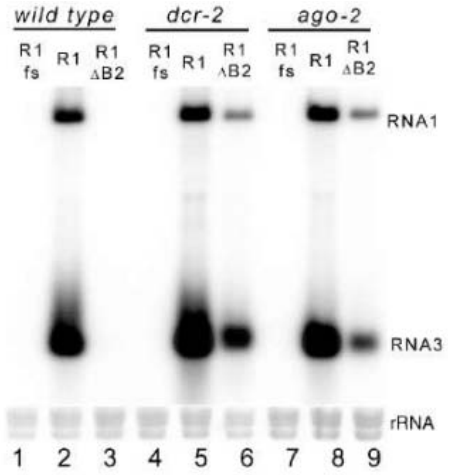

Fig. 1. Antiviral silencing in *Drosophila* embryos requires Dcr-2 and Ago-2. Northern blot detection of FHV RNA accumulation in *wt*, *dcr-2*^{L811fsX}, and *ago-2*^{414} embryos microinjected with in vitro synthesized transcripts R1, R1fs, and R1ΔB2, as shown in fig. S1.

To investigate whether the RNAi pathway protects *Drosophila* from virus infection, we injected adult flies of either WT or *dcr-2*^{L811fsX} genotype with purified FHV virions. The FHV isolate was of low virulence in WT flies, because about 50% of infected flies survived 15 days postinoculation (dpi) (Fig. 2A) despite a detectable virus load (Fig. 2B, lanes 1 to 6). Inoculation with the same dose of FHV resulted in 60% mortality by 6 dpi and 95% by 15 dpi in *dcr-2*^{L811fsX} flies (Fig. 2A). Mock inoculation with buffer had little effect on either WT or *dcr-2*^{L811fsX} flies for as long as observations were made. Both Northern and Western blot analyses revealed that the virus accumulated more rapidly and to much greater levels in *dcr-2*^{L811fsX} than WT flies (Fig. 2, B and C). Thus, *dcr-2* mutants exhibit enhanced disease susceptibility to FHV in comparison with WT flies, demonstrating that Dcr-2 is also required to mount an immune response that protects adult *Drosophila* against FHV infection.

R2D2 contains tandem double-stranded RNA (dsRNA)–binding domains and forms a heterodimer with Dcr-2 in vivo that is required for siRNA loading into RISC (*1*, *15*). We found that flies homozygous for a loss-of-function mutation in *r2d2* exhibited a phenotype of enhanced disease susceptibility to FHV infection similar to that of *dcr-2*^{L811fsX} (Fig. 2). Thus, R2D2 also participates in the innate immunity pathway that protects adult flies from FHV infection. Notably, although FHV accumulated to extremely high levels in both *dcr-2* and *r2d2* mutant flies, abundant viral siRNAs were detected only in *r2d2* mutant flies, and viral siRNAs were below the level of detection in *dcr-2*^{L811fsX} flies (Fig. 2D). Thus, FHV infection is detected by Dcr-2, leading to production of FHV siRNAs. However, R2D2 is not required for the production but is essential

[1]Graduate Program for Microbiology, [2]Department of Plant Pathology and Center for Plant Cell Biology, Institute for Integrative Genome Biology, [3]Department of Entomology, University of California, Riverside, CA 92521, USA. [4]Department of Biochemistry, Molecular Biology, and Cell Biology, Northwestern University, Evanston, IL 60208, USA.

*These authors contributed equally to this work.
†To whom correspondence should be addressed. E-mail: dingsw@ucr.edu

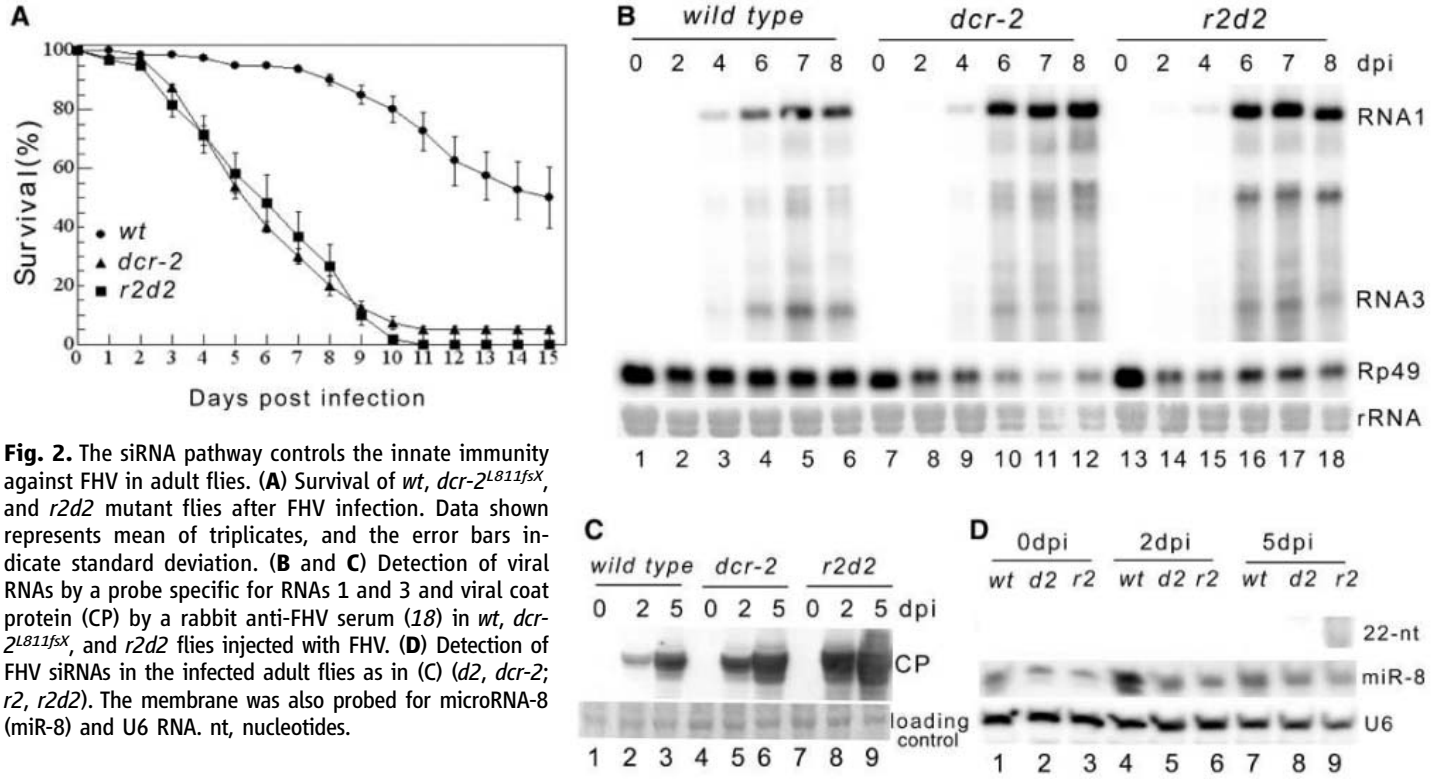

Fig. 2. The siRNA pathway controls the innate immunity against FHV in adult flies. (**A**) Survival of *wt*, *dcr-2*^{L811fsX}, and *r2d2* mutant flies after FHV infection. Data shown represents mean of triplicates, and the error bars indicate standard deviation. (**B** and **C**) Detection of viral RNAs by a probe specific for RNAs 1 and 3 and viral coat protein (CP) by a rabbit anti-FHV serum (*18*) in *wt*, *dcr-2*^{L811fsX}, and *r2d2* flies injected with FHV. (**D**) Detection of FHV siRNAs in the infected adult flies as in (C) (*d2*, *dcr-2*; *r2*, *r2d2*). The membrane was also probed for microRNA-8 (miR-8) and U6 RNA. nt, nucleotides.

for the function of viral siRNAs, which is consistent with the genetic requirements for processing the artificially introduced dsRNA (*1*, *15*).

To investigate whether the RNAi pathway in *Drosophila* is specific against nodaviruses and not other classes of RNA viruses, we assessed the susceptibility of WT, *dcr-2*^{L811fsX}, and *r2d2* mutant flies to cricket paralysis virus (CrPV). CrPV contains a nonsegmented plus-strand RNA genome but belongs to a group of picorna-like viruses (*16*). CrPV is substantially more virulent than FHV in *Drosophila*, because injection of CrPV at much lower titers resulted in mortality of 70% of WT flies by 15 dpi (Fig. 3A). We found that CrPV also induced enhanced disease susceptibility in both *dcr-2* and *r2d2* mutant flies (Fig. 3A). About 60% of the infected mutant flies were dead by 6 dpi, and more than 95% were dead by 15 dpi (Fig. 3A). In addition, Northern blots indicated that the virus accumulated more rapidly and to greater levels in the mutant flies (Fig. 3B). Thus, both *dcr-2* and *r2d2* are required for protection of *Drosophila* against CrPV.

CrPV infection of cultured S2 cells induced antiviral silencing, illustrated by detection of CrPV-specific siRNAs (Fig. 4A). Antiviral silencing against FHV in S2 cells induced by FR1gfp as described previously (*11*) was suppressed by CrPV superinfection, leading to derepression of green fluorescent protein (GFP) (Fig. 4B, left). Two ORFs are encoded by the CrPV RNA genome (*16*) (fig. S2). We did not observe suppression of antiviral silencing in S2 cells cotransfected with a plasmid expressing either the entire downstream ORF of CrPV or the individual mature virion proteins processed from the polyprotein (Fig. 4C, lanes 4 to 10). In contrast, RNAi suppression was detected after cotransfection with a plasmid expressing either the entire upstream ORF of CrPV or its N-terminal 140 codons (Fig. 4C, pA in lane 1). However, the suppressor activity was not detected after a frameshift mutation was introduced into pA (Fig. 4C, lane 2), thus identifying the N-terminal fragment of 140 amino acids of the CrPV nonstructural polyprotein as a VSR.

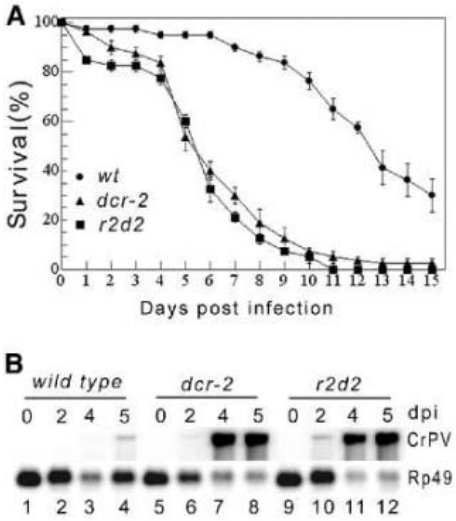

Fig. 3. Mutant *dcr-2* and *r2d2* flies exhibit enhanced disease susceptibility to CrPV. (**A**) Survival of *wt*, *dcr-2*^{L811fsX}, and *r2d2* mutant flies after CrPV infection. Data shown represents mean of triplicates, and the error bars indicate standard deviation. (**B**) Accumulation of CrPV genomic RNA in WT, *dcr-2*^{L811fsX}, and *r2d2* mutant adults injected with CrPV.

In *D. melanogaster*, Imd signaling is stimulated by Gram negative (Gram$^-$) bacterial infection, whereas Toll signaling is triggered by Gram positive (Gram$^+$) bacterial infection (*7*, *17*). To determine whether loss of the RNAi pathway initiated by Dcr-2 had an impact on the Toll and Imd signaling processes, we subjected WT, *dcr-2*^{L811fsX}, and *r2d2* mutant flies to immune challenge by inoculation with *Escherichia coli* (Gram$^-$) or *Micrococcus luteus* (Gram$^+$). Northern blot hybridizations detected substantial transcriptional induction of the antimicrobial peptide gene *Diptericin A* 6 hours postimmune challenge (hpi) with either *E. coli* or *M. luteus*, which declined at 24 hpi (fig. S3) as described (*17*). Similar induction patterns for *Diptericin A* were observed in *dcr-2*^{L811fsX} and *r2d2* mutant flies inoculated with Gram$^+$ and Gram$^-$ bacteria (fig. S3). Furthermore, we found that induction of either *Attacin A* or *Drosomycin* by Gram$^+$ and Gram$^-$ bacteria was also not altered in *dcr-2*^{L811fsX} and *r2d2* mutant flies as compared to WT flies (fig. S3). These results indicate that induction of antimicrobial peptide genes via Toll and Imd signaling pathways is not compromised in *dcr-2*^{L811fsX} and *r2d2* mutant flies.

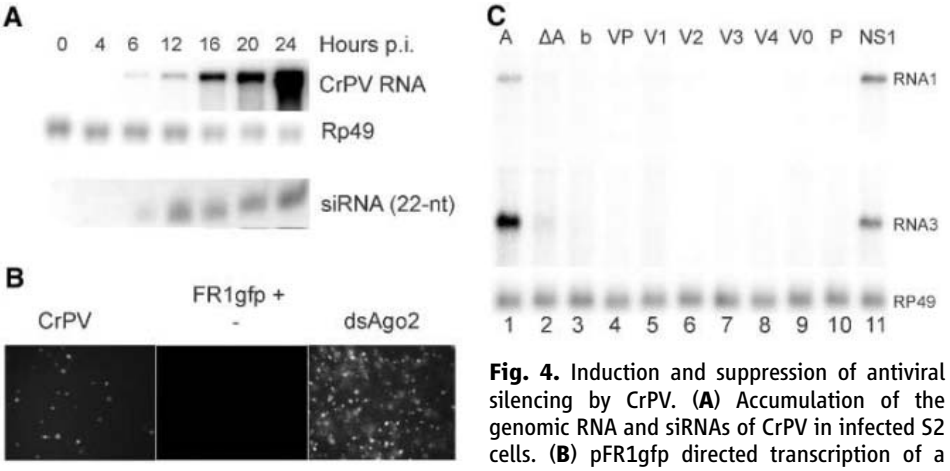

Fig. 4. Induction and suppression of antiviral silencing by CrPV. (**A**) Accumulation of the genomic RNA and siRNAs of CrPV in infected S2 cells. (**B**) pFR1gfp directed transcription of a recombinant FHV RNA1 in which the coding sequence for B2 was replaced by that of GFP. S2 cells were transfected with pFR1gfp alone (middle) or pFR1gfp plus either dsRNA-targeting Ago-2 (right) or CrPV superinfection (left). (**C**) Identification of CrPV RNAi suppressor. Cells were cotransfected with pFR1gfp and a plasmid as indicated on top of each lane (fig. S2), and total RNA was analyzed for the accumulation of pFR1gfp-encoded RNA1 and RNA3. P, the empty plasmid; VP, the virion protein precursor; V1, VP1; V2, VP2; V3, VP3; V4, VP4; V0, VP0 (precursor for VP3 and VP4); A, the first 140 codons of the upstream ORF; ΔA, a frameshift mutant of A; and b, the first 107 codons of the upstream ORF. NS1 is an RNAi suppressor of influenza A virus as described previously (*11*).

Nodaviruses and the polio-like CrPV belong to two different superfamilies of animal RNA viruses. We demonstrate that the same set of RNAi pathway genes is required for *Drosophila* defense against FHV and CrPV and that both viruses encode a potent VSR. These results collectively show that RNAi pathway functions as a common viral immunity mechanism in *Drosophila* and that RNAi suppression represents a general counterdefensive strategy used by insect viruses. Furthermore, a genetic requirement for Dcr-2, R2D2, and Ago-2 in antiviral silencing establishes a molecular framework for the innate immunity against viruses in *D. melanogaster*. None of Dcr-2, R2D2, and Ago-2 plays a detectable role in either the production or function of miRNAs in *D. melanogaster* (*1*). Thus, our work identifies the dsRNA-siRNA pathway of RNAi as providing the innate immunity against virus infection in *Drosophila* and establishes that dsRNA produced during virus replication acts as the pathogen trigger whereas Dcr-2 and Ago-2 act as host sensor and effector of the immunity, respectively. These results support and extend the previous findings on antiviral silencing in *C. elegans* (*4*, *5*).

Although NF-κB-like signaling in the Toll and Imd pathways do not appear to play a role in the RNAi-directed viral immunity mechanism in *D. melanogaster*, the fly mutant defective in the Janus kinase (JAK) Hopscotch exhibited a modest increase in susceptibility to infection with *Drosophila* C virus, suggesting an antiviral role for JAK–signal transducer and activator of transcription (STAT) signaling (*8*). Nonetheless, we believe that RNAi-based immunity is independent of JAK-STAT signaling, because virus infection is not known to induce the RNAi pathway in *Drosophila* (*8*) and FHV induction of the JAK-STAT responsive gene *vir-1* was unaltered in the *dcr-2* and *r2d2* mutants, as shown by our recent work. Because the Toll and Imd pathways are highly conserved in vertebrates (*7*), the *Drosophila* model established for RNAi may also be useful for the analyses of the innate antiviral immunity in vertebrates.

References and Notes

1. Y. Tomari, P. D. Zamore, *Genes Dev.* **19**, 517 (2005).
2. A. J. Hamilton, D. C. Baulcombe, *Science* **286**, 950 (1999).
3. H. W. Li, W. X. Li, S. W. Ding, *Science* **296**, 1319 (2002).
4. R. Lu *et al.*, *Nature* **436**, 1040 (2005).
5. C. Wilkins *et al.*, *Nature* **436**, 1044 (2005).
6. O. Voinnet, *Nat. Rev. Genet.* **6**, 206 (2005).
7. J. A. Hoffmann, *Nature* **426**, 33 (2003).
8. C. Dostert *et al.*, *Nat. Immunol.* **6**, 946 (2005).
9. R. A. Zambon, M. Nandakumar, V. N. Vakharia, L. P. Wu, *Proc. Natl. Acad. Sci. U.S.A.* **102**, 7257 (2005).
10. L. A. Ball, K. L. Johnson, *Adv. Virus Res.* **53**, 229 (1999).
11. W. X. Li *et al.*, *Proc. Natl. Acad. Sci. U.S.A.* **101**, 1350 (2004).
12. S. M. Hammond, S. Boettcher, A. A. Caudy, R. Kobayashi, G. J. Hannon, *Science* **293**, 1146 (2001).
13. K. Okamura, A. Ishizuka, H. Siomi, M. C. Siomi, *Genes Dev.* **18**, 1655 (2004).
14. Y. S. Lee *et al.*, *Cell* **117**, 69 (2004).
15. Q. Liu *et al.*, *Science* **301**, 1921 (2003).
16. J. E. Wilson, M. J. Powell, S. E. Hoover, P. Sarnow, *Mol. Cell. Biol.* **20**, 4990 (2000).
17. P. Irving *et al.*, *Proc. Natl. Acad. Sci. U.S.A.* **98**, 15119 (2001).
18. X. F. Dong, P. Natarajan, M. Tihova, J. E. Johnson, A. Schneemann, *J. Virol.* **72**, 6024 (1998).

19. We thank J. L. Imler for a stimulating discussion, A. Schneemann for providing CrPV and the anti-FHV serum, A. Raikhel for the bacterial strains, and members of the Ding and the Atkinson laboratories for comments and technical assistance. This project was supported by NIH grant AI052447 and U.S. Department of Agriculture grant 2005-35319-15331 (to S.W.D.). Partial support for this work was provided by NIH grants (to P.A. and R.W.C.).

Supporting Online Material

www.sciencemag.org/cgi/content/full/1125694/DC1
Materials and Methods
Figs. S1 to S3
References

1 February 2006; accepted 14 March 2006
Published online 23 March 2006;
10.1126/science.1125694
Include this information when citing this paper.

Hybridization Station

The a-Hyb Hybridization Station is an automated system for processing standard microarray slides that is suitable for integration into laboratory robotics and high-throughput settings. Its active circulatory system ensures efficient mixing and evenly distributes liquids over the microarray surface, thereby accelerating diffusion-limited processes and removing air bubbles. An accurate temperature control allows for standardization of incubation conditions, leading to greater reproducibility and reliability of the assays. It includes intuitive software that enables researchers to define conditions for each individual slide, such as hybridization temperature and supply of media. The user can handle to up four microarrays simultaneously in a microtiterplate-formatted slide carrier. The instrument is operated via touch screen.

Miltenyi Biotec For information +49 2204 8306-37 www.miltenyibiotec.com

Kits and Reagents

Trevigen's anti-8-oxo-dG antibody allows detection and quantitation of 8-hydroxyguanine in DNA, cell, and tissue samples and can be used in immunocytochemistry, enzyme-linked immunosorbent assays (ELISA), immunoprecipitation, and immunohistochemistry. The Glutathione Peroxidase Assay Kit can be used to measure glutathione-dependent peroxidases in plasma, erythrocyte lysates, tissue homogenates, and cell lysates. The kit is suitable for 96-well or cuvette format. The Universal 96-well PARP Assay Kit measures the incorporation of biotinylated poly(ADP-ribose) (PARP) onto histone proteins in a 96-well plate format. The assay is suitable for screening of PARP inhibitors and for measuring the activity of PARP in cell and tissue extracts. Important features of the assay include its colorimetric, nonradioactive format and its sensitivity down to 0.01 units of PARP per well.

Trevigen For information 800-873-8443 www.trevigen.com

Human Tumor Blots

Users can compare normal and tumor tissue proteins quickly and easily using tumor sets that are prepared with total protein extracts from normal and tumor tissue. Tumor Set I includes uterus, breast, cervix, ovary, testis, prostate, and rectum. Tumor Set II includes liver, lung, pancreas, stomach, thyroid, laryngopharynx, and skin. The user can choose the antibody and probe.

G-Bioscience/Geno Technology For information 800-628-7730 www.GBiosciences.com

Pathway Analysis Software

Version 4.0 of PathwayStudio (formerly PathwayAssist) contains powerful new tools for microarray data analysis and pathway dynamics simulation, as well as more than 1000 reconstructed pathways. PathwayStudio 4.0 scales from desktop to enterprise-wide, and allows scientists to reconstruct pathways, understand biology from microarray/proteomics data, predict drug side effects, and prioritize biomarkers in a complete, secure data management environment. New features and functionality include a simulation module to explore the dynamic behavior of pathways, new tools for building relevance networks from gene expression data, and the MedScan Reader biomedical literature browser.

Ariadne Genomics For information 847-644-1557 www.ariadnegenomics.com

Enhancer Dot-Blot

The Enhancer Dot-Blot allows for up to 384 dot blots of protein or nucleic acids on nitrocellulose or nylon membranes. This system concentrates liquid samples in a small area on a membrane through capillary action, thus enhancing signal strength. The system is supplied with sample application Tube-Strips and ready-to-use, pre-cut membranes, and there is no need for expensive equipment or vacuum pumps.

Genotech For information 314-991-6034 www.genotech.com

Desalting Spin Plates

The Zeba Desalt 96-well Plates are an effective tool for the efficient high-throughput removal of salt and small molecules (<1000 Da) from 20- to 100-μg samples, preparing them for downstream analysis, including mass spectrometry, high-performance liquid chromatography, capillary electrophoresis, metabolite screening, and assay development. The ready-to-use plates, which do not require resin dispensing or hydration, contain a high-performance resin that provides exceptional desalting (≥95%) and protein recovery, with minimal sample dilution for small molecules. One plate can be processed in 5 minutes.

Pierce. For information 815-968-0747 www.piercenet.com

Lentiviral Gene Set

A small hairpin RNA (shRNA) gene family set in lentiviral format is available for direct use in gene silencing. The Mission TRC shRNA Human Tumor Suppressor Gene Family is the first in a series of shRNA target sets that allow for rapid RNA interference cell-based screens in mammalian systems not easily manipulated by traditional siRNA. The lentiviral transduction particle format eliminates the need to propagate bacterial cells, purify plasmid DNA, or undertake the lengthy process of preparing virus, thus saving time and resources. Lentiviral-based shRNA can be used to create a stable knockdown in almost any mammalian cell types, including primary and nondividing cells.

Sigma-Aldrich. For information 800-521-8956 www.sigma-aldrich.com

Newly offered instrumentation, apparatus, and laboratory materials of interest to researchers in all disciplines in academic, industrial, and government organizations are featured in this space. Emphasis is given to purpose, chief characteristics, and availability of products and materials. Endorsement by *Science* or AAAS of any products or materials mentioned is not implied. Additional information may be obtained from the manufacturer or supplier by visiting www.science.labvelocity.com on the Web, where you can request that the information be sent to you by e-mail, fax, mail, or telephone.

ScienceCareers.org

Classified Advertising

For full advertising details, go to **www.sciencecareers.org** and click on **How to Advertise,** or call one of our representatives.

United States & Canada

E-mail: advertise@sciencecareers.org
Fax: 202-289-6742

JILL DOWNING
(CT, DE, DC, FL, GA, MD, ME, MA, NH, NJ, NY, NC, PA, RI, SC, VT, VA)
Phone: 631-580-2445

KRISTINE VON ZEDLITZ
(AK, AZ, CA, CO, HI, ID, IA, KS, MT, NE, NV, NM, ND, OR, SD, TX, UT, WA, WY)
Phone: 415-956-2531

KATHLEEN CLARK
Employment: AR, IL, LA, MN, MO, OK, WI, Canada; Graduate Programs; Meetings & Announcements (U.S., Canada, Caribbean, Central and South America)
Phone: 510-271-8349

EMNET TESFAYE
(Display Ads: AL, IN, KY, MI, MS, OH, TN, WV; Line Ads)
Phone: 202-326-6740

GABRIELLE BOGUSLAWSKI
(U.S. Recruitment Advertising Sales Director)
Phone: 718-491-1607

Europe & International

E-mail: ads@science-int.co.uk
Fax: +44 (0) 1223-326-532

TRACY HOLMES
Phone: +44 (0) 1223-326-525

HELEN MORONEY
Phone: +44 (0) 1223-326-528

CHRISTINA HARRISON
Phone: +44 (0) 1223-326-510

SVITLANA BARNES
Phone: +44 (0) 1223-326-527

JASON HANNAFORD
Phone: +81 (0) 52-789-1860

To subscribe to *Science*:
In U.S./Canada call 202-326-6417 or 1-800-731-4939
In the rest of the world call +44 (0) 1223-326-515

Science makes every effort to screen its ads for offensive and/or discriminatory language in accordance with U.S. and non-U.S. law. Since we are an international journal, you may see ads from non-U.S. countries that request applications from specific demographic groups. Since U.S. law does not apply to other countries we try to accommodate recruiting practices of other countries. However, we encourage our readers to alert us to any ads that they feel are discriminatory or offensive.

ScienceCareers.org
We know science AAAS

POSITIONS OPEN

The Thermal Biology Institute at Montana State University, Bozeman, seeks applicants for two tenure-track positions, one at the **ASSISTANT** or **JUNIOR ASSOCIATE LEVEL** and one at the level of **FULL PROFESSOR,** starting as soon as fall 2006.

We seek individuals who will continue the Institute's reputation for innovation and excellence by maintaining or creating an internationally recognized, externally funded program in thermal biology research in one or more of the following disciplines: microbiology, geochemistry, plant sciences, virology, biochemistry, metabolomics/genomics, environmental/ecological sciences, pre-biotic chemistry, or engineering. The successful applicant for the senior position will participate in shaping the future directions of the Institute and could potentially assume the position of Institute Director. The successful applicants for both positions will receive academic appointments in the College of Agriculture, College of Engineering, or College of Letters and Science, depending on their expertise, and will be expected to teach courses appropriate for their home Department. The successful applicants must have a demonstrated record of achievement or potential for excellence in research and teaching experience appropriate to rank. For complete application instructions, see the vacancy announcement at **website: http://www.montana.edu/msuinfo/jobs/faculty/** or contact: **Chair, Thermal Biology Institute Faculty Search, Montana State University, P.O. Box 173142, Bozeman, MT 59717.** Screening of applications will begin June 1, 2006, and continue until the positions are filled. For more information about Montana State University and the Thermal Biology Institute, please browse the applicable links at **websites: http://www.montana.edu** and **http://www.tbi.montana.edu.** *ADA/Equal Opportunity/Affirmative Action/Veterans Preference.*

FACULTY POSITIONS IN BIOINFORMATICS
University of Cincinnati
Molecular Genetics, Biochemistry, and Microbiology

As part of an ongoing initiative in bioinformatics at the University of Cincinnati, the Department of Molecular Genetics, Biochemistry, and Microbiology is searching for faculty candidates who fit within this program, specifically those studying regulatory genomics and networks in pathogenic processes such as cancer, cardiovascular disease, or microbial pathogenesis, or individuals involved in computational studies of protein structure. Successful applicants should have a demonstrated record of excellence in research, and be able to maintain an externally funded research program. The candidate will be expected to interact with the collegewide Bioinformatics/Computational Biology Program.

Our 25 full-time Departmental faculty maintain highly visible research programs in multiple areas including mutation, chromosome structure, differentiation, developmental and cancer biology, structural biology, signal transduction, membrane transport, viral and microbial pathogenesis, and molecular and cellular immunology. Our graduate program includes 40 graduate students, and an equal number of postdoctoral fellows train in the Department. Our structural biology program includes both nuclear magnetic resonance (NMR) and X-ray crystallography. We maintain core facilities for production of transgenic and knockout mice, and electron, confocal, and light microscopy, gene microarray analysis, proteomics, and imaging are available. These provide a breadth of research opportunities.

For further information, please see **website: http://www.molgen.uc.edu/logic/.** Applicants should submit curriculum vitae, brief description of research, and the names of three qualified references to: **Jerry B. Lingrel, Ph.D., Professor and Chair, Department of Molecular Genetics, Biochemistry, and Microbiology, P.O. Box 670524, Cincinnati, OH 45267-0524.**

POSITIONS OPEN

DIRECTOR OF PREMEDICINE AND GENERAL SCIENCE MAJORS

The Penn State Eberly College of Science seeks a faculty person to direct the two large, interdisciplinary, undergraduate majors within the college, one in premedicine and the other in general science. This will be a renewable, fixed-term, multiyear academic appointment, with the specific rank to be determined by the finalist's credentials. In addition to directing these two majors, this position will involve advising large numbers of students pursuing health professional careers, as well as communicating and interacting effectively with admissions officers at health professional schools across the country, particularly medical schools. The person also will chair the college's Health Sciences Preprofessional Evaluation Committee, which prepares letters of evaluation for most Penn State students applying for medical school admission. The position requires a Ph.D. in a biological science, with the expectation that the successful candidate will hold a faculty appointment in the Biology Department and teach courses in the area of human systems biology (i.e., physiology, anatomy, et cetera). The person will report to both the College's Associate Dean and the Head of the Biology Department. Prior teaching, research, administrative and student counseling/advising experience, as well as outstanding written and oral communication and interpersonal skills, are essential. Applications will be reviewed beginning May 15, 2006, and continuing until the position is filled, with a prospective start date in the coming academic year. Please provide curriculum vitae and the names of three references. Write to: **Premed/Science Director Search, P.O. Box SC, Penn State Eberly College of Science Human Resources, 512 Thomas Building, University Park, PA 16802; fax: 814-865-9492,** or by **e-mail: mlb1@psu.edu.** *Penn State is committed to Affirmative Action, Equal Opportunity, and the diversity of its workforce.*

ASSISTANT PROFESSOR
Department of Neuroscience, Pharmacology, and Physiology

In the position, the ideal candidate will teach interdisciplinary integrated medical curriculum. Teaching duties will include both basic and clinical pharmacology. A Ph.D. with postdoctoral experience (and concentration in pharmacology) required. Successful candidate must establish an independent and externally funded research program, as well as collaborate with other faculty in the development of a newly established Center for Chronic Disorders of Aging. Areas of research currently represented by the Center include cardiovascular disease, degenerative disease of the central nervous system (CNS), pain mechanisms and management; preference given to candidates whose research interest compliments these areas. Will be responsible for teaching medical and graduate students. Applications currently accepted for July 2006 start or earliest availability of best candidate. Send curriculum vitae with e-mail address, statement of research interest and the names and addresses of three references to: **Philadelphia College of Osteopathic Medicine, 4190 City Avenue, Human Resources Department, Philadelphia, PA 19131. Fax: 215-871-6505. E-mail: hr@pcom.edu. Website: http://www.pcom.edu.** *Equal Opportunity Employer.*

FACULTY POSITION IN WHEAT GENOMICS. The Department of Plant Pathology seeks applications for a tenure-track position. Candidate will have strong molecular biology skills and a proven track record in publications and extramural funding. Details at **website: http://www.plantpath.ksu.edu/.** Send curriculum vitae, statement of research and teaching interests, and three letters of reference to: **Bikram S. Gill, Department of Plant Pathology, 4024 Throckmorton Plant Sciences Center, Kansas State University, Manhattan, KS 66506-5502.** *Kansas State is an Equal Opportunity Employer.*

Careers in Aging Research

Ethnic and Minority Implications

Aging does not proceed along the same pathways and timelines in all populations. Recent work shows that even diseases—including Alzheimer's disease and others—can develop differently in some ethnic and minority groups. As a result, aging research offers new possibilities for careers at academic, government, and industrial organizations. BY MIKE MAY

"The aging of the American population is wholly unprecedented," says Daniel Perry, executive director of the Alliance for Aging Research. In *When I'm 64* (2006) from the U.S. National Research Council, the authors write: "By 2030 there will be about 70 million people in the United States who are older than 64, nearly 22 percent of the population." Even more significant from a health standpoint, Perry points out that the number of people 85 years of age or older will quadruple from 2000 to 2030. The authors of *When I'm 64* add that the 2030 population will be more ethnically and racially diverse. Perry says, "This is an enormous social change, and it brings challenges and opportunities for people in medical research."

Currently, the Caucasian population makes up about 84 percent of the elderly population in the United States, according to Perry. He adds, though, that this figure will drop to about 75 percent by 2030. The relative increase in the non-Caucasian population could trigger equal increases in some health problems—such as diabetes and high blood pressure—that afflict some minorities at high rates. "There's a lot to learn about what is driving those disparities," says Perry. "We want to improve the quality and length of life for people who are not currently enjoying the same opportunities for healthy aging."

Alliance for Aging Research
http://www.agingresearch.org

National Institute on Aging
http://www.nia.nih.gov

Pennsylvania State University
http://www.psu.edu

Disparate Data

The most interesting research "attracts new investigators," says J. Taylor Harden, assistant to the director for special populations at the National Institute on Aging of the U.S. National Institutes of Health. For example, she points out a recent study by Jonathan Skinner, John French Professor of Economics at the Dartmouth University School of Medicine. In *Circulation* in 2005, Skinner and his colleagues reported that risk-adjusted mortality from acute myocardial infarction is "significantly higher in [U.S.] hospitals that disproportionately serve blacks. A reduction in overall mortality at these hospitals could dramatically reduce black-white disparities in healthcare outcomes."

As another example of intriguing research, Harden points out a 2005 study in the *Archives of Neurology* by Christopher Clark, associate professor of neurology at the University of Pennsylvania Health System, and his colleagues. In the abstract to this article, Clark and his colleagues wrote: "Latino individuals are the largest minority group and the fastest growing population group in the United States, yet there are few studies comparing the clinical features of Alzheimer disease (AD) in this population with those found in Anglo (white non-Latino) patients." Clark and his colleagues found that "Latino patients had a mean age at symptom onset 6.8 years earlier ... than Anglo patients." In thinking about that CONTINUED »

Department of Health and Human Services (DHHS)
National Institutes of Health (NIH)
National Institute on Aging (NIA)

The mission of the NIA is to conduct research on the processes of aging and age-related diseases. The Intramural Research Program (IRP) is comprised of 11 scientific laboratories, a clinical research branch, a research resources support branch and 2 sections. Our research program includes the scientific disciplines of biochemistry, cell, developmental and molecular biology, genetics, physiology, immunology, neuroscience, neurogenetics, behavioral sciences, epidemiology, statistics, and clinical research and the medical disciplines of neurobiology, immunology, endocrinology, cardiology, rheumatology, hematology, oncology, and gerontology. Medical problems associated with aging are pursued in depth using the tools of modern laboratory and clinical research. The central focus of our research is to understand age-related changes in physiology and the ability to adapt to environmental stress. The NIA IRP provides a stimulating, academic setting for a comprehensive effort to understand aging through multidisciplinary investigator-initiated research. Find further information about the NIA IRP at **www.grc.nia.nih.gov**

The NIA is committed to the development of scientists, providing advanced biomedical research training in age-related research at all career stages. Salaries for all positions posted are commensurate with research experience, according to the NIH intramural pay scale. To apply for a postdoctoral position listed below, submit curriculum vitae with bibliography, three letters of reference, and a short statement of research goals to the correspondent. If you are unable to contact the correspondent using e-mail, mail your application to:

National Institute on Aging, Gerontology Research Center
Attn: Darryl M. Murray, Ph.D. Postdoctoral Recruitment Specialist, Mailbox 09
5600 Nathan Shock Drive, Baltimore, MD 21224-6825

Postdoctoral positions below are available to those with a Ph.D. or M.D. degree with less than 5 years postdoctoral training, unless otherwise stated in the ad.

Laboratory of Cellular and Molecular Biology **http://www.grc.nia.nih.gov/branches/lbc/lbc.htm**

Chromatin Remodeling and Gene Regulation in Lymphocytes: Two postdoctoral positions are available in the Chromatin Structure and Function Unit. Projects investigate the role of remodeling enzymes in lymphocytes, regulation of immunoglobulin and cytokine genes, and the function of purified remodeling enzymes in a cell-free system using model transcription units. Experience with ChIP or biochemical assays with purified proteins is desired. Experience in molecular biology/biochemistry is preferred.
Correspondent: Michael Pazin, Ph.D. Email: pazinm@grc.nia.nih.gov

Molecular Immunology - DNA Recombination and Repair: A postdoctoral position is available in Molecular Immunology Unit. Projects are focused on the mechanisms/regulation of DNA recombination and repair in lymphocytes, in particular V(D)J recombination and immunoglobulin gene conversion. Experimental approaches will include cell-line based in vivo systems and biochemical in vitro assays using purified (recombinant) proteins. Experience in molecular biology, biochemistry or a related field preferred.
Correspondent: Sebastian Fugmann, Ph.D. Email: fugmanns@grc.nia.nih.gov

Laboratory of Clinical Investigation **http://www.grc.nia.nih.gov/branches/lci/lci.htm**

Cartilage MRI & Integration of Cardiovascular Metabolism, Physiology, and Function: Two postdoctoral positions are available in the Nuclear Magnetic Resonance (NMR) Unit. 1) Conduct spectroscopic and imaging studies of bio-engineered and animal derived cartilage tissue. Experience with MRI imaging or NMR spectroscopy of connective tissue is preferred, but not required. 2) A joint position, in the Laboratory of Cardiovascular Sciences and the NMR Unit will focus on MRI and spectroscopic studies of myocardial metabolism related to congestive heart failure and beta-adrenergic stimulation and blockage of the heart in the living mouse. Expertise in cardiac or muscle physiology, or biological NMR spectroscopy or imaging preferred.
Correspondent: Richard Spencer, M.D., Ph.D. Email: spencer@helix.nih.gov

Inflammation and Insulin Signaling: A postdoctoral position is available in the Diabetes Section to conduct studies on molecular aspects of insulin signaling in mammalian cells that involve molecular, biochemical, and cellular approaches. Insulin resistance disorders will be studied at the molecular level with a focus on pro-inflammatory cytokine signaling. Prior experience in molecular biology is highly desirable; experience in protein biochemistry, cell biology, or animal investigations is required.
Correspondent: Michel Bernier, Ph.D. Email: bernierm@grc.nia.nih.gov

NIH AND DHHS ARE EQUAL OPPORTUNITY EMPLOYERS

National Institute on Aging

Department of Health and Human Services (DHHS)
National Institutes of Health (NIH)
National Institute on Aging (NIA)

Regulation of Insulin Secretion: The Diabetes Section is seeking a postdoctoral candidate to study the regulation of insulin secretion in the gut-pancreatic loop. In type 2 diabetes this loop is defective and the Section is attempting to understand the defect with the ultimate goal being its correction. Studies will use cell culture and whole animal models and many modern-day biological tools to investigate the intracellular mechanisms that regulate the release of factors in the gut.
Correspondent: Josephine Egan, M.D. Email: eganj@grc.nia.nih.gov

Laboratory of Immunology http://www.grc.nia.nih.gov/branches/li/li.htm

Regulation of Memory T Cell Response and Lifespan: Postdoctoral positions are available to study the mechanisms that control memory lymphocyte response and lifespan. Studies will include: 1) role of chromatin changes in regulating differential gene expression and function of memory T cells, and 2) role of homeostatic cytokines in regulation of memory T cell lifespan. Experience in molecular biology and cellular immunology is required.
Correspondent: Nan-ping Weng, M.D., Ph.D. Email: wengn@mail.nih.gov

Laboratory of Molecular Gerontology http://www.grc.nia.nih.gov/branches/lmg/lmg.htm

Antibody Diversity: A postdoctoral position is available to conduct research focusing on the identification of mechanisms for targeting hypermutation proteins to the immunoglobulin locus. Studies include the role of uracil as the lesion that initiates mutation. The effect of mismatch repair, base excision repair, and DNA polymerases will be analyzed biochemically and in mice. Experience in immunology, molecular biology, genetics, or biochemistry is required.
Correspondent: Patricia J. Gearhart, Ph.D. Email: gearhartp@grc.nia.nih.gov

Base Excision and Single-strand Break Repair: A postdoctoral position is available in the Structure and Function in Base Excision Repair Unit. Projects will couple molecular, biochemical, and cellular approaches and mouse models, to define the mechanisms of base excision and single-strand break repair, with emphasis on the contribution of oxidative DNA damage to cancer and neurodegeneration. Experience with molecular biology preferred; some experience in protein biochemistry, cell biology, or animal investigations is desirable.
Correspondent: David M. Wilson, III, Ph.D. Email: wilsonda@grc.nia.nih.gov

DNA Helicases: The Unit on DNA Helicases is recruiting a postdoctoral candidate to investigate the functions of DNA helicases defective in premature aging and cancer disorders. Genetic and biochemical approaches will be used to characterize the roles of DNA helicases in the maintenance of genome stability, in cellular DNA metabolic pathways and the mechanisms of unwinding by human DNA helicases.
Correspondent: Robert M. Brosh, Jr., Ph.D. Email: broshr@grc.nia.nih.gov

DNA Repair Mechanisms and Aging: A postdoctoral position is available to conduct studies that involve molecular, biochemical, and cellular approaches at the interphase of DNA repair mechanisms and aging. Human premature aging diseases will be studied at the molecular level with a focus on mitochondrial DNA repair. Experience in molecular biology preferred; some experience in protein biochemistry, cell biology, or animal investigations desirable.
Correspondent: Vilhelm A. Bohr, M.D., Ph.D., Chief Email: bohrv@grc.nia.nih.gov

Laboratory of Personality and Cognition http://www.grc.nia.nih.gov/branches/lpc/lpc.htm

Personality and Neuroimaging: Available postdoctoral position involves a project that interfaces the personality and neuroimaging programs and investigates the role of personality factors in relation to volumetric MRI data and PET studies. Databases of medical, personality, and neuroimaging data, including brain imaging studies of participants in the Baltimore Longitudinal Study of Aging will be used extensively. Expertise in the neurobiology of personality, an interest in the neural underpinnings of personality is desired. Familiarity with analysis and interpretation of structural and functional imaging data is preferred.
Correspondent: Paul Costa, Ph.D., Chief, LPC Email: costap@mail.nih.gov

Brain Physiology and Metabolism Section http://www.grc.nia.nih.gov/branches/lns/cpms.htm

Dynamics of Brain Phospholipid Metabolism: A postdoctoral position is available to quantify dynamics of brain phospholipid-fatty acid metabolism in relation to antibipolar disorder drug action, signal transduction, neuroinflammation, and polyunsaturated fatty acid nutrition. Rodent models will be used to measure incorporation into tissue lipids of intravenously injected radiolabeled arachidonic or docosahexaenoic acid. Techniques include GC/MS, HPLC and TLC, quantification procedures for tissue lipids, enzyme assays, radiotracer kinetics, molecular biology, and general biochemistry.
Correspondent: Stanley I. Rapoport, M.D., Chief Email: sir@helix.nih.gov

NIH AND DHHS ARE EQUAL OPPORTUNITY EMPLOYERS

National Institute on Aging

Careers in Aging Research

research, Harden says, "We want to make sure that our diagnostic tools are appropriate and help people if this is an issue for this population. For example, families might think about getting older members examined and get support in place if needed."


J. TAYLOR HARDEN

Better Behavior

No one is surprised to hear that aging research related to ethnic or minority populations covers many aspects of basic and medical science. Consequently, a wide variety of backgrounds could lead to work in this field. For example, Perry says, "There is a great deal of interest in people who understand the basic mechanisms of cellular biology, genetics, and proteins." He adds, "A person with strong credentials in immunology would also find much to do."

Aging research will also impact the pharmaceutical industry. Perry says, "Because our society supports medical investigations with the hope of affecting people's lives for the better, this field will increasingly be part of clinical trials and clinical medicine."

The work on aging in ethnic and minority populations will also explore psychological and sociological aspects. "Feelings of worth and belonging," says Perry, "are really determinant factors in aging. So there is a lot of interest in behavioral factors." Keith Whitfield, associate professor of biobehavioral health at Pennsylvania State University, agrees. He says, "There's a need for a solid understanding of the social and behavioral science of minority aging."

Wrongly, older adults are often considered less competent than younger people. The authors of *When I'm 64* write: "There is ample evidence to suggest that negative expectations and stereotypes about the competence of older adults pervade Western culture." Nonetheless, such expectations are often false. The authors go on to write that "there is also evidence of older adults serving important roles in society."

The impact of social factors could be especially relevant to neurological capabilities. For example, work by Whitfield and his colleagues suggests that social support might play a key role in preserving cognitive functioning among African-Americans. He says, "In the long run, this could be good for African-American families, because they often have strong kin networks. For example, the disproportionate rates of poverty among African-Americans lead to considerable custodial care by grandparents. It gives the grandparents activities and challenges, provides someone to take care of the children," and seems to ultimately benefit the cognitive health of the grandparents.

The Big Boom

"Aging research, in general, is a very hot area," says Perry, "given that we are now just five years from the date when the first baby boomer turns 65. We will soon go from about six thousand people turning 65 every day to close to ten thousand." This enormous increase in the older portion of the population alone will drive more interest in research on aging and also require more services for those people. "There couldn't be an area with more interest," Perry continues, "and the current health disparities for ethnic and minority populations will only become more stark, unless we find ways to extend life for all races and backgrounds."


DANIEL PERRY

In addition, the changes going on in the U.S. population create new opportunities. Whitfield says, "Even in tough financial times for many institutions of higher learning, there is a great interest in diversity and in aging." In addition, he says that no one knows the details of how aging varies in different ethnic and minority groups. "It's almost like we need to establish new starting points for much of our understanding of aging so we get it right."

The future opportunities in aging for ethnic and minority populations will also go beyond basic and applied research. "There will also be considerable work in health delivery services," says Perry. "We now have a shockingly small number of doctors, nurses, pharmacists, physical therapists, and so on who have extended education and credentials in geriatrics." He adds, "The number of doctors with qualifications in geriatric medicine is only about 3 percent." He thinks that will create a tremendous demand for such specialists in managed care organizations and hospitals.


KEITH WHITFIELD

Aging Interest

"In 1999," says Perry, "NIH identified health disparities as an area of special emphasis. It developed a minority aging review committee so that opportunities for jobs in this area will continue to grow." Along with that NIH emphasis, research funds should be available. "Funding for medical- and health-related science continues to outstrip physical sciences, chemistry, and so on," says Perry. Also, the aging population will probably enhance the pressure to fund research. "Every member of Congress has constituents who get sick or whose parents get sick," says Perry.

Many biotechnology companies also work on aging. Elan is developing a vaccine for Alzheimer's disease. Geron explores many therapies related to aging, including cell-based approaches to chronic diseases. Migenix also puts significant resources into treatments for degenerative diseases. "Even Genentech focuses a lot on aging," says Perry.

To make the greatest strides on aging for ethnic and minority populations, scientists might need a new approach. "We need to stop thinking that we can take things that have been studied in other groups and simply apply that to minorities," says Whitfield. "Results show that there are different patterns and causal pathways to similar outcomes." Those results—seeing new mechanisms of aging in some populations—open new opportunities for everyone in this field.

Mike May (mikemay@mindspring.com) is a publishing consultant for science and technology based in the state of Minnesota, U.S.A.

EMBL

The European Molecular Biology Laboratory, EMBL is an international research organisation with its Headquarters Laboratory in Heidelberg, Germany and four additional Units in Hinxton (the European Bioinformatics Institute, EBI), Grenoble, Hamburg, and Monterotondo. EMBL offers a highly collaborative, uniquely international culture. It fosters top quality, interdisciplinary research by promoting a vibrant environment consisting of young independent research groups with access to outstanding graduate students and postdoctoral fellows. High-level expertise is available in Computational Biology, diverse aspects of experimental Molecular Biology as well as Physics, Biophysics, Chemical Biology and instrument development.

Coordinator Position at EMBL

Structural and Computational Biology Unit

EMBL is searching for a Structural and Computational Biology Unit Coordinator, who will replace Luis Serrano to lead the Heidelberg Unit jointly with Peer Bork. The candidate will have an outstanding record in any aspect of Structural Biology or Systems Biology. He or she will have a broad scientific view, possess scientific vision and leadership skills, will wish to work in an open, collegial environment and will possess administrative competence. The candidate will lead a research group, will mentor younger faculty members and will ensure the maintenance of world class standards of research throughout the Unit. Further, he/she will participate in the collegial leadership of EMBL.

The Scientific Programme of EMBL emphasises experimental analysis at multiple levels of biological organisation, from the molecule to the organism, as well as Computational Biology, Bioinformatics and Systems Biology. Within this structure, the Structural and Computational Biology Unit occupies a critical position. The Unit applies a wide range of modern technologies to diverse biological problems. Current Group and Team Leaders are: Peer Bork, Bettina Böttcher, Elena Conti, Achilleas Frangakis, Anne-Claude Gavin, Toby Gibson, Rob Russell, Michael Sattler, Klaus Scheffzek, Reinhard Schneider, Dietrich Suck. In addition, several group leaders from other EMBL Units have joint appointments in Structural and Computational Biology. Due to the EMBL turnover system, the Unit composition is highly dynamic, and the Coordinator will play a critical role in the choice of new Group Leaders and thus in the research direction of the entire Unit. He/she will help integrate the Unit's research activities with those of the other Units in Heidelberg (Cell Biology and Biophysics, Developmental Biology, Gene Expression) and in EMBL's Outstations, particularly with the Structural Biology research at the Grenoble and Hamburg Units and Bioinformatics research at the EBI.

EMBL is an inclusive, equal opportunity employer offering attractive conditions and benefits appropriate to an international research organisation.

Further information on the position can be obtained from the EMBL Director General, Iain Mattaj (dg-office@embl.de).

About EMBL please visit www.embl.org.

Applicants should submit a curriculum vitae, quoting ref. no. S/06/50 in the subject line to: application@embl.de

EMBL, Personnel, Postfach 10.2209, D-69012 Heidelberg, Germany, Fax: +49 6221 387555

www.embl.org

Scientific Director, Center for Cancer Research, NCI

The Center for Cancer Research (CCR), National Cancer Institute (NCI), National Institutes of Health (NIH), Department of Health and Human Services (DHHS), is accepting applications for the position of Scientific Director (SD), Center for Cancer Research (CCR).

The CCR's mission is to reduce the burden of cancer through exploration, discovery and translation. The CCR is composed of approximately 195 Principal Investigators in 50 Laboratories, Branches and Programs. As one of the world's largest cancer research centers, the CCR takes advantage of the breadth of its researchers to foster interdisciplinary programs and facilitate translational research. Basic research is a strength of the CCR, with areas of investigation including immunology, carcinogenesis, human genetics, mouse genetics, viral oncology, HIV, chromatin biology, structural biology, DNA replication and recombination, signal transduction, apoptosis, cell cycle regulation, cytokines and chemokines, cellular, molecular and developmental biology, medicinal chemistry and natural products chemistry, molecular pharmacology, xenobiotic metabolism, radiation biology, computational biology and bioinformatics. Areas of excellence in clinical and translational research include cancer vaccines, clinical proteomics, molecular targets of cancer, molecular imaging, biologic mediators, cell-based therapies, immunotoxin therapy, radiation therapy, cancer genetics, molecular epidemiology, cancer prevention, multidrug resistance, clinical pharmacology, angiogenesis and molecular pathology.

The Scientific Director is responsible for the overall management and scientific direction of the intramural research program in the CCR, including the training and mentoring of tenure-track investigators and post-doctoral researchers assigned to the program. The SD must have a scientific vision for the program and administrative skills to manage it. The successful candidate must have an appropriate doctoral degree and experience directing large-scale cancer research programs. Salary is commensurate with experience.

All applicants should submit a letter indicating interest in the position, a statement of research interests, a career synopsis and brief bibliography, current curriculum vitae and complete bibliography, and the names and addresses of five references, by **May 31st**, to:

Dr. Dinah S. Singer, c/o Mr. Patrick Miller, 31 Center Drive, Suite 3A19, Bethesda, Maryland 20892.

Scientific Director for Clinical Research, NCI

The Center for Cancer Research (CCR), National Cancer Institute (NCI), National Institutes of Health (NIH), Department of Health and Human Services (DHHS) is accepting applications for the position of Scientific Director (SD) for Clinical Research.

The CCR's clinical mission is to conduct concept-based (science-driven) clinical trials that evaluate new therapies rather than testing existing ones, discover and develop molecularly targeted agents and combinations of agents for use in clinical trials, develop novel approaches to early cancer detection and prevention, develop and deliver novel technologies for molecular diagnosis of cancer, emphasize understudied diseases and cancers with increasing incidence or involving special populations, and develop better preclinical models and methods to expedite development of novel interventions for cancer.

The SD for Clinical Research is responsible for overseeing the clinical branches of the NCI and the critical bench to bedside translation of novel preclinical observations from CCR laboratories utilizing the unique resources of the NIH Clinical Center. S/he is responsible for oversight of the overall clinical program within the CCR and will work closely with the Director, CCR, to develop an outstanding overall intramural research program. As a specialized Cancer Center within the NCI portfolio, it is essential that the CCR clinical program is integrated both within the context of the intramural scientific program, as well as within the context of the overall NCI clinical program. The SD for Clinical Research is responsible for achieving an integrated clinical sciences program within the Intramural Research Program (IRP) that contributes substantially to the NCI mission and is highly valued across the clinical landscape. The SD will oversee the clinical agenda across all major clinical disciplines including surgical oncology, radiation oncology, medical oncology and pediatric oncology. In addition to these major disciplines, the SD will oversee the Experimental Transplant and Immunology Branch, the Laboratory of Pathology and the HIV and Aids Malignancy Branch.

The successful candidate must have an appropriate doctoral degree and experience directing large-scale cancer research programs. Salary is commensurate with experience.

All applicants should submit a letter indicating interest in the position, a statement of research interests, a career synopsis and brief bibliography, current curriculum vitae and complete bibliography, and the names and addresses of five references, by **May 31st**, to:

Dr. James Doroshow, c/o Mr. Patrick Miller, 31 Center Drive, Suite 3A19, Bethesda, Maryland 20892.

WWW.NIH.GOV

Deputy Director
Division of Cancer Biology

The Department of Health and Human Services(DHHS), National Institutes of Health(NIH), National Cancer Institute (NCI), is seeking a Deputy Director, Division of Cancer Biology (DCB), to participate in the scientific and administrative management of the Division. DCB has principal responsibility for the planning, direction, coordination and evaluation of a broad program of extramural research in cancer biology and etiology, with six Branches focused on cancer cell biology, tumor biology and metastasis, cancer immunology and hematology, DNA and chromosome aberrations, cancer etiology, and structural biology and biotechnology with an annual budget of over $800 million that supports grants, cooperative agreements, contracts and operating expenses. The Deputy Director participates in the planning of a coordinated program in the areas of cancer etiology, biology and immunology and is directly responsible for conducting a continuous review and evaluation of the Division's operations as they pertain to a broad program of grant supported activities designed to increase knowledge of cancer biology. The Deputy Director, DCB, will be appointed at a salary commensurate with his/her qualifications and experience. Full federal benefits include, leave, health and life insurance, retirement savings plan (401K equivalent).

Qualifications Required: The applicant must have a doctoral level degree (Ph.D.) Or medical degree (M.D.) with significant research experience. The applicant currently must be an experienced Senior Scientist and/or Science Administrator with considerable expertise and demonstrated recognition for achievements related to cancer biology research and documented experience in program planning, implementation and oversight and in grants management. The applicant must have significant administrative, managerial and supervisory experience.

How to apply: Applicants should send a brief biography, curriculum vitae, bibliography and the names and addresses of four references to: **Dinah A. Singer, Ph.D., Director, Division of Cancer Biology, National Cancer Institute, 6130 Executive Blvd., Building EPN, Room 5044, Rockville, MD 20852-7380.**

If you need additional information, please call **Mr. Stephen White at (301) 594-8905 or Mrs. Bridgette Tobiassen at (301) 594-8786. DEADINE FOR RECEIPT OF APPLICATIONS: May 31, 2006.**

Staff Scientist Position

Staff Scientist Position is available at the National Cancer Institute, National Institute of Health for candidates with at least three to five years of Post-doctoral experience in Molecular Biology and or Biochemistry. It is a GS-13 position with at starting salary of approximately $70,000 per year plus benefits. The candidate will be involved in studying the mechanism of nuclear export of mRNA in fission yeast. Submit cover letter, CV and provide names and address of three references to: **Ravi Dhar, BRL, CCR, NIH Bldg. 37 Rm. 6138, 9000 Rockville Pike, Bethesda, MD 20892-4260**. Telephone No: **301-496-0990, Email: dharr@mail.nih.gov**

Postdoctoral, Research and Clinical Fellowships at the National Institutes of Health

www.training.nih.gov/pdopenings

www.training.nih.gov/clinopenings

Train at the bench, the bedside, or both

Office of Intramural Training and Education
Bethesda, Maryland 20892-0240
800.445.8283

MRI Scientist Position
National Institute of Neurological Disorders and Stroke

With nation-wide responsibility for improving the health and well being of all Americans, the Department of Health and Human Services oversees the biomedical research programs of the National Institutes of Health.

The NIH MRI Research Facility (NMRF) in the National Institute of Neurological Disorders and Stroke is seeking an MRI scientist to support the human brain imaging studies conducted by the NIH investigators. NMRF offers state-of–the-art MRI facilities for users throughout the NIH. The NMRF is a part of the NIH In Vivo NMR Center which houses active research programs in brain and cardiac MRI. Four 3T MRI (GE) scanners and a 7T MRI (GE) scanner are available in the NMR Center for human brain research. The successful candidate will have a Ph.D. in a relevant field and interest in application of MRI to study brain function and disorders. Experience in MRI pulse sequence design and programming is required. Knowledge and interest in image processing or MRI hardware is desirable. In addition to collaborative research, the candidate will have the opportunity to initiate new projects that will impact ongoing research. Salary is very competitive and commensurate with education and experience.

Please send a CV and three letters of reference to **Dr. Lalith Talagala, NIH MRI Research Facility, National Institutes of Health, 10 Center Drive, Room B1D69, Bethesda, MD 20892-1060, Email: talagala@nih.gov.**

Positions @ NIH
THE NATIONAL INSTITUTES OF HEALTH

Health Research in a Changing World

Fighting Diseases and Improving Lives

Director, Office of Communications and Government Relations

The National Institute of Allergy and Infectious Diseases (NIAID), National Institutes of Health (NIH) in Bethesda, Maryland, seeks applications from exceptional candidates for the challenging position of Director, Office of Communications and Government Relations (OCGR), a career Federal position in the Senior Executive Service.

The Director, OCGR, is the senior Institute advisor on and provides management leadership for the legislative affairs, communications and public affairs, and related functions of the NIAID. In addition, the position is also responsible for bringing an organization-wide perspective and providing leadership in communicating about and coordinating the Institute's international research programs.

The NIAID is a $4.4 billion research organization that leads, supports, and conducts research to understand, treat, and prevent infectious, immunologic, and allergic diseases throughout the world. NIAID supports well over 100 major research programs and initiatives within three broad, distinct mission areas: Biodefense research, AIDS research, and the NIAID traditional research mission of immunologic and infectious disease. A full package of Civil Service benefits is available including retirement, health and life insurance, long-term care insurance, leave and a 401k equivalent savings plan. The complete vacancy announcement, along with mandatory qualifications requirements and application procedures, can be accessed via the NIH Home Page at: **http://www.jobs.nih.gov** under the Executive Job Openings section (Announcement Number NIAID-06-01SES). For questions, contact **Patti Brown** at **SeniorRe@od.nih.gov** or by calling 301-451-7340. Applications, including a statement addressing the qualifications requirements, must be received by close of business **May 15, 2006**.

We invite you to explore our Institute and other opportunities at **http://healthresearch.niaid.nih.gov/science**

Please reference "Science" on your resume

Scientific and Clinical Director

The National Center for Complementary and Alternative Medicine (NCCAM) seeks an accomplished, innovative neuroscientist and clinician to fill three pivotal roles: as Scientific Director and Clinical Director of its Intramural Research Program (IRP) and as Senior Investigator responsible for developing a new research program in mind-body medicine. This individual will report to the NCCAM Director and will be a member of the NCCAM leadership.

As Scientific Director, you will articulate and implement a vision and oversee research infrastructure for highly unified and mutually supportive laboratory and clinical programs in the conduct of bench-to-bedside and bedside-to-bench research related to CAM therapies.

As Clinical Director, you will chart a course and allocate resources for clinical research; recruit and oversee the activities of clinical staff and fellows; ensure appropriate design and conduct of clinical research protocols; and facilitate the integration of CAM practices into the training programs and delivery of care throughout the NIH Clinical Center.

As Senior Investigator, you will have substantial committed resources to create a cutting-edge program of clinically oriented laboratory research and clinical studies that exploit neuroscience disciplines to define the nature, mechanisms of action, safety, and efficacy of diverse CAM modalities that affect actions and interactions linking mind, body, and behavior.

This exceptional opportunity is available to a U.S. citizen, resident alien, or nonresident alien with valid employment authorization who is an accomplished neuroscientist with a U.S. medical license; a demonstrated record of senior-level management of a large, nationally recognized research program; a commitment to both basic and clinical research; and leadership skills that equip him/her to forge team efforts with colleagues within intramural programs across NIH.

Salary and benefits are commensurate with experience. Qualified individuals are encouraged to email their CV, bibliography, list of three references, and cover letter outlining their relevant experience and vision for leading the NCCAM IRP to: *nccamdirector-r@mail.nih.gov*

Subject Line: Scientific and Clinical Director Search

Application Deadline: July 14, 2006

Email receipt of applications and inquiries is preferred; however, candidates needing reasonable accommodation may fax application materials to 301-402-4741.

NCCAM
NATIONAL CENTER FOR COMPLEMENTARY AND ALTERNATIVE MEDICINE

NIH and DHHS are Equal Opportunity Employers

WWW.NIH.GOV

Director, Division of Extramural Activities
National Institute of Dental and Craniofacial Research
Note: the closing date for this announcement has been extended to May 12, 2006

The National Institute of Dental and Craniofacial Research (NIDCR), a major research component of the National Institutes of Health (NIH) and the Department of Health and Human Services, seeks an outstanding scientist to lead its Division of Extramural Activities (DEA) located at the National Institutes of Health in Bethesda, Maryland.

The Director, DEA, provides leadership and advice in developing, implementing, and coordinating the Institute's extramural programs and policies. S/he serves as a senior advisor to the Director and other Institute officials on issues related to policies and procedures for extramural affairs, and represents the Institute on extramural program and policy issues within the NIH, the Department and with outside organizations. The Director oversees the initial scientific review of applications assigned to the Institute, including program projects, research grants in response to RFAs, training grants, cooperative agreements, and R&D contracts, and ensures effective and proper grants management. S/he manages and monitors all business aspects of the Institute's grants, provides information and guidelines for grant applications, and oversees the closed session of the National Advisory Dental and Craniofacial Research Council. In addition, the Director undertakes program evaluation and planning activities in conjunction with the Institute's programmatic Centers and the Office of Science Policy and Analysis.
Applicants must possess a Ph.D., D.D.S./D.M.D., M.D., or equivalent degree, in a biomedical or related field and have in depth knowledge of NIH policies and procedures governing extramural research activities (research grants, cooperative agreements, and contracts). Applicants must be able to serve as a spokesperson for NIDCR with research institutions, science professionals, and the general public, and have proven experience in directing and managing NIH extramural activities, with the requisite administrative and interpersonal skills to meet the demands of program direction.

Interested applicants should send their curriculum vitae and bibliography, and the names and addresses of four references. Applications must be received by the closing date and should be sent to:

Ms. Carol M. Beasley, National Institute of Dental and Craniofacial Research, Building 31, Room 2C39, Bethesda, MD 20892-2290, E-mail: carol.Beasley@nih.gov., Fax: 301-402-4088. The closing date for this position is: **May 12, 2006**

Deputy Director
National Institute of Neurological Disorders and Stroke (NINDS)

The NINDS is seeking exceptional candidates for the position of Deputy Director to provide leadership and serve as an active partner with the Director in leading a $1.5 billion national research program in diseases of the nervous system (www.ninds.nih.gov). This position offers a unique and exciting opportunity for the right individual to share responsibility in providing strong and visionary leadership to an organization dedicated to uncovering new knowledge and technologies, both basic and clinical. Candidates are sought who have a commitment to scientific excellence and the energy, enthusiasm, and innovative thinking required to help lead a major research institute. Applicants must possess an M.D. degree, as well as senior-level research experience or knowledge of research programs in one or more NINDS scientific areas, including familiarity with clinical research. Applicants should also demonstrate the ability to think strategically, work collaboratively, and use a consultative approach to problem solving and decision making. The Deputy will be expected to represent, and speak for, the Director and Institute before high level Government officials, as well as various non-government organizations advocating for those with neurological disease. Opportunities exist to have activities in the NINDS intramural program. Salary is commensurate with experience and a full package of Civil Service benefits is available, including: retirement, health and life insurance, long term care insurance, leave and savings plan (401K equivalent).

With nationwide responsibility for improving the health and well being of all Americans, the Department of Health and Human Services oversees the biomedical research programs of the NIH. The NIH encourages the application and nomination of qualified women, minorities, and individuals with disabilities.

Applicants should send a cover letter, curriculum vitae and bibliography to **Thomas Insel, M.D., Chair, Search Committee, c/o Ms. Joellen Harper Austin, OD, NINDS, Building 31, Room 8A52, 31 Center Drive, Bethesda, MD 20892-2540**. For further information, please contact **Dr. Insel at 301-443-3673**. Applicants will be reviewed starting **May 1, 2006**. Additional applications will be considered until the position is filled.

Tenure-Track Positions (4)

Faculty of Environmental & Forest Biology

(1) WILDLIFE ECOLOGIST

(Assistant or Associate Professor, tenure track). Qualified candidates must demonstrate a primary interest in wildlife ecology and management. A Ph.D. in Wildlife Ecology or a related discipline is required. Preference will be given to candidates with a record of excellence in teaching, research, and outreach, commensurate with time since degree. Strong quantitative skills including population analysis, biometry and spatial analysis, strong field skills, and ability to mentor graduate and undergraduate students are also preferred. Application review begins **April 17, 2006**. For more information contact Dr. William Porter (wfporter@esf.edu, phone 315-470-6798).

(2) VERTEBRATE ECOLOGIST

(Assistant Professor, tenure track). The successful candidate will develop a teaching, research, and service program in vertebrate ecology including such subjects as physiological, behavioral, evolutionary, population, community and landscape ecology of organisms, populations, ecosystems or regional biotas. A Ph.D. related to ecology of amphibians, birds, mammals or reptiles is required and a significant focus on field-based research is desired. Application review begins **August 7, 2006**. For more information contact Dr. James P. Gibbs (jpgibbs@syr.edu, phone 315-470-6764) or Dr. Mark Lomolino (island@esf.edu, phone 315-470-6805).

(3) PLANT ECOLOGIST

(Assistant Professor, tenure track). The successful candidate will develop a teaching, research and service program in plant ecology. A Ph.D. in Plant Ecology or a related discipline, as well as a record of publication, grantsmanship and independent research are required. Preference will be given to candidates with strong field experience and quantitative skills and a record of excellence in teaching, mentoring, research and outreach. Application review begins **August 7, 2006**. For more information contact Dr. Robin Kimmerer (rkimmer@esf.edu, 315-470-6785).

(4) FOREST ENTOMOLOGIST

(Assistant Professor, tenure track). The successful candidate will be expected to develop a teaching, research and service program in forest entomology. Qualified candidates must demonstrate a primary interest in the biology and management of forest insects. A Ph.D. in entomology or a related discipline is required. Application review begins **September 1, 2006**. For more information contact Dr. Stephen A. Teale (sateale@esf.edu, 315-470-6758).

The College of Environmental Science and Forestry is part of the State University system in New York and its campus is contiguous with Syracuse University. It maintains a small-college atmosphere with low student faculty ratios where both teaching and research are emphasized. As one of the finest environmental biology programs in the world, ***The Faculty of Environmental and Forest Biology*** (www.esf.edu/efb) includes 37 scientists who provide a diverse and enriching education emphasizing concepts of biodiversity conservation, physiology, and ecology of plants, animals, fungi and microorganisms. Field biology forms a strong foundation for coursework and research experience, and the College operates five field stations including Cranberry Lake Biological Station (www.esf.edu/clbs), the 6,000 hectare Huntington Forest and associated Adirondack Ecological Center (www.esf.edu/aec), the Tully Field Station and the 1,600 hectare Heiberg Forest south of Syracuse, and the Thousand Islands Biological Station on the St. Lawrence River (www.esf.edu/tibs). Students also participate in international field experiences including those in Africa, Australia, Dominica, Ireland, New Zealand and Russia.

For more detailed descriptions and application procedures for each position, visit the **SUNY-ESF Human Resources website - www.esf.edu/hr/search/**

SUNY-ESF is an Equal Opportunity/Affirmative Action employer.

The **Department of Experimental Therapeutics** seeks highly qualified, basic science applicants for tenure-track appointments as assistant/associate professor.

ASSISTANT/ASSOCIATE PROFESSOR, PHARMACOGENOMICS

The successful candidate will possess demonstrated ability to conduct independent research and obtain peer-reviewed funding in the area of human genome sequencing, genotyping and/or other approaches for identifying host-specific variability and pharmacology; be published in human cancer genetics, pharmacology and/or therapy; and be responsible for building a program in pharmacogenomics in the new Center for Targeted Therapy.

Applicants should hold a doctoral level or medical degree with emphasis in researching the effects of genetic variability on anticancer drug or biologic toxicity and efficacy; the characterization of polymorphisms relevant to drug action; and the identification of novel, genomic targets for drug development. In addition, a demonstrated collaborative ability to interact with clinicians and translational researchers developing new cancer therapies is required.

Preference will be given to Ph.D. or Pharm.D. candidates with expertise in the clinical application of novel, anticancer agents with particular emphasis on pharmacology; knowledge of human genetics tools currently employed in cancer therapy; and excellent communication and interpersonal skills.

ASSISTANT/ASSOCIATE PROFESSOR, MOLECULAR DRUG DESIGN

The successful candidate will possess demonstrated ability to conduct independent research in the area of computer-based screening and design of novel anticancer agents and have a proven track record indicated by publications and grant funding. The position also will be responsible for building a program in computer-aided drug design in the new Center for Targeted Therapy.

Applicants should hold a doctoral level or medical degree with emphasis in computer-aided drug design and the ability to interact with basic researchers developing new cancer therapies. Preference will be given to Ph.D. or Pharm.D. candidates with experience in computer modeling and design of novel anticancer agents; knowledge in structural biology of molecular targets for cancer drug discovery and development; and excellent communication and interpersonal skills.

Please forward curriculum vitae; contact information for references; and a brief statement including accomplishments, current and proposed research objectives and plans to emerge as a leader in chosen area to:

Garth Powis, D.Phil., Chair
Department of Experimental Therapeutics – Unit 422
The University of Texas M. D. Anderson Cancer Center
1515 Holcombe Blvd., Houston, Texas 77030-4009

E-mail: ETDept@mdanderson.org

The **University of Texas M. D. Anderson Cancer Center** offers generous start-up funds and quality laboratory space, as well as the opportunity to collaborate with leading scientists in structural biology, molecular target identification, pharmacology, biological therapy, drug development and clinical testing throughout the department and institution.

THE UNIVERSITY OF TEXAS
MD ANDERSON
CANCER CENTER
Making Cancer History®

The establishment of the Center for Targeted Therapy (which will occupy one of six unique, 130,000 square feet, state-of-the-art facilities that form the Red and Charline McCombs Institute for the Early Detection and Treatment of Cancer, located on the south campus of M. D. Anderson Cancer Center) will allow researchers and clinicians alike the ability to coordinate all stages of the drug discovery and development process and design new, more effective and specific drugs with less toxicity, targeted for individualized therapy thus accelerating the delivery of new drug therapies from the research bench to the patient's bedside.
Our vision is nothing short of curing cancer.

M. D. Anderson Cancer Center is an equal opportunity employer and does not discriminate on the basis of race, color, national origin, gender, sexual orientation, age, religion, disability or veteran status except where such distinction is required by law. All positions at The University of Texas M. D. Anderson Cancer Center are security sensitive and subject to examination of criminal history record information. Smoke-free and drug-free environment.

Chair

Department of Molecular Genetics

A search for a new chair of the Department of Molecular Genetics at The University of Texas M. D. Anderson Cancer Center is underway with the goal of recruiting an individual of international stature to enhance M. D. Anderson's basic research portfolio. We are seeking someone who is interested in leading a world-class basic science department and who wishes to have a critical role in influencing the scientific direction of one of the most respected and renowned cancer centers in the country. Applications are encouraged from outstanding senior-level scientists working in the field of molecular genetics, cancer genetics, epigenetics, genomics, biochemical genetics, or a related area.

We are committed to providing such an individual with major resources to support the highest level of research in genetics and genomics. Besides a generous individual start-up package, these will include appointment to an endowed chair, multiple positions for recruiting new faculty, expansion of the department into additional space in our new George and Cynthia Mitchell Basic Science Research Building, and substantial administrative and infrastructure support for directing a major research department.

M. D. Anderson offers unparalleled opportunities to engage in interactions with clinical and translational researchers as well as basic scientists. As part of the Texas Medical Center, M. D. Anderson and its faculty participate in countless programs and interactions with the other academic and health components including Baylor College of Medicine, The University of Texas Health Science Center, Rice University, and Texas A&M Institute of Bioscience and Technology. The breadth and quality of biomedical science in the Texas Medical Center rivals that of any academic medical center in the world.

Individuals who might be interested in exploring this exciting opportunity should contact us preferably via e-mail and include their curriculum vitae and a brief statement of purpose. We are casting a wide net and particularly encourage individuals who are seeking a significant leadership challenge while maintaining a dynamic research program. The search will continue until the position is filled and candidates will be reviewed on an ongoing basis. Contact information:

William Klein, Ph.D.
Chair, Department of Biochemistry and Molecular Biology, Unit 1000
The University of Texas M. D. Anderson Cancer Center
1515 Holcombe Blvd., Houston, TX 77030
E-mail: whklein@mdanderson.org

THE UNIVERSITY OF TEXAS
MD ANDERSON
CANCER CENTER

Making Cancer History®

AWI Stiftung Alfred-Wegener-Institut für Polar- und Meeresforschung

Die Stiftung Alfred-Wegener-Insitut für Polar- und Meeresforschung (Stiftung AWI) in Bremerhaven ist eine von der Bundesrepublik Deutschland und den Ländern Freie Hansestadt Bremen, Brandenburg und Schleswig-Holstein gemeinsam finanzierte Großforschungseinrichtung in der Helmholtz Gemeinschaft Deutscher Forschungszentren (HGF).

Die Stiftung AWI betreibt in Kooperation mit nationalen und internationalen Partnern in einem multidisziplinären Ansatz Meeres- und Polarforschung, die physikalische, biologische, geologische und chemische Methoden einschließt. Mit der Entwicklung komplexer Modelle, der Analyse mariner Ökosysteme sowie der Untersuchung biogeochemischer Prozesse im Ozean, der Atmosphäre und im Eis leistet die Stiftung Beiträge zur globalen Umweltforschung. Neben der Forschung gehören die Koordination sowie die technische und logistische Unterstützung der Polar- und Meeresforschung in der Bundesrepublik Deutschland zu den Aufgaben der Stiftung.

Die Stiftung AWI hat zurzeit ein jährliches Budget von ca. 110 Mio. Euro und beschäftigt etwa 800 Mitarbeiter/Mitarbeiterinnen. Sie wird von einem Direktorium geleitet, das aus einem hauptamtlichen wissenschaftlichen Direktor, einem hauptamtlichen administrativen Direktor sowie zwei stellvertretenden nebenamtlichen Direktoren besteht.

Zum 1. November 2007 ist in der Stiftung AWI die Stelle des/der

Wissenschaftlichen Direktors/Direktorin

neu zu besetzen. Der/die wissenschaftliche Direktor/in führt den Vorsitz im Direktorium.

Der/die wissenschaftliche Direktor/in repräsentiert die Stiftung AWI nach außen. In seinen/ihren Aufgabenbereich fallen insbesondere die wissenschaftliche Entwicklung der Stiftung, die Forschungsplanung und die Erfolgskontrolle sowie der Ausbau der Einrichtung im nationalen und internationalen Wissenschaftsraum.

Die Aufgaben verlangen eine Persönlichkeit, die über eine hervorragende Qualifikation in der naturwissenschaftlichen Grundlagenforschung und über mehrjährige Erfahrungen in leitenden Funktionen des Forschungsmanagements verfügt. Strategisches Gestaltungsvermögen muss sich in der Person mit praktischer Überzeugungskraft sowie Integrations- und Durchsetzungsfähigkeit verbinden.

Die Bestellung erfolgt für die Dauer von fünf Jahren. Wiederbestellung ist möglich. Die Vergütung orientiert sich an dem Vergütungsrahmen für herausgehobene Hochschulprofessoren.

Die Stiftung AWI kooperiert eng mit der Universität Bremen. Eine gemeinsame Berufung auf eine W-3 Stelle an der Universität Bremen in Verbindung mit der ausgeschriebenen Stelle ist erwünscht.

Die Mitglieder der Helmholtz-Gemeinschaft haben sich die Förderung von Frauen in Führungspositionen zum Ziel gesetzt. Bewerbungen von Frauen werden daher begrüßt.

Bitte richten Sie Ihre Bewerbung mit entsprechenden Unterlagen innerhalb von 3 Wochen nach Erscheinen dieser Anzeige an: **Ministerialdirektor Reinhard Junker, Vorsitzender des Kuratoriums der Stiftung AWI, c/o Bundesministerium für Bildung und Forschung in 53170 Bonn**.

UAMS
COLLEGE OF MEDICINE
UNIVERSITY OF ARKANSAS FOR MEDICAL SCIENCES

CHAIR
DEPARTMENT OF MICROBIOLOGY & IMMUNOLOGY

The College of Medicine at the University of Arkansas for Medical Sciences (UAMS) invites applications and nominations for the position of Chair of the Department of Microbiology & Immunology. Candidates must have strong leadership experience in research, administration and education, evidence of scholarly accomplishments, and a strongly funded research program transportable to the UAMS College of Medicine. The successful candidate will be expected to foster the growth of innovative, high-quality research and educational programs within the department, and build intra- and interdepartmental research and training programs leading to collaborative grants. Responsibilities include leadership of an academic department to serve the University's four-fold mission of teaching, healing, searching and serving. The Department of Microbiology & Immunology has 21 full-time faculty members. It hosts active, NIH-funded research programs in infectious disease, pathogenic bacteriology and virology, cellular and molecular immunology, and tumor immunology. The environment nurtures scholarly, university-based research and collaborative relationships. For more information about the UAMS and its College of Medicine, please visit our website at **www.uams.edu**. This is an exceptional opportunity for a leader with the vision to bring a strong department to the next level of excellence.

Applications, nominations, and requests for information may be sent to: **Nancy J. Rusch, Ph.D., Chair, Search Committee for the Microbiology & Immunology Chair, Department of Pharmacology and Toxicology, The College of Medicine, University of Arkansas for Medical Sciences, 4301 W. Markham Street, Slot 611, Little Rock, AR 72205; Phone: (501) 686-8038; Email: nrusch@uams.edu.** Applicants submitting a letter of interest should include a curriculum vitae.

UAMS is an Equal Opportunity Employer, promoting workplace diversity.

DIRECTOR OF MAGNETIC RESONANCE RESEARCH CENTER

The Albert Einstein College of Medicine of Yeshiva University is seeking a Director for the Gruss Magnetic Resonance Research Center (MRRC). The Center is a shared scientific facility, currently housing a 4T large-bore human magnet research platform and a 9T small-bore animal system. It supports multiple human and animal research projects using spectroscopic imaging, fMRI, and MR imaging. In addition, the Department of Radiology operates 6 clinical magnet systems that are used for human research, both imaging and MRS. Two of these are 3.0T systems. There are plans for an additional two clinical magnets in the next two years.

The Director of the MRRC should be a scientist (MD, PhD or MD/PhD) with outstanding leadership qualities, management skills, and a strong research portfolio. The Director is expected to develop a faculty recruitment plan to appropriately staff the MRRC in collaboration with Einstein Administration, Directors of NIH-funded Centers and Departmental Chairs, as well as direct her/his own research program. The Director will also participate in building a Division of MR Research in the Department of Radiology. The individual should strive to build collaborations with non-MR scientists, and attend to the career development of young investigators with limited MR experience as well as those with significant MR scientific expertise. The Director will also participate in graduate-level teaching programs and be involved in training multidisciplinary investigators.

Interested applicants should write or e-mail a letter of intent and C.V. in an electronic format to: **Dr. E. Stephen Amis, Chair, MRRC Search Committee, Albert Einstein College of Medicine, Jack and Pearl Resnick Campus, 1300 Morris Park Avenue, 312 Belfer, Bronx, NY 10461; Tel: (718) 920-5113, Email: amis@aecom.yu.edu** We welcome applicants who will add diversity to our academic leadership and faculty. EOE

ALBERT EINSTEIN COLLEGE OF MEDICINE
Advancing science, building careers

University of Louisville
Executive Vice President for Research

The University of Louisville (**www.louisville.edu**) is a public university with undergraduate, graduate, and professional degree programs that enroll almost 22,000 students. Expecting to generate more than $170 million in grants and contracts in FY06, UofL faculty, students, and staff carry out research in the arts, sciences, music, business, engineering, social work, nursing, medicine, dentistry, public health, education, and law. The University of Louisville has aggressively and successfully competed for federal funding among top tier funded research universities, especially in the health sciences, and was recognized last year as growing faster in terms of NIH funding over the last five years than any other "research-extensive" university in the nation. Aspiring to achieve recognition as one of the world's premier metropolitan research universities, the University of Louisville is committed to a research environment conducive to creating and freely disseminating the best scholarly contributions and scientific discoveries.

The Executive Vice President for Research reports directly to the President and serves as a member of the four-person Office of the President leadership team (President, Executive Vice President and Provost, Executive Vice President for Health Affairs, and Executive Vice President for Research). The Executive Vice President is responsible for the strategic design and implementation of the University's Research Plan, a fundamental component of the University's goal of preeminence as a metropolitan research university. The position description and additional information about the opening can be found at **www.louisville.edu/president/news/searches**.

The successful candidate will have: a strong record in the application for and management of externally funded grants and/or contracts; university teaching experience and a record of scholarly activity suitable for a tenured senior faculty appointment; demonstrated leadership abilities; broad knowledge of research funding sources for scholarly activity across all disciplines; administrative experience with the ability to interact/lead effectively in a culturally and ethnically diverse community; knowledge of matters related to research compliance, conflict of interest, technology transfer and commercialization of research, special challenges and options for a rapidly growing research university, and opportunities and synergies for a major research university in a large metropolitan community.

Please direct inquiries, nominations, and applications to:
Drs. Don Miller and Beth Boehm
Co-Chairs, Search Committee
102 Grawemeyer Hall
University of Louisville
Louisville, KY 40292

The deadline for expressions of interest to the search committee is **May 1, 2006** but the co-chairs will continue to review nominations and applications throughout the recruitment process.

The University of Louisville is committed to a diverse workforce. We encourage applications from all interested people including women, ethnic minorities, veterans, and disabled individuals.

Opportunity in Parsippany, NJ

Vice President, New Products
GSK Consumer Healthcare R&D

As a world-leading pharmaceutical and consumer healthcare company, GlaxoSmithKline helps people "Do more, feel better & live longer". In a fiercely competitive multi-billion dollar market, GSK Consumer Healthcare R&D team supports the development of leading global brands in OTC medicines, oral care and nutritional healthcare drinks. Innovative and entrepreneurial, this science-driven center of excellence uses state-of-the-art facilities and leading edge technologies to stay at the forefront of new product research and development.

We are now looking for a cutting-edge candidate for the role of Vice President, within our R&D department at our *Innovation Center* in Parsippany, NJ, who will lead the R&D strategy for the development of innovatively new products within our dental care and cold sore product category. This product group already includes well-known brands such as Poligrip®, Polident®, and Abreva®.

Reporting to the Vice President, Innovation for GSK Consumer Healthcare R&D, ideal candidates will lead a team of R&D scientists toward the creation of innovative consumer healthcare products and product extensions within our dental care and cold sore business category. In addition, the position will establish and maintain effective scientific collaborations and relationships with academic, industry, regulatory, and key scientific opinion leaders in dental care, and manage the implementation of the future product development portfolio.

Please visit www.gsk.com/careers to learn more about this position and to apply online. Please reference Req. ID 32932. GlaxoSmithKline is dedicated to supporting you with career-long opportunities and learning. We offer a competitive benefit and compensation package, designed to attract and retain the very best.

GSK is proud to promote an open culture, encouraging people to be themselves and giving their ideas a chance to flourish. GSK is equal opportunity employer M/F/D/V.

Together we can make life better.

gsk GlaxoSmithKline

University of Michigan
Medical School

CHAIR
THE DEPARTMENT OF MOLECULAR AND INTEGRATIVE PHYSIOLOGY

The University of Michigan Medical School is seeking an academic leader to direct the teaching and research programs of its Department of Molecular and Integrative Physiology.

Qualifications include: a Ph.D. or M.D. degree or equivalent, international stature as a leader in an area of Physiology, a proven record of research and innovation, demonstrated commitment to medical education and significant experience in leadership roles.

Please submit your CV and response to:
University of Michigan
Medical School
c/o Office of the Dean
Attn: Martha Smith
M4101 Medical Sciences Building I
Ann Arbor, Michigan 48109-0624

The University is a Non-Discriminatory/ Equal Opportunity Employer.

Chair • Department of Pathology

Stony Brook University's School of Medicine invites nominations and applications for the Shirley Strum Kenny Chair of Pathology. The incumbent also serves as the Pathologist-in-Chief at Stony Brook University Hospital, a 504-bed facility that contains more than 60,000 square feet of laboratory space. Over 70 autopsies, 4,600 cytologies, 18,000 surgical, and 4.1 million laboratory determinations are performed annually. The Department of Pathology has a reputation of excellence in teaching, research, and clinical care. Currently comprised of 21 full-time faculty, it offers a full graduate track leading to the Ph.D. degree in Cellular and Molecular Pathology and a fully accredited residency program in Anatomic and Clinical Pathology. The School of Medicine has a major multidisciplinary initiative in cancer research underway in which the Department plays a critical role.

Required: Candidates should have a record of achievement in mentoring of faculty, conducting meritorious clinical or basic research, and overseeing academic and clinical programs. Clinical and/or basic research interest in cancer would be advantageous. Administrative experience in budgetary and personnel matters. Applicants must hold a medical degree, be qualified for a senior faculty appointment, and be eligible for medical licensure in New York State.

Nominations and applications that include curriculum vitae should be submitted to:
Dr. Martin Karpeh, Chair, Pathology Search Committee
c/o Patricia Marsicano, Health Sciences Center
Level 4-177, Stony Brook University
Stony Brook, NY 11794-8430

Equal Opportunity/Affirmative Action Employer. Visit *www.stonybrook.edu/cjo* for employment information.

STONY BROOK

University of Missouri Health Care

Research Faculty Position

The University of Missouri School of Medicine Department of Surgery is seeking outstanding candidates for two research faculty positions. Rank and appointment status are contingent upon qualifications.

The candidate should have experience in a field of research in which surgeons interface. This includes, but is not limited to, cancer, heart disease, inflammation, wound healing, trauma, and vascular biology. Candidate must demonstrate evidence of current or future potential for federal funding, show interests in teaching medical students and surgical residents, and have the desire to interact with surgical researchers in developing a vigorous, extramurally funded research program.

Applicants should send curriculum vitae to: **Steve Eubanks, M.D., Chairman, Department of Surgery, University of Missouri-Columbia, Health Sciences Center, One Hospital Drive, Columbia, Missouri 65212.**

E-mail: grotewielln@health.missouri.edu

Equal Opportunity/ Affirmative Action/ ADA Employer

Visit the Department of Surgery's Web site at http://www.surgery.missouri.edu/. Go to "Practice Opportunities".

DEAN

College of Food, Agricultural and Natural Resource Sciences

The University of Minnesota, the state's Land Grant University, invites applications and nominations for the position of Dean of the new College of Food, Agricultural and Natural Resource Sciences (CFANS). This new college will integrate and build on the exceptional strengths and comparative advantages of three existing University units: the College of Natural Resources; the College of Agricultural, Food and Environmental Sciences; and the Department of Food Science and Nutrition. CFANS currently consists of 285 faculty in 13 departments with areas of emphasis that include environmental sciences, policy, and management; food, nutrition and animal science; and plant sciences. The Bell Museum of Natural History and the Minnesota Landscape Arboretum, both nationally acclaimed public education facilities, the Cloquet Forestry Center, and 6 research and outreach centers located around the state will be administered by CFANS. The University is seeking a Dean, committed to academic excellence, who has a vision that builds on these strengths and will provide the leadership to achieve this vision. For more detailed discussion of this new College, visit **http://www.umn.edu/transforming_the_u** and **http://www.newcollege.umn.edu/Transition.html.**

The Dean will lead and manage the new college through a period of remarkable institutional transformation. The next Dean will be charged to position the college as one of the premier research and educational centers in the world dedicated to renewable resources, food systems and environmental research. An essential priority for the Dean will be to foster a cohesive collegiate community that will capitalize on new opportunities to pursue excellence in research, teaching, and outreach. The successful candidate must have the ability to provide visionary and innovative leadership with keen insights, skillful management, and an adroit ability to manage relationships across a wide spectrum of institutions and constituencies. As a senior academic officer, the Dean must work collaboratively within and across colleges to foster and promote exceptional academic degree programs and research projects. As an institutional leader, the Dean will be responsible for building coalitions and promoting outreach efforts that engage the University of Minnesota in responding to statewide, national and international issues. The Dean will be expected to work closely with a wide variety of external constituencies, including stakeholders from the non-profit and for-profit sectors, government and other educational organizations. In addition, successful candidates must successfully cultivate development and fundraising opportunities with the public and private sectors in support of the college's academic agenda.

Candidates must: a) have a Ph.D. or terminal degree in a relevant field and a significant record that combines research and scholarship activity with administrative or managerial experiences; b) present evidence of professional distinction and national or international recognition in their field that warrant a tenured full professorship in the college; and c) have a demonstrated track record of effective leadership and management in a complex organization. A faculty appointment may be included in the position if mutually desired. The position reports to the Senior Vice President for Academic Affairs and Provost and is a University of Minnesota senior administrative appointment, classified as a Professional and Administrative position. Salary, faculty rank, and tenure are negotiable based upon qualifications and experience. The preferred starting date for this position is July 1, 2006.

Applications will be reviewed immediately and will be accepted until the position is filled. Applications must include a letter of interest and a current resume or curriculum vitae. All applications and nominations will be held confidential until finalists are determined. Applications and letters of nomination should be sent to: **CFANS Dean Search, c/o Office of the Sr. Vice President for Academic Affairs and Provost, University of Minnesota, 234 Morrill Hall, 100 Church Street SE, Minneapolis, MN 55455. Telephone: (612) 625-0051. Fax: (612) 624-3814. E-mail: provost@umn.edu.**

UNIVERSITY OF MINNESOTA

The University of Minnesota is an Equal Opportunity Educator and Employer.

U.S. DEPARTMENT OF ENERGY
Office of Science
Office of Biological and Environmental Research
Intergovernmental Personnel Act (IPA)
Appointment for two Research Program Managers

The U.S. Department of Energy's (DOE) Office of Biological and Environmental Research (OBER), Office of Science, is soliciting applications from university scientists interested in a 2-year assignment (with an option for an additional 2 years) under an Intergovernmental Personnel Act (IPA) assignment. The respective incumbents will serve as research program managers in the Climate Change Research Division of OBER located in Germantown, Maryland. One assignee would serve as the research program manager for the Terrestrial Carbon Sequestration Research Program and manage selected components of DOE's Terrestrial Carbon Cycle Research Program. Information on these two programs is available at: **http://cdiac2.esd.ornl.gov/index.html** and **http://www.science.doe.gov/ober/CCRD/tcp.html**, respectively. A second IPA assignee would manage DOE's Integrated Assessment Research Program. Information on the Integrated Assessment Research Program is available at: **http://www.science.doe.gov/ober/CCRD/ia.html**. To ensure that research sponsored by these programs is effectively coordinated within and among these and other Climate Change Research Programs in DOE, the incumbents would be expected to work in a team setting with other program managers in OBER.

An IPA assignment is a temporary transfer of skilled personnel between the Federal Government and State or local governments, institutions of higher education, Native American tribal governments, and eligible non-Federal "other organizations," including Federally Funded Research and Development Centers. Assignments are implemented through written Assignment Agreements between DOE, the non-Federal employer, and the assignee. For information on Intergovernmental Personnel Act assignments, please refer to the DOE Directive on IPAs at **http://www.directives.doe.gov/cgi-bin/explhcgi?qry1347894433;doe-110**.

Individuals interested in either IPA assignment position are requested to send their resume to: **Dr. Jerry W. Elwood, Director, Climate Change Research Division, Department of Energy, SC-23.3/Germantown Building, 1000 Independence Avenue, SW, Washington, DC 20585-1290 (Phone: 301-903-3281, email: (jerry.elwood@science.doe.gov)**. Applicants are requested to describe their expertise and experience that would enable them to effectively manage the Terrestrial Carbon Sequestration Research and Carbon Cycle Research Program or manage the Integrated Assessment Research Program. These vacancies will remain open until filled. Prior to submitting an application, prospective applicants should know whether their employer would approve the temporary assignment through the IPA Assignment Agreement.

Postdoctoral Fellow

A postdoctoral fellow position is available in the laboratory of Mitchell J. Weiss, MD, Ph.D. at The Joseph Stokes, Jr. Research Institute of The Children's Hospital of Philadelphia, an interdisciplinary institution dedicated to conducting basic, clinical and translational research on conditions and diseases that affect children.

The postdoc candidate will investigate the role of transcription factors in controlling cell survival, growth and differentiation during normal hematopoiesis and leukemogenesis. The candidate will use mutant mice, embryonic stem cells and tissue culture cells to perform the studies. Applicants must have a doctoral degree in biochemistry, cell biology, molecular biology or a related field and the ability to work well in a team.

Postdoctoral fellows at The Children's Hospital of Philadelphia receive mentored training in a rich scientific and collaborative environment that includes the resources of the adjacent University of Pennsylvania. Visit **www.stokes.chop.edu** for more information about The Joseph Stokes, Jr. Research Institute and its research programs.

Interested individuals should submit their resume to: **www.stokes.chop.edu** and **weissmi@email.chop.edu.**

Hamilton Eye Institute
Research Center
Department of Ophthalmology

TENURE-TRACK FACULTY POSITION

The Department of Ophthalmology at The University of Tennessee Health Science Center is seeking an Assistant Professor to join the newly opened Hamilton Eye Institute Research Center, with outstanding core facilities for bioimaging and molecular genetics. The candidate should demonstrate the potential for establishing a vigorous, independent research program with extramural funding in retinal injury/degeneration, glaucoma, retinal development, or related areas. Generous startup support, newly renovated research space, and access to core research facilities will be provided. Candidates may participate in the teaching programs of the Graduate School of Health Sciences. Applicants must have PhD or MD degree.

Applicants should send a curriculum vitae, statement of research interests, and the names of three references to: **Eldon Geisert, Ph.D., Chair of the Recruiting Committee, Department of Ophthalmology, 930 Madison Ave., Ste. 731, University of Tennessee HSC, Memphis TN 38163**.

The University of Tennessee is an Affirmative Action/Equal Opportunity Employer.

STANFORD
UNIVERSITY

EXECUTIVE DIRECTOR
Global Climate and Energy Project

The Global Climate and Energy Project (GCEP) solicits applications for the position of Executive Director. GCEP is a ten-year, $225 million project devoted to fundamental science and engineering science research leading to new options for reducing greenhouse gas emissions associated with energy use. We seek a person of high stature in energy research with a demonstrated record of research in an energy area related to GCEP's research activities. The ideal candidate will be a research scientist or engineer who also has significant experience in developing and managing a research portfolio. We anticipate that this appointment will be made as a research faculty or senior fellow associated with a department or institute appropriate to the background of the successful candidate. Funding for this position will be provided by GCEP. The successful applicant will interact effectively with a broad range of Stanford colleagues, including physical, chemical, and biological scientists, and engineers, as well as representatives of the project sponsors. The search is open to applicants at the level of full professor or senior fellow. The position will remain open until filled.

Applications, including a curriculum vita, a statement outlining research interests and research management approach, and the names and addresses of three or more referees, should be sent by **May 15, 2006**, via either electronic or regular mail, to:

GCEP Executive Director Search Committee, 416 Escondido Mall
Stanford University
Stanford, CA 94305-2205
gcep_search@stanford.edu

Questions can be directed to **Prof. Franklin M. Orr, Jr.** at:
gcep_inquiries@stanford.edu

Information about GCEP can be found at: **http://gcep.stanford.edu**

Stanford University has a strong institutional commitment to the principle of diversity. In that spirit, we particularly encourage applications from women, members of ethnic minorities, and individuals with disabilities.

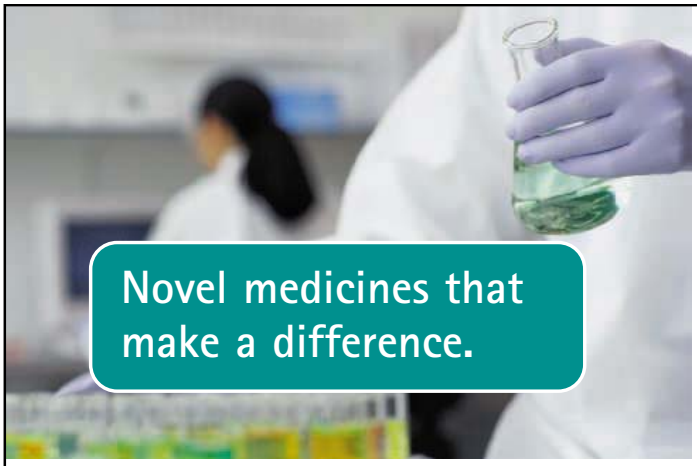

Merck is dedicated to discovering, developing and delivering novel medicines and vaccines that can make a difference in people's lives. But our mission also entails something more. As a Company, we seek to maintain high ethical standards and a culture that values honesty, integrity and transparency in all that we do.

Merck & Co., Inc. is currently hiring for the following positions:

Genetically Engineered Models - the focus of this group is to utilize "cutting edge" gene-targeting technologies and to pioneer new "disruptive technologies" to advance Merck's mission to develop medicines for unmet medical need.

- **Associate Director – Boston, MA (SCI002730)**
- **Sr. Program Manager – Rahway, NJ (SCI002728)**

Molecular Profiling is staffed by biologists with expertise in applying gene expression profiling and other high through put genomic technologies and analysis tools towards biomarker and new target discovery The following Lead Scientist positions are currently open:

Molecular Profiling – Guided Solutions

- **Sr. Research Biologist – Oncology – West Point, PA (SCI002690)**
- **Sr. Research Biologist – Neurology – West Point, PA (SCI002741)**

Molecular Profiling – Metabolic Diseases

- **Sr. Research Biologist – Rahway, NJ (SCI002740)**

Molecular Profiling – Proteomics is a cross-disciplinary team applying state of the art Fourier Transform Mass Spectrometry to identify and quantify altered protein levels and post translational modifications related to disease or therapeutic agents. Proteins and multi-analyte protein signatures may serve as pharmacodynamic, efficacy, or toxicity markers in preclinical and clinical drug development.

- **Research Chemist – Rahway, NJ (SCI002669)**
- **Sr. Research Chemist – Boston, MA (SCI002696)**
- **Sr. Research Chemist – Boston, MA (SCI002687)**

Please visit Merck's website at **www.merck.com/careers** and search for the SCI number referenced above to apply for the position you're interested in!

MERCK

www.merck.com

Merck is an equal opportunity employer—proudly embracing diversity in all of its manifestations.

ROSETTA INPHARMATICS

A wholly owned subsidiary of Merck & Co., Inc.

Rosetta Inpharmatics LLC is a wholly owned subsidiary of Merck & Co., Inc., located in Seattle, Washington. We conduct leading-edge genomic research and data analysis focused on how medical compounds affect biology, enabling more accurate selection of drug targets and more efficient drug development.

At **Rosetta,** we believe that employees who have a passion for the work they do - and are challenged by it - achieve results that often exceed expectations, and have an indelible impact on their team and the company. We foster an environment that encourages creativity, drive,teamwork, and the desire to improve the quality of human life through the advancement of drug discovery. If the same basic principles and values guide your career, we'd like to hear from you.

Rosetta Inpharmatics LLC is currently hiring for the following positions, located in Seattle, WA:

Informatics is a cross-disciplinary team of computational biologists, data analysts, software developers, DBAs, and laboratory scientists that researches, develops, integrates & applies cutting-edge methods, databases, and software solutions to empower drug discovery & development.

- **Sr. Research Scientist – Data Analyst**
- **Sr. Research Scientist – Pathway Analyst**
- **Bioinformatics Developer – Pathways**
- **Software Engineer – Database Development & Integration**
- **Bioinformatics Database Developer**

Biology/Gene Modification involves laboratory experiments directed at developing cutting-edge applications of RNA interference and DNA microarray technology. Research programs include the use of microarray technology for analysis of signal transduction pathways, and miRNA analysis and RNAi screens for target identification.

- **Sr. Research Biologist**

Gene Expression Laboratory is a high through put Microarray processing facility that generates high quality gene expression data.

- **ERP/JDE Administrator**
- **Sr. Manager, Customer Support Services**

Genetics is a team of computational scientists, bioinformaticians, and statistical geneticists that develop and apply methods to analyze and mine genetic/molecular profiling data in segregating mouse and human populations to elucidate complex human diseases and identify and validate novel targets for those diseases.

- **Sr. Statistical Geneticist**
- **Sr. Research Scientist – Network Analyst**
- **Sr. Research Biologist – Genetics**
- **Sr. Research Scientist – Genetic Analyst**
- **Sr. Statistical Geneticist – Group Leader**
- **Statistical Geneticist – Seattle, WA & Rahway, NJ**

Please visit the Rosetta web site to view job descriptions and apply: **www.rii.com.**

www.rii.com

Merck is an equal opportunity employer—proudly embracing diversity in all of its manifestations.

PRESIDENT / CEO

Foundation for Blood Research

Foundation for Blood Research
with
Faculty Appointment
Dartmouth Medical School

Dartmouth Medical School

The Foundation for Blood Research (FBR), is conducting a search for a President/CEO. This position includes a faculty appointment, for a suitable candidate, at Dartmouth Medical School (DMS). FBR is located in Scarborough, Maine, a suburb of Portland, Maine's largest city, close to the ocean, lakes, and beaches, and within driving distance to Dartmouth Medical School located in Hanover, New Hampshire. FBR's major areas of education, research and clinical testing include molecular genetics, prenatal screening, and rheumatic diseases.

The President of the Foundation for Blood Research is expected to direct scientific development and promote the fiscal health of the organization. The President will lead the institution in finding ways to identify, manage, and prevent human disease through clinical laboratory investigation and service, clinical epidemiology, outreach science and education, and public health program design and evaluation. The President will work closely with the Dean and senior personnel at Dartmouth Medical School to advance joint clinical research and outreach education activities. A medical degree is required, and the physician should be licensable in Maine and be (or have been) a Principal Investigator on grants awarded at the national or international level and have a record of peer-reviewed publications. Optimally, the candidate will have national stature and be experienced managing a group of scientists.

Applications: Send letter of interest and curriculum vitae to:

Chair, Search Committee
Foundation for Blood Research
P.O. Box 130
Scarborough, ME 04070-0130

www.fbr.org

EEOC

Assistant or Associate Professors

Department of Pharmacology and Experimental Therapeutics

Boston University School of Medicine

The Department of Pharmacology and Experimental Therapeutics at Boston University School of Medicine (**http://www.bumc.bu.edu/busm/pm**) invites applications for the position of Assistant or Associate Professor. Individuals with an interest in applying pharmacological principles to contemporary problems in neuroscience, translational neuroscience, or transdisciplinary research (such as neurotropic viruses; cancers of nervous tissue; oncogenes in synaptic plasticity; biomarkers; or medicinal chemistry) are encouraged to apply. The Department has strengths in a broad range of research areas including learning and memory, neuropeptides, substance abuse, neurodegenerative diseases, anxiety, and epilepsy. The Department awards a PhD in Pharmacology and Experimental Therapeutics, which may be combined with a joint PhD in Biomedical Neuroscience, or Cellular and Molecular Biology. The Department administers an active university-wide pharmacological sciences training program that is supported by an NIGMS T32 in Biomolecular Pharmacology.

Interested individuals should send a curriculum vitae to: **Dr. David H. Farb, Chairman, Department of Pharmacology and Experimental Therapeutics, Boston University School of Medicine, 715 Albany Street, L-603, Boston, MA 02118**.

An Equal Opportunity/Affirmative Action Employer.

POPULATION COUNCIL SEEKS DIRECTORS FOR NEW PROGRAMS

The Population Council is implementing a major strategic planning initiative and seeks program directors for three areas: HIV/AIDS; Poverty, Gender, and Youth; and Reproductive Health. The Council seeks to improve the well-being and reproductive health of current and future generations around the world. Activities include biomedical, social science, and health-related research, demographic analysis, development and introduction of appropriate biomedical products, innovative program development, evaluation, and scaling up.

The program directors will play a leading role in setting priorities for future program development and implementation; analysis and implementation of ongoing projects; allocation of unrestricted funds; fundraising; and representation of the Council to governments, NGOs, industry partners and donor agencies. Program directors will be headquartered in New York or Washington, DC and will work closely with staff members in 17 regional and country offices throughout the developing world. Send CV and cover letter to the attention of **Ms. Vivien Rabin, Director of Human Resources; Population Council, One Dag Hammarskjold Plaza, New York, NY 10017; jobs@popcouncil.org; fax #646-277-8243.**

For full job descriptions, including qualifications, go to: **http://www.popcouncil.org/opportunities/index.html**.

AA/EOE M-F

SENIOR SCIENTIST

BioProtection Systems Corporation (BPSC), an affiliated company to NewLink Genetics, is a vaccine development company located in the Iowa State University Research Park in Ames, Iowa. The company is developing innovative vaccine solutions utilizing the innate immune system against viral and bacterial pathogens. We are seeking an experienced individual to lead a creative group of scientists in the application of our proprietary vaccine technology.

Background/Qualifications: Ph.D. in Immunology or Virology with at least 5 years postdoctoral experience (preferably industrial) in immunology/infectious disease or vaccine research.

Responsibilities include, but are not limited to:

- Manage scientific team focused on anti-viral vaccine development including supervision and execution of work plans and projects.
- Develop cell-based and animal models for testing efficacy of anti-viral vaccine candidates.
- Apply knowledge of vaccine formulations and methods to maximize human immune responses to viral immunogens.
- Good written and verbal communication skills with a proven record in obtaining extramural funding.

Interested applicants should forward their cover letter and resume along with salary history/requirements to: **Joseph E. Nash, Business Manager, BioProtection Systems Corporation, 2901 South Loop Drive, Suite 3360, Ames, Iowa 50010-8646** or E-mail your resume to: **apply@bpsys.net**.

Looking for a great science career?

Get the experts behind you.
Visit www.ScienceCareers.org

Your career is too important to leave to chance. So to find the right job or get career advice, turn to the experts. At ScienceCareers.org we know science. And we are committed to helping take your career forward. Our knowledge is firmly founded on the expertise of *Science*, the premier scientific journal, and the long experience of AAAS in advancing science around the world. Put yourself in the picture with the experts in science. Visit www.ScienceCareers.org.


Science
AAAS
Marie Curie
1867-1934
Science
AAAS
Albert Einstein
1879-1955
ALBERT EINSTEIN and related rights ™/© of The Hebrew University of Jerusalem, used under license. Represented by The Roger Richman Agency, Inc., www.albert-einstein.net.
ScienceCareers.org
We know science
AAAS

POSITIONS OPEN

ASSISTANT PROFESSOR
Evolutionary Biology / Molecular Systematics

The Department of Botany at Oklahoma State University (OSU) **(website: http://botany.okstate.edu)** seeks to fill a tenure-track Assistant Professor position (start date negotiable), as part of an Oklahoma NSF Experimental Program to Stimulate Competitive Research (EPSCoR) initiative to develop plant virology statewide **(website: http://bioinfosu.okstate.edu/pvbe).** Successful candidates are expected to mentor students and develop extramurally funded experimental research on the molecular systematics or evolution of plants or plant viruses. Expertise in molecular biology and a working knowledge of bioinformatics are required. Opportunities exist for collaborative research in plant biology spanning Oklahoma's research universities and the S. R. Noble Foundation. Teaching duties will include appropriate undergraduate and graduate courses. A Ph.D. degree, strong publication record, and postdoctoral experience are required. Position will remain open until filled; for full consideration, submit a PDF containing vitae, statements of research and teaching interests, and contact information for three references by 26 May 2006, to **e-mail: paula.shryock@okstate.edu.** *OSU is an Equal Opportunity, Affirmative Action Employer. Women and minorities are encouraged to apply.*

DEPARTMENT OF PEDIATRICS
University of Colorado School of Medicine
Genetics and Basic Biology of Neurodevelopmental Disorders in Childhood

The Department of Pediatrics at the University of Colorado Health Sciences Center is seeking applications from senior investigators studying the genetic and cellular basis, animal models, or therapeutic approaches to neurodevelopmental disorders of childhood. The successful applicant will be a member of the Mental Retardation and Developmental Disabilities Research Center that has been funded by the National Institute of Child Health and Human Development for more than 35 years. Appointment will be at the **FULL** or **ASSOCIATE PROFESSOR** level, as appropriate.

Send curriculum vitae and statement of research interest to: **Richard A. Spritz, M.D., Professor and Director, Human Medical Genetics Program, University of Colorado Health Sciences Center, P.O. Box 6511, Mail Stop 8300, Aurora, CO 80045-0511.** Review of applications will begin on May 1, 2006, and continue until the position is filled.

The University of Colorado is committed to diversity and equality in education and employment.

POSTDOCTORAL POSITIONS
Department of Neurosciences
Medical University of South Carolina at Charleston

Postdoctoral positions are available in drug abuse or in primate cognitive neuroscience. Candidates will partake in the development of a new drug abuse laboratory at Medical University of South Carolina in Charleston (MUSC), or a new Carolina Primate Center located in Yemassee (60 to 90 minutes from Charleston). Applicants must have a strong academic record of independent research with a Ph.D. or M.D. degree and expertise in the neuroscience of drug abuse, or neurophysiology in behaving monkeys. Applicants must apply online at **website: http://www.musc.edu/hrm/careers/faculty.htm.** Position requisition number is 042486. Applicants should submit online curriculum vitae, names of three references, and a cover letter expressing their interest and qualifications to: **Gary Aston-Jones, Ph.D., Murray Chair of Excellence and Director, Carolina Primate Center, Department of Neurosciences, Medical University of South Carolina, 173 Ashley Avenue, BSB 403, Charleston, SC 29425.** *MUSC is an Equal Employment Opportunity/Affirmative Action Employer.*

POSITIONS OPEN

A **POSTDOCTORAL POSITION** is currently available for studies of endometriosis in nonhuman primates at the Oregon National Primate Research Center. The project will focus on the effects of steroid hormones and hormone antagonists on eutopic and ectopic rhesus macaque endometrium. The studies will also involve organ culture with nonhuman primate tissues. Requirements include a Ph.D. or equivalent, a strong background in reproductive biology, experience in immunocytochemistry, in situ hybridization and molecular biology, laboratory animal surgery, excellent skills in written and verbal English communication, data analysis, and the ability to work both independently and in collaboration with other team members. Salary will be commensurate with experience and NIH standards. Please submit a summary of research experience, curriculum vitae, a statement of research interests and three references to: **Ov Daniel Slayden, Division of Reproductive Sciences, Oregon National Primate Research Center, Oregon Health Sciences University, 505 N.W. 185th Avenue, Beaverton, OR 97006.**

GRADUATE STUDENT POSITIONS are available to work on the molecular biology of Anaplasma. The research will involve the development of attenuated strains through the use of genetic transformation and gene knockouts for potential use as vaccines. Prior experience with molecular biology techniques and veterinary infectious diseases is desirable. *Stipulations of the funding require applicants to be natives of Mexico, or a Central or South American country.* For further information or to make an application, please contact: **Dr. A.F. Barbet, Department of Infectious Diseases and Pathology, University of Florida, Box 110880, Gainesville, Florida 32611, U.S.A. (e-mail: barbet@ufl.edu).** Applications will be reviewed as received with at least one position beginning fall semester 2006.

Two University of California, San Francisco/Northern California Institute for Research and Education **POSTDOCTORAL POSITIONS** are available in areas including signal transduction, tumor cell biology, stem cell biology, neurosciences, and wound healing. Applicants with Ph.D. in biochemistry or cell and molecular biology will be considered. To apply send curriculum vitae and names of two references to **e-mail: careers@ncire.org** and reference job number 06-175 in the subject line. For questions you may write or e-mail: **Dr. Lilly Bourguignon, Ph.D., Department of Medicine, University of California at San Francisco and VAMC (111N), 4150 Clement Street, San Francisco, CA 94121 (e-mail: lilly.bourguignon.ucsf.edu).**

RESEARCH ASSISTANT PROFESSOR and **POSTDOCTORAL FELLOW POSITIONS** available to study the molecular mechanisms of integrin signaling and platelet activation. Candidates must have M.D. or Ph.D. Please submit curriculum vitae and names of three references by June 1, 2006, to: **Dr. Xiaoping Du, Department of Pharmacology (MC 868), University of Illinois at Chicago, 835 S. Wolcott Avenue, Chicago, IL 60612. E-mail: xdu@uic.edu.** *The University of Illinois is an Affirmative Action/Equal Opportunity Employer.*

RESEARCH ASSOCIATE with experience in protein studies. Send resume to: **Dr. McCrae, Case Western Reserve University, 10900 Euclid Avenue, Cleveland, OH 44106.** Must reference job code FF2006. *Equal Opportunity Employer.*

FELLOWSHIPS

The Weizmann Institute of science

will award a limited number of

Distinguished Postdoctoral Fellowships

known as

Koshland Scholars

The fellowships are available in all the fields of scientific research that are pursued at The Weizmann Institute in the following areas:

Biology, Chemistry, Computer Science
Physics, Mathematics, Biochemistry

All courses and seminars at the Institute are conducted in English.

Applications may be submitted at any time, but the awards will be made shortly after the usual deadlines for the submission of Fellowship applications: January 1 and May 15 of each year. Candidates for Koshland fellowships must be sponsored by a Faculty Member of the Weizmann Institute. Interested candidates are advised to contact prospective sponsors directly.

For additional information and application forms, consult the Feinberg Home Page at **http://www.weizmann.ac.il/feinberg** or write to: Postdoctoral Fellowships Program, The Feinberg Graduate School, The Weizmann Institute of Science, Rehovot 76100, Israel; Fax: 972-8-934-4114; e-mail: postdoc@weizmann.ac.il

The Weizmann Institute of Science invites outstanding Ph.D. students at universities abroad who are nearing graduation (or who have recently completed their Ph.D. studies) to visit the Institute for a few days, meet its scientists, explore postdoctoral research opportunities, and experience its warm and relaxed atmosphere. A limited number of such visits are subsidized by the Institute on a competitive basis. Those who are invited are under no obligation to the Institute to continue their postdoctoral studies here. For more details, see **http://www.weizmann.ac.il/feinberg/student_visit**

The Weizmann Institute was selected in 2005 to be the best place to work in academia outside the US. See link: **www.thescientist.com/2005/11/7/39/1**

POSITIONS OPEN

VETERINARY PATHOLOGIST

The Department of Pathobiology at the University of Florida College of Veterinary Medicine is seeking a Veterinary Pathologist for a tenure-track position at the rank of **ASSISTANT/ASSOCIATE** or **FULL PROFESSOR.** Applicants should have a D.V.M. or equivalent degree and a record of research accomplishment in infectious disease/emerging pathogens and/or immunologic mechanisms. Applicants having a Ph.D. degree and American College of Veterinary Pathologists certification are preferred. Primary responsibilities will be to conduct a competitive program in research and to teach pathology. Teaching may be at the professional, graduate, resident, and/or postdoctoral levels. The Department has excellent research facilities and programs in infectious disease and comparative immunology (**website: http://www.vetmed.ufl.edu/path.htm**). The University of Florida is developing a campus-wide program of excellence to study emerging pathogens. Applicants should submit a letter outlining professional goals, curriculum vitae, and a list of three references to:

Dr. William Castleman
Department of Pathobiology
College of Veterinary Medicine
P.O. Box 110880
University of Florida
Gainesville, FL 32611-0880

Informal inquiries are welcome (**e-mail: castlema@ufl.edu; telephone: 352-392-4700, extension 3920**). Review of applicants is ongoing and will continue until the position is filled. The start date is flexible and negotiable. *The University of Florida is an Equal Opportunity/Equal Access/Affirmative Action Employer.*

RESEARCH ASSOCIATE
(Assistant Professor)

The University of Chicago, the Ben May Institute for Cancer Research is seeking a full-time Research Associate (Assistant Professor) to examine the biological functions of c-June N-terminal kinase (JNK) using a range of molecular, cellular, and genetic approaches. Applicants should have Ph.D. degree, with strong background in immunology and virology. An outstanding publication record and at least three years of research experience in signal transduction are essential.

Qualified applicants must provide current curriculum vitae and bibliography, statement of research interest and goals, and full names, addresses, telephone and fax numbers, and e-mail addresses of at least three scholars who can provide academic references.

Application material should be sent to:

Barbara Patterson
Human Resources Administrator
The University of Chicago
The Ben May Institute for Cancer Research
929 E. 57th Street, CIS, W-421D
Chicago, IL 60637

The University of Chicago is an Affirmative Action/Equal Opportunity Employer.

POSTDOCTORAL POSITION AVAILABLE

Immediate opening for a motivated individual to study the regulation of lymphocyte development, activation, and antitumor immunity. The focus of the laboratory is on understanding the mechanisms by which Cbl, PKA, and microRNA influence intracellular signaling network required for lymphocyte lineage development and function. Successful candidate will join an expanding and well-equipped research team in a highly interactive research environment at Columbia University. Experience in immunology and molecular biology is essential.

Please send curriculum vitae and three letters of reference to:

Hua Gu, Ph.D., Department of Microbiology, Columbia University College of Physicians and Surgeons, HHSC, Room 6-611, 701 West 168th Street, New York, NY 10032; or **e-mail: hg2065@columbia.edu.**

Columbia University is an Affirmative Action/Equal Opportunity Employer.

POSITIONS OPEN

POSTDOCTORAL FELLOWSHIPS
Insect Virology/Ecological Risk Assessment
Sault Sainte Marie, Ontario, Canada

Two Postdoctoral Positions on development and risk assessment of genetically modified baculoviruses for forest insect pests are available. One Postdoctoral Fellowship is for risk assessment of genetically modified baculoviruses in a forest ecosystem. A Ph.D. with expertise in ecology and entomology is needed; additional expertise in mathematical modelling, insect pathology and molecular virology is advantageous (for details, contact **Dr. J. Cory** at **e-mail: jenny.cory@algomau.ca**). Another Postdoctoral Fellowship is on development and evaluation of modified spruce budworm baculoviruses carrying native host insect genes and control regions. A Ph.D. with experience in molecular virology and entomology is an asset (for details, contact **Dr. B. Arif** at **e-mail: barif@nrcan.gc.ca**). Contact and curriculum vitae to **Dr. Peter Krell** (University of Guelph) at **e-mail: pkrell@uoguelph.ca.**

POSTDOCTORAL FELLOW, IMMUNOLOGY

The Department of Pathology seeks a recent self-motivated Ph.D. for an NIH funded study seeking to define the cell mediated immune response to human polyomavirus BK. The position requires a working knowledge of immunoinformatics, ELISPOT and tetramer binding assays, epitope mapping, cell sorting, preparation of recombinant proteins in Baculovirus vectors, and DNA sequencing. More information about the Department is available at **websites: http://path.upmc.edu** and **http://path.upmc.edu/divisions/transpath.html.**

Respond with a cover letter, statement of interests, curriculum vitae, and contact information for three references references to: **Professor P.S. Randhawa, M.D.,** at **e-mail: randhawapa@msx.upmc.edu.**

ANNOUNCEMENTS

INDO-UNITED STATES SCIENCE AND TECHNOLOGY FORUM
Second Call for Proposal 2006

The Indo-United States Science and Technology Forum, established under an agreement between the governments of India and the United States of America, is an autonomous, not-for-profit society that promotes and catalyzes the Indo-U.S. bilateral collaborations in science, technology, engineering and biomedical research through substantive interaction among government, academia, and industry.

The Forum seeks to support innovative programs aimed to stimulate interactions that have a strong potential for generating follow-on activities and building long term Indo-U.S. science and technology relationships. The Forum promotes program that nurtures contacts between the young and mid-career scientists and technologists and fosters active public-private partnership in research and development.

The Forum solicits proposals thrice a year (January, May, and October) jointly submitted by the U.S. and Indian principal investigators from academia, government funded institutions/laboratories and private research and development entities for: (1) Knowledge research and development Networked and Public-Private Networked Indo-U.S. Centers. (2) Bilateral workshop, conference, symposium, training schools, et cetera. (3) Travel grants (i) To avail already awarded fellowship and sabbatical positions in U.S./India. (ii) For selected U.S. participants to attend international conferences / events in India. (iii) For specific exploratory/planning visits aimed at large scale collaborations.

Detailed format available at **website: http://www.indousstf.org.**

For further details and electronic submission, contact: **Arabinda Mitra, e-mail: amitra@indousstf.org** and **Michael Cheetham, e-mail: mcheetham@si.edu.**

Submission deadline: 15 June 2006. Award announcement: mid-September 2006.

Fulbright House, 12 Hailey Road, New Delhi-110 001, India. **Website: http://www.indousstf.org.**

MARKETPLACE